Friedrich-Schiller-Universität Jena

Chemisch-Geowissenschaftlichen Fakultät

Stimuli-responsive polymeric nanoparticles for biomedical applications

Dissertation

(kumulativ)

zur Erlangung des akademischen Grades

doctor rerum naturalium (Dr. rer. nat.)

vorgelegt dem Rat der Chemisch-Geowissenschaftlichen Fakultät der

Friedrich-Schiller-Universität Jena

von M. Sc. Turgay Yildirim

geboren am 1. Januar 1984 in Sariz (Türkei)

Gutachter:

1. .....

2. .....

Tag der öffentlichen Verteidigung: ……

Ayşu'ma

Table of Contents

Documentation of authorship

This section contains a list of the individual contributions to the publications reprinted in this thesis.

P1	C. Englert,[1] J. C. Brendel,[2] T. Majdanski,[3] T. Yildirim,[4] S. Schubert,[5] M. Gottschaldt,[6] N. Windhab,[7] U. S. Schubert,[8] "Pharmapolymers in the 21st century: Synthetic polymers in drug delivery applications", submitted.							
Author	**1**	**2**	**3**	**4**	**5**	**6**	**7**	**8**
Conceptual development	×	×			×	×	×	×
Preparation of the manuscript	×	×	×	×	×	×		
Correction of the manuscript		×	×	×	×	×	×	×
Proposed publication equivalent				0.5				

P2	T. Yildirim,[1] A. C. Rinkenauer,[2] C. Weber,[3] A. Traeger,[4] S. Schubert,[5] U. S. Schubert,[6] "RAFT made methacrylate copolymers for reversible pH-responsive nanoparticles", *J. Polym. Sci., Part A: Polym. Chem.* **2015**, *53*, 2711-2721.					
Author	**1**	**2**	**3**	**4**	**5**	**6**
Conceptual development	×			×	×	×
Polymer synthesis & characterization	×					
Nanoparticle synthesis & characterization	×					
Scientific discussions			×			
Cytotoxicity studies		×				
Preparation of the manuscript	×					
Correction of the manuscript		×	×	×	×	×
Proposed publication equivalent	1.0					

P3 T. Yildirim,[1,#] C. Matthaeus,[2,#] A. T. Press,[3] S. Schubert,[4] M. Bauer,[5] J. Popp,[6] U. S. Schubert,[7] "Uptake of retinoic acid-modified PMMA nanoparticles in LX2 and liver tissue by Raman imaging and intravital microscopy", *Macromol. Biosci.* **2017**, *DOI: 10.1002/mabi.201700064*. # Authors contributed equally.

Author	**1**	**2**	**3**	**4**	**5**	**6**	**7**
Conceptual development	×	×		×			
Polymer synthesis & characterization	×						
Nanoparticle synthesis & characterization	×						
Raman measurements		×					
Intravital microscopy measurements			×				
Preparation of the manuscript	×	×	×	×			
Correction of the manuscript	×	×	×	×	×	×	×
Proposed publication equivalent	1.0						

P4 T. Yildirim,[1] A. Traeger,[2] E. Preussger,[3] S. Stumpf,[4] C. Fritzsche,[5] S. Hoeppener,[6] S. Schubert,[7] U. S. Schubert,[8] "Dual responsive nanoparticles from a RAFT copolymer library for the controlled delivery of doxorubicin", *Macromolecules* **2016**, *49*, 3856-3868.

Author	**1**	**2**	**3**	**4**	**5**	**6**	**7**	**8**
Conceptual development	×							×
Polymer synthesis & characterization	×							
Nanoparticle synthesis & characterization	×			×		×		
Cytotoxicity studies			×		×			
Cellular uptake studies		×						
Preparation of the manuscript	×							
Correction of the manuscript		×	×	×	×	×	×	×
Proposed publication equivalent	1.0							

P5	T. Yildirim,[1] I. Yildirim,[2] R. Yanez-Macias,[3] S. Stumpf,[4] C. Fritzsche,[5] S. Hoeppener,[6] C. Guerrero-Sanchez,[7] S. Schubert,[8] U. S. Schubert,[9] "Dual pH and ultrasound responsive nanoparticles with pH triggered surface charge-conversional properties", *Polym. Chem.* **2017**, *8*, 1328-1340.

Author	**1**	**2**	**3**	**4**	**5**	**6**	**7**	**8**	**9**
Conceptual development	×								×
Polymer synthesis & characterization	×	×	×						
Nanoparticle synthesis & characterization	×			×		×			
Cytotoxicity studies					×				
Preparation of the manuscript	×								
Correction of the manuscript		×	×	×	×	×	×	×	×
Proposed publication equivalent	1.0								

P6	T. Yildirim,[1] A. Traeger,[2] P. Sungur,[3] S. Hoeppener,[4] C. Fritzsche,[5] I. Yildirim,[6] D. Pretzel,[7] S. Schubert,[8] U. S. Schubert,[9] "Polymersomes with endosomal pH induced vesicle-to-micelle morphology transition and a potential application for controlled doxorubicin delivery", submitted.

Author	**1**	**2**	**3**	**4**	**5**	**6**	**7**	**8**	**9**
Conceptual development	×								×
Polymer synthesis & characterization	×					×			
Nanoparticle synthesis & characterization	×		×	×					
Cellular uptake studies		×							
Cytotoxicity studies					×				
Comet assay studies							×		
Preparation of the manuscript	×								
Correction of the manuscript		×	×	×	×	×	×	×	×
Proposed publication equivalent	1.0								

Erklärung zu den Eigenanteilen des Promovenden/der Promovendin sowie der weiteren Doktoranden/Doktorandinnen als Koautoren an den Publikationen und Zweitpublikationsrechten bei einer kumulativen Dissertation

Für alle in dieser kumulativen Dissertation verwendeten Manuskripte liegen die notwendigen Genehmigungen der Verlage („Reprint permissions") für die Zweitpublikation vor.

Die Co-Autoren der in dieser kumulativen Dissertation verwendeten Manuskripte sind sowohl über die Nutzung, als auch über die oben angegebenen Eigenanteile informiert und stimmen dem zu.

Die Anteile der Co-Autoren an den Publikationen sind in diesem Kapitel aufgeführt (Documentation of authorship).

Ich bin mit der Abfassung der Dissertation als publikationsbasiert, d.h. kumulativ, einverstanden und bestätige die vorstehenden Angaben. Eine entsprechend begründete Befürwortung mit Angabe des wissenschaftlichen Anteils des Doktoranden/der Dokorandin an den verwendeten Publikationen werde ich parallel an den Rat der Falkultät der Chemisch-Geowissenschaftlichen Fakultät richten.

Turgay Yildirim	Datum	Ort	Unterschrift
Prof. Dr. Ulrich S. Schubert	Datum	Ort	Unterschrift

1. Introduction

Parts of this chapter have been published in: **P1**) C. Englert, J. C. Brendel, T. Majdanski, T. Yildirim, S. Schubert, M. Gottschaldt, N. Windhab, U. S. Schubert, "Pharmapolymers in the 21st century: Synthetic polymers in drug delivery applications", submitted.

Polymeric nanoparticles have attracted tremendous interest, in particular for controlled drug delivery applications. According to the National Nanotechnology Initiative, the term 'nanoparticle' refers to materials with dimensions between 1 and 100 nm. However, several materials are considered as nanoparticles in literature although they have larger dimensions (up to several hundred nanometers).[1] Nanoparticles in literature usually refer to liposomes, micelles, polymersomes, nanogels and polymer drug conjugates. Within this thesis, the focus will be on stable solid dispersions (prepared by nanoprecipitation of statistical copolymers), polymeric micelles and polymersomes (polymeric vesicles). In the last few decades, numerous polymeric nanoparticle based drug delivery systems have been used in various stages of clinical trials for the treatment of different diseases. These systems improve the therapeutic efficiency of the physically encapsulated or chemically conjugated drugs mainly by (i) improving the solubility of poorly water-soluble drugs, (ii) prolonging the circulation time, (iii) helping preferential accumulation at the tumor sites by the enhanced permeability and retention (EPR) effect[2] as well as by (iv) reducing systemic side effects.[3] Nevertheless, poor cellular internalization and premature drug release still limit the therapeutic efficacy. To circumvent these limitations, stimuli-responsive polymeric nanoparticles became the focus of considerable interest as a result of their on demand drug release ability as well as their tunable physicochemical properties.[4] In order to ensure the reliability and the reproducibility of the stimuli-responsive polymeric nanoparticle systems, synthesis of polymers with well-defined chemical composition, molar mass, high end group fidelity and low dispersity are crucial.[5] The development of reversible deactivation radical polymerization (RDRP) techniques during the last decades including nitroxide mediated polymerization (NMP),[6] atom transfer radical polymerization (ATRP)[7] and reversible addition fragmentation chain transfer (RAFT) polymerization[8] has tremendously simplified the synthesis of well-defined polymers. Among these polymerization methods, the RAFT polymerization process is probably the most commonly used one as a result of its tolerance of a wide variety of polymerization conditions and different functionalities in the monomers.[9] However, successful synthesis of the polymers is only the first step in reaching the goal; the polymers also need to be formulated into nanoparticles in a controlled and reproducible

way. Being facile, time-saving and cheap, nanoprecipitation represents a straightforward technique to fabricate nanoparticles.[10] The nanoprecipitation method usually relies on (i) dissolution of the polymer in a good solvent (an organic solvent that is miscible with water), (ii) self-assembly of the well-dissolved polymers into nanoparticles by exposure of polymer to water (non-solvent), and (iii) removing of organic solvents by evaporation (for low boiling point solvents) or by dialysis (for high boiling point organic solvents). Nanoprecipitation also allows efficient encapsulation of active ingredients into nanoparticles during the self-assembly process.[11]

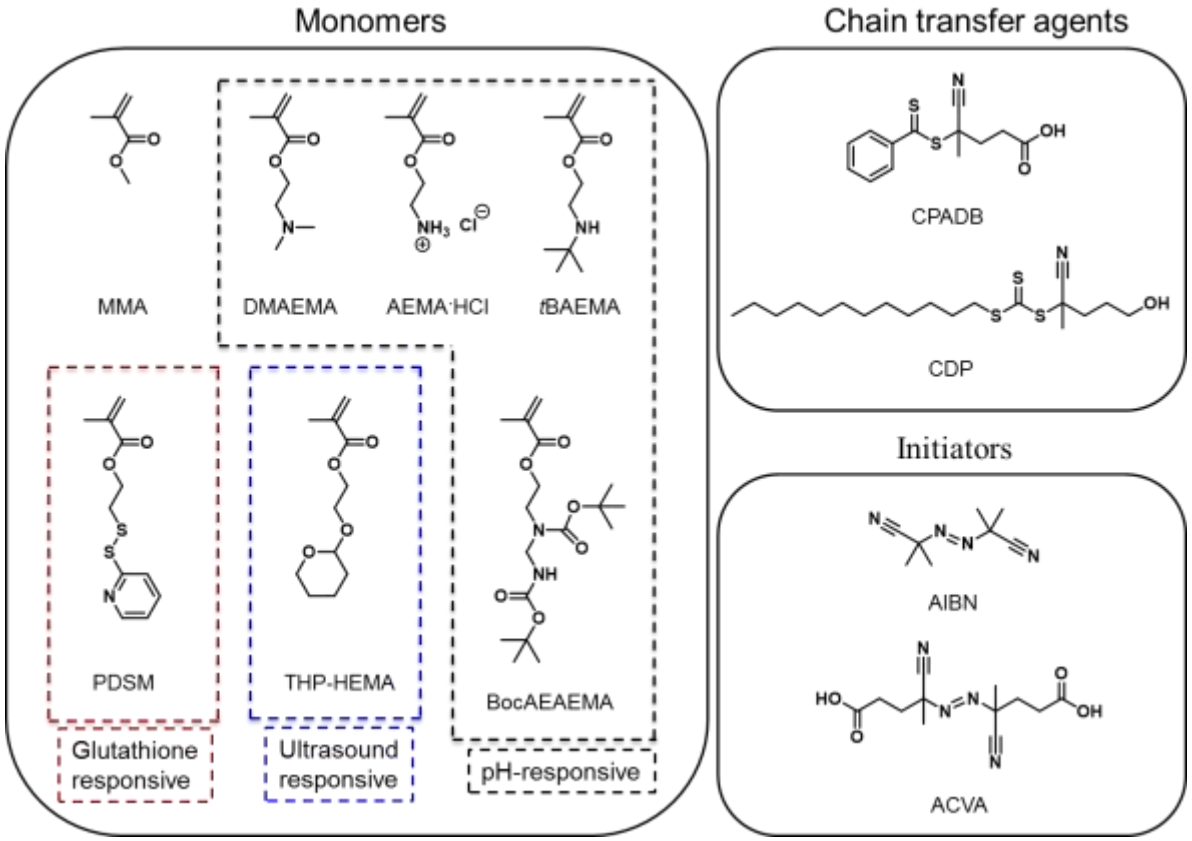

Figure 1.1 Schematic representation of the vinylic monomers polymerized *via* RAFT polymerization together with the corresponding investigated responses: methyl methacrylate (MMA), 2-(dimethylamino)ethyl methacrylate (DMAEMA), 2-aminoethyl methacrylate hydrochloride (AEMA·HCl), 2-(*tert*-butylamino)ethyl methacrylate (*t*BAEMA), pyridyldisulfide ethyl methacrylate (PDSM), 2-((tetrahydro-2H-pyran-2-yl)oxy)ethyl methacrylate (THP-HEMA), 2-((*tert*-butoxycarbonyl)(2-((*tert*-butoxycarbonyl)amino)ethyl)amino)-ethyl methacrylate (BocAEAEMA); chain transfer agents (CTA): 4-cyano-4-(phenylcarbonothioylthio) pentanoic acid (CPADB), 4-cyano-4-[(dodecylsulfanylthiocarbonyl)sulfanyl]pentanol (CDP); initiators: 2,2′-azobis(2-methylpropionitrile) (AIBN), 4,4′-azobis(4-cyanovaleric acid) (ACVA).

The aim of this thesis is to design and synthesize novel stimuli-responsive polymeric nanoparticle systems for controlled drug delivery applications. To this end, this thesis investigates (i) the synthesis of several novel amphiphilic stimuli-responsive statistical or block copolymers *via* RAFT copolymerization of various functional monomers (Figure 1.1), (ii) the self-assembly behavior of the polymers by nanoprecipitation, (iii) studies the stimuli-responsive behavior of the nanoparticles, and (iv) evaluates these nanoparticles for possible drug delivery applications. Stimuli-responsive nanoparticles, also known as "smart nanoparticles", can recognize the environmental stimuli and respond to it by changing their physical or chemical properties. The stimuli can be broadly classified into two main categories: (i) endogenous (biological) stimuli including pH value, glutathione (GSH) concentration,[12-13] enzyme activity[14] and receptor,[15-16] and (ii) exogenous stimuli (physical) such as temperature,[17-18] magnetic field,[19-20] light,[21] and ultrasound.[22-23] Among the endogenous stimuli, pH-responsiveness is maybe the most studied one due to the presence of physiological pH gradients within the body.[24] For instance, the extracellular pH value of inflammatory and tumor tissues is slightly more acidic (pH ~ 6.5−7.2) than normal tissues.[25] Following endocytosis, the pH value even drops to 5.0 in endosomes and 4.5 in the lysosomes. These physiological pH gradients are the reasons to formulate pH-responsive nanoparticles aiming (i) to release drugs at the target site of action and (ii) to tune the physical properties (e.g, size, surface charge and morphology) of the nanoparticles within the different parts of the physiological environment leading to enhanced safety and cellular uptake of the nanoparticles. There are two common routes to prepare pH-responsive polymeric nanoparticles: (i) By incorporating ionizable pendant groups into the polymers, (ii) by using pH-labile bonds within the backbone or the side chain of the corresponding polymers. Therefore, the pH-responsiveness of nanoparticles obtained from both routes relies mainly on the change of the hydrophobic-to-hydrophilic ratio of the polymers as a result of cleavage of the acid labile bonds or the ionization of the pendant groups. The hydrophobic-to-hydrophilic ratio of the nanoparticles is the key parameter, which determines the size, surface charge, morphology and solubility of the nanoparticles. Weakly basic amino groups represent interesting ionizable moieties to formulate biologically relevant pH-responsive nanoparticles due to their pH value dependent protonation/deprotonation abilities. Below their pK_a values, amino groups are protonated and become hydrophilic. In contrast, above their pK_a values amino groups become hydrophobic as a consequence of the deprotonation. The pH responsive behavior of the nanoparticles is affected by the amount and the chemical structure of the amino groups incorporated in the corresponding

copolymers. **Chapter 2** discusses the effect of various amino structures (primary, secondary and tertiary) on the pH responsive behavior of poly(methyl methacrylate) (PMMA) based nanoparticles. Most of the nanoparticle based drug delivery systems rely on the physical encapsulation of active molecules into nanoparticles during the formulation of the corresponding polymers. However, these systems usually exhibit some drawbacks including premature release of the cargo as well as insufficient loading.[26] Conjugation of polymers with bioactive molecules can overcome these limitations.[27] Primary amino groups enable the chemical conjugation of the bioactive molecules including proteins and peptides to the polymers.[28] In the second part of **Chapter 2**, chemical conjugation of the retinoic acid (RA) and a fluorescent dye (DY590) to a primary amino functional PMMA based copolymer is demonstrated. Moreover, formulation of the cationic nanoparticles and an application for label free Raman imaging as well as possible selectivity of RA for hepatic stellate cells (HSC) *via* intravital microscopy is discussed.

Apart from the pH value gradients within the physiological environment, the reductive environment of the cytosol compared to extracellular environments (100 to 1000 times higher glutathione (GSH) concentration than the extracellular GSH) also provides a rationale for the intracellular delivery of therapeutic agents.[29-30] Such GSH responsive nanoparticles are generally constructed by incorporating disulphide functionality at the side chain,[31] in the backbone (main chain),[32] or in the cross-linker.[33] The disulphide functionality can react with intracellular GSH *via* thiol–disulfide exchange reaction and can result in disruption of the nanoparticles leading to a cargo release. Pyridyldisulfide ethylmethacrylate (PDSM) is a well-known monomer that is commonly used to produce polymers with disulfide pendants.[34-36] **Chapter 3** describes the synthesis of the statistical copolymer library of PDSM with different compositions of 2-((*tert*-butoxycarbonyl)(2-((*tert*-butoxycarbonyl)amino)ethyl)amino)-ethyl methacrylate (BocAEAEMA) that contains primary and secondary amino groups in the side chain (after deprotection of the Boc-group).[37] Moreover, both glutathione and pH-responsiveness of respective nanoparticles and their potential application for the controlled delivery of doxorubicin (DOX) is demonstrated.

The surface charge of nanoparticles plays a crucial role on the cellular internalization, blood circulation, and the safety of the nanoparticles. For instance, it is well-known that positively charged nanoparticles are internalized faster by the cells than negatively charged and neutral nanoparticles as a result of their high interaction with the negatively charged cell membranes.[38]

However, the positively charged nanoparticles can interact with proteins in the bloodstream causing severe aggregation and rapid clearance from circulation. Moreover, positive charge can cause perturbation of the plasma membrane inducing cytotoxicity and immune response.[39] In contrast, neutral and negatively charged nanoparticles have less interaction with proteins and longer circulation times.[40] As a consequence, the construction of charge-conversional nanoparticles that are neutral or have negative surface charge values in the blood but become positively charged under a slightly acidic environment have become appealing for intravenous drug delivery systems. Drug delivery systems with these features are expected to combine the advantages of positively and negatively charged nanoparticles to improve the targeting efficiency.[41-42] **Chapter 4** demonstrates that random incorporation of the 2-(dimethylamino)ethyl methacrylate (DMAEMA) moieties into a 2-((tetrahydro-2H-pyran-2-yl)oxy)ethyl methacrylate (THP-HEMA) based hydrophobic polymer allows obtaining nanoparticles with pH-dependent surface charge conversion properties. Furthermore, it is shown that the disassembly pH value and the isoelectric point (IEP) of the nanoparticles can be systematically tuned by varying the amino content of the polymers. The majority of the reported stimuli responsive nanoparticle systems depend on the endogenous (biological) stimuli like endosomal pH value or GSH concentration. However, biological stimuli are complicated and can limit the control over the drug release. In contrast, exogenous stimuli are independent of the complex conditions of the biological environment, and they can be applied in a remotely and spatiotemporally controlled manner.[43] This can provide a precise control over the release of the encapsulated payloads. Among the exogenous stimuli, ultrasound has recently attracted a great deal of attention because of its noninvasiveness, lack of ionizing radiations, deeper penetration into the interior of the body as well as tunable frequency and time of treatment, which prevents damage to healthy tissue.[4, 44-45] **Chapter 4** shows that THP-HEMA based nanoparticles are responsive to ultrasound as a result of their relatively low glass transition temperatures (T_g) and lack of any crystallization temperatures (T_c). It is believed that nanoparticles that possess hydrophobic segments that have a low T_g value can respond to a stimuli by changing their morphologies.[46-48] In the second part of the **Chapter 4**, it is shown that polymersomes constructed by using a diblock copolymer of THP-HEMA with DMAEMA exhibit a morphology transition from vesicles at neutral pH values to micelles upon decreasing the pH value. Furthermore, the ability of this system for the controlled delivery of a hydrophilic anti-cancer drug doxorubicin hydrochloride (DOX·HCl) is demonstrated.

2. PMMA based cationic nanoparticles

Parts of this chapter have been published: **P2**) T. Yildirim, A. C. Rinkenauer, C. Weber, A. Traeger, S. Schubert, U. S. Schubert, *J. Polym. Sci., Part A: Polym. Chem.* **2015**, 53, 2711-2721; **P3**) T. Yildirim,[#] C. Matthäus,[#] A. T. Press, S. Schubert, M. Bauer, J. Popp, U. S. Schubert, *Macromol. Biosci.* **2017**, *DOI: 10.1002/mabi.201700064*. [#]Authors contributed equally.

Incorporation of amino groups into hydrophobic polymer chains enables to obtain pH responsive polymers and the corresponding cationic nanoparticles. In order to investigate the influence of the amino structure and the amount of the amino content on the pH responsive behavior of the nanoparticles, a series of statistical copolymers of PMMA with three different commercially available amino methacrylates including tertiary (DMAEMA), secondary (*t*BAEMA) and protonated primary amino functionalities (AEMA·HCI) were synthesized using the reversible addition-fragmentation chain transfer (RAFT) polymerization process (Scheme 2.1). 4-Cyano-4-(phenylcarbonothioylthio) pentanoic acid (CPADB) was chosen as chain transfer agent (CTA), because it has previously effectively mediated the RAFT polymerization of various amino methacrylates.[37, 49] In order to vary the amino content, two different feed ratios were used aiming to obtain 10% as well as 20% amino content for each monomer. Considering the possible cytotoxic effects of the amino groups and the required hydrophobicity of the copolymers for the capability to form nanoparticles *via* nanoprecipitation, the amino content in the copolymers was kept low (in between 9 and 21%). It is known that the deprotonated primary amino functional monomer AEMA can rearrange to its thermodynamically more stable isomer 2-hydroxyethyl methacrylamide.[49-50] Moreover, free primary amino groups in the polymerization mixture can decompose the dithiobenzoate moiety of the CTA.[51] To avoid these unwanted reactions, AEMA in its hydrochloride salt form was used for the polymerizations. For DMAEMA and *t*BAEMA copolymerizations (**P1** to **P4**) ethanol was used as solvent. However, methanol under reflux was used as solvent for the AEMA·HCl copolymerizations (**P5** and **P6**) as a result of the poor solubility of AEMA·HCl in ethanol. All copolymerizations were performed utilizing 2,2′-azobis(2-methylpropionitrile) (AIBN) as source of radicals. Purified copolymers were characterized by SEC measurements and ^{1}H NMR spectroscopy (Table 2.1). The calculated M_n values estimated by ^{1}H NMR are in good agreement with the theoretical values that are estimated using the [monomer] to [CTA] ratio and the monomer conversions.

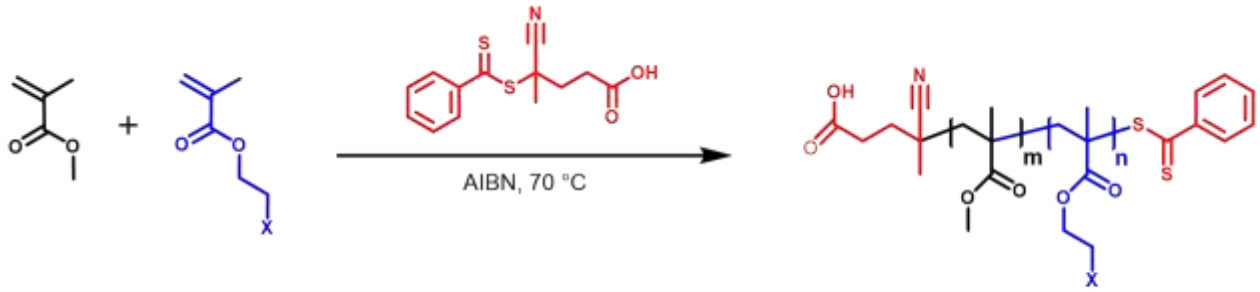

Scheme 2.1 Schematic representation of the RAFT copolymerization of MMA with amino-functionalized methacrylates.

Table 2.1 Selected characterization data of the MMA (M1) copolymers with corresponding amino methacrylates (M2).

Entry	**M2**	f(**M1**/**M2**)[a]	F(**M1**/**M2**)[b,d]	Conv. (%) **M1**	Conv. (%) **M2**	$M_{n,theo.}$[e] [g mol^{-1}]	DP[d] **M1**	DP[d] **M2**	M_n[d] [g mol^{-1}]	M_n[f] [g mol^{-1}]	$Đ$[f]
P1	DMAEMA	9	7.4	39[c]	45[c]	4,500	41	5.5	5,200	6,100	1.16
P2	DMAEMA	4	4	42[c]	50[c]	5,200	40	10	5,900	7,600	1.17
P3	*t*BAEMA	19	9.5	29[c]	70[c]	3,700	35	3.7	4,500	5,200	1.19
P4	*t*BAEMA	5.7	3.8	36[c]	72[c]	5,300	35	9.2	5,500	7,900	1.15
P5	AEMA·HCl	9	9.1	45[d]	44[d]	5,000	42	4.6	5,200	5,100	1.13
P6	AEMA·HCl	4	3.7	48[d]	52[d]	5,900	30	8.2	4,600	4,500	1.19
P7[g]	AEMA		9				45	5	5,200	5,300	1.18
P8[h]	AEMA		3.6				35	9.8	5,000	4,800	1.18

[a]Initial monomer feed ratio. [b]Monomer ratio in the isolated copolymer. [c]Determined by GC. [d]Determined by ^{1}H NMR spectroscopy. [e]Determined by the formula $M_{n,theo.} = [([M]_{M1}/[CTA] \times Conv. \times M_{M1}) + ([M]_{M2}/[CTA] \times Conv. \times M_{M2}) + (M_{CTA})]$. [f]Determined by SEC in $CHCl_3$ analysis (RI detection, PMMA calibration). [g]Deprotonated form of **P5**. [h]Deprotonated form of **P6**.

SEC measurements in chloroform revealed monomodal molar mass distributions for all polymers with low dispersities ($Đ < 1.2$). Before nanoparticle formulation, the copolymers of AEMA·HCl (**P5** and **P6**) were treated with Amberlyst® A21, which is a weak base, to obtain the desired primary amino-functionalized copolymers (**P7** and **P8**). After treatment with Amberlyst® A21, **P6**, which is soluble in water, became hydrophobic and water non-soluble (**P8**) as a result of deprotonation of the amino groups. Nanoparticles were formulated by nanoprecipitation of the synthesized tertiary (**P1** and **P2**), secondary (**P3** and **P4**) and primary (**P7** and **P8**) amino-functionalized PMMA based copolymers without using any stabilizers/surfactants. For nanoprecipitation, acetone was used as solvent and water was used as non-solvent. In order to vary the dimensions of the obtained nanoparticles, different formulation conditions were utilized such as two different dropping methods (dropping acetone polymer solution to water (AW) and

dropping water to acetone polymer solution (WA)) and two different initial acetone polymer solution concentrations. As commonly observed for the nanoprecipitation technique, nanoparticles with smaller diameters were obtained with the AW method compared to the WA process (Table 2.2).[52] Well-defined nanoparticles with positive zeta potential values could be obtained with all polymers by using initial acetone-polymer solution concentrations of 1 mg mL^{-1}. The positive zeta potentials of the nanoparticles are ascribed to the amino moieties into the polymers. SEM investigations revealed spherical shapes for all nanoparticles. Although nanoparticles with monomodal size distributions and low PDI values could be produced using DMAEMA (**P1** and **P2**) and AEMA (**P7** and **P8**) copolymers with an initial acetone-polymer solution concentration of 10 mg mL^{-1}, *t*BAEMA (**P3** and **P4**) copolymers yielded nanoparticles and undefined aggregates. This can be attributed to the lower pKa values of *t*BAEMA copolymers compared to the DMAEMA and AEMA copolymers preventing the nanoparticles to have an appreciable surface charge at neutral pH values. In agreement with this assumption, nanoparticles without any aggregation could be obtained using an acetate buffer with a pH value of 5.0 instead of using pure water (Table 2.2).

Table 2.2 Characterization results of the prepared nanoparticles.

Polymer	Method[a]	Z-average[b] [d, nm]		PDI[b]		Zeta potential[c] [mV]	
		c = 1 g L^{-1}	c = 10 g L^{-1}	c = 1 g L^{-1}	c = 10 g L^{-1}	c = 1 g L^{-1}	c = 10 g L^{-1}
P1	AW	152 ± 2	123 ± 1	0.16 ± 0.02	0.12 ± 0.01	+35 ± 4.4	+37 ± 0.3
	WA	340 ± 3	720 ± 18	0.11 ± 0.03	0.07 ± 0.05	+25 ± 4.3	+48 ± 1.1
P2	AW	184 ± 2	131 ± 2	0.16 ± 0.01	0.11 ± 0.04	+52 ± 0.4	+31 ± 0.7
	WA	473 ± 3	636 ± 4	0.18 ± 0.04	0.07 ± 0.05	+47 ± 0.4	+51 ± 0.7
P3	AW	126 ± 1	200 ± 1[d]	0.12 ± 0.02	0.19 ± 0.03[d]	+44 ± 3.3	+ 56 ± 9[d]
	WA	314 ± 3	1079 ± 28[d]	0.14 ± 0.04	0.26 ± 0.12[d]	+29 ± 0.4	+ 40 ± 3[d]
P4	AW	169 ± 2	158 ± 1[d]	0.15 ± 0.01	0.15 ± 0.03[d]	+36 ± 6.4	+ 41 ± 3[d]
	WA	331 ± 3	610 ± 12[d]	0.09 ± 0.05	0.14 ± 0.01[d]	+20 ± 2.1	+ 26 ± 2[d]
P7	AW	121 ± 1	110 ± 1	0.17 ± 0.01	0.14 ± 0.02	+56 ± 3.2	+59 ± 0.6
	WA	306 ± 2	339 ± 2	0.11 ± 0.02	0.10 ± 0.03	+61 ± 0.5	+64 ± 1.0
P8	AW	133 ± 1	182 ± 1	0.14 ± 0.02	0.08 ± 0.04	+54 ± 2.1	+59 ± 0.8
	WA	254 ± 3	582 ± 13	0.07 ± 0.05	0.17 ± 0.02	+53 ± 3.7	+61 ± 0.6

[a]AW, dropping acetone to water; WA, dropping water to acetone. [b]Average values of three DLS measurements. [c]Average values of three zeta potential measurements. [d]Nanoprecipitation with acetate buffer (pH = 5) as non-solvent.

In order to understand the pH responsive behavior of the nanoparticles, the suspensions were stored for 24 h at 37 °C at various pH values. Subsequently, changes in size and surface charge values were investigated by DLS and zeta potential measurements. The DLS measurements revealed that **P1** nanoparticles that contain 10% DMAEMA functionality are stable at slightly acidic pH values (3.4 to 6) but they aggregate at pH values 7 and 8 (Figure 2.3, A). The

aggregation of the nanoparticles is due to the decrease in the zeta potential values of the nanoparticles as a result of deprotonation of the DMAEMA moieties (Figure 2.3, B). It is known that van der Waals attractions become stronger than electrostatic repulsions causing aggregation when the absolute zeta potential values of the nanoparticles are lower than 20 mV.[53] In agreement with this, **P1** nanoparticles are stable at a pH value of 9 due to having zeta potential values beyond -20 mV. The negative zeta potential value of the **P1** nanoparticles at pH 9 can be attributed to a complete deprotonation of the DMAEMA groups and the carboxylic acid functionality of the utilized CTA into the polymer. Unlike **P1**, **P2** nanoparticles are stable at a pH value of 7. This is due to the higher DMAEMA content (20%) of **P2** leading to a sufficient character of the nanoparticles for stabilizing of the nanoparticles. Between the pH values 3.4 to 5 **P2** nanoparticles exhibited a significant increase in the PDI value and a tremendous decrease in the count rate, which is proportional to the size and the number of the nanoparticles. These observations are attributed to the dissolution of the nanoparticles at acidic pH values caused by the complete protonation of the DMAEMA groups. Furthermore, a control experiment with nanoparticles prepared using Eudragit® E100, which is a well-known coating polymer that exhibits dissolution at acidic media,[54] revealed similar results like **P2** nanoparticles. Nanoparticles deriving from **P3** and **P4** are stable at acidic pH values but they revealed a reduced stability around neutral pH values compared to DMAEMA nanoparticles. This could be due to bulky *tert*-butoxy group the *t*BAEMA that inhibits the protonation of the amino groups, resulting in low zeta potential values and accordingly causing aggregation of the nanoparticles. In contrast, AEMA containing nanoparticles (**P7** and **P8**) revealed improved stabilities around neutral pH values compared to DMAEMA nanoparticles. This is ascribed to the primary amino structure of the AEMA rendering nanoparticles to protonate easily under neutral conditions. **P7** nanoparticles are stable at acidic pH values. However, **P8** nanoparticles that contain 20% AEMA functionality revealed nanoparticle disassembly between pH values 3.4 to 5 as a result of the polymer dissolution. It is known that PMMA is nontoxic, whereas amino functional polymers usually induce toxic effects to the cells as a result of their undesired destructive interactions with the negatively charged cell membranes.[55] Therefore, cytotoxicity of the nanoparticles and the water soluble polymer **P6** on L929 cells was investigated (Figure 2.2).

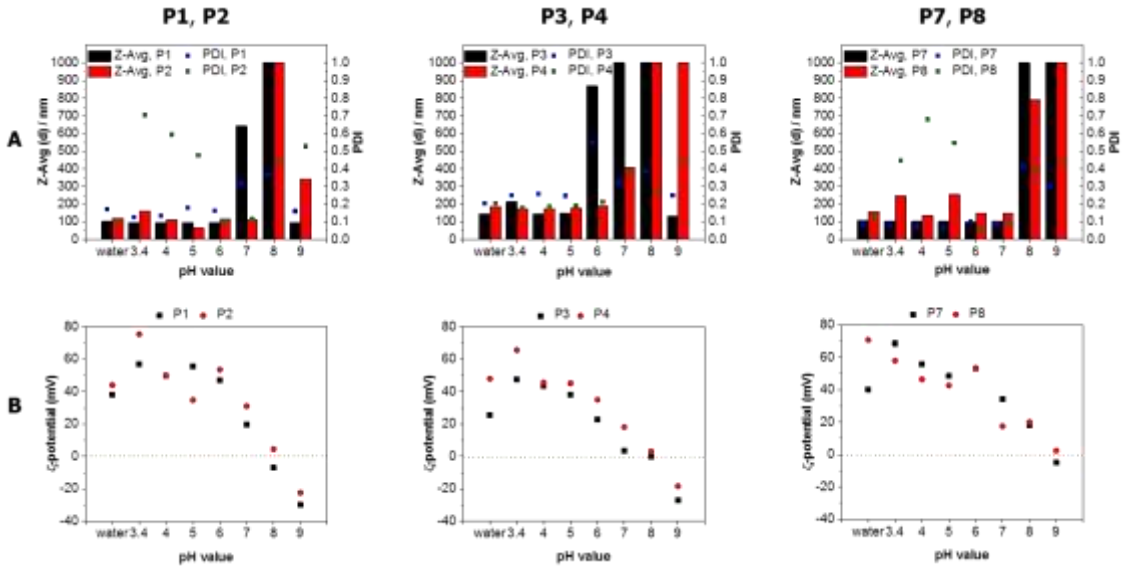

Figure 2.1 (A) Z-Average diameter (represented up to 1000 nm) and PDI values of nanoparticles as a function of the pH value. (B) Zeta potentials of the nanoparticles as a function of the pH value.

P6 revealed severe toxic effects on L929 cells after 24 h incubation. However, the nanoparticles prepared from **P8**, which is the deprotonated form of **P6**, did not show any cytotoxic effect under the same conditions. This is attributed to the decrease of the cationic character of the polymer after deprotonation.

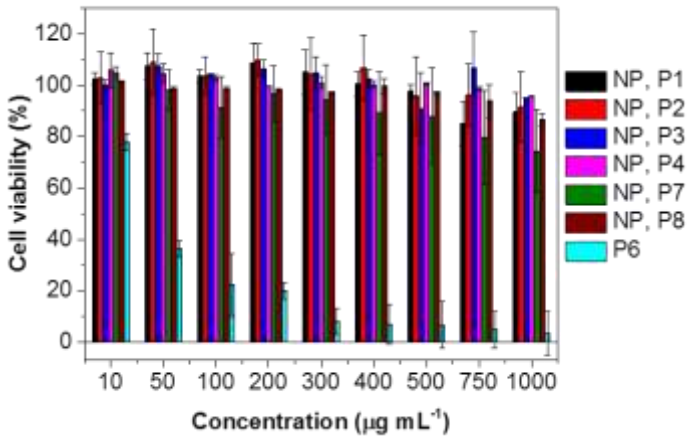

Figure 2.2 Cytotoxicity test of nanoparticles (NPs) that are prepared from **P1** to **P4**, **P7**, **P8** and water soluble polymer **P6** in L929 cells. Untreated cells on the same well plate were used as positive controls.

The majority of the nanoparticle based drug delivery systems count on the physical entrapment of therapeutic agents into nanoparticles during the self-assembly of the polymers in aqueous solution. However, these systems mainly suffer from a premature release of the cargo and an

insufficient loading. As a result, chemical conjugation of the active molecules to the polymers have become a common strategy to overcome these limitations.[27] Primary amino groups offer a number of postpolymerization modification approaches including Michael addition, formation of amides and imines, ring-opening of epoxy moieties and so on.[56] As a consequence, they are one of the most common functional groups that are amenable to conjugate bioactive molecules to the polymers. Raman microscopic imaging of cells and tissues have become an attractive tool due to its non-destructive and label-free approach. Raman imaging enables to image individual cellular components including endoplasmic reticulum, Golgi apparatus, vesicles and mitochondria.[57-59] Moreover, the intracellular uptake of molecules and particles can also be monitored by Raman imaging when their spectral contrast with respect to the cellular environment is sufficient. Molecules that have extended π-conjugated systems represent a very high Raman sensitivity as a result of their high Raman scattering cross sections. For instance, cellular uptake of the beta-carotene loaded PLGA nanoparticles could be investigated by Raman microscopy.[60] Raman spectroscopy has also been used to quantify vitamin A in hepatic stellate cells (HSCs) of the liver.[61] Retinoic acid (RA), that is a biosynthetic analogues (precursors) of vitamin A, has also desired features for direct observation by Raman spectroscopy.[62] Moreover, it is known that HSC take up vitamin A independent of their needs through cell-type specific receptors and store it in large vesicles located near their nuclei.[63-64] As a consequence, RA was covalently attached to a before synthesized primary amino functional PMMA based copolymer (**P5**, Table 2.1) to study the suitability of the RA conjugated polymeric nanoparticles for Raman imaging investigations. Furthermore, in order to investigate the possible selectivity of the RA bearing nanoparticles for HSCs the copolymer is additionally functionalized with a fluorescent dye. In order to prove the covalent coupling of RA to the polymer by SEC (UV detector) and UV-vis spectroscopy, the ω RAFT end-group of the polymer, which exhibits a strong UV absorption in a similar region like RA, was cleaved by following a procedure reported in literature before yielding a hydroxyl-terminated polymer (**P9**) (Scheme 3.1).[65] Before the coupling reactions, **P9** was treated with Amberlyst® A21 to deprotonate the polymer that contains HCl salt. Subsequently, DCC coupling was utilized to chemically attach RA to the pendant primary amino groups of the **P9**, resulting in a RA conjugated polymer (**P10**). Furthermore, amino groups of the **P10** and **P9** were functionalized with NHS ester functional fluorescent dye DY590, yielding **P11** and **P12**, respectively. Successful coupling of RA and DY590 to the polymers was confirmed by ^{1}H NMR spectroscopy, SEC and UV-vis spectroscopy. RA and/or DY590 bearing nanoparticles

were prepared by the nanoprecipitation of the modified polymers (**P10**, **P11** and **P12**). Cationic nanoparticles were obtained with diameters between 70 to 85 nm with monomodal size distributions and relatively low PDI values.

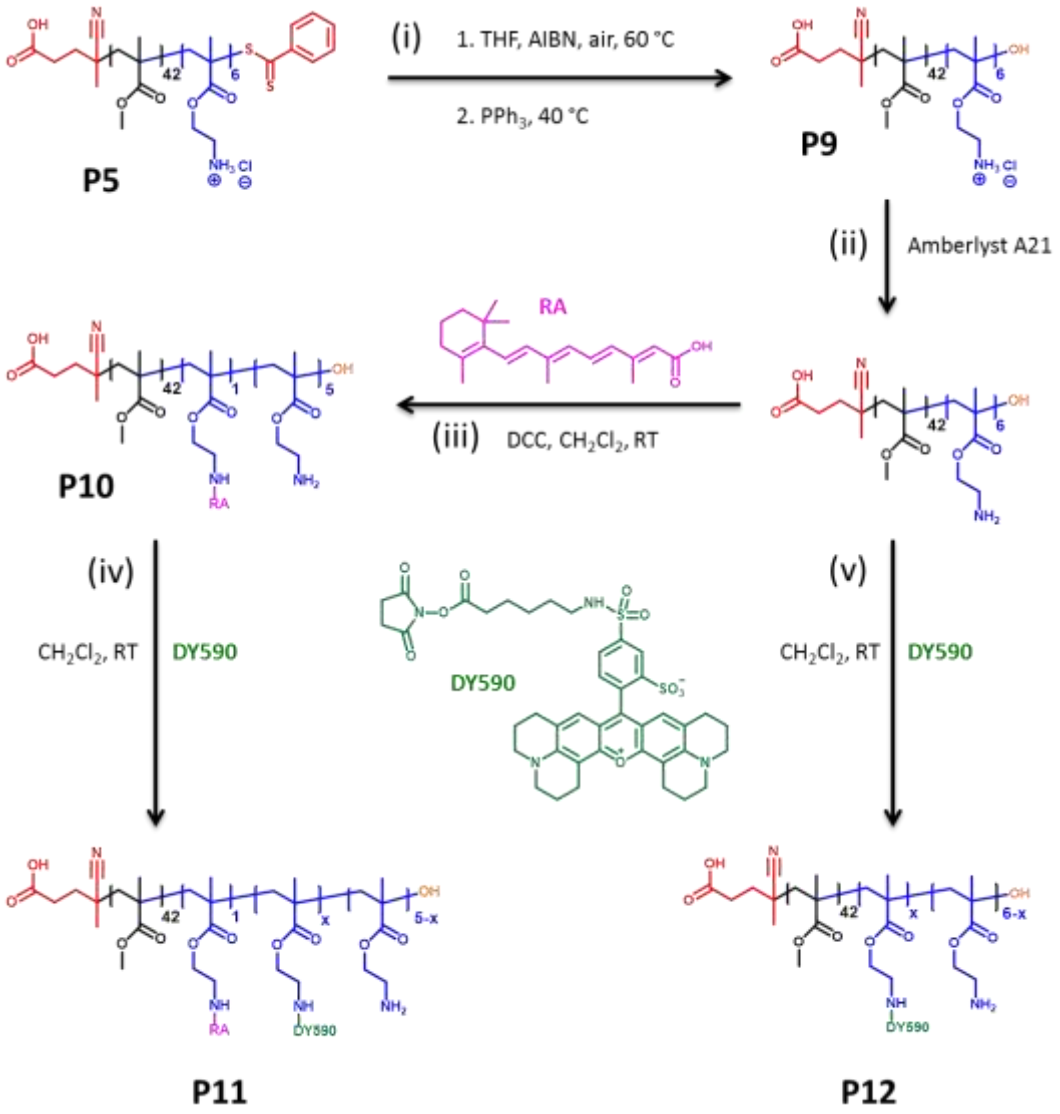

Scheme 2.2 Schematic representation of the (i) RAFT end group cleavage; (ii) deprotonation of **P9**; (iii) coupling of the retinoic acid (RA) to deprotonated form of **P19**; (iv and v) coupling of DY590 to **P10** and the deprotonated form of **P9**.

Figure 2.3 displays the Raman images of two LX2 cells incubated with RA conjugated (**P10**) nanoparticles for 1 and 3 h at a concentration of 50 mg mL^{-1} along with the corresponding spectral information. The cytosol is plotted in cyan, whereas the distribution of the nanoparticles is plotted in red. After 1 h, the endocytotic cellular uptake of the particles was clearly visible. Small vesicle-like inclusions in dimensions of 0.5 to 1 µm that are distributed throughout the

cytosol could be observed. The typical RA Raman band at 1596 cm^{-1} was distinctly visible in the corresponding endmember spectrum (in red). The cyan endmember spectrum corresponding to the cytosol has the appearance of typical Raman spectra of cells and reveals all of the typical protein bands. After 3 h, the cellular uptake of the particles was increased. Large inclusions of the particles were observed throughout the whole cell. Moreover, the typical RA Raman band at 1596 cm^{-1}, which is three times as intense compared to the 1 h incubation time, became the dominated band in the corresponding endmember spectrum. There was no change observed in the corresponding endmember spectrum of the cytosol.

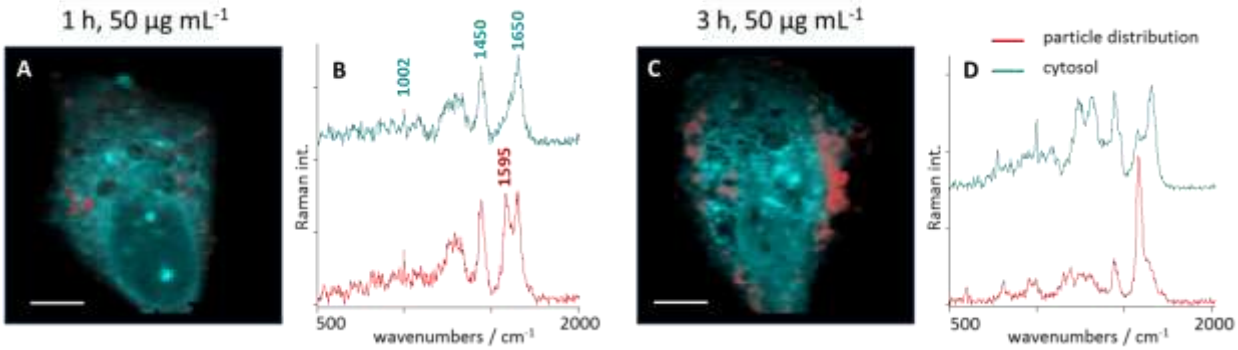

Figure 2.3 Raman images of LX2 cells incubated with P^{RA} nanoparticles for 1 hour (A) and 3 hours (C) along with the corresponding spectral information plotted in (B) and (D) respectively. The distribution of the nanoparticles is shown in red. Distinctly pronounced in the Raman spectra is the RA marker band at 1596 cm^{-1}. Scale bars represent 10 µm.

In order to track modified nanoparticles, *in vivo* intravital microscopy was used. Cationic nanoparticles prepared from DY590 conjugated polymers (**P11** and **P12)** entered to the cells located in the sinusoids (Figure 2.4). Greater occurring accumulations, in particular in the curves of the sinusoids, could be assigned to Kupffer cells and HSC. Smaller accumulations scattered along the sinusoids could be contributed to liver sinusoidal endothelia cells (LSECs). Kupffer cells, also known as stellate macrophages, are macrophages located in the liver and represent together with LSECs the immunological line of defense in the liver. It is known that cationic nanoparticles can be recognized and eliminated rapidly by immune cells in particular in the liver. Interestingly, the attachment of the RA did not alter the pharmacokinetics of the nanoparticles. These results indicate that surface charge of the nanoparticles should be carefully engineered to employ targeting moieties.

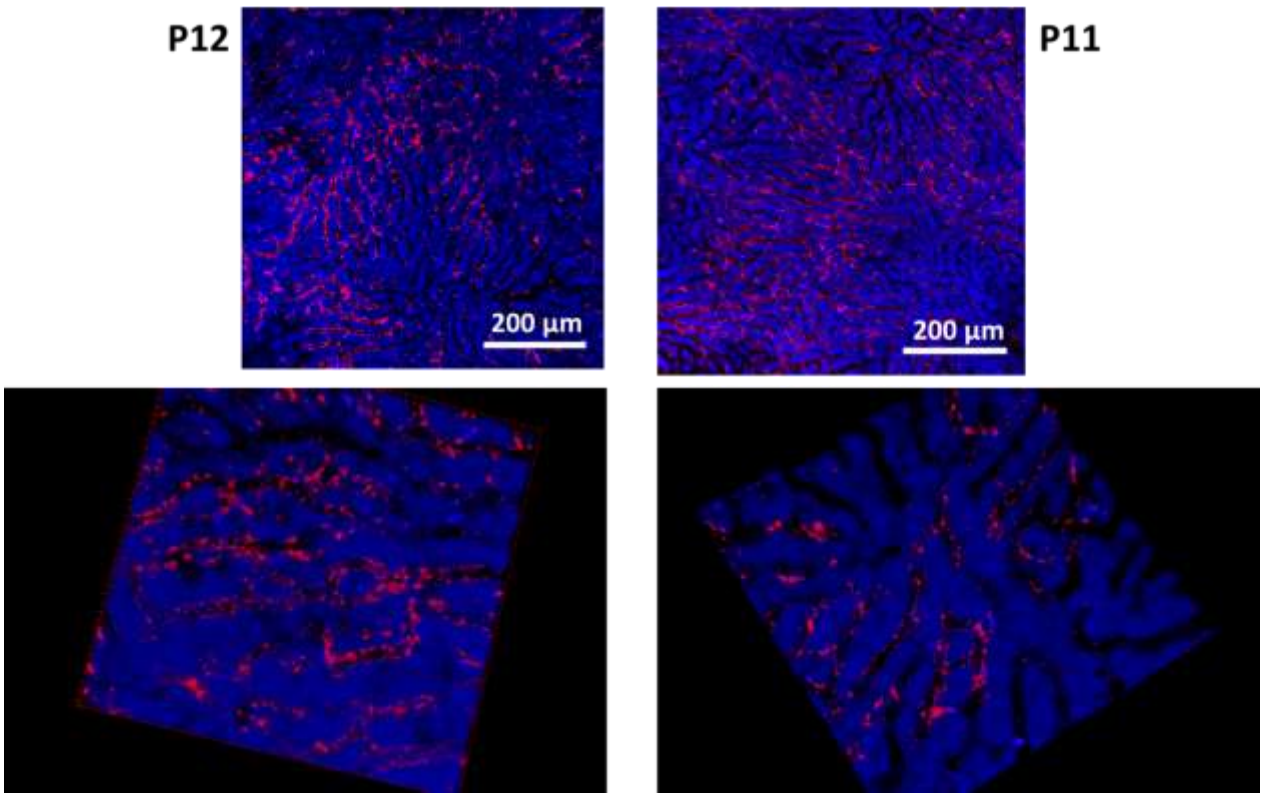

Figure 2.4 Hepatic uptake of DY590 conjugated polymeric nanoparticles without (**P12**) and with (**P11**) retinoic acid after 40 min.

3. Glutathione and pH-responsive nanoparticles for the controlled delivery of doxorubicin

Parts of this chapter have been published: **P4**) T. Yildirim, A. Traeger, E. Preussger, S. Stumpf, C. Fritzsche, S. Hoeppener, S. Schubert, U. S. Schubert, *Macromolecules* **2016**, *49*, 3856-3868.

In order to obtain a new glutathione and pH-responsive nanoparticle system, a library of well-defined statistical copolymers of pyridyldisulfide ethyl methacrylate (PDSM) with different compositions of 2-((*tert*-butoxycarbonyl)(2-((*tert*-butoxycarbonyl)amino)ethyl)amino) ethylmethacrylate (BocAEAEMA) were synthesized using the RAFT polymerization process (Scheme 3.1). PDSM is used as glutathione (GSH) responsive moiety since it contains a pyridyldisulfide functionality, which is reactive to free thiol moieties under ambient conditions.[66] AEAEMA that contains primary and secondary amino groups in the side chain is used as pH-responsive moiety.[37] It is known that block copolymer nanoparticles hide the hydrophobic segments of the polymers in the core of the micelles or in the bilayer of the vesicles.[67-68] In contrast, statistical copolymer assemblies can provide surface exposed hydrophobic moieties. We envisioned that surface exposed hydrophobic PDSM functionality can accelerate the GSH responsive behavior of the corresponding nanoparticles. As a consequence, a number of statistical copolymers with similar molar mass values but varying monomer compositions were synthesized.

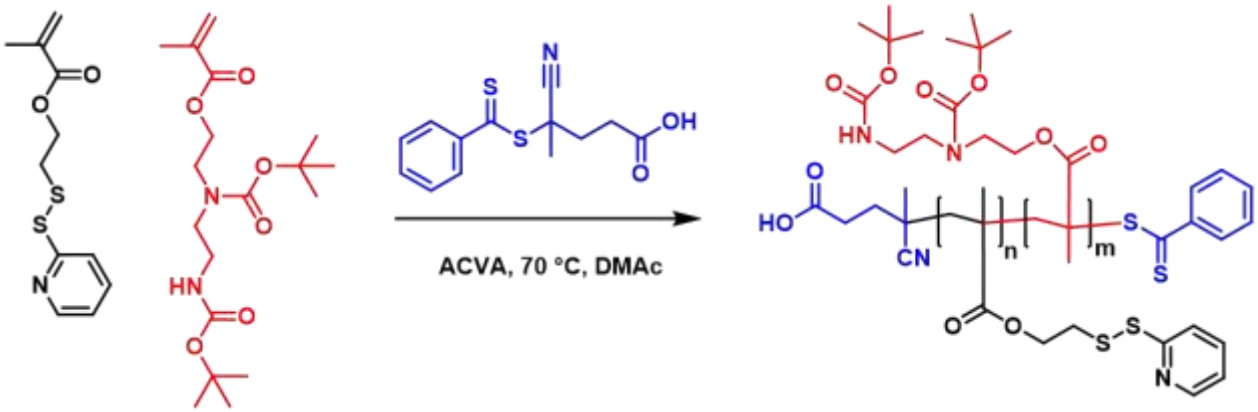

Scheme 3.1 Schematic representation of the RAFT copolymerization of PDSM with BocAEAEMA.

The isolated (co)polymers were characterized by ^{1}H NMR spectroscopy (Figure 3.1) and SEC measurements (Table 3.1). The DP values for each monomer and the according number average

molar mass (M_n) values were calculated by ^{1}H NMR end group analysis. SEC in DMAc revealed monomodal traces and low dispersities ($Đ < 1.2$) for all polymers.

Table 3.1 Selected characterization data of the PDSM (M1) copolymers with BocAEAEMA (M2).

Entry	Monomer/CTA/ ACPA	f(M1/ M2)[a]	F(M1/ M2)[b]	Conv. [%][c] M1/M2	$M_{n,theo.}$[d] [g mol^{-1}]	DP[c] M1/M2	M_n[c] [g mol^{-1}]	$M_{n,SEC}$[f] [g mol^{-1}]	$Đ$[f]
P13[g]	38.07/1/0.25			76/0	7,700	24/0	6,400	7,300	1.18
P14	37.19/1/0.25	19.0	19.1	78/60	7,700	23/1.2	6,600	7,000	1.13
P15	36.40/1/0.25	9.0	11.1	73/62	7,200	21/1.9	6,300	7,400	1.15
P16	35.62/1/0.25	5.7	7.5	87/67	8,300	24/3.2	7,600	8,300	1.14
P17	34.86/1/0.25	4.0	5.5	75/60	7,200	21/3.8	7,000	8,000	1.14
P18	33.42/1/0.25	2.3	3.5	78/70	7,600	19/5.5	7,200	9,200	1.13
P19	32.17/1/0.25	1.5	2.5	78/68	7,400	17/6.8	7,200	10,000	1.09
P20	29.86/1/0.25	0.7	1.0	83/74	7,700	11/11	7,200	9,700	1.12
P21[h]	25.92/1/0.25			0/69	6,900	0/18.3	7,100	7,600	1.08

[a]Initial monomer feed ratio. [b]Monomer ratio in the isolated copolymer. [c]Determined by ^{1}H NMR spectroscopy. [d]Determined by the formula $M_{n,theo.} = [([M]_{M1}/[CTA] \times Conv. \times M_{M1}) + ([M]_{M2}/[CTA] \times Conv. \times M_{M2}) + (M_{CTA})]$. [f]Determined by SEC in DMAc analysis (RI detection, PS calibration). [g]Homopolymer of the PDSM. [h]Homopolymer of the BocAEAEMA.

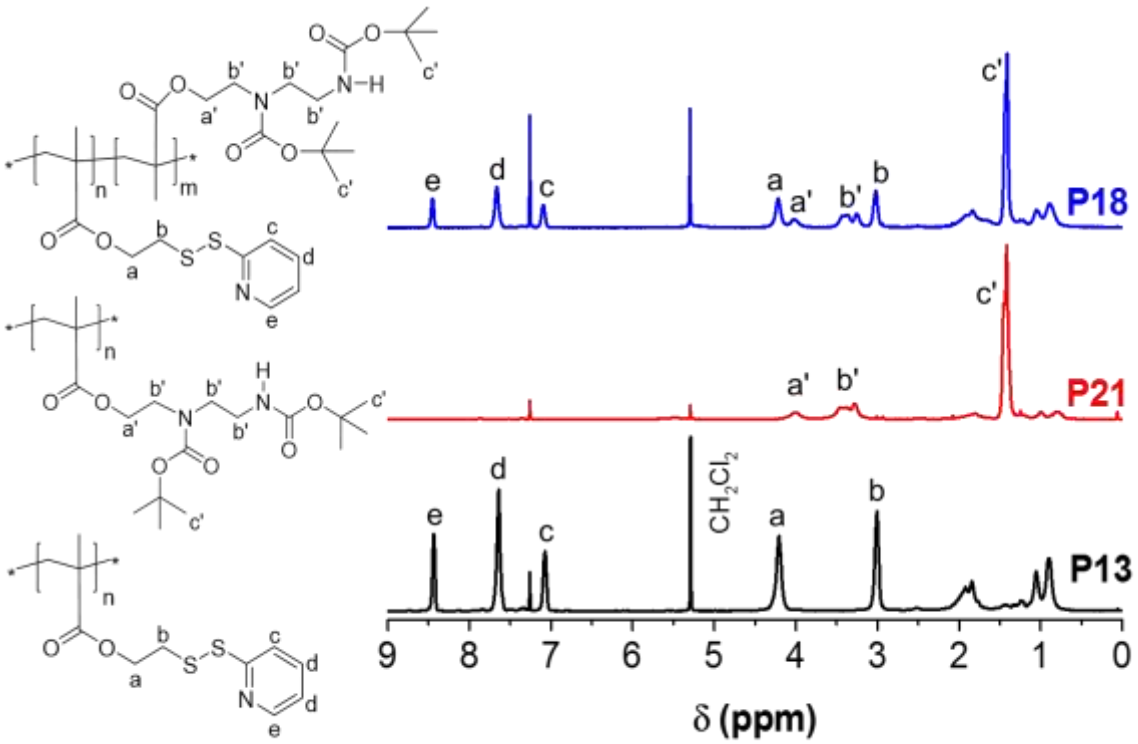

Figure 3.1 ^{1}H NMR spectra (300 MHz, $CDCl_3$) of **P1**, **P6**, and **P9** and the assignment of the peaks used to calculate the degree of polymerization (DP).

Prior to the nanoparticle formulation, the Boc-groups of the polymers were cleaved by treating with trifluoroacetic acid. The quantitative cleavage of the Boc-groups was proven by ^{1}H NMR spectroscopy by the disappearance of the *tert*-butoxy carbonyl proton signals at 1.41 ppm. Polymeric nanoparticles could be obtained by nanoprecipitation of the deprotected copolymers of **P14**, **P15**, and **P16** containing 5, 8, and 12 mol% AEAEMA functionality, respectively. However, with polymers that contain higher mol% AEAEMA, no well-defined nanoparticles could be obtained as a result of their insufficient hydrophobicity. Variations of the initial formulation conditions (initial acetone-polymer solution concentration, dropping methods) enabled to obtain cationic nanoparticles with diameters ranging from 50 to 460 nm (Table 3.2). SEM measurements revealed homogenous spherical shapes (Figure 3.2). An increase of the mol% of the AEAEMA content of the polymers caused a decrease of the nanoparticles size for both initial polymer concentrations. The decrease in the size of the nanoparticles with increasing AEMA content is attributed to the increase of the amount of charged groups in the polymer chains.[69]

Table 3.2 Selected characterization results of the prepared nanoparticles.

Entry	Z-average [d, nm][a]		PDI[a]		ζ-potential [mV][b]	
	c = 5 g L^{-1}	c = 5 g L^{-1}	c = 5 g L^{-1}	c = 5 g L^{-1}	c = 5 g L^{-1}	c = 5 g L^{-1}
P14	466 ± 4[c]	74 ± 1[d]	0.07 ± 0.02[c]	0.20 ± 0.01[d]	72 ± 5[c]	69 ± 3[d]
P15	274 ± 1[c]	51 ± 1[d]	0.11 ± 0.02[c]	0.26 ± 0.01[d]	62 ± 2[c]	72 ± 5[d]
P16	180 ± 1[c]	---[e]	0.05 ± 0.01[c]	---[e]	59 ± 3[c]	---[e]

[a]Average values of three DLS measurements. [b]Average values of three zeta potential measurements. [c]WA, dropping water to acetone. [d]AW, dropping acetone to water. [e]No well defined nanoparticles.

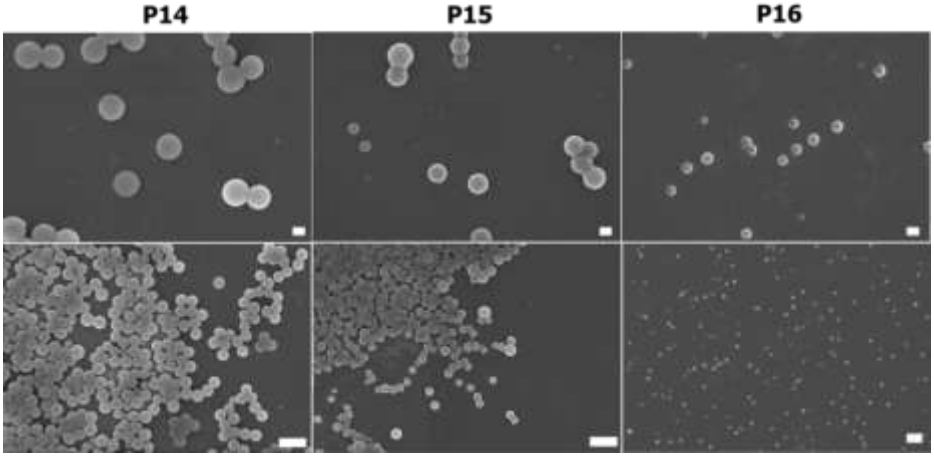

Figure 3.2 SEM images of nanoparticles that were prepared from **P14**, **P15**, and **P16** (5 mg mL^{-1}) by dropping water to acetone-polymer solution (WA). Upper scale bars represent 200 nm, lower scale bars represent 1000 nm.

In order to test the pH-responsive behavior of the nanoparticles, suspensions were titrated in the pH value range from 3.5 to 9, and the changes in size and zeta potential values were recorded simultaneously. The nanoparticles revealed stable size and PDI values at acidic pH values. However, a gradual increase in the size as well as in the PDI values of the nanoparticles was observed as the pH value increases. The nanoparticles were aggregated over a certain pH value. This is attributed to the deprotonation of the AEAEMA moieties of the polymers. In accordance with this, the zeta potential of the nanoparticles is inversely proportional to the pH value (Figure 3.3). The GSH responsive behavior of the nanoparticles was studied by monitoring the changes in particle size and the derived count rate over time in respond to 10 µM and 10 mM GSH concentration at 37 °C (Figure 3.4). These conditions mimic the GSH concentration in the blood and the cytosol, respectively. At a 10 µM GSH concentration, there was no change either in the nanoparticle size or in the derived count rate of the nanoparticles indicating the stability of the nanoparticles in the plasma. However, at a 10 mM GSH concentration, all nanoparticles exhibited an increase in size as well as a decrease in the derived count rate indicating a disassembly of the nanoparticles. The disassembly of the nanoparticles was attributed to the attachment of the GSH to the polymers *via* thiol-disulfide exchange reaction converting the amphiphilic copolymers into more hydrophilic polymers.

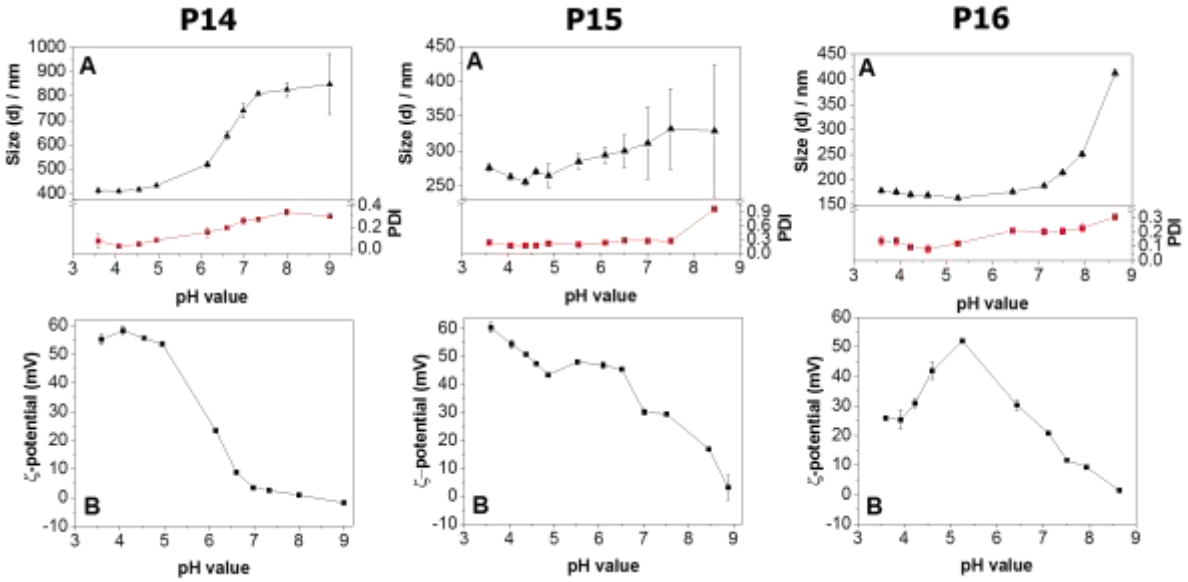

Figure 3.3 (A) Z-Average diameter and PDI values of the nanoparticles as a function of the pH value. (B) Zeta potentials of the nanoparticles as a function of the pH value.

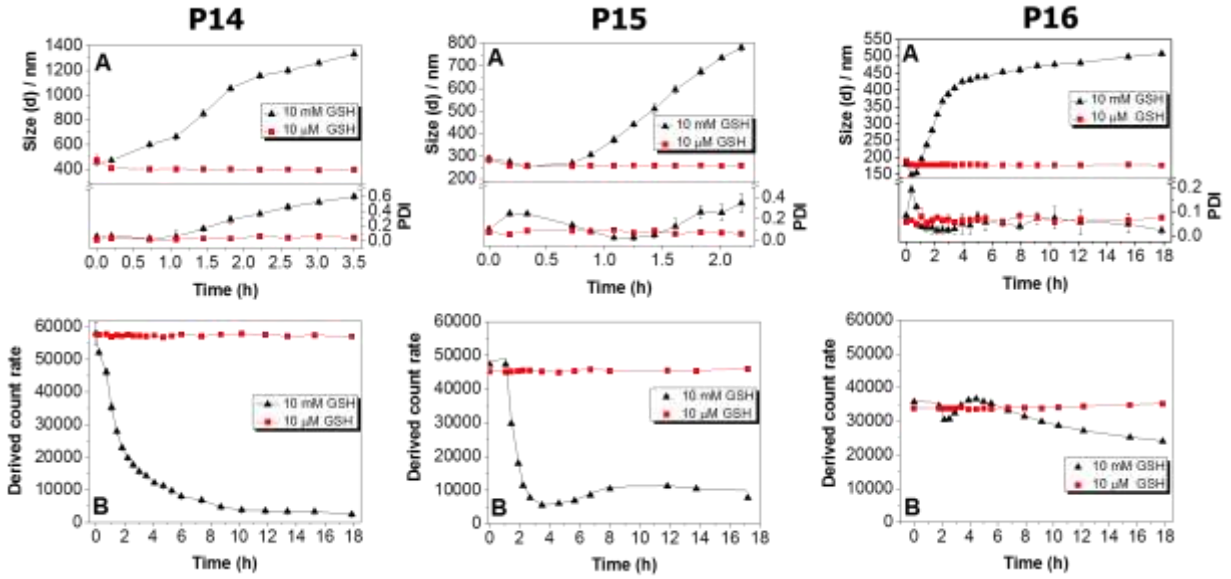

Figure 3.4 (A) Z-Average diameter and PDI values of the nanoparticles as a function of 10 µM and 10 mM GSH. (B) Derived count rate of the nanoparticles as a function of 10 µM and 10 mM GSH.

DOX was encapsulated into **P15** nanoparticles utilizing the nanoprecipitation method. DLS and zeta potential measurements revealed that DOX-loaded nanoparticles have a Z-average diameter of 130 nm, a PDI value of 0.1 and a zeta potential of +30 mV. The drug loading efficiency (19.2%) and drug loading content (1.9%) were calculated using a fluorescence intensity calibration function of DOX in pure water. The release experiments revealed that the DOX release was significantly enhanced with the trigger of 10 mM GSH compared to the physiological conditions. The cytotoxicity studies revealed that the nanoparticles and the deprotonated water soluble **P21** represented no cytotoxic effect on L929 cells after 48 h of incubation at concentrations up to 0.75 and 0.5 mg mL^{-1}, respectively (Figure 3.5 A). Above the indicated concentrations, nanoparticles and **P21** exhibited moderate toxic effects to the cells, which could be attributed to the amino functionality of the polymers.[15] DOX-loaded nanoparticles resulted in a cell death in a concentration and time dependent manner comparable with free DOX (Figure 3.5 B). The efficient cell death was attributed to the release of DOX from the nanoparticles in the intracellular environment inhibiting the proliferation of the cells. The intracellular trafficking of DOX-loaded nanoparticles in comparison with free DOX was followed in HEK cells using confocal laser scanning microscopy (CLSM) (Figure 3.6). DOX fluorescence was clearly observed in the cytosol and in the nuclei for cells treated with DOX-loaded nanoparticles after incubation for 6 h. This indicates that the DOX-loaded nanoparticles efficiently entered the cells, and the DOX was released from the nanoparticles by the intracellular triggers. A longer

incubation time (24 h) resulted in stronger DOX fluorescence inside the cell nuclei. Similar results were obtained with free DOX.

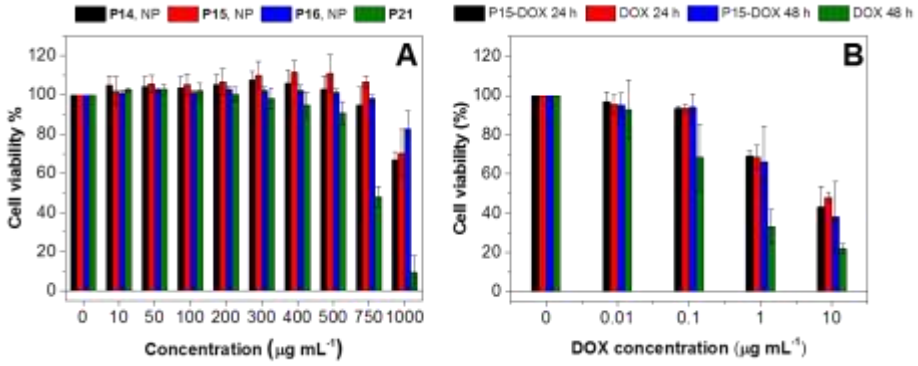

Figure 3.5 (A) Cytotoxicity test of nanoparticles (NPs) that were prepared from **P14**, **P15**, **P16**, and AEAEMA homopolymer **P21** in L929 cells. (B) Cytotoxicity test of DOX-loaded nanoparticles and free DOX. The relative viability is expressed as percentage to control cells not treated with NPs. Untreated cells on the same well plate were used as positive controls.

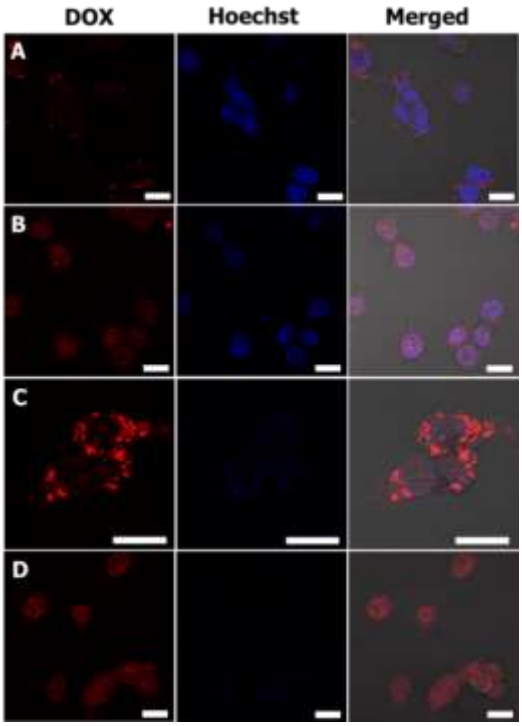

Figure 3.6 Live cell CLSM images of HEK cells incubated with DOX-loaded nanoparticles and free DOX at 1 μg/mL pure and encapsulated DOX. For each panel, the images from left to right show DOX fluorescence in cells (red), cell nuclei stained by Hoechst (blue), and overlays of the two images and a brightfield image. The scale bars correspond to 20 μm in all the images. (A) DOX-loaded nanoparticles, 6 h incubation; (B) free DOX, 6 h incubation; (C) DOX-loaded nanoparticles, 24 h incubation; (D) free DOX, 24 h incubation.

These results indicate that the prepared polymeric nanoparticles are promising vehicles for the controlled release of loaded pharmaceutical agents in the cytosol.

4. Effect of glass transition temperature on the stimuli responsive behavior of the nanoparticles

Parts of this chapter have been published: **P5**) T. Yildirim, I. Yildirim, R. Yanez-Macias, S. Stumpf, C. Fritzsche, S. Hoeppener, C. Guerrero-Sanchez, S. Schubert, U. S. Schubert, *Polym. Chem.* **2017**, *8*, 1328-1340; **P6**) T. Yildirim, A. Traeger, P. Sungur, S. Hoeppener, C. Fritzsche, I. Yildirim, D. Pretzel, S. Schubert, U. S. Schubert, submitted.

It is known that nanoparticles derived from THP functional polymers can be disrupted by ultrasound exposure.[70-71] Moreover, the THP group can be cleaved under acidic conditions.[32] As a consequence, a library of well-defined statistical copolymers of 2-((tetrahydro-2H-pyran-2-yl)oxy)ethyl methacrylate (THP-HEMA) with different compositions of 2-(dimethylamino) ethyl methacrylate (DMAEMA) were synthesized using the RAFT polymerization process to develop a novel ultrasound- and pH value responsive nanoparticle system with surface charge conversion from negative to positive at slightly acidic conditions (Scheme 4.1). In order to investigate comprehensively the effect of the DMAEMA content on the stimuli response of the corresponding nanoparticles, one homopolymer of THP-HEMA (**P22**) and four copolymers of THP-HEMA and DMAEMA (**P23** to **P26**) with 5 mol% of DMAEMA content increment (5 to 20 mol% DMAEMA) with similar molar mass values were synthesized utilizing a Chemspeed Swing-SLT automated parallel synthesizer.[72-73] Moreover, it is known that the ionizable carboxylic acid end-group of the CPADB could potentially affect the pH-responsive behavior of the corresponding nanoparticles.[74-75] To investigate the effect of functional CTA end groups on pH-responsive behavior of the nanoparticles, analogues of **P22** and **P26** (**P22OH** and **P26OH)** were synthesized by utilizing a non-ionizable hydroxyl functional chain transfer agent 4-cyano-4-((dodecylsulfanylthiocarbonyl)sulfanyl)pentanol (CDP).

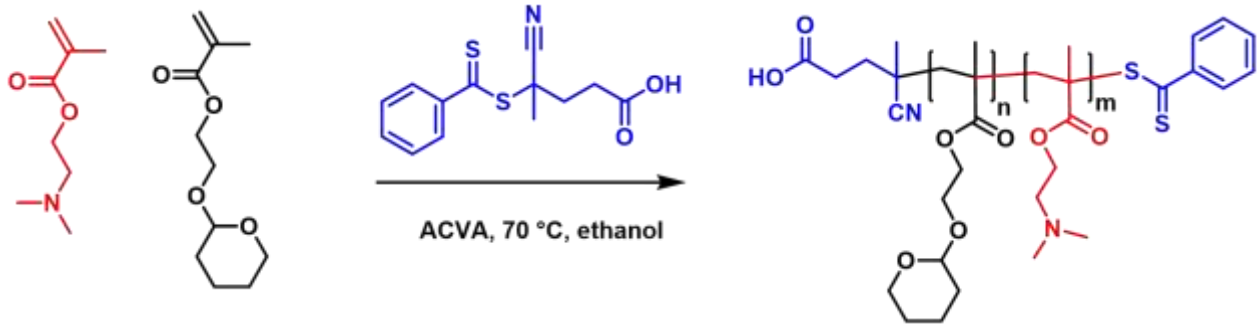

Scheme 4.1 Schematic representation of the RAFT copolymerization of THP-HEMA with DMAEMA.

Table 4.1 Selected characterization data of the THP-HEMA (M1) (co)polymers with DMAEMA (M2).

Entry	Monomer/ CTA/ACPA	f(M1/ M2)[a]	F(M1/ M2)[b]	Conv. [%][c] M1/M2	$M_{n,theo.}$[d] [g mol^{-1}]	DP[c] M1/M2	M_n[c] [g mol^{-1}]	$M_{n,SEC}$[e] [g mol^{-1}]	$Đ$[e]	T_g [°C][f]
P22	45.37/1/0.25			85/0	8,500	40/0	8,800	6,300	1.13	29.4
P22OH	45.37/1/0.25			90/0	9,000			6,800	1.24	-
P23	45.98/1/0.25	19	15.7	85/84	8,500	36/2.3	8,300	5,700	1.18	30.6
P24	46.61/1/0.25	9	8.2	80/90	8,100	33/4	7,800	5,600	1.18	28.0
P25	47.26/1/0.25	5.7	5.6	76/84	7,800	31/5.5	7,800	6,200	1.17	29.9
P6	47.92/1/0.25	4	4	84/87	8,500	29/7.3	7,600	6,300	1.18	29.1
P26OH	47.92/1/0.25	4	4	82/90	8,600			6,400	1.27	-

[a]Initial monomer feed ratio. [b]Monomer ratio in the isolated copolymer. [c]Determined by ^{1}H NMR spectroscopy. [d]Determined by the formula $M_{n,theo.} = [([M]_{M1}/[CTA] \times Conv. \times M_{M1}) + ([M]_{M2}/[CTA] \times Conv. \times M_{M2}) + (M_{CTA})]$. [e]Determined by SEC in $CHCl_3$ analysis (RI detection, PMMA calibration). [f]Determined by DSC analysis.

Differential scanning calorimetry (DSC) studies under nitrogen atmosphere revealed that polymers exhibit single T_g temperatures ranging from 29.1 to 30.6 °C. The pendant tertiary amino moieties of the polymers were quaternized by treating with an excess of methyl iodide in order to study the pH response of the nanoparticles prepared from permanently positively charged polymers (**P23q** to **P26q**). The nanoparticles were obtained from the synthesized (co)polymers (**P22** to **P26**, **P22OH**, **P26OH**, **P22q** to **P26q**) using the nanoprecipitation method. Quaternized polymers (**P23q** to **P26q**) resulted in smaller nanoparticles compared to unquaternized ones (**P23** to **P26**) for both dropping methods as a result of permanently charged groups in quaternized polymers (**P23q** to **P26q**).[69]

Table 4.2 Selected characterization results of the prepared nanoparticles.

Entry	Z-average [d, nm][a]		PDI[a]		ζ-potential [mV][b]	
	AW[c]	WA[d]	AW[c]	WA[d]	AW[c]	WA[d]
P22	108 ± 1	242 ± 3	0.14 ± 0.01	0.01 ± 0.01	- 31 ± 1	- 26 ± 1
P22OH	119 ± 1	223 ± 3	0.08 ± 0.02	0.08 ± 0.02	- 33 ± 1	- 25 ± 1
P23q	57 ± 1	182 ± 1	0.23 ± 0.01	0.06 ± 0.01	+ 29 ± 1	+ 37 ± 2
P24	98 ± 1	216 ± 3	0.13 ± 0.02	0.03 ± 0.01	+ 42 ± 1	+ 46 ± 6
P24q	42 ± 1	172 ± 2	0.26 ± 0.01	0.07 ± 0.02	+ 54 ± 3	+ 57 ± 1
P25	130 ± 1	233 ± 1	0.13 ± 0.01	0.01 ± 0.01	+ 48 ± 1	+ 30 ± 1
P25q	38 ± 1	120 ± 1	0.28 ± 0.01	0.11 ± 0.01	+ 65 ± 3	+ 48 ± 1
P26	120 ± 1	247 ± 2	0.11 ± 0.01	0.02 ± 0.01	+ 45 ± 1	+ 47 ± 1
P26OH	89 ± 1	229 ± 3	0.15 ± 0.11	0.05 ± 0.03	+ 42 ± 1	+ 51 ± 1
P26q	51 ± 1	138 ± 2	0.28 ± 0.01	0.01 ± 0.01	+ 48 ± 5	+ 63 ± 2
PMMA	-	187 ± 1	-	0.03 ± 0.03	-	- 18 ± 1

[a]Average values of three DLS measurements. [b]Average values of three ζ-potential measurements in pure water. [c]Dropping acetone to water. [d]Dropping water to acetone.

In order to investigate the effect of the pH value on the size and the surface charge of the nanoparticles, variations in the diameter and zeta potential values of the nanoparticles were

studied at different pH values after 1 h of incubation at 37 °C. **P22** nanoparticles possessed stable size and PDI values at neutral and basic pH values (pH = 7.4, 8, and 9) (Figure 4.1). Upon lowering the pH value below 7.4, a gradual increase in the size was observed. This is due to the decrease in the ζ-potential values from -66 mV at a pH value of 9 to -19 mV at a pH value of 6.3. In accordance with this, **P22** nanoparticles were precipitated around a pH value of 6.3. Below its isoelectric point (IEP) (the pH value at which the surface charge of the nanoparticles is zero), **P22** nanoparticles became positively charged. Lovett *et al.* reported that a carboxylic acid based CTA can be ionized in neutral media and protonated at acidic pH values leading to a nanoparticle ζ-potential conversion.[75] As a consequence, the observed IEP of the **P22** nanoparticles was first attributed to the protonation of the carboxyl end-group of the polymers. However, similar results were observed with **P22OH** nanoparticles that contain a hydroxyl functional CTA instead of a carboxyl functionality. Therefore, exhibition of IEPs for both polymers was attributed to the existence of THP-HEMA groups. In contrast to **P22** and **P22OH**, the **P24** nanoparticles were stable in the pH range from 4 to 6 with ζ-potential values higher than +58 mV as a result of protonated DMAEMA groups. At a pH value of 3.1, **P24** nanoparticles exhibited a significant decrease in size from 200 to 80 nm. This was ascribed to the protonation of the DMAEMA as well as the THP-HEMA groups. The protonation of the THP-HEMA moieties was expected to result in a cleavage of the cyclic acetal functionality of the THP-HEMA pendants. However, ^{1}H NMR studies revealed that even with an incubation in 0.1 acetic acid (pH = 3.1) at 37 °C for 24 h a negligible acetal group cleavage was observed indicating the slow cleavage of the THP-HEMA moieties. Between the pH values from 6.3 to 7.4, **P24** nanoparticles were aggregated due to the insufficient ζ-potential values (lower than ±20 mV) as a result of the deprotonated DMAEMA moieties. However, at a pH value of 8 and above, they became stable due to having ζ-potential values beyond -37 mV. In contrast to **P24**, the size of the **P25** decreased from 200 nm to 33 nm at pH 4. Moreover, prolonging the incubation time to 6 h resulted in dissolution of the polymers in acidic media as a result of the protonation of the DMAEMA groups. In agreement with this, **P26** nanoparticles that contain a higher DMAEMA content than **P25** revealed dissolution even at a pH value of 5. Moreover, it was observed that the IEP of the nanoparticles shifted to the higher pH values as the DMAEMA content of the polymers increases.

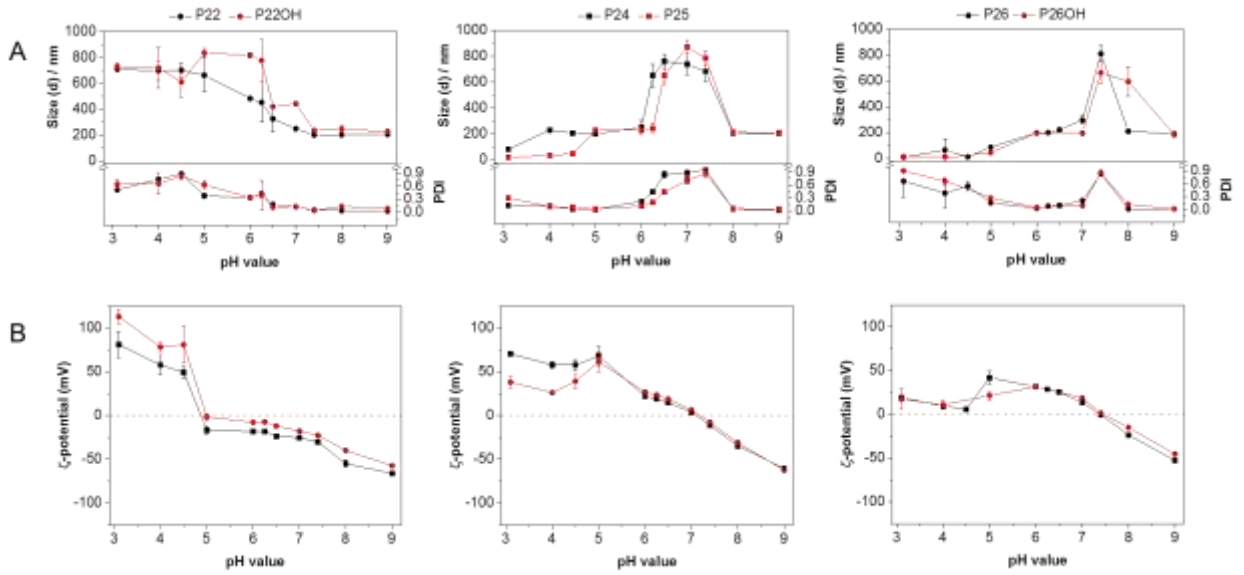

Figure 4.1 (A) Intensity-weighted size and PDI values of the nanoparticles as a function of the pH value. (B) ζ-Potential values of the nanoparticles as a function of the pH value.

Ultrasound responsiveness of the nanoparticles was investigated by exposing the nanoparticles to ultrasound with a power of 20 W and a frequency of 26 kHz. The variations in particle size, PDI value and derived count rate were recorded by DLS at intervals of 5 minutes of the ultrasound treatment. DLS measurements revealed a gradual increase in size and PDI values but a continuous decrease in the derived count rate upon prolonged ultrasound exposure for all nanoparticles due to the disassembly of the nanoparticles upon ultrasound treatment. In agreement with this, SEM measurements revealed that uniform spherical shapes of the nanoparticles distorted to irregular larger aggregates and some smaller structures. In a control experiment, PMMA nanoparticles did not show any response to the applied ultrasound. After ultrasound treatment no change in the ^{1}H NMR spectrum of the nanoparticles was observed. As a consequence, the ultrasound responsiveness of the nanoparticles was attributed to the elastic nature (low T_g values) of the corresponding THP-HEMA based polymers. In agreement with this assumption, a control experiment with poly(methyl acrylate) (PMA) (T_g = 16 °C) nanoparticles revealed similar responsive behavior to ultrasound. As a consequence, ultrasound behavior of the THP-HEMA based nanoparticles ascribed to their high motion abilities as a result of having low T_g values. Nile Red was used as a model compound to study the ability of the nanoparticles to encapsulate hydrophobic guest molecules. It is known that the fluorescence of Nile Red is sensitive to its environment.[76] Nanoparticles prepared from unquaternized polymers exhibited similar emission intensities as well as comparable emission wavelength maxima (Figure 4.2 A)

indicating that the cores of the nanoparticles have similar hydrophobicities. However, quaternized nanoparticles exhibited a gradual decrease in the emission intensity of Nile Red upon increasing the ratio of the quaternized DMAEMA content. Moreover, a continuous red shift in the emission wavelength maximum of Nile Red was observed as the quaternized DMAEMA content increased in the polymers (Figure 4.2 B). This indicates that simply by variation of the amount of the charged groups in the polymers the hydrophilicity of the core of the nanoparticles can be tuned. Additionally, dye release experiments demonstrated that release of Nile Red was significantly accelerated in acidic media or upon ultrasound exposure.

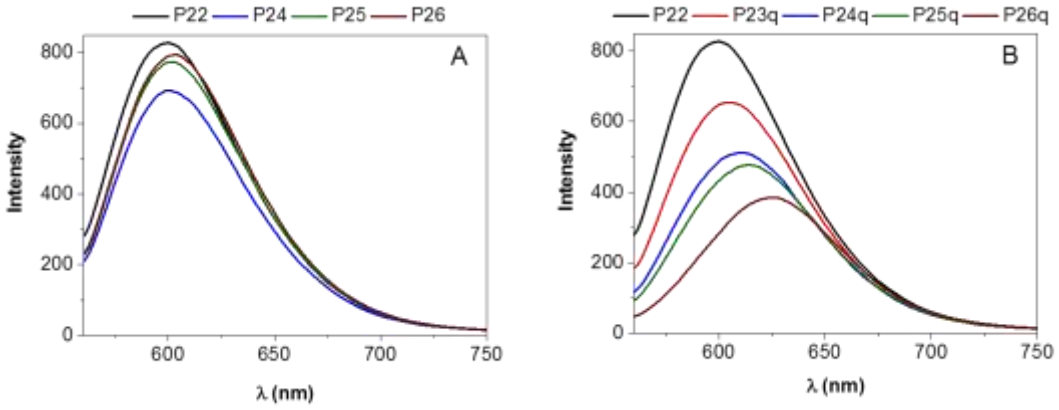

Figure 4.2 Fluorescence emission spectra of Nile Red encapsulated into nanoparticles (0.5 mg mL^{-1}) formed by **P22**, **P24** to **P26** (A) as well as **P22**, **P23q** to **P26q** (B).

Polymersomes, also known as polymeric vesicles, are hollow structures enclosed by a polymeric bimembrane composed from amphiphilic copolymers.[77-79] Polymersomes contain an aqueous interior and a hydrophobic membrane. As a consequence, they are capable to encapsulate both hydrophobic and hydrophilic molecules.[80] Stimuli responsive polymersomes usually release the encapsulated drugs in response to a certain stimuli by swelling, dissolution, precipitation or collapsing.[81] However, polymersomes can also undergo morphology transition in response to stimuli when their membranes have enough chain motilities.[46, 82] In particular, vesicle-to-micelle transitions are of particular interest for the controlled delivery of hydrophilic molecules as a result of offering a loss of aqueous cavities within the vesicles.[83-85] It is known that polymersomes can undergo shape transformations in response to stimuli when their membrane has a sufficient chain mobility. As a consequence, three well-defined diblock copolymers of poly((THP-HEMA)-*b*-DMAEMA) were synthesized by reversible addition-fragmentation chain transfer (RAFT) polymerization using a macro chain transfer approach (Scheme 4.2) in order to

obtain a polymersome system with pH value dependent morphology transition abilities. The macro chain transfer agent (**P27**) was synthesized by RAFT polymerization of THP-HEMA using CPADB as CTA. The mean DP of the **P27** was estimated to be 35 using ^{1}H NMR end group analysis. For the synthesis of diblock copolymers, **P27** was utilized as RAFT CTA and ACVA as initiator (Scheme 4.2).

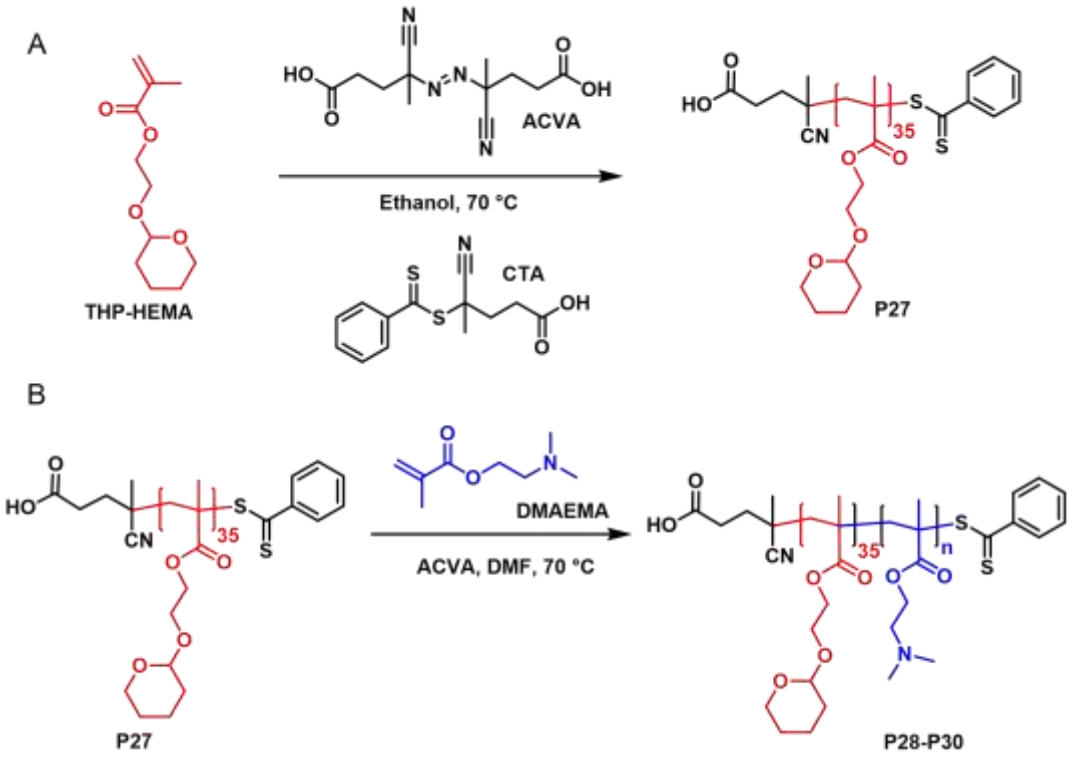

Scheme 4.2 (A) Schematic representation of the synthesis of **P27** *via* RAFT polymerization of THP-HEMA and (B) its subsequent chain extension with DMAEMA.

To identify the optimal monomer composition for a polymersome formation, the length of the p(THP-HEMA) block was kept constant and the DP of p(DMAEMA) block was systematically varied from 21 to 50 by variation of the [**P27**] to [DMAEMA] ratio or the polymerization time. The mean DPs of the DMAEMA block of the copolymers were calculated *via* ^{1}H NMR spectroscopy by comparing the integral values of the characteristic signals of DMAEMA with THP-HEMA. SEC analysis demonstrated a narrow molar mass distribution ($Đ$ < 1.1) for all polymers indicating the effectiveness of **P27** for the controlled RAFT polymerization of DMAEMA (Table 4.3). Differential scanning calorimetry (DSC) analysis revealed that all copolymers have single T_g temperatures in the range of 21 to 25 °C suggesting that THP-HEMA and DMAEMA block segments are thermodynamically miscible. Self-assembly behavior of the

amphiphilic diblock copolymers in water was investigated utilizing the nanoprecipitation method using dropping water into acetone polymer solutions with an initial polymer concentration of 5 mg mL^{-1}.

Table 4.3 Selected characterization data of the block copolymers (**P28** to **P30**).

Entry	DMAEMA/ mCTA[a]	mCTA/ ACVA[b]	Polym. time [h]	Conv. [%][c]	$DP_{theo.}$[d]	$M_{n,theo.}$[e] [g mol^{-1}]	DP[f]	M_n[g] [g mol^{-1}]	$M_{n,SEC}$[i] [g mol^{-1}]	$Đ$[i]	T_g[j]
P28	49.62/1	15/1	4	36	18	10,600	21	11,100	8,300	1.09	24.9
P29	49.62/1	15/1	8	58	29	12,400	30	12,500	9,300	1.08	23.4
P30	102.54/1	15/1	7	49	50	15,700	50	15,700	11,200	1.10	20.7

[a]Monomer to mCTA ratio. [b]mCTA to ACVA ratio. [c]Determined by ^{1}H NMR spectroscopy. [d]Determined by the formula $DP_{theo.}$ = [([M]/[mCTA] × Conv.]. [e]Determined by the formula $M_{n,theo.}$ = [([M]/[mCTA] × Conv. × M_{mCTA}) + (M_{mCTA})]. [f]Determined by ^{1}H NMR spectroscopy of isolated polymers. [g]Determined by the formula $M_{n,theo.}$ = [(DP × M_{DMAEMA}) + M_{mCTA}]. [i]Determined by SEC in DMAc analysis (RI detection, PS calibration). [j]Determined by DSC analysis.

A monomodal number distribution with an average hydrodynamic diameter (D_{av}) of 30 nm was observed by DLS for the **P28** suspensions. However, some small number of medium sized aggregates (D_{av} ~300 nm) could also be observed in the volume distribution. In accordance with this, cryo-TEM analysis exhibited predominantly polydisperse vesicles ranging from 20 to 90 nm diameters and some larger spherical aggregates (~200 nm). The bilayer thickness of the polymersomes was found to be around 8 ± 2 nm. DLS measurements revealed a monomodal number distribution (D_{av} = 15 nm) for the **P29** suspensions. Some larger structures were also observed in the DLS volume distribution with a D_{av} of 120 nm. Cryo-TEM measurements revealed a coexistence of spherical micelles with diameters around 12 nm and polydisperse vesicles which have diameters ranging from 30 to 180 nm. For the **P30** suspensions, DLS measurements showed a monomodal number distribution (D_{av} = 10 nm). In agreement with this, cryo-TEM analysis exhibited homogeneous spherical micelles that have diameters around 10 nm. These results indicate that the morphology of the suspensions changes from vesicles to spherical micelles as the block length of the DMAEMA increases as a result of the increased hydrophilicity, which correlates with before reported literature.[79] The hydrophilicity of the synthesized block copolymers can also be varied by the variation of the pH value of the environment as a result of the pH responsiveness of the DMAEMA block. As a consequence, the pH responsive behavior of the polymersomes was investigated by examining the variations in diameters and zeta potentials at different pH values after 3 h of incubation at 37 °C. The **P28** suspensions exhibited a stable size distribution at neutral pH values (pH = 7.0 and 7.4). However,

an increase in the diameter of the polymersomes was observed at a pH value of 8.0. This is due to the decrease of the ζ-potential of the polymersomes from +33 mV at pH 7.4 to +20 mV at pH 8.0 due to the partial deprotonation of the DMAEMA moieties. In accordance with this, the polymersomes were precipitated at pH value of 9.0 as a result of a further decrease of the ζ-potential from +20 mV to -11 mV. In contrast, a decrease of the pH value from neutral to acidic pH values resulted in a continuous decrease in the diameter and an increase in the ζ-potential values. Moreover, the turbid solution became transparent at acidic pH values.

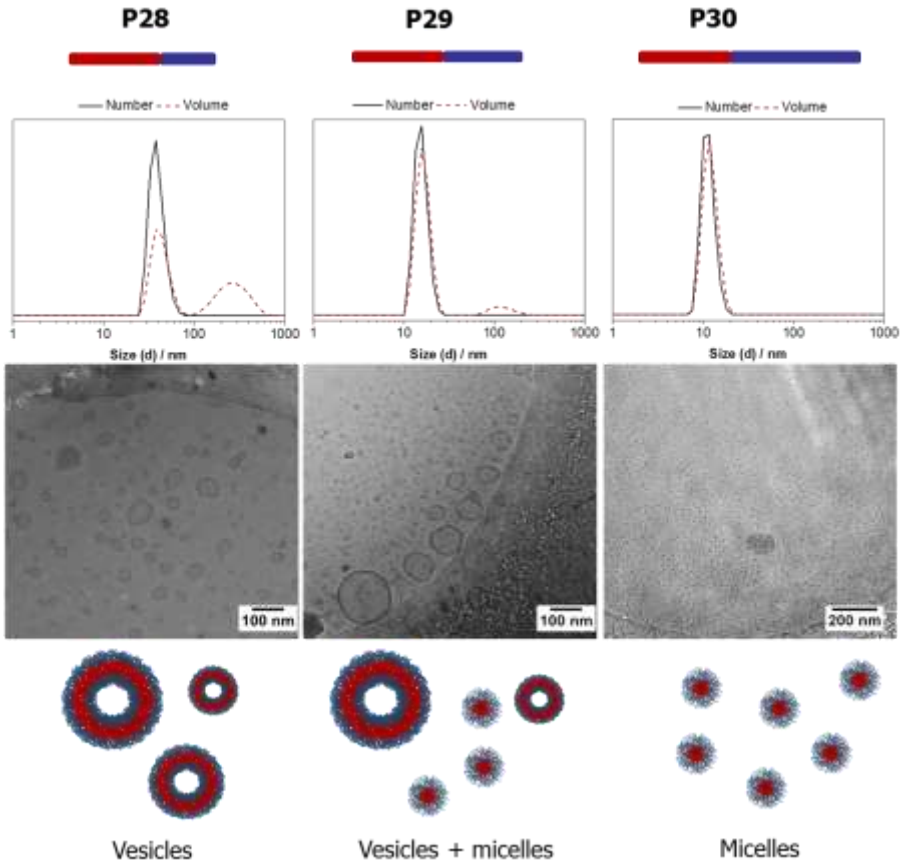

Figure 4.3 DLS plots and cryo-TEM images of the suspensions obtained from **P28**, **P29**, and **P30** in water (c = 2.5 mg mL^{-1}).

Cryo-TEM measurements revealed exclusively vesicular aggregates with clearly visible membranes at pH 7.4. On the contrary, only homogeneous spherical micelles were observed at a pH value of 5.0. As a consequence, the decrease in the diameter upon decreasing the pH to acidic values was correlated to the morphology transition from vesicles to micelles as a result of an increase of the polymer hydrophilicity. The critical aggregation concentration (CAC) of the polymersomes was calculated as 0.084 mg mL^{-1} using Nile Red as a fluorescent probe. The

calculated CAC of the polymersomes is slightly lower than the before reported values for p(THP-HEMA) copolymer based micelles.[32] The ability of polymersomes to encapsulate hydrophilic molecules was investigated using the water soluble anticancer drug doxorubicin hydrochloride (DOX). DOX was loaded in **P28** polymersomes utilizing nanoprecipitation. DLS measurements exhibited a number average diameter of 30 nm and a ζ-potential of +30 mV for the DOX-loaded polymersomes. Cryo-TEM investigations showed relatively uniform vesicular structures. The drug loading efficiency and drug loading content were calculated by fluorescence measurements as 30.7% and 1.5%, respectively. The DOX experiments revealed that DOX was released from the polymersomes faster at a pH value of 5.0 compared to 7.4. This was attributed to the morphology change of the polymersomes at acidic pH values to micelles that cause a loss of hydrophilic aqueous cavities.

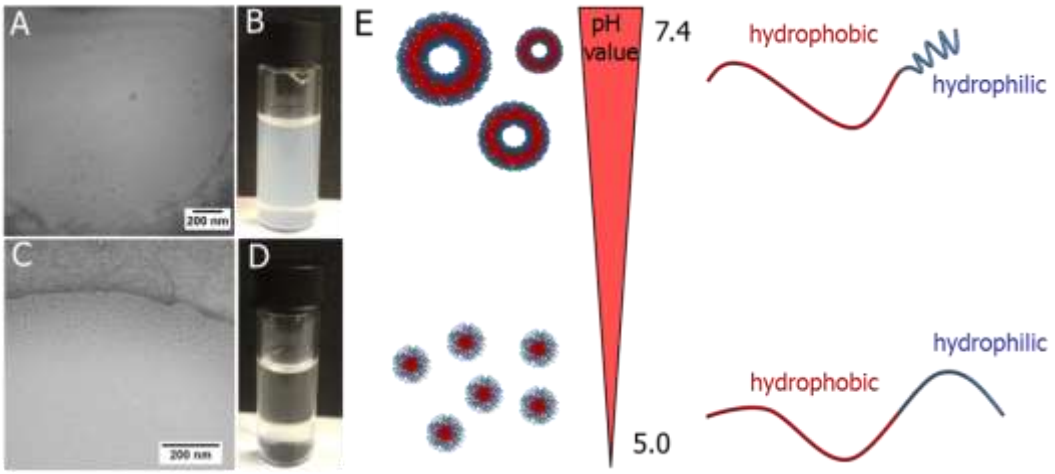

Figure 4.4 (A) Cryo-TEM image of the **P28** suspension at pH 7.4. (B) Photograph of vial containing the **P28** suspension at pH 7.4. (C) Cryo-TEM image of the **P28** suspension at pH 5.0. (D) Photograph of vial containing the **P28** suspension at pH 5.0. (E) Schematic illustration of the pH value change induced vesicle-to-micelle morphology transition as a result of an increase of the volume of hydrophilic blocks at acidic media.

The cytotoxicity studies of copolymer aqueous nanoparticle suspensions revealed that **P28** is not toxic to L929 cells after 48 h incubation up to a concentration of 250 µg mL^{-1}. However, the **P28** suspensions exhibited toxic effects to the cells starting from 300 mg mL^{-1} became more pronounced Figure 4.5 A). The cytotoxicity of **P28** suspensions was ascribed to the p(DMAEMA) block, which can induce toxic effects to cells as a result of its cationic character.[86-87] The **P29** suspensions revealed similar cell viabilities compared to **P28** at the tested concentrations. However, the **P30** suspensions that contains the longest p(DMAEMA) block

exhibited the highest toxic effects to the cells. Moreover, the cytotoxicity of the DOX-loaded polymersomes was also evaluated in comparison with free DOX (Figure 4.5 B). The results exhibited that DOX-loaded polymersomes had similar cell killing efficiencies as the free DOX.

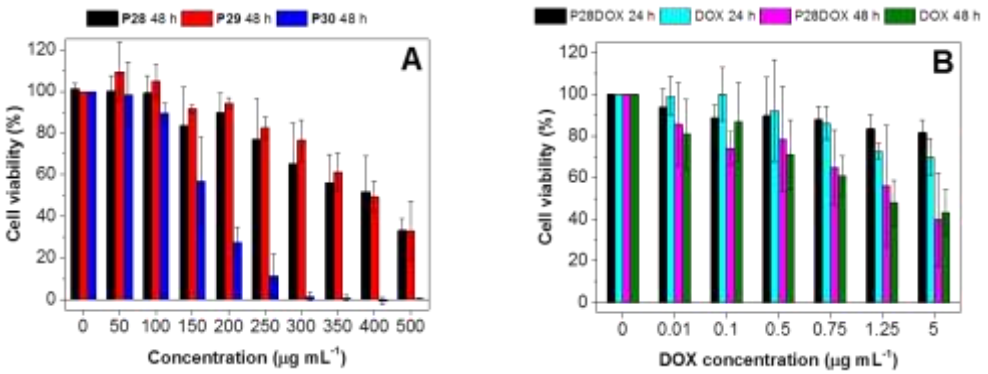

Figure 4.5 (A) Cytotoxicity test of **P28**, **P29**, and **P30** aqueous suspensions in L929 cells after 48 h incubation. (B) Cytotoxicity test of DOX·HCl encapsulated **P28** suspensions and free DOX·HCl in L929 cells. The relative viability is expressed as percentage to control cells not treated with NPs. Untreated cells on the same well plate were used as positive controls.

Confocal laser scanning microscopy (CLSM) was used to monitor the cellular uptake of the DOX loaded polymersomes and the free DOX. The red fluorescence of DOX was clearly observed in the nucleus of L929 cells after incubation for only 2 h indicating the efficient cellular uptake of DOX loaded polymersomes and the fast release of the DOX in the endo/lysosomes as a result of the morphology change. A longer incubation time of DOX loaded polymersomes to 24 h yielded a stronger DOX fluorescence. Similar results were obtained with free DOX. The cellular uptake of the DOX-loaded polymersomes and the free DOX were further quantified through flow cytometry. Flow cytometry results indicated that fluorescence intensity of the DOX-loaded polymersomes is higher than that of the free DOX after 2 h and this becomes even more pronounced for longer incubation times. This indicated that DOX-loaded polymersomes entered the cells faster than the free DOX. It is known that cationic nanoparticle systems can be uptaken by the cells even faster than small molecules including the free DOX.[88-90] Therefore, the faster uptake of the DOX-loaded polymersomes was attributed to their positive surface charges.

These results show that the glass transition temperature of the polymers represents an important parameter for the stimuli-responsive behavior of the nanoparticles.

5. Summary

Stimuli-responsive polymeric nanoparticles have recently gained tremendous attention, in particular in the field of controlled drug delivery as a result of offering prolonged circulation times and on demand delivery. The tailor-made design of stimuli-responsive nanoparticles mostly relies on the incorporation of desired stimuli-responsive motifs into the polymers. However, the challenge is to synthesize the corresponding polymers in a well-defined and reproducible way. In the context of the synthesis of stimuli-responsive polymers, the reversible addition fragmentation chain transfer (RAFT) polymerization process is advantageous compared to other techniques due to its high tolerance to various functional groups and polymerization conditions. After the synthesis of the stimuli responsive polymers, it is also crucial to formulate the resulting stimuli-responsive nanoparticles in a controlled way. Nanoprecipitation represents a facile and reliable way to produce polymeric nanoparticles. As a result, the RAFT polymerization process and the nanoprecipitation technique were selected as the methods of choice within this thesis for the synthesis of (multi)functional polymers and the formation of the corresponding nanoparticles.

The presented thesis represents an overview of (i) the synthesis of various new stimuli-responsive polymers with tailor-made functionalities and polymer structures, (ii) the formulation of stimuli-responsive nanoparticles *via* nanoprecipitation, (iii) the investigation of stimuli-responsive behavior of the nanoparticles, as well as (iv) the evaluation of synthesized nanoparticles for drug delivery applications (Figure 5.1).

It is shown that methyl methacrylate (MMA) could be copolymerized with various amino methacrylates including primary amino functional 2-aminoethyl methacrylate hydrochloride (AEMA·HCl), secondary amino functional 2-(*tert*-butylamino)ethyl methacrylate (*t*BAEAMA) and tertiary amino functional 2-(dimethylamino)ethyl methacrylate (DMAEMA) using the RAFT polymerization process. Furthermore, it is demonstrated that nanoprecipitation of these polymers yielded pH responsive PMMA based nanoparticles. The resulting nanoparticles exhibited a pH responsive behavior in a way that strongly depends on the amount and the chemical structure of the amino groups of the polymers. Additionally, it was proven that these nanoparticles can host hydrophobic compounds at neutral pH values and release them at acidic pH values as a result of their dissolution abilities.

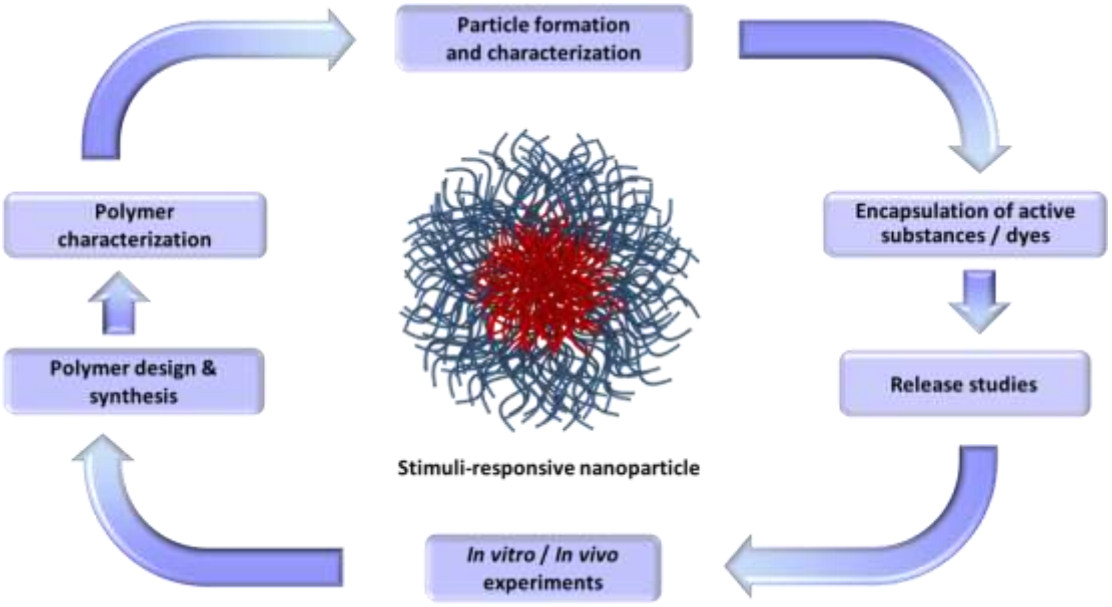

Figure 5.1 Schematic representation of the workflow of the represented studies in this thesis.

The primary amino groups enable the covalent conjugation of bioactive molecules to the polymers using various reactions. In this context it was demonstrated that retinoic acid and a fluorescent dye could be successfully coupled to the AEMA·HCl functionalized PMMA based copolymer. The utilization of the nanoprecipitation method for the modified polymers resulted in cationic nanoparticles. Raman imaging studies demonstrated that retinoic acid (RA) functionalized nanoparticles can be detectable in cells without any need of additional labels. Moreover, the conjugation of the dye allowed monitoring nanoparticles *via* intravital microscopy.

The incorporation of disulphide bridges into copolymer pendants enables the possibility to obtain glutathione responsive nanoparticles. To this end, the RAFT polymerization process was used for the preparation of a statistical copolymer library of pyridyldisulfide ethylmethacrylate (PDSM) with 2-((*tert*-butoxycarbonyl)(2-((tert-butoxycarbonyl)amino)ethyl)amino)-ethyl methacrylate (Boc-AEAEMA). The nanoprecipitation method was utilized to formulate nanoparticles. It was observed that an increase of the AEAEMA content leads to a decrease of the nanoparticles size. The resulting nanoparticles were found to be responsive both to the glutathione concentration as well as the pH value. It could be shown that these nanoparticles can encapsulate the antitumor drug doxorubicin hydrochloride, carry it into the cells and release it in a response to intracellular glutathione concentration and pH value change.

Exogenous stimuli responsive nanoparticles have also gained increased interest for drug delivery applications. Particular interest in this regards focused on the ultrasound responsiveness. The

RAFT polymerization process was used to synthesize a well-defined statistical copolymer library of 2-((tetrahydro-2H-pyran-2-yl)oxy)ethyl methacrylate (THP-HEMA) with DMAEMA with different monomer compositions. The nanoparticle suspensions of these polymers were prepared by nanoprecipitation method. The pH-responsive behavior of the nanoparticles showed that incorporation of DMAEMA units into THP-HEMA based nanoparticles can provide effective pH-dependent surface charge conversion features. Moreover, it was shown that the disassembly pH value and the isoelectric point (IEP) of the nanoparticles could be systematically tuned by varying the DMAEMA content of the polymers. The ultrasound responsiveness tests revealed that THP-HEMA nanoparticles are responsive to ultrasound as a result of their high chain mobility. Moreover, cytotoxicity studies demonstrated that positively charged nanoparticles at the pH value of the cell media exhibited toxic effects to the cells, whereas the negatively charged nanoparticles were biocompatible and not cytotoxic.

Besides sustaining ultrasound responsiveness, the high chain mobility of THP-HEMA based polymers can possibly allow to obtain nanoparticles that also exhibit morphology transition in a response to a stimulus. In this context, three different block copolymers of THP-HEMA and DMAEMA were synthesized *via* RAFT polymerization by utilization of p(THP-HEMA) as a macro chain transfer agent. The length of the p(THP-HEMA) block was kept constant, whereas the length of the p(DMAEMA) block was systematically varied. Self-assembly studies demonstrated that the block copolymer with the shortest p(DMAEMA) block favors polymersome formation in water, whereas an increase of the DP of the p(DMAEMA) resulted in micellar structures. It was demonstrated that polymersomes undergo a morphology transition from vesicles to micelles in response to a decrease of the pH value from neutral to acidic values. Furthermore, it was verified that the polymersomes are capable of encapsulating DOX and transporting it into cells.

In summary, this thesis presents the synthesis of new stimuli-responsive polymers and the formulation of their corresponding nanoparticles. The nanoparticle systems show promising properties for potential drug delivery applications.

6. Zusammenfassung

Polymere Nanopartikel, welche auf einen bestimmten Reiz reagiesen, haben vor kurzem eine enorme Aufmerksamkeit erlangt, insbesondere im Bereich der kontrollierten Arzneimittelabgabe, da sie längere Verweilzeiten haben und nach Bedarf liefern. Die maßgeschneiderte Gestaltung von solchen reaktionsfähigen Nanopartikeln beruht meist auf dem Einbau von gewünschten reaktiven Motiven in die Polymere, sogenannte stimuli-responsive Polymere. Die Herausforderung besteht jedoch darin, die entsprechenden Polymere in einer klar definierten und reproduzierbaren Weise zu synthetisieren. Im Rahmen der Synthese von stimuli-responsiven Polymeren ist die reversible Additions-Fragmentierungs-Kettentransfer (RAFT) Polymerisation im Vergleich zu anderen Techniken aufgrund ihrer hohen Toleranz gegenüber verschiedenen funktionellen Gruppen und Polymerisationsbedingungen vorteilhaft. Nach der Synthese der auf Stimuli reagierenden Polymere ist es auch entscheidend, die resultierenden stimuli-responsiven Nanopartikel kontrolliert zu formulieren. Die Nanofällung stellt eine einfache und zuverlässige Methode zur Herstellung von Polymer-Nanopartikeln dar. Somit wurden in dieser Arbeit RAFT-Polymerisationsverfahren und die Nanofällung als Methoden der Wahl für die Synthese von (multi) funktionellen Polymeren und die Formulierung zu entsprechenden Nanopartikeln ausgewählt.

Die vorliegende Arbeit stellt einen Überblick über (i) die Synthese verschiedener neuer stimuli-reaktionsfähiger Polymere mit maßgeschneiderten Funktionalitäten und Polymerstrukturen dar, (ii) die Formulierung von stimuli-reaktionsfähigen Nanopartikeln durch Nanofällung, (iii) die Untersuchung des stimuli-responsiven Verhaltens der Nanopartikel sowie (iv) die Auswertung von synthetisierten Nanopartikeln für Arzneimittelabgabeanwendungen (Abbildung 6.1).

Es konnte gezeigt werden, dass Methylmethacrylat (MMA) mit verschiedenen Aminomethacrylaten einschließlich primären Aminofunktionen 2-Aminoethylmethacrylat-hydrochlorid (AEMA·HCl), sekundären Aminofunktionen 2-(*Tert*-Butylamino) ethylmethacrylat (*t*BAEAMA) und tertiären Aminofunktionen 2-(Dimethylamino) ethylmethacrylat (DMAEMA) unter Verwendung von RAFT-Polymerisationsverfahren copolymerisiert werden könnte. Weiterhin wird gezeigt, dass die Nanofällung dieser Polymere PMMA-basierte Nanopartikel ergab, welche auf pH-Wertveränderungen reagieren. Dieses Verhalten hängt stark von der Menge und der chemischen Struktur der Aminogruppen der Polymere ab. Darüber hinaus wurde

bewiesen, dass diese Nanopartikel hydrophobe Verbindungen bei neutralen pH-Werten einschließen und sie bei niedrigen pH-Werten infolge ihrer Löslichkeit freisetzen können.

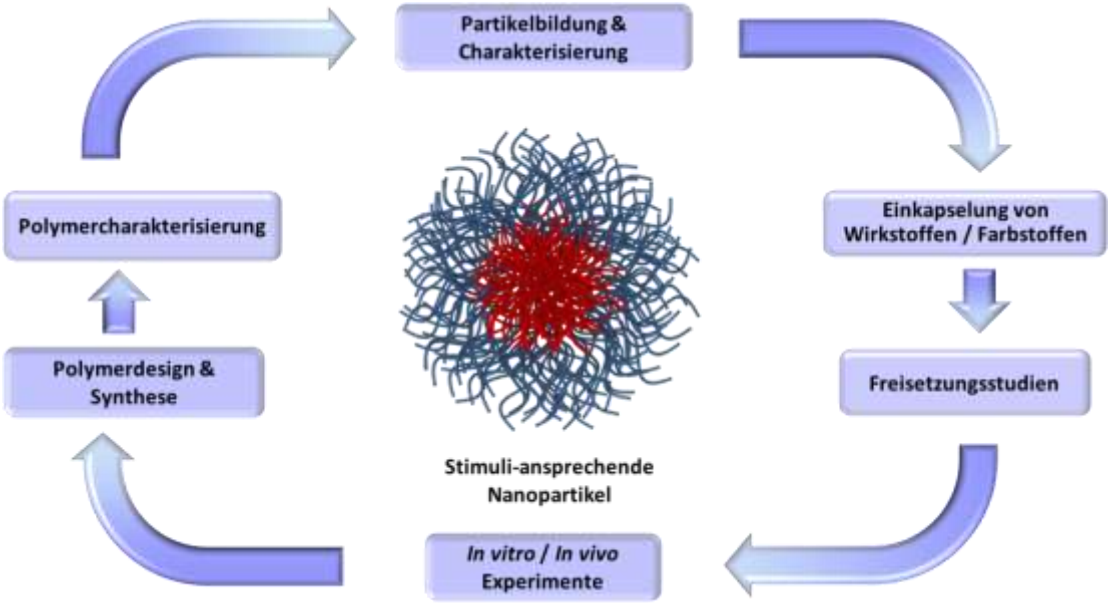

Abbildung 6.1 Schematische Darstellung des Arbeitsablaufs der dargestellten Studien in dieser Arbeit.

Die primären Aminogruppen erlauben die kovalente Anbindung von bioaktiven Molekülen an die Polymere mittels verschiedener Reaktionen. In diesem Zusammenhang wurde gezeigt, dass Retinolsäure (RA) und ein Fluoreszenzfarbstoff erfolgreich an das AEMA·HCl-funktionalisierte Copolymer auf PMMA-Basis gekoppelt werden konnten. Die Verwendung der Nanofällung für die modifizierten Polymere führte zu kationischen Nanopartikeln. Raman-Imaging-Studien zeigten, dass RA-funktionelle Nanopartikel in Zellen nachweisbar sind, ohne dass zusätzliche Marker benötigt werden. Darüber hinaus erlaubte die Konjugation des Farbstoffs die Überwachung von Nanopartikeln mit Hilfe der intravitalen Mikroskopie.

Der Einbau von Disulfidbrücken in Copolymer-Seitenketten ermöglicht die Herstellung von, redoxaktiven Nanopartikeln. Zu diesem Zweck wurde ein RAFT-Polymerisationsverfahren für die Herstellung einer statistischen Copolymerbibliothek von Pyridyldisulfid ethylmethacrylat (PDSM) mit 2-((*Tert*-Butoxycarbonyl)(2-((tert-butoxycarbonyl) amino) ethyl) amino) ethylmethacrylat (Boc-AEAEMA) verwendet. Die Nanofällung wurde erneut zur Formulierung von Nanopartikeln verwendet. Es wurde beobachtet, dass eine Erhöhung des AEAEMA-Gehalts zu einer Abnahme der Nanopartikelgröße führt. Es konnte weiterhin festgestellt werden, dass die resultierenden Nanopartikel sowohl auf die Glutathionkonzentration als auch auf den pH-Wert

ansprechen. Das Antitumor-Medikament Doxorubicin-Hydrochlorid wurde in die Nanopartikel eingekapselt, in die Zellen transportiert und entsprechend der intrazellulären Glutathion-Konzentration und der pH-Wert-Änderung freigesetzt.

Exogene stimuli-responsive Nanopartikel haben ebenfalls an Interesse für Anwendungen in der Arzneimittelabgabe gewonnen. Besonderes Interesse in dieser Hinsicht konzentriert sich auf Partikel, die auf Ultaschall reagieren. Das RAFT-Polymerisationsverfahren wurde verwendet, um eine definierte, statistische Copolymerbibliothek von THP-HEMA mit DMAEMA mit verschiedenen Monomerzusammensetzungen zu synthetisieren. Die Nanopartikel-Suspensionen dieser Polymere wurden nach dem Nanofällungsverfahren hergestellt. Das Verhalten der Nanopartikel zeigt, dass der Einbau von DMAEMA-Einheiten in THP-HEMA-basierte Nanopartikel zu einer Umwaldung der Oberflächenladung in Abhängigkeit der pH-Wertes führen kann. Darüber hinaus wurde gezeigt, dass der kritische-pH-Wert und der Isoelektrische Punket (IEP) der Nanopartikel systematisch durch Variation des DMAEMA-Gehaltes der Polymere abgestimmt werden konnten. Die Ultraschall empfindlich zeigt, dass THP-HEMA-Nanopartikel aufgrund ihrer hohen Kettenmobilität auf Ultraschall reagieren. Darüber hinaus zeigten Zytotoxizitätsstudien, dass positiv geladene Nanopartikel bei dem pH-Wert im Zellmedien toxisch für Zellen sind, während die negativ geladenen Nanopartikel biokompatibel und nicht zytotoxisch sind.

Neben der Sensibilität auf Ultraschall kann die hohe Kettenbeweglichkeit von THP-HEMA-basierten Polymeren möglicherweise zu, Nanopartikeln führen, die einen Morphologiewechsel als Reaktion auf einen Stimulus aufweisen. In diesem Zusammenhang wurden drei verschiedene Blockcopolymere von THP-HEMA und DMAEMA mittels RAFT-Polymerisation unter Verwendung von p(THP-HEMA) als Makro-Kettenübertragungsmittel synthetisiert. Die Länge des p(THP-HEMA)-Blocks wurde konstant gehalten, während die Länge des p(DMAEMA)-Blocks systematisch variiert wurde. Versuche zur Selbstorganisation zeigten, dass das Blockcopolymer mit dem kürzesten p(DMAEMA)-Block die Bildung von Vesikeln in Wasser begünstigt, während eine Erhöhung des DP des p(DMAEMA) zu mizellaren Strukturen führte. Es wurde gezeigt, dass Polymere einen Morphologieübergang von Vesikeln zu Micellen in Reaktion auf eine Abnahme des pH-Wertes von neutral zu sauer erfahren. Weiterhin wurde bestätigt, dass die Polymere in der Lage sind, DOX zu verkapseln und in Zellen zu transportieren.

Zusammenfassend stellt diese Arbeit die Synthese von neuartigen stimuli-responsiven Polymeren und die Formulierung ihrer entsprechenden Nanopartikel dar. Die Nanopartikel-Systeme weisen potentiell interessante Eigenschaften für mögliche Anwendungen als Medikamententransporter auf.

7. References

[1] O. C. Farokhzad, R. Langer, *ACS Nano* **2009**, *3*, 16-20.

[2] H. Maeda, *J. Control. Release* **2012**, *164*, 138-144.

[3] L. Zhang, F. X. Gu, J. M. Chan, A. Z. Wang, R. S. Langer, O. C. Farokhzad, *Clin. Pharmacol. Ther.* **2008**, *83*, 761-769.

[4] S. Mura, J. Nicolas, P. Couvreur, *Nat. Mater.* **2013**, *12*, 991-1003.

[5] G. Moad, *Polym. Chem.* **2017**, *8*, 177-219.

[6] C. J. Hawker, *J. Am. Chem. Soc.* **1994**, *116*, 11185-11186.

[7] J.-S. Wang, K. Matyjaszewski, *J. Am. Chem. Soc.* **1995**, *117*, 5614-5615.

[8] J. Chiefari, Y. K. Chong, F. Ercole, J. Krstina, J. Jeffery, T. P. T. Le, R. T. A. Mayadunne, G. F. Meijs, C. L. Moad, G. Moad, E. Rizzardo, S. H. Thang, *Macromolecules* **1998**, *31*, 5559-5562.

[9] C. Boyer, V. Bulmus, T. P. Davis, V. Ladmiral, J. Liu, S. Perrier, *Chem. Rev.* **2009**, *109*, 5402-5436.

[10] S. Schubert, J. J. T. Delaney, U. S. Schubert, *Soft Matter* **2011**, *7*, 1581-1588.

[11] C. Sanson, C. Schatz, J.-F. Le Meins, A. Soum, J. Thévenot, E. Garanger, S. Lecommandoux, *J. Control. Release* **2010**, *147*, 428-435.

[12] V. Bulmus, M. Woodward, L. Lin, N. Murthy, P. Stayton, A. Hoffman, *J. Control. Release* **2003**, *93*, 105-120.

[13] R. Wei, L. Cheng, M. Zheng, R. Cheng, F. Meng, C. Deng, Z. Zhong, *Biomacromolecules* **2012**, *13*, 2429-2438.

[14] W. Ke, J. Li, K. Zhao, Z. Zha, Y. Han, Y. Wang, W. Yin, P. Zhang, Z. Ge, *Biomacromolecules* **2016**, *17*, 3268-3276.

[15] P. Zhang, Y.-C. Chiu, L. H. Tostanoski, C. M. Jewell, *ACS Nano* **2015**, *9*, 6465-6477.

[16] N. Yamaguchi, L. Zhang, B.-S. Chae, C. S. Palla, E. M. Furst, K. L. Kiick, *J. Am. Chem. Soc.* **2007**, *129*, 3040-3041.

[17] B. Jeong, Y. H. Bae, S. W. Kim, *J. Control. Release* **2000**, *63*, 155-163.

[18] T. Kaiden, E. Yuba, A. Harada, Y. Sakanishi, K. Kono, *Bioconjugate Chem.* **2011**, *22*, 1909-1915.

[19] H. Oliveira, E. Pérez-Andrés, J. Thevenot, O. Sandre, E. Berra, S. Lecommandoux, *J. Control. Release* **2013**, *169*, 165-170.

[20] C. Sanson, O. Diou, J. Thévenot, E. Ibarboure, A. Soum, A. Brûlet, S. Miraux, E. Thiaudière, S. Tan, A. Brisson, V. Dupuis, O. Sandre, S. Lecommandoux, *ACS Nano* **2011**, *5*, 1122-1140.

[21] B. Yan, J.-C. Boyer, D. Habault, N. R. Branda, Y. Zhao, *J. Am. Chem. Soc.* **2012**, *134*, 16558-16561.

[22] W. Chen, J. Du, *Sci. Rep.* **2013**, *3*, 2162.

[23] J. L. Paris, M. V. Cabañas, M. Manzano, M. Vallet-Regí, *ACS Nano* **2015**, *9*, 11023-11033.

[24] W. Gao, J. M. Chan, O. C. Farokhzad, *Mol. Pharm.* **2010**, *7*, 1913-1920.

[25] X. Hu, Y. Zhang, Z. Xie, X. Jing, A. Bellotti, Z. Gu, *Biomacromolecules* **2017**, *18*, 649-673.
[26] J. Nicolas, *Chem. Mater.* **2016**, *28*, 1591-1606.
[27] J. Rautio, H. Kumpulainen, T. Heimbach, R. Oliyai, D. Oh, T. Jarvinen, J. Savolainen, *Nat. Rev. Drug Discov.* **2008**, *7*, 255-270.
[28] W. N. E. van Dijk-Wolthuis, P. van de Wetering, W. L. J. Hinrichs, L. J. F. Hofmeyer, R. M. J. Liskamp, D. J. A. Crommelin, W. E. Hennink, *Bioconjugate Chem.* **1999**, *10*, 687-692.
[29] F. Meng, W. E. Hennink, Z. Zhong, *Biomaterials* **2009**, *30*, 2180-2198.
[30] M. Huo, J. Yuan, L. Tao, Y. Wei, *Polym. Chem.* **2014**, *5*, 1519-1528.
[31] Y.-L. Li, L. Zhu, Z. Liu, R. Cheng, F. Meng, J.-H. Cui, S.-J. Ji, Z. Zhong, *Angew. Chem. Int. Ed.* **2009**, *48*, 9914-9918.
[32] A. Klaikherd, C. Nagamani, S. Thayumanavan, *J. Am. Chem. Soc.* **2009**, *131*, 4830-4838.
[33] R. Liu, X. Zhao, T. Wu, P. Feng, *J. Am. Chem. Soc.* **2008**, *130*, 14418-14419.
[34] L. Li, K. Raghupathi, C. Yuan, S. Thayumanavan, *Chem. Sci.* **2013**, *4*, 3654-3660.
[35] D. C. González-Toro, J.-H. Ryu, R. T. Chacko, J. Zhuang, S. Thayumanavan, *J. Am. Chem. Soc.* **2012**, *134*, 6964-6967.
[36] J.-H. Ryu, R. T. Chacko, S. Jiwpanich, S. Bickerton, R. P. Babu, S. Thayumanavan, *J. Am. Chem. Soc.* **2010**, *132*, 17227-17235.
[37] I. Kurtulus, G. Yilmaz, M. Ucuncu, M. Emrullahoglu, C. R. Becer, V. Bulmus, *Polym. Chem.* **2014**, *5*, 1593-1604.
[38] R. R. Arvizo, O. R. Miranda, M. A. Thompson, C. M. Pabelick, R. Bhattacharya, J. D. Robertson, V. M. Rotello, Y. S. Prakash, P. Mukherjee, *Nano Lett.* **2010**, *10*, 2543-2548.
[39] Y. Lee, K. Miyata, M. Oba, T. Ishii, S. Fukushima, M. Han, H. Koyama, N. Nishiyama, K. Kataoka, *Angew. Chem. Int. Ed.* **2008**, *47*, 5163-5166.
[40] E. C. Cho, J. Xie, P. A. Wurm, Y. Xia, *Nano Lett.* **2009**, *9*, 1080-1084.
[41] S. Chen, L. Rong, Q. Lei, P.-X. Cao, S.-Y. Qin, D.-W. Zheng, H.-Z. Jia, J.-Y. Zhu, S.-X. Cheng, R.-X. Zhuo, X.-Z. Zhang, *Biomaterials* **2016**, *77*, 149-163.
[42] J.-Z. Du, T.-M. Sun, W.-J. Song, J. Wu, J. Wang, *Angew. Chem. Int. Ed.* **2010**, *49*, 3621-3626.
[43] T. Manouras, M. Vamvakaki, *Polym. Chem.* **2017**, *8*, 74-96.
[44] L. Huang, C. Yu, T. Huang, S. Xu, Y. Bai, Y. Zhou, *Nanoscale* **2016**, *8*, 4922-4926.
[45] Y. Li, R. Tong, H. Xia, H. Zhang, J. Xuan, *Chem. Commun.* **2010**, *46*, 7739-7741.
[46] R. Salva, J.-F. Le Meins, O. Sandre, A. Brûlet, M. Schmutz, P. Guenoun, S. Lecommandoux, *ACS Nano* **2013**, *7*, 9298-9311.
[47] B. M. Discher, Y.-Y. Won, D. S. Ege, J. C.-M. Lee, F. S. Bates, D. E. Discher, D. A. Hammer, *Science* **1999**, *284*, 1143-1146.
[48] X. Li, I. V. Pivkin, H. Liang, G. E. Karniadakis, *Macromolecules* **2009**, *42*, 3195-3200.
[49] A. H. Alidedeoglu, A. W. York, C. L. McCormick, S. E. Morgan, *J. Polym. Sci., Part A: Polym. Chem.* **2009**, *47*, 5405-5415.
[50] A. Housni, H. Cai, S. Liu, S. H. Pun, R. Narain, *Langmuir* **2007**, *23*, 5056-5061.
[51] H. Willcock, R. K. O'Reilly, *Polym. Chem.* **2010**, *1*, 149-157.

[52] A. Vollrath, A. Schallon, C. Pietsch, S. Schubert, T. Nomoto, Y. Matsumoto, K. Kataoka, U. S. Schubert, *Soft Matter* **2013**, *9*, 99-108.
[53] A. Shalviri, H. K. Chan, G. Raval, M. J. Abdekhodaie, Q. Liu, H. Heerklotz, X. Y. Wu, *Colloids Surf., B* **2013**, *101*, 405-413.
[54] D. S. Kohane, D. G. Anderson, C. Yu, R. Langer, *Pharm. Res.* **2003**, *20*, 1533-1538.
[55] N. M. Schaeublin, L. K. Braydich-Stolle, A. M. Schrand, J. M. Miller, J. Hutchison, J. J. Schlager, S. M. Hussain, *Nanoscale* **2011**, *3*, 410-420.
[56] L. He, E. S. Read, S. P. Armes, D. J. Adams, *Macromolecules* **2007**, *40*, 4429-4438.
[57] S. F. El-Mashtoly, H. K. Yosef, D. Petersen, L. Mavarani, A. Maghnouj, S. Hahn, C. Kötting, K. Gerwert, *Anal. Chem.* **2015**, *87*, 7297-7304.
[58] M. Hedegaard, C. Matthäus, S. Hassing, C. Krafft, M. Diem, J. Popp, *Theor. Chem. Acc.* **2011**, *130*, 1249-1260.
[59] C. Matthäus, T. Chernenko, J. A. Newmark, C. M. Warner, M. Diem, *Biophys. J.* **2007**, *93*, 668-673.
[60] C. Matthäus, S. Schubert, M. Schmitt, C. Krafft, B. Dietzek, U. S. Schubert, J. Popp, *ChemPhysChem* **2013**, *14*, 155-161.
[61] K. Galler, R. P. Requardt, U. Glaser, R. Markwart, T. Bocklitz, M. Bauer, J. Popp, U. Neugebauer, *Sci. Rep.* **2016**, *6*, 24155.
[62] R. Álvarez, B. Vaz, H. Gronemeyer, Á. R. de Lera, *Chem. Rev.* **2014**, *114*, 1-125.
[63] R. Kawaguchi, J. Yu, J. Honda, J. Hu, J. Whitelegge, P. Ping, P. Wiita, D. Bok, H. Sun, *Science* **2007**, *315*, 820-825.
[64] W. S. Blaner, S. M. O'Byrne, N. Wongsiriroj, J. Kluwe, D. M. D'Ambrosio, H. Jiang, R. F. Schwabe, E. M. C. Hillman, R. Piantedosi, J. Libien, *Biochim. Biophys. Acta* **2009**, *1791*, 467-473.
[65] M. Dietrich, M. Glassner, T. Gruendling, C. Schmid, J. Falkenhagen, C. Barner-Kowollik, *Polym. Chem.* **2010**, *1*, 634-644.
[66] Z. Jia, L. Wong, T. P. Davis, V. Bulmus, *Biomacromolecules* **2008**, *9*, 3106-3113.
[67] J.-H. Ryu, S. Bickerton, J. Zhuang, S. Thayumanavan, *Biomacromolecules* **2012**, *13*, 1515-1522.
[68] L. Li, K. Raghupathi, C. Song, P. Prasad, S. Thayumanavan, *Chem. Commun.* **2014**, *50*, 13417-13432.
[69] A. Reisch, A. Runser, Y. Arntz, Y. Mély, A. S. Klymchenko, *ACS Nano* **2015**, *9*, 5104-5116.
[70] J. Xuan, M. Pelletier, H. Xia, Y. Zhao, *Macromol. Chem. Phys.* **2011**, *212*, 498-506.
[71] J. Wang, M. Pelletier, H. Zhang, H. Xia, Y. Zhao, *Langmuir* **2009**, *25*, 13201-13205.
[72] J. J. Haven, C. Guerrero-Sanchez, D. J. Keddie, G. Moad, S. H. Thang, U. S. Schubert, *Polym. Chem.* **2014**, *5*, 5236-5246.
[73] C. Guerrero-Sanchez, L. O'Brien, C. Brackley, D. J. Keddie, S. Saubern, J. Chiefari, *Polym. Chem.* **2013**, *4*, 1857-1862.
[74] N. J. W. Penfold, J. R. Lovett, N. J. Warren, P. Verstraete, J. Smets, S. P. Armes, *Polym. Chem.* **2016**, *7*, 79-88.

[75] J. R. Lovett, N. J. Warren, L. P. D. Ratcliffe, M. K. Kocik, S. P. Armes, *Angew. Chem. Int. Ed.* **2015**, *54*, 1279-1283.
[76] J.-H. Ryu, R. Roy, J. Ventura, S. Thayumanavan, *Langmuir* **2010**, *26*, 7086-7092.
[77] Y. Mai, A. Eisenberg, *Chem. Soc. Rev.* **2012**, *41*, 5969-5985.
[78] D. E. Discher, A. Eisenberg, *Science* **2002**, *297*, 967-973.
[79] J. Du, R. K. O'Reilly, *Soft Matter* **2009**, *5*, 3544-3561.
[80] A. Choucair, P. Lim Soo, A. Eisenberg, *Langmuir* **2005**, *21*, 9308-9313.
[81] F. Meng, Z. Zhong, J. Feijen, *Biomacromolecules* **2009**, *10*, 197-209.
[82] H. Yuan, C. Huang, S. Zhang, *Soft Matter* **2010**, *6*, 4571-4579.
[83] K. E. B. Doncom, C. F. Hansell, P. Theato, R. K. O'Reilly, *Polym. Chem.* **2012**, *3*, 3007-3015.
[84] C. Maiti, R. Banerjee, S. Maiti, D. Dhara, *Langmuir* **2015**, *31*, 32-41.
[85] J. R. Lovett, N. J. Warren, S. P. Armes, M. J. Smallridge, R. B. Cracknell, *Macromolecules* **2016**, *49*, 1016-1025.
[86] J. Cai, Y. Yue, D. Rui, Y. Zhang, S. Liu, C. Wu, *Macromolecules* **2011**, *44*, 2050-2057.
[87] Z. H. Wang, W. B. Li, J. Ma, G. P. Tang, W. T. Yang, F. J. Xu, *Macromolecules* **2011**, *44*, 230-239.
[88] Y. Chen, K. Ai, Y. Liu, L. Lu, *ACS Appl. Mater. Interfaces* **2014**, *6*, 655-663.
[89] X. Hu, X. Guan, J. Li, Q. Pei, M. Liu, Z. Xie, X. Jing, *Chem. Commun.* **2014**, *50*, 9188-9191.
[90] H. Deng, X. Zhao, J. Liu, L. Deng, J. Zhang, J. Liu, A. Dong, *J. Mater. Chem. B* **2015**, *3*, 9397-9408.

List of abbreviations

ACVA	4,4′-Azobis(4-cyanovaleric acid)
AEMA	2-Aminoethyl methacrylate
AEMA·HCI	2-Aminoethyl methacrylate hydrochloride
AIBN	2,2′-Azobis(2-methylpropionitrile)
ATRP	Atom transfer radical polymerization
BocAEAEMA	2-((*tert*-Butoxycarbonyl)(2-((tert-butoxycarbonyl)amino)ethyl)amino)-ethyl methacrylate
CAC	Critical aggregation concentration
CDP	4-Cyano-4-((dodecylsulfanylthiocarbonyl)sulfanyl)pentanol
CLSM	Confocal laser scanning microscopy
CPADB	4-Cyano-4-(phenylcarbonothioylthio) pentanoic acid
cryo-TEM	Cryo-transmission electron microscopy
CTA	Chain transfer agent
Đ	Dispersity
DCC	*N*,*N*'-Dicyclohexylcarbodiimide
DLS	Dynamic light scattering
DMAc	*N*,*N*-Dimethylacetamide
DMAEMA	2-(Dimethylamino)ethyl methacrylate
DMF	Dimethylformamide
DOX	Doxorubicin hydrochloride
DP	Degree of polymerization
DSC	Differential scanning calorimetry
GSH	Glutathione
HSC	Hepatic stellate cells
IEP	Isoelectric point
LSECs	Liver sinusoidal endothelia cells
MMA	Methyl methacrylate
M_n	Number average molar mass
NHS	*N*-Hydroxysuccinimide
NMP	Nitroxide mediated polymerization
NMR	Nuclear magnetic resonance
NP	Nanoparticle
PDI	Polydispersity index
PDSM	Pyridyldisulfide ethylmethacrylate
PLGA	Poly(lactide-*co*-glycolide)
PMA	Poly(methyl acrylate)
PMMA	Poly(methyl methacrylate)
RA	Retinoic acid
RAFT	Reversible addition fragmentation chain transfer
RDRP	Reversible deactivation radical polymerization
SEC	Size exclusion chromatography
SEM	Scanning electron microscopy
*t*BAEMA	2-(*tert*-Butylamino)ethyl methacrylate
T_c	Crystallization temperature
T_g	Glass transition temperature
THP-HEMA	2-((Tetrahydro-2H-pyran-2-yl)oxy)ethyl methacrylate

Curriculum vitae

01/01/1984	Born in Sariz, Turkey
2004-2010	Bogazici University, Istanbul, Turkey **Scientific degree**: Bachelor of Science
2010-2012	Bogazici University, Istanbul, Turkey **Scientific degree**: Master of Science **Topic**: "Synthesis of branched alkyl substituted phenylene derivatives as potential drug molecules active against prostate cancer" (Assoc. Prof. A. E. Acar)
2013-present	PhD student at the Institute of Organic Chemistry und Macromolecular Chemistry, Friedrich Schiller University Jena, Germany **Topic**: "Stimuli responsive polymeric nanoparticles for biomedical applications" (Prof. U. S. Schubert)

Jena, den 29.06.2017 _____

Publication list

Peer-reviewed publications:

1. **T. Yildirim**, A. C. Rinkenauer, C. Weber, A. Traeger, S. Schubert, U. S. Schubert, "RAFT made methacrylate copolymers for reversible pH-responsive nanoparticles", *J. Polym. Sci., Part A: Polym. Chem.* **2015**, *53*, 2711-2721.
2. **T. Yildirim**, A. Traeger, E. Preussger, S. Stumpf, C. Fritzsche, S. Hoeppener, S. Schubert, U. S. Schubert, "Dual responsive nanoparticles from a RAFT copolymer library for the controlled delivery of doxorubicin", *Macromolecules* **2016**, *49*, 3856-3868.
3. M. Sahn, **T. Yildirim**, M. Dirauf, C. Weber, P. Sungur, S. Hoeppener, U. S. Schubert, "LCST behavior of symmetrical PNiPAm-*b*-PEtOx-*b*-PNiPAm triblock copolymers", *Macromolecules* **2016**, *49*, 7257-7267.
4. I. Yildirim, T. Bus, M. Sahn, **T. Yildirim**, D. Kalden, S. Hoeppener, A. Traeger, M. Westerhausen, C. Weber, U. S. Schubert, "Fluorescent amphiphilic heterografted comb polymers comprising biocompatible PLA and PEtOx side chains", *Polym. Chem.* **2016**, *7*, 6064-6074.
5. **T. Yildirim**, I. Yildirim, R. Yanez-Macias, S. Stumpf, C. Fritzsche, S. Hoeppener, C. Guerrero-Sanchez, S. Schubert, U. S. Schubert, "Dual pH and ultrasound responsive nanoparticles with pH triggered surface charge-conversional properties", *Polym. Chem.* **2017**, *8*, 1328-1340.
6. C. Englert, J. C. Brendel, T. Majdanski, **T. Yildirim**, S. Schubert, M. Gottschaldt, N. Windhab, U. S. Schubert, "Pharmapolymers in the 21st century: synthetic polymers in drug delivery applications", submitted.
7. **T. Yildirim**,[#] C. Matthäus,[#] A. T. Press, S. Schubert, M. Bauer, J. Popp, U. S. Schubert, "Uptake of retinoic acid-modified PMMA nanoparticles in LX2 and liver tissue by

Raman imaging and intravital microscopy", *Macromol. Biosci.* **2017**, *DOI: 10.1002/mabi.201700064*. # Authors contributed equally.

8. **T. Yildirim**, A. Traeger, P. Sungur, S. Hoeppener, C. Fritzsche, I. Yildirim, D. Pretzel, S. Schubert, U. S. Schubert, "Polymersomes with endosomal pH induced vesicle-to-micelle morphology transition and a potential application for controlled doxorubicin delivery", submitted.

9. R. Yanez-Macias, I. Kulai, J. Ulbrich, **T. Yildirim**, P. Sungur, S. Hoeppener, R. Guerrero-Santos, U. S. Schubert, M. Destarac, C. Guerrero-Sanchez, S. Harrisson, "Thermosensitive spontaneous gradient copolymers with block and gradient-like features", *Polym. Chem.* **2017**, *DOI: 10.1039/C7PY00495H*.

10. I. Yildirim,[#] **T. Yildirim**,[#] D. Kalden, G. Festag, N. Fritz, C. Weber, S. Schubert, M. Westerhausen, U. S. Schubert, "Retinol initiated poly(lactide)s: Synthesis, nanoparticle formulation and stability investigation", *Polym. Chem.* **2017**, *DOI: 10.1039/C7PY00881C*. # Authors contributed equally.

Oral presentation:

1. **T. Yildirim**, U. S. Schubert, "Cationic nanoparticles from copolymers of MMA with amine-containing comonomers obtained *via* RAFT copolymerization." 3rd International Symposium on Controlled/Living Polymerization, May 1-4, 2014 Antalya, Turkey.

Poster presentations:

1. **T. Yildirim**, A. C. Rinkenauer, C. Weber, A. Traeger, S. Schubert, U. S. Schubert, "Reversible pH-responsive nanoparticles from a RAFT made copolymer library." EPF, June 21-26, 2015, Dresden, Germany.
2. **T. Yildirim**, S. Schubert, U. S. Schubert, "Dual responsive nanoparticles from a RAFT copolymer library for the controlled delivery of doxorubicin." KAUST Research Conference: Polymers – Designing Macromolecules for Applications, February 5-7, 2017, Thuwal, Kingdom of Saudi Arabia.

Acknowledgements

First of all, I would like to thank **Prof. Schubert** for giving me the opportunity to work in his group. It was a great pleasure to work in his well-equipped labs. I also want to thank him for his guidance and support.

Secondly, I want to thank **Dr. Stephanie Schubert** for her continuous support and supervision over the years. I also appreciate all the fruitful discussions.

Furthermore, I would like to express my gratitude to all the coworkers within or outside the Schubert group who cooperated with me over the years. I want to thank **Dr. Christine Weber** for introducing me to RAFT polymerization. I want to thank **Dr. Anja Traeger** for all the bio-experiments and lots of discussions as well as **Dr. Alexandra Rinkenauer**, **Carolin Fritzsche, Elisabeth Preussger** and **Dr. David Pretzel** for all the bio-assays. Also special thanks to **Dr. Stephanie Höppener, Steffi Stumpf** and **Pelin Sungur** for lots of TEM/SEM measurements. I gratefully acknowledge **Dr. Christian Matthaeus** for Raman imaging and **Dr. Adrian T. Press** for intravital microscopy studies. Special thanks to **Dr. Carlos Guerrero Sanchez** and **Roberto Yañez-Macias** for helping out on the use of robots. Thanks a lot **Martin Sahn** for the supply of oxazoline based macromonomer and **Michael Pröhl** for the supply of functional sugars. I would like to thank **Dr. Grit Festag** for SEC, **Dr. Wolfgang Günther** and **Gabriele Sentis** for NMR, **Nicole Fritz** for MS measurements. I thank **Dr. Uwe Köhn** for ordering**, Sandra Köhn** for supplying lab equipment. I also want to acknowledge **Dr. Jürgen Vitz** and **Renzo Paulus** for introduction to the instruments as well as for the software.

I thank to **Meike Leiske**, **Anne-Kristin Trützschler**, **Dr. Mathias Hartlieb**, **Martin Reifarth**, **Peng Wei** and **Daniel Schnoor** for their contribution to a nice working lab atmosphere. I thank **Dr. Johannes C. Brendel** and **Dr. Michael Gottschaldt** for all the useful discussions.

I thank to **Sylvia Braunsdorf** and **Franca Frister** for always being nice to me as well as for all the help with the paper work.

I especially thank my office friends for all the fun we have had; **Dr. Justyna Czaplewska** (thanks for the delicious food and nice conversations), **Tobias Majdanski** (thanks for nice soccer games and delicious food, I wish you and **Irmela** the best), **Christoph Englert** (thanks for the amazing bubble soccer game and for the help with university related paper work), **Susanne**

Seupel (a lot of thanks for your great help for transporting my mattress from Dresden to Jena (with **Oli**) as well as for helping with all the German official stuff), **Michael Pröhl** (thanks for the organization of a nice contest ☺).

I also want to thank my family: my brother **Turgut** for his support and his wife **Tugce** for bringing **Kerem** into the world as a gift to our family ☺, my brother **Kenan** for his continuous support, my parents and my mother-in law for supporting me throughout my PhD period.

At the end, I would like to thank my beloved wife (and colleague ☺) **Ilknur**. Without her support, patience and encouragement, this thesis would not have been possible.

Declaration of authorship / Selbständigkeitserklärung

Ich erkläre, dass ich die vorliegende Arbeit selbständig und unter Verwendung der angegebenen Hilfsmittel, persönlichen Mitteilungen und Quellen angefertigt habe.

I certify that the work presented here is, to the best of my knowledge and belief, original and the result of my own investigations, except as acknowledged, and has not been submitted, either in part or whole, for a degree at this or any other university.

Jena, den 29.06.2017 _____

Publications P1 to P6

P1: Reprinted by permission of C. Englert, J. C. Brendel, T. Majdanski, T. Yildirim, S. Schubert, M. Gottschaldt, N. Windhab, and U. S. Schubert.

P2: Reprinted by permission of Wiley VCH.

P3: Reprinted by permission of T. Yildirim, C. Matthaeus, A. T. Press, S. Schubert, M. Bauer, J. Popp, and U. S. Schubert.

P4: Reprinted by permission of the American Chemical Society. Copyright 2017

P5: Reprinted by permission of Royal Society of Chemistry.

P6: Reprinted by permission of T. Yildirim, A. Traeger, P. Sungur, S. Hoeppener, C. Fritzsche, I. Yildirim, D. Pretzel, S. Schubert, and U. S. Schubert.

Publication P1

"Pharmapolymers in the 21st century: Synthetic polymers in drug delivery applications"

C. Englert, J. C. Brendel, T. Majdanski, T. Yildirim, S. Schubert, M. Gottschaldt, N. Windhab, U. S. Schubert

Manuscript, submitted.

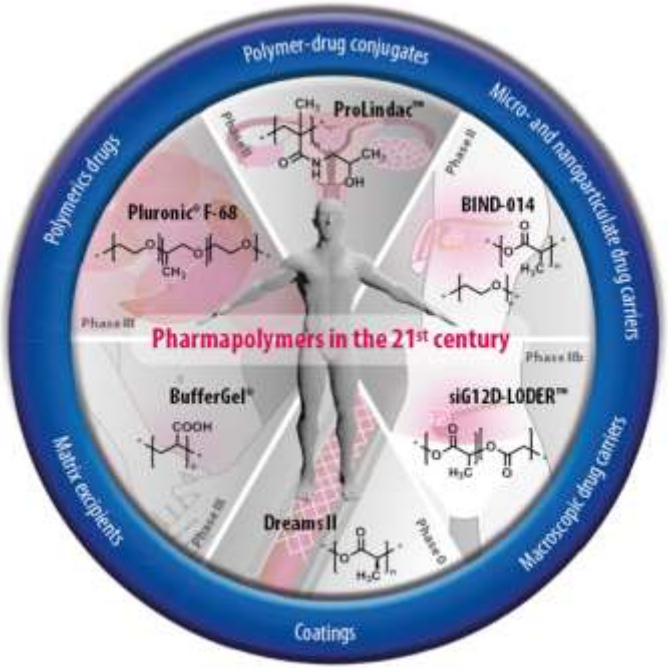

Pharmapolymers in the 21st Century:

Synthetic Polymers in Drug Delivery Applications

Christoph Englert,[a,b] Johannes C. Brendel,[a,b] Tobias C. Majdanski,[a,b] Turgay Yildirim,[a,b] Stephanie Schubert,[b,c] Michael Gottschaldt,[a,b] Norbert Windhab,[d] Ulrich S. Schubert[a,b,]*

[a] Laboratory of Organic and Macromolecular Chemistry (IOMC), Friedrich Schiller University Jena, Humboldtstrasse 10, 07743 Jena, Germany

[b] Jena Center for Soft Matter (JCSM), Friedrich Schiller University Jena, Philosophenweg 7, 07743 Jena, Germany

[c] Department of Pharmaceutical Technology, Friedrich Schiller University Jena, Otto-Schott-Strasse 41, 07747 Jena, Germany

[d] Evonik Nutrition and Care GmbH, Kirschenallee, Darmstadt 64293, Germany

Email: ulrich.schubert@uni-jena.de

Graphical abstract

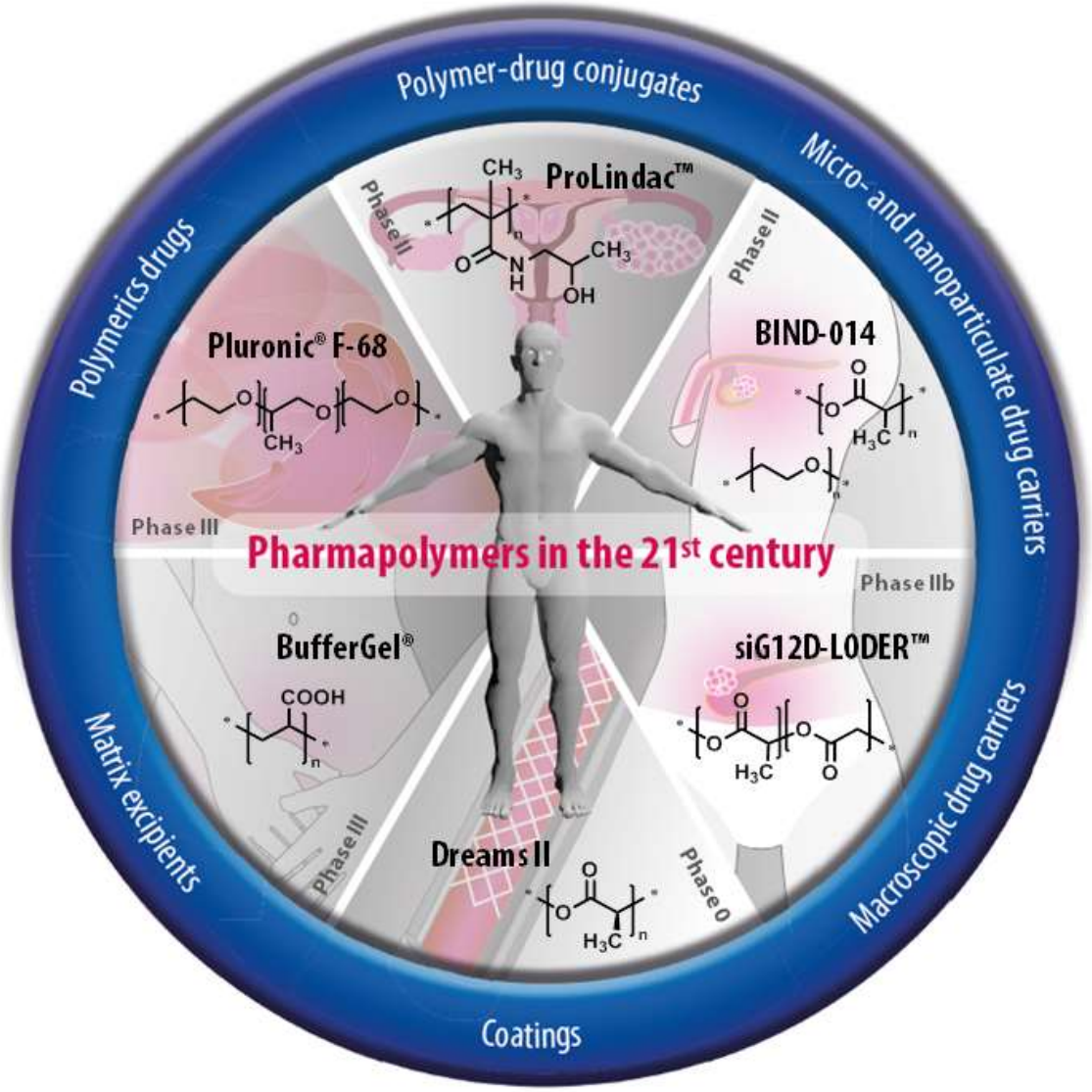

Abstract

The administration of drugs, as a main challenge of pharmaceutical and medicinal applications, has certainly benefited from the application of synthetic polymers. However, despite an enormous effort to develop new materials for drug delivery applications, only few of them have entered the market due to the hurdles of regulation, production, cost efficiency and both industrial's and patients' acceptance. In this review, we summarize all these classes of synthetic polymers, which are on the market as well as the latest developments in clinical trials, and describe their application in polymer-drug conjugates, as excipients, in nano-/microscopic and macroscopic drug carriers, as polymeric coatings, or as polymeric drugs. Our intention is to create a link between the underlying chemical structures, the properties of the polymers, and their area of application, where they are often just known by their trade names or abbreviations. In addition selected types of synthetic polymers are highlighted that feature interesting properties and have the potential to make it to the market in future.

FROM THE CONTENTS

1. Introduction

The administration of drugs is one of the main tasks within the area of pharmaceutical and medicinal applications. Drugs are defined as "articles intended for use in the diagnosis, cure, mitigation, treatment, or prevention of disease" and "articles (other than food) intended to affect the structure or any function of the body of man or other animals" by the Federal Food, Drug, and Cosmetic Act (FD&C Act). Starting in the early 1960s, controlled drug delivery research has broadened and has developed from macroscopic devices and implants (1970s and 1980s) to microscopic (1980s and 1990s) as well as nanoscopic systems.[1] Besides liposomes, nanocrystals, bio-compatible metal-organic frameworks and others, polymeric materials represent a useful option to fulfill the challenges of drug storage and delivery. They can be subdivided into natural, pseudo-synthetic and synthetic macromolecules. The latter offer several advantages compared to natural polymers like an easier synthesis of large quantities, nonsignificant batch-to-batch variations and countless possibilities for modifications to achieve the desired properties. These factors turn polymers into very promising candidates to solve numerous problems in drug administration.

In this review, we introduce the term 'Pharmapolymers', which describes synthetic polymers used during the administration of drugs. They are based on an artificially made polymeric backbone, excluding chemically modified natural polymer species plus dendrimers, which do not reveal a distribution in the number of repeating units per molecule (molar mass distribution). The first part comprises an overview of potential polymer classes, which are discussed concerning their suitability (structure, properties etc.) as potential drug delivery systems. This represents the basis for the following parts of the work. To be considered as drug delivery system, the polymer structure has to fulfill at least parts of the following requirements: Biocompatibility, biodegradability or complete chemical inertness as well as sufficient control over its synthetic structure. In 1999, Uhrich *et al.* already reviewed polymeric systems for controlled drug delivery.[2] Almost two decades later, this work misses completeness and the modern developments of the polymer classes applied nowadays. The second part summarizes all pharmapolymers which are currently or have previously been on the market subdivided according to their form of appearance. In addition, we included materials which are currently undergoing clinical trials. The main routes of drug administration discussed here are oral, topical and by injection (intravenous, intramuscular, subcutaneous). The third section highlights recent progress in research and exemplarily describes a few chosen *in vivo* studies to emphasize future prospects of pharmapolymers in drug delivery applications. On average, only one out of 5,000 compounds that enters pre-clinical studies (and only one out of 10 that enters clinical studies) becomes an approved drug after 10 years from the starting idea to the market approval.[2] The clinical phases necessary for market approval and a short description are listed in Table 1.

The present study is the most comprehensive summary of established synthetic polymers in drug administration so far, comprising far more than 100 polymeric products on the market and 70 under clinical investigations. Our intent is to provide a link between chemical structures as well as properties of the polymers and their area of application, where they are often just known by their trade names or abbreviations. Even so, the authors apologize in advance for all omissions since it is nearly impossible to keep track of the whole wealth of materials applied in drug delivery.

Table 1. Overview of clinical trial phases.

Phase	Primary goal	Secondary goal	Participants	Duration	Special Features
Preclinical	Checking for preliminary safety, efficacy and pharmacokinetic information (*in vitro* & *in vivo*)		-	Several years	
Phase 0	Pharmacokinetics (*i.e.* oral bioavailability and half-life of the drug)		10		Often skipped for phase I, subtherapeutic, doses too low to cause any therapeutic effect
Phase I	Checking for safety	Establish the max. tolerated dose, determine side effects, determine the metabolism and pharmacologic actions of drugs	20 to 100	Several months	Often first time tested in humans, subtherapeutic with ascending doses
Phase II	Checking for efficacy	Determine the common short-term side effects and risks	Several hundred	Up to 2 years	Therapeutic doses, "Proof of concept"
Phase III	Confirm findings in large patient population	Evaluate the overall risk-benefit ratio	300 to 3,000	1 to 4 years	Usually randomized controlled trials, pivotal studies for drug licensing
Phase IV	Testing long-term safety in diverse patient population	Identify additional, unusual side effects	"Real-life patients", several thousands	*Ongoing*	

2. Polymer classes

The Food and Drug Administration (FDA) is a federal agency of the United States Department of Health and Human Services, which is responsible for the monitoring of trading and safety standards in the food and drug industries in the United States. A large number of different polymer types are used in pharmaceutical research and applications nowadays, whether in an early scientific stage or already in FDA approved formulations. To fulfill specific requirements, often different polymer classes have to be combined to create smart solutions for specific problems. The following chapter discusses the most important polymer classes including individual representatives of pharmapolymers. All structures of homopolymer systems mentioned later in the application Chapter 3 or the future prospects Chapter 4 are marked in bold and can be found in Table 2.

2.1 Polyethers

The term polyether generally describes polymers that contain the ether functional group in their main chain. Although there are several FDA approved polyethers, they all reveal one major drawback: They lack biodegradability (referring to the degradation of the polymer backbone, independent of the molar mass of the respective polymer species).

Among them, **poly(ethylene glycol) (PEG)** (also poly(ethylene oxide) (PEO) for M_n >20,000 g mol^{-1}) represents probably the most well-known polyether in pharmaceutical applications. The oldest[3] and most frequently used method to synthesize PEG in laboratory and industrial scale is *via* anionic ring-opening polymerization of ethylene oxide[4] resulting in polymers with a wide range of possible molar masses and very low dispersities.[5] Cationic polymerization is also feasible, with the drawback of broad molar mass distribution due to backbiting reactions.[6] A variety of functionalized PEGs are offered from commercial sources, with different α and/or ω functionalities, *e.g.* methoxy groups, amines, or thiols. Furthermore, side group functionalized PEG derivatives are known in literature, *e.g.* functionalized with furfuryl.[7] PEG has several interesting advantages for pharmaceutical applications. It is water soluble, even at higher molar masses,[8] non-ionic, non-toxic and biocompatible. Furthermore, it was already approved by the FDA for different applications in foods, cosmetics and pharmaceuticals.[9] The success of PEG in the biomedical area started with the covalent decoration of bio(active) molecules,[10] often named PEGylation,[11] which will be described in detail in Chapter 3.1.1. One outstanding property of PEG is the so-called “stealth-effect”, discovered in 1990 for modified liposomes.[12] It describes the ability to protect molecules or nanoscopic objects against unspecific interactions with blood components (*e.g.* opsonization), by attaching specific proteins to the surface.[13] Until now, PEG is still regarded as the gold standard for stealth behavior. Furthermore, renal filtration was found to be decreased by the attachment of PEG which comes along with an increase of the molar masses. These two points lead to significantly elongated *in vivo* blood circulation times of formulations associated with PEG.[13-14] Besides all the advantages of PEG a few drawbacks have to be addressed as well.[15] With increasing molar mass of the polymers, PEG tends to accumulate within certain organs, which has to be avoided.[16] If, however, the applied product contains oligomers below 400 g mol^{-1} or becomes fragmented, toxic species can be produced by oxidation *in vivo*.[17] A second issue concerns the possibility of an immune response due to compliment C activation, which can lead to hypersensitive reactions and, consequently, to an anaphylactic shock.[18] Furthermore – despite the established large scale production – the anionic polymerization technique requires still an high effort, in particular considering the highly toxic and explosive monomer and the purification of the polymer for pharmaceutical applications (formaldehyde and 1,4-dioxane can occur as side products, which need to be excluded from pharmacological grade PEG). Nevertheless, PEG remains the most commonly used polymer in drug administration and can be considered as the standard.

Poly(propylene glycol) (PPG) (also named poly(propylene oxide): PPO) represents another polyether which is applied for drug delivery. The common way to synthesize PPG is anionic ring-opening polymerization with an alcoholate as initiator and a base as catalyst resulting in the atactic product. The change of the catalyst enables the synthesis of the isotactic product. However, like most mono-substituted epoxides, the monomer tends to induce chain transfer reactions during the polymerization limiting the maximum molar mass (M_n) of the resulting polymer to approximately 6,000 g mol^{-1}.[4-5] The water solubility of the polymer is, compared to PEG, reduced considerably, which causes an lower critical solution temperature (LCST) between 15 and 42 °C depending on the molar mass[19] ($LCST_{PEG} \approx 100$ °C),[20] whereas the biocompatibility is even more distinct as for PEG.[21] The polymer appears mostly as a central, non-ionic, hydrophobic, non-toxic segment in PEG-*b*-PPG-*b*-PEG block copolymers named poloxameres, which are also known by their trade names Pluronic®, Synperonic® and Kolliphor® (a subgroup are poloxamines consisting of an ethylene diamine core). The commercial products are available in various compositions. The polymerization of the block copolymer is similar to the PPG homopolymer synthesis. After the homopolymer is formed, ethylene oxide is added to the reaction, which then grows from both sides of the PPG homopolymer. The resulting products often contain admixtures, *e.g* homopolymer, di- and triblock polymers, which can be removed by chromatographic fractionation. Poloxameres are increasing the rate of wound and burn healing, which is the reason why they can be found in skin healing creams and skin substitutes. Furthermore, they form micelles in aqueous solution, making them attractive for drug delivery applications.

Poly(glycerol) (PG) represents an alternative for PEG and PPG in terms of solubility- and biological behavior. PG's are produced by anionic[22] or cationic[23] ring-opening polymerization of glycidol leading to branched polymer architectures. Using anionic ring-opening polymerization, high molar mass polymers comprising a relatively narrow distribution (up to 700,000 g mol^{-1} at dispersities of below 1.4) can be synthesized.[24] The main advantage of PG compared to PEG is the presence of hydroxyl groups at the main chain, which can be utilized to introduce additional functionalities to the polymer backbone.[25] If the alcohol group on the monomer is protected, a linear polymerization with molar masses (M_n) up to 30,000 g mol^{-1} can be accomplished.[26] Both, linear and hyperbranched PGs are fully biocompatible,[27] revealing even better profiles compared to PEG.[28] Similar to PEG, modifications with PG lead to an elongated circulation time.[29] A rather well-known example is poly(glycerol) polyricinoleate (PGPR) as food additive being considered by the FDA as general recognized as safe (GRAS) for human consumption (Code of Federal Regulations: 21 CFR 172.854). Several other poly(glycerol) esters are known for their application as emulsifier in food, cosmetics and pharmaceutical preparations.

2.2 Poly(ethylene imine)s

Poly(ethylene imine)s (PEI) are characterized by the presence of amine group functionalities within the polymer backbone, which determine their chemical and physical behavior. PEI reveals one of the highest cationic-charge-densities of all organic macromolecules.[30] Every third atom is an amine group of which every sixth nitrogen atom is protonated under physiological conditions.[30] This high charge density enables the interaction with the phosphate groups of genetic material leading to the formation of toroidal complexes that are readily endocytosed by cells.[31] This feature makes PEI a highly efficient vector for delivering oligonucleotides *in vitro* and *in vivo*.[32] It occurs in two different forms: Linear and branched PEI.

Branched poly(ethylene imine) (BPEI) can be synthesized by the ring-opening polymerization of unsubstituted aziridine as described in 1944 by Jones *et al.* leading to uncontrolled branching and chains with primary, secondary, and tertiary amine groups.[33] Increasing molar masses result in higher degrees of branching and, to this end, cross-linking becomes more likely. The handling of explosive and toxic aziridine requires safety precautions, which are often not applicable in most chemistry laboratories. The molar masses of commercially available BPEI cover the

complete range up to 750,000 g mol^{-1} (M_w), however, no dispersities are reported. The exact determination of the number average molar mass M_n of PEI is extremely complex and has been in the focus of several literature reports.[31a, 34] The synthesis of **linear poly(ethylene imine) (LPEI)** *via* hydrolysis of poly(2-alkyl-2-oxazoline)s was first described in the 1960s.[35] Therefore, linear 2-methyl or 2-ethyl substituted poly(2-oxazoline)s (POx) are mainly used as precursors. The hydrolysis can be performed under acidic[35b, 36] or basic conditions[35b, 37] and results in products hydrolyzed up to 97%. The molar mass of LPEI and its distribution is limited by the respective POx precursor. However, the living character of the cationic polymerization of POx (see Chapter 2.7) produces well-defined polymers with controlled molar masses and low dispersities, which comply with the biological demands for LPEI (M_n up to 25,000 g mol^{-1}, $Đ < 1.2$).[38] LPEI can be purchased in the range from 400 to 250,000 g mol^{-1} (M_w). The robust polymerization protocols tolerate a variety of comonomers, initiators, and quenchers, including allyl and aryl groups enabling the selective introduction of various functionalities to the LPEI backbone.[39] An alternative is the controlled partial hydrolysis of the amide bonds which has been studied in the last decades.[40] A further approach to LPEIs is the controlled polymerization of *N*-substituted aziridines followed by the deprotection of the amines.[37a] However, this route comes along with unwanted side reactions due to the harsh conditions or incomplete cleavage.[41] None of the products based on PEI have been approved by the FDA so far, which is mainly related to its cytotoxicity.

2.3 Polyesters

Polyester describe a class of polymers containing the ester functional group in their main chain which renders most of these polymers biodegradable.

One of the earliest polymers was **poly(caprolactone) (PCL)** synthesized by the Carothers team in the 1930's. PCL is a non-toxic, biodegradable, semi-crystalline aliphatic polyester, which is approved by the FDA for several applications, *e.g.* drug delivery systems, sutures, long-term implants and adhesion barriers as well as new tissue scaffold host systems. It is hydrophobic, but soluble in several solvents, can be blended with a variety of other materials and degrades very slowly under physiological conditions (from months to years) compared to other polyesters.[42] The main reason for the extended degradation time is the lack of enzymes suitable to hydrolyze the ester in the human body.[43] Furthermore, the hydrolysis time of PCL depends on the physical and chemical properties of the polymer, in particular the crystallinity and the molar mass. However, this degradation profile makes PCL very attractive for long term drug delivery devices or implants.[44] PCL degrades into 6-hydroxyhexanoic acid, which is less acidic than degradation products from other polyesters reducing the effect of autocatalysis occurring with the hydrolysis of polyesters. Besides the degradability, PCL exhibits a high permeability for most drug molecules. Furthermore, functional groups can be introduced for example by copolymerization, which enables an adjustment of several properties, including hydrophilicity, adhesivity and biocompatibility.[45] PCL can be synthesized in several ways, such as by anionic, cationic, coordination or free radical ring-opening polymerization (ROP) processes first described by Carothers for PLA. The most common synthesis routes comprise the ring-opening polymerization using metal catalysts which have to be removed afterwards and the often used polycondensation. A well-known catalyst for ROP is stannous octoate due to its high efficiency and its approval by the FDA as food additive.[46] The reported molar masses (M_n) range from 530 to 630,000 g mol^{-1}.[47] Numerous strategies to improve the degradation and mechanical properties of PCL, such as copolymerization and blending with different polymers, are described in literature.[42a, 44e, 48] The exceptional compatibility of PCL in blends is utilized to improve the material properties by mixing PCL with polysaccharides, PLA, chitosan and many more.[48-49]

Poly(lactic acid) (PLA) and **poly(glycolic acid) (PGA)** are aliphatic polyesters approved by the FDA for a wide range of applications. These materials are well-established in pharmaceutical industry as drug carriers and traditionally

applied as suture material.[50] Major advantages are their biocompatibility, biodegradability and their mechanical strength.[51] The degradation products are further non-toxic and can be cleared or consumed within bioprocesses occurring in the body, which makes them a powerful tool for *in vivo* delivery. Similar to PCL, the material properties such as degradation rate and mechanical strength depend on the structural features of the polymer including crystallinity and chain length.[52] High molar mass species are obtained by ROP[53] using stannous octoate as catalyst.[50b, 51a] Additional metal-free methods including enzymatic techniques are under investigation for the polycondensation of PLA.[52b, 54] PLA represents a stiff and hard polymer revealing versatile properties depending on the tacticity and molar mass. Compared to PGA it comprises an extra methyl group, and, therefore, a stereocenter, which results in three possible products: Poly(L-lactic acid) (PLLA), poly(D-lactic acid) (PDLA) and the mixture of both, poly(D-lactic acid-*co*-L-lactic acid) (PDLLA). PLLA and PDLA are semi-crystalline, while PDLLA is amorphous and, consequently, reveals the fastest degradation rate.[50c, 52b] Nevertheless, the hydrophobic methyl side group increases the steric hindrance and shields the ester bond from hydrolysis by water which results in a decreased degradation time compared to PGA. In consequence, PLA is a promising material for long term applications.[55] PGA has been known since 1954 as potential low cost fiber forming, highly crystalline polymer.[50b] However, the high sensitivity towards hydrolysis and the poor solubility in organic solvents limits its use for pharmaceutical applications.[47, 51b] The respective copolymer poly(lactic-*co*-glycolic acid) (PLGA) is probably the best established and studied polymer for pharmaceutical applications and tissue engineering.

Poly(oxalate)s (PO) represent another subgroup of polyesters, which is prepared by the ester interchange reaction of diols with the diester of the oxalic acid. In 1980, Shalaby *et al.* filed a patent for the preparation of polyalkylene oxalates from different aliphatic diols.[56] Since that time, POs and copoly(oxalate)s have been reported only a few times in literature. They represent a family of biocompatible and biodegradable polymers, which degrade hydrolytically (and comparatively rapid) into non-toxic products that can easily be removed from the body.[57] Oxalate-based polymers allow a facile control over their biodegradability, crystallinity and mechanical strength. Their hydrolytic stability and their mechanical properties are mainly influenced by the composition and hydrophobicity of the incorporated diol. Compared to the commercial biodegradable polymers PCL or PLGA, they exhibit faster degradation kinetics. This turns POs into useful materials for medical grade plastics and devices (*e.g.* syringes and scrub brushes).[58] Garcia and Miller established the oxalate metathesis polymerization using diols from renewable sources and without the need of any solvents. They obtained POs with molar masses (M_n) ranging from 40,000 to 70,000 g mol^{-1}.[58] Despite its biocompatibility and degradability none of the polymers in this class is yet approved by the FDA.

Poly(butylene terephthalate) (PBT) is obtained by the ester interchange reaction of 1,4-butanediol and terephthalic acid and subsequent polycondensation. Its resistance to solvents, heat and mechanical strongness turns PBT into a basic module in many electronic devices and home appliances. Considering biomedical application PBT has not gained much attention, yet.

2.4 Polycarbonates

Polycarbonates (PC) are a group of thermoplastic polymers containing carbonate links in their backbone, firstly discovered in 1898 by Alfred Einhorn.[59] After 50 years without commercialization, Schnell (Bayer AG, Germany) patented the synthesis of linear PCs in 1953.[60] In the same year, Fox (General Electric Company, USA) synthesized independently a branched PC.[61] Since the late 50's, PCs became frequently used in commercial applications. The excellent biocompatibility, non-toxic degradation products and the absence of autocatalytic degradation processes render aliphatic PCs interesting polymeric materials.[62] The polymers are commonly synthesized by polycondensation methods (step growth), as performed by the phosgenation of hydroxyl compounds or the

transesterification of diols with lower dialkyl carbonates.[63] Another approach is the utilization of CO_2 and oxiranes to produce "green" PCs (up to 100,000 g mol^{-1}, Đ < 1.2) *via* an addition polymerization,[64] whereas the low reactivity of CO_2 requires very efficient catalysts.[65] However, these polymerization techniques suffer from drawbacks such as the poor control over molecular parameters and broad molar mass distributions.[66] A suitable preparation method to obtain well-defined PC is the ring-opening polymerization (ROP) of cyclic carbonates (chain growth, "living"), which can be performed by both cationic and anionic polymerization. The ROP allows the control of molar masses (M_n) with low dispersities (30,000 g mol^{-1}, Đ < 1.1[67]) at fast polymerization rates and facilitates the formation of more complex architectures like block polymers[68] and star shaped polymers.[69] Furthermore, in contrast to polycondensation, no by-products are obtained from the polymerization. Compared to aliphatic polyesters (*i.e.* PCL or the copolymer PLGA), polycarbonates are degraded *in vivo* by surface erosion.[70] Their degradation does not cause an acidic environment, which may occur during polyester degradation and might be hazardous for loaded drugs or healthy tissues. PC resins are solely FDA approved for use as articles or components of articles intended for use in producing, manufacturing, packing, processing, preparing, treating, packaging, transporting, or holding food in accordance with defined conditions (21 CFR 177.1580). Nowadays, the design of functional cyclic carbonate monomers has gained increasing interest, comprising hydroxyl,[71] carboxyl,[72] amine,[73] alkene[74]/alkyne,[75] halogen,[76] azido[77] and sugar[78] pendant groups.

2.5 Poly(amino acid)s

Synthetic polypeptides are based on the same peptide bonds present in natural proteins and, therefore, exhibit a good biodegradability and excellent biocompatibility. Nevertheless, they are prepared by purely synthetic reaction processes and therefore included in this review.[79] As almost all types of amino acids can be applied for the polymerization, a large variety of different functionalities such as ionic or stimuli responsive side groups are accessible and complex superstructures including micelles and gels can be formed.[80] In 1906, Hermann Leuchs first reported the synthesis and polymerization of α-amino acid *N*-carboxyanhydrides (NCAs).[81] Since this time, NCAs have gained increasing interest for the synthesis of homo- and copolymers as well as cyclic polypeptides. A large number of reviews can be found dealing with the immense variety of synthetic procedures.[82] Nowadays, the most established way to obtain synthetic polypeptides is the ring-opening polymerization (ROP) of NCAs using amine-based initiators. Remarkable reactions have been developed to synthesize polypeptides and polypeptide-based copolymers with controlled molar masses and dispersities as well as complex architectures. Deming and co-workers reached macromolecules with M_n up to 500,000 g mol^{-1} (Đ < 1.2) by applying different transition-metal-based initiators in a living ROP.[83] Conventional amines as initiators allow the synthesis of polypeptides with 100,000 g mol^{-1} and comparable dispersities.[84] Side reactions can further be suppressed using ammonium chloride functionalized macro-initiators[85] or an organosilicon.[86] The functionalization of polypeptides has gained increasing attention in recent years. The introduction of various functional groups or stimuli-sensitive moieties to the side chains of the polypeptides render them particularly appealing for the design and development of multi-functional active biomaterials. The functionalization is mainly achieved by two approaches: I) The one-step ROP of NCA monomers, already containing the desired functional moieties or II) the post-polymerization modification of polypeptides. Reported modifications comprise click chemistry, in particular alkyne-azide cycloadditions and thiol-ene reactions, controlled free-radical polymerizations, aminolysis and transesterifications, which have extensively been reviewed.[82c, 87] The modularity of using unnatural amino acid derivatives as monomers leads to a versatility of polymer structures with molecular and physical properties far from those of proteins. Trifunctional amino acids, such as glutamic acid, lysine and aspartic acid, are often used to achieve structural viability within the respective polymer, in particular **poly(glutamic acid) (PGluA)**,[88] **poly(lysine)**[89] or **poly(aspartic acid)**.[90] The FDA classifies chosen poly(amino acid)s under the GRAS status for different food applications.

2.6 Poly(peptoid)s

In 1982, Farmer and Ariens introduced the term "peptoid" as a peptidomimetic/pseudopeptide that is able to mimic the biological action of peptides while not resembling them structurally.[91] One decade later, Bartlett and co-workers defined them more specifically as oligomers of *N*-substituted glycine (poly(α-peptoids)).[92] Nowadays, most reports of peptoids, *e.g.* those indexed in PubMed, refer to the mentioned *N*-substituted glycines or respective poly(β-/γ-peptoids). In both cases, side chains are attached to the amide nitrogen and make the polymer resistant to protease degradation.[93] **Poly(peptoid)s (PoP)** are particularly interesting due to their convenient synthesis, chemical diversity and biological relevance. They can be synthesized in a sequence defined (stepwise) or statistical (chain growth) manner.[94] They are routinely obtained in a stepwise procedure, particularly the submonomer solid phase synthesis developed by Zuckermann *et al.*,[95] and have been reviewed continuously.[96] This two-step sequence method does not require the protection of the backbone and a variety of primary amines (most of them commercially available) can be incorporated.[97] Monodisperse PoPs of 100 monomer units (M_n = 8,500 g mol^{-1}) have been synthesized by coupling together two submonomer-synthesized 50-mers.[98] The submonomer method represents a relatively inexpensive route compared to the preparation of the corresponding α-peptides.[99] Microwave heating can be used to accelerate the submonomer synthesis and increases the efficiency of coupling sterically hindered and electrostatically deactivated amines.[100] An alternative approach for their synthesis is the (living) ring-opening polymerization of *N*-substituted *N*-carboxyanhydride (NCA) monomers in solution or from solid substrates.[94b, 96b, 101] This chain growth polymerization yields PoPs with degrees of polymerization >100, but with limited sequence control.[102] Their structural similarity compared to peptides, their resistance against protease, the proteolytic stability, the convenient synthesis and their superior biocompatibility make PoPs an interesting class of materials for a variety of applications, *e.g.* as transfection and therapeutic agents,[103] diagnostic agent[104] and lung surfactant mimetic.[105] Optionally, they can be incorporated into polypeptides at specific sites.[106] Luxenhofer and co-workers could recently show the degradation of PoPs v*ia* oxidative degradation under biologically relevant conditions.[107] This polymer class is not yet approved by the FDA.

2.7 Poly(2-oxazoline)s

Concerning biocompatible, hydrophilic polymers, **poly(2-oxazoline)s (POx)** gained increasing attention.[15] This class of polymers was introduced in 1966 by four independent research groups.[35, 108] The polymers are prepared by a cationic ring-opening polymerization (CROP) of 2-substituted oxazolines resulting in repeating amide functionalities at the interface between polymer backbone and side chain. Since 2004, the microwave assisted synthesis is most commonly used to shorten reaction times from days to minutes.[109] As the CROP is not as sensitive as most anionic polymerization methods, the production of POx in a lab scale is comparably convenient, and a large variety of possible functionalization strategies can be applied.[110] Besides the variation of start- and end-groups, the 2-substitution of the monomer can be modulated within the borders of tolerated functionalities in a CROP. The achievable molar mass strongly depends on the used monomer. POx derivatives bearing short side chains (methyl or ethyl) are reported to be biocompatible[111] and even feature a stealth effect similar to PEG (see Chapter 3.1.2),[112] which turns these polymers into highly favorable materials for biomedical applications.[113] By the incorporation of longer side chains, the solubility behavior can be tailored creating systems being thermoresponsive or water insoluble.[114] Just as PEG, POx is not biodegradable. A degradation of the amide group leads to an abstraction of the side group rather than a decomposition of the backbone and, hence, the formation of linear poly(ethylene imine) (see Chapter 2.2). Since 2016, poly(2-ethyl-2-oxazoline) is approved by the FDA as indirect additive used in food contact substances (21 CFR 175.105).

2.8 Poly(*N*-acrylamide)s

Poly(*N*-acrylamide)s describe a polymer class that bear amide functionalities in the side chain. There is a large variety of monomers commercially available, however, the most commonly applied and studied polymers are doubtlessly poly(*N*-(2-hydroxypropyl)methacrylamide) and poly(*N*-isopropylacrylamide). Furthermore, poly(2-acrylamido-2-methylpropane sulfonate) is utilized.

Poly(*N*-(2-hydroxypropyl)methacrylamide) (PHPMA) is a hydrophilic, chemically and hydrolytically stable, biocompatible polymer, often described simply as "HPMA" in literature. Moreover, it mimics living tissue and features a well-established safety profile in the human body. Its hydroxyl group functionalities allow the convenient conjugation of drugs and targeting molecules. However, PHPMA-based polymers are nonbiodegradable, which limits their use for some pharmaceutical applications.[115] Otherwise, they are hydrophilic and known to be non-toxic in the rat, even at higher doses (30 g kg^{-1}).[116] PHPMA can be synthesized by conventional free radical polymerization of *N*-(2-hydroxypropyl) methacrylamide or by several controlled radical polymerization techniques including atom transfer radical polymerization (ATRP) and reversible addition-fragmentation chain transfer (RAFT) polymerization.[117] Other techniques include the post-polymerization modification of poly(pentafluorophenyl methacrylate) (PPFMA), which contains activated ester side chains, by reacting with 1-amino-2-propanol.[118] Compared to the free radical polymerization, controlled radical polymerization techniques provide access to a vast number of macromolecular architectures including PHPMA copolymers with improved control over the molar mass and dispersity.[119] Despite the extensive research effort spent on PHPMA, none of the materials has yet been approved by the FDA.

Poly(*N*-isopropylacrylamide) (PNIPAAm) is one of the most intensively studied temperature responsive polymers of the past four decades.[120] The PNIPAAm homopolymer exhibits a lower critical solution temperature (LCST) of around 33 °C in aqueous solution, which is close to the body temperature.[121] In addition, the LCST of PNIPAAm can be easily tuned by copolymerizing various functional monomers to alter the polymer backbone.[122] When the temperature is lower than the LCST, PNIPAAm is water soluble due to a complex H-bond network along the PNIPAAm chains. In contrast, at temperatures above the LCST PNIPAAm becomes water insoluble because of the destroyed H-bond network and the release of water molecules.[123] Due to this reversible transition in water, its good biocompatibility and low toxicity, PNIPAAm-based polymers are found in numerous biological and biomedical applications including controlled drug release, tissue engineering, bio-detection, bio-separation, smart microfluidic devices and biochips.[123-124] However, PNIPAAm is not biodegradable which limits its use in some pharmaceutical applications.[125] PNIPAAm can be synthesized by a variety of polymerization techniques including conventional free radical polymerization, ATRP, and RAFT polymerization of *N*-isopropylacrylamide.[120a, 126] Although an enormous progress has been made, to the best of our knowledge, there is no FDA approval of PNIPAAm-based materials, nor are there any materials under clinical investigation for drug delivery.

2.9 Polyphosphoesters

Polyphosphoesters are constructed by repeating phosphoester groups $(\text{-POR'-O-R-O-})_n$ in the main chain. They can be subdivided into polyphosphites, polyphosphonates, polyphosphoramidates and polyphosphates.[127]

Among them, **polyphosphates (PP)** (R' = OR^1) represent the most important class of polymers, due to their structural similarity with nucleic and teichoic acids.[128] Inorganic PPs are salts or esters of polymeric oxoanions built on tetrahedral phosphate (PO_4) units and occur as linear or branched forms, or cyclic ring structures. They are commonly synthesized by dehydration of orthophosphate (PO_4^{3-}) at an elevated temperature. Other methods include an olefin metathesis reaction *via* an acyclic diene and the ring-opening metathesis polymerization.[129]

A variety of synthetic methods has been summarized by Wang *et al.*.[130] PP can be found in all bacterial, fungal, plant or animal life forms. PP was first isolated from yeast by Lieberman[131] in 1888 and has been reviewed frequently since the 80's.[132] The numerous and different biological functions and their biocompatibility have made these materials the subject of several research areas investigating the substitution for adenosine triphosphate (ATP) in kinase reactions,[133] chelation of metals,[134] or their role in the physiological regulation of growth, development, stress, and deprivation.[135] PPs allow for numerous opportunities of modifications due to the pentavalent nature of the phosphorus atoms. Examples for such modifications are the introduction of double[136]/triple bonds,[137] hydroxy[138] and amine groups[139] to the side chain or polymer backbone. Since Yan and co-workers reported the synthesis of highly pure hyperbranched polyphosphates (HBPPs) *via* the self-condensing ring-opening polymerization, this method attracted considerable attention.[140] The convenient modification of the side group of the cyclic phosphate monomers resulted in a variety of structures and functionalities.[128] Well-defined PPs with approximately 30,000 g mol^{-1} (M_n) can be synthesized with dispersities $Đ < 1.1$[141] while also high molar mass PPs are possible (M_n = 150,000 g mol^{-1}).[142] Under physiological conditions, PPs can degrade into non-toxic, low molar mass species through the hydrolysis or enzymatic cleavage of the phosphate bond. The FDA classifies chosen PPs used in food under the GRAS status. They can be found in all types of food including baby food, meat, seafood and cheese according to the stipulated rules (food industry: < 5000 pm,[143] meat: < 0.5% weight of the final product[144]). Polyphosphates have shown to stabilize the protein structure, form a surface layer coagulated protein around meat or to retain the natural moisture of seafood.

2.10 Polysiloxanes

Materials composed of a backbone of alternating silicon and oxygen atoms with two alkyl or aryl moieties attached to the tetravalent silicon (-R_2Si-O-) are generally referred to as silicon polymers.[145] They can be considered as hybrid materials due to the combination of polar inorganic siloxane bonds (-Si-O-) in the backbone and organic alkyl or aryl side chains. Since the invention of the so-called "Direct Synthesis" of methylchlorosilane by Rochow and Müller (also called "Müller-Rochow-Process") in the early 1940s, polysiloxanes have been prepared industrially. This large scale production of silicon polymers is realized by an equilibration polymerization of cyclic and linear oligosiloxanes in the presence of an acid or a base as catalyst.[146] The method enables easy scale-up and cost effective production. However, it does not provide a good control over molar masses of the polymers and their dispersity. Only with the development of an ionic ring-opening polymerization using cyclic oligosiloxanes as monomers, well-defined polysiloxanes with defined molar masses and narrow dispersities became accessible.[147] Compared to the carbon-based polymers, silicon polymers feature superior physical and chemical properties in terms of thermal and oxidative stability, as well as flexibility combined with a low thermal glass transition temperature.[148]

Poly(dimethylsiloxane) (PDMS), for pharmaceutical applications better known as "dimethicone", bears two methyl groups on each silicon atom and represents the most prominent member of the silicone family. It is used in various pharmaceutical applications due to its excellent biocompatibility, low toxicity, optical transparency, gas permeability, high thermal stability, elasticity and low production costs.[149] However, due to the extreme hydrophobicity, PDMS-based materials suffer from low wettability and biofouling problems.[150] In consequence, increasing concerns arise about the safety of PDMS polymers in long term applications in blood contacting environments. To overcome these limitations, the focus of recent silicon related research has been concentrated on modifications to enhance the hydrophilicity and anti-fouling capability.[151] PDMS is not biodegradable in processes occurring *in vivo*; however, it slowly degrades within the environment to yield silica, carbon dioxide and water as non-toxic degradation products.[152] The FDA approved the use of PDMS in foods (except milk), cosmetic and pharmaceutical products (21 CFR 173.340).

2.11 Poly(vinyl ester/alcohol/ether)s

Poly(vinyl esters/alcohols/ethers) are all based on the polymerization of a vinyl group linked to an adjacent oxygen group. Poly(vinyl ester)s comprise polymer species, which are mainly prepared by free radical polymerization of vinyl esters. Technically important is **poly(vinyl acetate) (PVAc)**. More than one decade ago, the preparation of well-defined PVAc by controlled radical polymerization (M_n = 50,000 g mol^{-1}, Đ < 1.4) by "macromolecular design *via* interchange of xanthate"/reversible addition-fragmentation chain-transfer (MADIX/RAFT) polymerization became popular.[153] PVAc reveals a glass transition temperature (T_g) around room temperature. Since it is rather brittle below the T_g, plasticizers are usually added for improved flexibility. The homopolymer is often applied as adhesive in water-based emulsions. To overcome its stiffness, PVAc is often copolymerized with other monomers. Furthermore, PVAc can be partially or fully hydrolyzed to obtain the water-soluble **poly(vinyl alcohol) (PVA)**. It cannot be prepared by polymerization of the respective monomer vinyl alcohol since it is unstable. Depending on the length of the initial PVAc and the degree of hydrolysis under acidic or alkaline conditions, PVA with molar masses (M_n) from 20,000 to 400,000 g mol^{-1} can be obtained with varying solubility, tensile strength and adhesiveness.[154] It has a number of desirable properties like mechanical strength and high elasticity that make it a useful pharmapolymer. The hydroxyl groups are suitable for cross-linking (*e.g.* with ethylene glycol diglycidyl ether[155] or glutaraldehyde[156]) to create hydrogel networks with low or high swelling behavior in water. They have been well-established as drug delivery carriers. The FDA approved PVA for various uses, *e.g.* as indirect food additive in products, which are in contact with food (21 CFR 177.1670), as diluent in color additive mixtures for coloring shell eggs (21 CFR 73.1) and as ophthalmic demulcent (21 CFR 349.12).[154] Several microorganisms are able to degrade PVA as well as PVAc through enzymatic processes. The degradation by human enzymes has not been reported so far. The copolymer poly(ethylene-*co*-vinyl acetate) (PEVA) is often used in drug delivery research to slowly release a compound. Furthermore, it reveals only little or no reaction after implantation.

Since 1930, **poly(vinyl ether)s (PVE)** have been produced on an industrial scale. PVEs are polymers bearing the functional ether group in the side chain. They are made from the respective vinyl ethers *via* chain-growth polymerization. The functional versatility of the starting material allows the incorporation of alkyl or amine moieties. Different synthesis routes and industrial processes are described in literature.[157] Probably the most important PVE is the amphipathic butyl- and amine modified one (PBAVE) that has shown remarkable performances in trial experiments.

2.12 Poly(*N*-vinyl amide)s

Poly(*N*-vinyl amide)s describe a polymer class that comprises amide functionalities in the side chain. Compared to poly(*N*-acryl amide)s, the amide group is linked to the polymer backbone through the nitrogen atom. The most prominent representative is **poly(vinyl pyrrolidone) (PVP)**.

Linear PVP was first synthesized by Reppe in 1939 as one of the numerous products originating from acetylene chemistry. It is a water soluble, non-ionic, biocompatible and stable polymer, which is not metabolized by the organism.[158] In the very beginning during World War II, it was mainly used as plasma expander.[159] Today, it is well established in several products of cosmetic and pharmaceutical industry, *e.g.* as binder in pills. A special feature of PVP, also known as "povidone", is its possibility to form strong hydrogen bonds, which also explains its good solubility properties in water. Furthermore, the hydrogen bond formation enables complexation of polar compounds which increases the water solubility and the bioavailability, as reported for acetaminophen.[160] The complex formation constants as well as solubility properties were furthermore determined for several other substances.[161] It could be shown that PVP, similar to PEG, increases the water solubility and blood circulation time

for liposomes.[162] PVP is approved by the FDA for numerous applications, *e.g.* in food for human consumption (21 CFR 173.55). A reported method to synthesize PVP in laboratory scale is MADIX/RAFT polymerization. In industrial scale, it is synthesized by free radical polymerization in most cases, whereat a broad range of molar masses can be obtained. The commercially available polymers comprise ranges (M_w) from 2,000 to $2{,}500 \times 10^3$ g mol^{-1}.[163] In order to achieve high molar masses, a polymerization in aqueous solution is commonly applied using hydrogen peroxide as initiator. Organic solvents generally lead to low molar mass PVP. Using hydrogen peroxide as initiator, the solvent for the polymerization is of high importance for the final product, since it is responsible for the polymer end group. Other possibilities to create different functional endgroups include the usage of suitable transfer agents or specific chain capping agents. Post modifications are also possible but difficult to control, and the products are hard to purify. Another way to alter or to improve the polymer properties of PVP is copolymerization.[160] The synthesis is performed by radical polymerization in an organic solvent similar to the synthesis of the linear homopolymer. A frequently used comonomer is vinyl acetate (polymer: copovidone). The amount of vinyl acetate increases the hygroscopicity of the product, allowing the preparation of less brittle films, which is preferable for the use as soluble binder or film-forming agent.[161] One opportunity to obtain water insoluble PVP is cross-linking, resulting in so-called crospovidone. The ways to synthesize cross-linked PVP are versatile, reaching from the use of cross-linking agents or cross-linking monomers to subsequent cross-linking with peroxides. A well-known way to obtain highly cross-linked products is the so-called "popcorn polymerization". This method uses either an alkali hydroxide, yielding some bifunctional monomers, or a small amount of bifunctional monomers for cross-linking.[161, 164] The mechanism of this polymerization method is not well-determined, since it was primary observed as a side reaction in radical polymerization processes. It could be found that this polymerization starts by a highly reactive nucleus initiating the whole process, similar to the formation of popcorn.[165] Infrared measurements revealed that there is no structural difference between the cross-linked PVP obtained by popcorn polymerization and the linear PVP, but a difference was observed for chemically cross-linked PVP. Therefore the cross-linking of PVP *via* popcorn polymerization is essentially of a physical nature.[161] The cross-linked PVP is widely used in beverage and pharmaceutical industry. The good adsorptive properties are used to remove polyphenols or azo dyes from beverages. A rather well-known example in the pharmaceutical industry is the PVP-iodine complex which is used as disinfectant, also known as betaisodona and with several other trade names. Furthermore, crospovidone shows beneficial disintegration properties, thus it is used as additive in tablets promoting their break up and, therefore, speed up the drug release from solid dosage forms.[161, 166]

2.13 Poly(allylamine)s

Poly(allylamine) (PAAm) is a cationic polymer obtained from the radical or cationic polymerization of allylamine. While the backbone contains no nitrogen, as described for poly(ethylene imine), the polymer side chain contains primary amine groups which can be converted into secondary or tertiary amine functionalities. This turns PAAm into a highly promising gene delivery agent.[167] Poly(allylamine hydrochloride) in combination with an anionic polyelectrolyte (*e.g.* poly(styrene sulfonate)) can be used to form layer-by-layer adsorbed films.[168]

2.14 Poly((meth)acrylate)s

Poly(acrylate)s and poly(methacrylate)s are synthetic polymers of acrylic and methacrylic acids or their esters, respectively.[169] They are prepared on an industrial scale by free radical polymerization applying a variety of different methods, which include bulk, solution, suspension, and emulsion polymerization.[170] Poly(meth)acrylates can also be synthesized by various controlled radical polymerization techniques, which allow

a better control over molar mass, dispersity, polymer composition, and polymer architecture compared to free radical polymerization.[171] Poly(methacrylate)s generally display a higher glass transition temperature (T_g) and a lower decomposition temperature than the corresponding poly(acrylate)s.[172] The properties of poly(meth)acrylates can conveniently be tuned by varying the molecular structure of the ester side chain. These modifications enable access to polymers spanning the whole range from water to oil soluble or from brittle to elastic. The FDA has approved the safety of poly(meth)acrylates in several pharmaceutical applications, *e.g.* as basic components of food contact surfaces (21 CFR 177.1010).

Poly(acrylic acid) (PAA) and **poly(methacrylic acid) (PMAA)**, bearing a carboxylic acid unit on every second carbon atom of the main chain, are water soluble, weak anionic polyelectrolytes.[173] Besides their linear form they can be cross-linked by several cross-linking agents. The backbone of PAA and PMAA are not biodegradable, but they exhibit a low toxicity and excellent biocompatibility.[160] In aqueous solution, PAA and PMAA display a reversible coil-to-globule transition at pH 5. At lower pH values, these polymers undergo a transition to a compact globular conformation. However, if the pH value is increased, the chains expand into a fully solvated coil conformation due to the ionization of the carboxyl groups.[174] This reversible ionization of PAA and PMAA enables the formulation of pH- and ionic strength responsive materials. For instance, PAA-based hydrogels swell rapidly when placed in an aqueous environment due to the ionization of carboxyl groups. This feature makes PAA and its sodium salt (poly(sodium acrylate)) the most prominent materials for super absorbers, which are applied in diapers and membranes for hemodialysis or ultrafiltration.[175] Concerning drug delivery applications, PAA provides sufficient flexibility and excellent bioadhesion properties. Hence, they are frequently used for oral and mucosal contact applications such as tablets, oral suspensions and bioadhesives. An advantage of PAA is the convenient modification of the carboxyl side chains with alcohols or amines to introduce additional functionalities. In consequence, drugs and/or bioactive molecules can easily be attached to the PAA backbone in accordance with the concept of Ringsdorf.[176] **Poly(2-hydroxyethyl methacrylate) (PHEMA)** represents another water soluble, biocompatible poly(methacrylate) modified with hydroxyl functionalities in each repeating unit. These hydroxyl groups enable the material to form strong hydrogen bonds and make it very hydrophilic without need for charged side chains. As a consequence, PHEMA is often used as the main material for contact lenses. Moreover, the hydroxyl functionality of PHEMA can further be modified in post-polymerization reactions to conjugate any bio-active molecule.

Poly(methyl methacrylate) (PMMA) represents probably one of the best-known poly(methacrylate)s containing a methyl ester functionality at the side chain, which makes this material hydrophobic and non-soluble in water. PMMA was first developed in 1928 by Röhm, Chalmers and Bauer. The first commercial product was brought to the market in 1933 by the Rohm and Haas company under the trademark "Plexiglas®".[177] In the following years, PMMA rapidly became the most important plastic glass due to its excellent transparency and ease of production. Concerning pharmaceutical applications, PMMA is characterized by an excellent biocompatibility, convenient processability, low toxicity, minimal inflammatory reactions with tissues, and low production costs.[178] Being nonbiodegradable and fracture resistant, it is an essential material for implant materials, in particular in case of long term applications. PMMA-based materials have further found application in dermal fillers, bone cements, intraocular lenses and membranes in dialyzers for hemodialysis.[179] However, there are some limitations to the use of PMMA, which are related to its brittleness and shrinkage, the generation of voids during processing steps, a lack of adherence to bone tissue, and the heat created by the exothermic reaction during cement polymerization, which can damage bone tissue.[180] To overcome these problems, alternative poly(meth)acrylates are currently under investigation, in particular for use as long term implant materials. One example is **poly(*n*-butyl methacrylate) (PBMA)**, which possesses a butyl ester at the side chain. This material features a lower toxicity, a higher fracture toughness, and a better fatigue life, while reducing the exothermic effects compared to PMMA.[181]

Another important modification of poly(methacrylate) is **poly(2-dimethylaminoethyl methacrylate) (PDMAEMA)**, which contains an ionizable tertiary amine group. In water it may be protonated and becomes a weak cationic polyelectrolyte depending on the pH value. The pK_a value of the polymer depends on the composition as well as the molar mass, whereas values between 7 and 8 have been reported. Additionally, PDMAEMA exhibits LCST behavior in water depending on the molar mass of the polymer and the pH value of the solution.[182] However, the positive charge on the polymer causes these materials to be quite cytotoxic, which, in combination with the lack of biodegradability, limits its use in pharmaceutical applications.[183] Concerning drug delivery systems, the monomer DMAEMA is so far only applied as comonomer in combination with other methacrylates or methacrylic acid to modulate the overall charge and create a defined pattern for dissolution at specific pH values. Apart from changing the ester functionality or its alkyl moiety, physicochemical properties of the poly(meth)acrylates can also be altered by copolymerizing different functional monomers and by varying the monomer composition of the polymers. Incorporating the ionizable segments in the backbone of the polymers, such as amine and/or carboxyl groups, can render a tunable pH-dependent water solubility to the corresponding polymers. Accordingly, they are used for pH-dependent drug release applications due to salt formation.[184] These copolymers are more commonly known as EUDRAGIT® polymers in pharmaceutical industry and described in Chapter 3.

Furthermore, in addition to hydrogen and methyl groups, some other functionalities can be installed on the α-position of the acrylic backbone. For instance, acrylates with a nitrile group are called cyanoacrylates. Various alkyl groups can be added to the ester group, *e.g*. methyl, butyl, or hexyl. Cyanoacrylates polymerize rapidly in the presence of traces of water by an anionic polymerization mechanism to corresponding poly(cyanoacrylate)s. Therefore, they are commonly used as instant adhesives or "superglues".[185] For medical adhesive applications, cyanoacrylates with long alkyl groups are preferred since poly(cyanoacrylate)s with short groups can irradiate the tissues. Poly(cyanoacrylate)s, in particular **poly(isobutyl cyanoacrylate)** and **poly(isohexyl cyanoacrylate)**, have also been used in drug delivery applications. The installation of the heavier element fluorine on the α-position results in α-fluoroacrylates. Poly(α-fluoroacrylate)s can be obtained by the free radical polymerization of the α-fluoroacrylate.[186] Compared to the conventional (meth)acrylates these polymers exhibit better thermal and chemical stabilities. These polymers are mainly used for optical applications, but also found to be useful in cross-linked copolymers as polymer sequestrant.

2.15 Polyacrylonitriles

Polyacrylonitriles (PAN) are synthetic, semicrystalline organic polymers consisting of nitrile units attached to the carbon backbone. First synthesized in 1930 by Fikentscher and Heuck (IG Farben, Ludwigshafen),[187] it took more than 16 years for establishing the large scale production of PAN (brand name Orlon®) by Du Pont®.[188] Commercial PAN with high molar mass is synthesized by free radical polymerization of acrylonitrile. As a result, the control of the molar mass distribution is limited and high dispersities are obtained ($M_n < 10^6$ g mol^{-1}, $Đ > 3$). More controlled processes like the ATRP and the RAFT polymerization enable the control of the molar mass distribution for molar masses (M_n) up to 100,000 g mol^{-1} (ATRP[189]: $Đ < 1.3$; RAFT[190]: 60,000 g mol^{-1}, $Đ = 1.2$ to 1.4). In many cases, various vinyl monomers are copolymerized to modify the structure for final applications.[191] Anionic polymerization has been applied for the polymerization of PAN as well,[192] but this method results in branched structures, which affects the mechanical behavior of the PAN.[193] In general, the active nitrile groups in PAN can be converted to other functional groups like carboxyls (*via* hydrolysis)[194] and amines (*via* reduction),[195] which subsequently facilitate further modifications. Recently, Nataraj *et al.* reviewed the application of PAN-based nanofibers in various fields.[196] Several investigations have demonstrated that the relatively poor biocompatibility of the conventional PAN could be improved by bulk or surface modification.[197] Another simple and low-cost alternative modification is

blending.[198] The FDA approved the use of PAN in the production of semi-rigid and rigid acrylic plastics, which are intended for use in contact with food (21 CFR 177.1010).

2.16 Polyurethanes

Discovered 75 years ago, **polyurethanes (PU)** represent a versatile polymer class based on a modular structure which is generated by the combination of a variety of polyols and isocyanates as building blocks.[199] The urethane groups are formed in the polymer backbone by the polyaddition of respective isocyanates and alcohol groups. The chemical nature of the building blocks, the reaction sequence as well as the ratio of the OH/isocyanate components determines the properties of the polymers. Polyols with molar masses (M_n) larger than 1,000 g mol^{-1} are used to make soft and elastic PUs (*e.g.* PEG-diols) while short chains result in hard, rigid PUs (*e.g.* dipropylene glycol). The latter can be further supported by cross-linkages. The most common used isocyanates are aromatic diisocyanates (*e.g.* toluene and methylene diphenyl diisocyanate) since they reveal higher reactivity compared to aliphatic isocyanates (*e.g.* hexamethylene diisocyanates). Often the reaction of three components, in particular a diisocyanate, a bifunctional polyol and a dihydroxy chain extender, is described to form linear, segmented copolymers consisting of alternating hard and soft segments. The structural diversities and tailorable properties (*e.g.* biodegradability, blood compatibility, hydrophilicity) make these materials extremely versatile for bioapplications and other high-tech products.[200] Doubtless, the most prominent application for PUs are foams of different nature. The FDA approved PU resins for use as basic components of food contact surfaces (21 CFR 177.1680). Other materials, which are closely related to PUs, are polyureas (often summarized as polyurethanes); these are the product of the addition of isocyanates with amines.[201] In general PUs for biomedical applications are mainly found in gels of various sizes.

2.17 Polystyrenes

Polystyrenes (PS) are synthetic aromatic polymers made from the styrene monomers. The first commercially available polymers were manufactured by the company I. G. Farben in 1931.[202] The most prominent applications are the PS foams. Pioneering work on its polymerization was done by Natta (1960) and Ishihara (1986) who reported the synthesis of iso- (phenyl groups on the same side) and syndiotactic polystyrenes (phenyl groups on alternating sides of the backbone). The latter is commonly prepared in a so-called Ziegler-Natta-polymerization.[203] This kind of polymerization uses metallocene catalysts in order to control the orientation of the monomer in the moment of addition.[204] Further synthesis routes comprise radical, anionic as well as cationic polymerization. The syndiotactic PS exhibits a crystallization rate, which is around two orders of magnitude larger than the isotactic form. Several routes for the synthesis of functional materials are described in literature, comprising *in situ* functionalization, post-polymerization modification or the application of pre-functionalized monomers.[205] For instance, the introduction of sulfonic acid groups in the para-position of the benzene ring turns the resulting PS into the water soluble **poly(styrene sulfonic acid)**. Different cross-linking agents have been incorporated into the PS resins, including the most commonly applied divinylbenzene, but also other monomers have been used to adjust different solvation properties (*e.g.* dimethacrylate, tetraethylene glycol).[206] Basically, PS is hard and rather brittle and occurs in the solid or foam state. It is a widely used plastic for packaging where hygiene is important. Above its glass transition temperature (100 °C) it becomes liquid, while cooling down results in rigidity again. Using this temperature behavior, PS can be processed *via* extrusion, molding or vacuum forming.[207] PS is approved by the FDA as food packaging material (21 CFR 177.1640) updated in 2013 by the Plastics Foodservice Packaging Group.[208]

2.18 Polyanhydrides

Polyanhydrides are commonly obtained by the dehydration reaction between diacids by either melt polycondensation or solution polymerization to form the functional group (-O-CO-R-CO-). Different structures, their characterization and biocompatibility have extensively been reviewed.[209] The polymers were prepared with the intention to obtain a material that should degrade within the time range of their application due to the presence of the most reactive functional group available for degradation on the basis of passive hydrolysis.[210] They degrade *in vivo* into non-toxic monomer counterparts, which can be eliminated from the body as metabolites. High molar mass polyanhydrides (M_n up to 30,000 g mol^{-1}) can be synthesized by utilizing heterogenic coordination catalysts.[211] Often used monomers are the naturally occurring sebacic acid (**poly(sebacic acid)**, FDA: 21 CFR 175.105) and the 1,3-bis(4-carboxyphenoxy)-propane (**poly(*bis*-(p-carboxyphenoxy)propane**). While aromatic polyanhydrides can fragment after exposure to water, resulting in a rapid release of water-soluble drugs, copolymers prepared from fatty acids (*e.g.* sebacic acid) show controlled degradation rates from days to years. The copolymer poly(styrene-*co*-maleic anhydride) was approved by the FDA as indirect food additive for use as articles or components of articles that contact food items (21 CFR 177.1820).

Containing the functional groups in the side chain, **poly(maleic anhydride)** represents another form of polyanhydrides made from maleic anhydride in the presence of free radical catalysts and various organic bases, among others.[212] It is mainly used as comonomer, *e.g.*, for the polymerization with styrene (poly(styrene-*co*-maleic anhydride)). A unique feature is the preparation of almost perfectly alternating copolymers which are the first polymers that were used for drug conjugates.

2.19 Polyolefins

Polyolefins describe a class of polymers obtained from a simple alkene (olefin) as monomer. These materials are produced in million ton scales and are the most common plastics used in commodity products. Besides radical processes or the frequently used coordination polymerization, the living alkene polymerization method catalyzed by transition metal complexes is becoming more and more popular to synthesize polyolefins with a precise molar mass control as well as a wide array of polymer architectures.[213] Their properties are mainly determined by their molar mass and degree of crystallinity (from liquid-like to rigid plastics). All practical or commercial relevant polyolefines are poly-α-olefins. The FDA approved **poly(ethylene)** for use as basic component of food contact surfaces (21 CFR 177.1520). It represents the simplest representative and most common plastic, which is made from ethylene in the presence of the Ziegler-Natta catalyst.[214]

Further often used olefins are **poly(isobutylene)** (by cationic polymerization of isobutylene),[215] the non-reactive fluoropolymer **poly(vinylidene fluoride) (PVDF)** (by radical polymerization of vinylidene difluoride)[216] and **poly(hexafluoropropylene) (PHFP)**. *Bis*functional polyolefins like **poly(octa-1,7-diene)** can be used for cross-linking reactions to obtain network architectures.

700 **Table 2.** Overview of polymer classes that exhibit pharmaceutical relevance.

POLYMER CLASS	STRUCTURE	R	NAME (ABBREVIATION)	WATER SOLUBILITY	BIODEGR.[a] (Y/N)	APPLICATION (see corresponding chapter)
Polyether	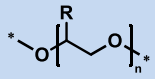	H	Poly(ethylene glycol) (PEG)	Good	N	Polymer-drug conjugates, solid colloidal dispersions, polyplexes, microgels, hydrogels, solid implants and inserts, matrix excipients
		CH_3	Poly(propylene glycol) (PPG)	LCST ~ 50 °C	N	Solid colloidal dispersions, polyplexes, matrix excipients, polymeric drugs
		OH	Poly(glycerol) (PG)	Good	N	Future prospects
		CH_2Cl	Poly(epichlorohydrin) (Poly(chlormethyl)oxiran)	No	N	Polymeric drugs
	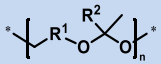		Poly(ketal) (PK)	Dependent on R^2	Y	Future prospects
Poly(ethylene imine)	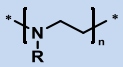	H	Linear poly(ethylene imine) (LPEI)	Good for > 70 °C	N	Polyplexes, hydrogels, future prospects
		CH_2CH_2NHR	Branched poly(ethylene imine) (BPEI)	Good	N	Polyplexes, hydrogels, future prospects
Polyester	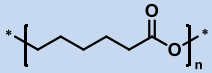		Poly(caprolactone) (PCL)	Degradation	Y	Drug-eluting stents, future prospects
	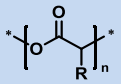	H	Poly(glycolic acid) (PGA)	Degradation	Y	Solid colloidal dispersions, hydrogels, solid implants and inserts, drug-eluting stents, future prospects
		CH_3	Poly(lactic acid) (PLA) (*i.e.* PDLLA, PLLA and PDLA)	Degradation	Y	Solid colloidal dispersions, hydrogels, solid implants and inserts, drug-eluting stents, future prospects
	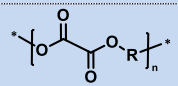		Poly(oxalate) (PO)	Degradation	Y	Future prospects
	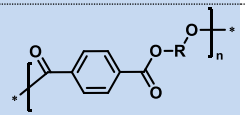	$(CH_2)_4$	Poly(butylene terephthalate) (PBT)	Degradation (> 60 °C)	Y	Microgels
Polycarbonate	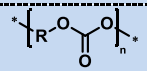			Good	Y	Future prospects
Poly(amino acid)	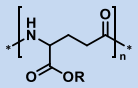	H	Poly(γ-glutamic acid) (PGluA)	Good	Y	Polymer-drug conjugates, future prospects
			Poly(γ-glutamate) (PGlu)	Good	Y	Solid colloidal dispersions, nanogels
	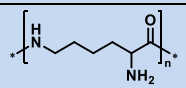		Poly(lysine)	Good	Y	Polyplexes, future prospects

	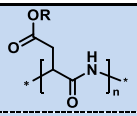		α-Poly(aspartate) (PAs)	Good	Y	Solid colloidal dispersions
Poly(peptoid)	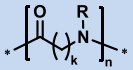		(PoP)	Good	Y	Future prospects
Poly(2-oxazoline)	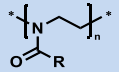		(POx)	Good (only for CH_3, C_2H_5)	N	Polymer-drug conjugates, future prospects
Poly(*N*-acrylamide)	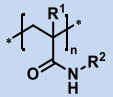	R^1 = H; R^2 = $CH(CH_3)_2$	Poly(*N*-isopropylacrylamide) (PNiPAAm)	Depending on temp.	N	Future prospects
		R^1 = CH_3; R^2 = $CH_2CH(CH_3)(OH)$	Poly(*N*-(2-hydroxypropyl)-methacrylamide) (PHPMA)	Good	N	Polymer-drug conjugates, future prospects
Polyphosphoester	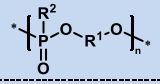	R^2 = OR	Poly(phosphate) (PP)	Good	Y (Depend. on R^2)	Future prospects
Polysiloxane		R^1,R^2 = CH_3	Poly(dimethylsiloxane) (PDMS, dimethicone)	No	N	Hydrogels, solid implants and inserts, matrix excipients, future prospects
Poly(vinyl ester/alcohol/ether)	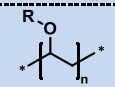	$COCH_3$	Poly(vinyl acetate) (PVAc)	Good	Y	Solid implants and inserts, drug-eluting stents, Future prospects
	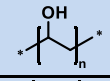		Poly(vinyl alcohol) (PVA)	Good	Y	Microgels, solid implants and inserts, solid oral dosage forms, matrix excipients
	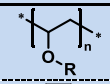		Poly(vinyl ether) (PVE)	No	N	Polymer-drug conjugates
Poly(*N*-vinyl amide)	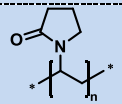		Poly(vinyl pyrrolidone) (PVP)	Good	N	Hydrogels, drug-eluting stents, matrix excipients, future prospects
Poly(allylamine)	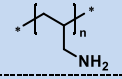		(PAAm)	Good	?	Polymeric drugs, future prospects
Poly(acrylate)		R^1 = H; R^2 = H	Poly(acrylic acid) (PAA)	Good	N	Hydrogels, matrix excipients, future prospects
		R^1 = H; R^2 = CH_3	Poly(methyl acrylate)	No	N	Solid oral dosage forms
		R^1 = H; R^2 = C_2H_5	Poly(ethyl acrylate)	No	N	Solid oral dosage forms
		R^1 = F; R^2 = H	Poly(2-fluoroprop-2-enoate)	Good	N	Polymeric drugs
Poly(methacrylate)		R = H	Poly(methacrylic acid) (PMAA)	Good	N	Microgels, solid oral dosage forms, future prospects
		R = CH_3	Poly(methyl methacrylate) (PMMA)	No	N	Solid implants and inserts, solid oral dosage forms, matrix excipients, future prospects

		R = C_4H_9	Poly(*n*-butyl methacrylate) (PBMA)	No	N	Drug-eluting stents, matrix excipients
		R = $CH_2CH_2N(CH_3)_2$	Poly(dimethylaminoethyl methacrylate) (PDMAEMA)	Good	N	Solid oral dosage forms, matrix excipients, future prospects
		R = $CH_2CH_2N(C_2H_5)_2$	Poly(diethylaminoethyl methacrylate) (PDEAEMA)	Depending on pH value	N	Solid oral dosage forms
		R = $CH_2CH_2N(CH_3)_3^+$	Poly(trimethylammonioethyl methacrylate chloride) (PTMAEMA)	Depending on pH value	N	Solid oral dosage forms
		R = CH_2CH_2OH	Poly(2-hydroxyethyl methacrylate) (PHEMA)	Good (low molar masses)	N	Hydrogels
Poly(cyanoacrylate)		R = $CH_2CH(CH_3)_2$	Poly(isobutyl cyanoacrylate)	No	N	Solid colloidal dispersions
		R = $(CH_2)_3CH(CH_3)_2$	Poly(isohexyl cyanoacrylate)	No	N	Solid colloidal dispersions
Polyacrylonitrile	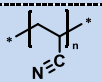		(PAN)	Good (in aq. inorganic salt solutions)	N	Hydrogels, future prospects
Polyurethane	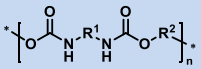		(PU)	No	Y	Hydrogels, solid implants and inserts
Polystyrene	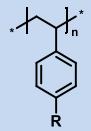	H	(PS)	No	N	Polymer-drug conjugates, drug-eluting stents, polymeric drugs, future prospects
		SO_3H	Poly(styrene sulfonic acid)	Good	N	Polymeric drugs
		$[-CHCH_2]_n$	Poly(divinylbenzene)	No	N	Polymeric drugs
Polyanhydride	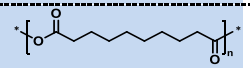		Poly(sebacic acid)	Decomposition	Y	Solid implants and inserts
	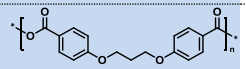		Poly(*bis*-(p-carboxy-phenoxy)propane)	Decomposition	Y	Solid implants and inserts
	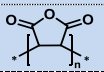		Poly(maleic anhydride)	Decomposition	N	Polymer-drug conjugates, future prospects
Polyolefin		R^1 = H; R^2 = H	Poly(ethylene)	No	N	Solid implants and inserts, drug-eluting stents
		R^1 = CH_3; R^2 = CH_3	Poly(isobutylene)	No	N	Drug-eluting stents
		R^1 = F; R^2 = F	Poly(vinylidene fluoride) (PVDF)	No	N	Drug-eluting stents
	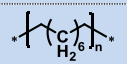		Poly(octa-1,7-diene)	No	N	Polymeric drugs
			Poly(hexafluoropropylene) (PHFP)	No	N	Drug-eluting stents

[a] Biodegradability in this review designates the potential of polymer chain cleavage by enzymes or proteases (Y = yes, N = no).

3. Polymers in pharmaceutical applications

The following chapter describes different forms of applications of pharmapolymers which are already available on the market or currently undergoing clinical trials. The current clinical status and the respective NTC number (clinicaltrials.gov identifier) usually refer to the official webpage https://clinicaltrials.gov/. In some cases, the availability and the approved indication of use for the applied materials vary between countries. The described forms of appearance include polymer-drug conjugates, drug carrier systems in scales ranging from nano- to macroscopic size, polymers as coatings and matrix excipients as well as polymeric drugs.

3.1 Polymer-drug conjugates

The conjugation to polymers is a well-established technique to improve the properties of therapeutically active substances. In the last decades, numerous polymers have been tested for this purpose. The cytostatic agents that have been mainly used for preparing polymer-drug conjugates are doxorubicin (DOX), camptothecin (CPT), paclitaxel (TXL) and platinum complexes (Figure 1), but also other, more specialized drugs are conjugated.

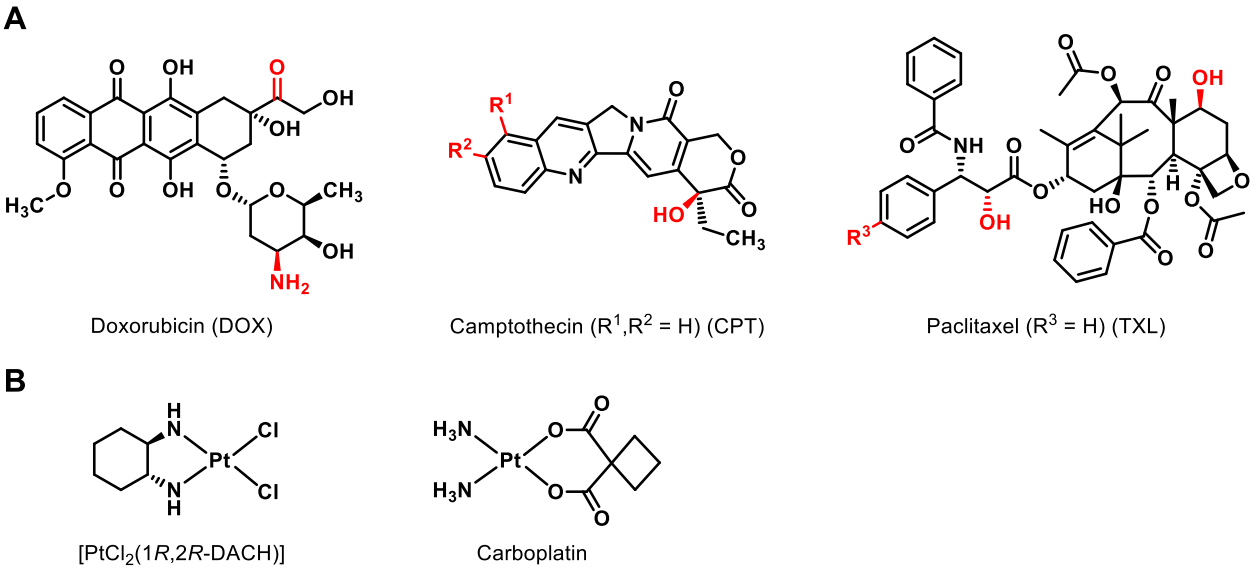

Figure 1. Schematic representation of the structures of the most common cytostatic agents used for preparing polymer-drug conjugates. A) Literature reported conjugation sites (marked in red) and B) selected examples for platinum complexes.

3.1.1 PEG conjugates

One of the first and probably the most well-known example is the attachment of poly(ethylene glycol) (PEG), also called PEGylation. In drug delivery, PEGylation can be subdivided into three categories: The attachment of PEG to proteins, to small drug molecules and to other polymers. The latter is often related to the formation of nanocarriers, which are described in detail in Chapter 3.2. With the attachment of PEG chains, some of the beneficial properties of this polymer are transferred to the pharmacological active compounds, which can improve

the accessibility of drugs in biological systems.[15, 217] Pioneered by Davis and his colleagues, the first PEGylation was successfully demonstrated on a protein.[10a] The initial goal was the protection from destruction during the delivery process. As an unexpected finding, the authors observed that the PEGylation improved the pharmacokinetic and pharmacodynamics of the protein.[218] Similar observations are found for small drug molecules, which often suffer from poor solubility and, therefore, low bioavailability. The attachment of PEG strongly improves their properties by adapting the beneficial properties of the PEG polymer.

PEGylation of proteins. Since the first PEGylation of a protein, a variety of accessible functional groups on protein surfaces has been explored as potential linking sites. In general, the functionalization with PEG introduces several advantageous properties compared to the native protein. PEGylated proteins show an improved pharmacokinetic and pharmacodynamic, which is related to an increased water solubility, an increased stability, shielding from metabolic enzymes, a reduced immunogenicity and retarded renal clearance (due to stealth behavior) leading to an elongated blood circulation time.[11b] Depending on the molar mass of the attached PEG chains, the clearance by the kidneys can also be circumvented.[15, 218-219] The conjugation additionally reduces the immunogenicity of the native protein, increases its stability and prolongs the biological half-life which helps to reduce the frequency of administration. In the last decade, several new conjugation methods have been developed, allowing a more effective and selective attachment of PEG polymers. The PEGylation techniques of proteins can be separated into first and second generation.[220] The first generation is performed using short PEGs (M_n = 5,000 to 12,000 g mol^{-1}) being randomly bound to the protein surface. A disadvantage when using a PEG-diol is the formation of a high content of protein dimers, trimers and even fully cross-linked materials. In consequence, the α-methylated mPEGs are preferred to avoid this problem, although minor contaminations with PEG-diol are still present.[221] As activation agents or linkers between the protein and the PEG chains, cyanuric chloride, tresyl chloride and many more compounds are applied.[11a, 222] The second generation of PEGylation improved the selectivity of the attachment to specific areas of the protein while reducing the influences on the protein structure. Common groups for functionalization are maleimide targeting free thiol groups, NHS activated acids reacting with amines, benzotriazoles, which create a pH-responsive linkage, and aldehydes such as propionaldehyde. Furthermore, second generation PEGs allow an easier purification and removal of remaining PEG-diol, *e.g.* in the case of PEG with activated acids up to 97% of the remaining diol content can be removed by ion-exchange chromatography.[218] PEGylation techniques forming disulfide bridges enable the site specific PEGylation to the few free cysteine residues on the protein surface, which minimizes the loss of biological activity, but preserves the low immunogenicity. A rather new method is described by DeFrees *et al.* called glycopegylation. This method basically uses enzymes for *N*-acetylgalactosamine (GalNAc) glycosylation at specific serine and threonine residues, which subsequently conjugate to salic acid conjugated PEG by enzymatic transfer.[223] These improvements on the conjugation methods allow the synthesis of drug conjugates with well-defined amounts of PEG and selective binding to non-active parts of the protein.[224] A more detailed overview on different protein PEGylation techniques is given by Roberts *et al.*.[11d]

Considering the above mentioned improvements on the synthesis, in particular the excellent selectivity of conjugation and the general benefits like the improved pharmacokinetics, it is not surprising that a number of PEGylated proteins already entered the market and several new materials are in clinical trials. Overall, thirteen different PEGylated proteins are nowadays approved and commercialized (Table 3). The first clinically approved PEGylated protein drug was the enzyme Adagen® (Enzon Pharmaceuticals). After its approval, several other PEGylated protein drugs found their way to commercialization and entered clinical trials within a short period of time. A milestone in the pharmaceutical development was certainly the approval of Macugen®, being the first approved aptamer used as therapeutic agent in humans.[225] The latest protein drug that has been approved by the Food and Drug Administration (FDA, Nov. 2015) is the PEGylated full length Factor VIII (Adynovate®) for use in patients aged 12 years and older suffering from haemophilia A and.[226] Once approved by the FDA or European

Medicines Agency (EMA), established PEGylated proteins are investigated in clinical trials. Due to the large number of clinical studies, only a selection of investigated diseases can be found in Table 3.

Table 3. PEGylated proteins and small drugs on the market approved by the FDA and EMA as well as their use for other diseases.

TRADE NAME	CONJUGATE	INDICATION/USE	MANCUFACTURER	M_n (PEG) (g mol^{-1}) [# of PEGs/drug molecule]	CURRENT CLINICAL TRIALS ON …
			PROTEIN		
Adagen®	PEG-Adenosine Deaminase	SCID[a]	Enzon Pharmaceuticals	5,000 [11 to 17]	Severe combined immunodeficiency disease
Oncaspar®	PEG-Asparaginase	Leukaemia	Enzon Pharmaceuticals	5,000 [69 to 82]	Various cancers (neoplasms, multiple myeloma)
PegIntron®, ViraferonPeg®	PEG-Interferon-α2b	Hepatitis C	Schering-Plough	12,000 [1]	Hepatitis B, various cancers (*e.g.* fallopian tube-, ovarian-, peritoneal cavity cancer, neoplasm, melanoma), HIV Infection
	PEG-Interferon-α2a	Hepatitis C	Hoffman-La Roche	40,000 [1 branched]	Hepatitis B, various cancers (*e.g.* kidney cancer, leukemia), HIV infection
Somavert®	PEG-Human growth hormone mutein antagonist	Acromegaly	Pfizer	5,000 [4 to 6]	Different neoplasms (colorectal, lung, breast, prostatic)
Neulasta®	PEG-G-CSF[b]	Neutropenia	Amgen®	20,000 [1]	Various cancers (*e.g.* breast cancer)
Macugen® (Pegaptanib)	PEG-anti-VEGF aptamer	WARMD	OSI Pharmaceuticals/ Pfizer	40,000 [1 branched]	Wet age related macular degeneration
Mircera®	PEG-Erytropoietin	AACKD	Hoffman-La Roche	30,000 [1]	Various cancers (*e.g.* breast, prostate cancer, lymphoma, neoplasms)
Cimzia®	PEG-anti-TNF Fab[c]	Rheumatoid arthritis & Crohn's disease (RACD)	UCB Cares®	40,000 [1 branched]	RACD
Krystexxa® (Pegloticase)	PEG-Uricase	Chronic gout	Horizon Pharma	10,000 [9 per homo-tetramer (4)]	Chronic kidney disease stage 5
Omontys®	Peginesatide	AACKD	Affymax/Takeda[d]	40,000 [1 branched]	Anaemia associated with chronic kidney disease
Lonquex® (Lipegfilgrastim)	Glycopegylated G-CSF	Neutropenia[e]	TEVA	20,000 [1]	Various cancers (*e.g.* breast, ovarian cancer)
Plegridy®	PEG-interferon beta 1a	Relapsing multiple sclerosis (RMS)	Biogen™	20,000 [1]	RMS
Adynovate®	PEG-Factor VIII (full-length Coagulation Factor VIII) (BAX 855)	Haemophilia A[a]	Shire	20,000 [2]	Different blood diseases (von Willebrand Disease, thrombosis)
			SMALL DRUG		
Moventig® (EU: Movantik®) (Naloxegol)	PEG-Naloxone[b]	Opioid-induced constipation	AstraZeneca	< 1,000 [1]	

[a] Only approved by the FDA, [b] G-CSF: Granulocyte-colony stimulating factor, [c] approved for different disease in U.S. and E.U. (Nektar®), [d] withdrawn by Takeda, [e] Only approved by the EMA.

Selected PEGylated protein drugs in clinical trials. Due to the high number of materials in clinical trials, we only like to highlight a few materials in late stages of clinical testing (phase III) used for different kinds of diseases (Table 4).

Inherent bleeding disorder due to a deficiency or dysfunction of coagulation proteins is called haemophilia (A in case of Factor VIII, B in case of Factor IX). The only treatment of haemophilia patients is the intravenous injection of the deficient coagulation factors, prophylactic or in case of acute trauma. A drawback of native coagulates is their short half-life (FVIII 8: 12 h, FIX 18: 24 h) and the resulting frequent need for administration. In comparison, PEGylated FVIII and FIX show extended half-life and increased blood concentration after injection.[227] Besides the FDA approved PEGylated recombinant Factor VIII several other products are currently undergoing clinical trials including PEGylated Factor IX proteins. These drugs differ mainly in the way of PEG-binding, the chain length of the PEG or the modification of the protein (mutant Factor VIII (K1804C)).[227b, 227c, 228] The aim of these modifications is of course an increased activity.[229] Two conjugates are currently undergoing clinical trials in phase III (N8-GP and N9-GP).[230] The effects of these products are discussed in detail in literature.[227c, 231] Age related macular degeneration (AMD) is a medical condition causing blurred or impeded vision on focused objects, which in case of the more common wet AMD is related to the formation of abnormal blood vessels in the middle part of the retina. Initiated by the approval of the previously mentioned Macugen®, further PEGylated protein aptamers are under investigation, such as Fovista®. In contrast to Macugen®, Fovista® is developed to inhibit the platelet-derived growth factor (PDGF) and, therefore, the formation of abnormal vessel growth. For the treatment of AMD, it is combined with ranibizumab, an anti-Vascular Endothelial Growth Factor (anti-VEGF), and just passed the clinical trials phase II and entered phase III showing significantly improved results compared to native ranibizumab.

Patients with an inactive recombinant phenylalanine ammonia lyase suffer from an enrichment of phenylalanine (Phe) or hyperphenylalaninemia, which is mainly caused by a recessive gene disorder and results in mental retarding, if not recognized and treated timely.[232] A possible treatment is an enzyme substitution therapy. However, injections of pure phenylalanine ammonia-lyase (PAL) have only a short half-life and low activity in gastric secretions. In consequence, research focused on the development of more efficient forms realized by site-directed mutagenesis and PEG modifications. As a result, the concentration of Phe in blood could be decreased significantly and the symptoms are diminished.[233] Another PEGylated protein that reached phase III clinical trials is Peglispro,[234] a PEGylated insulin for the application as long term drug for diabethis mellitus patients. It could be shown that Peglispro has improved pharmakokinetic and pharmakodynamic profiles and, preferentially, hepatic *versus* peripheral action compared to insulin glargine. Nevertheless, end of 2015 the development of the project was discontinued by the supplier Lilly due to late stage observations regarding liver fat changes leading to unresolved questions.[235]

Table 4. PEGylated proteins under active clinical trials in phase III.

NAME	PEGYLATED PROTEIN	INDICATION/USE	MANUFACTURER	M_n (PEG) (g mol^{-1}) [# of PEGs/drug molecule]	IDENTIFIER NUMBER
N8-GP	Glycopegylated recombinant coagulation Factor VIII (K1804C)	Haemophilia A	Novo Nordisk®	40,000 [1]	NCT01489111
N9-GP	PEGylated recombinant Factor IX	Haemophilia B	Novo Nordisk®	40,000 [1]	NCT02141074
Fovista®	PEGylated anti-platelet-derived growth factor	Age related macular degeneration	Ophthotech/ Nektar®	40,000 [1 branched]	*e.g.* NCT01944839
Pegvaliase	PEGylated recombinant PAL enzyme[a]	Phenylketonuria	BioMarin®	20,000 [1]	NCT01819727

[a] PAL: Phenylalanine ammonia lyase.

PEGylation of small molecule drugs. In comparison to proteins, small molecules provide only a limited number of reactive side chains that are suitable for modifications. The lack of functional side groups in linear PEGs makes the coupling capacity of small molecules a critical issue. In order to improve the loading capacity, different architectures were investigated, *e.g.* forked, multi-arm, star-like and dendritic or branched polymers for the conjugation of small molecule drugs.[236] [217b, 237] Despite the immense research effort, it took a comparably long time for PEGylated small molecule drugs to enter the market. Small molecule drugs, such as antitumor agents, often suffer from poor solubility, high toxicity, rapid excretion and untargeted biodistribution. Therefore, conjugation of PEG represents an obvious way to improve their profiles. However, until now PEG-Naloxone (Moventig®) is, to the best of our knowledge, the first and only marketed PEGylated small molecule drug (approved by FDA and EMA) (Table 3). PEG-Naloxone is applied for treatment of opioid-induced constipation and approved for adult patients with chronic non-cancer pain.[217a] Being approved in 2014, Moventig® entered the market comparably late considering that PEGylation of proteins is performed for decades. Li *et al.* summarized 20 to 25 PEGylated small molecules at different stages of development and several research examples which show that PEGylated small molecules principally have improved properties. However, those examples failed in clinical trials due to a reduced activity, an inherent instability or their toxicity.[237b] Nevertheless, with the first approval of a PEGylated small drug we are confident that further examples will follow.

A list of PEGylated small molecule drugs undergoing clinical trials is given in Table 5. NKTR-181 is a PEGylated agonist for the μ-opioid receptor developed by Nektar®. Currently, it undergoes clinical trials in phase III.[238] Modified opoids are the most common medication types to treat chronic pain. In preclinical and clinical trials, the PEG modified drug revealed a slower uptake by the central nervous system (CNS) due to a reduced crossing of the blood-brain barrier (BBB), resulting in fewer CNS related side effects.[239] The aim of NKTR-181 is the treatment of patients with chronic low back pain (SUMMIT-07).[240]
Etirinotecan pegol comprises the prodrug irinotecan which is conjugated to a 20,000 g mol^{-1} four arm PEG by a degradable linker. Irinotecan is widely used as chemotherapeutical agent.[241] After enzymatic hydrolysis of the linker, it metabolizes into SN38, a potent topoisomerase I inhibitor and the active moiety of irinotecan, resulting in a 1000-fold increased activity in comparison to irinotecan itself.[242] The conjugation to PEG using slowly hydrolysable linkers based on esters aims at an application as long-acting agent with continuous and targeted drug release. In consequence, the concentration of SN38 is reduced in the plasma and undesired side effects are diminished.[243] As a result of the beneficial properties observed in phase II, Etirinotecan pegol is now undergoing clinical trials in phase III for advanced breast cancer and brain metastases in the US (Onzeald™).[243] In addition to this trial, further studies in different stages are currently ongoing to test its use for other cancerous diseases. In phase II of clinical trials, toxic side-effects associated with common chemotherapies appeared less frequent or were completely absent.[244] These preliminary results make etirinotecan pegol an attractive and interesting candidate for chemotherapies in the future. Other PEGylated small molecules produced by Nektar® are in earlier stages of clinical trials (I and II), including EZN-2208 for advanced solid tumors/lymphoma, and NKTR-171 for neuropathic pain.[238, 245]

Table 5. PEGylated small molecule drugs undergoing active clinical trials.

NAME	PEGYLATED DRUG	INDICATION/USE	MANUFACTURER	M_n (PEG) (g mol^{-1}) [# of PEGs/drug molecule]	STATUS
NKTR-181	n.a.	Neuropathic pain	Nektar®	< 1,000	Phase III (*e.g.* NCT01619839)
NKTR-102 (US: Onzeald™)	Etirinotecan pegol (SN38)	Several cancer	Nektar®	20,000 [1 four-arm]	Phase III (*e.g.* NCT01492101)

EZN-2208	SN38	Several cancer	Enzon Pharmaceuticals	40,000 [1 four-arm]	Phase II (*e.g.* NCT00520637)
NKTR-171	n.a.	Neuropathic pain	Nektar®	< 1,000	Phase I[246]

n.a.: not applicable.

3.1.2 Non-PEG conjugates

Some limitations of PEGylation have emerged specifically including an increased occurrence of immunogenic reactions and the accumulation in tissues which is a result of the nondegradability.[247] Hypersensitivity has been observed in some cases, which diminishes the benefits of PEGylation in case of some patient populations.[248] Even though PEG is not biodegradable, degradation occurred under certain circumstances (light, heat etc.) with the possibility of a build-up of toxic side products while stored.[15] Nevertheless, PEG is currently still the most tested and best understood polymer available with the longest clinical track record, but research efforts have increased to develop alternative materials addressing these limitations of PEG and adding further functionalities to polymer-drug conjugates. The number of potential alternatives for PEGylation has increased tremendously in the last years.[249] Requirements for potential substitutes for PEG include a high water-solubility, non-toxicity, non-immunogenicity, low accumulation during a therapy and clearance from the body.[250] Besides natural polymers such as heparin, dextran, chitosan, hyaluronic acid and human serum albumin, several synthetic polymers have emerged as suitable conjugate alternatives to PEG. In the following chapter we focus on these synthetic PEG alternatives and summarize all materials which entered clinical trials or the market already (Table 6).

Poly(styrene-*co*-maleic anhydride). The conjugation of poly(styrene-*co*-maleic anhydride) to the antitumor protein neocarzinostatin (SMANCS) was the first clinically approved polymer-drug conjugate (Zinostatin Stimalmer®) and is to this date the only non-PEG polymer-protein therapeutic that made it to the market. Maeda *et al.* reported the synthesis of SMANCS in the late 1970's. The copolymer consisting of styrene and maleic anhydride (SMA) was partially modified (30 to 50%) with butanol which was found to provide considerable hydrophobicity (Figure 2). Once added into aqueous solution, the residual anhydrides open and quickly form the acid. The modified SMA polymer chains were covalently linked to neocarzinostatin (NCS).[251] This characteristic enables dispersion in the phase-contrast agent lipiodol used in lymphangiography and, therefore, local administration through the feeding artery of the primary cancer, in particular liver cancer, of patients.[252] With the aid of X-ray, a precise localization of SMANCS to tumor tissue became realizable. Preclinical studies revealed the highest tumor-blood ratio (> 2.500) of the prodrug location ever reported for targeting approaches.[253] Maeda mentioned for the first time the importance of passive tumor targeting by the "enhanced permeability and retention effect" (EPR effect) describing that molecules of certain sizes (M_n = 30,000 to 50,000 g mol^{-1})[254] tend to accumulate preferentially in tumor tissue not in normal tissue.[255] Recently, lipiodol has been proven to be essential for the anti-tumor activity of SMANCS.[256] The protein conjugate successfully passed the clinical phases with high response rates (36 to 40%).[257] SMANCS received its approval for the market in 1990 (Japan) as part of the treatment of hepatocellular carcinoma and is distributed by Astellas Pharma (formerly Yamanouchi).[258] The highest chance of success is given in a 'patient-individualized treatment' (dose per tumor size/area) and follow-up treatments are only administered if the tumor is not regressing. Despite the efforts made to develop novel polymer carriers, the modified copolymer SMA remains the only commercialized synthetic alternative to PEG. However, a few other types of polymers or their drug conjugates, respectively, have been evaluated in clinical studies and mainly comprise poly(*N*-(2-hydroxypropyl)methacrylamide) (PHPMA) and poly(glutamic acid) (PGluA).

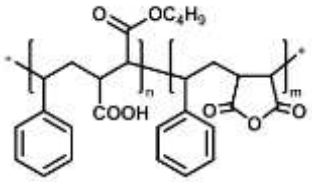

Figure 2. Schematic representation of the chemical structure of poly(styrene-*co*-maleic anhydride/acid/ester).

Poly(*N*-(2-hydroxypropyl)methacrylamide) (PHPMA). Testing conjugates of the PHPMA with anthracyclines, the homopolymers and respective copolymers were found to be chemically inert in biological media and showed no immunogenic response.[259] The first polymer-drug conjugate that entered clinical trials was the PHPMA conjugate PK1 (FCE28068), which included doxorubicin (DOX) covalently bound by a tetrapeptide linker.[116] The peptide (Gly-Phe-Leu-Gly) is stable in the plasma, but can be cleaved off by lysosomal enzymes of tumor cells[260] enabling the controlled release of the DOX within the tumor cell.[261] In addition, the conjugate has shown to concentrate within the solid tumor models of rats.[262] After phase I studies revealed signs of activity and a 5-fold decrease in toxicity compared to the pure anthracycline,[116] phase II trials on application for breast, non-small cell lung and colon cancer were initiated. Positive responses were indicated for breast and for non-small cell lung, while none were observed in case of colorectal cancer. A related compound to PK1, named PK2 (FCE28069), was modified by incorporation of a galactosamine group, which was designed to increase the uptake in liver tumor cells by interaction with the asialoglycoprotein receptor. After the PHPMA-DOX-galactosamine conjugate was investigated in preclinical studies,[263] the phase I trial revealed that the maximum tolerated dose (MTD) was reduced to approximately half the value of PK1, although the molar mass and the loading ratio were similar.[264] An increased uptake due to the hepatic targeting was confirmed by planar imaging and single photon emission computed tomography (SPECT) with ^{123}I-labeled PK2, while the conjugate without galactosamine (PK1) revealed no effect. However, despite showing promising results, both clinical studies (PK1 and PK2) were discontinued for undisclosed reasons.

For decades, platinum complexes have represented a major class of chemotherapeutics, which have been used for the treatment of solid tumors. Although numerous different Pt analogues have been investigated in preclinical and clinical studies, cis-, carbo-, and oxaliplatin are the only metal-based anticancer agents in routine clinical use. Recently, the drug conjugates AP5280 and AP5286 have entered clinical trials. A diamine platinum(II) (AP5280) or a diaminocyclohexane platinum(II) (AP5286) moiety, respectively, are bound to a dicarboxylate ligand that is linked to PHPMA *via* the tetrapeptide spacer Gly-Phe-Leu-Gly.[265] This cathepsin B sensitive linker has already been mentioned for PK1 and PK2. For AP5280, preclinical studies revealed a high antitumor efficiency and increased MTD compared to the established clinical standards cis- and carboplatin.[266] In the case of AP5286, we can only refer to a handful of references that claim phase I trials that are currently ongoing.[236, 267] Abeona Therapeutics (formerly Access Pharmaceuticals) has decided to focus on a third generation polymer which is based on an improved polymer carrier.[115] ProLindac™ (AP5346) represents a 25,000 g mol^{-1} (M_w) polymer delivery vehicle based on PHPMA, to which a diaminocyclohexane (DACH) platinum is conjugated.[268] The pH-sensitive linker causes a more rapid release of the platinum in environments of low pH value, as it is typically found in many tumor sites. ProLindac™ is currently in clinical development phase II in cancer patients with solid tumors. The phase I/II monotherapy study on patients with recurrent ovarian cancer has been completed and demonstrated efficiency and safety.[268-269] This opens the field for further clinical studies of ProLindac™ in combination with other chemotherapeutic agents, *e.g.* TXL.[270] Two other PHPMA conjugates, which entered clinical phase I trials, are bound to TXL or CPT, respectively. In the case of TXL (PNU-166945), the drug is conjugated to the PHPMA backbone *via* the previously mentioned enzymatically degradable tetrapeptide linker. One patient with advanced breast cancer had a partial response. The study had to be discontinued due to severe neurotoxic effects observed in additional rat studies.[271] PNU-166148 is a copolymer consisting of HPMA, very few units of *N*-(2-hydroxypropyl)methacryloyl glycinamide and methacrylamide units, to which CPT is bound through the degradable Gly-6-amino-hexanoyl-Gly spacer (**Figure 3**). The conjugate was developed by Pharmacia and Upjohn to overcome problems in the clinical delivery of CPT, which are related to the limited solubility of the active form (closed lactone ring) or the poor activity of the more soluble open ring form. With conjugation of the closed form of CPT to the copolymer, the solubility was maintained while the drug can be released by the pH-dependent or enzymatic degradation of the linker. There are three different phase I studies described in literature.[272]

The obtained results revealed changes in the pharmacokinetics of CPT with a prolonged half-life for both carrier-bound and released-CPT. However, the studies lacked answers to potential pharmacodynamic benefits, and revealed no sign of significant antitumor activity. The toxicities of the studied conjugates were similar to the pure compound CPT. Therefore, Pharmacia and Upjohn decided to discontinue further clinical development of PNU-166148.

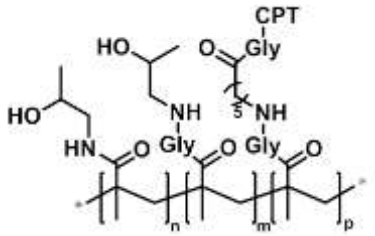

Figure 3. Schematic representation of the chemical structure of the camptothecin(CPT)-conjugate of the copolymer PNU-166148.

All PHPMA conjugates which have been investigated in clinical studies are exclusively applied for cancer treatment. Although PHPMA is well-established as a biocompatible drug carrier and a promising alternative to PEG, protein conjugates of this polymer class are less developed. However, in recent years, the research on PHPMA copolymers for the treatment of non-cancerous diseases has increased tremendously (see Chapter 4). These innovative and promising developments in the rational design, synthesis, and evaluation of novel PHPMA copolymer-drug conjugates have been highlighted elsewhere.[273]

Poly(glutamic acid) (PGluA). PGluA represents a well-established type of polymer which frequently appears in clinical studies. The conjugate with TXL (CT-2103) is one of the few successful polymer-drug conjugates to date which is known under the name Opaxio™ (formerly as Xyotax™, CTI BioPharma). It has already successfully finished phase III trials where it proved its efficacy against ovarian and non-small cell lung cancer in combination with other standard chemotherapeutics.[274] Opaxio™ features an extremely high loading capacity (~37 wt% TXL) compared to other polymer conjugates. Key advantages of the material are the inherent biodegradability of the polymer backbone and the related release of TXL or its derivatives *in vitro* and *in vivo* by enzymatic cleavage in the presence of cathepsin B.[275] In 2006, CTI BioPharma planned a new phase III study of 1,500 women suffering from ovarian cancer with the aim to improve survival rates. Two years later, CTI announced that the European Medicines Agency (EMA) has accepted to review CTI's Marketing Authorization Application for Opaxio™ for first-line treatment of patients with non-small cell lung cancer.[276] We expect that Opaxio™ will be on the market for the treatment of different types of cancer in the near future. In a similar manner, CPT was conjugated to PGluA (CT-2106) and the polymer-drug conjugate has already finished a phase I study (advanced solid malignancy).[277] According to an exclusive record, a phase II study on the treatment of advanced metastatic ovarian cancer was completed, but no results were published so far (NCT00291837).

Poly(2-oxazoline)s (POx). The conjugation of the FDA-approved dopamine agonist, rotigotine (high affinity for the subclass of dopamine receptors in the brain that mediate dopamine signaling), to a poly(2-ethyl-2-oxazoline) (PEtOx) backbone (SER-214) resulted in a stimulant, which displayed an impressive efficacy *in vivo*.[278] The continuous dopaminergic stimulation profile provided by SER-214 represents a powerful tool in the treatment of the Parkinson's disease. In October 2015, Serina Therapeutics started to recruit participants for a clinical phase I study (NCT02579473). Serina Therapeutics is furthermore offering a versatile POx-platform (POZ™) for multiple applications in drug delivery.[279]

Poly(vinyl ether) (PVE). Arrowhead Pharmaceuticals follows a concept of covalent attachment of the genetic material to the polymer backbone with triggered intracellular release. This platform is named Dynamic PolyConjugate (DPC). DPCs are composed of an amphipathic butyl- and amine PVE (PBAVE, **Figure 4**) that has shown the best transfection performance in trial and error experiments.[280] To this backbone, GalNAc as hepatic targeting ligand and PEG are attached as

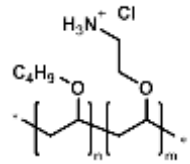

Figure 4. Schematic representation of the chemical structure of the amphipathic butyl- and amine poly(vinyl ether) (PBAVE).

well as a siRNA that is linked *via* a disulfide bond.[281] Once taken up by a cell, PEG and GalNAc are split off and the membrane-disrupting PBAVE is exposed to promote the endosomal escape (Figure 5). The siRNA is then released in the cytosol under the existing reducing conditions. ARC-520, ARC-521 and ARC-AAT are the formulations in clinical trials for the treatment of liver related diseases that are based on the DPC platform.

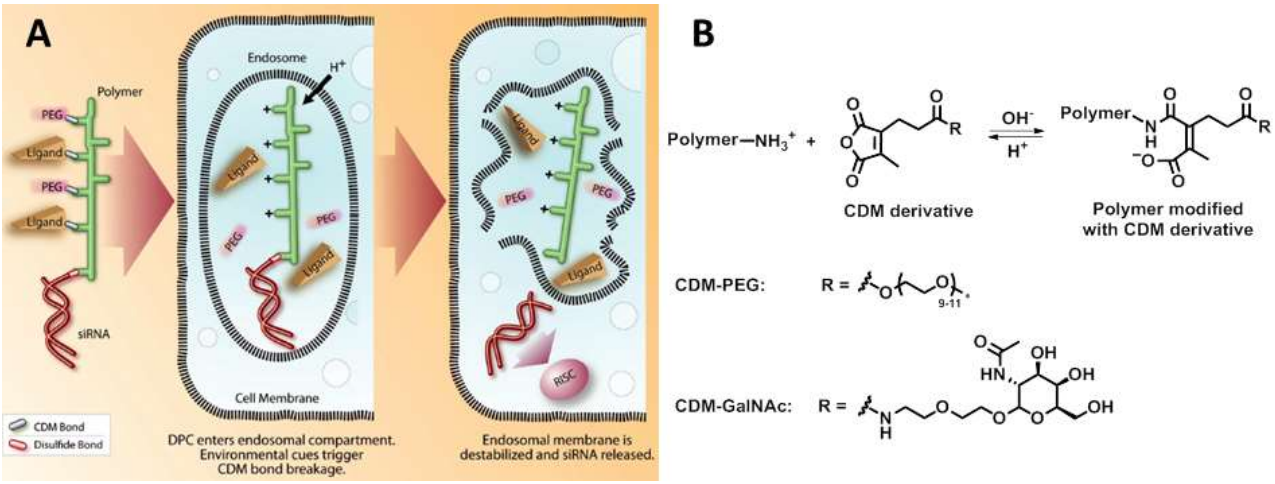

Figure 5. The proposed mechanism of siRNA delivery. A) Schematic representation of the siRNA Dynamic PolyConjugate (DPC), its cellular uptake, disassembly in the low pH environment of the endosome, and release of the siRNA into the cytoplasm of the target cell (CDM = Carboxylated dimethyl maleic acid); B) mechanism of pH-sensitive CDM chemistry and the structures of the CDM derivatives used in this study. Depicted is the reaction of CDM with free tertiary amines on the polymer, which is reversible under acidic conditions. Reprinted from [281] with permission of National Academy of Sciences, Copyright (2017).

Table 6. Synthetic polymer-drug conjugates in clinical trials (PEG-alternatives).

TRADE NAME	POLYMER SYSTEM	DRUG	INDICATION/USE	MANUFACTURER	STATUS
Zinostatin Stimalmer® (SMANCS)	Poly(styrene-*co*-maleic anhydride)	NeoCardioStatin	Hepatocellular carcinoma	Astellas Pharma	Market
PK1, FCE28068	PHPMA	DOX	Lung and breast cancers	Pfizer	Phase II (NCT00003165, Disc.)
PK2, FCE28069	PHPMA	DOX-Galactosamine	Hepatocellular carcinoma	Pfizer	Phase I[264] (Disc.)
AP5280	PHPMA	Carboplatin platinate	Various cancers	Abeona Therapeutics	Phase I/II[282]
AP5286			Various cancers	Abeona Therapeutics	Phase I[236]
ProLindac™, AP5346	PHPMA	DACHplatin	Ovarian, melanoma & colorectal cancers	Abeona Therapeutics	Phase II (NCT00415298)
PNU-166945	PHPMA	TXL	Various cancers (Breast cancer)	Pfizer	Phase I[271] (Disc.)
PNU-166148	PHPMA	CPT (MAG)	Various cancers	Pfizer	Phase I (NCT00004076, Disc.)
OPAXIO™, CT-2103, Paclitaxel poliglumex, (formerly Xyotax™)	PGluA	TXL	Lung, ovarian, colorectal, breast & esophageal cancers	CTI BioPharma	Market

CT-2106	PGluA	CPT	Colorectal, lung & ovarian cancers	CTI BioPharma	Phase II (NCT00291837)
SER-214	POx	Rotigotine	Parkinson's Disease	Serina Therapeutics	Phase I (NCT02579473)
ARC-AAT	PBAVE	siRNA	Liver disease associated with alpha-1 antitrypsin deficiency	Arrowhead Pharmaceuticals	Phase II (NCT02900183)
ARC-520	PBAVE	siRNA	Hepatitis B	Arrowhead Pharmaceuticals	Phase II (*e.g.* NCT02065336, NCT02738008)
ARC-521	PBAVE	siRNA	Hepatitis B	Arrowhead Pharmaceuticals	Phase I (NCT02797522)

DOX: doxorubicin, DACH: diaminocyclohexane, TXL: paclitaxel, MAG: (20-O-(N-methacryloyl-glycyl-aminohexanoyl-glycyl)), CPT: camptothecin.

3.2 Micro- and nanoparticulate drug carriers

Polymeric micro- and nanoparticulate drug carriers for active pharmaceutical ingredients (APIs) have been in the focus of intense research since the mid 90's. In the best case, the API is protected during the delivery and released in a controlled way at the targeted site, which reduces the required frequency of administration, the therapeutic dose, and the possibility of adverse side effects, reducing issues related to patients' compliance.[283] The term 'microparticle' by definition refers to particles with dimensions between 100 nm and 100 µm, while particles are called 'nanoparticles' if their size ranges from 1 to 100 nm.[284] However, several materials are considered as nanoparticles in literature although they slightly exceed the defined limit, but still exhibit similar properties. Therefore, we do not strictly comply with the given definition, but subdivide the materials according to their properties or the route of administration, respectively. Nevertheless, the size of all mentioned nanoparticles does not exceed 500 nm, which is still accepted.[284]

In the context of this review, the terms polymeric micro- and nanoparticles summarize stable solid dispersions (prepared by emulsion polymerization of monomers or direct dispersion of premade polymers), which also include polymeric micelles (including cross-linked micelles) or vesicles (often called polymersomes) as well as modified liposomes, and polymer-based micro- and nanogels, but also polyplexes. The latter are formed by electrostatic interactions between genetic materials (DNA, siRNA, mRNA) and cationically charged hydrophilic polymers in solution. The different sizes of nano- and microparticles obviously influence their properties as for example nanoparticles have a reduced tendency to aggregate in comparison to microparticles. Concerning drug delivery applications, the size influences key parameters like the distribution within the body, the ability to cross biological barriers, or the uptake into cells. Larger microparticles, for example, need to be delivered directly to the site of action, but they also remain at this location and act as a depot releasing their payload over weeks, *e.g.* by slow degradation of the microparticles. On the contrary, nanoparticles distribute in the body and cross barriers, but they are also able to penetrate into leaky vascular tissue usually observed in tumors and inflamed sites.[285] Moreover, they are small enough to enter cells *via* pinocytosis, which is the "cell drinking" of any cell type, while microparticles are only taken up by phagocytosis. As a consequence of these variations in the properties, the question of the right size of the drug delivery vehicle strongly depends on the application and the route of administration. The most common way of administration is certainly the oral uptake. The main challenges for particulate carriers are the protection of the drug during the harsh conditions in the gastrointestinal (GI) tract and the transport through the GI epithelium including a mucus layer as additional barrier.[286] For the direct targeting of the GI barrier layers itself, particles of about 2 µm reveal the best adsorption after oral application.[283] Smaller nanoparticles are found to cross these barriers, but for a more detailed understanding the area of oral

administration of nanosized materials still requires significant basic research.[287] In pulmonary administrations, particles around 5 µm penetrate deeply in the smaller airways of the lung, which is well-suitable for topical treatment.[288] In contrast, 1 to 2 µm particles are able to deposit in the capillary-rich alveoli, where systemic drug delivery is targeted. Nanoparticles can be exhaled if they are not immobilized by aggregation or in suspension as droplets. In the case of an intravitreal, subcutaneous or intramuscular administration, microspheres are preferably in the order of 10 to 250 µm to avoid uptake by macrophages while minimizing inflammatory reactions. For local administration in the brain, the microspheres should not be larger than 100 µm to preserve the structure of the brain. Considering intravenous nanotherapies, particles should preferably have a size below 200 nm to increase the circulation time in the blood stream and avoid filtration by the spleen or clearance by renal excretion.[289] The probably most difficult route of administration is the transport through the skin, which represents a natural barrier against particle penetration if not damaged.[290] Common nano- and microparticles (above 10 nm) are not able to cross the stratum corneum, but may accumulate in the hair follicles (300 to 600 nm sized particles).[291] An overview of these different routes of administration and the suitable size range is given in Figure 6.

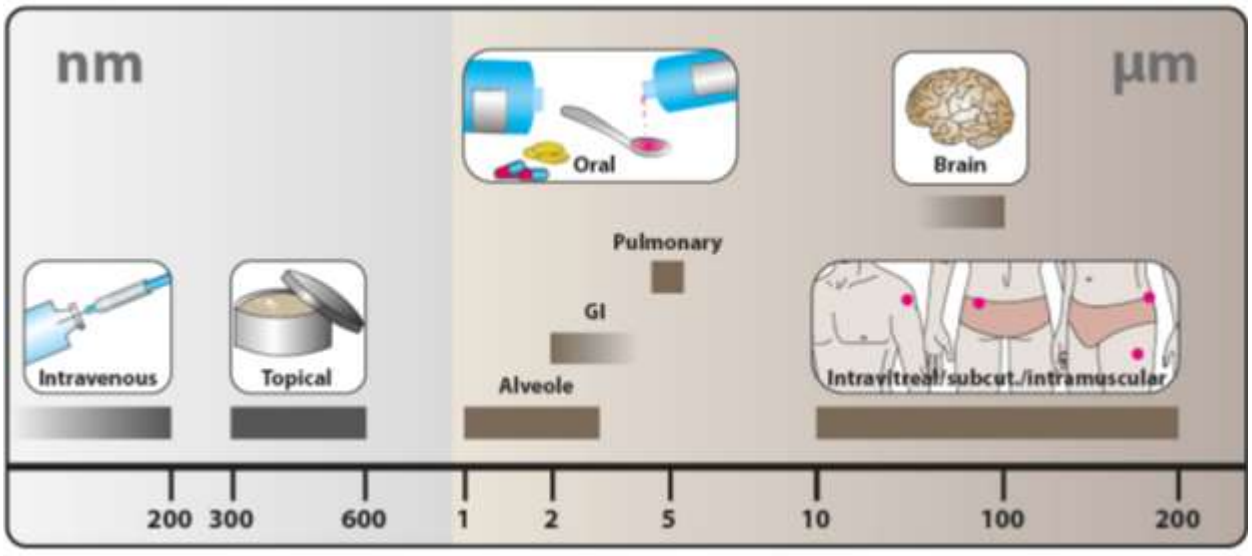

Figure 6. Overview of different routes of administration of micro- and nanoparticulate drug carriers; GI: gastrointestinal tract.

3.2.1 Solid colloidal dispersions

Microparticle dispersions. For the local and continuous delivery of APIs, injections of degradable microparticles certainly are the most commonly chosen route of administration. The particles are usually produced by emulsion techniques, *i.e.* the polymer and the drug are dissolved in a suitable organic solvent and the mixture is suspended in water, while the solvent is evaporated by continuous stirring. Additional surfactants such as PVA might be added to stabilize the resulting particles. Besides the classic procedure more sophisticated double (multiple) emulsion techniques were developed for example to encapsulate water soluble compounds, but also other methods like spray drying or precipitation

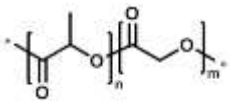

Figure 7. Schematic representation of the chemical structure of poly(lactic-*co*-glycolic acid) (PLGA).

techniques are applied.[292] As polymers poly(lactide acid) and the copolymer poly(lactic-*co*-glycolic acid) (PLGA, Figure 7) are the most accepted and also approved materials for microparticle formation. The tunable biodegradability of the polymer (by varying molar mass, structure (end-group) and composition (lactic acid/glycolide ratio)) and morphology of the particles enables PLA/PLGA to be easily engineered regarding their aimed distribution and release profiles. Marketed products of PLGA microparticles include long-acting dosage forms with *in vivo* life-times ranging from 2 to 80 weeks if administered as a gluteal intramuscular or abdominal subcutaneous depot for peptides, proteins but also small molar mass drugs.[293] Table 7 provides an overview of marketed PLGA microparticle products (no other polymers are used in marketed microparticle formulations) treating various diseases such as cancer and psychological disorders. They are also used in dentistry as local antibiotics and in animal husbandry for deworming.

An innovative route of administration is the *in situ* formation of biodegradable matrices after the liquid carrier (*e.g.* DMSO) has diffused quickly from the polymeric solution towards surrounding tissue. Risperidone ISM® represents a PLGA microparticle releasing risperidone for the treatment of schizophrenia. Clinical phase II trials have been successfully performed (NCT02086786).[294]

Table 7. List of marketed controlled release parenteral microspheres based on PLGA.

TRADE NAME	DRUG	INDICATION/USE	MANUFACTURER[a]
Risperdal Consta®	Risperidone	Schizophrenia	Janssen
Zoladex®	LHRH agonists	Prostate cancer	AstraZeneca
Lupron Depot®, Eligard®, Enantone®/Trenantone®	Leuprolide	Prostate cancer	AbbVie, TOLMAR Pharmaceuticals, Takeda
Decapeptyl®, Trelstar®, Pamorelin®	Triptorelin	Prostate cancer	Ferring Pharmaceuticals, Allergan™, Ipsen Pharma
Profact Depot®, Suprefact Depot®	Buserelin	Prostate cancer, endometriosis	Sanofi
Bydureon®	Exenatide	Diabetis	AstraZeneca
Sandostatin® LAR, Somatuline® LA	Octreotide	Acromegaly, diarrhea	Novartis
Nutropin Depot®	Somatropin	Growth hormone deficiency	Genentech/Alkermes® (disc.)
Vivitrol®	Naltrexone	Opioid- & alcohol dependence	Alkermes®
Arestin®	Minocycline HCl	Peridontal disease	Valeant® (disc.)
Longrange®	Eprinomectine	Parasitic disease	Merial (Sanofi)

[a] Selection thereof.

The versatility and unique properties of PLGA and PLA certainly promote the domination of the market of these materials considering microparticles for drug delivery. As a consequence, it is no surprise that further developments, which are currently in clinical trials, are also based almost exclusively on these polymers. To the best of our knowledge, only two alternatives have at least entered the stage of clinical testing. The first one is a microparticulate formulation consisting of paclitaxel and a biodegradable polyphosphoester (NCT00005046).

The polymer is a copolymer of short PLA oligomers and ethyl phosphate (P(DAPG-EOP)) (Figure 8).[295] The microparticles (Paclimer®) were injected into the peritoneal cavity for treatment of recurrent ovarian cancer.[296] The study (phase I) verified the beneficial properties of the material ensuring a controlled and continuous release over more than eight weeks. However, the presence of polymer filaments after several months indicated a slow degradation and caused a marked inflammatory response. The second one is the microsphere Retin-A Mikro® (Valeant®), which is based on the Microsponge® technology comprising styrene, divinylbenzene and methyl methacrylate and the starting material ethylene glycol dimethacrylate in its polymer backbone.[297] Tretinoin is encapsulated in the polymer in the application form of a skin cream that slowly releases the active medication to treat acne vulgaris.

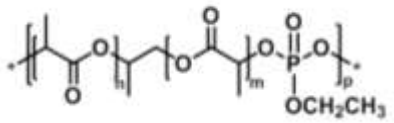

Figure 8. Schematic representation of the chemical structure of the copolymer consisting of short PLA oligomers and ethyl phosphate (P(DAPG-EOP)).

Amphiphilic block copolymer micelles. Polymeric micelles are created by dispersion of a block copolymer consisting of a hydrophobic and a hydrophilic domain. The block-like and amphiphilic structure is essential for polymeric micelles and their self-assembly behavior.[284] In contrast to small molecule surfactants, polymeric micelles often seem to be not dynamic, which means that there is almost no exchange of polymer molecules between the aggregates, and the polymeric micelles are kinetically frozen.[298] However, in most cases these exchange dynamics are simply not investigated as the experiments require long acquisition times (up to several days or weeks) to provide a detectable signal. According to its definition, polymeric micelles are still in an equilibrium with its dissolved polymer chain.[284] Consequently, the formation and stability of the micelles depend on the concentration. However, with increasing size of the hydrophobic block this equilibrium can be shifted towards the formation of micelles, and the critical micelle concentration (CMC) might be below the detection limit.[299] Nevertheless, a common concept to overcome any stability issues related to polymeric micelles is the cross-linking of the micellar core, which ideally can be used to covalently entrap the API.[300] The research and development of polymeric micelles has a very strong focus on cancer therapy. The toxic and undesirable side effects of chemotherapeutic agents are supposed to be diminished by using these nanoparticulate carrier systems.[301] The low lymphatic drainage of tumors and the highly vasculature tumor tissue results in an enhanced penetration and retention (EPR) effect of the micelles, which consequently yields a passive targeting of tumor tissue. Even more efficient is the use of micelles bearing targeting moieties, which allow selective recognition of specific receptors that are overexpressed in cancer cells. Recently published review articles cover the outcomes of clinical research and also show the results of preclinical studies in terms of polymeric nanoparticles in cancer therapy.[301-302] However until now, none of these formulations reached FDA approval for cancer therapy. Only one micellar delivery system is on the South Korean market (Table 8).[303] Genexol® PM is a paclitaxel encapsulating polymeric micelle consisting of a block copolymer of methoxy-PEG and poly(D,L-lactic acid) (Figure 9A).[304]

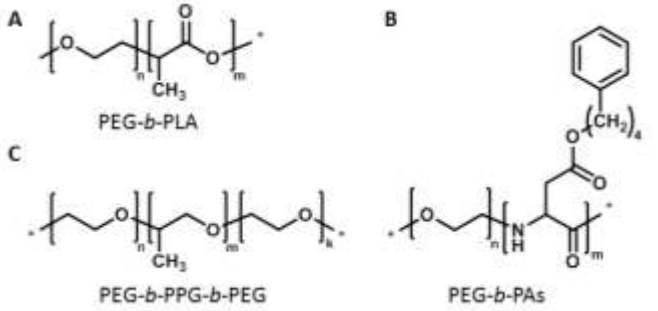

Figure 9. Schematic representation of the chemical structures of the block copolymers of A) methoxy-PEG and poly(D,L-lactic acid) (Genexol® PM); B) PEG and esterified PAs (4-phenyl-1-butanol) (NK105); C) PEG and PPG (also called Pluronic®, SP1049C).

Nevertheless, a considerable number of micellar systems are currently undergoing clinical trials in various stages. In the following, we provide an overview of the various materials, which are clinically tested, and exemplarily describe the applications where these materials are in latest stage of clinical trials. In general, most of these micellar

formulations are also in preclinical/clinical trials for treatment of other cancerous diseases, which shows the potential of polymeric nanoparticles in cancer therapy in future. A good example is the block copolymer PEG-*b*-PLA which is identical to the material used in Genexol® PM. This polymer is further used for the formulation of docetaxel encapsulating PEG-*b*-PLA polymeric micelles with similar sizes (20 to 50 nm) named Nanoxel®-PM, which is in clinical phase I.[305] Other materials also take advantage of the generally accepted use of PEG for the hydrophilic block. In contrast, a variety of different polymers is used for the hydrophobic block. NK105 uses a block copolymer of PEG and partially hydrophobized poly(aspartate) (PAs) (esterification of the carboxylic groups with 4-phenyl-1-butanol, Figure 9B) for the delivery and release of docetaxel.[306] SP1049C is a mixture of non-ionic PEG-*block*-PPG-*block*-PEG copolymers (Pluronic® L61, Pluronic® F127, Figure 9C) that form a micelle to encapsulate doxorubicin.[307] SP1049C has the state as an orphan drug for gastric cancer as approved by the FDA.

With the effort to improve the specifity of nanoparticles, targeted strategies were developed and already entered clinical trials. BIND-014 is the outcome of a combinatorial library of nanoparticles based on PEG-*b*-PLA and PEG-*b*-PLGA that encapsulate docetaxel and bear a prostate-specific membrane antigen (PSMA) on the micelle surface. PSMA is a tumor antigen preferentially expressed on prostate cancer cells and vasculature of non-prostate solid tumors.[308] The PSMA substrate analog inhibitor S,S-2-(3-(5-amino-1-carboxypentyl)-ureido)-pentanedioic acid (ACUPA) is covalently attached to a PEG-*b*-PLA. A mixture of PEG-*b*-PLA and PEG-*b*-PLA-ACUPA is finally used for the micelle formation in a microfluidic supported emulsion/solvent evaporation process. BIND-014 was the best performing candidate in terms of particle size, drug loading, targeting ligand density, PEG/PLA ratio and so on. The same technology (Accurins® technology) was recently used to deliver a selective Aurora B kinase inhibitor, AZD2811, that induces apoptosis in tumor cells.[309] Increased encapsulation efficiency and reduced drug leakage could be achieved by simple ion pairing of AZD2811 and are currently tested in phase 1 studies. Preclinical studies using the same Accurins® portfolio involve BIND-510 (encapsulated drug: Vincristine, PEG-*b*-PLA with PSMA targeting) and others as proposed by BIND Therapeutics.[310] A critical point is that the physical entrapment of drugs can be associated with drug leakage before reaching the side of action.

Therefore, the covalent attachment *via* labile linkers to the polymer backbone can be advantageous. A popular system is a block copolymer of PEG and polyglutamate. The polyaminoacid is able to complex different platinum complexes, which renders the polymer amphiphilic. NC-6004 is delivering *cis*-platin and already entered clinical phase III. The same concept is applied for NC-4016 in phase I, using 1,2-diaminocyclohexane platinum (DACHplatin) to modify PEG-*b*-PGlu block copolymers. Also other anti-cancer drugs were covalently attached to the PGlu block: NK012 is functionalized with SN-38, a camptothecin derivative, and completed clinical phase II for the treatment of breast and lung cancer. A similar system using poly(amino acid) is NK911, with DOX covalently linked to the carboxy groups of the copolymers of PEG and PAs. NK911 revealed less stability and more drug release but also higher accumulation at other cell regions compared to liposomal doxorubicin (Doxil®).[311] Clinical phase I finished in 2004 and did not recruit for phase II until now. There are only few examples of materials in clinical trials that are not aiming at the treatment of cancer. SEL-068 is a PEG-*b*-PLGA-based micelle loaded with peptides for the treatment of nicotine addiction.[312] This nicotine vaccine creates nicotine specific antibodies that bind free nicotine and prevent it from crossing the BBB. The same particle platform (Synthetic Vaccine Particle (SVP™)) is used for the design of SEL-110 in antigen-specific immunotherapy. SEL-110 is loaded with specific protein- or peptide antigens and rapamycin and aims to prevent unwanted anti-drug-antibodies from forming.[313]

Table 8. List of active clinical trials using amphiphilic block copolymer micelles.

TRADE NAME	POLYMER SYSTEM	DRUG	INDICATION/USE	MANUFACTURER	STATUS
Genexol® PM (US: Cynviloq™, IG-001)	PEG-*b*-PLA	Docetaxel	Breast, lung, ovarian cancer	Samyang Biopharm	Market (South Korea)

Nanoxel®-PM (Docetaxel-PNP)	PEG-*b*-PLA	Docetaxel	Solid tumors	Samyang Biopharm	Phase I (NCT02274610)
NK105	PEG-*b*-PAs	Docetaxel	Gastric, breast cancer	NanoCarrier®	Phase III (NCT01644890)
SP1049C	PEG-*b*-PPG-*b*-PEG (Pluronic® L61, F127[a])	DOX	Adenocarcinoma	Supratek Pharm	Phase II[307]
BIND-014 (Accurins® technology)	PEG-*b*-PLGA, PEG-*b*-PLA	Docetaxel	Solid tumors	BIND Therapeutics/ Pfizer	Phase II (*e.g.* NCT01812746, NCT01792479,)
AZD2811 (Accurins® technology)	PEG-*b*-PLA	AZD2811	Solid tumors	AstraZeneca	Phase I (NCT02579226)
NC-6004	PEG-*b*-PGlu	Cisplatin	Solid tumors	NanoCarrier®	Phase III (NCT02043288)
NC-4016	PEG-*b*-PGlu	DACHplatin	Solid tumors	NanoCarrier®	Phase I[314]
NK012	PEG-*b*-PGlu	SN-38	Breast, lung, colorectal cancer	Nippon Kayaku	Phase II (*e.g.* NCT00951613, NCT00951054)
NK911	PEG-*b*-PAs	DOX	Pancreatic, colorectal cancer	n.a.	Phase I[311] (disc.)
SEL-068	PEG-*b*-PLGA	TLR agonist and T cell helper peptide	Nicotine addiction	Selecta Biosciences	Phase I (NCT01478893)
SEL-110	PEG-*b*-PLGA	Rapamycin, peptide antigen	Production of anti-drug antibodies, unwanted immune response	Selecta Biosciences	Phase I (NCT02648269)

DOX: doxorubicin, DACH: diaminocyclohexane; [a] L = liquid, F = flake/solid, the first one or two digits (in a three-digit number) in the code, multiplied by 300, indicates the approximate molar mass of the PPG block and the last digit of this code × 10 provides the percentage PEG content; n.a.: not applicable.

Nanoparticle dispersions. Besides the large number of micellar structures made from amphiphilic block copolymers only few systems have entered clinical studies, which are solid nanoparticle dispersions prepared by nanoprecipitation or emulsion polymerization (Table 9). CRLX101 is a nanoparticle formulation consisting of a statistical copolymer based on β-cyclodextrin and PEG, that is hydrophobized by conjugation of CPT to the cyclodextrin ring *via* an acid labile glycine linker.[315] The current studies are recruiting participants for several clinical studies in cancer therapy, which shows the potential of this formulation as novel nanomedical device. CRLX301 has recently started phase IIa and uses the same polymer platform as CRLX101 but with docetaxel as active agent.[316] While the previously mentioned system is still stabilized by the amphiphilic character of the polymer, DOX-Transdrug is a solid nanoparticle dispersion that is produced by emulsion polymerization of isohexyl cyanoacrylate in the presence of DOX. DOX-Transdrug is used for the treatment of liver cancer by local injection *via* the hepatic artery and has recently entered clinical phase III. This system was also successfully applied to pass the BBB for the therapy of glioblastomas as observed in rats.[317] Another acrylate-based nanocarrier is prepared in a comparable way resulting in mitoxantrone (dihydroxyanthracenedione, DHAD) encapsulating poly(isobutyl cyanoacrylate) nanoparticles (DHAD-PBCA-NP). The formulation shows good efficacy in treating liver cancer and, thus, enhances the survival period.[318] DHAD-PBCA-NP reached clinical phase II but did not continue since 2009.

Table 9. List of active clinical trials using nanoparticle dispersions.

TRADE NAME	POLYMER SYSTEM	DRUG	INDICATION/USE	MANUFACTURER	STATUS
CLRX101 (IT-101)	P(EG-*co*-cyclodextrin)	CPT	Lung cancer, renal cell carcinoma	Cerulean™	Phase II (*e.g.* NCT02010567, NCT02769962)

CRLX301	P(EG-*co*-cyclodextrin)	Docetaxel	Solid tumors	Cerulean™	Phase I/IIa (NCT02380677)
Livatag® (DOX-Transdrug)	Poly(isohexyl cyanoacrylate) coated with Tween 80	DOX	Liver cancer	Onxeo	Phase III (NCT01655693)
DHAD-PBCA-NP	Poly(isobutyl cyanoacrylate)	Mitoxantrone	Liver cancer	n.a.	Phase II[318] (Disc.)

CPT: campthothecin, DOX: doxorubicin; n.a.: not applicable.

Modified liposomes. Liposomes are structurally slightly different species also using polymers in a nanoparticular device. They are composed of phospholipids, which self-assemble into lipid bilayers (able to incorporate lipophilic molecules) surrounding an aqueous core (able to incorporate hydrophilic molecules).[319] For improving the desired properties, the phospholipids can be covalently modified with polymers or targeting functions resulting in surface modified liposomes. For example, PEG is generally used to improve the circulation and drug retention. In addition to the stealth effect, PEG is acting as spacer molecule between lipid structures and targeting functions. Besides Doxil® being the most prominent example of a PEG-containing liposome on the market[320] there are also Lipodox®,[321] Oncodox® PEG[322] and Lipoplatin™[323] showing good performances in cancer treatment with DOX and cisplatin, respectively, as APIs (Table 10). The heat-responsive liposomal formulation ThermoDox® is now recruiting patients for a phase III study of PEGylated liposomal DOX.

Table 10. List of PEG-modified liposomes on the market or in active clinical trials in phase III.

TRADE NAME	DRUG	INDICATION/USE	MANUFACTURER	STATUS
Doxil® (Caelyx®)	DOX	Ovarian cancer, AIDS-related Kaposi's sarcoma, multiple myeloma	Janssen	Market
Lipodox®	DOX	Metastatic carcinoma of the ovary, metastatic breast cancer, AIDS related Kaposi's Sarcoma	Sun Pharma	Market
Oncodox® PEG	DOX	Ovarian cancer, breast cancer, AIDS related Kaposi's Sarcoma	Ciplamed	Market
Lipoplatin™	Cisplatin	Pancreatic cancer, head and neck cancer, mesothelioma, breast cancer, non-cell lung cancer	Regulon	Phase III[324]
ThermoDox®	DOX	Primary liver cancer, breast cancer	Celsion	Phase III (NCT02112656)

DOX: doxorubicin.

3.2.2 Polyplexes

The delivery of small molecules either encapsulated or conjugated to yield apoptosis in cancer cells is only one strategy in cancer therapy. The pharmaceutical industry also holds promise on gene therapy. However, to transport genetic material such as plasmid DNA (pDNA), short interfering RNA (siRNA) and messenger RNA (mRNA) into body cells these structures must be protected against degradation and shielded to avoid clearance. A common way is the complexation of the negatively charged genetic material with cationically charged polymers *via* electrostatic interactions. The result is a so-called polyplex, which ideally should mimic the nature of viruses and result in efficient gene delivery and transfection without showing an immune response. Poly(ethylene imine) (PEI) and its variations are among the most studied materials for this purpose. In contrast to other cationic polymers, linear and branched PEI are capable of mediating endosomal escape, which is essential for transfection.[325] Other prominent examples are poly(L-lysine) or poly(2-(dimethylamino)ethyl methacrylate) (PDMAEMA).[326] In general, it can be said that only pDNA and RNA therapeutics passed preclinical studies so far for clinical trials.[325, 327]

Different PEI formulations and modifications that all resolved general toxicity issues of PEI *in vitro* and *in vivo* reveal encouraging results in clinical phases (Table 11). SNS01-T is a jetPEI® formulation, *i.e.* a linear PEI dissolved in a special buffer system. Although the precise composition is undisclosed, it is expected to have a molar mass (M_n) of about 22,000 g mol^{-1}. The polyplex contains both a B-cell-specific expression pDNA and a siRNA, which suppresses hypusinated eIF5A. A reduction of eIF5A levels was found to sensitize myeloma cells to apoptosis.[328] CYL-02 is also based on jetPEI® as transfection agent and in clinical phase II for pDNA delivery. It strongly inhibits tumor progression and dissemination of pancreatic cancer after intratumoral administration using endoscopic ultrasound.[329] A promising intravenously administered system is a polyplex of the pDNA BC-819 with PEI. BC-819/PEI targets cancer cells that generally express the H19 gene, which activates Diphtheria Toxin A (DTA) and leads to cell death, whereas healthy cells that are also exposed to the pDNA are not affected. In 2016, BC-819 was announced to commence phase III.[330] In addition, BioCancell developed a dual-DTA expression system named BC-821, which is a pDNA that is again transfected with PEI and switches the distinct promoters H19 and IGF2-P4.[331] The dual expression system may have the benefit of enhanced cancer cell toxicity and a higher chance that at least one of the promoters will be active in any tumor. A further pDNA PEI-based formulation in clinical trials is EGEN-001. It contains a cholesterol modified low molar mass branched PEI that is also PEGylated.[332] EGEN-001 is designed for direct injection into cancerous tissue where it increases the local concentration of interleukin 12 (IL-12) in the tumor microenvironment. IL-12 has several functions, amongst them it is known to potentiate antitumoral functions of the host immune system.[333] The delivery of a RNA sequence is also in the focus of Celsion by using the TheraSilence™ technology platform.[334] In general, the intrinsic cytotoxicity of PEI is a serious problem in the transfer to a FDA approved PEI-based product.

The benefit of non-viral siRNA delivery is to selectively silence gene expression *in vivo*. The first targeted (siRNA) nanoparticle formulation in clinical trials is denoted as CALAA-01.[335] The polymer matrix is a cationic cyclodextrin containing polymer prepared by polycondensation of a diamine-functionalized cyclodextrin and dimethyl suberimidate leading to a polyamidine. Adamantyl functionalized PEG with and without human transferrin ligands is complexed with the cyclodextrin moieties for steric stabilization and also for the targeting ability of the polyplexes. CALAA-01 completed phase I in 2012 but did not proceed further. However, this study was the first evidence that systemically administered siRNA induces RNA interferences in humans.[336]

In the early days of gene therapy, the discovery of interferon caused much excitement. Various forms of interferon are produced by virally infected cells and interfere with further viral growth and, thus, show promise in antitumor and antiviral therapy. The synthetic double-stranded RNA (dsRNA), an interferon that consists of a pair of polyinosinic and polycytidylic acids, is condensed with poly(L-lysine) and supplemented with carboxymethylcellulose to form Hiltonol®.[337] Probably the first clinical study using this system was already conducted in 1978.[338] Nowadays, there are many clinical trials of Poly-ICLC for various types of cancer. However, Poly-ICLC is also in clinical trials to test its efficacy as adjuvant (to boost the immune response) in HIV-infected patients. A further polylysine-based polyplex is a PEGylated version that demonstrated an effect for cystic fibrosis patients after administration of the complexed pDNA carrying the cystic fibrosis transmembrane regulator-encoding gene to the nasal mucosa in an early phase I study.[339]

Although cancer is certainly the most prominent disease to be treated by polyplex-based gene delivery, the treatment of other human diseases can also benefit of the approach if applied at the right site or by using targeting functions. The DermaVir patch is a topical application of a pDNA, encoding the entire HIV genome minus the integrase gene that is formulated with mannosylated jet-PEI® in a glucose solution.[340] For this purpose, the stratum corneum needs to be interrupted to deliver the polyplex to the Langerhans cells to be transported to the lymph nodes in order to express the HIV antigens. The DermaVir therapeutic vaccination completed phase II but did not proceed further maybe due to infection risks of the skin. A different pDNA vaccination that already started phase III trials is ASP0113. It is designed to suppress the activation of the cytomegalovirus (CMV) in transplant recipients. It basically consists of two plasmids encoding CMV glycoprotein B and phosphoprotein 65, respectively,

formulated with poloxamer, a triblock PEG-*b*-PPG-*b*-PEG (CRL1005), and a mixture of alkyl-benzyldimethylammonium chlorides (BAK, alkyl chains: C12, C14, C16, C18).[341] The hydrophobic cationic surfactant BAK and the hydrophilic CRL1005 self-assemble with the pDNA into nanoparticles.

Table 11. List of active clinical trials using polyplexes.

TRADE NAME	POLYMER SYSTEM	DRUG	INDICATION/USE	MANUFACTURER	STATUS
SNS01-T	LPEI (jetPEI®)	pDNA, siRNA	Multiple myeloma	Sevion Therapeutics	Phase II (NCT01435720)
CYL-02	LPEI (jetPEI®)	pDNA	Pancreatic adenocarcinoma	InvivoGen	Phase II (NCT02806687)
BC-819/PEI (DTA-H19)	BPEI	DNA	Bladder cancer, ovarian cancer, pancreatic adenocarcinoma	BioCancell	Phase II (NCT00595088)
EGEN-001 (GEN-1)	Cholesterol and PEG-modified PEI	DNA	Ovarian, tubal, colorectal peritoneal cancer	GOG® Foundation	Phase II (NCT01118052)
CALAA-01	Cationic cyclodextrin, adamantane modified PEG	siRNA	Solid tumors	Calando Pharmaceuticals	Phase I (NCT00689065) (disc.)
Hiltonol® (Poly-ICLC)	Polylysine, carboxymethyl cellulose	dsRNA	Brain tumor, non-small cell lung cancer, skin cancer, breast cancer	Oncovir	Phase II (*e.g.* NCT01984892, NCT02423863)
			HIV		Phase I/II (NCT02071095)
DermaVir (LC002)	Mannosylated LPEI (jetPEI®)	DNA	HIV vaccine	Genetic Immunity	Phase II (NCT00711230)
ASP0113 (VCL-CB01, formerly TransVax®)	PEG-*b*-PPG-*b*-PEG, (CRL1005)	DNA	CMV vaccine	Vical	Phase III (NCT01877655)

pDNA: plasmid deoxyribonucleic acid, siRNA: small interfering ribonucleic acid, dsRNA: double-stranded ribonucleic acid, CMV: cytomegalovirus.

3.2.3 Micro-/Nanogels

Microgels. ‚Microgels' (IUPAC name) are defined as hydrogel microparticles (also mentioned as 'microhydrogels' or 'hydrogel microspheres') formed by water soluble polymers which are physically or chemically cross-linked. In physical gels, the cross-linking points of the network are formed by non-covalent or supramolecular interactions, such as hydrogen bonds, ionic or hydrophobic interactions, respectively. On the other side covalent bonds form the links of the network in chemical gels, *i.e.* cross-linking of ready polymers on functional groups or polymerization of multivalent monomers. These three-dimensional networks fill the size gap between dendrimers/polymers (10 to 20 nm) and macroscopic hydrogels (see Chapter 3.3.1) comprising sizes from 100 nm to 100 µm according to the definition of microparticles.[342] Microgel systems possess high capacity for drug loading, are mostly biocompatible, and can be modified for biodegradability, which represent the key points to design an effective drug delivery system. Their structure features some key advantages in comparison to dendritic systems including their superior swelling behavior, the opportunity to introduce responsive modalities, and the presence of suitable gaps for encapsulation of other compounds (without the need of a chemical attachment). Besides their application as drug delivery systems, they have shown promising potential for use in adjacent fields such as diagnostics, antiviral compounds, and embolic therapies.[343] Microgel-based formulations for drug delivery have shown significant enhancements in effectiveness and safety considering certain anti-cancer drugs or other pharmaceutically active compounds, which was confirmed by numerous *in vivo* studies. Despite this progress, only very few microgels have been explored in clinical studies and several safety issues have to be overcome. The challenges in terms of cargo

delivery and their efficient clearance once they have accomplished their mission *in vivo* demand careful engineering of the microgels. This remains challenging due to the complexity of the systems and the unique structural features. To date, there are only three microgel systems based on synthetic polymers that are approved for use as drug delivery system. They are all used in the treatment of hepatocellular carcinoma (Table 12). DC Bead® is an embolic hydrogel microsphere product that is capable of being loaded with anthracycline drugs just before administration in a transarterial chemoembolization (TACE) procedure. TACE is a minimally invasive (non-surgical) procedure performed by an interventional radiologist. In this process, the microgel is not just delivering the drug, but also occludes the arteries supplying the tumor. DC Bead® is composed of a biocompatible PVA hydrogel, which has been modified with the ionic monomer sodium 2-acrylamido-2-methylpropanesulfonate (AMPS, Figure 10). The latter enables the electrostatic loading and delivery of chemotherapeutic drugs. The beads are produced by an inverse emulsion polymerization and are available in sizes from 100 to 900 µm.[344] Injected into the local artery, the formulation occludes the blood flow to the target tissue and delivers a local and sustained dose of the drug directly to the tumor. DC Bead® is approved as anti-tumor formulation with doxorubicin (DEBDOX™)[345] and irinotecan (DEBIRI™).[346] Current research is focusing on an increase of the drug doses of administered drug.[347] In addition, the microbeads can be loaded with idarubicin (IDASPHERE II) by the interaction of the positively charged protonated amine group of idarubicin hydrochloride with the sulphonate of the DC Beads®.[348] They are currently in randomized phase II studies. Special radiopaque beads (RO Beads), which are also based on the DC Bead® platform, have been investigated to not only be pharmacologically active, but allow the imaging of the active site in a rabbit VX2 liver tumor model by X-ray scans. These RO Beads were covalently modified with a triiodobenzyl group to allow a better traceability in comparison to DC beads® which were loaded with a soluble contrast agent.[349] The first commercially available RO bead, LC Bead LUMI™, was cleared by the FDA for the chemoembolization of hypervascular tumors and arteriovenous malformations.[350]

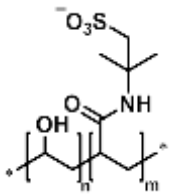

Figure 10. Schematic representation of the chemical structure of P(VA-co-2-acrylamido-2-methylpropane sulfonate).

Other commercialized microgels include the Tandem® microspheres, which are spherical, biocompatible, non-resorbable hydrogel cores based on cross-linked poly(methacrylic acid) (PMAA).[351] They are subdivided into two classes of microspheres, Oncozene® and Embozene®, which are both available in a size range from 40 to 100 µm. The latter features an additional outer layer of CeloNova's proprietary Polyzene®-F, a poly(bis(trifluoroethoxy)phosphazene) (Figure 11), which is introduced to enhance biocompatibility and reduce inflammation. These materials have been optimized for loading with a variety of drugs (Table 12). Current studies focus on the use of DOX (NCT02141906) or idarubicin,[352] loaded in the Oncozene® microspheres. Hepasphere™ represents another hydrogel microsphere, which is approved for clinical use and commercially available (in the range from 30 to 200 µm). In general, DOX is loaded into a polymer network of poly(vinyl alcohol-*co*-acrylic acid).[353] The microsphere binds drugs with the same mechanism as DC Bead®, using carboxylate instead of sulfonate groups. Recent developments in the treatment of hepatocellular carcinoma with Hepasphere™ were summarized by Malagari *et al.*.[354] LifePearl® is a PEG-based embolization hydrogel that can be loaded with chemotherapeutic agents to treat primary hyper vascular tumors or liver metastasis. The microspheres are biocompatible, hydrophilic, and precisely calibrated.[355]

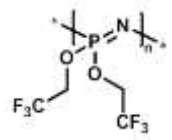

Figure 11. Schematic representation of the chemical structure of poly(bis(trifluoroethoxy)phosphazene) (Polyzene®-F).

A new injectable formulation for the delivery of IFN-α 2b is Locteron®, which is one of the few systems for continuous release of proteins that reached late-stage clinical trials. It is a microparticulate formulation encapsulating a protein which is suspended in an injection vehicle prior to subcutaneous administration.

The technology is based on PolyActive® – a variety of biodegradable poly(ether ester) segmented copolymers based on PEG and PBT. The polymers absorb water up to 65% of their weight resulting in a hydrogel network. Biolex Therapeutics announced that its remaining asset (phase III) for the treatment of hepatitis C virus (HCV) and hepatitis B virus (HBV) is finally commercialized.[356]

Nanogels. When the size of microgels is in submicron range (1 to 100 nm), they are usually specified as nanogels ('nanohydrogels', 'hydrogel nanospheres').[357] Although significant effort has been dedicated into their research,[358] there is only a limited number of nanogel systems under clinical investigations that are based on synthetic polymers. A new gel-based approach with the ability to form a depot (Medusa®) has been developed by Flamel Technologies (today: Avadel Pharmaceuticals). It enables a controlled drug release within an adjustable time ranging from one day up to one week without the often observed initial burst effect or a decreasing activity. The formulation will be administered as a subcutaneous injection. The polymer platform is based on poly(α-glutamate) (hydrophilic), where vitamin E is grafted onto (Figure 12). The resulting amphiphilic polymer spontaneously forms stable nanogels (20 to 50 nm) when dissolved in water due to the hydrophobic domains of vitamin E.[359] Different cargos (*e.g.* peptide, protein, small molecule) can be loaded into the nanogel simply by mixing the two components, and the uptake into the nanogel is solely based on non-covalent, hydrophobic and electrostatic interactions. The formulations with several therapeutic proteins (*e.g.* IL-2, IFN-α 2b and IFN-β 1a) revealed a release period of one week in animal models.[360] Clinical phase I trials were performed on the application of the interferon IFN-α 2b, which was administered to patients with genotype 1 hepatitis C virus (HVC), and the outcomes were compared to the established treatment with the respective PEGylated interferon PegIntron® (Table 3). The study demonstrated a favorable antiviral activity and safety profile using the Medusa® technology.[361] A phase II study followed (over a period of 12 weeks) in order to compare this formulation to PegIntron®, which was combined with ribavirin.[362] Currently, Avadel Pharmaceuticals explores the product Medusa® exenatide, which is called a once-a-week formulation. After successful preclinical studies on the administration to minipigs (June 2014), the company reported the completion of phase 1b trials for type 2 diabetes mellitus.[363]

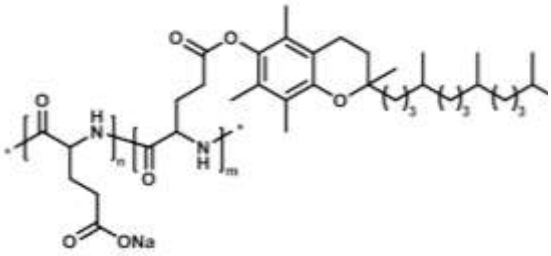

Figure 12. Schematic representation of the chemical structure of vitamin E-grafted poly(α-glutamate) (α-PGlu).

Table 12. Micro- and nanogels based on synthetic polymers on the market or in clinical trials.

TRADE NAME	SUBNAME	POLYMER SYSTEM	DRUG	INDICATION/USE	MANUFACTURER	STATUS
			Microgel			
DC Bead® (US: LC Bead®)	DEBDOX™	P(VA-*co*-AMPS)	DOX	Malignant hypervascular tumor	BTG	Market
	DEBIRI™	P(VA-*co*-AMPS)	Irinotecan	Metastatic colorectal cancer	BTG	Market
	IDASPHERE II	P(VA-*co*-AMPS)	Idarubicin	Liver cancer	Federation Franco-phone de Cancer-ologie Digestive	Phase II (NCT02185768)
Tandem®	Oncozene®	PMAA	DOX, epirubicin, idarubicin, irinotecan	Neurovascular arteriovenous malformations, hypervascular tumors	CeloNova BioSciences	Market
	Embozene®	PMAA + Polyzene®-F				Market

HepaSphere™ (US: QuadraSphere®)		Poly(VA-*co*-AA)	DOX	Hepatocellular carcinoma	Merit Medical®	Market
LifePearl®		PEG	DOX, irinotecan	Hyper vascular tumor, liver metastasis	Terumo	Market
PolyActive®	Locteron® (OctoPlus)	PEG-*b*-PBT (Multiblocks)	IFN-α 2b	Hepatitis C virus	Biolex Therapeutics	Phase III (NCT00863239)
			Nanogel			
Medusa®		α-PGlu grafted with vitamin E	IL-2, IFN-α 2b, IFN-β 1a, exenatide	Various cancers, viral infections	Avadel Pharmaceuticals	Phase I/II[363]

DOX: doxorubicin.

3.3 Macroscopic drug carriers

3.3.1 Hydrogels

Hydrogels. Hydrogels represent macroscopic, hydrophilic polymer networks, which are able to absorb water or aqueous biological fluids in amounts ranging up to multiple times of their own mass. In analogy to microgels, they can be subdivided by their type of cross-linking, *i.e.* chemical or physical cross-linking. Hydrogels are able to imitate natural living tissue more than any other class of synthetic biomaterials due to their high water content, soft consistency and porosity. Undoubtedly, their most advanced application field is their usage as contact lenses, in particular in form of soft lenses. However, the relatively low drug loading capacity and the burst release upon ocular administration is a challenge that has to be overcome. To date, no drug loaded contact lens is on the market.

An advanced alternative to frequent application of eye drops for steroid therapy is the hydrogel punctum plug Dextenza™. The dexamethasone loaded depot for ophthalmic drug delivery is based on branched PEG and represents the first sustained release ophthalmic product that entered phase III trials (**Table 13**).[364] As cross-linker, a molecule with four arms is used bearing complimentary reactive sites on each end which are not further described in literature. Very recently, Ocular Therapeutix™ announced positive results from this clinical trial for the treatment of post-surgical ocular inflammation and pain.[365] It is placed through the punctum (natural opening in the eye lid) into the lacrimal canaliculus and allows a controlled delivery of corticosteroid to the eye (Figure 13). After an application period of four weeks, the hydrogel degrades and liquefies through bulk hydrolysis[366] and naturally exits the nasolacrimal system. Besides the treatment of post-operative inflammation, as well as allergic conjunctivitis (phase III), the system is studied in phase II trials to treat the inflammatory dry eye disease.

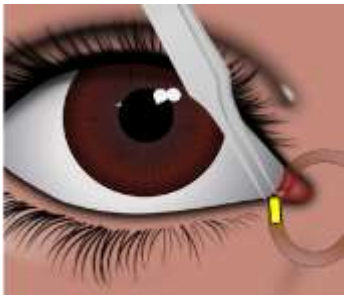

Figure 13. The hydrogel plug Dextenza™ (loaded with dexamethasone to treat inflammatory dry eye disease) is placed through the punctum (natural opening in the eye lid) into the lacrimal canaliculus and allows a controlled delivery of corticosteroid too the eye.

Besides ocular applications, hydrogels represent a promising platform for injection into the human body which facilitates the well-controlled administration of drugs at the desired rate and site. An overview of recent patent applications has been given by Calo and Khutoryanskiy.[367] A successful example for a hydrogel-based (non-ocular) drug delivery system is the vaginal insert Propess® (US: Cervidil®) used to induce cervical ripening, which is on the market since 1995. The network consists of polyurethane (PU) obtained from the cross-linking of PEG-diol and diisocyanates units (Figure 14) and releases the previously loaded drug dinoprostone continuously over a period of 12 h. This release is induced by the swelling of the hydrogel when it is placed in the moist vaginal environment.[368]

Based on a similar polymer system, Moraxen® represents a hydrogel that features a slow, controlled release of morphine sulfate over a whole day and is mainly used to relieve pain related to end-stage cancer.[369] It is used for rectal delivery, but it is not considered a classic suppository. The hydrogel is rather a reservoir type device which has to be removed and replaced if needed due to the lack of biodegradability. In 2008, Marillion Pharmaceuticals and Cytokine PharmaSciences announced that they signed a license agreement concerning the delivery system Pilobuc™, which is a buccal insert containing pilocarpine for the treatment of symptoms associated with primary and secondary Sjögren's syndrome, *e.g.* xerostomia.[370] Pilobuc™ is based on a PU hydrogel system, which is an adaption of the marketed products Propess® and Moraxen®.[371] It is placed between the buccal mucosa and gingiva at the back of the mouth.[371] In 2015, the phase II trial for the treatment of xerostomia has been discontinued.[372] A second controlled release system for vaginal delivery is Mysodelle®/Myspess® (US: Misodel®), which is based on a similar cross-linked system, synthesized from PEG, 1,2,6-hexanetriol and dicyclohexylmethane-4,4'-diisocyanate. The drug misoprostol, which is applied for the induction of labor, is released from a reservoir over a period of 24 h. The product is equipped with a withdrawal tape that enables rapid removal when active labor begins.[373] The product Supprelin® LA is a hydrogel system that is used as subcutaneous insert. The system acts as a reservoir and releases histrelin acetate (gonadotropin-releasing hormone agonist) for the treatment of children with central precocious puberty. The drug decreases the luteinizing hormone levels and the serum concentration of sex steroids. The formulation is composed of 2-hydroxyethyl methacrylate (HEMA), 2-hydroxypropyl methacrylate, trimethylolpropane trimethacrylate, benzoin methyl ether, di(4-tert-butylcyclohexyl) peroxydicarbonate (Perkadox-16) and Triton X-100 (non-ionic surfactant).[374] Histrelin acetate is continuously delivered over a period of 12 months until the implant has to be removed as it is nonbiodegradable.[375] Another subcutaneous insert based on a similar polymer reservoir release system of histrelin acetate is Vantas®,[376] which is indicated to treat the symptoms of advanced prostate cancer.

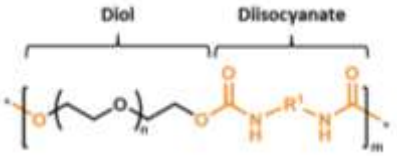

Figure 14. Schematic representation of the chemical structure of polyurethane (orange: urethane unit) obtained by a diol (*i.e.* PEG-diol) and a diisocyanate (R^1 = aliphatic, aromatic moiety).

Aquamere® and Aquatrix® II are types of hydrogel-based devices, which are produced by Hydromer®. The trademark Aquamere® comprises several hydrogels based on poly(vinyl pyrrolidone) (PVP) containing PU segments acting as cross-linker.[377] The materials are mainly used for topical applications, but some are applied in oral drug delivery systems. The product line includes four different polymer types (H-, A-, C- and S-series) which contain various comonomers to adjust the properties of the final hydrogel. The H-series products are solutions of PVP and hydrophilic PU that facilitate high viscosity, superb film formation properties and excellent compatibility. Based on the same polymer system as the H-series, the A-series exhibits polymers that are dispersed in ethanol for quick drying. The C-series products of cationic grafted PDMAEMA/PVP copolymers and hydrophilic PU have excellent adhesion and greater substantivity to skin and hair than H-series while maintaining excellent film forming properties. The S-series contains unique silicone-based copolymers of dimethiconylacrylate/PVP and hydrophilic PU, exhibiting a low viscosity and silky feel without oily residue. As a consequence, they are used for applications where sheen or tack reduction is required. The products under the trademark Aquatrix® II are sold as two separate aqueous solutions, forming a hydrogel upon mixing and result in superior cohesive and elastic properties. One part is a solution of PVP in water and the other one contains either chitosan or PEI depending on the specific product.[378] The resulting network can be loaded with active cosmetic and pharmaceutical ingredients by addition to the aqueous solution prior to the gel formation. Another hydrogel system, Hypan® is based on a segmented copolymer structure consisting of hard blocks (PAN sequences, good mechanical properties) and soft blocks (hydrophilic derivatives of acrylic acid obtained by controlled partial hydrolysis of PAN, good water binding capability) whereby more than one block of each kind is present per chain.[379] Hypan® hydrogels are used for the treatment of colon diseases and various cancers. The materials can be processed by extrusion and injection molding, which represent rather unusual methods considering hydrogels. Hypan® is produced and sold by

Hymedix.[380] SQZ Gel™ is a hydrogel system for oral medication composed of chitosan and PEG, which allows a pH-sensitive release of diltiazem hydrochloride to treat hypertension.[369, 381] In the basic environment of the gut, the swollen network shrinks and releases the drug.

Smart Hydrogel™ is a blend of the polymers PAA and PEG-*b*-PPG-*b*-PEG (Pluronic®) that forms a gel when it is warmed to body temperature. Once injected at the desired body surface, it gels and enables a constant dosing of drugs *in situ* for hours.[382] Increasing temperatures result in the aggregation of the hydrophobic ends of adjacent Pluronic®-PAA molecules and, therefore, the formation of micelles. In this conformation, the hydrophilic ends connect with each other to form a network that provides rigidity and structure to the mixture.[383] An intensely investigated thermo-gelling hydrogel is the Oncogel™ system, which is a network loaded with paclitaxel (TXL). It is currently investigated for its application in the treatment of different cancer types.[384] As an example, it has been proven to be effective in the treatment of malignant gliomas in rat models.[385] The physically cross-linked hydrogel by itself is known under the trade name ReGel® and consists of an amphiphilic triblock copolymer (PLGA-*b*-PEG-*b*-PLGA).[386] The system is soluble at low temperatures (< 15 °C), but upon injection into the body, ReGel® forms a gelled depot. The temperature increase towards the critical gelation temperature results in hydrophobic interactions of the PLGA segments and a strong micellar aggregation.[387] As a consequence, the entrapped active compounds are released for systemic/local delivery over several weeks. OncoGel™ has been evaluated in clinical studies on solid tumors[388] and in combination with radiotherapy on esophageal cancer.[389] A recent phase IIb study failed as it showed no impact on the tumor in patients with esophageal cancer. Based on these results, BTG has discontinued its clinical studies and its search for new partners to further develop OncoGel™.[390] Nevertheless, they will continue studies on ReGel® as a drug delivery technology.

Table 13. Hydrogels based on synthetic polymers on the market or in clinical trials.

TRADE NAME	POLYMER SYSTEM	DRUG	INDICATION/USE	MANUFACTURER	STATUS
DEXTENZA™	PEG	Dexamethasone	Post-operative inflammation, allergic conjunctivitis	Ocular Therapeutix™	Phase III[364]
			Inflammatory dry eye disease	Ocular Therapeutix™	Phase II[364]
Propess® (US: Cervidil®)	PU (PEG-diol)	Dinoprostone, 10 mg (prostaglandin E_2/PGE_2)	Induction of labor	Ferring Pharmaceuticals	Market
Moraxen®	PU (PEG-diol)	Morphine sulfate	End-stage cancer pain	BTG, PAION	Market
Pilobuc™	PU (PEG-diol)	Pilocarpine	Sjögren's syndrome (Xerostomia)	Ferring Pharmaceuticals	Phase II[372] (Disc.)
Mysodelle®, Myspess® (US: Misodel®)	PU (PEG-diol)	Misoprostol, 200 µg (prostaglandin E_1/PGE_1)	Induction of labor	Ferring Pharmaceuticals	Market
Supprelin® LA	2-Hydroxyethyl/propyl methacrylate, trimethylolpropane trimethacrylate	Histrelin acetate	Treatment of children with central precocious puberty	Endo®	Market
Vantas®	2-Hydroxyethyl/propyl methacrylate, trimethylolpropane trimethacrylate	Histrelin acetate	Advanced prostate cancer	Endo®	Market

Aquamere®	PVP and PVP-grafted copolymers (cl[a]: PU segments) (H-, A-, C-, S-series)	*Broad range of cosmetic & drug ingredients*	Topical and oral drug delivery	Hydromer®	Market
Aquatrix® II	PVP (cl: Chitosan), PVP (cl: PEI)	*Broad range of cosmetic & drug ingredients*	Drug delivery matrices (*i.e.* transdermal)	Hydromer®	Market
Hypan®	Multiblocks of PAN-b-PAA	[b]	Colon diseases, various cancers	Hymedix	Market
SQZ Gel™	PEG, Chitosan (blend)	Diltiazem	Hypertension	BTG, Macromed	Market
Hycore-V™, Hycore-R™	*Not discclosed*	Metronidazole	Vaginal and rectal infections	BTG , PAION	Market
Smart Hydrogel™	PAA, Pluronic® (blend)	*Broad range of drug ingredients*	Drug delivery matrices	MedLogic Global	Market
OncoGel™	PLGA-*b*-PEG-*b*-PLGA (ReGel®)	TXL	Esophageal cancer Recurrent glioma	BTG	Phase IIb[390] (disc.) Phase I/II (NCT00479765)

TXL: paclitaxel; [a] cl = cross-linker; [b] Hymedix has developed a line of seven products for the chronic wound care market. Which of them are used for drug delivery applications has not been described in publicly available resources.[380]

3.3.2 Solid implants and inserts

Solid drug delivery devices, which are implanted or simply inserted into natural orifices, possess several advantages over parenteral or oral dosage forms. Besides the site specific drug administration and, hence, significantly lower doses of the applied drugs, implantable or insertable devices usually allow a sustained and continuous release of the therapeutic agents. Furthermore, the medication by implantable devices guarantees a better patient compliance and acceptance than frequent injections or the taking of several pills a day. In this chapter, we focus on passive delivery devices that provide continuous release over time periods ranging from weeks to several years without the need for replenishment. These systems are particularly applied for the delivery of highly potent drugs, which work at low doses such as hormones. Numerous commercial systems are available for applications ranging from the prevention of HIV and the treatment of glaucoma to various methods for contraception.

Vaginal inserts. Currently, five different vaginal rings are commercially available (Table 14). For decades, silicone elastomers (PDMS-based) are used for their fabrication due to the low weight, high flexibility and excellent biocompatibility of these materials. Estring® and Femring® are used for hormone replacement therapy, whereas Progering® represents a contraceptive. Fertiring® combines both applications. The only commercialized vaginal ring that is based on poly(ethylene-*co*-vinyl acetate) (PEVA, Figure 15) is NuvaRing® for contraception. Numerous vaginal rings based on PDMS are currently under clinical investigations, which are not only used for contraception but also as prevention for sexually transmitted diseases. Milprosa™ and NES/EE already went through clinical phase III and are close to commercialization. The most advanced microbicide ring, dapivirine (DPV) Ring-004, was designed for HIV prevention and is in phase III trials.[391] Different rings for the controlled and simultaneous delivery of preventives for HIV (maraviroc, levonorgestrel) have recently entered clinical phase I. UPA-CVR, a vaginal ring releasing ulipristal acetate, is already investigated in clinical phase II studies.[392] The trend goes towards multifunctional applicable drug reservoirs. The dual protection vaginal ring of CONRAD is currently in phase I trials. It consists of two segments, which are based on different aliphatic polyether-based PUs from the Tecoflex® family (variable in

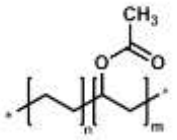

Figure 15. Schematic representation of the chemical structure of poly(ethylene-*co*-vinyl acetate) (PEVA).

hardness and hydrophilicity based on varying contents of PEG and poly(tetramethylene ether glycol) (PTMEG)). The system is optimized to deliver a high flux of tenofovir (HIV/herpes prevention) from one segment and a low flux of levonorgestrel (contraception) from the other.[393] Another polyurethane-based ring entering clinical trials is VR101, which releases glycerin to counteract vaginal dryness. Currently, the Population Council is developing a PEVA ring for simultaneous delivery of medivir-150 (targets HIV), carrageenan (targets human papilloma virus (HPV) and herpes simplex virus-2 (HSV-2)), zinc acetate (targets HIV and HSV-2) and levonorgestrel (targets unintended pregnancy).[394]

Another option for reliable contraception is the insertion of an intrauterine device (IUD, **Figure 16**). The hormonal IUD's are usually made of PDMS (Table 14). The levonorgestrel-releasing system Mirena® was approved by the FDA in 2000, after it had been used in Europe since 1991. A new version of Mirena®, called Skyla® (U.K.: Jaydess®), which is based on the same mechanism of action, was introduced to the US market in 2013. It features a smaller size and a reduced dose of the released hormone levonorgestrel. The latest IUD entering the market (Liletta®) was approved by the FDA in 2015 and exhibits similar characteristics (shape and dose of released levonorgestrel) compared to Mirena®. Intrauterine copper contraceptives (*e.g.* Paragard®) are not described herein, although their monofilament threads and T-frames are usually made of polyethylene (PE).

Figure 16. Schematic representation of an intrauterine device (IUD).

Table 14. Vaginal inserts on the market and selected inserts in clinical trials.

TRADE NAME	POLYMER SYSTEM	DRUG	INDICATION/USE	MANUFACTURER	STATUS
			VAGINAL RING		
Estring®	PDMS	17β-Estradiol	Hormone replacement (menopause)	Pfizer	Market
Femring®	PDMS	17β-Estradiol-3-acetate	Hormone replacement (menopause)	Allergan	Market
Progering®	PDMS	Progesterone	Contraception	Population Council, Grünenthal	Market (South America)
Fertiring®	PDMS	Progesterone	Contraception & hormone replacement (menopause)	Population Council, Grünenthal	Market
NuvaRing®	PEVA	Etonogestrel & ethinyl estradiol	Contraception	Merck & Co.	Market
Milprosa™	PDMS	Progesterone	Contraception	Ferring Pharmaceuticals	Phase III[395]
NES/EE	PDMS	Nestorone® (NES) & ethinyl estradiol	Contraception	Population Council	Phase III finished (NCT00455156)
NES/E2	PDMS	Estradiol & nestorone® (NES)	Contraception	Population Council	Phase II (NCT02626208)
DPV-Ring	PDMS	Dapivirine (DPV), (DPV Ring-004)	HIV prevention	IPM	Phase III finished[396]
		DPV/ levonorgestrel			Phase I (NCT02855346)
		DPV/maraviroc			Phase I (NCT01363037)

UPA-CVR	PDMS	Ulipristal acetate	Contraception	HRA Pharma, Population Council	Phase II[392]
Dual protection	PU, PEG & PTMEG (Tecoflex™, Lubrizol Corp.)	Levonorgestrel, tenofovir	Contraception & HIV/herpes prevention	CONRAD	Phase I (NCT02235662)
VR101	PU	Glycerin	Vaginal dryness	J3 Bioscience (formerly ViroPan)	Phase 0 (NCT02029053)
			INTRAUTERINE DEVICE		
Mirena®	PDMS	Levonorgestrel	Contraception	Bayer, Population Council	Market (as Levosert® in GB)
Skyla®	PDMS	Levonorgestrel	Contraception	Bayer	Market (as Jaydess® in GB)
Liletta® (LNG20)	PDMS	Levonorgestrel	Contraception	Allergan, Odyssea Pharma	Market

Subcutaneous implants. An effective contraception can further be accomplished by subcutaneous implants which are implanted at the inside of the upper arm (Figure 17) and continuously release hormones into the blood. After discontinuing the production of Norplant® (silicone capsules containing levonorgestrel),[397] Norplant® II (Jadelle®) was developed, which consists of small rods based on PDMS (Table 15). Once inserted, Norplant® II lasts up to 5 years. Utilizing the same mechanism of action, Sino-Implant II (two thin, flexible silicone rods) represents one of the most effective birth control products with annual pregnancy rates below 1%.[398] The product is considered for four years of use, so far.[399] Another type of subdermal implant is Nexplanon®, which is based on a PEVA copolymer. Nexplanon® reveals two main advantages compared to its predecessor Implanon®, which is replaced gradually: I) The easier insertion that avoids placing the implant too deep under the skin; II) the rod allows localization *via* X-ray since it is radiopaque due to the addition of 15 mg barium sulphate.[400] Despite showing great promise for being another contraceptive alternative, the development of PCL-based Capronor releasing levonorgestrel was abandoned in the 1990s due to skin irritation and stability in storage issues. Furthermore, there were concerns about removal of the device and a long release tail.[401] However, the single, tubular implant was able to achieve up to one year of ovulation suppression. [402] Very recently, the FDA approved another implant based on PEVA, called Probuphine®, which is the first device for the continuous release of buprenorphine. It is used for the maintenance treatment of opioid dependence as part of a complete treatment program including counseling and psychosocial support. Probuphine® consists of four rods that are implanted under the skin on the inside of the upper arm and provides treatment for six months.[403] VC-01™ is a subcutaneous implant currently under clinical investigation (phase I/II) to treat diabetes type I. It is composed of ViaCyte's Encaptra® drug delivery technology (made of undisclosed polymers[404]) and is used to deliver human embryonic stem cells (pancreatic PEC-01™ cells).

Figure 17. Schematic representation of the implantation of a subcutaneous implant. Reprinted from Acta Cir. Bras. 2009, *24*, 7-12. with permission of Creative Commons Corporation (2009).

Table 15. Subcutaneous implants on the market and in clinical trials.

TRADE NAME	POLYMER SYSTEM	DRUG	INDICATION/USE	MANUFACTURER	STATUS
Jadelle® (Norplant® II)	PDMS	Levonorgestrel	Contraception	Bayer, Population Council	Market (not in US)
Sino-Implant II	PDMS	Levonorgestrel	Contraception	Shanghai Dahua Pharmaceuticals	Market (as Zarin®, Fem-plant®, Trust®, Simplant® etc. registered in 24 countries)
Nexplanon®	PEVA	Etonogestrel	Contraception	Merck & Co.	Market
Capronor	PCL	Levonorgestrel	Contraception	RTI International	Phase II[401] (disc.)
Probuphine®	PEVA	Buprenorphine HCl	Opioid dependence	Titan & Braeburn™ Pharmaceuticals	Market
VC-01™	*undisclosed* (Encaptra®)	PEC-01™ cells[a]	Diabetes type 1	ViaCyte	Phase I/II (NCT02239354)

[a] Embryonic stem cell–derived precursors of insulin-producing beta cells.

Ocular implants and inserts. Implantable or insertable devices are well-established for the local treatment of eye diseases. Ocusert® Pilo was one of the first ocular delivery devices and represents an ocular insert, which is placed in the lower cul-de-sac of the eye to be used for the treatment of glaucoma (Table 16).[405] It contains a core reservoir consisting of pilocarpine and alginic acid and a framework of hydrophobic poly(ethylene-*co*-vinyl acetate) (PEVA) membrane that regulates diffusion of pilocarpine. However, the product has been withdrawn from the market, which is mainly related to the difficulties (in particular for elderly people) replacing the insert.[406] The first intravitreal implant was Vitrasert®. This ganciclovir pellet was used for the treatment of cytomegalovirus retinitis. The antiviral medication is coated by nondegradable layer of impermeable PEVA, which is sandwiched in between two permeable layers of PVA. This design enables a well-controlled rate of release of the drug by the diffusion only through the areas where no impermeable material is present. As a consequence, reimplantation is necessary after 5 to 8 months.[407] Due to market forces, Vitrasert® has not been produced since 2014, and all remaining implants have passed their expiration dates.[408] Retisert® followed as the second generation of reservoir-based implants, which are used for treatment of chronic noninfectious uveitis (Figure 18).[409] This implant for sustained release consists of a silicon laminate and PVA coating, which control the release of fluocinolone acetonide (FA). Further studies have proven the potential of this device in the treatment of edema (caused by diabetes) and central retinal vein occlusions.[410] Another implant for the delivery of FA and the treatment of diabetic macular edema is Iluvien®. This rod-like device is based on polyimide tubes (Figure 19) with a PVA membrane at the caps. Due to its small size, it can remain in the cavity even after the whole drug has been released. A similar, small rod-like device, which is injected into the white of the eye, is Ozurdex®. This system is designed to deliver the corticosteroide dexamethasone also applied for the treatment of macular edema. In contrast to previous devices, the use of degradable PLGA allows the dissolution of the implant and, therefore, eliminates the need of surgically removal. Another biodegradable PLGA-based implant is Surodex®, which is a rod-shaped device inserted into the anterior chamber after a cataract surgery in order to control postoperative inflammation.[407]

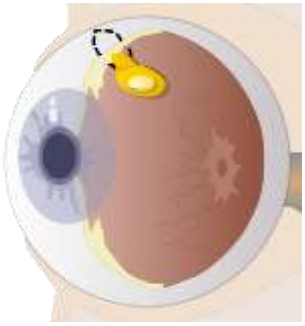

Figure 18. Schematic representation of the reservoir-based Retisert® implant.

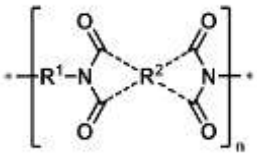

Figure 19. Schematic representation of the chemical structure of polyimides.

Further ophthalmic inserts (*e.g.* I-vation™ or Helios™), which are currently under clinical investigations, have been nicely reviewed elsewhere.[407, 411]

Table 16. Ocular implants and inserts on the market and in clinical trials.

TRADE NAME	POLYMER SYSTEM	DRUG	INDICATION/USE	MANUFACTURER	STATUS
Ocusert® Pilo	PEVA	Pilocarpine	Treatment of glaucoma	Johnson & Johnson, Alza Cooperation	Market (withdrawn)
Vitrasert®	PVA, PEVA (Versa™ platform)	Ganciclovir	Cytomegalovirus retinitis	Auritec Pharmaceuticals	Market (withdrawn)
Retisert®	PVA, PDMS (Versa™ platform)	Fluocinolone acetonide	Chronic non-infectious uveitis	Valeant® (Bausch & Lomb), Auritec Pharmaceuticals	Market
Iluvien®	Polyimide, PVA	Fluocinolone acetonide	Diabetic macular edema	AlimeraSciences	Market
Ozurdex®	PLGA (Novadur®)	Dexamethasone	Diabetic macular edema	Allergan	Market
Surodex®	PLGA, hydroxypropyl methylcellulose	Dexamethasone	Postcataract surgery inflammation	Oculex Pharmaceuticals	Market (China, Singapore, etc.)
I-vation™	PMMA, PEVA	Triamcinolone acetonide	Diabetic macular edema	SurModics	Phase II finished (NCT00692614)
Helios™	PDMS	Bimatoprost	Intraocular pressure (IOP)-lowering	ForSight™ VISION5	Phase II (NCT02537015)
*	PLGA	Brimonidine tartrate	Retinitis pigmentosa	Allergan	Phase II (NCT00661479)
			Age-related macular degeneration	Allergan	Phase II (NCT00658619)

* No trade name listed.

Implants for deeper tissue. While the majority of implantable devices comprises subcutaneous or ocular systems, which do not require major surgery to be applied, replaced or removed, a few devices were developed to be implanted into deeper tissue in the body (Table 17). Based on a biodegradable polymer (a copolymer of *bis*-(*p*-carboxyphenoxy)propane and sebacic acid called Polifeprosan 20) the Gliadel® wafer is approved for the treatment of malignant glioma.[412] It is inserted into cavities resulting after the surgical removal of the tumor in the brain (Figure 20) and will be degraded by the body to release the cytostatic drug carmustine. Another commercialized implant for the application in deeper tissue is Propel® based on the biodegradable polymer PLGA.[413] This steroid-eluting device is implanted after surgery into the nose to assist in the treatment of chronic sinusitis.

Figure 20. Schematic representation of the inserted Gliadel® wafer (polymer system) in the brain.

The presented implant systems reflect only a selection of currently commercially available systems. Besides, a large pipeline of polymer-based implant delivery technologies has been studied in promising clinical trials. The biodegradable implant siG12D-LODER™ (PLGA-based) is inserted into the tumor and releases a siRNA drug against KRASG12D over four months. In combination with chemotherapy it is used as targeted therapy for locally advanced pancreatic cancer (phase IIb).[414] Restora™ represents a transmucosal PU steroid-eluting device[415] for thirty day treatment of sinusitis (phase II/III).[416] In contrast, LiRIS® is a pretzel-shaped silicone tube that could be inserted into the bladder, releasing lidocaine over two weeks in females with interstitial cystitis (phase II).[417]

Table 17. Implants for deeper tissue on the market and in clinical trials.

TRADE NAME	POLYMER SYSTEM	DRUG	INDICATION/USE	MANUFACTURER	STATUS
Gliadel® Wafer	Polifeprosan 20[a]	Carmustine	Malignant glioma	Arbor Pharmaceuticals	Market
Propel®	PLGA, PEG	Mometasone furoate	Chronic sinusitis	Intersect® ENT	Market
siG12D-LODER™	PLGA (Loder™)	siRNA therapeutic (KRASG12D)	Pancreatic tumor	Silenseed	Phase IIb (NCT01676259)
Restora™	PU	Steroid	Sinusitis	SinuSys™	Phase II/III (NCT02627794)
LiRIS®	PDMS	Lidocaine	Interstitial cystitis/ bladder pain syndrome	Allergan	Phase II (*e.g.* NCT01475253, NCT01824303)

[a] Polifeprosan 20 (poly[bis (p-carboxy-phenoxy)] propane and sebacic acid).

Several companies are working continuously on new technologies (*e.g.* Medidur™, DebioStar™, Duros®, MedLaunch™), which can be used as polymer platform for different drugs. Implanted drug-eluting stents are described in Chapter 3.4.2 as the polymers are used as coatings in that case. Implanted devices built up from hydrogel networks, *e.g.* Supprelin® LA and Vantas®, are described in Chapter 3.3.1.

3.4 Coatings

3.4.1 Solid oral dosage forms

Despite the complexity of the related uptake mechanism, oral administration of pharmaceutical compounds is the preferred route for the drug delivery applications due to the ease of ingestion, the avoidance of painful procedures, its versatility, the high patient compliance, reduced sterility constraints, and flexibility of dosage form design (*e.g.* solids: Powder, granules, capsules).[418] In addition, the oral uptake allows patients to conveniently self-administer drugs without the need of any health care professionals.[419] But the oral delivery of pharmaceuticals remains challenging for several reasons: I) The typical transit time in the gut (from mouth to anus) is about 30 hours, which limits the use of drugs that aim at longer dosing times;[420] II) the physiological parameters and the biological environment of the gastrointestinal (GI) tract can vary quite significantly from one stage to the next. For example, the pH value of the saliva in the mouth is usually in the range of 5.8 and 7.4. Inside the stomach the pH value decreases dramatically to 1 (extremely acidic) and increases back to 7 (neutral) in the bowels; III) the food and beverage intake causes dynamic changes in the concentration of bile salts, lipids, carbohydrates and digestive enzymes throughout the GI tract that can interact with the drug;[421] IV) finally, before reaching the bloodstream, the drug has to overcome some anatomical obstacles including the degradative environment in the lumen and traversing the mucosa and epithelial cells. However, one of the main concerns remains the patient compliance considering the oral uptake of pharmaceuticals, in case the drugs have disagreeable taste and require frequent dosing. As a result of these limitations, various functional coatings based on polymers have been designed to improve the efficacy of the oral route of administration. These polymer coatings are mainly applied to solid dosage forms, *i.e.* tablets, granulates and capsules, with the aim to achieve selective delivery of active ingredients to a particular gastrointestinal (GI) tract, such as the small intestine or the large bowel, or to improve the patient compliance by improving the odor or masking the taste. Since the established systems comprise proven and versatile materials, there doesn't exist an immediate need for new polymer systems.

Polymer coatings for site specific delivery. The release of a drug at a specific site in the GI guarantees an optimized uptake into the blood stream or activity of the delivered active ingredient at the desired side, but avoids complications with other parts of the tract. Several polymer-based coatings have been developed to target various sites of the GI. An enteric polymer coating prevents the release of the drug in the gastric environment and facilitates the release in the small intestine or in the colon. This enables: I) The protection of the stomach from some drugs, which may cause stomach ulcers, such as aspirin, diclofenac and naproxen; II) the protection of special pharmaceutical compounds such as proton pump inhibitors (PPIs) (*e.g.* omeprazole or pantoprazole) against the acidic environment in the stomach, and, III) the targeting of the small intestine or colon.[422] Enteric coatings contain carboxylic acid groups, which remain in an unionized (protonated) form at low pH values and, therefore, are insoluble in the acidic aqueous environment of the stomach.[169] However, as the pH value increases in the small intestine, the carboxylic acids become deprotonated (negatively charged), which results in the dissolution of the polymers in the intestinal fluid.[423] Table 18 summarizes marketed poly(meth)acrylate copolymers, which are used for enteric coatings, including their chemical composition, product form and the pH value at which they become soluble. The critical pH value for dissolution of the polymers mainly depends on the content of the carboxylic acid and esterified groups. The different dissolution properties of enteric coatings enable targeting specific areas of the intestine. For example, EUDRAGIT® L100-55 and EUDRAGIT® L100 dissolve above pH value of 5.5 and 6.0, respectively, and are used for targeting the small intestine, whereas EUDRAGIT® S100 and EUDRAGIT® FS 30D (Figure 21) dissolve above pH value of 7.0 and are used for colon targeting.[424] In addition, the release of the encapsulated drugs can further be controlled by the thickness of the coating material or simply by blending the different enteric polymers in different ratios.[422]

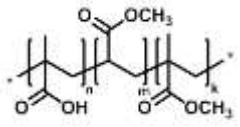

Figure 21. Schematic representation of the chemical structure for the copolymer poly(MAA-*co*-methyl acrylate-*co*-MMA), named EUDRAGIT® FS 30D.

Table 18. Marketed poly(meth)acrylates as enteric coatings.

TRADE NAME	PRODUCT FORM	POLYMER SYSTEM	DISSOLUTION pH	MANUFACTURER
EUDRAGIT® L 100-55	Powder	Poly(MAA-*co*-ethyl acrylate) 1:1	Soluble > pH 5.5	Evonik
EUDRAGIT® L 30D-55	Aqueous dispersion 30%			
Kollicoat® MAE 30 DP	Aqueous dispersion 30%		Soluble > pH 5.5	BASF
Kollicoat® MAE 100 P	Powder			
EUDRAGIT® L 100	Powder	Poly(MAA-*co*-MMA) 1:1	Soluble > pH 6.0	Evonik
EUDRAGIT® L 12.5	Organic solution 12.5%			
EUDRAGIT® S 100	Powder	Poly(MAA-*co*-MMA) 1:2	Soluble > pH 7.0	Evonik
EUDRAGIT® S 12.5	Organic solution 12.5%			
EUDRAGIT® FS 30D	Aqueous dispersion 30%	Poly(MAA-*co*-methyl acrylate-*co*-MMA) 7:3:1	Soluble > pH 7.0	Evonik

Apart from enteric coatings, sustained release coating polymers releasing the drug over time can also be used for modified/controlled release applications. These polymers lack ionizable groups and they are not soluble in the entire GI tract. However, they can swell with exposure to the gastrointestinal fluids and, consequently, release the active ingredients by a diffusion-controlled mechanism. These polymer coatings are mainly used in prolonged-action dosage forms. EUDRAGIT® RL and RS, which contain 10% or 5% quaternary ammonium groups, respectively,

as well as the neutral EUDRAGIT® NE and NM, which are the copolymers of ethyl acrylate and methyl methacrylate, are preferred coating materials for a sustained release. Table 19 includes marketed poly(meth)acrylate based copolymers which are used for sustained release coatings and their chemical composition as well as dissolution properties.

Table 19. Various marketed poly(meth)acrylates for sustained release.

TRADE NAME	PRODUCT FORM	POLYMER SYSTEM	PROPERTIES	ADVANTAGES
EUDRAGIT® RL 30 D	Aqueous dispersion 30%	Poly(ethyl acrylate-*co*-MMA-*co*-TMAEMA) 1:2:0.2	Insoluble, high permeability, pH-independent swelling	Customized release profiles by combination of RL and RS grades in different ratios, suitable for matrix structures
EUDRAGIT® RL PO	Powder			
EUDRAGIT® RL 100	Granules			
EUDRAGIT® RL 12.5	Organic solution 12.5%			
EUDRAGIT® RS 30 D	Aqueous dispersion 30%	Poly(ethyl acrylate-*co*-MMA-*co*-TMAEMA) 1:2:0.1	Insoluble, low permeability, pH-independent swelling	
EUDRAGIT® RS PO	Powder			
EUDRAGIT® RS 100	Granules			
EUDRAGIT® RS 12.5	Organic solution 12.5%			
EUDRAGIT® NE 30 D	Aqueous dispersion 30%	Poly(ethyl acrylate-*co*-MMA-*co*-TMAEMA) 2:1:0	Insoluble, low permeability, pH-independent swelling	No plasticizer required, highly flexible, suitable for matrix structures
EUDRAGIT® NE 40 D	Aqueous dispersion 40%			
EUDRAGIT® NM 30 D	Aqueous dispersion 30%			

TMAEMA = trimethylammonioethyl methacrylate chloride.

Polymer coatings for odor or taste masking. Polymer coatings are also applied to protect the sensitive ingredients from environmental influences such as light and moisture or to mask the unpleasant taste of the formulations.[169, 425] Methacrylates containing tertiary amino groups are commonly applied for masking the taste and moisture protection (Table 20). These pH-responsive polymer coatings take advantage of the differences in pH values between the oral cavity (pH 5.8 to 7.4) and the stomach (pH 1 to 3.5).[426] The polymers are insoluble in water at the neutral pH value of the saliva. Therefore, they suppress the release of the drug, which usually exhibit an unpleasant taste, and the diffusion of water molecules to the core of the system protecting any moisture sensitive ingredients. However, they become protonated and water-soluble at acidic conditions resulting in the release of the content in the stomach or in the small intestine.

Table 20. Marketed pH-responsive poly(meth)acrylates as protective coatings.

TRADE NAME	PRODUCT FORM	POLYMER SYSTEM	DISSOLUTION pH	MANUFACTURER
EUDRAGIT® E 100	Granules	Poly(BMA-*co*-DMAEMA-*co*-MMA) 1:2:1	Soluble < pH 5.0	Evonik
EUDRAGIT® E 12.5	Organic solution 12.5%			
EUDRAGIT® E PO	Powder			
Kollicoat® Smartseal 30D	Aqueous dispersion	Poly(MMA-*co*-DEAEMA[a]) 7:3	Soluble < pH 5.0; Stable in saliva	BASF

[a] DEAEMA= diethylaminoethyl methacrylate.

Apart from these pH-responsive methacrylates, some other water soluble synthetic polymers, including vinyl polymers and hydrophilic copolymers, are also applied for masking unpleasant tastes or protecting against moisture (Table 21). These polymers do not contain any ionic groups, which decreases the risk of chemical interactions with any other ingredient of the formulation.[425]

Table 21. Marketed water soluble synthetic polymers as protective coatings.

TRADE NAME	PRODUCT FORM	POLYMER SYSTEM	MANUFACTURER
Kollidon®	Powder	PVP	BASF
Kollicoat® IR	Powder	PVA-PEG-graft copolymer	BASF
Kollicoat® Protect	Powder	PVA-PEG-graft copolymer (Kollicoat® IR), PVA	BASF
Opadry® AMB	Powder	PVA	Colorcon®

Moreover, the previously mentioned enteric polymers (see Table 18) and coatings for sustained release (see Table 19) can also be used for taste masking and moisture protection if they provide a sufficient suppression of the drug release in the mouth and prevent moisture to pass into the formulation. However, to realize the desired fast drug release after swallowing, relatively thin coatings are applied.[425] Table 22 represents selected examples of commercialized drug formulations which are coated with EUDRAGIT® polymers.

Table 22. Examples for marketed dosage forms coated with EUDRAGIT® polymers.

TRADE NAME	POLYMER SYSTEM	DRUG	INDICATION/USE	MANUFACTURER
Clipper®	EUDRAGIT® L 100-55	Beclometasone dipropionate	Inflammatory bowel disease	Chiesi
Colo-Pleon®	EUDRAGIT® L 100-55	Sulfasalazine	Inflammatory bowel disease	Sanofi-Aventis
Entocort®	EUDRAGIT® L 100-55	Budesonide	Inflammatory bowel disease	Prometheus Lab.
Salofalk®	EUDRAGIT® L 100	Mesalazine	Inflammatory bowel disease	Dr. Falk Pharma
Ipocol®	EUDRAGIT® S 100	Mesalazine	Inflammatory bowel disease	Sandoz
Budenofalk®	EUDRAGIT® S 100 & EUDRAGIT® L 100	Budesonide	Inflammatory bowel disease	Dr. Falk Pharma
Premique®	EUDRAGIT® NE 30 D	Conjug. estrogens & medroxyprogesterone acetate (MPA)	Hormone replacement therapy for estrogen deficiency symptoms in postmenopausal women within an intact uterus	Pfizer
Nutrizym 22	EUDRAGIT® L 30 D	Pancreatin BP	Symptomatic relief of pancreatic exocrine insufficiency such as in fibrocycstic disease of the pancreas & chronic pancreatitis	Merck Serono
Convulex® CR	EUDRAGIT® RL 30 D	Sodium valproate	Epilepsy and bipolar disorder	G. L. Pharma GmbH
Amisulpride film-coated tablets	EUDRAGIT® E 100	Amisulpride	Acute & chronic schizophrenic disorders	Lek Pharmaceuticals D. D., Salutas Pharma GmbH
Adanif® XL	EUDRAGIT® E	Nifedipine	Hypertension, prophylaxis of chronic stable angina pectoris	Focus Pharmaceuticals

3.4.2 Drug-eluting stents

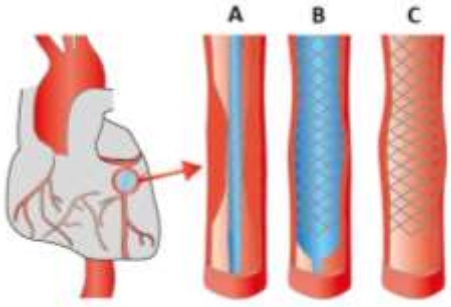

Figure 22. General mechanism of the insertion of a stent. A) Insertion of the stent by an inflatable catheter; B) expansion of the stent by the attached ballon; C) removal of the ballon.

Coronary artery disease (CAD) is a heart disease, which is considered to be one of the leading causes of death worldwide.[427] The lining of the coronary arteries, which guarantee the blood supply to heart muscle, becomes harder and stiffer, and, finally, the artery's diameter is narrowed due to the accumulation of plaque on their inner walls (atherosclerosis). The percutaneous transluminal coronary angioplasty (PTCA) is a well-established method to counteract the symptoms of the CAD. However, this treatment is not sufficient as the risks of early abrupt closure, intimal hyperplasia and late restenosis are considerably high, if it is not accompanied by further therapies.[428] An early approach to overcome these limitations resulted in the development of bare metal stents (BMS).[429] BMS are devices, which are first inserted in the narrowed coronary artery by an inflatable catheter. At the side of action, the BMS gets expanded by the attached balloon and acts as a mechanical scaffold to recover the original dimensions of the vessel (Figure 22).[430] Despite an initial improvement, the implantation of the BMS commonly results in an in-stent restenosis (ISR) due to the migration of vascular smooth cells within the stents.[431] The first attempts to prevent this restenosis by systematic drug delivery systems failed. As a consequence, focus was set on the development of drug-eluting stents (DES). These systems carry an antiproliferative drug, which is incorporated into a polymer coating of the BMS. The drugs are directly released at the injured sites to prevent the ISR by the suppression of the neointimal growth.[432] The first generation of DES comprises the sirolimus-eluting stent (Cypher®) and the paclitaxel-eluting stent (Taxus®), which are made of a stainless steel (SS) scaffold coated with the polymers poly(*n*-butyl methacrylate) (PBMA) and poly(ethylene-*co*-vinyl acetate) (PEVA) or poly(styene-*b*-isobutyelene-*b*-styrene) (PSIBS), respectively. The application of these modified stents resulted in a remarkable reduction of the usually occurring restenosis. However, safety concerns have been raised regarding the possibility of late stent thrombosis in case of a long term use.[433] In recent years, a second generation of DES has been developed with the aim to improve the efficacy and the long term safety of the stents. For this purpose, stent frames with thinner struts were introduced, and novel, more effective drugs were incorporated compared to the first generation DES. Similar to the first generation, these DES still use synthetic, nonbiodegradable polymers such as PBMA, PEVA, PSIBS, poly(hexafluoropropylene) (PHFP), and poly(vinylidene fluoride) (PVDF), sometimes in combination with a phosphorylcholine polymer (PCh) (Figure 23),[434] as coating materials of a metal surface. Table 23 summarizes all DES approved by the FDA that use polymer coatings.[428-429, 431, 435] Keeping in mind that the above mentioned polymers are nonbiodegradable, these coatings remain on the stent even after the drug is fully released, which may induce local hypersensitivity, inflammation and delayed vascular healing resulting in the development of late stent thrombosis.[436]

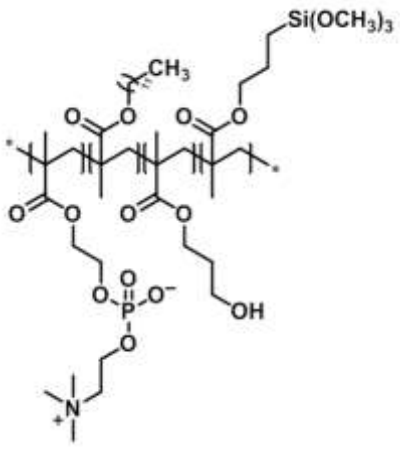

Figure 23. Schematic representation of the chemical structure of an exemplary phosphorylcholine polymer (PCh, PC technology™).

Table 23. Drug-eluting stents (DES) with nonbiodegradable polymers as coating materials on the market or in clinical trials.

TRADE NAME	STENT PLATFORM[a]	POLYMER SYSTEM	DRUG	DRUG RELEASE (DAYS)	MANUFACTURER	APPROVAL
Cypher®	SS	PEVA, PBMA, PCh	Sirolimus	40% (5); 85% (30); 100% (90)	Cordis Corporation	FDA[b]
Taxus®	SS	Poly(styrene-*b*-isobutylene-*b*-styrene)	TXL	<10% (28)	Boston Scientific	FDA
Promus PREMIER™	Pt-Cr	PBMA, poly(vinylidene-*co*-hexafluoropropylene)	Everolimus	71% (28); 100% (120)	Boston Scientific	FDA
Xience V®	Co-Cr	PBMA, poly(vinylidene-*co*-hexafluoropropylene)	Everolimus	80% (28); 100% (120)	Abbot Vascular	FDA
Endeavor®	Co-Cr	PCh	Zotarolimus	75% (2); 95% (15); 100% (28)	Metronic	FDA
Endeavor® Resolute	Co-Cr	Blend of PVP, poly(hexyl methacrylate)-*co*-PVP-*co*-PVAc and PBMA-*co*-PVAc (BioLinx)	Zotarolimus	50% (7); 70% (28); 100% (31)	Metronic	FDA
Firebird2®	Co-Cr	Poly(styrene-butylenes-styrene)	Sirolimus	50% (7); 90% (30)	Essen Technology (Beijing)	Phase IV (NCT01257373)

TXL: paclitaxel; [a] Pt-Cr: platinum chromium, SS: stainless steel, Co-Cr: cobalt chromium; [b] FDA approved stents also have CE approvals.

These issues have promoted the recent development of stents coated with fully biodegradable polymers such as PLGA and PLA. A successful example is the everolimus-eluting stent, which consist of a platinum chromium (Pt-Cr) platform coated with a biodegradable PLGA copolymer. A summary of FDA and CE approved DES based on biodegradable polymers are listed in Table 24.[429, 437]

Table 24. Drug-eluting stents (DES) with biodegradable polymers as coating materials.

TRADE NAME	STENT PLATFORM[a]	POLYMER SYSTEM	DRUG	DRUG RELEASE (DAYS)	MANUFACTURER	STATUS
Synergy™	Pt-Cr	PLGA	Everolimus	50% (60); 100% (90)	Boston Scientific	FDA[b]
Axxess™	Nitinol	PLA	Biolimus A9	45% (30)	Biosensors	CE
BioMatrix Flex™	SS	PLA	Biolimus A9	45% (30)	Biosensors	CE
Nobori®	SS	PLA	Biolimus A9	45% (30)	Terumo	CE
Supralimus®	SS	PLLA-PLGA-PCL-PVP	Sirolimus	100% (48)	SMT	CE
Orsiro	Co-Cr	PLLA + silicon carbide	Sirolimus	50% (30); 80% (90)	Biotronik	CE
BioMime™	Co-Cr	PLLA + PLGA	Sirolimus	100% (30)	Meril	CE
Inspiron®	Co-Cr	PLLA, PDLLGA	Sirolimus	60% (10); 100% (45)	Scitech Medical	Phase IV (NCT01856088)
Firehawk®	Co-Cr	PDLLA	Sirolimus	90% (90)	MicroPort Medical	CE
DESyne® BD	Co-Cr	PLA	Novolimus™	90% (90)	Elixir®	CE
MiStent SES®	Co-Cr	PLGA	Sirolimus	100% (270) (sustained release)	Micell Technologies	CE
Tivoli®	Co-Cr	PLGA	Sirolimus	50% (7); 80% (28)	Essen Technology (Beijing)	Phase III (NCT02448524)

[a] Pt-Cr: platinum chromium, SS: stainless steel, Co-Cr: cobalt chromium; [b] FDA approved stents also have CE approvals.

Although the above mentioned efforts have increased the efficacy and lifetime of stents, it has to be kept in mind that even after the degradation of the polymer coatings the metal scaffold (BMS) remains in the artery, which still might cause restenosis.[438] As a consequence, the development of fully biodegradable stents has gained considerable attention. Several fully degradable DES have been investigated clinically or are still in clinical trials, but so far only the evorolimus-eluting stent Absorb™ is FDA approved and the Novolimus™-eluting DESolve® is CE approved for commercial use in coronary patients (Table 25).[429, 439] In addition to these fully degradable systems, dual drug-eluting stents (DDES) are tested to deliver both anti-proliferative and pro-healing agents reducing the occurrence of stent thrombosis. Although some of the DDES have shown promising results in clinical trials, the Combo stent (OrbusNeich) is the only marketed DDES, which has CE approval. Combo stent uses stainless steel as stent platform and elutes the sirolimus and CD-34 antibody as drugs from a biodegradable polymer matrix that achieves the complete release within 30 days. Unfortunately, the chemical formulation of the used polymer matrix is not specified. Moreover, since the DDES in clinical trials are either polymer free or use no synthetic polymers, readers are referred to literature for more information.[429]

Table 25. Drug-eluting stents (DES) with fully biodegradable scaffolds and coatings.

TRADE NAME	STENT PLATFORM	POLYMER SYSTEM	DRUG	DRUG RELEASE (DAYS)	MANUFACTURER	STATUS
Absorb™	PLLA	PDLLA	Evorolimus	80% (28)	Abbot Vascular	FDA approval
DESolve®	PLLA	PLLA	Novolimus™	100% (180 to 270)	Elixir®	CE approval
Dreams I	Mg[a]	PLGA	TXL	100% (90)	Biotronik	Phase 0 (NCT01168830)
Dreams II	Mg	PLLA	Sirolimus	n.a.	Biotronik	Phase 0 (NCT01960504)
ReZolve2	PTD-PC[b]	n.a.	Sirolimus	Majority of drug (90)	REVA	Clinical study[c] (NCT01845311)

[a] Mg, magnesium; [b] PTD-PC, poly-tyrosine-derived polycarbonate; [c] status not clear; n.a.: not applicable.

3.5 Polymers as matrix excipients

Besides the previously described application forms, several synthetic polymers are added to pharmaceutical dosage forms. By definition they have to be inactive ingredients (all materials other than the API) in final drug products to belong to the so-called excipients.[440] The FDA provides an online database comprising all inactive ingredients approved for certain formulations for their particular route of administration, amount and concentration (also the polymers used for coatings, *e.g.*, several Eudragit® products, can be found here, see Chapter 3.4.1).[441] Excipients have undergone a paradigm shift from being “inert ingredients” to “functional ingredients”. For instance, polymers on one hand act as binders in tablets, capsules and granules, as solubilizing, lyophilizing, wetting or taste masking agents[442] but also as mucoadhesives.[443] They are referred to provide sustained release of drugs, to solubilize and protect them from degradation or to enhance their bioavailability. They ensure mucus permeability of the formulation and enhance the probability for the drug to permeate epithelial barriers (intestinal, nasal, pulmonary).[444] Thus, in fact they are used to modulate the overall efficacy of a drug and are, therefore, major components in so-called modified release (MR) drug delivery systems. Based on the solubility and permeability of an API, a Biopharmaceutical Classification System (BCI) has been introduced grouping the APIs into 4 classes (I to IV).[445] According to FDA, an API is for instance highly soluble when its highest clinical dose strength is soluble in 250 mL of aqueous media over a pH range of 1 to 7.5 at 37.5 °C, and it is considered to be highly permeable if the absorption of an orally administered dose in humans is > 90% when determined using mass balance or in comparison to an intravenous reference dose.[446] Such API is referred to as a class I API and can be more easily

delivered *via e.g.* an oral dosage form. For class II drugs (low solubility and high permeability) different formulation strategies have to be applied to deliver them orally, *e.g.* as polymeric amorphous solid dispersion.[447] Related to this, polymer matrix excipients can be classified as hydrophilic or hydrophobic matrices. The class of hydrophilic matrices is dominated by different celluloses (most often hydroxypropyl methylcellulose, HPMC) and polysorbates (both not subject of this review), but also PVP and PEG as synthetic polymers are used.
Due to the vast number of products on the market containing synthetic polymers as matrix excipients, herein only an impression of the most superficial functions of each polymer class is provided followed by an arbitrary selection of commercially available dosage forms. Often polymers can be included into formulations to fulfill several tasks depending on the formulation technology. Therefore, assignment of a certain polymer or polymer class to a particular function, dosage form or manufacturing process is difficult since it can perform different functions in different dosage forms (Table 26).

Eudragit®. Different poly(methacrylate)s (Eudragits®) are most frequently applied as synthetic hydrophobic matrices.[448] For instance, Eudragit® NE 30 D can serve as a coating material or can be processed into a tablet formulation acting as matrix (with up to 20 wt%), *e.g.* by wet granulation or direct compression of powders. The drug and other excipients are partially impregnated with the polymer. Subsequent compression results in embedment of the drug in a sponge-like network of thin polymer layers. The polymer network controls the penetration of digestive fluid into the tablet as well as the diffusion of the dissolved drug through the pores. In this way, a time controlled release and pH value independent formulation for sustained-release formulation can be realized. Eudragit® E PO (EE) is a cationic copolymer based on dimethylaminoethyl methacrylate, butyl methacrylate, and methyl methacrylate (for exact composition, see Table 20). It is soluble in gastric fluid up to pH 5, thus the drug release can be controlled to occur only in acidic environment. It is frequently used as a coating agent due to its film forming capability, but also finds application as a binder in tablets prepared by direct compression in 10% to 50% concentration. The coating of solid oral dosage forms is highlighted separately in Chapter 3.4.1.

Carbomer. "Carbomers" (Carbopol™) are high molar mass poly(acrylic acid)s (PAA), sometimes cross-linked with small amounts of allyl ethers of polyalcohols. The different numbers in the labels of carbomers (934, 934p, 940, 941) denote their different molecular sizes as well as the use of benzene during the manufacturing process. If benzene is not used during the manufacture, carbomers of type a, b or c are distinguished according to the viscosity of their solutions in water. They are most commonly used in cosmetic industry but also in tablet formulations, in particular for oral mucoadhesive controlled drug delivery systems.[449] Carbomers can absorb large amounts of water, thus increasing in volume up to 1,000 times to form gels and thick solutions that are stable and resistant to spoilage. Usually, carbomers are provided as a dried, white powder. Carbomers are considered to be generally regarded as safe by the FDA, although high concentrations may lead to eye and skin irritation.

Polycarbophil. Poly(acrylic acid) cross-linked with divinyl glycol is named polycarbophil. It is a bulk-forming laxative that increases the amount of water in stools to make them softer and easier to pass. Polycarbophil is used to treat constipation and to help to maintain regular bowel movements. It has been developed as pharmaceutical polymer with superior bioadhesive properties used in the field of controlled drug delivery systems. It could be used as a highly efficient thickener, bioadhesive agent, suspending aid and emulsion stabilizer when dispersed in water or other polar solvents.[450] Polycarbophil can also be used as a controlled release polymer in oral solid dose applications (*e.g.* Striant®). Typical usage levels for achieving controlled release characteristics in tablets manufactured by aqueous granulation are 5 wt% to 10 wt%, depending on the drug properties, co-excipients and processing parameters.

Dimethicone. Poly(dimethylsiloxane) (PDMS) is widely used under the name "dimethicone"' as lubricant and conditioning agent, but is also present in tablet capsules (*e.g.* Keflex®). An orally administered dosage form is the

over-the-counter drug "simethicone" (mixture of 90% to 99% of PDMS with siliciumdioxide, see Chapter 3.6). It is also used as excipient in tablets and capsules (*e.g.* Antara®). The presence of PDMS was found in many registered drugs, including familiar ones such as Augmentin™, Maalox®, and VapoSteam™, just to name a few examples.

Poly(ethylene glycol) (PEG). PEG is frequently used as stealth polymer covalently coupled to drugs (Chapter 3.1) or in micro- and nanoparticulate drug delivery systems (Chapter 3.2),[15] but also as matrix excipients in oral and parenteral dosage forms and more.[451] PEG is mainly added to solubilize poorly water soluble drugs to enhance their bioavailability and to reduce inter-subject variability of plasma concentrations. In particular, clear liquid PEG with low molar masses (M_n) of 300 to 600 g mol^{-1} is frequently used to solubilize poorly water soluble drugs in soft gelatin or HPMC capsules for oral application (*e.g.* Cetirizine capsules) and for almost all parenteral formulations (*e.g.* Robaxin®, Ativan®). PEG with molar masses (M_n) exceeding 4,000 g mol^{-1} is found in hard shell capsules, which is related to the administered drugs and the required stability of the capsules during passage.[452] Another reason is that the solubility of most drugs in PEG drops significantly upon dilution with water (leading to re-precipitation of the drug). Therefore, also surfactants are often added, which reduce the risk of precipitation of the drug from the PEG solution (*e.g.* phosphadidylcholine or polysorbat 80). Other solubility enhancers are further added to increase the solubility of drugs in PEG. These are commonly used ionizing agents; for acidic compounds (*e.g.* ibuprofen or naproxen) bases are added and for basic compounds (*e.g.* thioridazin or ranitidine) acids. Furthermore, hydrophilic polymers (*e.g.* povidone or cellulose derivatives) are added for the same reason. Administration of capsules results in increased rates of absorption and faster achievement of maximum plasma concentration, as shown for instance for the Ibuprofen containing soft gel capsules Spalt-Liqua® compared to a standard tablet formulation.[453] PEG (*i.e.* PEG 1000 and PEG 540) serves as a formulation base for some suppositories to dissolve the active substance in order to allow enhanced bioavailability by facilitating effective and complete release of the active substance in the body. Rather high molar mass PEGs are used to coat suppositories, providing elasticity and lubricity.

Poloxamer. Poloxamers represent another important group in the field of polymer excipients, which are triblock amphiphilic copolymers of the structure PEG-*b*-PPG-*b*-PEG (also known as Pluronic® from BASF). They are used for drug delivery as formulation excipients. They act as surfactants, emulsifying agents, solubilizing agents, dispersing agents, and as *in vivo* absorbance enhancers. They are also used in topical dosage forms, rectal suppositories, for the modification of the surface of hydrophobic drugs,[454] for drug delivery,[455] as micelles and micellar drug formulations for gene delivery,[456] and as components in formulations for transdermal drug delivery.[457] Because of the different customized block-lengths in the copolymers various poloxamers exist. Due to their inertness, a few poloxamers are on the rather tight list of excipients that were officially approved by the European Pharmacopoeia as well as the U.S. Pharmacopoeia even for human parenteral administration acting as dispersing, emulsifying and coemulsifying excipient, as tablet lubricant or wetting agent.

Poly(vinyl pyrrolidone) (PVP). PVP, also known as "povidone", is used in the pharmaceutical industry as a synthetic polymer vehicle for dispersing and suspending drugs. It has multiple uses, including as a binder for tablets and capsules, a film former for ophthalmic solutions, to aid in flavoring liquids and chewable tablets, and as an adhesive for transdermal systems. In oral dosage forms it is also added as a wicking agent to facilitate the entry of water to the inner surface of the core of the tablet by the formation of channels. A wide range of vinyl pyrrolidone homopolymers (povidone k12 to k90) with different molar masses are also available from BASF under the name Kollidon®. The k number refers to the mean molar mass of the PVP. The polymers with higher k-values (*i.e.* k90) are not usually administered by injection since their high molar masses prevent excretion by the kidneys and lead to accumulation in the body. The best-known example of PVP formulations is povidone-iodine, an important disinfectant. "Crospovidones" (polyplasdones, polyvinylpolypyrrolidone) are synthetic, insoluble, cross-linked

homopolymers of *N*-vinyl-2-pyrrolidone. They are insoluble in water, though they still absorb water and swell very rapidly generating a swelling force. As a consequence, they are used as disintegrants and dissolution agents for solid oral dosage forms and are even effective for poorly soluble dosage forms. Such orally disintegrating tablets have emerged as one of the novel solid oral dosage forms with the potential to deliver a wide range of drug candidates.[458] Polyplasdone™ XL crospovidone (Ashland) is a commonly used polyplasdone.

Poly(vinyl alcohol). Poly(vinyl alcohol) (PVA) as a water-soluble synthetic polymer is used to increase viscosity in pharmaceuticals but also as a lubricant and protectant in ophthalmic preparations (known as "artificial tears").[459] PVA is often found in over-the-counter eye redness and eye lubricant drops (Liquifilm Tears). PVA is the lubricant, and works by providing moisture to the eye, which helps to relieve dryness and protects the eye from becoming more irritated sometimes in combination with, for instant, phenylephrine.

Table 26. Selected examples of synthetic polymers as matrix excipients.

TRADE NAME	POLYMER SYSTEM	PREDOMINANT DOSAGE FORMS USED IN …	FUNCTION IN DOSAGE FORMS AS MATRIX EXCIPIENT
Eudragit®	P(MAA-*co*-MMA)	Oral	Film former, tablet binder, tablet diluent
Carbomer/Carbopol™	PAA	Ophthalmic	Mucoadhesive , viscosity enhancer, thickening agent
Polycarbophil	Poly(acrylic acid) cross-linked with divinyl glycol	Oral, vaginal gels	Mucoadhesive
Dimethicone	PDMS	Oral	Antifoaming agent, emollient
Poly(ethylene glycol)	PEG	Oral, parenteral, rectal	Ointment base, plasticizer, solvent, suppository base, tablet and capsule lubricant, mucoadhesive, tablet binder, thickening agent
Poloxamer/Pluronic®	PEG-*b*-PPG-*b*-PEG	Parenteral	Dispersing agent, emulsifying and coemulsifying agent, solubilizing agent, tablet lubricant, wetting agent, non-ionic surfactant
Povidone	PVP	Oral, ophthalmic	Disintegrant, dissolution aid, suspending agent, tablet binder
Crosspovidone	Polyvinylpolypyrrolidone (highly cross-linked povidone)	Oral	Tablet disintegrant
Copolyvidone	P(VP-*co*-VAc)	Oral	Film-former, granulating agent, tablet binder
Poly(vinyl alcohol)	PVA	Ophthalmic	Viscosity enhancer, lubricant & protectant

3.5.1 Oral dosage forms

Oral drug delivery combines several advantages and is, as already described, the most frequently used route for introducing drugs into the body.[460] The drug absorption depends on different factors making this process a complex one. One important issue is the solubility of the API's in the GI fluids to enable oral absorption (see coating of solid oral dosage forms, Chapter 3.4.1). Indeed, more than 50% of potential new drug candidates are expected to be lipophilic and have poor aqueous solubility.[461] In recent years, polymeric excipients have been widely used to overcome low solubility and formulation difficulties. Furthermore, various new solid formulations have been developed using technologies that involve polymer excipients. Selected examples of commercial oral drug formulations containing different synthetic polymers as matrix excipients are summarized in Table 27. Further oral products containing PEGs are nicely summarized by Gullapalli *et al.*.[451a]

1898 **Table 27**. Selected examples of oral drug formulations on the market containing different synthetic polymers as matrix excipients.

NAME	DRUG[a]	POLYMER SYSTEM	INDICATION/ USE	MANUFACTURER
Diethylpropion	Diethylpropion hydrochloride	Carbomer homopolymer type a	Treatment of obesity (anorexiant)	Lannett
Metformin	Metformin hydrochloride	Carbopol® 974P NF	Blood sugar control in people with type 2 diabetes	Aurobindo Pharma Limited
Alfuzosin	Alfuzosin hydrochloride	Carbomer homopolymer type b	Benign prostatic hyperplasia	Aurobindo Pharma Limited
Macrobid®	Nitrofurantoin	Carbomer 934[b]	Urinary tract infection	Norwich Pharmaceuticals
Striant®	Testosterone	Polycarbophil	Treatment of hypogonadism	Columbia Laboratories
Keflex®	Cephalexin	Dimethicone	Bacterial infection, skin or soft tissue infection, bladder infection, upper respiratory tract infection	Advancis Pharmaceutical
Antara®	Fenofibrate	Simethicone	Lowering high cholesterol & triglyceride levels in the blood	Lupin
Zarontin®	Ethosuximide	PEG 400[c]	Prevention and control of a certain type of seizure	Pfizer
Advil®	Ibuprofen	PEG 600	Pain relief for headaches, migraines & minor arthritis	Pfizer
Lybrel®	Ethinyl estradiol/ levonorgestrel	PEG 400, PEG 1450	Abnormal uterine bleeding, birth control, ovarian cysts, endometriosis, polycystic ovary syndrome	Wyeth
Augmentin™	Amoxicillin/clavulanic acid	PEG 4000, PEG 6000, dimethicone	Antibiotic (beta-lactamase inhibitors) for short term treatment of a wide range of infections caused by bacteria	GlaxoSmithKline
Lipofen®	Fenofibrate	PEG 8000, PEG 20000	Primary hypercholesterolemia, mixed dyslipidemia, severe hypertriglyceridemia	Cipher™
Maalox®	Aluminium & magnesium hydroxide/calcium carbonate	Simethicone	Acid indigestion, heartburn & sour stomach	Novartis
VapoSteam™	Camphor	PDMS, poloxamer 124[d]	Cold symptoms	Vick
Alprazolam	Alprazolam	Poloxamer 188 (Pluronic F 68)	Anxiety, panic disorder, depression, tinnitus, dysautonomia	TEVA
Accretropin™	Somatropin (recombinant human growth hormone (r-hGH))	Poloxamer 188 (Pluronic F 68)	Pediatric growth hormone deficiency, Turner syndrome	Cangene Corporation
Famciclovir	Famciclovir (guanosine analogue antiviral drug)	Poloxamer 407 (Pluronic F 127 NF)	Herpes zoster, herpes simplex	Apotex
Endocet®	Acetaminophen/oxycodone	Povidone	Chronic pain	Endo®
Naproxen	Naproxen	Povidone	Back pain, ankylosing spondylitis, sciatica, bursitis, tendonitis	TEVA
Cetirizine	Cetirizine hydrochloride	Povidone k29/32	Allergic rhinitis, urticaria	Northstar Rx LLC
Tinidazole	Tinidazole	Povidone k12	Bacterial vaginitis, trichomoniasis, giardiasis, amebiasis	Roxane Laboratories
Adenovirus vaccine		Plasdone C (PVP)	Adenovirus type 4 & type 7 vaccination	Barr Labs
Isoptin® SR	Verapamil hydrochloride	PEG, Povidone	Cluster headaches, migraine prevention, arrhythmia, high blood pressure	Ranbaxy Pharmaceuticals
Opana® ER	Oxymorphone	PVA, PEG	Narcotic analgesic	Endo®
BuPROPion	Bupropion hydrochloride	PVA, copovidone, povidone	SSRI induced sexual dysfunction, major depressive disorder, anxiety	Actavis

[a] All mentioned drugs are used in various drug formulations. However, in most cases they do not comprise a polymeric matrix excipient; [b] carbomer codes (*e.g.* 934) are an indication of molar mass and the specific components of the polymer; [c] PEG # (*e.g.* PEG 400) indicates the average molar mass of the specific PEG (*i.e.* 400 g mol^{-1}); [d] the first two digits code the molar mass of the PPG core, and the last digit codes the PEG content.

3.5.2 Parenteral dosage forms

Parenteral dosage forms describe all forms of administration avoiding any part of the gastrointestinal tract. The advantages of parenteral injection through the skin or other external boundary tissue are immediate systemic drug availability and rapid onset of action, as well as a long-term drug delivery by the formation of a depot or reservoir at the injection site. The sustained release of the drugs results from its long-acting property and its residence in the blood stream or the bone. However, the use of excipients for injectable drugs is more limited than for oral administration.[462] The application of novel excipients or the increase of their established concentration requires additional safety studies, which impedes the continuous progress of novel matrix excipients. Therefore, the well-established PEG is still the method of choice for polymeric excipients (Table 28).[451a] In comparison to compounds that are soluble and stable in a PEG vehicle (formulation as solution), insufficient solubility requires the formulation as suspension. Therefore, higher molar mass PEGs are used as suspending agents (viscosifying) to prevent setting of the dispersed material and to maintain homogeneity.

Table 28. Selected examples of parenteral drug formulations on the market containing PEG as matrix excipients.

TRADE NAME	DRUG	POLYMER SYSTEM	INDICATION/ USE	MANUFACTURER
		Solutions		
VePesid®	Etoposide	PEG 300[a]	Antineoplastic	Bristol-Myers Squib
Robaxin®	Methacarbamol	PEG 300	CNS depressant, musculoskeletal relaxant	Wyeth
Busulfex® (Myleran®)	Busulfan	PEG 400	Preparatory regimen prior to allogeneic hematopoietic progenitor stem cell transplantation	Otsuka Pharmaceutical
Ativan®	Lorazepam	PEG 400	Antianxiety, anticonvulsant	Biovail Laboratories
Persantine®	Dipyridamole	PEG 600	Coronary vasodilator	Boehringer Ingelheim (disc.)
		Extended-release suspensions		
Bioclate™	Antihemophilic factor VIII	PEG 3350	Prevention of bleeding episodes in persons with hemophilia A, control the bleeding related to surgery or dentistry in a person with hemophilia	Baxter Healthcare, Genetics Institute
Depo-Provera®	Medroxyprogesterone acetate	PEG 3350	Contraception	Pfizer
Depo-Medrol Lidocaine®	Methylprednisolone acetate, lidocaine	PEG 3350	Osteoarthritis, rheumatoid arthritis, acute & subacute bursitis	Pfizer
Aristocort® Forte	Triamcinolone	PEG 3350	Asthma, atopic dermatitis, drug hypersensitivity reactions	Sandoz
Invega Sustenna®	Paliperidone palmitate	PEG 4000	Schizophrenia	Janssen

[a] PEG # (*e.g.* PEG 300) indicates the average molar mass of the specific PEG (*i.e.* M_n = 300 g mol^{-1}).

3.5.3 Rectal, vaginal and urethral dosage forms

Suppositories. Suppositories are one type of solid dosage forms and can be administered rectal,[463] vaginal,[464] and to a much lesser extent, urethral. Although there are different suppository types, the systemic absorption is limited

to the rectal absorption, while the other two forms are mainly intended for local action. The rectal route is the method of choice if the oral dosage is not possible because of nausea, incapability of swallowing, or if the patient is unconscious. Different advantages and disadvantages of rectal administration have been nicely summarized by Vora and AliChisty.[463] The suppositories should melt or dissolve in the respective fluids in order to release the drug. Depending on the drug and the site of action different "suppository bases" are used, mainly fatty and oleaginous bases as well as water soluble and water miscible bases. Whereas the former ones are mostly derived from cocoa butter (also cottonseed oil, vegetable oils) the latter ones contain reasonable amounts of various PEGs of different molar masses (Table 29).[463] Certain PEG polymers may be used singly as suppository bases, but more commonly, formulas call for compounds of two or more molar masses mixed in various proportions as needed to yield a finished product of satisfactory hardness and dissolution time. Since the water miscible suppositories dissolve in body fluids and need not be formulated to melt at body temperature, they can be formulated with much higher melting points and thus may be safely stored at room temperature.

Table 29. Selected examples of suppositories on the market containing PEG as matrix excipients.

TRADE NAME	DRUG	POLYMER SYSTEM	INDICATION/ USE	MANUFACTURER
		Rectal		
THE MAGIC BULLET™	Bisacodyl	PEG	Relief of occasional constipation	Concepts in Confidence, USA
Acephen™	Acetaminophen	PEG 100 stearate[a]	Reduction of fever, relieve minor aches, pains & headache	G & W Laboratories
Indocin®	Indomethacin	PEG 3350,PEG 8000	Severe rheumatoid arthritis, ankylosing spondylitis, osteoarthritis, gouty arthritis	G & W Laboratories
Numorphan®	Oxymorphone	PEG 1000, PEG 3350	Relief of moderate to severe pain	Endo®
		Vaginal		
AVC	Sulfanilamide	PEG 400, PEG 3350	Treatment of Candida albicans infections	Monarch
Encare®	Nonoxynol-9	PEG	Contraception	Thompson Medical
Endometrin®	Progesterone	PVP	Help to become & stay pregnant	Ferring
		Urethral		
MUSE®	Alprostadil	PEG 1450, PEG 400	Treatment of erectile dysfunction (male)	Meda Pharmaceuticals

[a] PEG # (*e.g.* PEG 100) indicates the average molar mass of the specific PEG (*i.e.* M_n = 100 g mol^{-1}).

Gels. Gels have been established as useful dosage form for vaginal applications of different drugs endowed with moisturizing and lubrication effect, physiological pH restoring effect, as contraceptive, and as labor inducer.[465] They represent semi-solid systems comprising small amounts of solid, dispersed in a large volume of liquid. Gels show several advantages over other vaginal drug delivery systems such as higher bioavailability, safety, versatility, and economical savings.[466] Among the common natural derivatives (cellulose, chitosan etc.), PAA derivatives are mainly used as synthetic polymeric excipients (Table 30). Thanks to the high content in water, gels based on mucoadhesive polymers, without addition of drugs, are proposed for moisturization of the vagina in cases of vaginal dryness. Such Vaginal gels contain polycarbophil that forms the basis of well-consolidated marketed products (*e.g.* Replens®, Miphil®).[467]

Table 30. Selected examples of vaginal gels on the market containing different synthetic polymers as matrix excipients.

TRADE NAME	DRUG	POLYMER SYSTEM	INDICATION/ USE	MANUFACTURER
Zidoval®	Metronidazole	Carbomer 974P[a]	Bacterial vaginosis	Meda Pharmaceuticals
Metrogel®	Metronidazole	Carbomer 934P	Inflammatory papules & pustules of rosacea	Galderma
Replens®		Polycarbophil	Vaginal dryness	Church & Dwight
RepHresh® (Miphil®)		Polycarbophil	Vaginal dryness, bacterial vaginosis	Sanol
Advantage S	Nonoxynol-9	Carbomer 934P, polycarbophil	Contraception	Columbia Laboratories
Crinone®	Progesterone	Carbomer 934P, polycarbophil	Infertile women with progesterone deficiency, secondary amenorrhea	Watson
Conceptrol®	Nonoxynol-9	Povidone	Contraception	Revive

[a] Carbomer codes (*e.g.* 974P) are an indication of molar mass and the specific components of the polymer.

3.5.4 Ophthalmic dosage forms

Typically, gels with high water content but with certain viscosity are applied in ophthalmic drug formulations. To impart a high viscosity and a water content > 90%, in particular carbomers/carbopols™[468] and poloxamers[469] are used (Table 31). The polymers have to prolong the contact time on the ocular surface and to slow down the drug elimination. Eye drops represent an alternative dosage form to achieve therapeutic concentrations of drugs in ocular tissues. Thereby, the topical administration is effective for molecules with poor ocular uptake or poor efficacy-to-safety ratio when given systematically. The poor bioavailability and therapeutic response exhibited by conventional ophthalmic solutions due to pre-corneal elimination of the drug may be overcome by the use of *in situ* gel forming systems. *In situ* gelling systems increase the viscosity by changing the pH value or temperature in the pre-corneal region and lead to an increase of drug bioavailability by slowing drainage. Poloxamers possess thermal gelling properties and are frequently included in ophthalmic formulations to improve the ocular bioavailability of drugs by increasing the viscosity.[470] Future prospects are the delivery of peptides and proteins with the help of stimuli-responsive polymers.[471]

Table 31. Selected examples of ophthalmic drug formulations on the market containing different synthetic polymers as matrix excipients.

TRADE NAME	DRUG	POLYMER SYSTEM	DOSAGE FORM	INDICATION/ USE	MANUFACTURER
Pilopine HS®	Pilocarpine hydrochloride	Carbopol 940	Gel	Control intraocular pressure	Alcon Laboratories
Zirgan®	Ganciclovir	Carbomer	Gel	Acute herpetic keratitis (dendritic ulcers)	Bausch & Lomb
RESTASIS®	Cyclosporine	Carbomer copolymer type A	Emulsion	Chronic dry eye	Allergan
AzaSite®	Azithromycin	Poloxamer 407/ polycarbophil (DuraSite®)	Solution	Bacterial conjunctivitis	Akorn
ALREX®	loteprednol etabonate	Povidone	Suspension	Seasonal allergic conjunctivitis	Bausch & Lomb
Refresh Redness Relief®	Phenylephrine hydrochloride	PVA	Solution	Eye redness & dryness	Allergan

3.6 Polymeric drugs

Polymers that act as pharmaceutically active ingredients are relatively rare. Besides several attempts already in the 1960s, poly(ethylene sulfonate) and poly(maleic anhydride-*co*-divinylether) (DIVEMA) were studied for their effects, *e.g.* as anti-tumor agents, but failed due to toxicity issues. The pharmaceutical industry remarked strong doubts that a polymer can be a therapeutic agent in diseases where small molecules failed.[472] Major concerns were the presumably high dispersity (Đ) and the structural heterogeneity, in particular with regard to regulatory issues. However, in the last years a new market grew up with polymeric drugs that are approved and have defined and well-characterized structural features. The polymer characteristics but also the administration routes strongly influence the therapeutic effect of the polymeric drugs.

Polymeric sequestrants. One field of application is the removal of detrimental species from the gastrointestinal (GI) tract in a selective manner. Such polymeric sequestrants work as therapeutic agents and are able to bind and subsequently eliminate harmful species that were either ingested or produced by the human body itself. These polymers are usually ion exchange resins in the form of hydrogels that are not adsorbed by the GI tract. For the treatment of hyperkalemia (*i.e.* high levels of potassium ions in the serum, which can cause abnormal heart rhythms and other health problems), a sodium polystyrene sulfonate (Kayexalate®) is used as cation-exchange resin since decades (Table 32).[473] However, the high levels on resulting sodium may cause other critical effects.[474] Recently, Valtessa® was approved as a new medication to treat hyperkalemia.[475] This cross-linked polymer based on calcium 2-fluoroprop-2-enoate, divinylbenzene and octa-1,7-diene (also named patiromer) with a calcium-sorbitol counterion is established as a formulation of 100 µm beads.

Patients suffering from chronic or end-stage renal diseases often have elevated serum phosphate concentrations (hyperphosphatemia) that can be treated with sevelamer hydrochloride marketed under the brand name Renagel®, which is a poly(allylamine) cross-linked with epichlorohydrin (Figure 24).[476] Comparing to this, Renvela®, a sevelamer carbonate, shows fewer side effects. Bile acid sequestrants are one strategy in the treatment of elevated cholesterol levels. Cholestyramine (quarternized ammonium groups attached to poly(styrene-co-divinylbenzene)) and colestipol (copolymer of diethylenetriamine and epichlorohydrin) are polymeric therapeutics that bind bile acid, which is necessary for the production of cholesterol in the liver, but both therapeutics lack on low clinical efficiency.[477] Besides diverse other amine containing cross-linked polymers that entered clinical trials, Colestilan (poly(2-methylimidazol-*co*-(chlormethyl)oxiran) and Colesevelam hydrochloride (poly(allylamine) with 1-chloro-2,3-epoxypropane, (6-(allylamino)-hexyl)trimethylammonium chloride and *N*-allyldecylamine) are already on the market and show better performances as bile acid sequestrants for the treatment of hypercholesterolemia.[478] Micronized crospovidone can be used in the treatment of diarrhea based on its ability to form complexes with toxins.[164b]

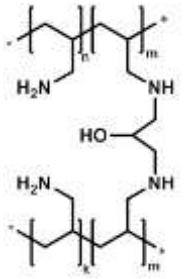

Figure 24. Schematic representation of the chemical structure for sevelamer, a poly(allylamine) cross-linked with epichlorohydrin (hydrochloride: Renagel®, carbonate: Renvela®).

For binding and removing toxins, originating *e.g.* from bacteria, such ion exchange resins are not efficient enough. More specific binding sides are necessary to reach multivalency. Tolevamer®, a high molar mass poly(styrene sulfonic acid), is such a toxin binder that is used to treat diarrhea.[479] However, this alternative to antibiotics failed in final clinical trials. The concept of multivalency is also used in research for the treatment of viruses, but none of them did reach the market yet. For example, specific peptides, that are conjugated to different polymer backbones, are able to protect cells from the anthrax toxin action.[480] A linear poly(acrylamide) bearing the C-glycoside of sialic acid shows antiviral activity against the influenza virus.[481] As preventional medicine for HIV infections, a naphthalene sulfonate polymer (PRO-2000®) was developed but also

failed in clinical phase studies.[482] The development of fat binding hydrogel-like polymers for the treatment of human obesity is also a growing area of research. Such polymers should inhibit fat hydrolysis and absorb unhydrolyzed fat droplets. They are based on *e.g.* poly(acrylamide)s, poly(meth)acrylates and other polymers that contain both cationic and hydrophobic moieties.[483] An even higher efficiency is aimed by additional conjugation of a lipase inhibitor to the polymer backbone (GT 389-255).[484]
Dimethicone (PDMS) and Espumisan® (dimethicone compounded with 4 to 7% silicone dioxide) are used as active pharmaceutical ingredients (API) in medicinal products such as chewable tablets, granulations, tablets, capsules, suspensions and drops.[485] These polymers are used in gastroenterology to relieve flatulence, tension in stomach, bowel colic and gastric ulceration due to their anti-foaming and anti-flatulent properties.[486] Moreover, simethicone can be used prior to upper GI endoscopy to reduce the amount of air bubbles and foam.[487] This increases the visibility during the procedure and provides the possibility of more accurate evaluation of the mucosa and consequently decreases the endoscopy duration.

Synthetic analogues of antigens. There are basically only very few polymeric drugs that are not related to sequestration of small molecules. They act as synthetic analogues of specific disease-associated antigens for systemic therapy. The first developed drug as such is glatiramer acetate (also known and marketed as Copaxone®). Glatiramer acetate is a copolymer of four L-amino acids (alanine, lysine, glutamic acid, and tyrosine in a molar ratio of 4.2 : 3.4 : 1.4 : 1.0) that are randomly copolymerized in a ring-opening polymerization of the corresponding amino acid anhydrides.[488] Glatiramer acetate acts *via* immunomodulation of pathways involved in the pathogenesis of multiple sclerosis. However, the complete mode of action is not yet fully understood. Patients suffering from multiple sclerosis demonstrate a significant decrease in the number of relapses and rate of progression when treated with glatiramer acetate. A recent study also shows a reduction of symptoms in patients with the Rett syndrome.[489] There was also a clinical trial where age-related macular degeneration could successfully be treated with glatiramer acetate.[490] The most recent research goes to other poly(amino acid) combinations that might also show a high potential as drugs for modulating immune responses.[491]

Miscellaneous polymeric drugs. Another polymeric drug is the commonly used highly purified non-ionic surfactant poloxamer 188, a block copolymer consisting of PEG-*b*-PPG-*b*-PEG (Pluronic® F-68). It is used in treating sickle cell disease to reduce inflammation and pain.[492] Clinical trials showed rheologic, cytoprotective, anti-adhesive and antithrombotic effects that help to reduce the overall duration of painful episodes of patients suffering from the sickle cell disease. The trials passed phase III (NCT00004408) but the drug (Flocor®) did not come to the market yet. An innovative approach is the PolyHeal™ technology, using negatively charged microspheres (~ 5 µm). They consist of nonbiodegradable, medical grade polystyrene (PS) in a suspension of serum-free nutrient medium. Cells and macromolecules are able to attach to the surface of the microspheres and to participate in the wound healing process. Further polymer-based wound healing dressings have been nicely summarized by Ghadi *et al.*.[493]

Table 32. Selected examples of polymeric drugs on the market.

TRADE NAME	POLYMER SYSTEM	INDICATION/USE	MANUFACTURER
Kayexalate®	Cross-linked sodium poly(styrene sulfonate)	Hyperkalemia	Sanofi
Valtessa®	Cross-linked calcium 2-fluoroprop-2-enoate, divinylbenzene, octa-1,7-diene (patiromer)	Hyperkalemia	Relypsa
Renagel®	Cross-linked poly(allylamine) (sevelamer hydrochloride)	Hyperphosphatemia	Sanofi (Genzyme)

Renvela®	Cross-linked poly(allylamine) (sevelamer carbonate)	Hyperphosphatemia	Sanofi (Genzyme)
BindRen® (Colestilan)	Cross-linked poly(2-methylimidazol-*co*-(chlormethyl)oxiran)	Hypercholesterolemia	Mitsubishi Tanabe Pharma
Welchol®, Cholestagel® (Colesevelam)	Cross-linked poly(allylamine)	Hypercholesterolemia	Sanofi (Genzyme)
Espumisan®	PDMS (simethicone)	Flatulence	Berlin-Chemie
Copaxone®	Glatiramer acetate	Multiple sclerosis	TEVA
PolyHeal™	PS	Wound healing	TEVA

4. Future prospects and concluding remarks

Besides the previously described systems on the market or in clinical trials, a large variety of polymer-based materials are currently under preclinical investigations, and these materials show immense potential concerning drug delivery applications. In the following chapter, we highlight a few exemplarily chosen systems used for pharmaceutical applications, which in our opinion hold an enormous potential and will certainly be in forthcoming clinical studies.

Polymer-drug conjugates. Although polymer-drug conjugates are under investigation for several decades now, the research interest in this field is still unabated. PEGylation has certainly dominated the area so far, but increasing concerns about its immunogenicity have promoted the development of new polymers and their conjugates. Some of these materials already reached the stage of clinical testing (conjugates of poly(*N*-(2-hydroxypropyl)methacrylamide (PHPMA), poly(2-oxazoline) (POx), see Chapter 3.1.2), and based on their performance more conjugates are currently in preclinical studies. The latest investigations, however, focused on the development of biodegradable polymers such as polyphosphoesters to substitute the nondegradable PEG. In the following some of the most promising systems are described.

Nondegradable polymers for drug conjugates. Among the vinyl based materials prepared by radical polymerizations PHPMA had certainly the highest impact on the area of polymer-drug conjugates. Due to the good compatibility and shielding capacity it is no surprise that more studies are ongoing. Besides the previously described drug conjugations, PHPMA has, *e.g.*, successfully been conjugated to NPC1161 (8-[(4-amino-1-methylbutyl) amino]-5-[3,4-dichlorophenoxy]-6-methoxy-4-methylquinoline), an 8-aminoquinoline analog with anti-leishmanial activity, and already passed successfully preclinical studies (*in vivo*).[494] In combination with *N*-acetylmannosamine (ManN) in the side chains, this polymer conjugate represents a promising candidate for clinical studies with reduced toxicity and increased efficiency of anti-leishmanial drugs for the treatment of visceral leishmaniasis. Mannose-grafted systems allow a selective delivery of anti-leishmanial drugs and a maximization of the potential of the drug to destroy the parasite at the site where it resides by mimicking the invasion process (mannose-dependent receptor-mediated endocytosis).

Further candidates based on vinyl polymers, which are close to be tested in clinical studies, rely on established systems, such as the Dynamic PolyConjugate (DPC) products: ARC-F12 (thrombosis, angioedema, inhibits the production of factor 12), ARC-LPA (cardiovascular diseases, reduces the production of apolipoprotein A), and ARC-HIF2 (clear cell renal cell carcinoma, first candidate to target tissue outside of the liver).[495]

During the last two decades, the class of POx has gained increasing attention for biomedical and drug delivery applications. Besides the already mentioned first POx conjugate (SER-214) under clinical investigations, several studies deal with the conjugation to drugs or proteins. The first report on a protein coupled to POx was published in 1990 by Miyamata *et al.*.[496] Preparing POx with a carboxylic acid as end-group allowed to attach the polymer to amine groups of the protein (lysine groups) using DCC/NHS chemistry. Other publications also show the increasing thermal stability,[497] as well as a decreasing rate of aggregation[498] using POx ligated proteins. The coupling of carboxy functionalized POx using NHS chemistry is the most common reaction for protein conjugation,[499] alongside using pyromelitic anhydride,[500] CuAAc,[501] reductive amination,[499b] native chemical ligation,[502] or the direct reaction of a protein with the living chain end of the polymerization.[503] Luxenhofer *et al.* recently summarized poly(2-oxazoline) drug and protein conjugates in different stages of their preclinical investigations.[113b] An interesting feature of POx is the versatility of the various types of oxazolines allowing to alter the properties and functionalities of the resulting polymers. For example, it was demonstrated that the cellular uptake can be influenced by the choice of the oxazoline monomer and architecture[499a, 503] and *in vivo* investigations showed a low immune response, as well as an increased circulation of POxylated proteins.[504] Besides these protein conjugates, POx was also conjugated to small molecule drugs in order to alter their pharmacokinetics. The anticancer drug Ara-C[498] as well as the antibiotic ciprofloxacin[505] showed similar behavior when conjugated to PEtOx as comparable PEG conjugates. In summary, it seems that in terms of biocompatibility and pharmacokinetic POxylation and PEGylation have very similar effects,[506] however, from a synthetic point of view the properties of POx can be altered with relative ease compared to PEG, just by changing the type of monomer used rendering POx a highly versatile tool.

A further alternative are zwitterionic polymers, that are mainly represented by polycarboxybetaine, polysulfobetaine and poly(methacryloyloxyethyl phosphorylcholine) (Figure 25). They are postulated to partially substitute the current benchmark polymer for protein conjugates, PEG, and to take a key role in the future of protein therapeutics.[507] These polymers are able to maintain the stability of proteins without diminishing their binding affinity, which represents a major improvement over the current PEGylation technique. An interesting example for this class of polymers is the hyperbranched copolymer poly(3-ethyl-3-(hydroxymethyl)oxetane)-*co*-(carboxybetaine) which is used as a biomimetic material in drug delivery carriers.[508] Another promising candidate is poly(carboxybetaine methacrylate) that was modified with the charged drug DOX.[509] The resulting conjugate features a low cytotoxicity, prolonged circulation time and a controlled release of DOX under mild acid conditions. Studies on tumor-bearing mice showed a tumor-inhibition rate of 55% without resulting in any body weight loss which usually accompanies this treatment. As previously mentioned, zwitterionic polymers are very promising materials to maintain the bioactivity of proteins. In this context, Chen and co-workers synthesized a zwitterionic block copolymer poly(methyl acrylic acid-*b*-sulfobetaine methacrylate) to modify a protein drug (uricase).[510] They demonstrated that the stability of the enzyme is improved without causing any destructive effects on its bioactivity by the conjugation of a zwitterionic copolymer with a short poly(methyl acrylic acid) block.

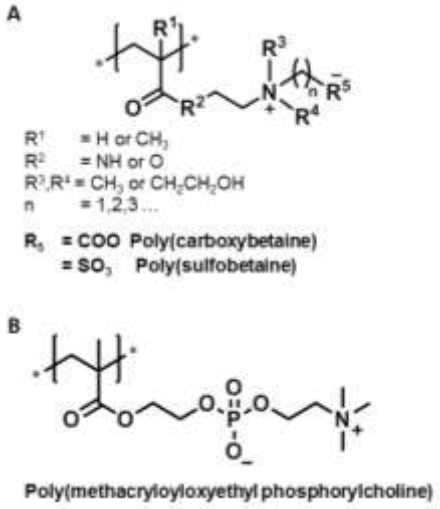

Figure 25. Schematic representation of the chemical structures of zwitterionic polymers: A) Poly(carboxybetaine) (R_5 = COO^-) and poly(sulfobetaine) (R_5 SO_3^-); B) poly(methacryloyloxyethyl phosphorylcholine).

Degradable polymers for drug conjugates. Undoubtedly, the degradability in biological relevant environment or at least the possibility for excretion of the applied polymers is a key aspect for their application in drug delivery. As a consequence, the nondegradable nature of many polymer conjugates using PEG or PHPMA has certainly hindered their progression towards market approval, although many of them have progressed into clinical development. Despite the efficiency of these materials, the safety of their administration is of utmost importance, and therefore it would not be surprising, if biodegradable polymer conjugates will have a much higher probability of clinical success.

Polyphosphoesters (PPE) represent a promising class of polymers which is not only biocompatible, but also degradable under physiological conditions. These alternatives have already been proposed as PEG substitutes in polymeric prodrugs.[130, 132d, 511] The simple and versatile adjustment of the hydrophobicity and polyvalence by attachment of different pendant ester groups of the variation of the backbone in PPEs allows the formation of fully biodegradable polymer-drug or -protein conjugates ("PPEylation"[512]) as well as the encapsulation of different drugs (*e.g.* low-molar-mass drugs, proteins, DNA, and plasmids) depending on the functionalities of the polymers. Recently, Zhang *et al.* presented a novel drug system containing ultra-high levels of drug loading *via* covalent attachment.[513] In this case, PEG-*b*-PPE-based paclitaxel (TXL) drug conjugates were synthesized by organocatalyst-promoted ring-opening polymerization (ROP) followed by click-reaction-based conjugation of PTX to the PPE block of the copolymer. The resulting amphiphilic polymer forms micelles with a loading capacity of 65 wt% of PTX and demonstrated to be effective against several cancer cell lines. In another study, dual pH-sensitive nanoparticles (PPC-Hyd-DOX-DA) have been designed, which are able to reverse their surface charges when exposed to tumor tissue to facilitate cell uptake.[514]

Polymers based on repeating ester units are another potential biodegradable class of polymers which is intensively investigated for polymer-drug conjugate approaches and also possesses a wide range of functionalities and properties.[515] Among them, polycarbonates have recently received much attention for protein/peptide conjugation.[516] Hedrick and co-workers demonstrated the synthesis of functional polycarbonates by ROP starting from the monomer pentafluorophenyl 5-methyl-2-oxo-1,3-dioxane-5-carboxylate (MTC-OC_6F_5, Figure 26). The active pentafluorophenyl esters enable a substitution with suitable nucleophiles such as alcohols and amines and, thus, the functionalization with other active groups.[517] The versatility of this approach was demonstrated by the preparation of numerous functional polycarbonates, which are of particular relevance to polymer-drug conjugates, including polycarbonates with PEG,[516] hydroxyl-containing[518] and zwitterionic side-chains.[519] Recently, Cheng *et al.* reported an *in vivo* efficacy for the first example of a polymeric therapeutic based on polycarbonates for the treatment of systemic methicillin-resistant *Staphylococcus aureus* (MRSA) infection. Other novel functional nanocarriers for biomedical applications have been extensively reviewed by numerous research groups, highlighting these polycarbonate-based degradable alternatives to PEG with minimal toxicity.[518, 520]

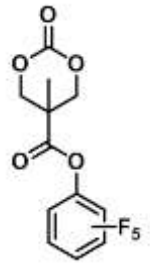

Figure 26. Schematic representation of the chemical structure of pentafluorophenyl 5-methyl-2-oxo-1,3-dioxane-5-carboxylate (MTC-OC_6F_5).

Micro- and nanoparticulate drug carriers. Although polymer-drug conjugates have certainly made a huge impact in the research area of synthetic pharmapolymers, great promises have been expected from particulate drug carrier systems. The versatility and diversity of potential materials used for their preparation allows a flexible design with tailor made properties, which has certainly resulted in the success of various systems in clinical trials or on the market. However, several issues still have to be addressed and the potential of these systems has by far not been fully exploited. The transfer of degradability to nondegradable polymers often represents a missing link between the design of advanced materials and their use in biomedical applications. To fulfill the criteria of degradability

appropriate units have to be integrated into the main chain during the synthesis. Another big issue in the application of particles, in particular microparticles, for drug delivery is the initial burst release.[521] This problem can be overcome by choosing the optimal conditions for the formulation processing or by changing the properties of the drug or the polymer itself to prevent polymer-drug separation. Doubtless, the main challenge is the targeted delivery that is necessary for cancer and some other diseases to perform better than conventional medications. An analysis of over 100 cancer studies has shown that in the average only 0.7% of injected particles reach their targets.[522] And what is more surprising, this number did not change within the last 10 years. Reasons for this are the increased immunogenicity and plasma protein adsorption *in vivo*, which masks the targeting molecules and also results in decreased blood circulation times.[301] Consequently, targeted nanoparticles behave with the same or less efficacy than untargeted particles. Even the often studied EPR effect only yielded poor delivery efficiency and shows the lack of 'proof-of-concept' studies to be translated to patient care.[522] A better understanding of the *in vivo* nanoparticle transport is necessary and can be accomplished by quantitative analysis with subsequent collection of all the information in databases including organization and interpretation of the data also with the help of computational tools. Such open excess databases are already established and supported by several programs (*e.g.* DaNa2.0[523] and Cancer Nanomedicine Repository[524]). Only a translation from research to the patient might stimulate the application of nanotechnology for treating human diseases as promised.

Solid colloidal dispersions. One strategy is the use of copolymers of PLGA and PEG making the particles more hydrophilic and in consequence more suitable for protein delivery.[525] The hydrophilic domains facilitate a slow and controlled release by diffusion. Further improvements on the release profiles and an additional increase in the loading capacity could be achieved by a triblock copolymer system consisting of PLGA, PEG and poly(allyl glycidyl ether); the latter can also be used to conjugate targeting ligands.[526] Several other systems based on these classic release mechanisms of drugs (diffusion through water filled pores, diffusion through the polymer matrix, osmotic pumping, and erosion) encapsulated in polymeric nano- and microparticles are currently still under intensive investigation in *in vitro*, *in vivo* and preclinical studies.[527] However, besides these systems rapid progress has been made in the development of stimuli-responsive nano- and microparticles as smart alternatives within the last years.[528] In this case, the release can be triggered by internal (coming from the cells/tissue itself) or external (coming from outside) stimuli. Such triggers can for example be temperature, light, ultrasound, pH-value, redox environment, or specific biomolecules and enzymes.[528] The development of more efficient targeting structures may further improve the efficiency of nano-/microparticles. For example, particles carrying siRNA and targeting molecules are able to simultaneously attack numerous pathways.[529] The given examples display only a small fraction of the numerous systems in development. The wide field of polymeric materials with countless variations in constitution, conformation, configuration, and molar mass will definitely yield nano- and microparticles that have the potential to show efficacy beyond the current products in clinical stages and on the market. However, a translation from bench to bedside is more cost- and time efficient if the polymeric material is already used in pharmaceutical products.[308] An interesting study shows the beneficial properties of doxorubicin (DOX) loaded PLGA microparticles that could be used in transarterial chemoembolization (TACE) instead of recently developed PLGA based microgels.[530] Such PLGA microparticles allow a re-entry into the tumor feeding arteries after an initial TACE trial combined with higher drug release rates. A further important step is the development of a robust and scalable process for the fabrication of micro-/nanoparticles with reproducible quality and the subsequent GMP (good manufacturing practice) production in kilogram quantities.

An interesting alternative to PLGA is poly(caprolactone) (PCL), which has a slower degradation rate than PLGA (up to one year), a high permeability for the diffusion of small molecules and does not generate an acidic environment after degradation often causing the destabilization of proteins.[531] Up to now, PCL is most commonly used in tissue engineering. Its use as therapeutic molecule delivery system is still limited since PCL carriers reveal in many cases low encapsulation efficiency, burst release and low bioactivity. In contrast, besides its beneficial slow

degradation rate, PCL is a rubbery at room temperature, which allows high permeability for many drugs. In recent years, PCL-materials have been intensively investigated in *in vitro* and *in vivo* biocompatibility and efficiency studies in order to deliver drugs, genetic materials and proteins. They have been nicely reviewed by Venkatraman and co-workers.[532] One example is the encapsulation of chloramphenicol in PCL-Pluronic® composite nanoparticles (CAM-PCL-NP). These systems exhibited significantly enhanced anti-MRSA (*methicillin-resistant Staphylococcus aureus*) activity against ten clinical isolates of MRSA strains. Compared to free-chloramphenicol treatment, the *in vivo* study of CAM-PCL-NPs in MRSA-infected burn-wound mice models revealed quicker efficiency in MRSA clearance and an improved survival rate.[533] Preclinical studies of a further formulation named NC-6300 show promising results in mice and are now under way for clinical studies in Japan.[534] In NC-6300, epirubicin is attached *via* an acide-labile hydrazone bond to PEG-PAs, which can be beneficial due to a better controlled release kinetic. Further attempts are also in the development of targeted drug delivery systems, which was already shown, *e.g.* by attaching several anti-TF antibodies resulting in an enhanced antitumor activity against TF-high expressing human pancreatic cancer cells, a subunit toolbox with insensibly large possible combinatorial combinations of desired bio-functionality and evolutionary optimization techniques.[535]

Polyplexes. Cationic polymers have already been bloomed over years as non-viral vectors in gene therapy. They show tremendous potential in treating different types of cancer and genetic disorders without using conventional drugs. One approach is to develop alternative gene delivery platforms by creating higher ordered macromolecular structures such as multi-component supramolecules or 2D and 3D scaffolds.[536] Another approach is to enhance existing vector platforms (*e.g.* by functionalization). For instant, the successful clinical application of the gold standard poly(ethylene imine) (PEI) for gene delivery depends mainly on three factors: I) The enhancement of the transfection efficiency; II) the reduction of toxicity, and, III) the ability of the vectors to overcome numerous biological barriers after systemic or local administration. Current research is focusing on the design of biodegradable[537] and more biocompatible derivatives[538] by modifying the PEI backbone. Very recently, our group introduced a new generation of linear PEI (3rd generation, Figure 27) bearing multiple functional groups comprising cationic functionalities, cell viability increasing functional groups as well as a third group of functionalities which can be used, *e.g.*, for targeting molecules.[38] One promising opportunity is the conjugation of glutathione moieties to the cationic backbone which enables the transport of genetic materials and, simultaneously, the passage through an hCMEC/D3 endothelial cell layer mimicking the highly selective blood-brain barrier (BBB) within a microfluidically perfused biochip.[539] Cationic methacrylate copolymers are another upcoming polymer platform able to interact with genetic material. Poly(2-dimethylaminoethyl methacrylate) (PDMAEMA) has shown promising gene transfection activity due to its cationic character.[540] Jiang and co-workers synthesized PEGylated PDMAEMA/DNA polyplexes for efficient brain-targeted gene delivery in mice. As mentioned for phosphates, inorganic safe materials will add an important basis for composites with synergistic functions.[541]

Figure 27. Schematic representation of the general chemical structure for the 3rd generation LPEI which describes the presence of multiple functional units comprising cationic functionalities (blue), cell viability increasing functional groups (black) as well as further functionalities (orange, *e.g.* targeting molecules).

Microgels. The importance of degradability has also been recognized for the design of carrier gels and, in particular, micro- and nanosized structures. One quite established example is a PEG microgel, which contains degradable PLGA sequences. Injecting them into the cavity of sheep shoulder joint, the new PEG-hydrogel microspheres were compared to nondegradable microgels with regard to location, degradation and inflammation.[542] The degradable microgel offers several advantages over the nondegradable material considering drug delivery in synovial tissue as it reduces the intensity of inflammatory reactions triggered in synovium. An interesting strategy for the continuous *in vivo* expression of a protein is the direct delivery of an *ex vivo* modified

cell encapsulated in a gel structure to shield it from the immune system. Sonnet *et al.* have developed a PEG-diacrylate (PEGDA) microgel with allogeneic carrier cells transduced with an adenovirus expressing BMP2 for bone regeneration.[543] The PEGylated microsphere system shields the cell and, thus, suppresses the destructive inflammatory processes. Within 3 weeks, a 5 mm long femur defect in a rat model was healed completely through secretion of 100-fold lower levels of protein compared to similar studies using recombinant protein. For the future, this class of injectables opens the macroscopic functional embodiment space staying close to a minimal invasive paradigm replacing larger drug eluting devices.

Nanogels. Besides the already discussed Medusa® technology (Chapter 3.2.3), the only nanogel examples that have been evaluated under clinical trials are based on a polysaccharide structure, *e.g.* cholesterol-bearing pullulan (CHP) network,[544] which are described elsewhere.[545] However, researchers still consider tailored nanogel systems as a very promising platform for drug delivery applications.[546] Recent successful studies prove the efficiency of nanogels by targeting multiple immune cell subsets in the draining lymph nodes.[547] In contrast to other gel materials, these systems are fabricated by the synthesis of mesoporous silica (MS) particles (200 nm) as templates and subsequent infiltration with pyridine dithioethylamine (PDA) modified poly(methacrylic acid) (PMAA-PDA). The infiltration of cysteamine (SH) modified PMAA (PMAASH) leads to a cross-linking by disulfide exchange followed by template removal. Further PEGylation of these PMAA nanogels did not affect their cellular association *in vitro*, but improved their lymphatic drainage *in vivo* (mice).
Similar to other nanoparticulate systems, the integration of stimuli responsive polymers promises access to carriers with local control of the cargo release. Recently, a new type of dual-responsive nanogel with tunable volume phase transition temperature and redox-labile properties was investigated.[548] The nanogel system is constructed from a copolymer based on vinylcaprolactam (VCL) and HPMA cross-linked with *N*,*N*'-*bis*(acryloyl)cystamine (P(VCL-s-s-HPMA)). The hydrophilicity of the nanogel allows a stable blood circulation at 37 °C. A higher temperature of the tumor tissue forces the nanogel to turn into a hydrophobic state which enhances its cell uptake. Upon the entrance into the tumor cells, a redox-triggered degradation of the nanogel (due to the presence of disulfide bonds) leads to a burst drug release. *In vivo* studies (A549 tumor-bearing mice) revealed that these nanogels can significantly limit the tumor growth with no side effects to normal tissues. These results underline the immense potential of the dual-responsive biodegradable nanogels for cancer therapy. Many other nanogel systems have been investigated *in vivo* based on polymers such as PMAA (drugs: DOX/TXL[549]), PEG (siRNA[550]), PEI (AZT 5'-triphosphate[551]), PEG-*b*-PGluA (17-AAG/DOX[552]; cisplatin/TXL[553]) and $PMEO_3MA$-*b*-PPFPMA (siRNA[554]). Considering the ongoing effort for the development of such carrier systems, we are certain that first nanogel materials will soon enter clinical trials.

Macroscopic drug carriers. They probably represent the most versatile application forms of pharmapolymers comprising the wide range of hydrogels and solid implants and inserts. The general trend is towards the creation of multiple functional systems. In our opinion, in particular the application of hydrogel systems will change significantly. Sensor and conditional release/activity can be established and are already shown for vaccination on animal trial stage.[555]

Hydrogels. The most common application form for hydrogels is certainly their use in contact lenses, but surprisingly they are not used as drug delivery vehicles so far, which is probably related to the loss of lens quality accompanied with the release. The recent development of new techniques to design contact lenses enables an extended drug release over a few weeks without any significant impact on the lens properties. Compared to alternative eye drops, these contact lenses revealed safety, efficacy and increased bioavailability in *in vivo* studies.[556] Corresponding contact lenses, placed on the cornea, release drugs into the post-lens (between lens and cornea) and reveal a prolonged contact time with the cornea.[557] The increased efficiency (35× higher than delivery with drops[558]) allows the delivery of drugs over extended time periods (which eliminates the need for multiple

dosing) while decreasing side effects since less drug amount is needed. Further ocular applications are the development of hydrogels based on poly(2-hydroxyethyl methacrylate) (PHEMA)[559] or poly(dimethyl siloxane) (PDMS),[560] which may serve as drug delivery agents for the anterior segment of the eye. The latter is also used for punctual plugs releasing cyclosporine A for a period of 3 months.[561] In the last years, immense effort has been put into the development of devices for ocular drug delivery,[562] and we are convinced that suitable systems will enter the market soon.

A real innovation is the non-hormonal contraceptive "Reversible inhibition of sperm under guidance" (RISUG®, Figure 28) for men developed by Guha and co-workers based on poly(styrene-*co*-maleic anhydride).[563] It represents a long acting and reversible alternative to a vasectomy as the polymer can be flushed with another injection of a dissolver.[564] It has been patented in several countries including India, China and the United States. While clinical phase III is already ongoing in India,[565] the Parsemus Foundation began to develop a similar polymer contraceptive inspired by RISUG® for the rest of the world in 2010 (Vasalgel™).[566] After one year of successful *in vivo* studies, they recently announced the start of first clinical trials in the second half of 2017 and a commercial launch in 2018.[567]

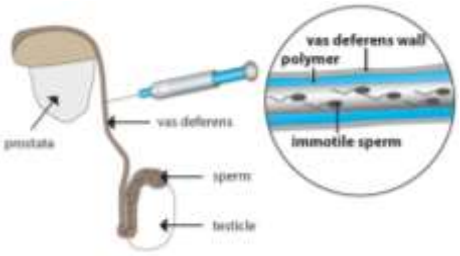

Figure 28. The work principle of "Reversible inhibition of sperm under guidance" (RISUG®): A) The hydrogel is injected into the vas deferens connected to each testicle; B) it coats the wall of the vas deferens. When sperm gets into contact with the wall it becomes unable to swim.

Besides the classic hydrogels, the development of so-called interpenetrating polymer networks (IPN) has expended enormously in the field of controlled release and targeted drug delivery in the last decades.[568] Introduced in 1960 by Miller,[569] IPN's are defined as "polymers comprising two or more networks which are at least partially interlaced on a molecular scale but not covalently bonded to each other and cannot be separated unless chemical bonds are broken" (IUPAC[570]). They represent a subgroup of physical gels. The blending of natural and/or synthetic polymers opens the field for the design of new controlled release systems for a variety of drugs and broadens the range of their properties.[571] IPNs reveal several advantages like an excellent swelling behavior, improved responsiveness and mechanical strength, which play an important role in drug delivery systems and differentiate them from single networks (such as hydrogels). Even if *in vitro* and *in vivo* data have been extensively studied and reviewed,[568, 571-572] and the number of patents on this technology is increasing frequently, IPN drug-loaded systems have not found their way into clinical studies up to now, and, hence, commercialization, so far. Their complexity due to the combination of various different properties has hindered a major breakthrough in pharmaceutical applications so far. The current research is still at the academic level, but in our opinion, IPNs are expected to receive much more attention in the future.

Coatings. Colon specific drug delivery has gained considerable attention not only considering colon associated diseases but also for the safe delivery of therapeutic peptides and proteins to the blood stream as the activity of proteolytic enzymes is far lower compared to the upper GI tract.[573] The marketed dosage forms that aim the site specific delivery of the drugs usually depend on the pH variations in the GI tract. However, the pH value difference between the small intestine and the colon is not high enough. This limits the efficient colon targeting in particular when the distal colon is targeted. Therefore, to achieve an efficient colon targeting, variations in the environment comparing the small and the large intestine are exploited in several *in vivo* studies, which include changes in the pH value, the different microbial enzymatic activity, the fluctuating intraluminal pressure or the transit time. Dosage forms which are coated with innovative colon targeting polymers have been extensively reviewed elsewhere.[574] However, it should be noted that novel polymers with unknown safety data always require additional safety assessment. Therefore, most of these studies use polymers with well-established safety profiles

for coatings. Hence, we do not envisage new marketed dosage forms with novel complex polymeric coatings in near future.

5. Concluding remark

The presented review attempted to provide a comprehensive overview of the current state of synthetic polymers used for drug delivery applications, so-called 'pharmapolymers'. Within the last decades, the impact of synthetic polymers has resulted in tremendous advances in chemical synthesis and analysis. The contribution highlights the current market situation and clinical status of respective polymers while paying attention to underlying chemical structures. In addition, we highlight upcoming trends in the development of new pharmapolymers, which in our opinion will have a tremendous impact on the market situation soon. However, we also summarize the obstacles these materials still have to overcome to the market for drug delivery applications. Our review comprises a detailed description of the most important polymer classes and their fields of application. Application forms like polymer-drug conjugates, drug carrier systems in scales ranging from nano- to macroscopic size, polymers as coatings and matrix excipients as well as polymeric drugs are described. We hope that providing a link between the properties and structures of these systems and their area of application helps scientists from different research fields where the systems are often just known by their trade names or abbreviations.

Acknowledgements

We acknowledge funding from the collaborative research center ChemBioSys (SFB 1127) by the German Science Foundation (DFG) and from the Thüringer Ministerium für Wirtschaft, Wissenschaft, und Digitale Gesellschaft (TMWWDG, ProExzellenz II, NanoPolar). M.G. is grateful for the funding by the DFG (GO 1100/4-1) and JB thanks the DFG for granting a fellowship (BR 4905/2-1). Furthermore, we thank Dr. Matthias Hartlieb for helpful comments.

Keywords

Pharmapolymers • drug delivery • market • clinical trials • structure-activity relationships

References

[1] A. S. Hoffman, *J. Control. Release* **2008**, *132*, 153-163.

[2] K. E. Uhrich, S. M. Cannizzaro, R. S. Langer, K. M. Shakesheff, *Chem. Rev.* **1999**, *99*, 3181-3198.

[3] a) P. J. Flory, *J. Am. Chem. Soc.* **1940**, *62*, 1561-1565; b) M. Szwarc, *Nature* **1956**, *178*, 1168-1169.

[4] A.-L. Brocas, C. Mantzaridis, D. Tunc, S. Carlotti, *Prog. Polym. Sci.* **2013**, *38*, 845-873.

[5] S. Penczek, M. Cypryk, A. Duda, P. Kubisa, S. Słomkowski, *Prog. Polym. Sci.* **2007**, *32*, 247-282.

[6] R. Hoogenboom, *Polyethers and Polyoxazolines*, in *Handbook of ring-opening polymerization* (Eds.: P. Dubois, O. Coulembier, J.-M. Raquez), Wiley-VCH, **2009**, pp. 141-164.

[7] a) B. Obermeier, F. Wurm, C. Mangold, H. Frey, *Angew. Chem. Int. Ed.* **2011**, *50*, 7988-7997; b) C. Mangold, F. Wurm, H. Frey, *Polym. Chem.* **2012**, *3*, 1714-1721; c) M. J. Barthel, T. Rudolph, S. Crotty, F. H. Schacher, U. S. Schubert, *J. Polym. Sci., Part A: Polym. Chem.* **2012**, *50*, 4958-4965.

[8] R. Kjellander, E. Florin, *J. Chem. Soc., Faraday Trans. 1* **1981**, *77*, 2053-2077.

[9] S. N. S. Alconcel, A. S. Baas, H. D. Maynard, *Polym. Chem.* **2011**, *2*, 1442-1448.

[10] a) A. Abuchowski, T. van Es, N. C. Palczuk, F. F. Davis, *J. Biol. Chem.* **1977**, *252*, 3578-3581; b) A. Abuchowski, J. R. McCoy, N. C. Palczuk, T. van Es, F. F. Davis, *J. Biol. Chem.* **1977**, *252*, 3582-3586.

[11] a) F. M. Veronese, *Biomaterials* **2001**, *22*, 405-417; b) F. M. Veronese, G. Pasut, *Drug Discovery Today* **2005**, *10*, 1451-1458; c) G. Pasut, F. M. Veronese, *Adv. Drug Delivery Rev.* **2009**, *61*, 1177-1188; d) M. J. Roberts, M. D. Bentley, J. M. Harris, *Adv. Drug Delivery Rev.* **2012**, *64*, 116-127.

[12] a) A. L. Klibanov, K. Maruyama, V. P. Torchilin, L. Huang, *FEBS Lett.* **1990**, *268*, 235-237; b) G. Blume, G. Cevc, *Biochim. Biophys. Acta Biomembr.* **1990**, *1029*, 91-97.

[13] S. Schöttler, G. Becker, S. Winzen, T. Steinbach, K. Mohr, K. Landfester, V. Mailänder, F. R. Wurm, *Nat. Nanotechnol.* **2016**, *11*, 372-377.

[14] a) V. P. Torchilin, V. S. Trubetskoy, *Adv. Drug Delivery Rev.* **1995**, *16*, 141-155; b) C. Monfardini, F. M. Veronese, *Bioconjugate Chem.* **1998**, *9*, 418-450.

[15] K. Knop, R. Hoogenboom, D. Fischer, U. S. Schubert, *Angew. Chem. Int. Ed.* **2010**, *49*, 6288-6308.

[16] a) A. Bendele, J. Seely, C. Richey, G. Sennello, G. Shopp, *Toxicol. Sci.* **1998**, *42*, 152-157; b) D. G. Rudmann, J. T. Alston, J. C. Hanson, S. Heidel, *Toxicol. Pathol.* **2013**, *41*, 970-983.

[17] D. A. Herold, K. Keil, D. E. Bruns, *Biochem. Pharmacol.* **1989**, *38*, 73-76.

[18] a) A. Chanan-Khan, J. Szebeni, S. Savay, L. Liebes, N. M. Rafique, C. R. Alving, F. M. Muggia, *Ann. Oncol.* **2003**, *14*, 1430-1437; b) J. Szebeni, *Toxicology* **2005**, *216*, 106-121.

[19] S. Dai, K. C. Tam, *Langmuir* **2004**, *20*, 2177-2183.

[20] S. Saeki, N. Kuwahara, M. Nakata, M. Kaneko, *Polymer* **1976**, *17*, 685-689.

[21] J. R. Fowles, M. I. Banton, L. H. Pottenger, *Crit. Rev. Toxicol.* **2013**, *43*, 363-390.

[22] M. Schömer, C. Schüll, H. Frey, *J. Polym. Sci., Part A: Polym. Chem.* **2013**, *51*, 995-1019.

[23] P. Kubisa, *J. Polym. Sci., Part A: Polym. Chem.* **2003**, *41*, 457-468.

[24] R. K. Kainthan, E. B. Muliawan, S. G. Hatzikiriakos, D. E. Brooks, *Macromolecules* **2006**, *39*, 7708-7717.

[25] M. A. Quadir, R. Haag, *J. Control. Release* **2012**, *161*, 484-495.

[26] A. Thomas, S. S. Müller, H. Frey, *Biomacromolecules* **2014**, *15*, 1935-1954.

[27] a) B. Klajnert, W. Walach, M. Bryszewska, A. Dworak, D. Shcharbin, *Cell Biol. Int.* **2006**, *30*, 248-252; b) R. K. Kainthan, J. Janzen, E. Levin, D. V. Devine, D. E. Brooks, *Biomacromolecules* **2006**, *7*, 703-709.

[28] M. I. Ul-Haq, B. F. L. Lai, R. Chapanian, J. N. Kizhakkedathu, *Biomaterials* **2012**, *33*, 9135-9147.

[29] K. Maruyama, S. Okuizumi, O. Ishida, H. Yamauchi, H. Kikuchi, M. Iwatsuru, *Int. J. Pharm.* **1994**, *111*, 103-107.

[30] O. Boussif, F. Lezoualc'h, M. A. Zanta, M. D. Mergny, D. Scherman, B. Demeneix, J. P. Behr, *Proc. Natl. Acad. Sci. U.S.A.* **1995**, *92*, 7297-7301.

[31] a) W. T. Godbey, K. K. Wu, A. G. Mikos, *J. Control. Release* **1999**, *60*, 149-160; b) W. T. Godbey, M. A. Barry, P. Saggau, K. K. Wu, A. G. Mikos, *J. Biomed. Mater. Res.* **2000**, *51*, 321-328.
[32] U. Lungwitz, M. Breunig, T. Blunk, A. Göpferich, *Eur. J. Pharm. Biopharm.* **2005**, *60*, 247-266.
[33] G. D. Jones, A. Langsjoen, S. M. M. C. Neumann, J. Zomlefer, *J. Org. Chem.* **1944**, *09*, 125-147.
[34] K. A. Gibney, I. Sovadinova, A. I. Lopez, M. Urban, Z. Ridgway, G. A. Caputo, K. Kuroda, *Macromol. Biosci.* **2012**, *12*, 1279-1289.
[35] a) T. Kagiya, S. Narisawa, T. Maeda, K. Fukui, *J. Polym. Sci. Part B* **1966**, *4*, 441-445; b) D. A. Tomalia, D. P. Sheetz, *J. Polym. Sci., Part A: Polym. Chem.* **1966**, *4*, 2253-2265.
[36] a) R. Tanaka, I. Ueoka, Y. Takaki, K. Kataoka, S. Saito, *Macromolecules* **1983**, *16*, 849-853; b) L. Tauhardt, K. Kempe, K. Knop, E. Altuntaş, M. Jäger, S. Schubert, D. Fischer, U. S. Schubert, *Macromol. Chem. Phys.* **2011**, *212*, 1918-1924.
[37] a) T. Saegusa, H. Ikeda, H. Fujii, *Macromolecules* **1972**, *5*, 108; b) T. Saegusa, S. Kobayashi, A. Yamada, *Macromolecules* **1975**, *8*, 390-396.
[38] T. Bus, C. Englert, M. Reifarth, P. Borchers, M. Hartlieb, A. Vollrath, S. Hoeppener, A. Traeger, U. S. Schubert, *J. Mater. Chem. B* **2017**, *5*, 1258-1274.
[39] K. Aoi, A. Motoda, M. Ohno, K. Tsutsumiuchi, M. Okada, T. Imae, *Polym. J.* **1999**, *31*, 1071-1078.
[40] a) J. H. Jeong, S. H. Song, D. W. Lim, H. Lee, T. G. Park, *J. Control. Release* **2001**, *73*, 391-399; b) H. M. L. Lambermont-Thijs, J. P. A. Heuts, S. Hoeppener, R. Hoogenboom, U. S. Schubert, *Polym. Chem.* **2011**, *2*, 313-322; c) H. P. C. Van Kuringen, J. Lenoir, E. Adriaens, J. Bender, B. G. De Geest, R. Hoogenboom, *Macromol. Biosci.* **2012**, *12*, 1114-1123.
[41] M. Jaeger, S. Schubert, S. Ochrimenko, D. Fischer, U. S. Schubert, *Chem. Soc. Rev.* **2012**, *41*, 4755-4767.
[42] a) A.-C. Albertsson, I. Varma, *Adv. Polym. Sci.* **2002**, *157*, 1-40; b) Q. Chen, G. Thouas, *Biomaterials: A Basic Introduction*, CRC Press (Taylor & Francis Group), Boca Raton, Florida, **2014**.
[43] B. Azimi, P. Nourpanah, M. Rabiee, S. Arbab, *J. Eng. Fiber. Fabr.* **2014**, *9*, 74-90.
[44] a) P. A. Gunatillake, R. Adhikari, *Eur. Cells Mater. J.* **2003**, *5*, 1-16; b) A. G. A. Coombes, S. C. Rizzi, M. Williamson, J. E. Barralet, S. Downes, W. A. Wallace, *Biomaterials* **2004**, *25*, 315-325; c) V. R. Sinha, K. Bansal, R. Kaushik, R. Kumria, A. Trehan, *Int. J. Pharm.* **2004**, *278*, 1-23; d) H. Sun, L. Mei, C. Song, X. Cui, P. Wang, *Biomaterials* **2006**, *27*, 1735-1740; e) X. Wei, C. Gong, M. Gou, S. Fu, Q. Guo, S. Shi, F. Luo, G. Guo, L. Qiu, Z. Qian, *Int. J. Pharm.* **2009**, *381*, 1-18.
[45] M. A. Woodruff, D. W. Hutmacher, *Prog. Polym. Sci.* **2010**, *35*, 1217-1256.
[46] M. Labet, W. Thielemans, *Chem. Soc. Rev.* **2009**, *38*, 3484-3504.
[47] C. Zhang, *Biodegradable polyesters: Synthesis, properties, applications*, in *Biodegradable polyesters*, Wiley-VCH, **2015**, pp. 1-24.
[48] K. Chavalitpanya, S. Phattanarudee, *Energy Procedia* **2013**, *34*, 542-548.
[49] a) A. Sarasam, S. V. Madihally, *Biomaterials* **2005**, *26*, 5500-5508; b) D. M. García Cruz, J. L. Gomez Ribelles, M. Salmerón Sánchez, *J. Biomed. Mater. Res. B* **2008**, *85*, 303-313.
[50] a) J. C. Middleton, A. J. Tipton, *Biomaterials* **2000**, *21*, 2335-2346; b) V. Singh, M. Tiwari, *Int. J. Polym. Sci.* **2010**, *2010*, 1-23; c) M. S. Lopes, A. L. Jardini, R. M. Filho, *Procedia Eng.* **2012**, *42*, 1402-1413.
[51] a) R. A. Jain, *Biomaterials* **2000**, *21*, 2475-2490; b) B. D. Ulery, L. S. Nair, C. T. Laurencin, *J. Polym. Sci., Part B: Polym. Phys.* **2011**, *49*, 832-864; c) H. K. Makadia, S. J. Siegel, *Polymer* **2011**, *3*, 1377-1397; d) B. Behera, *J. Med. Pharm. Innov.* **2013**, *1*, 1-5; e) B. Azimi, P. Nourpanah, M. Rabiee, S. Arbab, *J. Eng. Fiber. Fabr.* **2014**, *9*, 47-66.
[52] a) H. Tsuji, *Macromol. Biosci.* **2007**, *7*, 1299; b) P. Gentile, V. Chiono, I. Carmagnola, P. V. Hatton, *Int. J. Mol. Sci.* **2014**, *15*, 3640-3659.
[53] W. H. Carothers, G. L. Dorough, F. J. v. Natta, *J. Am. Chem. Soc.* **1932**, *54*, 761-772.

[54] C. C. Erbetta, R. J. Alves, J. M. Resende, R. F. Freitas, R. G. Sousa, *J. Biomater. Nanobiotechnol.* **2012**, *3*, 208-225.
[55] a) M. Jamshidian, E. A. Tehrany, M. Imran, M. Jacquot, S. Desobry, *Compr. Rev. Food Sci. Food Saf.* **2010**, *9*, 552-571; b) C. Engineer, J. Parikh, A. Raval, *Trends Biomater. Artif. Organs* **2011**, *25*, 79-85.
[56] S. W. Shalaby, D. D. Jamiolkowski, US 4140678 A, **1980**.
[57] a) S. J. Holland, B. J. Tighe, P. L. Gould, *J. Control. Release* **1986**, *4*, 155-180; b) J. Shin, K.-N. Yeh, *J. Appl. Polym. Sci.* **1999**, *74*, 921-936; c) L. Finelli, N. Lotti, A. Munari, *Eur. Polym. J.* **2002**, *38*, 1987-1993; d) S. Kim, K. Seong, O. Kim, S. Kim, H. Seo, M. Lee, G. Khang, D. Lee, *Biomacromolecules* **2010**, *11*, 555-560.
[58] J. J. Garcia, S. A. Miller, *Polym. Chem.* **2014**, *5*, 955-961.
[59] A. Einhorn, *Justus Liebigs Ann. Chem.* **1898**, *300*, 135-155.
[60] H. Schnell, *Angew. Chem.* **1956**, *68*, 633-640.
[61] D. Fox*, Polyesters: History*, in *High performance polymers: Their origin and development* (Eds.: R. B. Seymour, G. S. Kirshenbaum), Springer, **1986**, pp. 67-70.
[62] a) D. J. A. Cameron, M. P. Shaver, *Chem. Soc. Rev.* **2011**, *40*, 1761-1776; b) H. Seyednejad, A. H. Ghassemi, C. F. van Nostrum, T. Vermonden, W. E. Hennink, *J. Control. Release* **2011**, *152*, 168-176; c) Y. Zhang, H. F. Chan, K. W. Leong, *Adv. Drug Delivery Rev.* **2013**, *65*, 104-120.
[63] F. Suriano, O. Coulembier, J. L. Hedrick, P. Dubois, *Polym. Chem.* **2011**, *2*, 528-533.
[64] A. Cyriac, S. H. Lee, J. K. Varghese, E. S. Park, J. H. Park, B. Y. Lee, *Macromolecules* **2010**, *43*, 7398-7401.
[65] a) M. Taherimehr, P. P. Pescarmona, *J. Appl. Polym. Sci.* **2014**, *131*, 41141; b) R.-R. Ang, L. Tin Sin, S.-T. Bee, T.-T. Tee, A. A. H. Kadhum, A. R. Rahmat, B. A. Wasmi, *J. Cleaner Prod.* **2015**, *102*, 1-17.
[66] K. Sehanobish, T. Pham, H. C. P. Bosnyak, in *Polymeric Materials Encyclopedia, Vol. 8* (Ed.: J. C. Salamone), CRC Press (Taylor & Francis Group), **1996**, p. 5697.
[67] J. Xu, F. Prifti, J. Song, *Macromolecules* **2011**, *44*, 2660-2667.
[68] a) Y. Shibasaki, H. Sanada, M. Yokoi, F. Sanda, T. Endo, *Macromolecules* **2000**, *33*, 4316-4320; b) C. Yang, Z. Y. Ong, Y.-Y. Yang, P. L. R. Ee, J. L. Hedrick, *Macromol. Rapid Commun.* **2011**, *32*, 1826-1833; c) S. M. Guillaume, *Eur. Polym. J.* **2013**, *49*, 768-779; d) R. P. Brannigan, A. Walder, A. P. Dove, *J. Polym. Sci., Part A: Polym. Chem.* **2014**, *52*, 2279-2286.
[69] a) H. Wu, Y. Ji, Z. Li, X. Wang, Q. Zhang, S. Cui, W. Wu, J. Liu, K. Guo, *J. Polym. Sci., Part A: Polym. Chem.* **2015**, *53*, 729-736; b) C. Yang, S. Q. Liu, S. Venkataraman, S. J. Gao, X. Ke, X. T. Chia, J. L. Hedrick, Y. Y. Yang, *J. Control. Release* **2015**, *208*, 93-105.
[70] Z. Zhang, R. Kuijer, S. K. Bulstra, D. W. Grijpma, J. Feijen, *Biomaterials* **2006**, *27*, 1741-1748.
[71] a) M. Acemoglu, S. Bantle, T. Mindt, F. Nimmerfall, *Macromolecules* **1995**, *28*, 3030-3037; b) E. J. Vandenberg, D. Tian, *Macromolecules* **1999**, *32*, 3613-3619.
[72] T. F. Al-Azemi, K. S. Bisht, *Macromolecules* **1999**, *32*, 6536-6540.
[73] F. Sanda, J. Kamatani, T. Endo, *Macromolecules* **2001**, *34*, 1564-1569.
[74] P. G. Parzuchowski, M. Jaroch, M. Tryznowski, G. Rokicki, *Macromolecules* **2008**, *41*, 3859-3865.
[75] R. C. Pratt, F. Nederberg, R. M. Waymouth, J. L. Hedrick, *Chem. Commun.* **2008**, 114-116.
[76] J. Mindemark, T. Bowden, *Polymer* **2011**, *52*, 5716-5722.
[77] X. Zhang, Z. Zhong, R. Zhuo, *Macromolecules* **2011**, *44*, 1755-1759.
[78] a) Y. Shen, X. Chen, R. A. Gross, *Macromolecules* **1999**, *32*, 2799-2802; b) F. Suriano, R. Pratt, J. P. K. Tan, N. Wiradharma, A. Nelson, Y.-Y. Yang, P. Dubois, J. L. Hedrick, *Biomaterials* **2010**, *31*, 2637-2645.
[79] a) T. J. Deming, *Prog. Polym. Sci.* **2007**, *32*, 858-875; b) Y. Shen, X. Fu, W. Fu, Z. Li, *Chem. Soc. Rev.* **2015**, *44*, 612-622.

[80] a) A. Lavasanifar, J. Samuel, G. S. Kwon, *Adv. Drug Delivery Rev.* **2002**, *54*, 169-190; b) C. Li, *Adv. Drug Delivery Rev.* **2002**, *54*, 695-713; c) Y. Bae, K. Kataoka, *Adv. Drug Delivery Rev.* **2009**, *61*, 768-784; d) S. F. M. van Dongen, H.-P. M. de Hoog, R. J. R. W. Peters, M. Nallani, R. J. M. Nolte, J. C. M. van Hest, *Chem. Rev.* **2009**, *109*, 6212-6274; e) S. Hehir, N. R. Cameron, *Polym. Int.* **2014**, *63*, 943-954.

[81] H. Leuchs, *Ber. Deutsch. Chem. Ges.* **1906**, *39*, 857-861.

[82] a) H. R. Kricheldorf, *Angew. Chem. Int. Ed.* **2006**, *45*, 5752-5784; b) N. Hadjichristidis, H. Iatrou, M. Pitsikalis, G. Sakellariou, *Chem. Rev.* **2009**, *109*, 5528-5578; c) C. Deng, J. Wu, R. Cheng, F. Meng, H.-A. Klok, Z. Zhong, *Prog. Polym. Sci.* **2014**, *39*, 330-364.

[83] T. J. Deming, *J. Polym. Sci., Part A: Polym. Chem.* **2000**, *38*, 3011-3018.

[84] T. Aliferis, H. Iatrou, N. Hadjichristidis, *Biomacromolecules* **2004**, *5*, 1653-1656.

[85] a) I. Dimitrov, H. Schlaad, *Chem. Commun.* **2003**, 2944-2945; b) J.-F. Lutz, D. Schütt, S. Kubowicz, *Macromol. Rapid Commun.* **2005**, *26*, 23-28.

[86] H. Lu, J. Cheng, *J. Am. Chem. Soc.* **2007**, *129*, 14114-14115.

[87] a) C. He, X. Zhuang, Z. Tang, H. Tian, X. Chen, *Adv. Healthcare Mater.* **2012**, *1*, 48-78; b) H. Lu, J. Wang, Z. Song, L. Yin, Y. Zhang, H. Tang, C. Tu, Y. Lin, J. Cheng, *Chem. Commun.* **2014**, *50*, 139-155.

[88] A. Ogunleye, A. Bhat, V. U. Irorere, D. Hill, C. Williams, I. Radecka, *Microbiology* **2015**, *161*, 1-17.

[89] I.-L. Shih, Y.-T. Van, M.-H. Shen, *Mini-Rev. Med. Chem.* **2004**, *4*, 179-188.

[90] S. Roweton, S. J. Huang, G. Swift, *J. Environ. Polym. Degrad.* **1997**, *5*, 175-181.

[91] P. S. Farmer, E. J. Ariens, *Trends Pharmacol. Sci.* **1982**, *3*, 362-365.

[92] R. J. Simon, R. S. Kania, R. N. Zuckermann, V. D. Huebner, D. A. Jewell, S. Banville, S. Ng, L. Wang, S. Rosenberg, C. K. Marlowe, *Proc. Natl. Acad. Sci. U.S.A.* **1992**, *89*, 9367-9371.

[93] a) K. Kirshenbaum, A. E. Barron, R. A. Goldsmith, P. Armand, E. K. Bradley, K. T. V. Truong, K. A. Dill, F. E. Cohen, R. N. Zuckermann, *Proc. Natl. Acad. Sci. U.S.A.* **1998**, *95*, 4303-4308; b) R. N. Zuckermann, *Pept. Sci.* **2011**, *96*, 545-555.

[94] a) J. W. Robinson, H. Schlaad, *Chem. Commun.* **2012**, *48*, 7835-7837; b) J. Sun, R. N. Zuckermann, *ACS Nano* **2013**, *7*, 4715-4732; c) A. Birke, D. Huesmann, A. Kelsch, M. Weilbaecher, J. Xie, M. Bros, T. Bopp, C. Becker, K. Landfester, M. Barz, *Biomacromolecules* **2014**, *15*, 548-557; d) K. Klinker, R. Holm, P. Heller, M. Barz, *Polym. Chem.* **2015**, *6*, 4612-4623

[95] R. N. Zuckermann, J. M. Kerr, S. B. H. Kent, W. H. Moos, *J. Am. Chem. Soc.* **1992**, *114*, 10646-10647.

[96] a) R. M. J. Liskamp, D. T. S. Rijkers, J. A. W. Kruijtzer, J. Kemmink, *ChemBioChem* **2011**, *12*, 1626-1653; b) R. Luxenhofer, C. Fetsch, A. Grossmann, *J. Polym. Sci., Part A: Polym. Chem.* **2013**, *51*, 2731-2752; c) A. M. Rosales, R. A. Segalman, R. N. Zuckermann, *Soft Matter* **2013**, *9*, 8400-8414; d) A. S. Knight, E. Y. Zhou, M. B. Francis, R. N. Zuckermann, *Adv. Mater.* **2015**, *27*, 5665-5691; e) C. Secker, S. M. Brosnan, R. Luxenhofer, H. Schlaad, *Macromol. Biosci.* **2015**, *15*, 881-891.

[97] A. S. Culf, R. J. Ouellette, *Molecules* **2010**, *15*, 5282.

[98] H. K. Murnen, A. R. Khokhlov, P. G. Khalatur, R. A. Segalman, R. N. Zuckermann, *Macromolecules* **2012**, *45*, 5229-5236.

[99] S. M. Miller, R. J. Simon, S. Ng, R. N. Zuckermann, J. M. Kerr, W. H. Moos, *Bioorg. Med. Chem. Lett.* **1994**, *4*, 2657-2662.

[100] a) H. J. Olivos, P. G. Alluri, M. M. Reddy, D. Salony, T. Kodadek, *Org. Lett.* **2002**, *4*, 4057-4059; b) B. C. Gorske, S. A. Jewell, E. J. Guerard, H. E. Blackwell, *Org. Lett.* **2005**, *7*, 1521-1524.

[101] D. Zhang, S. H. Lahasky, L. Guo, C.-U. Lee, M. Lavan, *Macromolecules* **2012**, *45*, 5833-5841.

[102] a) M. Schneider, C. Fetsch, I. Amin, R. Jordan, R. Luxenhofer, *Langmuir* **2013**, *29*, 6983-6988; b) N. Gangloff, C. Fetsch, R. Luxenhofer, *Macromol. Rapid Commun.* **2013**, *34*, 997-1001.

[103] a) S. Lohan, G. S. Bisht, *Mini Rev. Med. Chem.* **2013**, *13*, 1073-1088; b) K. H. A. Lau, *Biomater. Sci.* **2014**, *2*, 627-633.
[104] a) C. M. Gao, A. Y. Yam, X. Wang, E. Magdangal, C. Salisbury, D. Peretz, R. N. Zuckermann, M. D. Connolly, O. Hansson, L. Minthon, H. Zetterberg, K. Blennow, J. P. Fedynyshyn, S. Allauzen, *PLoS ONE* **2010**, *5*, e15725; b) M. M. Reddy, R. Wilson, J. Wilson, S. Connell, A. Gocke, L. Hynan, D. German, T. Kodadek, *Cell* **2011**, *144*, 132-142.
[105] a) S. L. Seurynck, J. A. Patch, A. E. Barron, *Chem. Biol.* **2005**, *12*, 77-88; b) N. J. Brown, J. Johansson, A. E. Barron, *Acc. Chem. Res.* **2008**, *41*, 1409-1417.
[106] a) C. A. Olsen, *ChemBioChem* **2010**, *11*, 152-160; b) B.-C. Lee, R. N. Zuckermann, *ACS Chem. Biol.* **2011**, *6*, 1367-1374.
[107] J. Ulbricht, R. Jordan, R. Luxenhofer, *Biomaterials* **2014**, *35*, 4848-4861.
[108] a) W. Seeliger, E. Aufderhaar, W. Diepers, R. Feinauer, R. Nehring, W. Thier, H. Hellmann, *Angew. Chem. Int. Ed.* **1966**, *5*, 875-888; b) T. G. Bassiri, A. Levy, M. Litt, *J. Polym. Sci. Part B* **1967**, *5*, 871-879.
[109] a) F. Wiesbrock, R. Hoogenboom, C. H. Abeln, U. S. Schubert, *Macromol. Rapid Commun.* **2004**, *25*, 1895-1899; b) K. Kempe, C. R. Becer, U. S. Schubert, *Macromolecules* **2011**, *44*, 5825-5842; c) C. Englert, A. M. Schwenke, S. Hoeppener, C. Weber, U. S. Schubert, *Adv. Polym. Sci.* **2016**, *274*, 209-240.
[110] B. Guillerm, S. Monge, V. Lapinte, J.-J. Robin, *Macromol. Rapid Commun.* **2012**, *33*, 6000-6016.
[111] a) J. Kronek, Z. Kroneková, J. Lustoň, E. Paulovičová, L. Paulovičová, B. Mendrek, *J. Mater. Sci.: Mater. Med.* **2011**, *22*, 1725-1734; b) R. Luxenhofer, G. Sahay, A. Schulz, D. Alakhova, T. K. Bronich, R. Jordan, A. V. Kabanov, *J. Control. Release* **2011**, *153*, 73-82; c) M. Bauer, S. Schroeder, L. Tauhardt, K. Kempe, U. S. Schubert, D. Fischer, *J. Polym. Sci., Part A: Polym. Chem.* **2013**, *51*, 1816-1821.
[112] a) M. C. Woodle, C. M. Engbers, S. Zalipsky, *Bioconjugate Chem.* **1994**, *5*, 493-496; b) S. Zalipsky, C. B. Hansen, J. M. Oaks, T. M. Allen, *J. Pharm. Sci.* **1996**, *85*, 133-137.
[113] a) R. Hoogenboom, *Angew. Chem. Int. Ed.* **2009**, *48*, 7978-7994; b) R. Luxenhofer, Y. Han, A. Schulz, J. Tong, Z. He, A. V. Kabanov, R. Jordan, *Macromol. Rapid Commun.* **2012**, 1613-1631; c) V. R. de la Rosa, *J. Mater. Sci.: Mater. Med.* **2014**, *25*, 1211-1225.
[114] C. Weber, R. Hoogenboom, U. S. Schubert, *Prog. Polym. Sci.* **2012**, *37*, 686-714.
[115] R. Duncan, M. J. Vicent, *Adv. Drug Delivery Rev.* **2010**, *62*, 272-282.
[116] P. A. Vasey, S. B. Kaye, R. Morrison, C. Twelves, P. Wilson, R. Duncan, A. H. Thomson, L. S. Murray, T. E. Hilditch, T. Murray, S. Burtles, D. Fraier, E. Frigerio, J. Cassidy, *Clin. Cancer Res.* **1999**, *5*, 83-94.
[117] a) J. Kopeček, H. Bažilová, *Eur. Polym. J.* **1973**, *9*, 7-14; b) M. Teodorescu, K. Matyjaszewski, *Macromolecules* **1999**, *32*, 4826-4831; c) C. W. Scales, Y. A. Vasilieva, A. J. Convertine, A. B. Lowe, C. L. McCormick, *Biomacromolecules* **2005**, *6*, 1846-1850.
[118] a) M. Eberhardt, P. Théato, *Macromol. Rapid Commun.* **2005**, *26*, 1488-1493; b) M. I. Gibson, E. Fröhlich, H.-A. Klok, *J. Polym. Sci., Part A: Polym. Chem.* **2009**, *47*, 4332-4345.
[119] B. S. Tucker, B. S. Sumerlin, *Polym. Chem.* **2014**, *5*, 1566-1572.
[120] a) M. Heskins, J. E. Guillet, *J. Macromol. Sci. Chem. Ed.* **1968**, *A2*, 1441-1455; b) K. Dušek, D. Patterson, *J. Polym. Sci. Part. A-2* **1968**, *6*, 1209-1216.
[121] a) H. Wei, S.-X. Cheng, X.-Z. Zhang, R.-X. Zhuo, *Prog. Polym. Sci.* **2009**, *34*, 893-910; b) A. Halperin, M. Kröger, F. M. Winnik, *Angew. Chem. Int. Ed.* **2015**, *54*, 15342-15367.
[122] Z. M. O. Rzaev, S. Dinçer, E. Pişkin, *Prog. Polym. Sci.* **2007**, *32*, 534-595.
[123] T. Sun, G. Qing, *Adv. Mater.* **2011**, *23*, H57-H77.
[124] a) Y. Guan, Y. Zhang, *Soft Matter* **2011**, *7*, 6375-6384; b) Y. Lu, M. Ballauff, *Prog. Polym. Sci.* **2011**, *36*, 767-792; c) C. Li, Y. Ma, H. Niu, H. Zhang, *ACS Appl. Mater. Interfaces* **2015**, *7*, 27340–27350;

d) L. D. Blackman, D. B. Wright, M. P. Robin, M. I. Gibson, R. K. O'Reilly, *ACS Macro Lett.* **2015**, *4*, 1210-1214; e) H. Hathaway, D. R. Alves, J. Bean, P. P. Esteban, K. Ouadi, J. Mark Sutton, A. T. A. Jenkins, *Eur. J. Pharm. Biopharm.* **2015**, *96*, 437-441.

[125] H. M. Mansour, M. Sohn, A. Al-Ghananeem, P. P. DeLuca, *Int. J. Mol. Sci.* **2010**, *11*, 3298.

[126] a) F. Ganachaud, M. J. Monteiro, R. G. Gilbert, M.-A. Dourges, S. H. Thang, E. Rizzardo, *Macromolecules* **2000**, *33*, 6738-6745; b) G. Masci, L. Giacomelli, V. Crescenzi, *Macromol. Rapid Commun.* **2004**, *25*, 559-564.

[127] T. Steinbach, E. M. Alexandrino, C. Wahlen, K. Landfester, F. R. Wurm, *Macromolecules* **2014**, *47*, 4884-4893.

[128] J. Liu, W. Huang, Y. Pang, D. Yan, *Chem. Soc. Rev.* **2015**, *44*, 3942-3953.

[129] a) F. Marsico, M. Wagner, K. Landfester, F. R. Wurm, *Macromolecules* **2012**, *45*, 8511-8518; b) T. Steinbach, E. M. Alexandrino, F. R. Wurm, *Polym. Chem.* **2013**, *4*, 3800-3806.

[130] Y.-C. Wang, Y.-Y. Yuan, J.-Z. Du, X.-Z. Yang, J. Wang, *Macromol. Biosci.* **2009**, *9*, 1154-1164.

[131] L. Lieberman, *Ber. Chem.-Ges.* **1888**, *21*, 598-607.

[132] a) I. S. Kulaev, V. M. Vagabov, *Adv. Microb. Physiol* **1983**, *24*, 83-171; b) A. Kornberg, *J. Bacteriol.* **1995**, *177*, 491-496; c) I. S. Kulaev, V. M. Vagabov, T. V. Kulakovskaya, *The biochemistry of inorganic polyphosphates*, John Wiley & Sons, **1979**; d) T. Steinbach, F. R. Wurm, *Angew. Chem. Int. Ed.* **2015**, *54*, 6098-6108; e) X. Wang, H. C. Schröder, W. E. G. Müller, *Biotechnol. J.* **2016**, *11*, 11-30.

[133] a) A. Kornberg, S. R. Kornberg, E. S. Simms, *Biochim. Biophys. Acta* **1956**, *20*, 215-227; b) S. R. Kornberg, *Biochim. Biophys. Acta* **1957**, *26*, 294-300.

[134] a) R. P. Elliott, R. P. Straka, J. A. Garibaldi, *Appl. Microbiol.* **1964**, *12*, 517-522; b) A. Momeni, M. J. Filiaggi, *Langmuir* **2014**, *30*, 5256-5266.

[135] A. Kornberg, N. N. Rao, D. Ault-Riché, *Annu. Rev. Biochem.* **1999**, *68*, 89-125.

[136] J.-Z. Du, T.-M. Sun, S.-Q. Weng, X.-S. Chen, J. Wang, *Biomacromolecules* **2007**, *8*, 3375-3381.

[137] S. Zhang, A. Li, J. Zou, L. Y. Lin, K. L. Wooley, *ACS Macro Lett.* **2012**, *1*, 328-333.

[138] W.-J. Song, J.-Z. Du, N.-J. Liu, S. Dou, J. Cheng, J. Wang, *Macromolecules* **2008**, *41*, 6935-6941.

[139] J. Wang, H.-Q. Mao, K. W. Leong, *J. Am. Chem. Soc.* **2001**, *123*, 9480-9481.

[140] J. Liu, W. Huang, Y. Zhou, D. Yan, *Macromolecules* **2009**, *42*, 4394-4399.

[141] Y. Iwasaki, E. Yamaguchi, *Macromolecules* **2010**, *43*, 2664-2666.

[142] J. Libiszowski, K. Kałużynski, S. Penczek, *J. Polym. Sci. Polym. Chem. Ed.* **1978**, *16*, 1275-1283.

[143] J. A. Obritsch, D. Ryu, L. E. Lampila, L. B. Bullerman, *J. Food Prot.* **2008**, *71*, 1401-1405.

[144] A. S. Naidu, *Natural food antimicrobial systems*, CRC Press (Taylor & Francis Group), **2000**.

[145] E. Yilgör, I. Yilgör, *Prog. Polym. Sci.* **2014**, *39*, 1165-1195.

[146] a) L. Wilczek, J. Chojnowski, *Makromol. Chem.* **1983**, *184*, 77-90; b) A. Mitra, D. A. Atwood, *Polysiloxanes & polysilanes*, in *Encyclopedia of inorganic chemistry* (Ed.: R. B. King), John Wiley & Sons, **2006**.

[147] a) P. Cancouët, E. Daudet, G. Hélary, M. Moreau, G. Sauvet, *J. Polym. Sci., Part A: Polym. Chem.* **2000**, *38*, 826-836; b) A. Saxena, S. Rajaraman, M. Leatherman, *Macromolecules* **2007**, *40*, 752-755; c) M. D. Ninago, A. J. Satti, J. A. Ressia, A. E. Ciolino, M. A. Villar, E. M. Vallés, *J. Polym. Sci., Part A: Polym. Chem.* **2009**, *47*, 4774-4783.

[148] A. Colas, *Dow Corning, Life Sciences* **2005**.

[149] R. De Jaeger, M. Gleria, *Inorganic Polymers*, Nova Science Publishers, **2007**.

[150] H. Zhang, M. Chiao, *J. Med. Biol. Eng.* **2015**, *35*, 143-155.

[151] a) H. Schmolke, S. Demming, A. Edlich, V. Magdanz, S. Büttgenbach, E. Franco-Lara, R. Krull, C.-P. Klages, *Biomicrofluidics* **2010**, *4*, 44113; b) K. M. Kovach, J. R. Capadona, A. S. Gupta, J. A. Potkay, *J. Biomed. Mater. Res. A* **2014**, *102*, 4195-4205; c) M. A. Rufin, J. A. Gruetzner, M. J. Hurley, M. L. Hawkins, E. S. Raymond, J. E. Raymond, M. A. Grunlan, *J. Mater. Chem. B* **2015**, *3*, 2816-2825.

[152] C. Stevens, *Int. J. Cosmet. Sci.* **1998**, *20*, 296-304.
[153] M. H. Stenzel, L. Cummins, G. E. Roberts, T. P. Davis, P. Vana, C. Barner-Kowollik, *Macromol. Chem. Phys.* **2003**, *204*, 1160-1168.
[154] C. C. DeMerlis, D. R. Schoneker, *Food Chem. Toxicol.* **2003**, *41*, 319-326.
[155] I. Orienti, R. Trere, B. Luppi, F. Bigucci, T. Cerchiara, G. Zuccari, V. Zecchi, *Arch. Pharm.* **2002**, *335*, 89-93.
[156] S. M. More, R. V. Kulkarni, B. Sa, N. V. Kayane, *J. Appl. Polym. Sci.* **2010**, *116*, 1732-1738.
[157] G. Schröder, *Poly(vinyl ethers)*, in *Ullmann's encyclopedia of industrial chemistry*, Wiley-VCH, Weinheim, Germany, **2000**.
[158] M. G. Tardajos, M. Nash, Y. Rochev, H. Reinecke, C. Elvira, A. Gallardo, *Macromol. Chem. Phys* **2012**, *213*, 529-538.
[159] W. Reppe, *Angew. Chem.* **1953**, *65*, 577-578.
[160] V. G. Kadajji, G. V. Betageri, *Polymers* **2011**, *3*, 1972.
[161] V. Bühler, *Kollidon: Polyvinylpyrrolidone excipients for the pharmaceutical industry*, BASF, Ludwigshafen, Germany, **2008**.
[162] a) V. P. Torchilin, *J. Microencapsulation* **1998**, *15*, 1-19; b) Z. Zhu, C. Xie, Q. Liu, X. Zhen, X. Zheng, W. Wu, R. Li, Y. Ding, X. Jiang, B. Liu, *Biomaterials* **2011**, *32*, 9525-9535.
[163] F. Fischer, S. Bauer, *Chem. Unserer Zeit* **2009**, *43*, 376-383.
[164] a) F. Haaf, A. Sanner, F. Straub, *Polym. J.* **1985**, *17*, 143-152; b) M. B. Mohamed, M. K. Talari, M. Tripathy, A. B. A. Majeed, *Int. J. Drug Formulation Res.* **2012**, *3*, 13-28.
[165] W. Strohmeier, P. Hartmann, *Z. Naturforsch. B* **1964**, *19*, 655.
[166] a) P. S. Mohanachandran, P. G. Sindhumol, T. S. Kiran, *Int. J. Pharm. Sci. Rev. Res.* **2011**, *6*, 105-109; b) R. Bala, S. Khanna, P. Pawar, *Asian J. Pharm. Clin. Res.* **2012**, *5*, 8-14; c) M. Mangal, S. Thakral, M. Goswami, P. Ghai, *Int. J. Pharm. Pharm. Sci. Res.* **2012**, *2*, 26-35.
[167] M. Wytrwal, C. Leduc, M. Sarna, C. Goncalves, M. Kepczynski, P. Midoux, M. Nowakowska, C. Pichon, *Int. J. Pharm.* **2015**, *478*, 372-382.
[168] J. M. C. Lourenço, P. A. Ribeiro, A. M. Botelho do Rego, F. M. Braz Fernandes, A. M. C. Moutinho, M. Raposo, *Langmuir* **2004**, *20*, 8103-8109.
[169] K. Nollenberger, J. Albers, *Int. J. Pharm.* **2013**, *457*, 461-469.
[170] P. F. Holmes, M. Bohrer, J. Kohn, *Prog. Polym. Sci.* **2008**, *33*, 787-796.
[171] a) P. Kwiatkowski, J. Jurczak, J. Pietrasik, W. Jakubowski, L. Mueller, K. Matyjaszewski, *Macromolecules* **2008**, *41*, 1067-1069; b) E. Yoshida, *Colloid. Polym. Sci.* **2011**, *289*, 1625-1630; c) T. Yildirim, A. C. Rinkenauer, C. Weber, A. Traeger, S. Schubert, U. S. Schubert, *J. Polym. Sci., Part A: Polym. Chem.* **2015**, *53*, 2711-2721.
[172] F. Fleischhaker, A. P. Haehnel, A. M. Misske, M. Blanchot, S. Haremza, C. Barner-Kowollik, *Macromol. Chem. Phys.* **2014**, *215*, 1192-1200.
[173] K. Terao, *Poly(acrylic acid) (PAA)*, in *Encyclopedia of polymeric nanomaterials* (Eds.: Shiro Kobayashi, Klaus Müllen), Springer, Berlin, Heidelberg, Germany, **2014**, pp. 1-6.
[174] T. Swift, L. Swanson, M. Geoghegan, S. Rimmer, *Soft Matter* **2016**, *12*, 2542-2549.
[175] J. E. Elliott, M. Macdonald, J. Nie, C. N. Bowman, *Polymer* **2004**, *45*, 1503-1510.
[176] a) A. Bernkop-Schnürch, C. Egger, M. Elhassan Imam, A. H. Krauland, *J. Control. Release* **2003**, *93*, 29-38; b) G. M. Eichenbaum, P. F. Kiser, A. V. Dobrynin, S. A. Simon, D. Needham, *Macromolecules* **1999**, *32*, 4867-4878.
[177] S. Hochheiser, *Rohm and Haas: History of a chemical company*, University of Pennsylvania Press, Philadelphia, Pennsylvania, **1986**.
[178] U. Ali, K. J. B. A. Karim, N. A. Buang, *Polym. Rev.* **2015**, *55*, 678-705.
[179] a) F. Galli, S. Benedetti, U. Buoncristiani, M. Piroddi, C. Conte, F. Canestrari, E. Buoncristiani, A. Floridi, *Kidney Int.* **2003**, *64*, 748-755; b) T. G. Tihan, M. D. Ionita, R. G. Popescu, D. Iordachescu,

Mater. Chem. Phys. **2009**, *118*, 265-269; c) A. Gomaa, R. M. H. Lee, C. S. C. Liu, *Eye* **2011**, *25*, 1090-1093; d) M. Khandaker, M. B. Vaughan, T. L. Morris, J. J. White, Z. Meng, *Int. J. Nanomed.* **2014**, *9*, 2699-2712.

[180] A. Bhowmick, S. Banerjee, R. Kumar, P. Kundu, *Biomedicine and Nanotechnology* **2013**, *254*, 135-167.

[181] C. Migliaresi, L. Fambri, J. Kolarik, *Biomaterials* **1994**, *15*, 875-881.

[182] R. Yañez-Macias, I. Alvarez-Moises, I. Perevyazko, A. Lezov, R. Guerrero-Santos, U. S. Schubert, C. Guerrero-Sanchez, *Macromol. Chem. Phys.* **2017**, accepted.

[183] Y.-Z. You, D. S. Manickam, Q.-H. Zhou, D. Oupický, *J. Control. Release* **2007**, *122*, 217-225.

[184] T. Yildirim, A. Traeger, E. Preussger, S. Stumpf, C. Fritzsche, S. Hoeppener, S. Schubert, U. S. Schubert, *Macromolecules* **2016**, *49*, 3856-3868.

[185] B. Burns*, Polycyanoacrylates*, in *Encyclopedia of polymer science and technology* (Ed.: H. F. Mark), John Wiley & Sons, **2016**, pp. 1-27.

[186] J. M. Cracowski, V. Montembault, D. Bosc, B. Améduri, F. Odobel, L. Fontaine, *J. Polym. Sci., Part A: Polym. Chem.* **2009**, *47*, 1403-1411.

[187] H. Finkentscher, C. Heuck, DE 654989 C, **1930**.

[188] H. R. Clyde, US 2404713 A, **1946**.

[189] H. Dong, W. Tang, K. Matyjaszewski, *Macromolecules* **2007**, *40*, 2974-2977.

[190] M. Kopeć, P. Krys, R. Yuan, K. Matyjaszewski, *Macromolecules* **2016**, *49*, 5877-5883.

[191] a) P. Bajaj, K. Sen, S. H. Bahrami, *J. Appl. Polym. Sci.* **1996**, *59*, 1539-1550; b) P. Bajaj, T. V. Sreekumar, K. Sen, *J. Appl. Polym. Sci.* **2001**, *79*, 1640-1652; c) D. F. Grishin, I. D. Grishin, *Russ. Chem. Rev.* **2015**, *84*, 712.

[192] a) Y. Nakano, K. Hisatani, K. Kamide, *Polym. Int.* **1994**, *35*, 207-213; b) A. V. Novoselova, V. V. Shamanin, L. V. Vinogradova, *Polym. Sci. Ser. B Polym. Chem.* **2009**, *51*, 205-211.

[193] H. Ono, K. Hisatani, K. Kamide, *Polym. J.* **1993**, *25*, 245-265.

[194] M. L. Gupta, B. Gupta, W. Oppermann, G. Hardtmann, *J. Appl. Polym. Sci.* **2004**, *91*, 3127-3133.

[195] N. Arsalani, R. Rakh, E. Ghasemi, A. A. Entezami, *Iran. Polym. J.* **2009**, *18*, 623-632.

[196] S. K. Nataraj, K. S. Yang, T. M. Aminabhavi, *Prog. Polym. Sci.* **2012**, *37*, 487-513.

[197] C. Dizman, D. O. Demirkol, S. Ates, L. Torun, S. Sakarya, S. Timur, Y. Yagci, *Colloids Surf., B* **2011**, *88*, 265-270.

[198] M. Amirilargani, A. Sabetghadam, T. Mohammadi, *Polym. Adv. Technol.* **2012**, *23*, 398-407.

[199] O. Bayer, H. Rinke, W. Siefken, L. Orthner, H. Schild, DRP 728981 (13. Nov. 1937), I. G. Farben, Chem. Zbl., **1940**.

[200] a) P. A. Gunatillake, R. Adhikari, G. P. Felton*, Biodegradable polyurethanes: design, synthesis, properties and potential applications*, in *Biodegradable polymers: Processing, degradation and applications* (Ed.: Gary P. Felton), Nova Science Publishers, Hauppauge (New York), **2011**, pp. 431-470; b) G. T. Howard, *Int. Biodeterior. Biodegrad.* **2002**, *49*, 245-252; c) T. Thomson, *Polyurethanes as specialty chemicals: principles and applications*, CRC Press (Taylor & Francis Group), Boca Raton, Florida, **2005**.

[201] K. Uhlig, *Discovering polyurethanes*, Carl Hanser, München, Germany, **1999**.

[202] B. Tieke, *Makromolekulare Chemie: Eine Einführung*, John Wiley & Sons, **2014**.

[203] a) G. Natta, P. Corradini, I. W. Bassi, *Nuovo. Cima.* **1960**, *15*, 68-82; b) N. Ishihara, T. Seimiya, M. Kuramoto, M. Uoi, *Macromolecules* **1986**, *19*, 2464-2465.

[204] W. Kaminsky, *Metalorganic catalysts for synthesis and polymerization: recent results by Ziegler-Natta and metallocene investigations*, Springer Science & Business Media, Berlin, Germany, **1999**.

[205] P. Zinck, F. Bonnet, A. Mortreux, M. Visseaux, *Prog. Polym. Sci.* **2009**, *34*, 369-392.

[206] C. A. McNamara, M. J. Dixon, M. Bradley, *Chem. Rev.* **2002**, *102*, 3275-3300.

[207] J. Maul, B. G. Frushour, J. R. Kontoff, H. Eichenauer, K.-H. Ott, C. Schade, *Polystyrene and styrene copolymers*, in *Ullmann's encyclopedia of industrial chemistry*, Wiley-VCH, **2000**.
[208] http://plasticfoodservicefacts.com/Safety-of-Styrene-Based-Polymers-for-Food-Contact, last accessed 16.01.2017.
[209] N. Kumar, R. S. Langer, A. J. Domb, *Adv. Drug Delivery Rev.* **2002**, *54*, 889-910.
[210] A. Göpferich, J. Tessmar, *Adv. Drug Delivery Rev.* **2002**, *54*, 911-931.
[211] A. J. Domb, R. Langer, *J. Polym. Sci., Part A: Polym. Chem.* **1987**, *25*, 3373-3386.
[212] N. G. Gaylord, *J. Macromol. Sci., Rev. Macromol. Chem.* **1975**, *C13*, 235-261.
[213] G. J. Domski, J. M. Rose, G. W. Coates, A. D. Bolig, M. Brookhart, *Prog. Polym. Sci.* **2007**, *32*, 30-92.
[214] a) P. Cossee, *J. Catal.* **1964**, *3*, 80-88; b) G. Fink, R. Mülhaupt, H. H. Brintzinger, *Ziegler Catalysts: Recent Scientific Innovations and Technological Improvements*, Springer, Berlin, Heidelberg, Germany, **2012**.
[215] J. E. Puskas, Y. Chen, Y. Dahman, D. Padavan, *J. Polym. Sci., Part A: Polym. Chem.* **2004**, *42*, 3091-3109.
[216] A. J. Lovinger, *Poly(vinylidene fluoride)*, in *Developments in crystalline polymers, Vol. 1* (Ed.: D. C. Bassett), Springer, Dordrecht, Netherlands, **1982**, pp. 195-273.
[217] a) A. Grigoletto, K. Maso, A. Mero, A. Rosato, O. Schiavon, G. Pasut, *J. Drug Delivery Sci. Technol.* **2016**, *32*, 132–141; b) P. Mishra, B. Nayak, R. K. Dey, *Asian J. Pharm. Sci.*, *11*, 337–348.
[218] J. M. Harris, R. B. Chess, *Nat. Rev. Drug Discovery* **2003**, *2*, 214-221.
[219] A. Kolate, D. Baradia, S. Patil, I. Vhora, G. Kore, A. Misra, *J. Control. Release* **2014**, *192*, 67-81.
[220] V. B. Damodaran, C. J. Fee, *Eur. Pharm. Rev.* **2010**, *15*, 18.
[221] a) A. Kozlowski, J. Milton Harris, *J. Control. Release* **2001**, *72*, 217-224; b) P. L. Turecek, M. J. Bossard, F. Schoetens, I. A. Ivens, *J. Pharm. Sci.* **2016**, *105*, 460-475.
[222] a) I. Zundorf, T. Dingermann, *Die Pharmazie* **2014**, *69*, 323-326; b) M. A. Croyle, Q. C. Yu, J. M. Wilson, *Hum. Gene Ther.* **2000**, *11*, 1713-1722.
[223] S. DeFrees, Z.-G. Wang, R. Xing, A. E. Scott, J. Wang, D. Zopf, D. L. Gouty, E. R. Sjoberg, K. Panneerselvam, E. C. M. Brinkman-Van der Linden, R. J. Bayer, M. A. Tarp, H. Clausen, *Glycobiology* **2006**, *16*, 833-843.
[224] a) S. Brocchini, A. Godwin, S. Balan, J.-w. Choi, M. Zloh, S. Shaunak, *Adv. Drug Delivery Rev.* **2008**, *60*, 3-12; b) G. Pasut, F. M. Veronese, *J. Control. Release* **2012**, *161*, 461-472.
[225] E. W. M. Ng, D. T. Shima, P. Calias, E. T. Cunningham, D. R. Guyer, A. P. Adamis, *Nat. Rev. Drug Discovery* **2006**, *5*, 123-132.
[226] http://www.fda.gov/NewsEvents/Newsroom/PressAnnouncements/ucm472643.htm, last accessed 16.01.2017.
[227] a) I. A. Ivens, A. Baumann, T. A. McDonald, T. J. Humphries, L. A. Michaels, P. Mathew, *Haemophilia* **2013**, *19*, 11-20; b) M. V. Ragni, *Drugs* **2015**, *75*, 1587-1600; c) M. Laffan, *Br. J. Haematol.* **2016**, *172*, 23-31; d) R. Stidl, S. Fuchs, M. Bossard, J. Siekmann, P. L. Turecek, M. Putz, *Haemophilia* **2016**, *22*, 54-64.
[228] a) E. Blasko, L. Leong, D. S. Sim, L. Tang, E. Ho, J. Wu, K. Z. Kauser, B. Subramanyam, *Blood* **2014**, *124*, 1471-1471; b) T. T. Wynn, B. Gumuscu, *J. Blood Med.* **2016**, *7*, 121-128.
[229] H. R. Stennicke, M. Kjalke, D. M. Karpf, K. W. Balling, P. B. Johansen, T. Elm, K. Øvlisen, F. Möller, H. L. Holmberg, C. N. Gudme, E. Persson, I. Hilden, H. Pelzer, H. Rahbek-Nielsen, C. Jespersgaard, A. Bogsnes, A. A. Pedersen, A. K. Kristensen, B. Peschke, W. Kappers, F. Rode, L. Thim, M. Tranholm, M. Ezban, E. H. N. Olsen, S. E. Bjørn, *Blood* **2013**, *121*, 2108-2116.
[230] a) P. W. Collins, G. Young, K. Knobe, F. A. Karim, P. Angchaisuksiri, C. Banner, T. Gürsel, J. Mahlangu, T. Matsushita, E. P. Mauser-Bunschoten, J. Oldenburg, C. E. Walsh, C. Negrier, *Blood*

2014, *124*, 3880-3886; b) T. E. Coyle, M. T. Reding, J. C. Lin, L. A. Michaels, A. Shah, J. Powell, *J. Thromb. Haemost.* **2014**, *12*, 488-496.
[231] F. Peyvandi, I. Garagiola, S. Seregni, *J. Thromb. Haemost.* **2013**, *11*, 84-98.
[232] a) M. J. de Groot, M. Hoeksma, N. Blau, D. J. Reijngoud, F. J. van Spronsen, *Mol. Genet. Metab.* **2010**, *99*, S86-S89; b) J. B. Hennermann, S. Roloff, C. Gebauer, B. Vetter, A. von Arnim-Baas, E. Mönch, *Mol. Genet. Metab.* **2012**, *107*, 294-301.
[233] A. Bélanger-Quintana, A. Burlina, C. O. Harding, A. C. Muntau, *Mol. Genet. Metab.* **2011**, *104*, S19-S25.
[234] C. Sorli, *Am. J. Med.*, *127*, S39-S48.
[235] T. Hirose, *Diabetol. Int.* **2016**, *7*, 16-17.
[236] R. Haag, F. Kratz, *Angew. Chem. Int. Ed.* **2006**, *45*, 1198-1215.
[237] a) X. Pang, H.-L. Du, H.-Q. Zhang, Y.-J. Zhai, G.-X. Zhai, *Drug Discovery Today* **2013**, *18*, 1316-1322; b) W. Li, P. Zhan, E. De Clercq, H. Lou, X. Liu, *Prog. Polym. Sci.* **2013**, *38*, 421-444.
[238] M. Swierczewska, K. C. Lee, S. Lee, *Expert Opin. Emerging Drugs* **2015**, *20*, 531-536.
[239] http://fibromyalgianewstoday.com/2015/03/04/novel-drug-treats-chronic-pain-without-side-effects-danger-abuse/, last accessed 16.01.2017.
[240] http://www.nektar.com/pipeline/rd-pipeline/nktr-181, last accessed 16.01.2017.
[241] U. Hoch, C.-M. Staschen, R. K. Johnson, M. A. Eldon, *Cancer Chemother. Pharmacol.* **2014**, *74*, 1125-1137.
[242] A. Patnaik, K. P. Papadopoulos, A. W. Tolcher, M. Beeram, S. Urien, L. J. Schaaf, S. Tahiri, T. Bekaii-Saab, F. M. Lokiec, K. Rezaï, A. Buchbinder, *Cancer Chemother. Pharmacol.* **2013**, *71*, 1499-1506.
[243] http://www.nektar.com/pipeline/rd-pipeline/onzeald, last accessed 16.01.2017.
[244] a) http://www.fda.gov/downloads/AdvisoryCommittees/CommitteesMeetingMaterials/Drugs/OncologicDrugsAdvisoryCommittee/UCM426178.pdf, last accessed 16.01.2017; b) E. A. Perez, A. Awada, J. O'Shaughnessy, H. S. Rugo, C. Twelves, S.-A. Im, P. Gómez-Pardo, L. S. Schwartzberg, V. Diéras, D. A. Yardley, D. A. Potter, A. Mailliez, A. Moreno-Aspitia, J.-S. Ahn, C. Zhao, U. Hoch, M. Tagliaferri, A. L. Hannah, J. Cortes, *Lancet Oncol.* **2015**, *16*, 1556-1568.
[245] Z. Hong, *Curr. Bioact. Compd.* **2011**, *7*, 3-7.
[246] E. C. Emery, A. P. Luiz, J. N. Wood, *Expert Opin. Ther. Targets* **2016**, *20*, 975-983.
[247] a) E. M. Pelegri-O'Day, E.-W. Lin, H. D. Maynard, *J. Am. Chem. Soc.* **2014**, *136*, 14323-14332; b) Y. Qi, A. Chilkoti, *Curr. Opin. Chem. Biol.* **2015**, *28*, 181-193.
[248] S. Shah, T. Prematta, N. F. Adkinson, F. T. Ishmael, *J. Clin. Pharmacol.* **2013**, *53*, 352-355.
[249] R. Duncan, *Nat. Rev. Cancer* **2006**, *6*, 688-701.
[250] A. Godwin, K. Bolina, M. Clochard, E. Dinand, S. Rankin, S. Simic, S. Brocchini, *J. Pharm. Pharmacol.* **2001**, *53*, 1175-1184.
[251] a) H. Maeda, J. Takeshita, R. Kanamaru, *Int. J. Pept. Protein Res.* **1979**, *14*, 81-87; b) H. Maeda, M. Ueda, T. Morinaga, T. Matsumoto, *J. Med. Chem.* **1985**, *28*, 455-461.
[252] N. Ohtsuka, T. Konno, Y. Miyauchi, H. Maeda, *Cancer* **1987**, *59*, 1560-1565.
[253] T. Konno, H. Maeda, *Targeting chemotherapy of hepatocellular carcinoma*, in *Neoplasms of the liver* (Eds.: Kunio Okuda, Kamal G. Ishak), Springer, Tokyo, Japan, **1987**, pp. 343-352.
[254] P. Caliceti, F. M. Veronese, *Adv. Drug Delivery Rev.* **2003**, *55*, 1261-1277.
[255] Y. Matsumura, H. Maeda, *Cancer Res.* **1986**, *46*, 6387-6392.
[256] H. Ishii, J. Furuse, M. Nagase, Y. Maru, M. Yoshino, T. Hayashi, *Jpn. J. Clin. Oncol.* **2003**, *33*, 570-573.
[257] T. Taguchi, T. Saito, J. Ota, I. Nakao, K. Ohashi, H. Nakamura, T. Konno, *Gan to kagaku ryoho* **1991**, *18*, 1665-1675.
[258] M. J. Vicent, R. Duncan, *Trends Biotechnol.* **2006**, *24*, 39-47.

[259] a) B. Rihova, M. Bilej, V. Vetvicka, K. Ulbrich, J. Strohalm, J. Kopecek, R. Duncan, *Biomaterials* **1989**, *10*, 335-342; b) B. Rihova, K. Ulbrich, J. Kopecek, P. Mancal, *Folia Microbiol.* **1983**, *28*, 217-227.
[260] P. M. Loadman, M. C. Bibby, J. A. Double, W. M. Al-Shakhaa, R. Duncan, *Clin. Cancer Res.* **1999**, *5*, 3682-3688.
[261] P. Rejmanová, J. Kopeček, R. Duncan, J. B. Lloyd, *Biomaterials* **1985**, *6*, 45-48.
[262] J. Cassidy, R. Duncan, G. J. Morrison, J. Strohalm, D. Plocova, J. Kopecek, S. B. Kaye, *Biochem. Pharmacol.* **1989**, *38*, 875-879.
[263] R. Duncan, L. C. Seymour, L. Scarlett, J. B. Lloyd, P. Rejmanová, J. Kopecek, *Biochim. Biophys. Acta* **1986**, *880*, 62-71.
[264] L. W. Seymour, D. R. Ferry, D. Anderson, S. Hesslewood, P. J. Julyan, R. Poyner, J. Doran, A. M. Young, S. Burtles, D. J. Kerr, *J. Clin. Oncol.* **2002**, *20*, 1668-1676.
[265] E. Gianasi, M. Wasil, E. G. Evagorou, A. Keddle, G. Wilson, R. Duncan, *Eur. J. Cancer* **1999**, *35*, 994-1002.
[266] X. Lin, Q. Zhang, J. R. Rice, D. R. Stewart, D. P. Nowotnik, S. B. Howell, *Eur. J. Cancer* **2004**, *40*, 291-297.
[267] a) http://www.prnewswire.com/news-releases/access-expands-its-polymer-platinate-program-71728437.html, last accessed 16.01.2017; b) R. Tong, J. Cheng, *Polym. Rev.* **2007**, *47*, 345-381.
[268] D. P. Nowotnik, E. Cvitkovic, *Adv. Drug Delivery Rev.* **2009**, *61*, 1214-1219.
[269] D. P. Nowotnik, *Curr. Bioact. Compd.* **2011**, *7*, 21-26.
[270] https://www.clinicaltrialsregister.eu/ctr-search/search?query=2010-020030-25, last accessed 16.01.2017.
[271] J. M. Meerum Terwogt, W. W. ten Bokkel Huinink, J. H. Schellens, M. Schot, I. A. Mandjes, M. G. Zurlo, M. Rocchetti, H. Rosing, F. J. Koopman, J. H. Beijnen, *Anticancer drugs* **2001**, *12*, 315-323.
[272] a) N. E. Schoemaker, C. van Kesteren, H. Rosing, S. Jansen, M. Swart, J. Lieverst, D. Fraier, M. Breda, C. Pellizzoni, R. Spinelli, M. G. Porro, J. H. Beijnen, J. H. M. Schellens, W. W. ten Bokkel Huinink, *Br. J. Cancer* **2002**, *87*, 608-614; b) D. Bissett, J. Cassidy, J. S. de Bono, F. Muirhead, M. Main, L. Robson, D. Fraier, M. L. Magnè, C. Pellizzoni, M. G. Porro, R. Spinelli, W. Speed, C. Twelves, *Br. J. Cancer* **2004**, *91*, 50-55; c) F. M. Wachters, H. J. M. Groen, J. G. Maring, J. A. Gietema, M. Porro, H. Dumez, E. G. E. de Vries, A. T. van Oosterom, *Br. J. Cancer* **2004**, *90*, 2261-2267.
[273] a) X.-M. Liu, S. C. Miller, D. Wang, *Adv. Drug Delivery Rev.* **2010**, *62*, 258; b) J. Kopeček, P. Kopečková, *Adv. Drug Delivery Rev.* **2010**, *62*, 122-149.
[274] a) H. Ross, P. Bonomi, C. Langer, M. O'Brien, K. O'Byrne, L. Paz-Ares, A. Sandler, M. Socinski, F. Oldham, J. Singer, *J. Clin. Oncol.* **2006**, *24*, abstr. 7039; b) C. J. Langer, K. J. O'Byrne, M. A. Socinski, S. M. Mikhailov, K. Leśniewski-Kmak, M. Smakal, T. E. Ciuleanu, S. V. Orlov, M. Dediu, D. Heigener, A. J. Eisenfeld, L. Sandalic, F. B. Oldham, J. W. Singer, H. J. Ross, *J. Thorac. Oncol.* **2008**, *3*, 623-630; c) M. E. R. O'Brien, M. A. Socinski, A. Y. Popovich, I. N. Bondarenko, A. Tomova, B. T. Bilynsky˘ı, Y. S. Hotko, V. L. Ganul, I. Y. Kostinsky, A. J. Eisenfeld, L. Sandalic, F. B. Oldham, B. Bandstra, A. B. Sandler, J. W. Singer, *J. Thorac. Oncol.* **2008**, *3*, 728-734.
[275] P. Bonomi, *Expert Rev. Anticancer Ther.* **2007**, *7*, 415-422.
[276] http://www.prnewswire.com/news-releases/european-regulatory-agency-accepts-cell-therapeutics-incs-marketing-authorization-application-for-xyotaxtm-for-lung-cancer-for-review-56983987.html, last accessed 16.01.2017.
[277] J. Homsi, G. R. Simon, C. R. Garrett, G. Springett, R. De Conti, A. A. Chiappori, P. N. Munster, M. K. Burton, S. Stromatt, C. Allievi, P. Angiuli, A. Eisenfeld, D. M. Sullivan, A. I. Daud, *Clin. Cancer Res.* **2007**, *13*, 5855-5861.

[278] K. L. Eskow Jaunarajs, D. G. Standaert, T. X. Viegas, M. D. Bentley, Z. Fang, B. Dizman, K. Yoon, R. Weimer, P. Ravenscroft, T. H. Johnston, M. P. Hill, J. M. Brotchie, R. W. Moreadith, *Mov. Disord.* **2013**, *28*, 1675-1682.
[279] http://serinatherapeutics.com/, last accessed 16.01.2017.
[280] D. H. Wakefield, J. J. Klein, J. A. Wolff, D. B. Rozema, *Bioconjugate Chem.* **2005**, *16*, 1204-1208.
[281] D. B. Rozema, D. L. Lewis, D. H. Wakefield, S. C. Wong, J. J. Klein, P. L. Roesch, S. L. Bertin, T. W. Reppen, Q. Chu, A. V. Blokhin, J. E. Hagstrom, J. A. Wolff, *Proc. Natl. Acad. Sci. U.S.A.* **2007**, *104*, 12982-12987.
[282] J. M. Rademaker-Lakhai, C. Terret, S. B. Howell, C. M. Baud, R. F. de Boer, D. Pluim, J. H. Beijnen, J. H. M. Schellens, J.-P. Droz, *Clin. Cancer Res.* **2004**, *10*, 3386-3395.
[283] V.-T. Tran, J.-P. Benoît, M.-C. Venier-Julienne, *Int. J. Pharm.* **2011**, *407*, 1-11.
[284] M. Vert, K.-H. Hellwich, M. Hess, P. Hodge, P. Kubisa, M. Rinaudo, F. Schué, *Pure Appl. Chem.* **2012**, *84*, 377-410.
[285] D. S. Kohane, *Biotechnol. Bioeng.* **2007**, *96*, 203-209.
[286] J. Renukuntla, A. D. Vadlapudi, A. Patel, S. H. S. Boddu, A. K. Mitra, *Int. J. Pharm.* **2013**, *447*, 75-93.
[287] A. C. Hunter, J. Elsom, P. P. Wibroe, S. M. Moghimi, *Nanomed. Nanotechnol. Biol. Med.* **2012**, *8, Supplement 1*, S5-S20.
[288] F. Ungaro, I. d' Angelo, A. Miro, M. I. La Rotonda, F. Quaglia, *J. Pharm. Pharmacol.* **2012**, *64*, 1217-1235.
[289] K. Letchford, H. Burt, *Eur. J. Pharm. Biopharm.* **2007**, *65*, 259-269.
[290] T. W. Prow, J. E. Grice, L. L. Lin, R. Faye, M. Butler, W. Becker, E. M. T. Wurm, C. Yoong, T. A. Robertson, H. P. Soyer, M. S. Roberts, *Adv. Drug Delivery Rev.* **2011**, *63*, 470-491.
[291] A. Firooz, S. Nafisi, H. I. Maibach, *Int. J. Pharm.* **2015**, *495*, 599-607.
[292] V. Lassalle, M. L. Ferreira, *Macromol. Biosci.* **2007**, *7*, 767-783.
[293] G. Singh, T. Kaur, R. Kaur, A. Kaur, *Int. J. Pharm. Pharm. Sci.* **2014**, *1*, 30-42.
[294] http://www.rovi.es/ficheros/notas/ingles/185i.pdf., last accessed 16.01.2017.
[295] W. Dang, I. R. Garver, DE 60023138 T2, **2006**.
[296] D. K. Armstrong, G. F. Fleming, M. Markman, H. H. Bailey, *Gynecol. Oncol.* **2006**, *103*, 391-396.
[297] S. Kaity, S. Maiti, A. Ghosh, D. Pal, A. Ghosh, S. Banerjee, *J. Adv. Pharm. Technol. Res.* **2010**, *1*, 283-290.
[298] T. Nicolai, O. Colombani, C. Chassenieux, *Soft Matter* **2010**, *6*, 3111-3118.
[299] G. Riess, *Prog. Polym. Sci.* **2003**, *28*, 1107-1170.
[300] M. Talelli, M. Barz, C. J. F. Rijcken, F. Kiessling, W. E. Hennink, T. Lammers, *Nano Today* **2015**, *10*, 93-117.
[301] E. Pérez-Herrero, A. Fernández-Medarde, *Eur. J. Pharm. Biopharm.* **2015**, *93*, 52-79.
[302] Y. Min, J. M. Caster, M. J. Eblan, A. Z. Wang, *Chem. Rev.* **2015**, *115*, 11147-11190.
[303] C. Oerlemans, W. Bult, M. Bos, G. Storm, J. F. W. Nijsen, W. E. Hennink, *Pharm. Res.* **2010**, *27*, 2569-2589.
[304] http://www.samyangbiopharm.com/eng/productintroduce/injection01, last accessed 16.01.2017.
[305] S.-W. Lee, M.-H. Yun, S. W. Jeong, C.-H. In, J.-Y. Kim, M.-H. Seo, C.-M. Pai, S.-O. Kim, *J. Control. Release* **2011**, *155*, 262-271.
[306] K. Kato, K. Chin, T. Yoshikawa, K. Yamaguchi, Y. Tsuji, T. Esaki, K. Sakai, M. Kimura, T. Hamaguchi, Y. Shimada, Y. Matsumura, R. Ikeda, *Invest. New Drugs* **2012**, *30*, 1621-1627.
[307] J. W. Valle, A. Armstrong, C. Newman, V. Alakhov, G. Pietrzynski, J. Brewer, S. Campbell, P. Corrie, E. K. Rowinsky, M. Ranson, *Invest. New Drugs* **2011**, *29*, 1029-1037.

[308] J. Hrkach, D. Von Hoff, M. M. Ali, E. Andrianova, J. Auer, T. Campbell, D. De Witt, M. Figa, M. Figueiredo, A. Horhota, S. Low, K. McDonnell, E. Peeke, B. Retnarajan, A. Sabnis, E. Schnipper, J. J. Song, Y. H. Song, J. Summa, D. Tompsett, G. Troiano, T. Van Geen Hoven, J. Wright, P. LoRusso, P. W. Kantoff, N. H. Bander, C. Sweeney, O. C. Farokhzad, R. Langer, S. Zale, *Sci. Transl. Med.* **2012**, *4*, 128ra139-128ra139.

[309] S. Ashton, Y. H. Song, J. Nolan, E. Cadogan, J. Murray, R. Odedra, J. Foster, P. A. Hall, S. Low, P. Taylor, R. Ellston, U. M. Polanska, J. Wilson, C. Howes, A. Smith, R. J. A. Goodwin, J. G. Swales, N. Strittmatter, Z. Takáts, A. Nilsson, P. Andren, D. Trueman, M. Walker, C. L. Reimer, G. Troiano, D. Parsons, D. De Witt, M. Ashford, J. Hrkach, S. Zale, P. J. Jewsbury, S. T. Barry, *Sci. Transl. Med.* **2016**, *8*, 325ra317.

[310] a) L. Cadzow, K. Arnold, D. Thrasher, J. Nolan, A. Horhota, E. Lewis-Clark, J. Wright, S. Low, *Mol. Cancer Ther.* **2015**, *14*, C184; b) http://www.businesswire.com/news/home/20150924005171/en/BIND-Therapeutics-Announces-Pfizer-Exercises-Option-Advance, last accessed 16.01.2017.

[311] Y. Matsumura, T. Hamaguchi, T. Ura, K. Muro, Y. Yamada, Y. Shimada, K. Shirao, T. Okusaka, H. Ueno, M. Ikeda, N. Watanabe, *Br. J. Cancer* **2004**, *91*, 1775-1781.

[312] L. Pittet, D. Altreuter, P. Ilyinskii, C. Fraser, Y. Gao, S. Baldwin, M. Keegan, L. Johnston, T. Kishimoto, *J. Immunol.* **2012**, *188*, 75.11.

[313] R. A. Maldonado, R. A. LaMothe, J. D. Ferrari, A. H. Zhang, R. J. Rossi, P. N. Kolte, A. P. Griset, C. O'Neil, D. H. Altreuter, E. Browning, L. Johnston, O. C. Farokhzad, R. Langer, D. W. Scott, U. H. von Andrian, T. K. Kishimoto, *Proc. Natl. Acad. Sci. U.S.A.* **2015**, *112*, E156-165.

[314] T. Ueno, K. Endo, K. Hori, N. Ozaki, A. Tsuji, S. Kondo, N. Wakisaka, S. Murono, K. Kataoka, Y. Kato, T. Yoshizaki, *Int. J. Nanomed.* **2014**, *9*, 3005-3012.

[315] S. Eliasof, D. Lazarus, C. G. Peters, R. I. Case, R. O. Cole, J. Hwang, T. Schluep, J. Chao, J. Lin, Y. Yen, H. Han, D. T. Wiley, J. E. Zuckerman, M. E. Davis, *Proc. Natl. Acad. Sci. U.S.A.* **2013**, *110*, 15127-15132.

[316] D. Lazarus, S. Kabir, S. Eliasof, *Cancer Res.* **2012**, *72*, 5643.

[317] S. Wohlfart, A. S. Khalansky, C. Bernreuther, M. Michaelis, J. Cinatl Jr, M. Glatzel, J. Kreuter, *Int. J. Pharm.* **2011**, *415*, 244-251.

[318] Q. Zhou, X. Sun, L. Zeng, J. Liu, Z. Zhang, *Nanomed. Nanotechnol. Biol. Med.* **2009**, *5*, 419-423.

[319] B. S. Pattni, V. V. Chupin, V. P. Torchilin, *Chem. Rev.* **2015**, *115*, 10938-10966.

[320] https://www.doxil.com/, last accessed 16.01.2017.

[321] http://www.fda.gov/drugs/informationondrugs/approveddrugs/ucm292721.htm, last accessed 16.01.2017.

[322] http://www.ciplamed.com/content/oncodox-peg-injection, last accessed 16.01.2017.

[323] G. P. Stathopoulos, *Anti-Cancer Drugs* **2010**, *21*, 732-736.

[324] G. P. Stathopoulos, D. Antoniou, J. Dimitroulis, P. Michalopoulou, A. Bastas, K. Marosis, J. Stathopoulos, A. Provata, P. Yiamboudakis, D. Veldekis, N. Lolis, N. Georgatou, M. Toubis, C. Pappas, G. Tsoukalas, *Ann. Oncol.* **2010**, *21*, 2227-2232.

[325] U. Lächelt, E. Wagner, *Chem. Rev.* **2015**, *115*, 11043-11078.

[326] Y. Lee, K. Kataoka, *Adv. Polym. Sci.* **2012**, 95-134.

[327] a) R. Kanasty, J. R. Dorkin, A. Vegas, D. Anderson, *Nat. Mater.* **2013**, *12*, 967-977; b) H. Yin, R. L. Kanasty, A. A. Eltoukhy, A. J. Vegas, J. R. Dorkin, D. G. Anderson, *Nat. Rev. Genet.* **2014**, *15*, 541-555.

[328] C. A. Taylor, Z. Liu, T. C. Tang, Q. Zheng, S. Francis, T.-W. Wang, B. Ye, J. A. Lust, R. Dondero, J. E. Thompson, *Mol. Ther.* **2012**, *20*, 1305-1314.

[329] L. Buscail, B. Bournet, F. Vernejoul, G. Cambois, H. Lulka, N. Hanoun, M. Dufresne, A. Meulle, A. Vignolle-Vidoni, L. Ligat, N. Saint-Laurent, F. Pont, S. Dejean, M. Gayral, F. Martins, J. Torrisani, O.

Barbey, F. Gross, R. Guimbaud, P. Otal, F. Lopez, G. Tiraby, P. Cordelier, *Mol. Ther.* **2015**, *23*, 779-789.
[330] http://www.biocancell.com/lead-program/bc-819/, last accessed 16.01.2017.
[331] I. J. Matouk, D. Halle, M. Gilon, A. Hochberg, *J. Transl. Med.* **2015**, *13*, 1-12.
[332] J. G. Fewell, M. Matar, G. Slobodkin, S.-O. Han, J. Rice, B. Hovanes, D. H. Lewis, K. Anwer, *J. Control. Release* **2005**, *109*, 288-298.
[333] R. D. Alvarez, M. W. Sill, S. A. Davidson, C. Y. Muller, D. P. Bender, R. L. DeBernardo, K. Behbakht, W. K. Huh, *Gynecol. Oncol.* **2014**, *133*, 433-438.
[334] http://celsion.com/pages/pipeline, last accessed 16.01.2017.
[335] M. E. Davis, *Mol. Pharmaceutics* **2009**, *6*, 659-668.
[336] M. E. Davis, J. E. Zuckerman, C. H. J. Choi, D. Seligson, A. Tolcher, C. A. Alabi, Y. Yen, J. D. Heidel, A. Ribas, *Nature* **2010**, *464*, 1067-1070.
[337] H. B. Levy, G. Baer, S. Baron, C. E. Buckler, C. J. Gibbs, M. J. Iadarola, W. T. London, J. Rice, *J. Infect. Dis.* **1975**, *132*, 434-439.
[338] A. S. Levine, H. B. Levy, *Cancer Treat. Rep.* **1978**, *62*, 1907-1912.
[339] M. W. Konstan, P. B. Davis, J. S. Wagener, K. A. Hilliard, R. C. Stern, L. J. H. Milgram, T. H. Kowalczyk, S. L. Hyatt, T. L. Fink, C. R. Gedeon, S. M. Oette, J. M. Payne, O. Muhammad, A. G. Ziady, R. C. Moen, M. J. Cooper, *Hum. Gene Ther.* **2004**, *15*, 1255-1269.
[340] F. Lori, J. Trocio, N. Bakare, L. M. Kelly, J. Lisziewicz, *Vaccine* **2005**, *23*, 2030-2034.
[341] a) J. Hartikka, A. Geall, V. Bozoukova, D. Kurniadi, D. Rusalov, J. Enas, J.-H. Yi, A. Nanci, A. Rolland, *J. Gene Med.* **2008**, *10*, 770-782; b) M. A. Kharfan-Dabaja, T. Nishihori, *Expert Rev. Vaccines* **2015**, *14*, 341-350.
[342] A. L. Sisson, R. Haag, *Soft Matter* **2010**, *6*, 4968-4975.
[343] A. V. Kabanov, S. V. Vinogradov, *Angew. Chem. Int. Ed.* **2009**, *48*, 5418-5429.
[344] A. L. Lewis, M. V. Gonzalez, S. W. Leppard, J. E. Brown, P. W. Stratford, G. J. Phillips, A. W. Lloyd, *J. Mater. Sci. Mater. Med.* **2007**, *18*, 1691-1699.
[345] G. Bruixola, R. García, F. Gomez, C. Escoín, L. Palomar, H. de la Cueva, J. J. Martínez, A. Santaballa, *Ann. Oncol.* **2015**, *26*, iii6-ii9.
[346] O. K. Akinwande, P. Philips, P. Duras, S. Pluntke, C. Scoggins, R. C. Martin, *Cardiovasc. Interv. Radiol.* **2015**, *38*, 361-371.
[347] A. L. Lewis, M. R. Dreher, V. O'Byrne, D. Grey, M. Caine, A. Dunn, Y. Tang, B. Hall, K. D. Fowers, C. G. Johnson, K. V. Sharma, B. J. Wood, *J. Mater. Sci. Mater. Med.* **2016**, *27*, 13.
[348] M. Boulin, P. Hillon, J. P. Cercueil, F. Bonnetain, S. Dabakuyo, A. Minello, J. L. Jouve, C. Lepage, M. Bardou, M. Wendremaire, P. Guerard, A. Denys, A. Grandvuillemin, B. Chauffert, L. Bedenne, B. Guiu, *Alimentary Pharmacology & Therapeutics* **2014**, *39*, 1301-1313.
[349] R. Duran, K. Sharma, M. R. Dreher, K. Ashrafi, S. Mirpour, M. Lin, R. E. Schernthaner, T. R. Schlachter, V. Tacher, A. L. Lewis, S. Willis, M. den Hartog, A. Radaelli, A. H. Negussie, B. J. Wood, J.-F. H. Geschwind, *Theranostics* **2016**, *6*, 28-39.
[350] https://www.btgplc.com/media/press-releases/first-patient-treated-with-lc-bead-lumi-radiopaque-embolic-bead-supported-by-philips-live-image-guidance/, last accessed 16.01.2017.
[351] U. Fritz, O. Fritz, T. A. Gordy, R. Wojcik, J. Blummel, A. Kuller, US 9107850 B2, **2009**.
[352] B. Guiu, A. Schmitt, S. Reinhardt, A. Fohlen, T. Pohl, M. Wendremaire, A. Denys, J. Blümmel, M. Boulin, *J. Vasc. Interv. Radiol.* **2015**, *26*, 262-270.
[353] E. de Luis, J. I. Bilbao, J. A. G. J. Ciércoles, A. Martínez-Cuesta, A. de Martino Rodríguez, M. D. Lozano, *Cardiovasc. Interv. Radiol.* **2008**, *31*, 367-376.
[354] K. Malagari, A. Pomoni, D. Filippiadis, D. Kelekis, *Hepat. Oncol.* **2015**, *2*, 147-157.

[355] http://www.terumo-europe.com/en-emea/interventional-oncology/loco-regional-treatment/drug-elutable-microspheres-tace/lifepearl%C2%AE-microspheres, last accessed 16.01.2017.
[356] http://www.marketwired.com/press-release/biolex-sells-lex-system-to-synthon-and-initiates-sale-of-locteron-1653466.htm, last accessed 16.01.2017.
[357] J. Alemán, A. V. Chadwick, J. He, M. Hess, K. Horie, R. G. Jones, P. Kratochvíl, I. Meisel, I. Mita, G. Moad, *Pure Appl. Chem.* **2007**, *79*, 1801-1829.
[358] a) M. Hamidi, A. Azadi, P. Rafiei, *Adv. Drug Delivery Rev.* **2008**, *60*, 1638-1649; b) K. S. Soni, S. S. Desale, T. K. Bronich, *J. Control. Release* **2016**, *240*, 109-126.
[359] http://www.avadel.com/research-pipeline/innovative-technologies/medusa-/, last accessed 16.01.2017.
[360] Y. P. Chan, R. Meyrueix, R. Kravtzoff, F. Nicolas, K. Lundstrom, *Expert Opin. Drug Deliv.* **2007**, *4*, 441-451.
[361] L. Jorgensen, H. M. Nielson, *Delivery Technologies for Biopharmaceuticals: Peptides, Proteins, Nucleic Acids and Vaccines*, JohnWiley & Sons, West Sussex (U. K.), **2009**.
[362] http://www.marketwired.com/press-release/flamel-technologies-medusar-formulated-interferon-alpha-demonstrates-favorable-antiviral-nasdaq-flml-1673013.htm, last accessed 16.01.2017.
[363] http://adisinsight.springer.com/drugs/800040952, last accessed 16.01.2017.
[364] http://www.ocutx.com/pipeline/dexamethasone-punctum-plug, last accessed 16.01.2017.
[365] https://www.drugs.com/clinical_trials/ocular-therapeutix-announces-successful-topline-results-both-inflammation-pain-primary-efficacy-17243.html, last accessed 16.01.2017.
[366] C. Blizzard, A. Desai, A. Driscoll, *J. Ocul. Pharmacol. Ther.* **2016**, *32*, 595-600.
[367] E. Caló, V. V. Khutoryanskiy, *Eur. Polym. J.* **2015**, *65*, 252-267.
[368] http://www.ferringusa.com/pi/cervidil., last accessed 16.01.2017.
[369] P. Gupta, K. Vermani, S. Garg, *Drug Discovery Today* **2002**, *7*, 569-579.
[370] http://www.businesswire.com/news/home/20080225005425/en/Marillion-Pharmaceuticals-Cytokine-PharmaSciences-Announce-License-Agreement, last accessed 16.01.2017.
[371] J. Gibson, J. A. Halliday, K. Ewert, S. Robertson, *Br. Dent. J.* **2007**, *202*, E17.
[372] http://adisinsight.springer.com/drugs/800020054, last accessed 16.01.2017.
[373] https://docetp.mpa.se/LMF/Misodel%20vaginal%20delivery%20system%20ENG%20PAR.pdf, last accessed 16.01.2017.
[374] http://www.supprelinla.com/, last accessed 16.01.2017.
[375] L. A. Silverman, E. K. Neely, G. B. Kletter, K. Lewis, S. Chitra, O. Terleckyj, E. A. Eugster, *J. Clin. Endocrinol. Metab.* **2015**, *100*, 2354-2363.
[376] http://www.vantasimplant.com/, last accessed 16.01.2017.
[377] http://www.hydromer.com/cosmetic/aquamere.pdf, last accessed 16.01.2017.
[378] http://www.hydromer.com/cosmetic/aquatrix.pdf, last accessed 16.01.2017.
[379] V. A. Stoy, *J. Biomater. Appl.* **1988**, *3*, 552-604.
[380] http://www.bloomberg.com/research/stocks/private/snapshot.asp?privcapId=711690, last accessed 16.01.2017.
[381] R. C. Rathi, J. Bark, K. D. Fowers*, SQZgelTM*, in *Modified-release drug delivery technology* (Eds.: M. J. Rathbone, J. Hadgraft, M. S. Roberts, M. E. Lane), CRC Press (Taylor & Francis Group), Salt Lake City, Utah, **2008**, pp. 153-162.
[382] https://hum-molgen.org/companies/profile.php3/413-gelmed, last accessed 16.01.2017.
[383] D. E. Newton, *Chemistry of New Materials*, Facts On File, New York, **2007**.
[384] N. L. Elstad, K. D. Fowers, *Adv. Drug Delivery Rev.* **2009**, *61*, 785-794.

[385] B. Tyler, K. D. Fowers, K. W. Li, V. R. Recinos, J. M. Caplan, A. Hdeib, R. Grossman, L. Basaldella, K. Bekelis, G. Pradilla, F. Legnani, H. Brem, *J. Neurosurg.* **2010**, *113*, 210-217.
[386] G. Bonacucina, M. Cespi, G. Mencarelli, G. Giorgioni, G. F. Palmieri, *Polymers* **2011**, *3*, 779-811.
[387] M. McKenzie, D. Betts, A. Suh, K. Bui, L. D. Kim, H. Cho, *Molecules* **2015**, *20*, 20397-20408.
[388] S. J. Vukelja, S. P. Anthony, J. C. Arseneau, B. S. Berman, C. Casey Cunningham, J. J. Nemunaitis, W. E. Samlowski, K. D. Fowers, *Anticancer Drugs* **2007**, *18*, 283-289.
[389] G. A. DuVall, D. Tarabar, R. H. Seidel, N. L. Elstad, K. D. Fowers, *Anticancer Drugs* **2009**, *20*, 89-95.
[390] http://www.scripintelligence.com/researchdevelopment/BTG-discontinues-paclitaxel-gel-after-Phase-IIb-failure-313595, last accessed 16.01.2017.
[391] http://ipmglobal.org/our-work/our-products/dapivirine-ring/phase-iii-results, last accessed 16.01.2017.
[392] http://pipeline.ctiexchange.org/products/upa-vaginal-ring, last accessed 16.01.2017.
[393] J. T. Clark, M. R. Clark, N. B. Shelke, T. J. Johnson, E. M. Smith, A. K. Andreasen, J. S. Nebeker, J. Fabian, D. R. Friend, P. F. Kiser, *PLoS ONE* **2014**, *9*, e88509.
[394] S. R. Ugaonkar, A. Wesenberg, J. Wilk, S. Seidor, O. Mizenina, L. Kizima, A. Rodriguez, S. Zhang, K. Levendosky, J. Kenney, M. Aravantinou, N. Derby, B. Grasperge, A. Gettie, J. Blanchard, N. Kumar, K. Roberts, M. Robbiani, J. A. Fernández-Romero, T. M. Zydowsky, *J. Control. Release* **2015**, *213*, 57-68.
[395] http://www.tevapharm.com/news/phase_iii_study_of_teva_s_milprosa_progesterone_vaginal_ring_published_in_fertility_and_sterility_03_13.aspx, last accessed 16.01.2017.
[396] http://www.ipmglobal.org/content/ipms-dapivirine-ring-may-offer-significant-hiv-protection-when-used-consistently-new-data, last accessed 16.01.2017.
[397] D. Ramchandran, U. D. Upadhyay, *Population Reports* **2007**, 1-19.
[398] A. Lendvay, R. Otieno-Masaba, S. K. Azmat, A. Wheeless, W. Hameed, B. T. Shaikh, S. Kuria, M. J. Steiner, M. Chen, P. J. Feldblum, *Contraception* **2014**, *89*, 197-203.
[399] http://www.dahua-sh.com/, last accessed 16.01.2017.
[400] S. Palomba, A. Falbo, A. Di Cello, C. Materazzo, F. Zullo, *Gynecol. Endocrinol.* **2012**, *28*, 710-721.
[401] https://pipeline.ctiexchange.org/fillpdf?fid=105&nid=869, last accessed 16.01.2017.
[402] V. Halpern, R. M. Stalter, D. H. Owen, L. J. Dorflinger, A. Lendvay, K. H. Rademacher, *Contraception* **2015**, *92*, 3-9.
[403] http://www.fda.gov/NewsEvents/Newsroom/PressAnnouncements/ucm503719.htm, last accessed 16.01.2017.
[404] E. Dolgin, *Nat. Med.* **2014**, *20*, 9-11.
[405] http://www.medicinenet.com/pilocarpine-ophthalmic_ocular_system/article.htm, last accessed 16.01.2017.
[406] D. B. Troy, J. P. Remington, P. Beringer, *Remington: The science and practice of pharmacy*, Lippincott Williams & Wilkins, Philadelphia, Pennsylvania, **2006**.
[407] J. Wang, A. Jiang, M. Joshi, J. Christoforidis, *Mediators Inflammation* **2013**, *2013*, 780634.
[408] W. A. Pearce, S. Yeh, H. F. Fine, *Ophthalmic surgery, lasers & imaging retina* **2016**, *47*, 103-107.
[409] A. C. Anselmo, S. Mitragotri, *J. Control. Release* **2014**, *190*, 15-28.
[410] M. Cabrera, S. Yeh, T. A. Albini, *J. Ophthalmol.* **2014**, *2014*, 5.
[411] a) Q. D. Nguyen, E. B. Rodrigues, M. E. Farah, W. F. Mieler, D. V. Do, *Retinal pharmacotherapeutics: Retinal pharmacotherapeutics*, in *Developments in ophthalmology* (Ed.: F. Bandello), Karger, **2016**; b) N. Kuno, S. Fujii, *Ocular Drug Delivery Systems for the Posterior Segment: A Review*, Retina Today May/June, **2012**.
[412] http://www.gliadel.com/, last accessed 16.01.2017.
[413] http://propelopens.com/, last accessed 16.01.2017.

[414] T. Golan, E. Z. Khvalevsky, A. Hubert, R. M. Gabai, N. Hen, A. Segal, A. Domb, G. Harari, E. B. David, S. Raskin, Y. Goldes, E. Goldin, R. Eliakim, M. Lahav, Y. Kopleman, A. Dancour, A. Shemi, E. Galun, *Oncotarget* **2015**, *6*, 24560-24570.
[415] http://www.drug-dev.com/Main/Back-Issues/ADVANCED-DELIVERY-DEVICES-Implantable-DrugEluting-1006.aspx, last accessed 16.01.2017.
[416] http://sinusys.com/, last accessed 16.01.2017.
[417] M. J. Cima, H. Lee, K. Daniel, L. M. Tanenbaum, A. Mantzavinou, K. C. Spencer, Q. Ong, J. C. Sy, J. Santini, C. M. Schoellhammer, D. Blankschtein, R. S. Langer, *J. Control. Release* **2014**, *190*, 157-171.
[418] S. V. Sastry, J. R. Nyshadham, J. A. Fix, *Pharm. Sci. Technol. Today* **2000**, *3*, 138-145.
[419] M. W. Tibbitt, J. E. Dahlman, R. Langer, *J. Am. Chem. Soc.* **2016**, *138*, 704-717.
[420] G. Traverso, R. Langer, *Nature* **2015**, *519*, S19.
[421] a) F. Kong, R. P. Singh, *J. Food Sci.* **2008**, *73*, R67-R80; b) F. J. O. Varum, G. B. Hatton, A. W. Basit, *Int. J. Pharm.* **2013**, *457*, 446-460.
[422] C. S. Leopold, *Pharm. Sci. Technol. Today* **1999**, *2*, 197-204.
[423] S. D. Hussan, R. Santanu, P. Verma, V. Bhandari, *IOSR J. Pharm.* **2012**, *2*, 5-11.
[424] a) S. Thakral, N. K. Thakral, D. K. Majumdar, *Expert Opin. Drug Deliv.* **2013**, *10*, 131-149; b) C. Lautenschläger, C. Schmidt, D. Fischer, A. Stallmach, *Adv. Drug Delivery Rev.* **2014**, *71*, 58-76.
[425] S. Joshi, H. U. Petereit, *Int. J. Pharm.* **2013**, *457*, 395-406.
[426] T. Yoshida, T. C. Lai, G. S. Kwon, K. Sako, *Expert Opin. Drug Deliv.* **2013**, *10*, 1497-1513.
[427] M. A. Hanson, M. T. Fareed, S. L. Argenio, A. O. Agunwamba, T. R. Hanson, *Prim. Care* **2013**, *40*, 1-16.
[428] T. Hu, J. Yang, K. Cui, Q. Rao, T. Yin, L. Tan, Y. Zhang, Z. Li, G. Wang, *ACS Appl. Mater. Interfaces* **2015**, *7*, 11695-11712.
[429] Y. Huang, H. C. A. Ng, X. W. Ng, V. Subbu, *J. Control. Release* **2014**, *193*, 188-201.
[430] W. Khan, S. Farah, A. J. Domb, *J. Control. Release* **2012**, *161*, 703-712.
[431] J. Iqbal, J. Gunn, P. W. Serruys, *Br. Med. Bull.* **2013**, *106*, 193-211.
[432] A. E. Alahmar, A. D. Grayson, M. Andron, M. Egred, E. D. Roberts, B. Patel, R. K. G. Moore, K. Albouaini, M. Jackson, R. A. Perry, *Int. J. Cardiol.* **2009**, *132*, 398-404.
[433] T. Palmerini, G. Biondi-Zoccai, D. Della Riva, A. Mariani, P. Genereux, A. Branzi, G. W. Stone, *J. Am. Coll. Cardiol.* **2013**, *62*, 1915-1921.
[434] S. L. Chin-Quee, S. H. Hsu, K. L. Nguyen-Ehrenreich, J. T. Tai, G. M. Abraham, S. D. Pacetti, Y. F. Chan, G. Nakazawa, F. D. Kolodgie, R. Virmani, N. N. Ding, L. A. Coleman, *Biomaterials* **2010**, *31*, 648-657.
[435] a) D. M. Martin, F. J. Boyle, *Med. Eng. Phys.* **2011**, *33*, 148-163; b) T. Tada, R. A. Byrne, S. Cassese, L. King, S. Schulz, J. Mehilli, A. Schömig, A. Kastrati, *Am. Heart J.* **2013**, *165*, 80-86; c) B. D. Gogas, M. McDaniel, H. Samady, S. B. I. King, *Trends Cardiovasc. Med.* **2014**, *24*, 305-313.
[436] A. M. Sammel, D. Chen, N. Jepson, *Heart, Lung and Circulation* **2013**, *22*, 495-506.
[437] a) G. G. Stefanini, B. Kalesan, P. W. Serruys, D. Heg, P. Buszman, A. Linke, T. Ischinger, V. Klauss, F. Eberli, W. Wijns, M.-C. Morice, C. Di Mario, R. Corti, D. Antoni, H. Y. Sohn, P. Eerdmans, G.-A. van Es, B. Meier, S. Windecker, P. Jüni, *Lancet* **2011**, *378*, 1940-1948; b) K. Upendra, B. Sanjeev, *Minerva Cardioangiol.* **2012**, *60*, 23-31; c) P. A. Lemos, I. Bienert, *Expert Rev. Med. Devices* **2013**, *10*, 295-300; d) D. J. Kereiakes, I. T. Meredith, S. Windecker, R. Lee Jobe, S. R. Mehta, I. J. Sarembock, R. L. Feldman, B. Stein, C. Dubois, T. Grady, S. Saito, T. Kimura, T. Christen, D. J. Allocco, K. D. Dawkins, *Circ. Cardiovasc. Interv.* **2015**, *8*, e002372; e) L. O. Jensen, P. Thayssen, M. Maeng, J. Ravkilde, H. S. Hansen, S. E. Jensen, H. E. Bøtker, K. Berencsi, J. F. Lassen, E. H. Christiansen, *Am. Heart J.* **2015**, *170*, 210-215.
[438] W. Chen, T. C. J. Habraken, W. E. Hennink, R. J. Kok, *Bioconjugate Chem.* **2015**, *26*, 1277-1288.

[439] B. D. Gogas, V. Farooq, Y. Onuma, P. W. Serruys, *Hellenic J. Cardiol.* **2012**, *53*, 301-309.
[440] https://www.drugs.com/inactive/, last accessed 16.01.2017.
[441] http://www.accessdata.fda.gov/scripts/cder/iig/index.cfm, last accessed 16.01.2017.
[442] H. Sohi, Y. Sultana, R. K. Khar, *Drug Dev. Ind. Pharm.* **2004**, *30*, 429-448.
[443] B. Karolewicz, *Saudi Pharm. J.* **2016**, *24*, 525-536.
[444] K. Babiuch, M. Gottschaldt, O. Werz, U. S. Schubert, *RSC Advances* **2012**, *2*, 10427-10465.
[445] G. L. Amidon, H. Lennernas, V. P. Shah, J. R. Crison, *Pharm. Res.* **1995**, *12*, 413-420.
[446] http://www.fda.gov/downloads/Drugs/Guidances/ucm070246.pdf., last accessed 16.01.2017.
[447] S. Baghel, H. Cathcart, N. J. O'Reilly, *J. Pharm. Sci.* **2016**, *105*, 2527-2544.
[448] O. M. Y. Koo, *Pharmaceutical Excipients: Properties, Functionality, and Applications in Research and Industry*, John Wiley & Sons, **2016**.
[449] a) A. K. Singla, M. Chawla, A. Singh, *Drug Dev. Ind. Pharm.* **2000**, *26*, 913-924; b) G. P. Andrews, T. P. Laverty, D. S. Jones, *Eur. J. Pharm. Biopharm.* **2009**, *71*, 505-518.
[450] Z. Zhu, Y. Zhai, N. Zhang, D. Leng, P. Ding, *Asian J. Pharm. Sci.* **2013**, *8*, 218-227.
[451] a) R. P. Gullapalli, C. L. Mazzitelli, *Int. J. Pharm.* **2015**, *496*, 219-239; b) A. D'Souza A, R. Shegokar, *Expert Opin. Drug Deliv.* **2016**, *13*, 1257-1275.
[452] E. T. Cole, D. Cadé, H. Benameur, *Adv. Drug Deliv. Rev.* **2008**, *60*, 747-756.
[453] T. Schettler, S. Paris, M. Pellett, S. Kidner, D. Wilkinson, *Clin. Drug Investig.* **2001**, *21*, 73-78.
[454] Q. T. Shubhra, J. Tóth, J. Gyenis, T. Feczkó, *Polym. Rev.* **2014**, *54*, 112-138.
[455] a) G. Dumortier, J. L. Grossiord, F. Agnely, J. C. Chaumeil, *Pharm. Res.* **2006**, *23*, 2709-2728; b) J. J. Escobar-Chávez, M. López-Cervantes, A. Naik, Y. Kalia, D. Quintanar-Guerrero, A. Ganem-Quintanar, *J. Pharm. Pharm. Sci.* **2006**, *9*, 339-358.
[456] a) A. V. Kabanov, E. V. Batrakova, V. Y. Alakhov, *J. Control. Release* **2002**, *82*, 189-212; b) E. V. Batrakova, A. V. Kabanov, *J. Control. Release* **2008**, *130*, 98-106.
[457] E. A. Yapar, O. Ynal, *Trop. J. Pharm. Res.* **2012**, *11*, 855-866.
[458] A. Al-Khattawi, A. R. Mohammed, *Expert Opin. Drug Deliv.* **2013**, *10*, 651-663.
[459] N. Krishna, F. Brow, *Am. J. Ophthalmol.* **1964**, *57*, 99-106.
[460] N. Debotton, A. Dahan, *Med. Res. Rev.* **2017**, *37*, 52-97.
[461] A. Dahan, J. M. Miller, *AAPS J.* **2012**, *14*, 244-251.
[462] C. G. Wermuth, D. Aldous, P. Raboisson, D. Rognan, *The Practice of Medicinal Chemistry*, Academic Press, Elsevier Science, San Diego, California, **1996**.
[463] L. Shargel, I. Kanfer, *Generic drug product development: Specialty dosage forms*, CRC Press (Taylor & Francis Group), **2016**.
[464] S. Garg, K. R. Tambwekar, K. Vermani, A. Garg, C. L. Kaul, L. J. Zaneveld, *Pharm. Technol.* **2001**, 15.
[465] J. das Neves, M. F. Bahia, *Int. J. Pharm.* **2006**, *318*, 1-14.
[466] M. Justin-Temu, F. Damian, R. Kinget, G. Van Den Mooter, *J. Womens Health (Larchmt.)* **2004**, *13*, 834-844.
[467] C. M. Caramella, S. Rossi, F. Ferrari, M. C. Bonferoni, G. Sandri, *Adv. Drug Delivery Rev.* **2015**, *92*, 39-52.
[468] J. H. Guo, *Drug Deliv. Technol.* **2003**, *3*.
[469] D. R. Devi, P. Sandhya, B. N. V. Hari, *J. Pharm. Sci. Res.* **2013**, *5*, 159-165.
[470] H. Almeida, M. H. Amaral, P. Lobao, J. M. Lobo, *Drug Discov. Today* **2014**, *19*, 400-412.
[471] P. Mahlumba, Y. Choonara, P. Kumar, L. du Toit, V. Pillay, *Molecules* **2016**, *21*, 1002.
[472] P. Dhal, S. R. Holmes-Farley, C. Huval, T. Jozefiak, *Adv. Polym. Sci.* **2006**, *192*, 9-58.
[473] B. B. Gerstman, R. Kirkman, R. Platt, *Am. J. Kidney Dis.* **1992**, *20*, 159-161.
[474] Z. Harel, S. Harel, P. S. Shah, R. Wald, J. Perl, C. M. Bell, *Am. J. Med.* **2013**, *126*, 264.e269-224.

[475] M. R. Weir, G. L. Bakris, D. A. Bushinsky, M. R. Mayo, D. Garza, Y. Stasiv, J. Wittes, H. Christ-Schmidt, L. Berman, B. Pitt, *N. Engl. J. Med.* **2015**, *372*, 211-221.
[476] E. A. Slatopolsky, S. K. Burke, M. A. Dillon, *Kidney Int.* **1999**, *55*, 299-307.
[477] W. H. Mandeville, D. I. Goldberg, *Curr. Pharm. Des.* **1997**, *3*, 15-28
[478] a) M. H. Davidson, *Expert Opin. Pharmacother.* **2007**, *8*, 2569-2578; b) T. Suzuki, K. Oba, Y. Igari, N. Matsumura, K. Watanabe, S. Futami-Suda, H. Yasuoka, M. Ouchi, K. Suzuki, Y. Kigawa, H. Nakano, *J. Nippon Med. Sch.* **2013**, *80*, 211-217.
[479] T. J. Louie, J. Peppe, C. K. Watt, D. Johnson, R. Mohammed, G. Dow, K. Weiss, S. Simon, J. F. John, G. Garber, S.-C. Taber, D. M. Davidson, *Clin. Infect. Dis.* **2006**, *43*, 411-420.
[480] E. M. Nestorovich, S. M. Bezrukov, *Expert Opin. Drug Discovery* **2014**, *9*, 299-318.
[481] J. D. Reuter, A. Myc, M. M. Hayes, Z. Gan, R. Roy, D. Qin, R. Yin, L. T. Piehler, R. Esfand, D. A. Tomalia, J. R. Baker, *Bioconjugate Chem.* **1999**, *10*, 271-278.
[482] J. Balzarini, L. Van Damme, *Lancet* **2007**, *369*, 787-797.
[483] D. Concagh, V. R. Garigapati, S. R. Holmes-Farley, C. C. Huval, T. H. Jozefiak, W. H. Mandeville, K. K. Shackett, WO 2001005408 A1, **2001**.
[484] I. Melnikova, D. Wages, *Nat. Rev. Drug Discovery* **2006**, *5*, 369-370.
[485] A. Colas, L. Aguadisch, *Chim. Nouv.* **1997**, *15*, 1779.
[486] K. Mojsiewicz-Pieńkowska*, Review of current pharmaceutical applications of polysiloxanes (silicones)*, in *Handbook of polymers for pharmaceutical technologies* (Eds.: V. K. Thakur, M. K. Thakur), John Wiley & Sons, **2015**, pp. 363-381.
[487] M. Ahsan, L. Babaei, A. Gholamrezaei, M. H. Emami, *Diagn. Ther. Endosc.* **2011**, *2011*, 4.
[488] N. J. Carter, G. M. Keating, *Drugs* **2012**, *70*, 1545-1577.
[489] A. Djukic, J. Feldman, H. P. Frey, J. Jankowski, R. Holtzer, S. Moshe, H. Muzumdar, S. Rose, R. Shinnar, S. Shinnar, *Eur. J. Paediatr. Neurol.* **2015**, *19*, S8.
[490] G. Landa, O. Butovsky, J. Shoshani, M. Schwartz, A. Pollack, *Curr. Res.* **2008**, *33*, 1011-1013.
[491] J. Kovalchin, J. Krieger, M. Genova, K. Collins, M. Augustyniak, A. Masci, T. Hittinger, B. Kuca, G. Edan, C. Braudeau, M. Rimbert, U. Patel, E. Mascioli, E. Zanelli, *J. Neuroimmunol.* **2010**, *225*, 153-163.
[492] E. P. Orringer, J. F. Casella, K. I. Ataga, M. Koshy, P. Adams-Graves, L. Luchtman-Jones, T. Wun, M. Watanabe, F. Shafer, A. Kutlar, M. Abboud, M. Steinberg, B. Adler, P. Swerdlow, C. Terregino, S. Saccente, B. Files, S. Ballas, R. Brown, S. Wojtowicz-Praga, J. M. Grindel, *JAMA* **2001**, *286*, 2099-2106.
[493] R. Ghadi, A. Jain, W. Khan, A. Domb, *Wound Healing Biomaterials-Volume 2: Functional Biomaterials* **2016**, 203.
[494] A. Nan, S. L. Croft, V. Yardley, H. Ghandehari, *J. Control. Release* **2004**, *94*, 115-127.
[495] http://arrowheadpharma.com/pipeline/, last accessed 16.01.2017.
[496] M. Miyamoto, K. Naka, M. Tokumizu, T. Saegusa, *Macromolecules* **1989**, *22*, 1604-1607.
[497] F. Manzenrieder, R. Luxenhofer, M. Retzlaff, R. Jordan, M. G. Finn, *Angew. Chem. Int. Ed.* **2011**, *50*, 2601-2605.
[498] A. Mero, G. Pasut, L. D. Via, M. W. M. Fijten, U. S. Schubert, R. Hoogenboom, F. M. Veronese, *J. Control. Release* **2008**, *125*, 87-95.
[499] a) J. Tong, R. Luxenhofer, X. Yi, R. Jordan, A. V. Kabanov, *Mol. Pharmaceutics* **2010**, *7*, 984-992; b) A. Mero, Z. Fang, G. Pasut, F. M. Veronese, T. X. Viegas, *J. Control. Release* **2012**, *159*, 353-361.
[500] a) S. Konieczny, C. P. Fik, N. J. H. Averesch, J. C. Tiller, *J. Biotechnol.* **2012**, *159*, 195-203; b) S. Konieczny, C. Krumm, D. Doert, K. Neufeld, J. C. Tiller, *J. Biotechnol.* **2014**, *181*, 55-63.
[501] T. Lühmann, M. Schmidt, M. N. Leiske, V. Spieler, T. C. Majdanski, M. Grube, M. Hartlieb, I. Nischang, S. Schubert, U. S. Schubert, L. Meinel, *ACS Biomater. Sci. Eng.* **2017**, *3*, 304–312.

[502] M. Schmitz, M. Kuhlmann, O. Reimann, C. P. R. Hackenberger, J. Groll, *Biomacromolecules* **2015**, *16*, 1088-1094.
[503] W. H. Velander, R. D. Madurawe, A. Subramanian, G. Kumar, G. Sinai-Zingde, J. S. Riffle, C. L. Orthner, *Biotechnol. Bioeng.* **1992**, *39*, 1024-1030.
[504] T. X. Viegas, M. D. Bentley, J. M. Harris, Z. Fang, K. Yoon, B. Dizman, R. Weimer, A. Mero, G. Pasut, F. M. Veronese, *Bioconjugate Chem.* **2011**, *22*, 976-986.
[505] M. Schmidt, S. Harmuth, E. R. Barth, E. Wurm, R. Fobbe, A. Sickmann, C. Krumm, J. C. Tiller, *Bioconjugate Chem.* **2015**, *26*, 1950-1962.
[506] M. Bauer, C. Lautenschlaeger, K. Kempe, L. Tauhardt, U. S. Schubert, D. Fischer, *Macromol. Biosci.* **2012**, *12*, 986-998.
[507] B. Cao, Q. Tang, G. Cheng, *J. Biomater. Sci., Polym. Ed.* **2014**, *25*, 1502-1513.
[508] X. Wang, X. Sun, G. Jiang, R. Wang, R. Hu, X. Xi, Y. Zhou, S. Wang, T. Wang, *J. Appl. Polym. Sci.* **2013**, *128*, 3289-3294.
[509] Z. Wang, G. Ma, J. Zhang, W. Lin, F. Ji, M. T. Bernards, S. Chen, *Langmuir* **2014**, *30*, 3764-3774.
[510] W. Lin, H. Zhang, J. Wu, Z. Wang, H. Sun, J. Yuan, S. Chen, *J. Mater. Chem. B* **2013**, *1*, 2482-2488.
[511] Z. Zhao, J. Wang, H.-Q. Mao, K. W. Leong, *Adv. Drug Delivery Rev.* **2003**, *55*, 483-499.
[512] T. Steinbach, F. R. Wurm, *Biomacromolecules* **2016**, *17*, 3338-3346.
[513] S. Zhang, J. Zou, M. Elsabahy, A. Karwa, A. Li, D. A. Moore, R. B. Dorshow, K. L. Wooley, *Chem. Sci.* **2013**, *4*, 2122-2126.
[514] J.-Z. Du, X.-J. Du, C.-Q. Mao, J. Wang, *J. Am. Chem. Soc.* **2011**, *133*, 17560-17563.
[515] E. Falco, M. Patel, J. Fisher, *Pharm. Res.* **2008**, *25*, 2348-2356.
[516] S. Tempelaar, L. Mespouille, O. Coulembier, P. Dubois, A. P. Dove, *Chem. Soc. Rev.* **2013**, *42*, 1312-1336.
[517] D. P. Sanders, K. Fukushima, D. J. Coady, A. Nelson, M. Fujiwara, M. Yasumoto, J. L. Hedrick, *J. Am. Chem. Soc.* **2010**, *132*, 14724-14726.
[518] A. C. Engler, X. Ke, S. Gao, J. M. W. Chan, D. J. Coady, R. J. Ono, R. Lubbers, A. Nelson, Y. Y. Yang, J. L. Hedrick, *Macromolecules* **2015**, *48*, 1673-1678.
[519] J. M. W. Chan, X. Ke, H. Sardon, A. C. Engler, Y. Y. Yang, J. L. Hedrick, *Chem. Sci.* **2014**, *5*, 3294-3300.
[520] a) Z. Y. Ong, K. Fukushima, D. J. Coady, Y.-Y. Yang, P. L. R. Ee, J. L. Hedrick, *J. Control. Release* **2011**, *152*, 120-126; b) J. Feng, R.-X. Zhuo, X.-Z. Zhang, *Prog. Polym. Sci.* **2012**, *37*, 211-236; c) W. Chen, F. Meng, R. Cheng, C. Deng, J. Feijen, Z. Zhong, *J. Control. Release* **2014**, *190*, 398-414.
[521] S. D. Allison, *Expert Opin. Drug Deliv.* **2008**, *5*, 615-628.
[522] S. Wilhelm, A. J. Tavares, Q. Dai, S. Ohta, J. Audet, H. F. Dvorak, W. C. W. Chan, *Nat. Rev. Mater.* **2016**, *1*, 16014.
[523] http://www.nanopartikel.info/en/, last accessed 16.01.2017.
[524] http://inbs.med.utoronto.ca/cnr/, last accessed 16.01.2017.
[525] H. Otsuka, Y. Nagasaki, K. Kataoka, *Adv. Drug Delivery Rev.* **2003**, *55*, 403-419.
[526] R. Rietscher, J. A. Czaplewska, T. C. Majdanski, M. Gottschaldt, U. S. Schubert, M. Schneider, C.-M. Lehr, *Int. J. Pharm.* **2016**, *500*, 187-195.
[527] a) T. Sun, Y. S. Zhang, B. Pang, D. C. Hyun, M. Yang, Y. Xia, *Angew. Chem. Int. Ed.* **2014**, *53*, 12320-12364; b) N. Kamaly, B. Yameen, J. Wu, O. C. Farokhzad, *Chem. Rev.* **2016**, *116*, 2602-2663.
[528] M. Karimi, A. Ghasemi, P. S. Zangabad, R. Rahighi, S. M. M. Basri, H. Mirshekari, M. Amiri, Z. S. Pishabad, A. Aslani, M. Bozorgomid, *Chem. Soc. Rev.* **2016**, *45*, 1457-1501.
[529] J. E. Zuckerman, M. E. Davis, *Nat. Rev. Drug Discovery* **2015**, *14*, 843-856.
[530] J. W. Choi, J.-H. Park, S. Y. Baek, D.-D. Kim, H.-C. Kim, H.-J. Cho, *Colloids Surf., B* **2015**, *132*, 305-312.
[531] D. Y. Wong, S. J. Hollister, P. H. Krebsbach, C. Nosrat, *Tissue Engineer.* **2007**, *13*, 2515-2523.

[532] D. Mondal, M. Griffith, S. S. Venkatraman, *Int. J. Polym. Mater.* **2016**, *65*, 255-265.
[533] S. Kalita, B. Devi, R. Kandimalla, K. K. Sharma, A. Sharma, K. Kalita, A. C. Kataki, J. Kotoky, *Int. J. Nanomed.* **2015**, *10*, 2971-2984.
[534] a) A. Takahashi, Y. Yamamoto, M. Yasunaga, Y. Koga, J.-i. Kuroda, M. Takigahira, M. Harada, H. Saito, T. Hayashi, Y. Kato, T. Kinoshita, N. Ohkohchi, I. Hyodo, Y. Matsumura, *Cancer Sci.* **2013**, *104*, 920-925; b) Y. Matsumura, *Jpn. J. Clin. Oncol.* **2014**, *44*, 515-525.
[535] A. Sugaya, I. Hyodo, Y. Koga, Y. Yamamoto, H. Takashima, R. Sato, R. Tsumura, F. Furuya, M. Yasunaga, M. Harada, R. Tanaka, Y. Matsumura, *Cancer Sci.* **2016**, *107*, 335-340.
[536] S. Y. Wong, J. M. Pelet, D. Putnam, *Prog. Polym. Sci.* **2007**, *32*, 799-837.
[537] a) C.-H. Ahn, S. Y. Chae, Y. H. Bae, S. W. Kim, *J. Control. Release* **2002**, *80*, 273-282; b) M. L. Forrest, J. T. Koerber, D. W. Pack, *Bioconjugate Chem.* **2003**, *14*, 934-940; c) C. Englert, M. Hartlieb, P. Bellstedt, K. Kempe, C. Yang, S. K. Chu, X. Ke, J. M. García, R. J. Ono, M. Fevre, R. J. Wojtecki, U. S. Schubert, Y. Y. Yang, J. L. Hedrick, *Macromolecules* **2015**, *48*, 7420-7427.
[538] a) S. Taranejoo, J. Liu, P. Verma, K. Hourigan, *J. Appl. Polym. Sci.* **2015**, *132*, 42096; b) C. Englert, M. Fevre, R. J. Wojtecki, W. Cheng, Q. Xu, C. Yang, X. Ke, M. Hartlieb, K. Kempe, J. M. Garcia, R. J. Ono, U. S. Schubert, Y. Y. Yang, J. L. Hedrick, *Polym. Chem.* **2016**, *7*, 5862-5872.
[539] C. Englert, A.-K. Trützschler, M. Raasch, T. Bus, P. Borchers, A. S. Mosig, A. Traeger, U. S. Schubert, *J. Control. Release* **2016**, *241*, 1-14.
[540] S. Agarwal, Y. Zhang, S. Maji, A. Greiner, *Mater. Today* **2012**, *15*, 388-393.
[541] Y. Qian, Y. Zha, B. Feng, Z. Pang, B. Zhang, X. Sun, J. Ren, C. Zhang, X. Shao, Q. Zhang, X. Jiang, *Biomaterials* **2013**, *34*, 2117-2129.
[542] L. Bédouet, F. Pascale, L. Moine, M. Wassef, S. H. Ghegediban, V.-N. Nguyen, M. Bonneau, D. Labarre, A. Laurent, *Int. J. Pharm.* **2013**, *456*, 536-544.
[543] C. Sonnet, C. L. Simpson, R. M. Olabisi, K. Sullivan, Z. Lazard, Z. Gugala, J. F. Peroni, J. M. Weh, A. R. Davis, J. L. West, E. A. Olmsted-Davis, *J. Orthop. Res.* **2013**, *31*, 1597-1604.
[544] M. Molina, M. Asadian-Birjand, J. Balach, J. Bergueiro, E. Miceli, M. Calderon, *Chem. Soc. Rev.* **2015**, *44*, 6161-6186.
[545] Y. Tahara, K. Akiyoshi, *Adv. Drug Delivery Rev.* **2015**, *95*, 65-76.
[546] A. Sharma, T. Garg, A. Aman, K. Panchal, R. Sharma, S. Kumar, T. Markandeywar, *Artif. Cells Nanomed. Biotechnol.* **2016**, *44*, 165-177.
[547] S. De Koker, J. Cui, N. Vanparijs, L. Albertazzi, J. Grooten, F. Caruso, B. G. De Geest, *Angew. Chem. Int. Ed.* **2016**, *55*, 1334-1339.
[548] Y. Tian, Y. Wang, S. Shen, X. Jiang, Y. Wang, W. Yang, *Part. Part. Syst. Charact.* **2015**, *32*, 1092-1101.
[549] S. Jin, J. Wan, L. Meng, X. Huang, J. Guo, L. Liu, C. Wang, *ACS Appl. Mater. Interfaces* **2015**, *7*, 19843-19852.
[550] M. Da, S. M. Tian, J. Baryza, J. C. Luft, J. M. DeSimone, *Mol. Pharmaceutics* **2015**, *12*, 3518-3526.
[551] T. Gerson, E. Makarov, T. H. Senanayake, S. Gorantla, L. Y. Poluektova, S. V. Vinogradov, *Nanomed. Nanotechnol. Biol. Med.* **2014**, *10*, 177-185.
[552] S. S. Desale, S. M. Raja, J. O. Kim, B. Mohapatra, K. S. Soni, H. Luan, S. H. Williams, T. A. Bielecki, D. Feng, M. Storck, V. Band, S. M. Cohen, H. Band, T. K. Bronich, *J. Control. Release* **2015**, *208*, 59-66.
[553] S. S. Desale, K. S. Soni, S. Romanova, S. M. Cohen, T. K. Bronich, *J. Control. Release* **2015**, *220, Part B*, 651-659.
[554] L. Kaps, L. Nuhn, M. Aslam, A. Brose, F. Foerster, S. Rosigkeit, P. Renz, R. Heck, Y. O. Kim, I. Lieberwirth, D. Schuppan, R. Zentel, *Adv. Healthcare Mater.* **2015**, *4*, 2809-2815.
[555] P. Tomakidi, T. Steinberg, W. Weber, D. Laird, R. Gübeli, EP 2455104 B1, **2013**.
[556] K. H. Hsu, S. Gause, A. Chauhan, *J. Drug Delivery Sci. Technol.* **2014**, *24*, 123-135.

[557] L. Xinming, C. Yingde, A. W. Lloyd, S. V. Mikhalovsky, S. R. Sandeman, C. A. Howel, L. Liewen, *Cont. Lens Anterior Eye* **2008**, *31*, 57-64.
[558] C.-C. Li, A. Chauhan, *Ind. Eng. Chem. Res.* **2006**, *45*, 3718-3734.
[559] A. Ribeiro, F. Veiga, D. Santos, J. J. Torres-Labandeira, A. Concheiro, C. Alvarez-Lorenzo, *Biomacromolecules* **2011**, *12*, 701-709.
[560] C.-C. Peng, A. Chauhan, *J. Control. Release* **2011**, *154*, 267-274.
[561] C. Gupta, A. Chauhan, *J. Control. Release* **2011**, *150*, 70-76.
[562] a) A. M. Ribeiro, A. Figueiras, F. Veiga, *J. Pharm. Pharm. Sci.* **2015**, *18*, 683-695; b) S. Kirchhof, A. M. Goepferich, F. P. Brandl, *Eur. J. Pharm. Biopharm.* **2015**, *95*, 227-238.
[563] S. K. Guha, US 5488075 A, **1996**.
[564] N. K. Lohiya, I. Alam, M. Hussain, S. R. Khan, A. S. Ansari, *Indian. J. Med. Res.* **2014**, *140*, 63-72.
[565] N. K. Lohiya, R. Suthar, A. Khandelwal, S. Goyal, A. S. Ansari, B. Manivannan, *Int. J. Androl.* **2010**, *33*, e198-e206.
[566] https://www.parsemusfoundation.org/projects/vasalgel/, last accessed 16.01.2017.
[567] https://www.parsemusfoundation.org/contraceptives/two-steps-forward/, last accessed 16.01.2017.
[568] A. Lohani, G. Singh, S. S. Bhattacharya, A. Verma, *J. Drug Delivery* **2014**, *2014*, 11.
[569] J. R. Millar, *J. Chem. Soc.* **1960**, 1311-1317.
[570] A. D. Jenkins, P. Kratochvíl, R. F. T. Stepto, U. W. Suter, *Pure Appl. Chem.* **1996**, *68*, 2287.
[571] T. M. Aminabhavi, M. N. Nadagouda, U. A. More, S. D. Joshi, V. H. Kulkarni, M. N. Noolvi, P. V. Kulkarni, *Expert Opin. Drug Deliv.* **2015**, *12*, 669-688.
[572] E. S. Dragan, *Chem. Eng. J.* **2014**, *243*, 572-590.
[573] L. F. A. Asghar, S. Chandran, *J. Pharm. Pharm. Sci.* **2006**, *9*, 327-338.
[574] a) L. Palugan, M. Cerea, L. Zema, A. Gazzaniga, A. Maroni, *J. Drug Delivery Sci. Technol.* **2015**, *25*, 1-15; b) A. Maroni, M. D. Del Curto, L. Zema, A. Foppoli, A. Gazzaniga, *Int. J. Pharm.* **2013**, *457*, 372-394.

Publication P2

"RAFT made methacrylate copolymers for reversible pH-responsive nanoparticles"

T. Yildirim, A. C. Rinkenauer, C. Weber, A. Traeger, S. Schubert, U. S. Schubert

J. Polym. Sci., Part A: Polym. Chem. **2015**, *53,* 2711-2721.

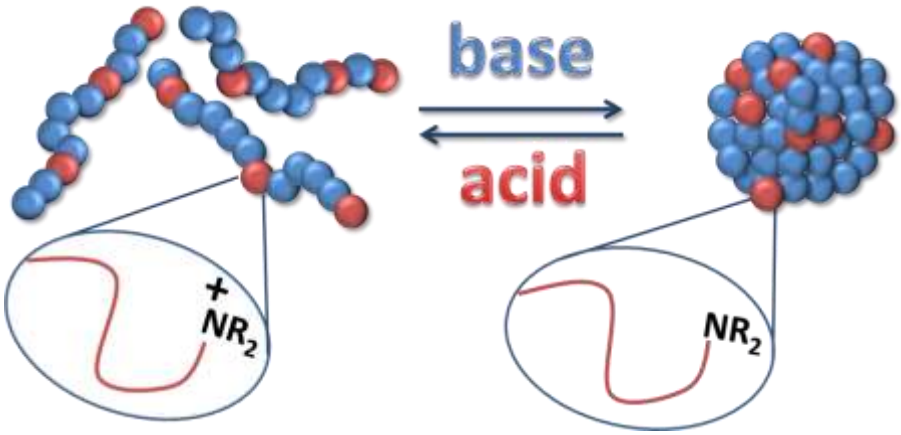

RAFT Made Methacrylate Copolymers for Reversible pH-Responsive Nanoparticles

Turgay Yildirim,[1,2] Alexandra C. Rinkenauer,[1,2] Christine Weber,[1,2] Anja Traeger,[1,2] Stephanie Schubert,[2,3] Ulrich S. Schubert[1,2]

[1]Laboratory of Organic and Macromolecular Chemistry (IOMC), Friedrich Schiller University Jena, Humboldtstr. 10, 07743 Jena, Germany
[2]Jena Center for Soft Matter (JCSM), Friedrich Schiller University Jena, Philosophenweg 7, 07743 Jena, Germany
[3]Institute of Pharmacy, Department of Pharmaceutical Technology, Friedrich Schiller University Jena, Otto-Schott-Str. 41, 07745 Jena, Germany
Correspondence to: U.S. Schubert; (E-mail: ulrich.schubert@uni-jena.de)

Received 1 May 2015; accepted 1 June 2015; published online 2 July 2015
DOI: 10.1002/pola.27734

ABSTRACT: In this study, we designed and investigated pH-responsive nanoparticles based on different ratios of monomers with primary, secondary or tertiary amino groups. For this purpose, copolymers of methyl methacrylate (MMA) with different compositions of amino methacrylates (2-(dimethylamino)ethyl methacrylate (DMAEMA), 2-(*tert*-butylamino)ethyl methacrylate (*t*BAEMA) and 2-aminoethyl methacrylate hydrochloride (AEMA·HCl)) were synthesized using the reversible addition-fragmentation chain transfer (RAFT) polymerization process. The controlled nature of the radical polymerization was demonstrated by kinetic studies. All copolymers show low dispersities ($Đ_M < 1.2$) with amino contents between 9 and 21 mol %. For the nanoparticle formation, nanoprecipitation with subsequent solvent evaporation was used. All suspensions were characterized by dynamic light scattering (DLS) and scanning electron microscopy (SEM). Different initial conditions of the formulations resulted in differently sized nanoparticles that have monomodal size distributions, relatively narrow polydispersity index (PDI) values and positive zeta potential values. The pH-stability test results demonstrated that, depending on the structure and amount of the amino content, the obtained nanoparticles reveal a reversible pH-response, such as dissolution at acidic pH values. The ability of the nanoparticles to encapsulate guest molecules was confirmed by pyrene fluorescence studies. The cytotoxicity assay results showed that the nanoparticles did not have any significant cytotoxic effect. © 2015 Wiley Periodicals, Inc. J. Polym. Sci., Part A: Polym. Chem. **2015**, *53*, 2711–2721

KEYWORDS: copolymerization; nanoparticles; nanoprecipitation; pH-responsive polymers; pH-responsive nanoparticles; polymerization kinetics; RAFT polymerization; self-assembly

INTRODUCTION Stimuli-responsive polymeric nanoparticles recently gained increasing attention due to their potential applications in numerous fields, in particular for pharmaceutical applications.[1–3] Depending on the chemical composition, such "smart" nanoparticles respond to external and/or internal stimuli by physicochemical changes driven by temperature,[4] light,[5] redox reaction,[6] ultrasound,[7] or pH value.[8] Among these, pH-responsive nanoparticles are regarded as highly promising vehicles for the selective delivery of pharmaceutical agents to the diseased tissues. Due to the fact that cancer cells have an abnormal acidic extracellular environment,[9] the pH-sensitivity of the matrix material can trigger the release of the encapsulated drugs. Several pH-responsive nanoparticle systems were reported to increase the efficacy of anticancer drugs in cancer therapy.[10–12] Moreover, a drug delivery vehicle with pH-responsive shedding would be useful for endosomal escape due to the acidification of the late endosome and lysosome.[13]

There are two main strategies to fabricate polymeric pH-responsive nanoparticle systems. The first category comprises the nanoparticles prepared from polymers that have pH-sensitive bonds, such as hydrazone or acetal bonds.[14,15] The second category involves the nanoparticle formation from polymers containing ionizable segments, such as amino and/or carboxyl groups.[16,17] Although there are several methodologies to prepare polymeric nanoparticles,[18] most of the pH-responsive structures in literature are based on the supramolecular self-assembly of copolymer micelles. However, the instability of the micelles below their critical micelle concentration represents a serious drawback.[19]

Additional Supporting Information may be found in the online version of this article.

© 2015 Wiley Periodicals, Inc.

Moreover, uniform size and morphology of the assembled structure is confined with block type copolymers that are harder to synthesize compared to statistical copolymers,[20] also in terms of upscaling.

In this study, a library of well-defined copolymers of methyl methacrylate (MMA) with three amino comonomers with ionizable segments (2-(dimethylamino)ethyl methacrylate (DMAEMA), 2-(*tert*-butylamino)ethyl methacrylate (*t*BAEMA) and 2-aminoethyl methacrylate hydrochloride (AEMA·HCl)) were synthesized via RAFT polymerization (Scheme 1) to obtain a novel pH-responsive drug delivery vehicle for the controlled release of loaded pharmaceutical agents in acidic environment.[21] MMA was used as main monomer in the copolymer chains due to the required hydrophobicity for the nanoparticle formation. DMAEMA, *t*BAEMA, and AEMA·HCl were used as comonomers since their polymers act as weak polybases with pKa values between 7.6 and 8.[22–24] All nanoparticles were prepared by means of nanoprecipitation[25,26] of the synthesized copolymers. To investigate a possible effect of the amino content on the pH-response of corresponding nanoparticles, the copolymer composition was varied by using different monomer feed ratios. Compared to the well-known pH-responsive systems, such as Eudragit E100,[27] the main advantage of our approach is the possibility to tune the nanoparticle's size, solubility, amino content and distribution of the amino moieties along the polymer chain, which could improve loading and release profiles of the pharmaceutical agents encapsulated.

EXPERIMENTAL SECTION

Materials

The monomers methyl methacrylate (MMA), 2-(*N,N*-dimethylamino)ethyl methacrylate (DMAEMA), 2-(*tert*-butylamino)ethyl methacrylate (*t*BAEMA) and 2-aminoethyl methacrylate hydrochloride (AEMA·HCl) were purchased from Sigma Aldrich and purified by stirring in the presence of inhibitor remover prior to use. 2,2′-Azobis(iso-butyronitrile) (AIBN) was purchased from Acros and recrystallized from methanol prior to use. 4-Cyano-4-(phenylcarbonothioylthio) pentanoic acid (CPADB), Amberlyst® A21, 1,3,5-trioxane, inhibitor remover and pyrene were purchased from Sigma Aldrich. AlamarBlue was obtained from Life Technologies. If not stated otherwise, cell culture materials, cell culture media, and solutions were obtained from PAA. All other chemicals were obtained from standard suppliers and used without purification unless specified.

Instruments and Methods

Proton nuclear magnetic resonance (^{1}H NMR) spectra were recorded at room temperature in $CDCl_3$ or CD_3OD on a Brucker Avance 300 MHz using the residual solvent resonance as an internal standard. The chemical shifts are given in ppm.

Gas chromatography (GC) measurements were performed on a Shimadzu GC-2010 instrument.

Size-exclusion chromatography (SEC) measurements were performed on two different setups: (SEC in $CHCl_3$) Shimadzu system equipped with a SCL-10A system controller, a LC-10AD pump, a RID-10A refractive index detector and a PSSSDV-linear S column (5 μm particle size; Polymer Standards Service GmbH, Mainz, Germany) at 40 °C using a chloroform, triethylamine and 2-propanol (94:4:2) mixture as eluent at a flow rate of 1 mL min^{-1}. The system was calibrated with PMMA standards ($M_p = 410$ to 88,000 g mol^{-1}); (SEC in DMAc) Agilent 1200 series equipped with a G1310A pump, a G1315D DA detector, a G1362A RI detector, and PSS GRAM 30 Å/1000 Å (10 μm particle size) columns in series at 40 °C using *N,N*-dimethylacetamide (DMAc) with 2.1 g L^{-1} LiCl as eluent at a flow rate of 1 mL min^{-1}. The system was calibrated with PMMA standards ($M_p = 505$ to 981,000 g mol^{-1}).

Chlorine analysis was carried out on a Titrator TLalpha 20 instrument.

Dynamic light scattering (DLS) was performed on a Zetasizer Nano ZS (Malvern Instruments, Herrenberg, Germany). After an equilibration time of 180 s, 3 × 30 runs were carried out at 25 °C ($\lambda = 633$ nm). The counts were detected at an angle of 173°. Each measurement was performed in triplicate. The mean particle size was approximated as the effective (Z-average) diameter and the width of the distribution as the polydispersity index of the particles (PDI) obtained by the cumulants method assuming a spherical shape.

Electrophoretic light scattering was used to measure the electrokinetic potential, also known as zeta potential. The measurements were performed on a Zetasizer Nano ZS (Malvern Instruments, Herrenberg, Germany) by applying laser Doppler velocimetry. For each measurement, 10 runs were carried out using the slow-field and fast-field reversal mode at 150 V. Each experiment was performed in triplicate at 25 °C.

For scanning electron microscopy (SEM), 5 μL of the suspensions were placed on a mica surface and dried overnight at room temperature under atmospheric pressure. Afterwards, images were taken using a Gemini 1530 type LEO field emission scanning electron microscope (Carl-Zeiss AG, Germany). The samples were coated with a thin layer (4 nm) of platinum via sputter coating using a Bal-TEC 020 HR Sputtering Coater.

For the cytotoxicity tests a Tecan Infinite 200 Pro fluorescence microplate reader (Crailsheim, Germany) was used.

The fluorescence spectra of pyrene solutions were recorded on a Jasco FP-6500 fluorometer applying an excitation wavelength of 335 nm. The emission spectra were recorded from 350 to 600 nm. The excitation and emission bandwidths were 3.0 and 3.0 nm, respectively. For the pH-response test of the nanoparticles a BioShake instrument (Analytik Jena AG, Germany) was used.

Synthesis

RAFT Polymerization

MMA was copolymerized with three different amino methacrylates (DMAEMA, *t*BAEMA and AEMA·HCl) using CPADB as chain transfer agent (CTA) and AIBN as initiator. The initial

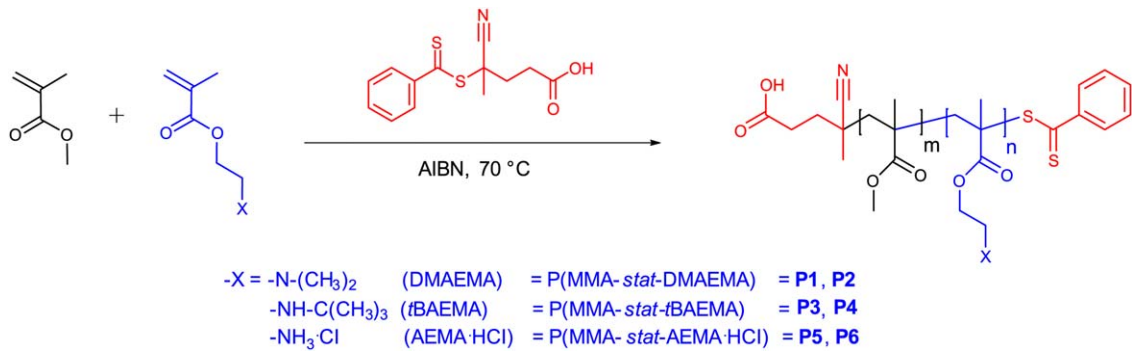

SCHEME 1 Schematic representation of the RAFT copolymerization of MMA with amino-functionalized methacrylates. [Color figure can be viewed in the online issue, which is available at wileyonlinelibrary.com.]

monomer feed ratios of the monomers were varied whereas the overall monomer to CTA ratio was kept constant at 100. All polymerizations were carried out at 70 °C in an oil bath. The copolymerizations with DMAEMA and *t*BAEMA (**P1–P4**) were performed in a 2 M ethanolic solution. Methanol was used as solvent for the copolymerizations with AEMA·HCl (**P5–P6**). The polymerization conditions are summarized in Table 1. An exemplary RAFT copolymerization procedure (Table 1, **P1**) is as follows: 30 g MMA (0.300 mol), 5.234 g DMAEMA (0.033 mol), 930 mg CPADB (3.329 mmol), and 137 mg AIBN (0.832 mmol) were dissolved in ethanol in a 250 mL two-necked round-bottom flask equipped with a magnetic stir bar. The total volume of the reaction mixture was 166 mL. After degassing for 4 h by argon purging, the t_0 sample for GC was taken and the flask was immersed in a preheated oil bath under stirring at 70 °C. After 10 h, the polymerization was stopped by cooling to room temperature and exposing to air. Monomer conversions were determined via GC by using the reaction solvent (ethanol) as internal standard. The polymer was purified by precipitating in cold hexane (approximately six times). The resulting pink colored polymer was dried under high vacuum at room temperature until constant weight to produce an overall yield of 40%. The number average molar mass (M_n) and molar mass dispersities were determined by two different SEC systems by using PMMA standards. SEC in $CHCl_3$: $M_n = 6100$ g mol^{-1} and $Đ_M = 1.16$. SEC in DMAc: $M_n = 6300$ g mol^{-1} and $Đ_M = 1.13$. ^{1}H NMR ($CDCl_3$, 300 MHz): $\delta = 7.87$, 7.52 and 7.36 (Ar-H, CPADB), 4.13 (—$OCH_2CH_2NH(CH_3)_2$), 3.60 (—OCH_3), 2.64 (—$OCH_2CH_2NH(CH_3)_2$), 2.4–0.7 (backbone) ppm.

The degree of polymerization (DP) for each polymer was calculated from the signal integrals in the ^{1}H NMR spectrum of the purified copolymer using the following equations:

$$DP_{MMA} = \frac{I(\text{peak } a)/3}{I(\text{peak } c)/2} \quad (1)$$

$$DP_{DMAEMA} = \frac{I(\text{peak } b)/2}{I(\text{peak } c)/2}, \quad (2)$$

with I(a) corresponding to the integral of methyl proton peaks of the MMA at 3.60 ppm, *I(b)* corresponding to the integral of methylene proton peaks of the DMAEMA at 4.13 ppm, and I(c) corresponding to the integral of two aromatic protons of the dithiobenzoate end group at 7.87 ppm. Molar mass values were calculated by using the following equation:

$$M_{n,NMR} = (DP_{MMA} \times M_{MMA}) + (DP_{DMAEMA} \times M_{DMAEMA}) + M_{CTA}, \quad (3)$$

in which the molar mass of the MMA, DMAEMA and RAFT agent are 100.12, 157.21, and 279.38 g mol^{-1}, respectively.

Kinetic Study of the Polymerizations

During each polymerization, aliquots of 0.2 mL were taken periodically from the reaction mixture by a syringe purged with argon. From each sample, conversions were calculated via GC (**P1**-**P4**) or ^{1}H NMR (**P5**-**P6**) by using the reaction solvents (**P1**-**P4**) or 1,3,5-trioxane (**P5**-**P6**) as internal standards. Molar masses and dispersities were determined via SEC analysis ($CHCl_3$, RI detection).

TABLE 1 RAFT Copolymerization Conditions of MMA (**M1**) and Corresponding Amino-Functionalized Methacrylates (**M2**)[a]

Entry	**M2**	**M1**/**M2**/CTA/AIBN	Solvent	Polymerization Time [h]
P1	DMAEMA	90/10/1/0.25	Ethanol	10
P2	DMAEMA	80/20/1/0.25	Ethanol	10
P3	*t*BAEMA	95/5/1/0.25	Ethanol	13
P4	*t*BAEMA	85/15/1/0.25	Ethanol	10
P5[b]	AEMA·HCl	90/10/1/0.25	Methanol	9
P6[b]	AEMA·HCl	80/20/1/0.25	Methanol	10

[a] All polymerizations were carried out at total monomer concentrations of 2 mol L^{-1}.

[b] Polymerization was carried out under reflux.

Deprotonation of the Polymers

Ion exchange resin Amberlyst A21® was used to deprotonate **P5** and **P6**. For a typical deprotonation reaction, **P5** was dissolved in methanol, mixed with Amberlyst® A21 and stirred for 1 h at room temperature. Subsequently, the corresponding polymer **P7** was obtained by filtration, precipitation into ice-cold hexane and by removal of the volatiles under reduced pressure at room temperature. ^{1}H NMR ($CDCl_3$, 300 MHz): $\delta = 7.87$, 7.52, and 7.36 (Ar-H, CPADB), 4.00 (—$OCH_2CH_2NH_2$), 3.60 (—OCH_3), 2.97 (—$OCH_2CH_2NH_2$), 2.5–0.7 (backbone) ppm. SEC in $CHCl_3$: $M_n = 5300$ g mol^{-1} and $Đ_M = 1.15$, SEC in DMAc: $M_n = 9000$ g mol^{-1} and $Đ_M = 1.10$. Elemental anal. found: C 58.31%, H 8%, N 1.73%, S 0.85%, Cl 1.01%.

Preparation of the Nanoparticle Suspensions

For nanoprecipitation, the corresponding polymers (**P1**, **P2**, **P3**, **P4**, **P7,** and **P8**) were dissolved in acetone at a concentration of 1 or 10 mg mL^{-1}, respectively, and subsequently added dropwise to deionized water under continuous stirring at 500 rpm (acetone to water, AW method). For the water to acetone (WA) method, deionized water was added drop-wise to the acetone polymer solution under stirring at 500 rpm. The acetone/water (solvent/nonsolvent) ratio was kept constant at 0.5 for all suspensions. After removal of the acetone by stirring overnight at room temperature (GC analysis ensured complete removal of acetone), all suspensions were diluted to the final volume of 10 mL. The nanoparticles were characterized by DLS (performed in pure water) and SEM without filtration.

pH-Response Test of the Nanoparticles

For the pH stability test of the nanoparticles ($c = 0.3$ mg mL^{-1}), 0.0667 M acetate buffer (pH values 3.4, 4, 5, 6) and 0.0667 M tris buffer (pH values 7, 8, 9) were used. 500 μL of nanoparticle suspensions were mixed with 500 μL of buffer solutions in Eppendorf tubes and stored at 37 °C while mixing at 200 rpm in a BioShake instrument. After 24 h, DLS and zeta potential measurements were performed (particle concentration of 0.15 mg mL^{-1} in all corresponding buffer systems).

Fluorescence Spectroscopic Study of the Nanoparticles

1 mL stock solution of pyrene (6×10^{-5} mol L^{-1}) in acetone was added to 1 mL nanoparticle suspensions (0.15 mg mL^{-1} polymer concentrations) at various pH values. The samples were incubated at 37 °C for 24 h to remove acetone and to give a final pyrene concentration of 3×10^{-5} mol L^{-1}.

Cell Lines, Culture Conditions, and Cytotoxicity Test of Nanoparticles

The L929 (CCL-1, ATCC) cell lines used in the cytotoxicity experiments were maintained in DMEM culture media supplemented with 10% fetal calf serum (FCS), 100 μg mL^{-1} streptomycin and 100 IU mL^{-1} penicilin. The cells were cultured at 37 °C in humidified 5% CO_2 atmosphere. The cytotoxicity was tested with L929 cells, as this sensitive cell line is recommended by ISO10993-5 ($n = 6$). In detail, cells were seeded at 10 cells per well in a 96-well plate and incubated for 24 h. No cells were seeded in the outer wells. Afterwards, the media were replaced by fresh media and incubated for 30 min. The nanoparticle suspensions were added in the end concentration range from 10 to 1000 μg mL^{-1}, and the cells were incubated at 37 °C for further 24 h. Subsequently, the medium was replaced by fresh media and AlamarBlue as recommended by the supplier. After incubation for 4 h, the fluorescence was measured at Ex 570/Em 610 nm, with untreated cells on the same well plate serving as controls.

RESULTS AND DISCUSSION

A series of amino-functionalized PMMA based copolymers was synthesized via RAFT polymerization due to its versatility and suitability for the synthesis of well-defined amino methacrylate copolymers.[28,29] Three different commercially available amino methacrylates that have tertiary (DMAEMA), secondary (*t*BAEMA) and protonated primary amine functionalities (AEMA·HCl) were used as comonomers. The utilized CTA CPADB has previously been successfully applied to mediate the RAFT polymerization of amino methacrylates.[29,30] [M]/[CTA] was kept constant at a ratio of 100/1 with a monomer concentration of 2 mol L^{-1} in order to obtain relatively low molar mass polymers, considering the increased toxicity of high molar mass polycations.[31] Depending on previous research in our group, the [CTA]/[AIBN] ratio was kept at 1/0.25 regarding polymerization rate and control over the molar mass.[32] All polymerizations were carried out in ethanol at 70 °C, except for **P5**-**P6**, where methanol under reflux was used as solvent because of the poor solubility of AEMA·HCl in ethanol. The primary amine containing monomer AEMA can easily rearrange to its thermodynamically more stable isomer 2-hydroxyethyl methacrylamide, and the dithiobenzoate moiety of the CTA is prone to an aminolysis reaction if the free amine monomer is used.[24] Thus, the hydrochloride salt of the monomer AEMA was used for the polymerization. Two different initial monomer feed ratios were applied for each copolymerization to vary the amino content in the copolymers. The amino methacrylate content in the copolymers was kept low (in between 9 and 21) due to the required hydrophobicity of the copolymers for the capability to form nanoparticles via nanoprecipitation.

Kinetic Studies

The distribution of the amine functionality among the PMMA chain might be an important parameter that could affect the particle formation or structure. To obtain information about the sequence arrangements of the monomers in the PMMA based copolymer chains, kinetic studies were performed for each copolymerization. The obtained data from the kinetic studies of the RAFT copolymerizations of MMA with 10 mol% comonomer (DMAEMA, *t*BAEMA and AEMA·HCl, respectively) are displayed in Figure 1. The corresponding data derived from the kinetic studies with 20 mol% comonomer content are given in the supporting information (Supporting

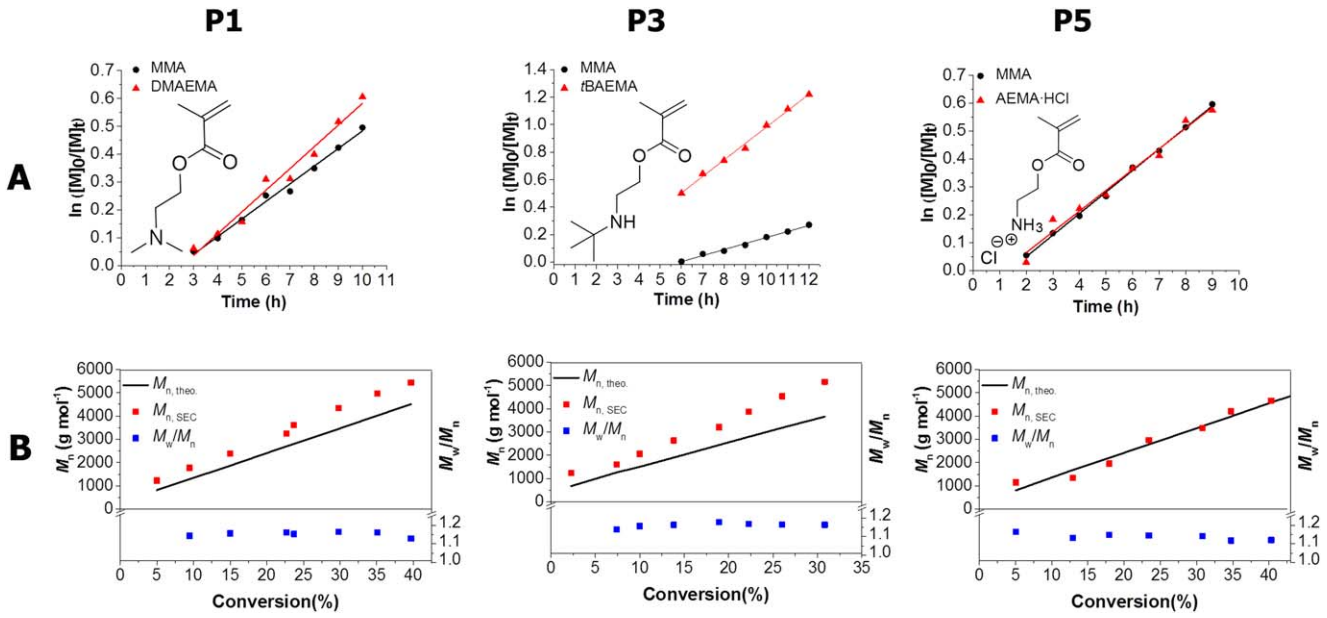

FIGURE 1 Kinetic studies of the RAFT copolymerization of MMA with 10 mol% comonomer DMAEMA (**P1**), *t*BAEMA (**P3**) and AEMA·HCl (**P5**). [M]/[CPADB]/[AIBN] = 100/1/0.25; $[M]_0 = 2$ mol L^{-1}. Polymerization conditions for (**P1** and **P3**): Solvent ethanol, $T = 70$ °C. Polymerization conditions for **P5**: Solvent methanol under reflux. (A) Semilogarithmic kinetic plots. (B) M_n and M_w/M_n evolution with total monomer conversion. [Color figure can be viewed in the online issue, which is available at wileyonlinelibrary.com.]

Information Fig. S2). Analysis of the kinetic samples by means of SEC in $CHCl_3$ revealed monomodal molar mass distributions that shift to lower elution volumes throughout the course of the polymerization (Supporting Information Fig. S1). The molar mass M_n was found to increase linearly with respect to the total monomer conversion (**B**, Fig. 1). These results indicate the controlled nature of the RAFT polymerization.

The semilogarithmic kinetic plots are linear (**A**, Fig. 1) for both monomers in each copolymerization, indicating a pseudo first order polymerization behaviour. At the beginning of the DMAEMA and AEMA·HCl polymerizations, induction periods of around 2 h were observed for each monomer, which is often reported for RAFT polymerizations.[33–36] However, for *t*BAEMA copolymerizations an increase in the induction period of the MMA was observed. This is due to the selective addition of the *t*BAEMA to the growing polymer chains at the beginning of the polymerizations.

The slopes of MMA and DMAEMA in the semilogarithmic plot, which are directly proportional to the polymerization rates of MMA and DMAEMA, respectively, are close to each other, which indicates that both monomers are consumed at close rates. In accordance to the results of the kinetic studies, the ratio of the monomers in the isolated copolymers is similar to the initial monomer feed ratio. These results are also in a good agreement with the reported reactivity ratios of MMA and DMAEMA for the RAFT and free radical copolymerizations ($r_{MMA} \sim 0.8$, $r_{DMAEMA} \sim 0.9$).[37,38] Therefore, it can be concluded that MMA and DMAEMA arrange in the polymer chain in a random sequence.

In contrast, the increased slope of the *t*BAEMA in the semilogarthmic plot reveals that *t*BAEMA is consumed faster than MMA. Indeed, the compositions in the isolated polymers deviated significantly from the initial monomer feed ratios in favor of *t*BAEMA at moderate monomer conversions. The reported relative reactivity ratios of MMA ($r_{MMA} \sim 0.7$) and *t*BAEMA ($r_{tBAEMA} \sim 1.4$)[39] for the free radical copolymerization are in a good agreement with these results. Thus, it can be concluded that the copolymers of MMA and *t*BAEMA display a gradient composition.[40,41]

To the best of our knowledge there are no relative reactivity ratios reported for the copolymerization of MMA and AEMA·HCl. However, almost identical slopes of MMA and AEMA·HCl in the semilogarithmic plot hint towards a random arrangement of the monomers along the polymer chain for both 10 as well as 20 mol% AEMA·HCl.

The kinetic plots for the copolymerizations of same monomers with different initial monomer feed ratios revealed similar results (Supporting Information Fig. S2).

Copolymer Synthesis and Characterization

Based on the results obtained from preliminary kinetic studies, the final copolymers were synthesized under similar conditions with a total M/CTA of 100 aiming at 10 as well as 20% amino content for each monomer. All polymerizations were stopped at moderate monomer conversions to exclude undesired coupling reactions that could take place at higher monomer conversions. Each purified polymer was characterized by ^{1}H NMR spectroscopy and SEC measurements on two systems (Table 2).

TABLE 2 Selected Characterization Data of the MMA (**M1**) Copolymers with Corresponding Amino Methacrylates (**M2**)

Entry	M2	f(M1/M2)[a]	F(M1/M2)[b,c]	Conv. (%) M1 M2	$M_{n,\,theo.}$[d] (g mol^{-1})	DP[c] M1 M2	M_n[c] (g mol^{-1})	M_n[e] (g mol^{-1})	$Đ_M$[e]	M_n[f] (g mol^{-1})	$Đ_M$[f]
P1	DMAEMA	9	7.4	39[g] 45[g]	4,500	41 5.5	5,200	6,100	1.16	6,300	1.13
P2	DMAEMA	4	4	42[g] 50[g]	5,200	40 10	5,900	7,600	1.17	7,800	1.15
P3	*t*BAEMA	19	9.5	29[g] 70[g]	3,700	35 3.7	4,500	5,200	1.19	7,100	1.17
P4	*t*BAEMA	5.7	3.8	36[g] 72[g]	5,300	35 9.2	5,500	7,900	1.15	11,900	1.16
P5	AEMA·HCl	9	9.1	45[c] 44[c]	5,000	42 4.6	5,200	5,100	1.13	9,200	1.15
P6	AEMA·HCl	4	3.7	48[c] 52[c]	5,900	30 8.2	4,600	4,500	1.19	11,000	1.15
P7[h]	AEMA		9			45 5	5,200	5,300	1.18	9,000	1.10
P8[i]	AEMA		3.6			35 9.8	5,000	4,800	1.18	10,000	1.15

[a] Initial monomer feed ratio.
[b] Monomer ratio in the isolated copolymer.
[c] Determined by ^{1}H NMR spectroscopy.
[d] Determined by the formula $M_{n,theo.} = [([M]_{M1}/[CTA] \times Conv. \times M_{M1}) + ([M]_{M2}/[CTA] \times Conv. \times M_{M2}) + (M_{CTA})]$.
[e] Determined by SEC in $CHCl_3$ analysis (RI detection, PMMA calibration).
[f] Determined by SEC in DMAc analysis (RI detection, PMMA calibration).
[g] Determined by GC.
[h] Deprotonated form of **P5**.
[i] Deprotonated form of **P6**.

The compositions of the isolated copolymers (F(M1/M2), Table 2) were calculated from the ^{1}H NMR spectra by using the integrals of appropriate signals derived from both comonomers (methyl proton signal "a" for MMA and methylene proton signal "b" for the amino monomers in Fig. 2, see the experimental section for details). Although DMAEMA and AEMA·HCl copolymers had close initial monomer feed ratios and monomer compositions in the polymers, *t*BAEMA copolymers revealed a composition drift. These results are in accordance with the kinetic studies of the corresponding monomers described above. However, by adjustment of the corresponding monomer feed ratios it was possible to obtain two sets of polymers that contained 10 and 20 mol% of amine comonomer, respectively. All ^{1}H NMR spectra clearly indicate the presence of the dithiobenzoate end-groups derived from the CTA (signals of the aromatic protons at 7.3–7.9 ppm) enabling an estimation of the DP for MMA and for each amino methacrylate. The according number average molar mass (M_n) values calculated by ^{1}H NMR are in good agreement with the theoretical values that were calculated from the [monomer] to [CTA] ratio and the monomer conversions. It should be noted that the ^{1}H NMR spectrum of **P6** was measured in methanol due to the insufficient solubility of **P6** in $CDCl_3$.

The isolated copolymers were analysed using two different SEC systems, which both revealed monomodal traces for all polymers with low dispersity values ($Đ_M < 1.2$) (Fig. 3, Supporting Information Fig. S3, Table 2). In general, higher M_n values were obtained from both SEC systems using PMMA calibration compared to the M_n values calculated from the ^{1}H NMR spectra. This is attributed to the difference in hydrodynamic volumes of the polymers in both eluents that

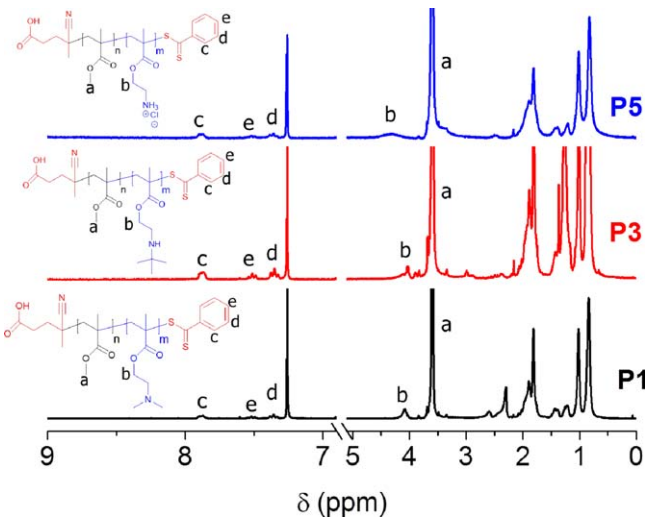

FIGURE 2 ^{1}H NMR spectra (300 MHz, $CDCl_3$) of **P1**, **P3,** and **P5** and the assignment of the peaks used to calculate the DP. [Color figure can be viewed in the online issue, which is available at wileyonlinelibrary.com.]

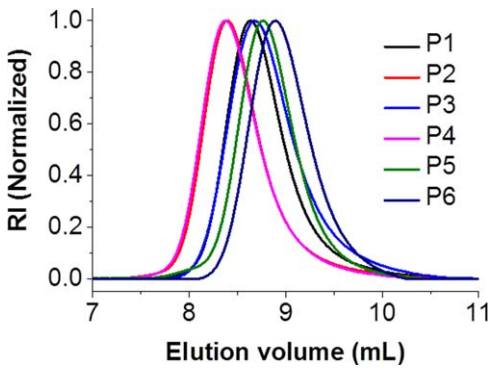

FIGURE 3 Normalized SEC traces in $CHCl_3$ (RI detection, eluent: $CHCl_3$) of isolated copolymers of **P1**-**P6**. [Color figure can be viewed in the online issue, which is available at wileyonlinelibrary.com.]

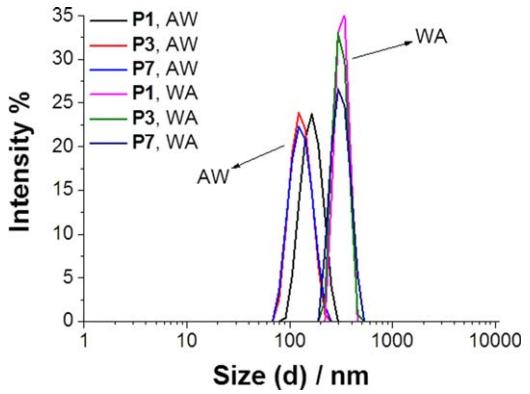

FIGURE 4 Intensity size distributions of nanoparticles in water (**P1**, **P3,** and **P7**) with the initial acetone-polymer concentration of 1 mg mL^{-1}, prepared by dropping acetone-polymer solution to water (AW) or dropping water to acetone-polymer solution (WA). [Color figure can be viewed in the online issue, which is available at wileyonlinelibrary.com.]

are used in these SEC systems compared to PMMA homopolymers. In particular the polar eluent of the SEC in DMAc apparently results in an increased hydrodynamic volume of the amine-containing polymers, which directly leads to an increased apparent molar mass.

Finally the charged copolymers that contain AEMA·HCl (**P5**-**P6**) were treated with Amberlyst® A21 to obtain the desired primary amino-functionalized copolymers (**P7**-**P8**). Elemental analysis results demonstrated a significant decrease in the chlorine content after the deprotonation reactions (Supporting Information Table S1). Both SEC systems revealed no change after the deprotonation reactions (Supporting Information Figs. S4–S7), which ensures the absence of disulfide bond formation, which could possibly occur subsequent to an end group cleavage of the polymers with Amberlyst® A21. It should also be noted that the ^{1}H NMR spectrum of **P8** (Supporting Information Fig. S15) was measured in $CDCl_3$ instead of MeOD since the polymer solubility after deprotonation changed dramatically, indicating the decreased polarity of the deprotonated polymer.

Preparation of Nanoparticle Suspensions

Polymeric nanoparticles were prepared from the synthesized tertiary (**P1**, **P2**), secondary (**P3**, **P4**) and primary (**P7**, **P8**) amino-functional MMA based copolymers by means of nanoprecipitation with subsequent solvent evaporation without any need of stabilizers/surfactants. The acetone/water ratio was kept at 0.5 for all suspensions. In order to obtain differently sized nanoparticles, two different initial acetone-polymer solution concentrations (1 mg mL^{-1}, 10 mg mL^{-1}) and two different dropping methods (dropping acetone polymer solution to water (AW) and dropping water to acetone polymer solution (WA)) were applied for each polymer. In general, smaller nanoparticles were obtained with dropping acetone polymer solution to water (AW) than dropping water to acetone polymer solution (WA) (Fig. 4), which is commonly observed for the nanoprecipitation method.[42] For the initial acetone-polymer solution concentration of 1 mg mL^{-1}, nanoparticles with monomodal size distributions (Fig. 4) and low polydispersity (PDI) values (Table 3) were obtained from all polymers.

However, with the initial acetone-polymer concentration of 10 mg mL^{-1}, nanoparticles with monomodal size distributions could only be obtained from the copolymers that contained DMAEMA and AEMA (**P1**, **P2**, **P7,** and **P8**), which both have a random comonomer distribution. In contrast, the gradient copolymers of *t*BAEMA (**P3**-**P4**) yielded nanoparticles and undefined aggregates which result in multimodal size distributions and high PDI values. This might be due to the tightly spaced amino groups along the polymer chain,

TABLE 3 Characterization Results of the Prepared Nanoparticles

		Z-average[b] [d, nm]		PDI[b]		Zeta potential[c] [mV]	
Polymer	Method[a]	$c = 1$ g L^{-1}	$c = 10$ g L^{-1}	$c = 1$ g L^{-1}	$c = 10$ g L^{-1}	$c = 1$ g L^{-1}	$c = 10$ g L^{-1}
P1	AW	152 ± 2	123 ± 1	0.16 ± 0.02	0.12 ± 0.01	+35 ± 4.4	+37 ± 0.3
	WA	340 ± 3	720 ± 18	0.11 ± 0.03	0.07 ± 0.05	+25 ± 4.3	+48 ± 1.1
P2	AW	184 ± 2	131 ± 2	0.16 ± 0.01	0.11 ± 0.04	+52 ± 0.4	+31 ± 0.7
	WA	473 ± 3	636 ± 4	0.18 ± 0.04	0.07 ± 0.05	+47 ± 0.4	+51 ± 0.7
P3	AW	126 ± 1	200 ± 1[d]	0.12 ± 0.02	0.19 ± 0.03[d]	+44 ± 3.3	+ 56 ± 9[d]
	WA	314 ± 3	1079 ± 28[d]	0.14 ± 0.04	0.26 ± 0.12[d]	+29 ± 0.4	+ 40 ± 3[d]
P4	AW	169 ± 2	158 ± 1[d]	0.15 ± 0.01	0.15 ± 0.03[d]	+36 ± 6.4	+ 41 ± 3[d]
	WA	331 ± 3	610 ± 12[d]	0.09 ± 0.05	0.14 ± 0.01[d]	+20 ± 2.1	+ 26 ± 2[d]
P7	AW	121 ± 1	110 ± 1	0.17 ± 0.01	0.14 ± 0.02	+56 ± 3.2	+59 ± 0.6
	WA	306 ± 2	339 ± 2	0.11 ± 0.02	0.10 ± 0.03	+61 ± 0.5	+64 ± 1.0
P8	AW	133 ± 1	182 ± 1	0.14 ± 0.02	0.08 ± 0.04	+54 ± 2.1	+59 ± 0.8
	WA	254 ± 3	582 ± 13	0.07 ± 0.05	0.17 ± 0.02	+53 ± 3.7	+61 ± 0.6

[a] AW, dropping acetone to water; WA, dropping water to acetone.
[b] Average values of three DLS measurements.
[c] Average values of three zeta potential measurements.
[d] Nanoprecipitation with acetate buffer (pH = 5) as nonsolvent.

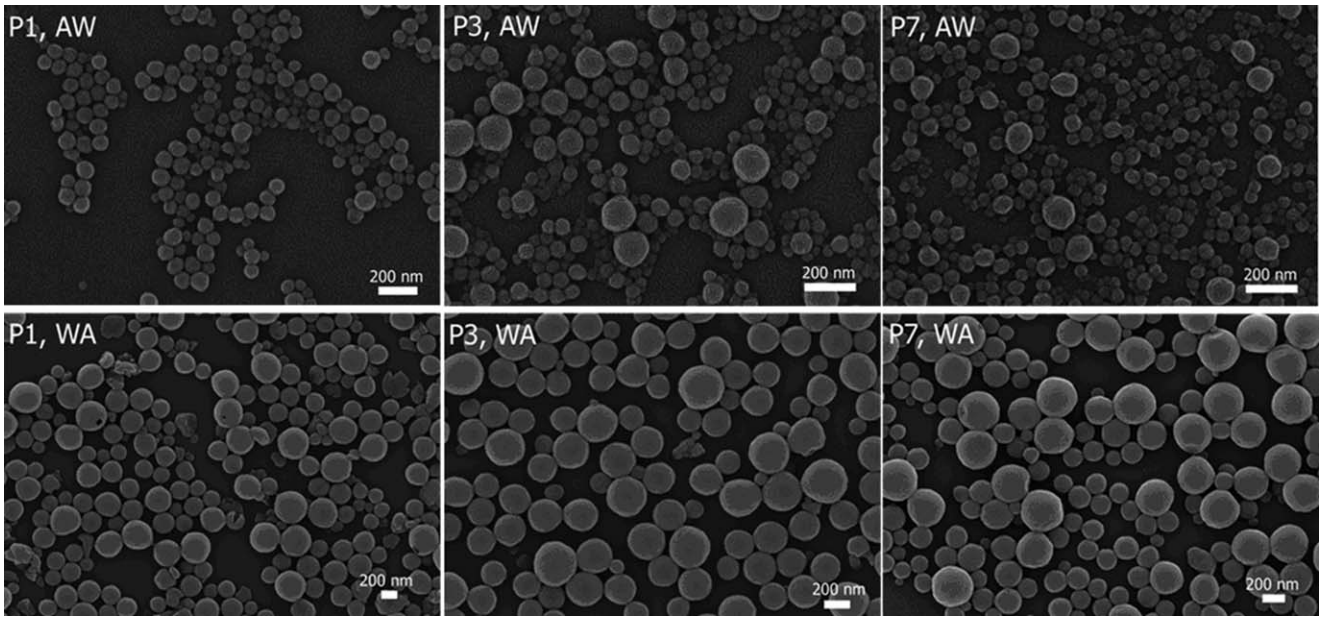

FIGURE 5 SEM images of nanoparticles that were prepared from **P1**, **P3,** and **P7** (1 mg mL^{-1}) by dropping acetone-polymer solution to water (AW) or dropping water to acetone-polymer solution (WA).

which result in strong intrachain electrostatic repulsion causing retardation of the protonation of the amino groups.[43] This would result in lower pKa values of gradient *t*BAEMA copolymers, although all used amino methacrylate monomers have similar pKa values[22–24] and prevent the nanoparticles from acquiring an appreciable cationic character at neutral pH values. Thus, favored van der Waals attraction results in particle aggregation. To support this assumption, instead of pure water an acetate buffer system with a pH value of 5 was used as nonsolvent for the nanoprecipitaion of **P3** and **P4** with an initial acetone-polymer concentration of 10 mg mL^{-1}. In this case, nanoparticles with monomodal size distributions and low PDI values could be obtained, presumably due to the electrostatic stabilization of the nanoparticles as a consequence of protonation of the closely spaced amino chains at acidic pH values. By dropping acetone-polymer solution to water (AW), small nanoparticles with comparable sizes (Z-average diameter between 110 and 184 nm) were obtained for both initial acetone-polymer concentrations ($c = 1$ mg mL^{-1}, $c = 10$ mg mL^{-1}, for **P3** and **P4** at pH 5). The acetone-polymer concentration did not affect the nanoparticle size significantly. However, by dropping water into acetone-polymer solution, relatively smaller nanoparticles (Z-average diameter between 254 and 473 nm) were formed at an initial acetone-polymer concentration of 1 mg mL^{-1} compared to 10 mg mL^{-1} (Z-average diameter between 339 and 720 nm) (Fig. 4). As intended, the zeta potential of all suspensions shows positive values in between +20 to +64 mV indicating a high colloidal stability. The long term stability of the nanoparticle suspensions was tested at room temperature for three weeks, showing no change in size and size distributions. SEM investigations revealed that all nanoparticles have spherical shapes (Fig. 5, Supporting Information Figs. S16–S18).

pH-Response Test of the Nanoparticles

The pH-responsive behavior behavior was tested by storing nanoparticle suspensions at various pH values. Dilute buffer systems were used to prevent salting out effects. The DLS measurements (**A**, Fig. 6) revealed that nanoparticles from **P1** at pH 7 to 8 were not stable and are significantly larger with higher PDI values compared to water suspensions. Undefined aggregates were also observed at pH 7 to 8. This can be explained by the low zeta potential of the nanoparticle suspensions (**B**, Fig. 6) at these pH values. At low zeta potential values, van der Waals attractions become stronger than electrostatic repulsions, which result in aggregation. In general, stable colloidal dispersions have zeta potentials beyond ±20 mV.[44] In agreement with this, **P1** nanoparticles are stable at pH values of 3.4, 4, 5, 6 and 9 with relatively high absolute zeta potentials. It should be noted that **P1** nanoparticles have negative zeta potentials at pH 9 as already reported for the p(DMAEMA) microgels above their isoelectric point.[45] Unlike **P1**, **P2** nanoparticles did not show any sign of instability at pH 7, only at pH values of 8 and 9 due to the higher DMAEMA content in **P2**, meaning a stronger cationic character. At pH values of 3.4 to 5, **P2** nanoparticles are protonated and dissolve as already reported for DMAEMA functional micelles at acidic conditions. The dissolution is also monitored by the significant decrease in the derived count rate obtained from DLS measurements that is directly proportional to the size and the number of the nanoparticles.[46] A subsequent increase of the pH value back to the initial pH value of 7.5 resulted in a significant increase in the derived count rate and a Z-average diameter slightly larger than the original nanoparticles (Z-average diameter = 180 nm, PDI = 0.38), which hints toward the reversible dissolution ability of the nanoparticles. Furthermore, the copolymer **P2** itself also revealed complete

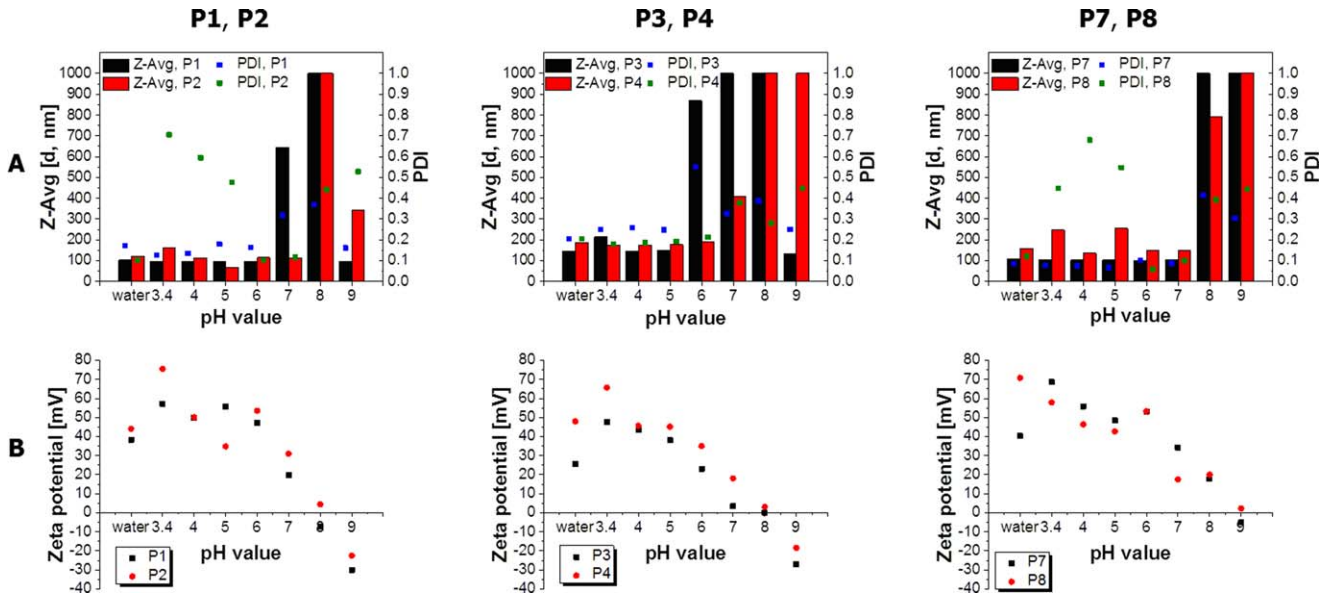

FIGURE 6 (A) Z-Average diameter (represented up to 1000 nm) and PDI values of nanoparticles as a function of the pH value. **(B)** Zeta potentials of the nanoparticles as a function of the pH value. [Color figure can be viewed in the online issue, which is available at wileyonlinelibrary.com.]

dissolution in aqueous media (0.3 mg/mL) at a pH value of 3.4. A dynamic increase of the pH value to the pH value of 7.5 resulted in spontaneous nanoparticle formation; DLS measurements ensured the nanoparticle formation (Z-average diameter = 124 nm, PDI = 0.34). In contrast, copolymer **P1** did not show any solubility in acidic aqueous media. Similar results were also obtained with nanoparticles prepared from Eudragit E100 as a reference pH-responsive material (Supporting Information Fig. S19).[27]

Due to the tightly spaced *t*BAEMA moieties that prevent protonation at neutral pH values, nanoparticles of **P3** and **P4** demonstrated less stability around neutral pH values compared to the DMAEMA functional nanoparticles. As shown in Figure 6, **P3** nanoparticles aggregate between pH 6 to 8 and **P4** nanoparticles aggregate between pH 7 to 9 as a consequence of the low zeta potential values. At acidic pH values, **P3** and **P4** nanoparticles were both stable due to the protonation of the *t*BAEMA. It should be noted that there was no nanoparticle dissociation observed even for **P4** that contains 21% *t*BAEMA.

Nanoparticles derived from the AEMA copolymers (**P7** and **P8**) revealed a higher stability compared to the DMAEMA and *t*BAEMA based nanoparticles around neutral pH values. Compared to the DMAEMA and *t*BAEMA nanoparticles, higher isoelectric points of the AEMA nanoparticles at a pH value around 9, as estimated from Figure 6(B), also support the higher stability of the AEMA based nanoparticles around neutral pH values. This can be explained by the primary amino structure of the AEMA that renders nanoparticles to protonate easily under neutral conditions. As shown in Figure 6, **P7** and **P8** nanoparticles are stable at pH values of 6 and 7 with relatively high zeta potential values. However, they tend to aggregate at pH values of 8 and 9 as a consequence of the low zeta potential values. Although **P7** nanoparticles are stable at pH values of 3.4, 4, and 5, **P8** nanoparticles with larger amino content were protonated and dissolved at these pH values.

Fluorescence Spectroscopic Study of the Nanoparticles

Pyrene as hydrophobic fluorescent probe was encapsulated as a model drug in **P2** and **P8** nanoparticles due to their dissolution ability at acidic pH values. The fluorescence emission spectra of pyrene against **P2** nanoparticles at various pH values are shown in Figure 7. Pyrene in pure water is

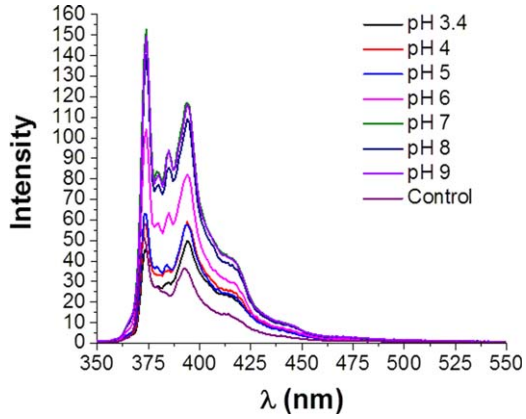

FIGURE 7 Fluorescence emission spectra of pyrene (6×10^{-5} mol L^{-1}) against **P2** nanoparticles (0.15 mg mL^{-1}) at various pH values. Pyrene in pure water was used as control. [Color figure can be viewed in the online issue, which is available at wileyonlinelibrary.com.]

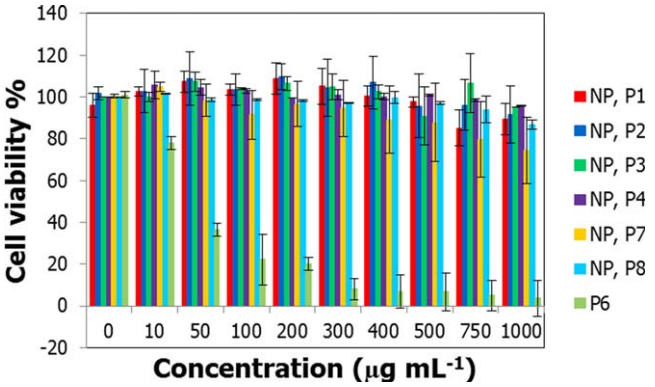

FIGURE 8 Cytotoxicity test of nanoparticles (NPs) that were prepared from **P1**, **P2**, **P3**, **P4**, **P7**, **P8** and water soluble polymer **P6** in L929 cells. The relative viability is expressed as percentage to control cells not treated with nanoparticles. Untreated cells on the same well plate were used as positive controls. Data represent means ± SD, $n \geq 6$. [Color figure can be viewed in the online issue, which is available at wileyonlinelibrary.com.]

used as control. The total intensities of the emission spectra of the nanoparticle suspensions at pH values from 7 to 9 are significantly higher compared to the emission intensity of the control. This indicates that pyrene is transferred into the hydrophobic domains of the nanoparticles and/or aggregates. However, at pH values of 3.4 to 5, the emission intensity of the pyrene is similar to the intensity of the control, which clearly reveals the dissolution of **P2** nanoparticles at these pH values. **P8** nanoparticles showed similar results (Supporting Information Fig. S20). However, compared to the same concentration of **P2** nanoparticles they have lower pyrene fluorescence intensities at pH values 7 to 9. This can be due to the lower hydrophobicity of the **P8** nanoparticles compared to the **P2** nanoparticles, meaning that **P2** might show in general higher encapsulation efficiencies for hydrophobic drugs.

Cytotoxicity of the Nanoparticles in L929 Cells

To evaluate the cytotoxicity of the nanoparticles, one nanoparticle sample of each copolymer prepared from 1 mg mL^{-1} AW technique and water soluble polymer **P6** was investigated at the indicated concentrations (Fig. 8). The cytotoxicity assay results showed that the nanoparticles did not have any significant cytotoxic effect on L929 cells after 24 h incubation at up to 1 mg mL^{-1}. These results are promising in comparison to the previous reports because cationic nanoparticles have frequently been associated with toxic effects in cell studies.[47,48] It should be noted that nanoparticles based on PMMA are known as nontoxic, whereas homopolymers based on PDMAEMA and PAEMA are known to be toxic.[49] **P6** showed a severe toxic effect on the cells, which is due to the primary amino functional AEMA moieties in the copolymer. However, nanoparticles, which are derived from **P8** (the deprotonated form of **P6**), are nontoxic. This might be due to the change of the cationic charge of the polymer. **P8** contains pH-responsive primary amines that are not fully protonated at the pH values applied. This leads to a decreased water solubility enabling nanoparticle formation. Due to the fact that the cationic charges are mainly responsible for cytotoxicity, the reduced charge content possibly also results in less destructive effects on the cell membrane.[50] Moreover, it was already demonstrated that cationic polyplexes with a comparable size to the nanoparticles show less cytotoxic effects in contrast to the free cationic polymer chains.[51] The cytotoxicity of single cationic polymer chains is based on the disruption of the lipid double layer by the formation of nanoscale pores or membrane thinning (2 to 5 nm).[52] Thus, the reduced cytotoxicity of the nanoparticle can be attributed to the combination of reduced cationic charge and less disruptive cell membrane interaction.

CONCLUSIONS

A library of well-defined copolymers of MMA with DMAEMA, *t*BAEMA and AEMA·HCl was synthesized via RAFT polymerization by varying the initial monomer feed ratios to alter the amino content in the copolymers and in the corresponding nanoparticle. The controlled nature of the polymerizations was certified by kinetic studies. By variation of the initial formulation conditions during the nanoprecipitation method, such as polymer concentration and dropping method, well-defined nanoparticles from the synthesized copolymers with varying sizes were successfully prepared. Moreover, pH-stability tests demonstrated that, depending on the structure and amount of the amino functionality in the copolymers, the corresponding nanoparticles reveal a pH response. Fluorescence spectroscopic studies of pyrene as model drug revealed the dissolution of two nanoparticle batches at acidic pH values. Moreover, none of these nanoparticles exhibited any cytotoxic effect on L929 cells.

The results encourage the use of these polymeric nanoparticles as novel carriers for the controlled release of loaded pharmaceutical agents in acidic environment, for example, cancer cells or endosomal cellular compartments. To optimize the release profile, the polymeric composition can be varied. Future investigations will deal with the controlled release of active payloads such as anticancer drugs but also with the delivery and release of genetic material, where the cationic moieties might favor the encapsulation efficiency and the burst release from endosome.

ACKNOWLEDGMENTS

We acknowledge funding from the Carl-Zeiss Foundation (JCSM Strukturantrag and fellowship for C.W.) and the Thüringer Ministerium für Wirtschaft, Wissenschaft, und Digitale Gesellschaft (TMWWDG, ProExzellenz II, NanoConSens). We also express our gratitude to Steffi Stumpf for help in the SEM investigations, Carolin Fritzsche for cell studies, and Dr. Michael Wagner, Dr. Antje Vollrath and Dr. Christian Pietsch for helpful discussion.

REFERENCES AND NOTES

1 R. Cheng, F. Meng, C. Deng, H.-A. Klok, Z. Zhong, *Biomaterials* **2013**, *34*, 3647–3657.

2 Y. Li, W. Xiao, K. Xiao, L. Berti, J. Luo, H. P. Tseng, G. Fung, K. S. Lam, *Angew. Chem. Int. Ed.* **2012**, *51*, 2864–2869.

3 M. Motornov, Y. Roiter, I. Tokarev, S. Minko, *Prog. Polym. Sci.* **2010**, *35*, 174–211.

4 B. Jeong, Y. H. Bae, S. W. Kim, *J. Control. Release* **2000**, *63*, 155–163.

5 B. Yan, J.-C. Boyer, D. Habault, N. R. Branda, Y. Zhao, *J. Am. Chem. Soc.* **2012**, *134*, 16558–16561.

6 J. Wang, X. Sun, W. Mao, W. Sun, J. Tang, M. Sui, Y. Shen, Z. Gu, *Adv. Mater.* **2013**, *25*, 3670–3676.

7 S.-F. Lee, X.-M. Zhu, Y.-X. J. Wang, S.-H. Xuan, Q. You, W.-H. Chan, C.-H. Wong, F. Wang, J. C. Yu, C. H. K. Cheng, K. C.-F. Leung, *ACS Appl. Mater. Interfaces* **2013**, *5*, 1566–1574.

8 R. Liu, D. Li, B. He, X. Xu, M. Sheng, Y. Lai, G. Wang, Z. Gu, *J. Control. Release* **2011**, *152*, 49–56.

9 N. E. Sounni, A. Noel, *Clin. Chem.* **2013**, *59*, 85–93.

10 Y. Lee, S. Fukushima, Y. Bae, S. Hiki, T. Ishii, K. Kataoka, *J. Am. Chem. Soc.* **2007**, *129*, 5362–5363.

11 E. S. Lee, K. Na, Y. H. Bae, *Nano Lett.* **2005**, *5*, 325–329.

12 S. Ganta, H. Devalapally, A. Shahiwala, M. Amiji, *J. Control. Release* **2008**, *126*, 187–204.

13 C. Clawson, L. Ton, S. Aryal, V. Fu, S. Esener, L. Zhang, *Langmuir* **2011**, *27*, 10556–10561.

14 Y. Bae, S. Fukushima, A. Harada, K. Kataoka, *Angew. Chem. Int. Ed.* **2003**, *42*, 4640–4643.

15 E. R. Gillies, J. M. J. Fréchet, *Bioconjugate Chem.* **2005**, *16*, 361–368.

16 J. Ko, K. Park, Y.-S. Kim, M. S. Kim, J. K. Han, K. Kim, R.-W. Park, I.-S. Kim, H. K. Song, D. S. Lee, I. C. Kwon, *J. Control. Release* **2007**, *123*, 109–115.

17 G.-H. Hsiue, C.-H. Wang, C.-L. Lo, C.-H. Wang, J.-P. Li, J.-L. Yang, *Int. J. Pharm.* **2006**, *317*, 69–75.

18 C. E. Mora-Huertas, H. Fessi, A. Elaissari, *Int. J. Pharm.* **2010**, *385*, 113–142.

19 A. W. Jackson, D. A. Fulton, *Polym. Chem.* **2013**, *4*, 31.

20 A. Honglawan, H. Ni, D. Weissman, S. Yang, *Polym. Chem.* **2013**, *4*, 3667.

21 G. Moad, E. Rizzardo, S. H. Thang, *Polymer* **2008**, *49*, 1079–1131.

22 S.-i. Yamamoto, J. Pietrasik, K. Matyjaszewski, *Macromolecules* **2008**, *41*, 7013–7020.

23 A. J. Morse, D. Dupin, K. L. Thompson, S. P. Armes, K. Ouzineb, P. Mills, R. Swart, *Langmuir* **2012**, *28*, 11733–11744.

24 L. He, E. S. Read, S. P. Armes, D. J. Adams, *Macromolecules* **2007**, *40*, 4429–4438.

25 H. Fessi, F. Puisieux, J. P. Devissaguet, N. Ammoury, S. Benita, *Int. J. Pharm.* **1989**, *55*, R1–R4.

26 S. Schubert, J. J. T. Delaney, U. S. Schubert, *Soft Matter* **2011**, *7*, 1581–1588.

27 D. Kohane, D. Anderson, C. Yu, R. Langer, *Pharm. Res.* **2003**, *20*, 1533–1538.

28 A. H. Alidedeoglu, A. W. York, C. L. McCormick, S. E. Morgan, *J. Polym. Sci., Part A: Polym. Chem.* **2009**, *47*, 5405–5415.

29 I. Kurtulus, G. Yilmaz, M. Ucuncu, M. Emrullahoglu, C. R. Becer, V. Bulmus, *Polym. Chem.* **2014**, *5*, 1593.

30 G. Moad, J. Chiefari, Y. K. Chong, J. Krstina, R. T. A. Mayadunne, A. Postma, E. Rizzardo, S. H. Thang, *Polym. Int.* **2000**, *49*, 993–1001.

31 J. M. Layman, S. M. Ramirez, M. D. Green, T. E. Long, *Biomacromolecules* **2009**, *10*, 1244–1252.

32 M. W. M. Fijten, R. M. Paulus, U. S. Schubert, *J. Polym. Sci., Part A: Polym. Chem.* **2005**, *43*, 3831–3839.

33 J. B. McLeary, J. M. McKenzie, M. P. Tonge, R. D. Sanderson, B. Klumperman, *Chem. Commun.* **2004**, 1950–1951.

34 J. Bigot, B. Charleux, G. Cooke, F. Delattre, D. Fournier, J. Lyskawa, F. Stoffelbach, P. Woisel, *Macromolecules* **2009**, *43*, 82–90.

35 A. J. D. Magenau, N. Martinez-Castro, D. A. Savin, R. F. Storey, *Macromolecules* **2009**, *42*, 8044–8051.

36 W. Zhang, L. Liu, X. Zhuang, X. Li, J. Bai, Y. Chen, *J. Polym. Sci. Part A: Polym. Chem.* **2008**, *46*, 7049–7061.

37 S. G. Roy, K. Bauri, S. Pal, A. Goswami, G. Madras, P. De, *Polym. Int.* **2013**, *62*, 463–473.

38 P. Cotanda, D. B. Wright, M. Tyler, R. K. O'Reilly, *J. Polym. Sci., Part A: Polym. Chem.* **2013**, *51*, 3333–3338.

39 S.H. Hong, V.M. McHung, Review of preparation and properties of polymers from copolymerization of aprotic acrylic monomers with protic acrylic monomers. Technical Report. Chemical Research, Development and Engineering Center, Aberdeen Proving Ground, MD. Available at: http://www.dtic.mil/cgibin/GetTRDoc?Location=U2&doc=GetTRDoc.pdf&AD=ADA197467; 1988, accessed on September 1, **2014**.

40 K. Matyjaszewski, M. J. Ziegler, S. V. Arehart, D. Greszta, T. Pakula, *J. Phys. Org. Chem.* **2000**, *13*, 775–786.

41 Y. K. Chong, T. P. T. Le, G. Moad, E. Rizzardo, S. H. Thang, *Macromolecules* **1999**, *32*, 2071–2074.

42 A. Vollrath, D. Pretzel, C. Pietsch, I. Perevyazko, S. Schubert, G. M. Pavlov, U. S. Schubert, *Macromol. Rapid. Commun.* **2012**, *33*, 1791–1797.

43 H. Lee, S. H. Son, R. Sharma, Y.-Y. Won, *J. Phys. Chem. B* **2011**, *115*, 844–860.

44 A. Shalviri, H. K. Chan, G. Raval, M. J. Abdekhodaie, Q. Liu, H. Heerklotz, X. Y. Wu, *Colloids Surf. B* **2013**, *101*, 405–413.

45 L. Hu, L.-Y. Chu, M. Yang, H.-D. Wang, C. Hui Niu, *J. Colloid Interface Sci.* **2007**, *311*, 110–117.

46 S. J. Wallace, J. Li, R. L. Nation, B. J. Boyd, *Drug Deliv. Transl. Res.* **2012**, *2*, 284–292.

47 H. Zhang, T. Xia, H. Meng, M. Xue, S. George, Z. Ji, X. Wang, R. Liu, M. Wang, B. France, R. Rallo, R. Damoiseaux, Y. Cohen, K. A. Bradley, J. I. Zink, A. E. Nel, *ACS Nano* **2011**, *5*, 2756–2769.

48 P. H. M. Hoet, L. Gilissen, B. Nemery, *Toxicol. Appl. Pharm.* **2001**, *175*, 184–190.

49 C. He, J. Liu, X. Ye, L. Xie, Q. Zhang, X. Ren, G. Zhang, C. Wu, *Langmuir* **2008**, *24*, 10717–10722.

50 N. M. Schaeublin, L. K. Braydich-Stolle, A. M. Schrand, J. M. Miller, J. Hutchison, J. J. Schlager, S. M. Hussain, *Nanoscale* **2011**, *3*, 410–420.

51 Y. Yue, F. Jin, R. Deng, J. Cai, Y. Chen, M. C. M. Lin, H.-F. Kung, C. Wu, *J. Control. Release* **2011**, *155*, 67–76.

52 S. Hong, P. R. Leroueil, E. K. Janus, J. L. Peters, M.-M. Kober, M. T. Islam, B. G. Orr, J. R. Baker, M. M. Banaszak Holl, *Bioconjug. Chem.* **2006**, *17*, 728–734.

Supporting Information

RAFT made methacrylate copolymers for reversible pH-responsive nanoparticles

Turgay Yildirim,[a,b] Alexandra C. Rinkenauer,[a,b] Christine Weber,[a,b] Anja Traeger,[a,b] Stephanie Schubert,[b,c] Ulrich S. Schubert[a,b]*

[a]Laboratory of Organic and Macromolecular Chemistry (IOMC), Friedrich Schiller University Jena, Humboldtstr. 10, 07743 Jena, Germany

[b]Jena Center for Soft Matter (JCSM), Friedrich Schiller University Jena, Philosophenweg 7, 07743 Jena, Germany

[c]Institute of Pharmacy, Department of Pharmaceutical Technology, Friedrich Schiller University Jena, Otto-Schott-Str. 41, 07745 Jena, Germany

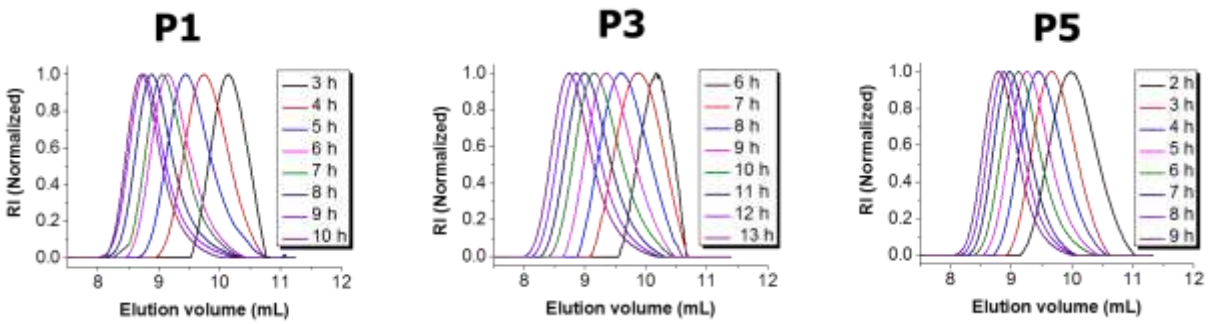

Figure SI-1 Overlay of the SEC traces ($CHCl_3$) from kinetic studies of the RAFT copolymerization of MMA with 10% comonomer: DMAEMA (**P1**), *t*BAEMA (**P3**) and AEMA·HCl (**P5**). [M]/[CPADB]/[AIBN] = 100/1/0.25; $[M]_0$ = 2 mol L^{-1}. Polymerization conditions for (**P1** and **P3**): Solvent ethanol, T = 70 °C. Polymerization conditions for **P5**: Solvent methanol under reflux.

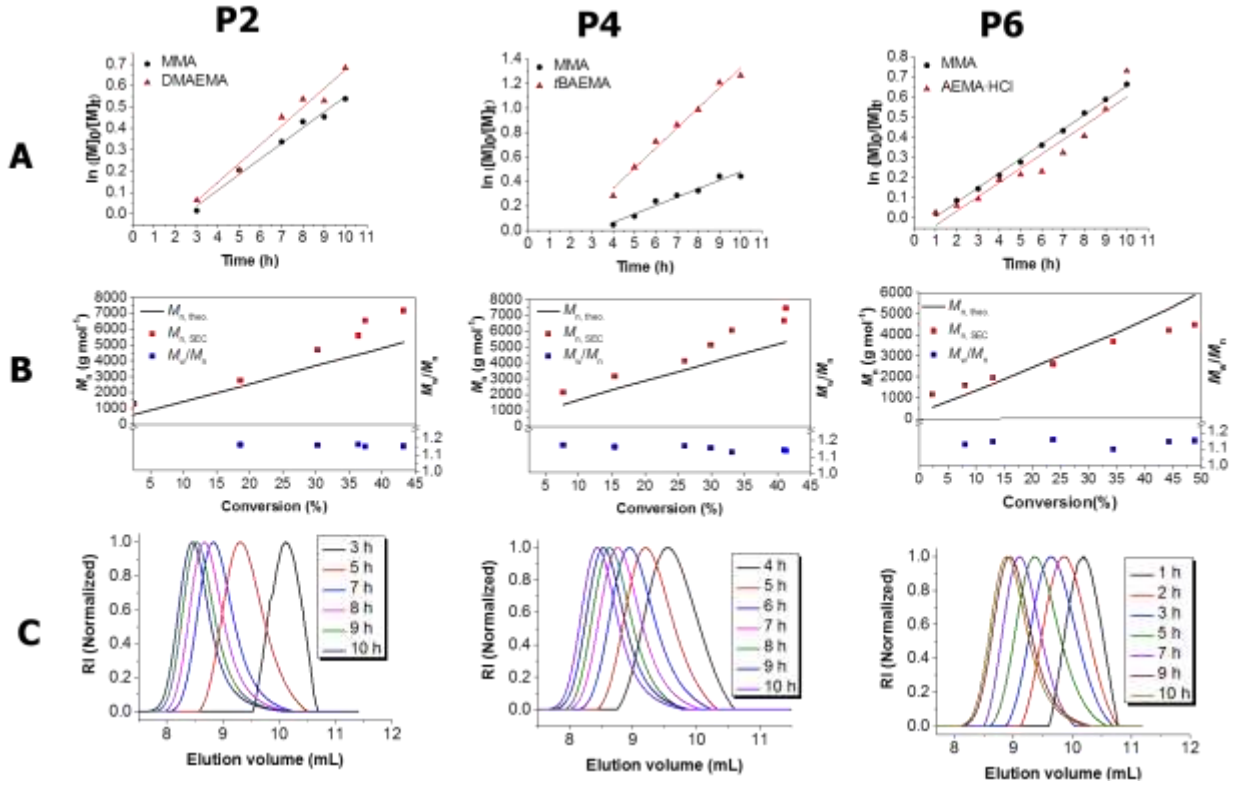

Figure SI-2 Kinetic studies of the RAFT copolymerization of MMA with 20 mol% comonomer DMAEMA (P2), *t*BAEMA (P4) and AEMA·HCl (P6). [M]/[CPADB]/[AIBN] = 100/1/0.25; $[M]_0$ = 2 mol L^{-1}. Polymerization conditions for (P2 and P4): Solvent ethanol, T = 70 °C. Polymerization conditions for P6: Solvent methanol under reflux. (A) Semilogarithmic kinetic plots. (B) M_n and M_w/M_n evolution with total monomer conversion. (C) SEC overlay traces ($CHCl_3$).

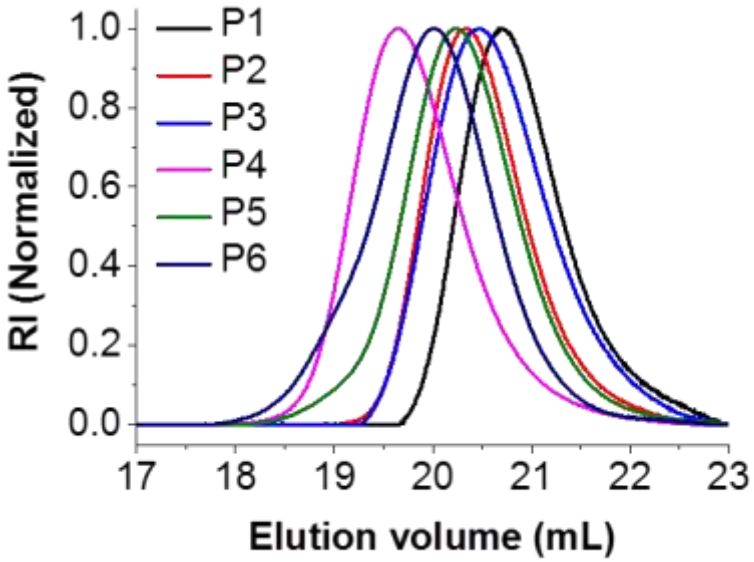

Figure SI-3 Normalized SEC traces (DMAc, RI detection) of the isolated copolymers of **P1**-**P6**.

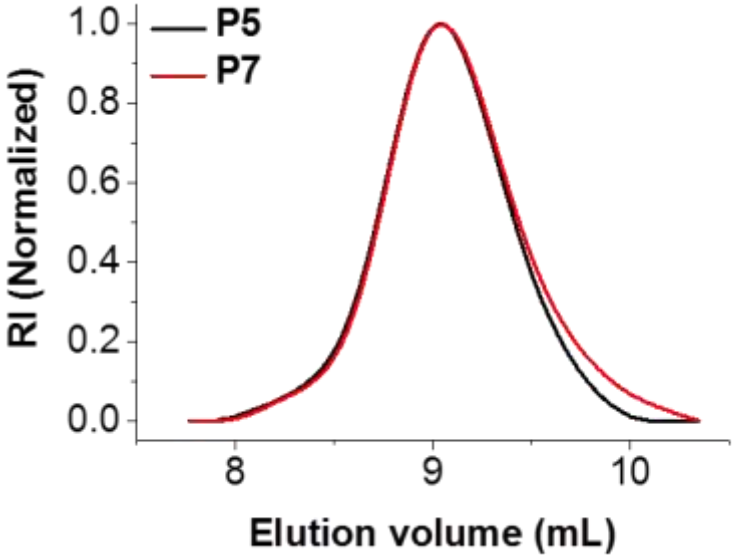

Figure SI-4 Normalized SEC traces ($CHCl_3$, RI detection) of the isolated copolymers **P5** and **P7**.

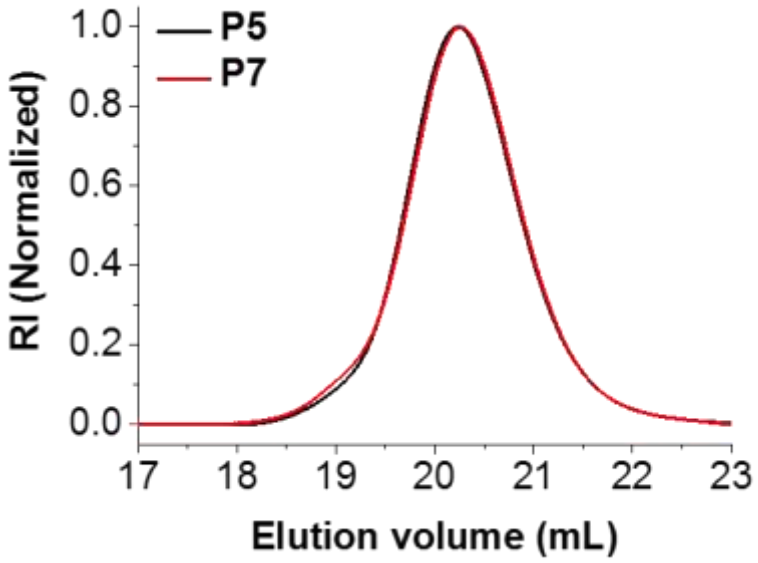

Figure SI-5 Normalized SEC traces (DMAc, RI detection) of isolated copolymers **P5** and **P7**.

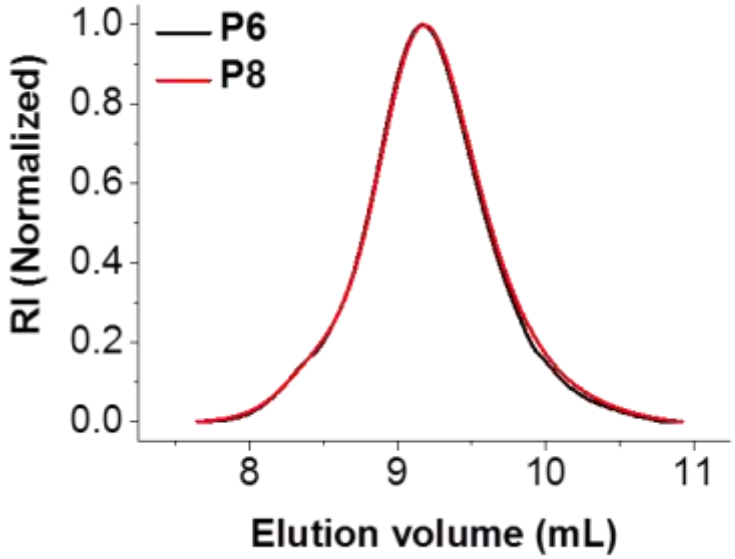

Figure SI-6 Normalized SEC traces ($CHCl_3$, RI detection) of isolated copolymers **P6** and **P8**.

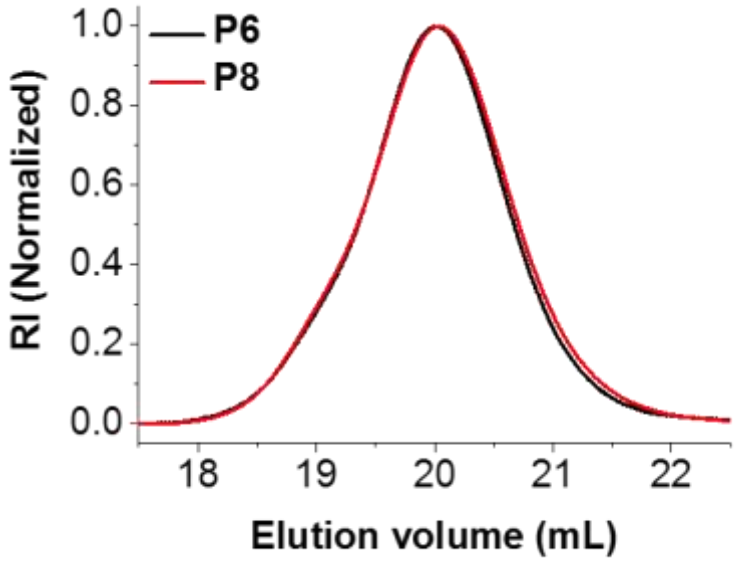

Figure SI-7 Normalized SEC traces (DMAc, RI detection) of isolated copolymers **P6** and **P8**.

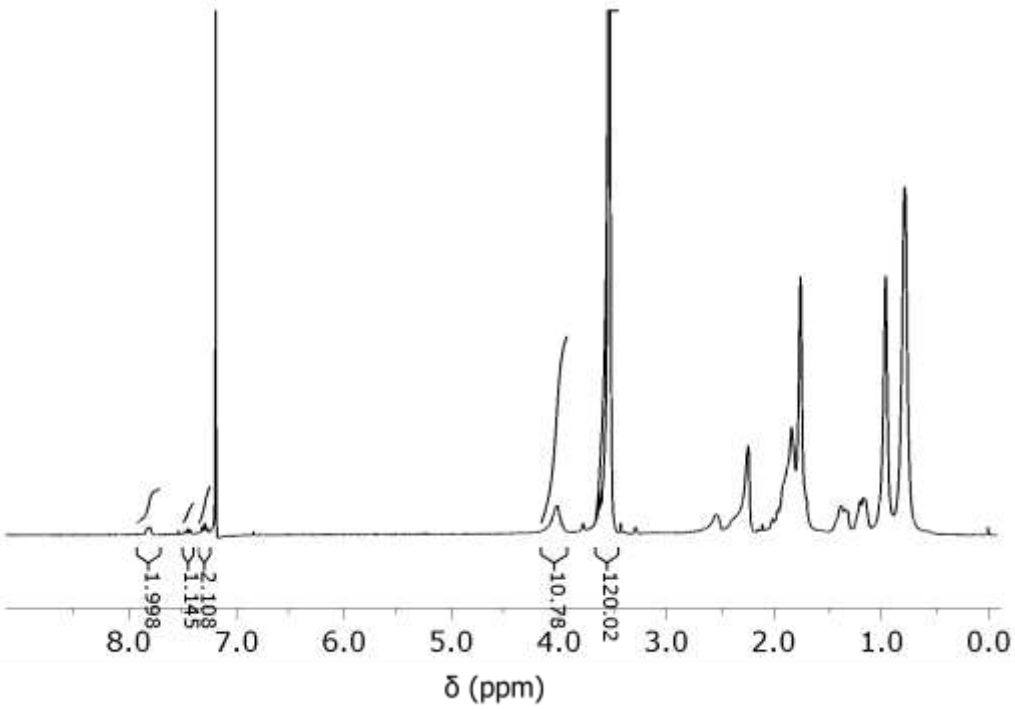

Figure SI-8 ^{1}H NMR spectrum (300 MHz, $CDCl_3$) of **P1**.

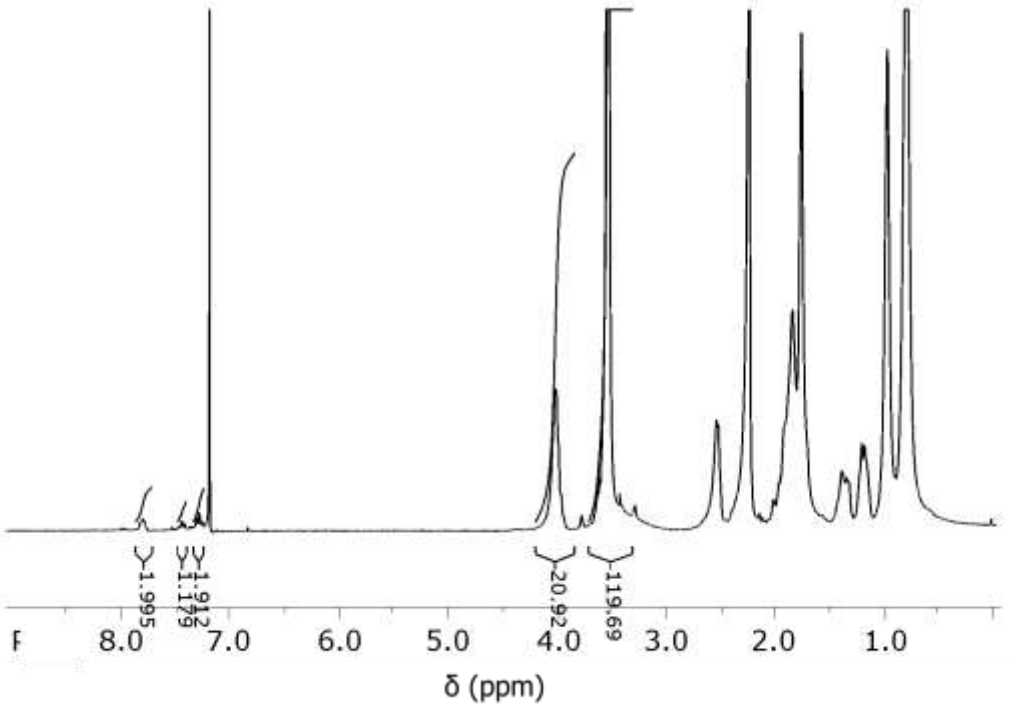

Figure SI-9 ^{1}H NMR spectrum (300 MHz, $CDCl_3$) of **P2**.

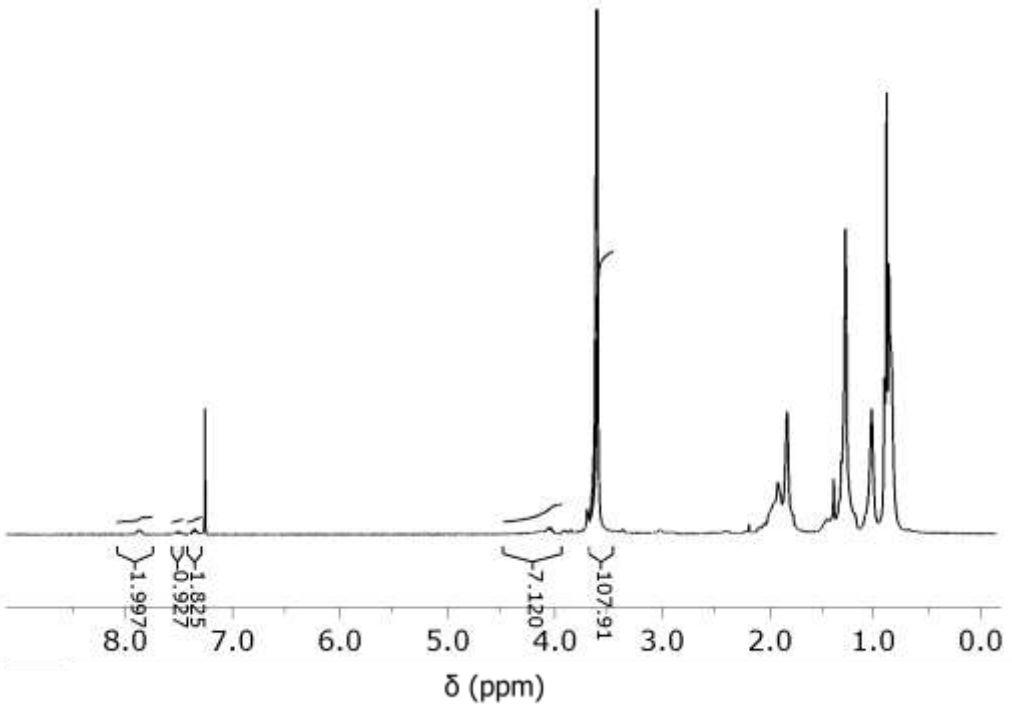

Figure SI-10 ^{1}H NMR spectrum (300 MHz, $CDCl_3$) of **P3**.

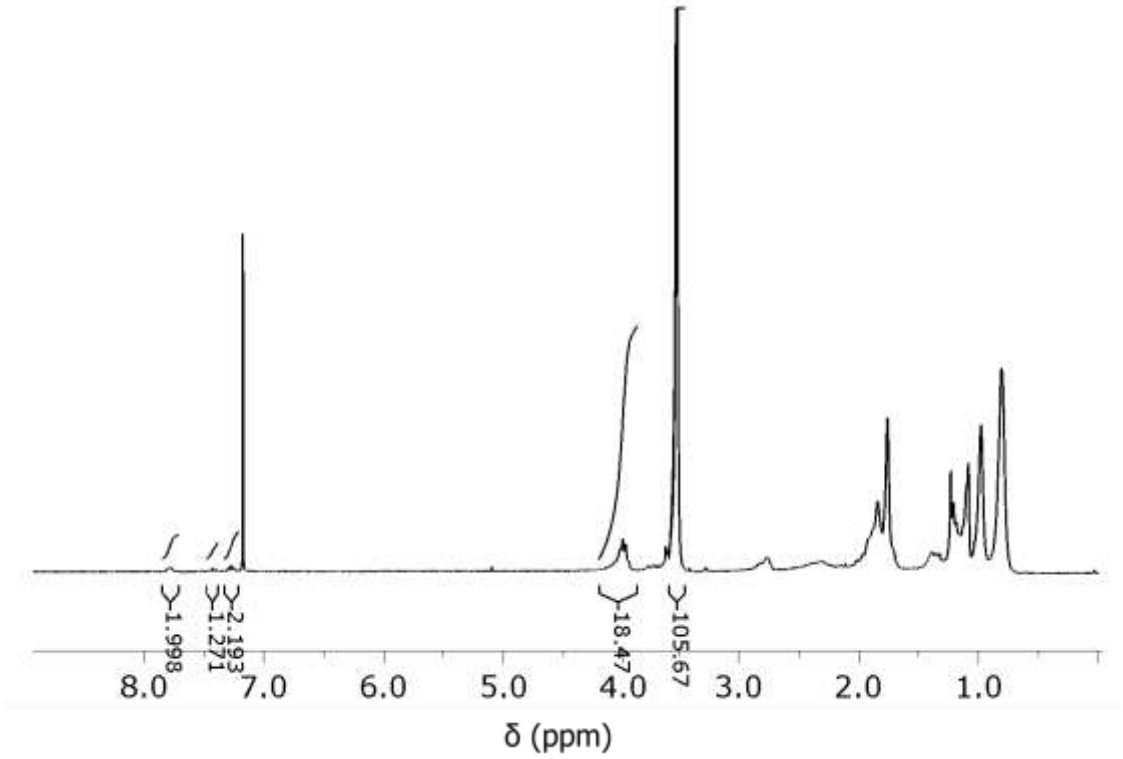

Figure SI-11 ^{1}H NMR spectrum (300 MHz, $CDCl_3$) of **P4**.

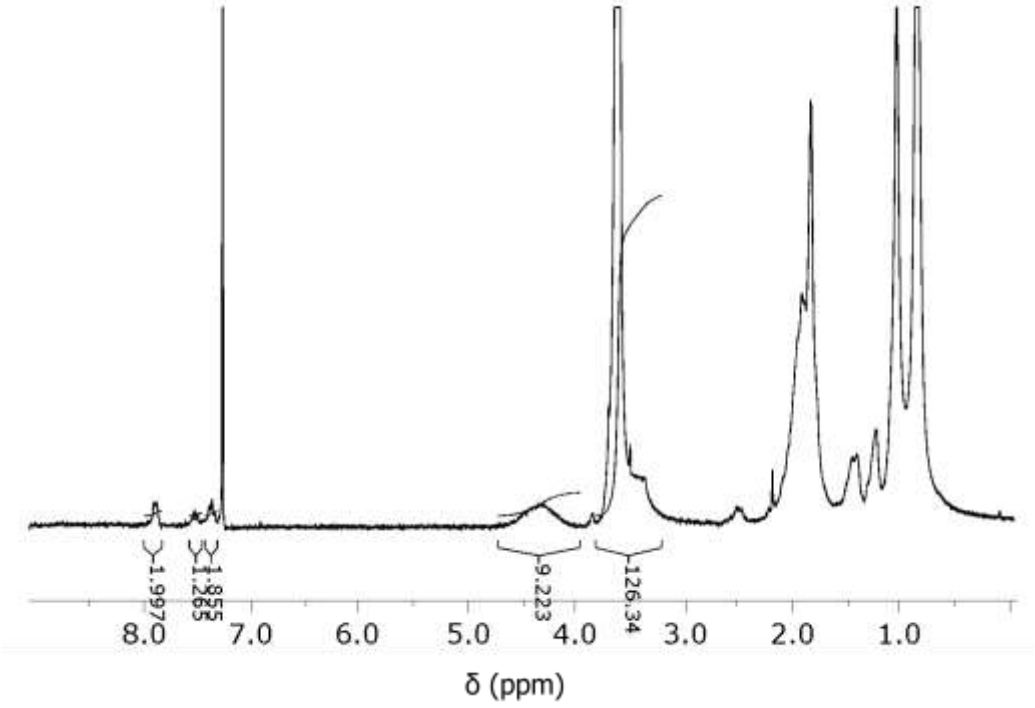

Figure SI-12 ^{1}H NMR spectrum (300 MHz, $CDCl_3$) of **P5**.

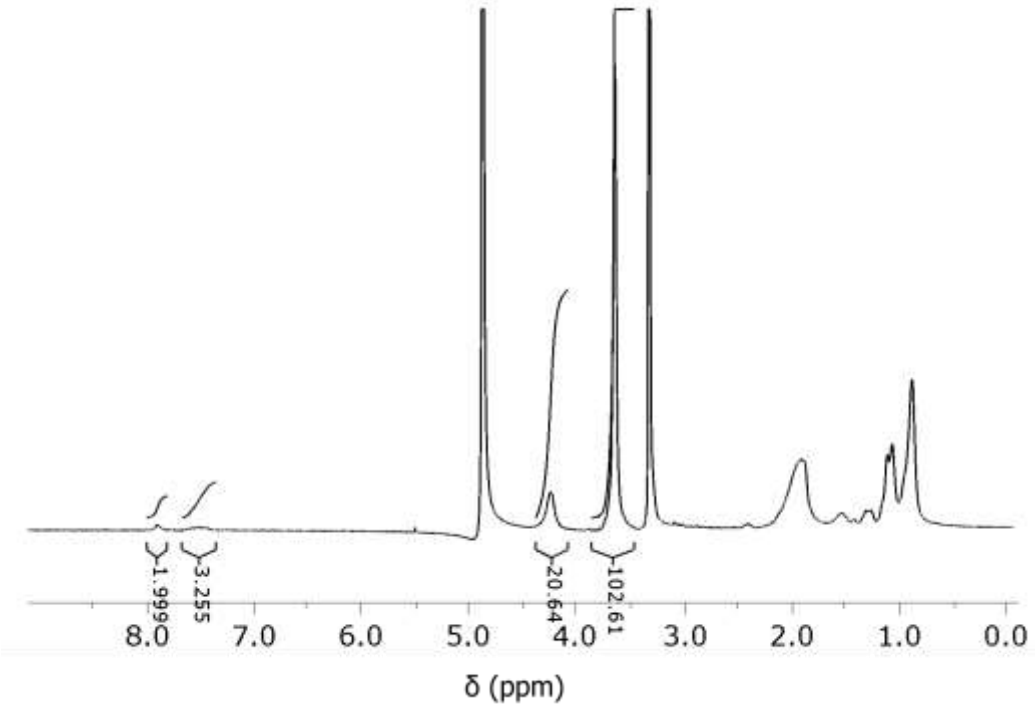

Figure SI-13 ^{1}H NMR spectrum (300 MHz, MeOD) of **P6**.

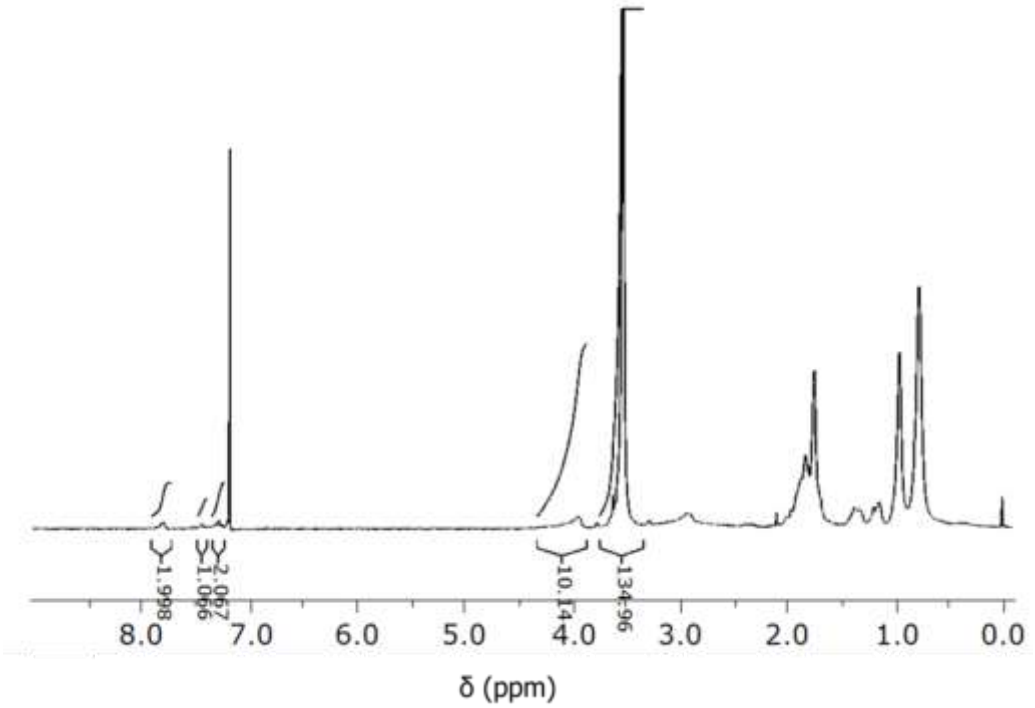

Figure SI-14 ^{1}H NMR spectrum (300 MHz, $CDCl_3$) of **P7**.

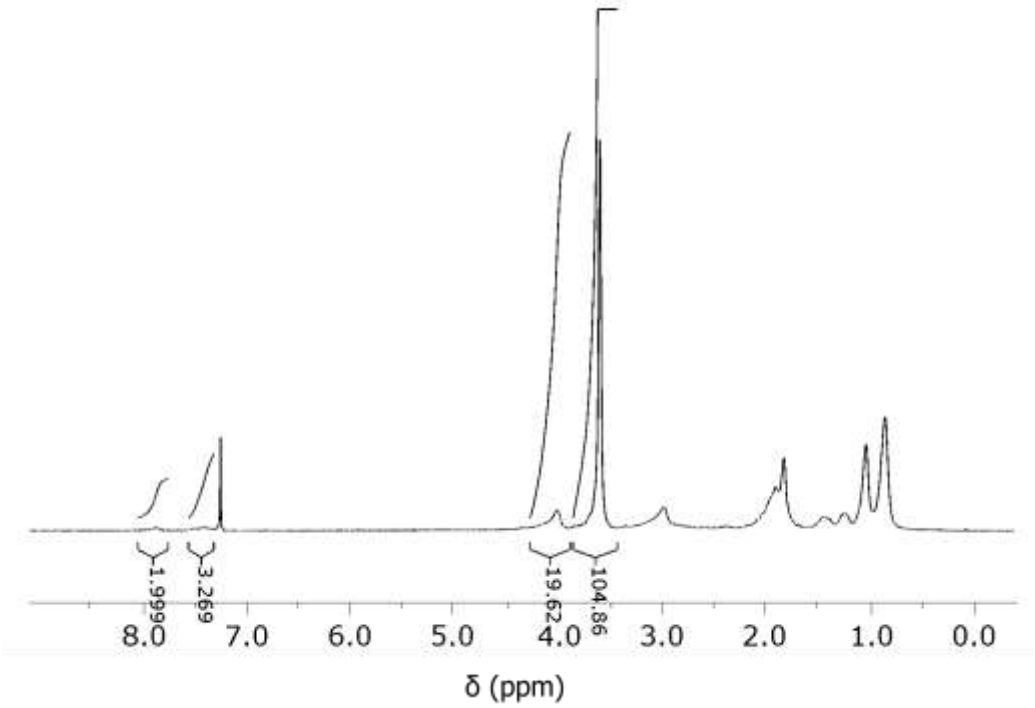

Figure SI-15 ^{1}H NMR spectrum (300 MHz, $CDCl_3$) of **P8**.

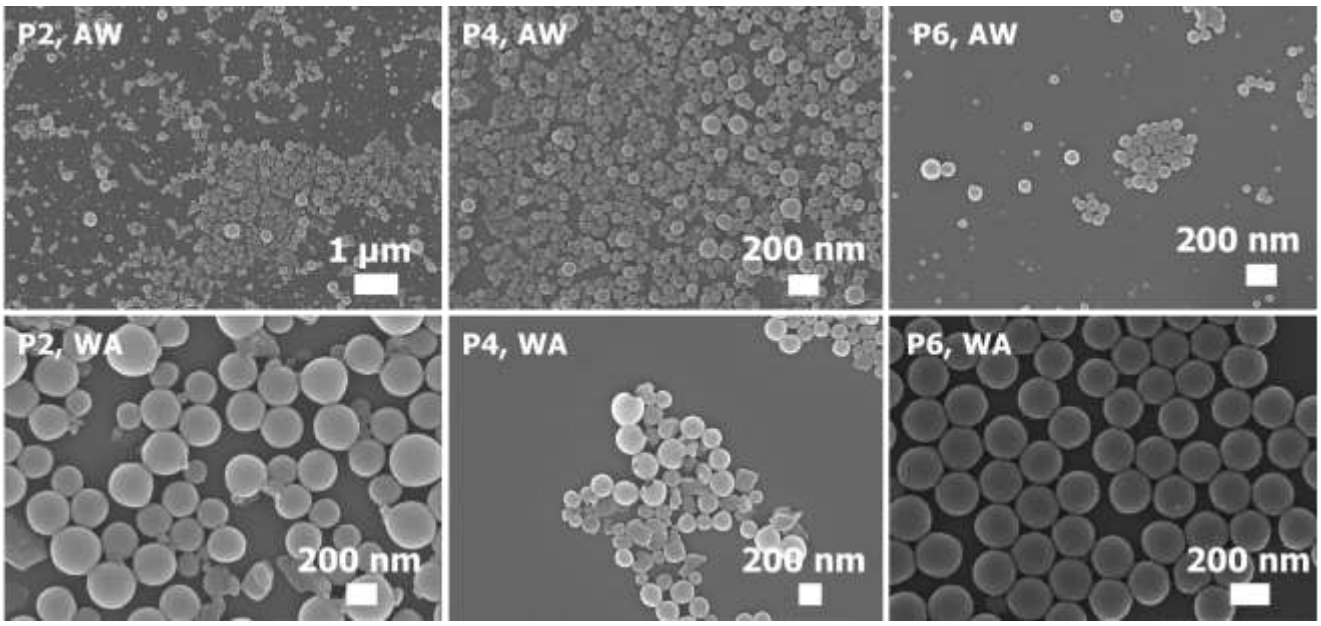

Figure SI-16 SEM images of nanoparticles that were prepared from **P2**, **P4** and **P8** (1 mg mL^{-1}) by dropping acetone-polymer solution to water (AW) or dropping water to acetone-polymer solution (WA).

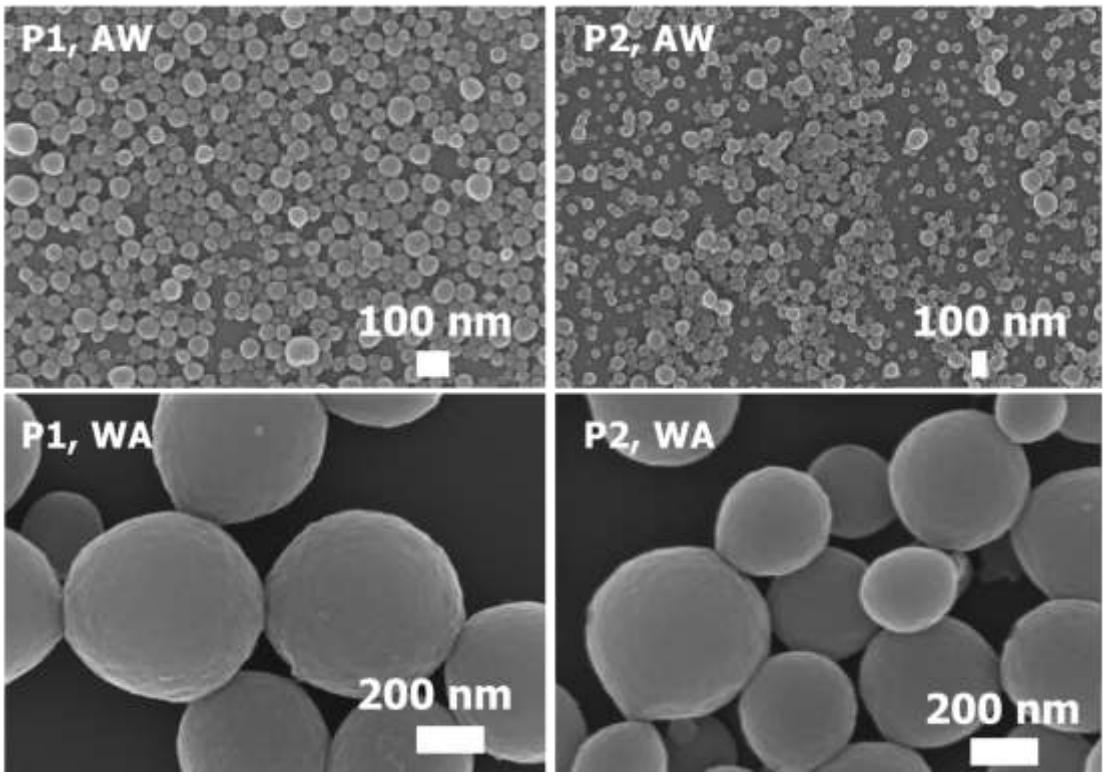

Figure SI-17 SEM images of nanoparticles that were prepared from **P1** and **P2** (10 mg mL^{-1}) by dropping acetone-polymer solution to water (AW) or dropping water to acetone-polymer solution (WA).

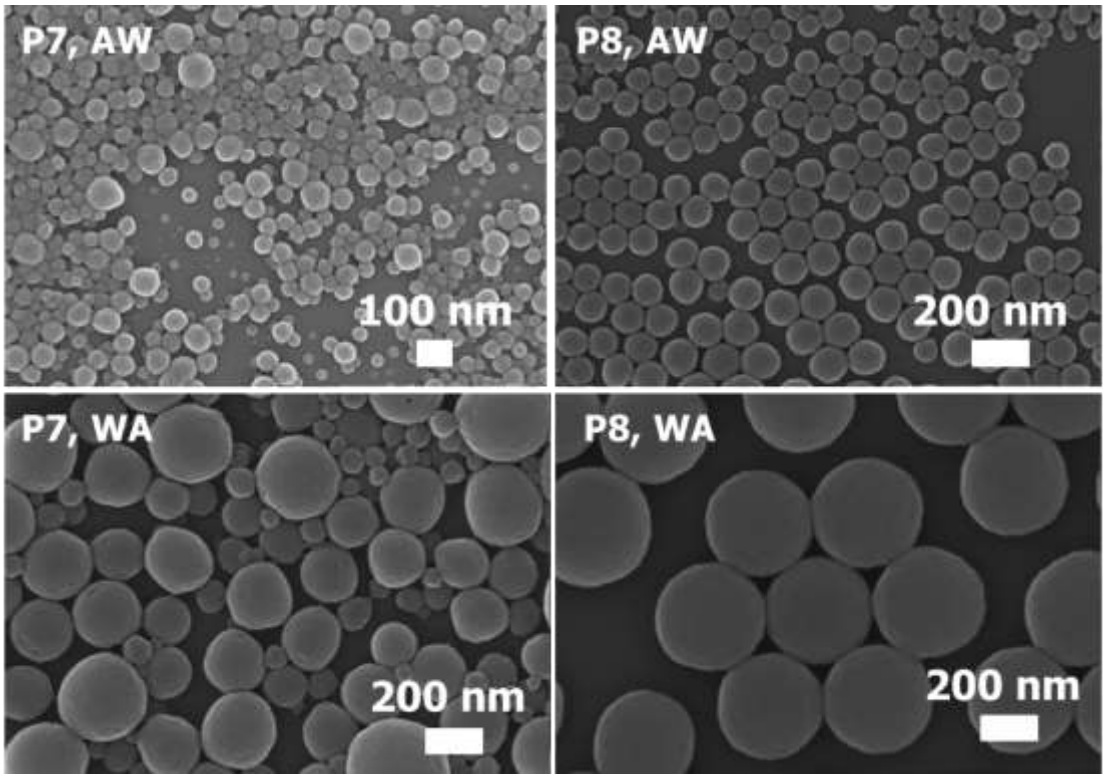

Figure SI-18 SEM images of nanoparticles that were prepared from **P7** and **P8** (10 mg mL^{-1}) by dropping acetone-polymer solution to water (AW) or dropping water to acetone-polymer solution (WA).

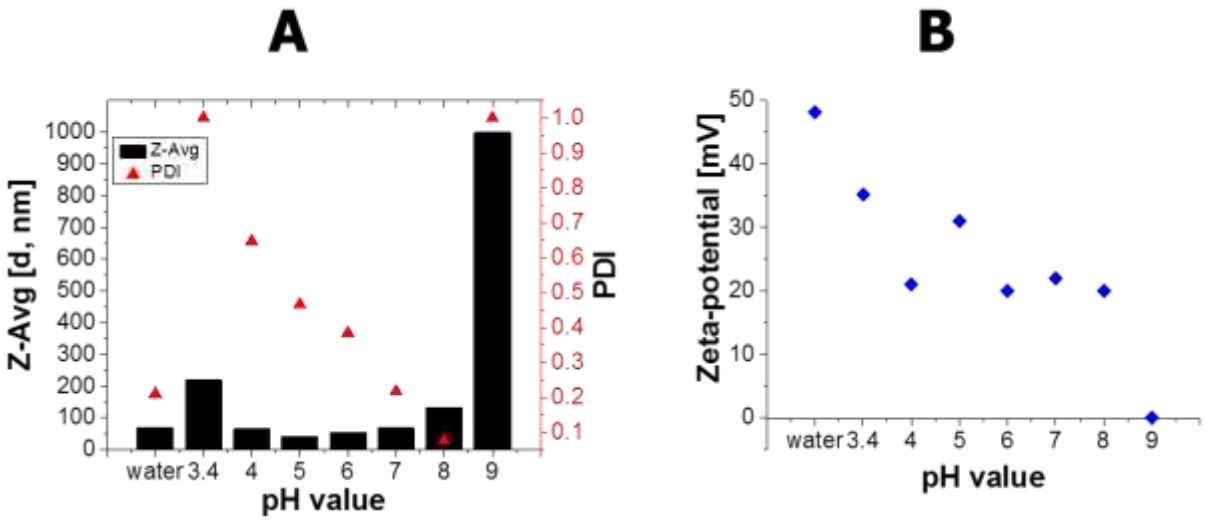

Figure SI-19 (A) Z-Average diameter (represented up to 1000 nm) and PDI values of Eudragit E100 nanoparticles as a function of the pH value. **(B)** Zeta potential of the Eudragit E100 nanoparticles as a function of the pH value.

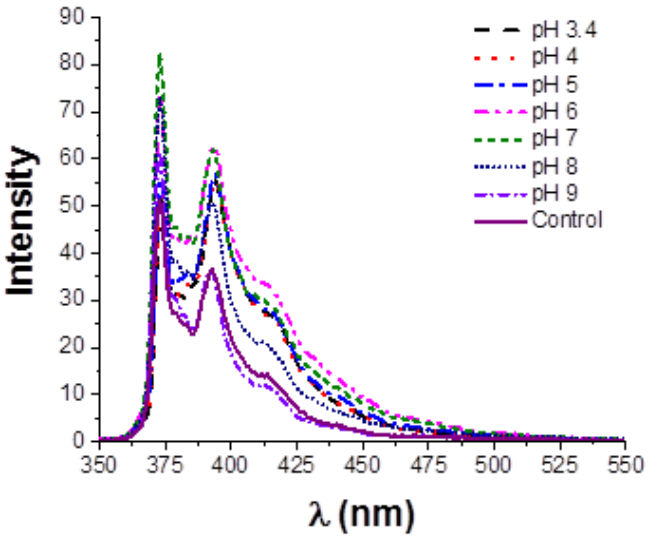

Figure SI-20 Fluorescence emission spectra of pyrene (6×10^{-5} mol L^{-1}) with **P8** nanoparticles (0.15 mg mL^{-1}) at various pH values. Pyrene in pure water was used as control.

Table SI-1 C, H, N, S and Cl contents (mass % in dry sample) in the copolymers of **P5**, **P6**, **P7** and **P8** that were determined by elemental analysis.

Polymer	C	H	N	S	Cl
P5	56.30	7.86	1.73	0.81	3.03
P7	58.31	8.00	1.73	0.85	1.01
P6	52.97	7.85	2.95	0.94	4.92
P8	55.80	7.75	3.02	0.89	0.92

Publication P3

“Uptake of retinoic acid-modified PMMA nanoparticles in LX2 and liver tissue by Raman imaging and intravital microscopy”

T. Yildirim, C. Matthaeus, A. P. Press, S. Schubert, M. Bauer, J. Popp, U. S. Schubert

Macromol. Biosci. **2017**, *DOI: 10.1002/mabi.201700064.*

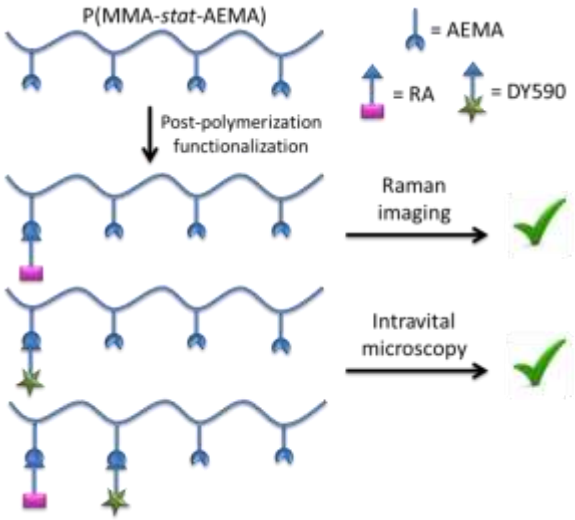

DOI: 10.1002/mabi.

Uptake of retinoic acid-modified PMMA nanoparticles in LX-2 and liver tissue by Raman imaging and intravital microscopy[a]

Turgay Yildirim,[#] Christian Matthäus,[#] Adrian T. Press, Stephanie Schubert, Michael Bauer, Jürgen Popp,* Ulrich S. Schubert*

Turgay Yildirim, Prof. Ulrich S. Schubert
Laboratory of Organic and Macromolecular Chemistry (IOMC), Friedrich Schiller University Jena, Humboldtstr. 10, 07743 Jena, Germany
E-mail: ulrich.schubert@uni-jena.de

Dr. Christian Matthäus, Prof. Dr. Jürgen Popp
Leibniz Institute of Photonic Technology (IPHT), Albert-Einstein-Straße 9, 07745 Jena, Germany
Institute of Physical Chemistry and Abbe Center of Photonics, Friedrich Schiller University Jena, Helmholtzweg 4, 07743 Jena, Germany

Dr. Adrian T. Press, Prof. Dr. Michael Bauer
Jena University Hospital, Department of Anesthesiology and Intensive Care Medicine, Am Klinikum 1, 07747 Jena, Germany

Dr. Stephanie Schubert
Institute of Pharmacy, Department of Pharmaceutical Technology, Friedrich Schiller University Jena, Otto-Schott-Str. 41, 07745 Jena, Germany

Turgay Yildirim, Dr. Christian Matthäus, Dr. Adrian T. Press, Dr. Stephanie Schubert, Prof. Dr. Michael Bauer, Prof. Dr. Jürgen Popp, Prof. Dr. Ulrich S. Schubert
Jena Center for Soft Matter (JCSM), Friedrich Schiller University Jena, Philosophenweg 7, 07743 Jena, Germany

Abstract

A primary amino functionalized methyl methacrylate (MMA) based statistical copolymer is covalently coupled with retinoic acid (RA) and a fluorescent dye (DY590) in order to investigate the feasibility of the RA containing polymeric nanoparticles for Raman imaging studies, and to study the possible selectivity of RA for hepatic stellate cells (HSC) via

[a] **Supporting Information** is available online from the Wiley Online Library or from the author.
[#] Authors contributed equally.

intravital microscopy. Cationic nanoparticles are prepared by utilizing the nanoprecipitation method using modified polymers. Raman studies show that RA functional nanoparticles can be detectable in all tested cells without any need of additional label. Moreover, intravital microscopy indicates that DY590 is eliminated through the hepatobiliary route but not if used as covalently attached tracing molecule for nanoparticles. However, it is a suitable probe for sensitive detection of polymeric nanoparticles.

1. Introduction

Polymeric nanoparticles have gained a great interest for potential applications such as imaging, diagnostics and targeted drug delivery. Most of these systems rely on the physical encapsulation of active molecules into nanoparticles during the self-assembly of the corresponding polymers in aqueous solution. However, these systems usually exhibit some drawbacks such as insufficient loading and premature release of the cargo. Conjugation of polymers with bioactive molecules can overcome these limitations.[1] In this study, retinoic acid (RA) was covalently attached to a primary amino functionalized methyl methacrylate (MMA) based statistical copolymer via an amide bond to investigate the feasibility of the retinoic acid containing polymeric nanoparticles for receptor mediated uptake by hepatic stellate cell (HSC) a resident perisinusoidal cell that is mainly responsible for liver cirrhosis.[2-4] These cells regulate sinusoidal blood flow in health and disease and are known to take up and store vit. A through receptors for a retinol binding protein.[5] Because of a relatively long conjugated π-bond system, retinol derivatives have very unique Raman properties, which make them ideal for Raman microscopic imaging studies in cell cultures. In order to further test the receptor mediated targeting concept and the possible selectivity of the retinoic acid for hepatic stellate cells *in vivo*, the copolymer was functionalized with a fluorescent dye with an activated ester. Retinoic acid and dye functionalized polymers were then subsequently self-assembled into nanoparticles *via* the nanoprecipitation method, and their cellular uptake mechanisms were investigated by Raman and intravital microscopy.

Over the past 10 years, Raman microscopic spectroscopy and imaging has become an attractive tool to spectroscopically characterize individual cells. The spatial resolution is analogous to conventional as well as fluorescence microscopy and only diffraction limited. By introducing a pinhole into the pathway of the collected light, Raman microscopy can also be applied confocally. Based on the collected spectral information, it is possible to image

individual cellular components or organelles, such as nucleus, endoplasmic reticulum, Golgi apparatus, vesicles or mitochondria.[6-8] Apart from subcellular structures it is possible to monitor the intracellular uptake of individual species (*e.g.* molecules and particles) based on their spectral properties. If the spectral contrast with respect to the cellular environment is sufficient, individual species can be monitored directly. It is also possible to introduce molecular functionalities possessing a unique Raman signature. Very popular in that respect is the introduction of deuterium by exchanging the hydrogens of a molecule. Consequently, the chemical properties remain unaltered, however, the spectroscopic features change significantly by shifting the observed scattering intensities of the CH/CD bonds by about 1000 wavenumbers. The concept of stable isotopic labeling has for instance been applied to study uptake dynamics of individual amino acids, deuterated lipids and liposomal nanoparticles.[9-13]

Very high Raman sensitivity, because of high Raman scattering cross sections, offer molecules with π-conjugation. Examples of molecular families with high π-conjugation are carotenoids or porphyrins. Recently, Raman microscopy has been applied to study the uptake efficiency of beta-carotene loaded PLGA nanoparticles.[14] The penetration of beta-carotene into skin has also been studied. Retinol or vitamin A as another member of the carotenoid family has also ideal properties for direct observation by Raman spectroscopy. Only recently, Raman spectroscopy has been used to quantify vitamin A in hepatic stellate cells (HSCs) of the liver.[15] HSCs are known to take up vitamin A independent of their needs though cell-type specific receptors[5] and store it in large vesicles located near their nuclei.[16] They serve as vitamin A storage and control its availability and, thereby, also protect from vitamin A intoxication. Besides controlling vitamin A availability,[17] HSC control the production and deposition of extracellular matrix proteins, mostly collagen, and intrahepatic blood pressure. Upon activation, HSCs contract and troch the sinusoids thereby limiting their diameter, increasing intrahepatic resistance and decreasing blood flow through the liver. HSC activation

occurs after a vast of stimuli. Chronic activation leads not only to an increased local and systemic blood pressure and transformation of HSCs to fibroblasts.[18] Activated HSCs are in a permanent contracted state, lose their vitamin A storage ability, exhibit a high proliferative capacity and deposit great amounts of extracellular matrix increasing liver stiffness and impairing many of its functions. While this state, referred to as liver fibrosis, is reversible in the beginning when the activating stimulus is removed, further activation of the liver ultimately processes to liver cirrhosis where the only remaining causative treatment is a liver transplantation. Novel targeted therapeutic strategies aim towards preventing the activation of HSCs and limiting their proliferative capacity[19] as well the deposition of collagen[4, 20] in an activating state. Different strategies including targeted nitric oxide release[21] in hepatic stellate cells or different antisense-based methods to suppress genes involved in the transcription, translation, protein-folding, activation or excretion of collagen are used successfully in experimental studies.[22] Due to the location of HSCs around the capillaries in the liver, sufficient concentrations of a drug remains challenging and different methods are applied to deliver molecules to HSCs based on their feature to take up and store vitamin A in the previously mentioned “need-independent” manner.

2. Results and discussion

For the presented *in vitro* and *in vivo* studies three different polymeric particles were synthesized. As the major aspect of the study is to investigate the possible selectivity of the retinoic acid for hepatic stellate cells three different PMMA based particle were synthesized. Retinoic acid functionalized particles can be directly monitored by Raman microscopy, which is ideal to monitor intracellular uptake behavior on the single cellular level. Because Raman imaging is usually very time consuming and therefore limited in the field of view (FOV), retinoic acid-modified PMMA particles were also functionalized with DY590 as a

fluorescence label. As a blind test for the in vivo studies pure PMMA particles were also labeled with DY590.

2.1. Polymer synthesis

A statistical copolymer (p(MMA-*stat*-AEMA·HCl) (**P^{RAFT}**)) of methyl methacrylate (MMA) and 2-aminoethyl methacrylate hydrochloride (AEMA·HCl) was synthesized via the reversible addition-fragmentation chain transfer (RAFT) polymerization as described earlier.[23] It was characterized by size-exclusion chromatography (SEC) showing a number-average molar mass (M_n) of 5,100 g mol^{-1} with a dispersity ($Đ$) of 1.13. The degree of polymerization for MMA and AEMA·HCl was estimated by ^{1}H NMR spectroscopy as 42 and 6, respectively. For functionalization with retinoic acid (RA), the amino functionalities of **P^{RAFT}** were modified with RA (Scheme 1). However, the ω RAFT end-group of **P^{RAFT}** exhibits a strong UV absorption, which is in a similar region with RA. As a consequence, in order to prove the covalent coupling of RA to the polymer by the SEC (UV detector) and UV-vis spectrophotometry, the ω RAFT end-group of the polymer was cleaved by following a procedure reported in literature before, yielding hydroxyl-terminated polymer (**P^{OH}**) (Scheme 1).[24] The cleavage of the RAFT end-group is indicated by a color change from pink to white. UV-vis spectroscopy further verified the cleavage of the ω RAFT end-group by the disappearance of UV absorbance at 305 nm in chloroform (Figure S1). In agreement with this, SEC analysis using UV detection at 300 nm of the polymer before and after end-group removal confirmed the complete elimination of the RAFT end-group by the disappearance of the UV absorption (Figure S3). In contrast, SEC analysis with RI detection revealed no significant changes in the M_n and $Đ$ values (Figure S2). The ^{1}H NMR spectrum also confirmed the disappearance of the ω RAFT end-group signals (δ = 7.84, 7.48, and 7.35 ppm) (Figure S4).

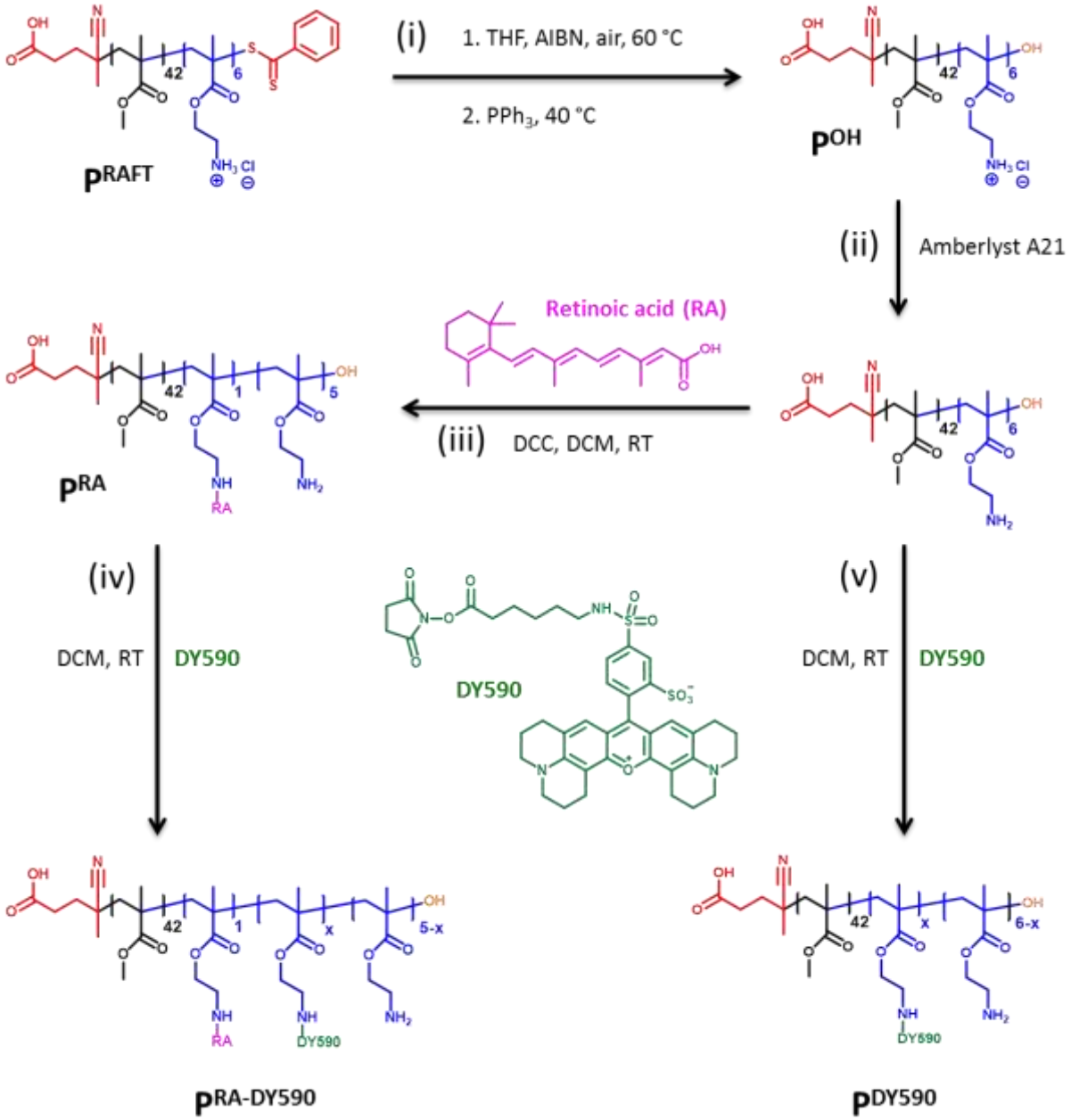

Scheme 1. Schematic representation of the (i) RAFT end group cleavage; (ii) deprotonation of $\mathbf{P^{OH}}$; (iii) coupling of the retinoic acid (RA) to deprotonated form of $\mathbf{P^{OH}}$; (iv and v) coupling of DY590 to $\mathbf{P^{RA}}$ and deprotonated form of $\mathbf{P^{OH}}$.

2.2. Coupling of retinoic acid and DY590 to P^{OH} and nanoparticle formulation

The charged polymer that contains HCl salt was treated with Amberlyst® A21 before coupling reactions to obtain the desired primary amino-functionalized polymer (Scheme 1). Subsequently, RA was covalently conjugated to the pendant primary amino groups of the $\mathbf{P^{OH}}$ by DCC coupling, yielding RA conjugated polymer ($\mathbf{P^{RA}}$) (Scheme 1). Covalent conjugation of the RA to the polymer was confirmed by ^{1}H NMR, SEC and UV-vis spectrophotometry.

After the coupling reaction, various characteristic signals of RA appeared without any shift in the ^{1}H NMR spectrum of $\mathbf{P^{RA}}$ compared to the spectrum of the $\mathbf{P^{OH}}$, indicating the covalent attachment of RA to the polymer without any isomerization (Figure S5). By comparing the relative signal intensity ratio of methyl protons of MMA (δ = 3.60 ppm, peak "a" in Figure S5) (calibrated to DP = 42) to methine protons of RA (δ = 5.82 ppm, peak "c" in Figure S5), the RA content in one $\mathbf{P^{RA}}$ chain was estimated as 1. SEC reveals a slight increase in the molar mass value after RA coupling caused by the increased hydrodynamic volume of the copolymer in chloroform after RA conjugation (Figure S6). Due to the conjugated polyene chain, RA has a strong UV absorbance at λ_{max} = 365 nm in chloroform. The λ_{max} of the RA in chloroform was blue shifted by 8 nm after coupling to the $\mathbf{P^{OH}}$ (Figure S7), which could be attributed due to the stacked polyene chains.[25] Moreover, SEC analysis of the $\mathbf{P^{RA}}$ with overlapping RI and UV signals (at 340 nm) confirms the covalent attachment of the RA to the polymer (Figure S8). In a next step, NHS ester functional fluorescent dye DY590 was covalently coupled to the primary amino groups of the $\mathbf{P^{RA}}$ and $\mathbf{P^{OH}}$ by using an amine NHS ester amidification reaction, resulting in $\mathbf{P^{RA\text{-}DY590}}$ and $\mathbf{P^{DY590}}$, respectively (Scheme 1). SEC (RI detector) showed no significant molar mass or dispersity changes after the coupling reaction (Figure S9-10), indicating DY590 has no impact on the hydrodynamic size of the polymers. DY590 has a strong UV absorption at λ_{max} = 578 nm in chloroform (Figure S11). After the coupling reactions, λ_{max} of the DY590 in chloroform was red shifted by 4 nm for both polymers (PRA-DY590 and PDY590) (Figure S11-12). SEC analysis of $\mathbf{P^{RA}}$ and $\mathbf{P^{OH}}$ with UV detection at 600 nm revealed no signal, but DY590 coupled polymers ($\mathbf{P^{RA\text{-}DY590}}$ and $\mathbf{P^{DY590}}$) exhibited intense signals, which overlap with their respective RI signals (Figure S13-14). This confirms the covalent coupling of DY590 to the polymers. The disappearance of the UV signals (at 600 nm) at high elution volumes in SEC analysis proved that there was no free DY590 left after each reaction. Therefore, by comparing the initial feed ratios of the polymer

and the DY590, it was assumed that one of every 39 polymer chain contains one DY590 molecule.

Polymeric nanoparticles were prepared from the synthesized RA and DY590 coupled polymers ($\mathbf{P^{RA}}$, $\mathbf{P^{RA\text{-}DY590}}$ and $\mathbf{P^{DY590}}$) by nanoprecipitation with subsequent solvent evaporation method.[26-27] Nanoparticles with monomodal size distributions (Z-average diameters between 73 and 85 nm) with relatively narrow polydispersity index (PDI) values were obtained for all polymers (Table S1, Figure S15). All suspensions exhibit positive ζ-potential values as a consequence of the primary amino functionality of the copolymers (Table S1).[28]

2.3. Raman imaging of particle uptake

LX-2 human liver cells where incubated with $\mathbf{P^{RA}}$ nanoparticles at a concentration of 50 µg/mL for two time intervals of 1 and 3 hours. The time intervals were chosen according to previous incubation experiments with particle systems of similar size. Figure 1 displays the Raman spectra of pure RA and the $\mathbf{P^{RA}}$ nanoparticles. The spectrum of RA is clearly dominated by the Raman intensity of the C=C symmetric stretching vibrations of the conjugated π-bonds at 1594 cm^{-1}. The Raman spectrum of the RA modified nanoparticles still exhibits this intensity as the most prominent Raman band. All other spectral features originate from vibrations of the polymeric matrix for instance the CH stretching vibrations at 2954 cm^{-1}, the C=O stretching of the ester bonds of the methacrylate or CH scissoring vibrations at 1452 cm^{-1}.

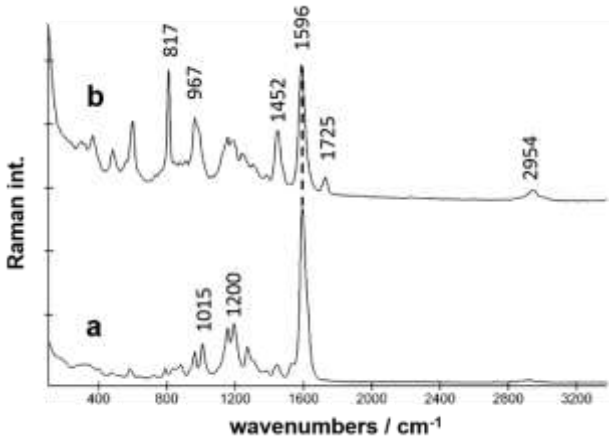

Figure 1. Raman spectra of RA (retinoic acid) (a) and RA modified methacrylate ($\mathbf{P^{RA}}$) polymeric nanoparticles (b).

Figures 2A and 2C show the Raman images of two LX-2 cells incubated with $\mathbf{P^{RA}}$ NPs for 1 and 3 hours at a concentration of 50 mg/mL. The distribution of the nanoparticles is plotted in red, the cytosol in cyan. The associated spectral information is plotted in corresponding colors in Figures 2B and 2D. The Raman images were reconstructed using a typical spectral unmixing algorithm, which searches a given dataset for the most dissimilar spectral components, usually refered to as endmembers. Usually the number of endmembers can be set to the number of molecular species that can be observed, as for instance proteins, lipids and in the reported examples retinoic acid. For Raman imaging of individual cells usually 3 to 4 endmembers are sufficient to reconstruct the image. Because a water immersion objective was used one spectral endmember always corresponds to the plain surrounding water.[7] After 1 hour, the endocytotic uptake of the particles is clearly visible. Small vesicle-like inclusions on the order of 0.5 to 1 µm are distributed throughout the cytosol. The corresponding endmember spectrum (also in red) distinctly shows the typical RA Raman band at 1596 cm^{-1}. The other Raman bands of the red spectrum are typical Raman bands of proteins and can be assigned to vibrations of the protein backbones and their residues. Characteristic protein bands are for instance the C=O stretching vibrations of carbonyl groups at 1650 cm^{-1}, usually refered to as amide I band, CH_2 scissoring deformations of methylene groups at 145 cm^{-1}, or the all

symmetric phenylalanine ring breathing at 1002 cm^{-1}. Interestingly, only the very strong RA associated 1596 cm^{-1} band is represented in the observed endmember spectra, none of the other methacrylic polymer bands is distinctly visible. However, all of these bands overlay with the spectral features of the proteins and are, therefore, more likely masked by these, as early degradation of the nanoparticles is not very likely. The cyan endmember spectrum associated with the cytosol exhibits all of the typical protein bands and has the appearance of typical Raman spectra of cells.

The Raman image in Figure 2C shows the particle distribution after 3 hours. The uptake is apparently continuously increased and has reached a level where in some regions of the cytosol individual endocytotic vesicles cannot be resolved or have aggregated in sizes of several micrometers. Large inclusions of the particles can be observed throughout the whole cell. The corresponding endmember spectrum is now dominated by the RA marker band at 1596 cm^{-1}. The band is three times as intense compared to the 1 hour incubation time. In addition, also the region below the marker band is now altered and bears additional features of the RA spectrum. The endmember associated with the cytosol again exhibits all typical protein bands.

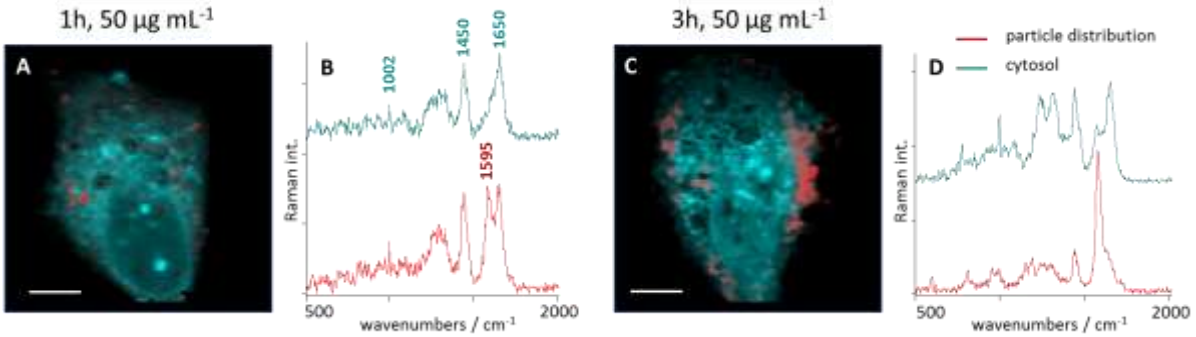

Figure 2. Raman images of LX-2 cells incubated with $\mathbf{P^{RA}}$ nanoparticles for 1 hour (A) and 3 hours (C) along with the corresponding spectral information plotted in (B) and (D) respectively. The distribution of the nanoparticles is shown in red. Distinctly pronounced in the Raman spectra is the RA marker band at 1596 cm^{-1}.

Several cells have been imaged by Raman microscopy for the two incubation intervals to assure an observation of representative uptake patterns. In Figure 3, the Raman images of five

cells for both incubation times are presented. The top row shows the results for the incubation of 1 hour. Similar to the image already discussed for Figure 2A, all cells exhibit small vesicle-like inclusions due to endocytosis. No enhanced aggregation in the vicinity of the cellular membranes was observed and the distribution is random. Vesicle size and number are on the same order. The size of the endocytes does not reflect the size of the nanoparticles, which might be a hint for more than one particle per endocyte. For 3 hours of incubation, the uptake is significantly increased. All cells show amounts of particles that fill entire fractions of the cytosol and a level of saturation is apparent. For longer incubation times, the cell survival rate critically decreased. The spectral information associated with the Raman images shows similar increases in intensity as discussed for Figure 2 (data not shown).

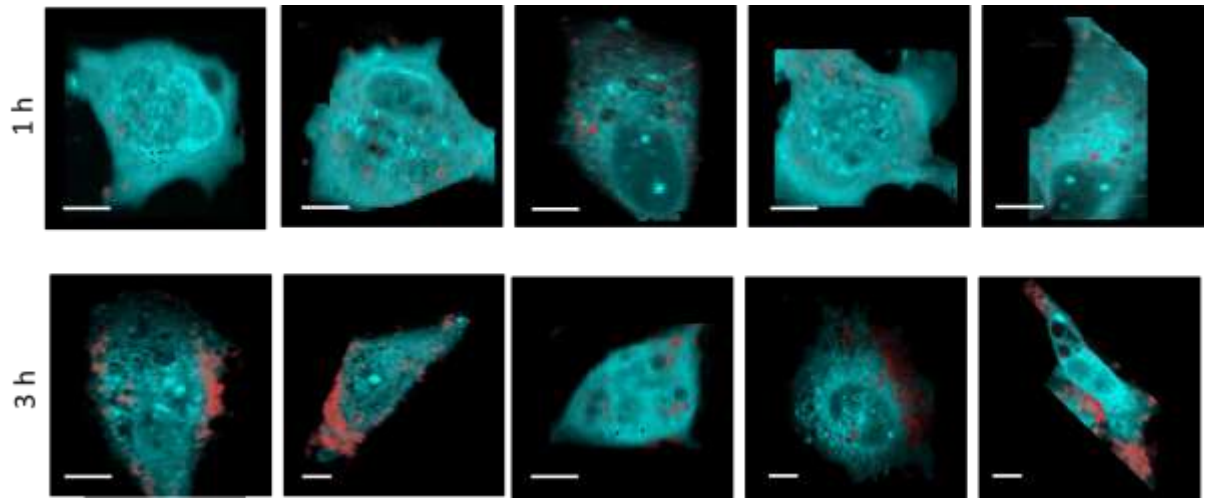

Figure 3. LX-2 cells incubated with $\mathbf{P^{RA}}$ nanoparticles for 1 hour (top row) and 3 hours (bottom).

It is important to note at this point that no native intracellular retinol or retinol derivatives was observed in untreated cells, which is in contrast to previous Raman experiments on hepatic stellate cells freshly extracted from rat or mouse liver.[29-30] It is not entirely clear why for the LX-2 cells we did not observe the presence of any retinol derivatives by Raman spectroscopy. A very crucial aspect for Raman measurements in general, is that the sensitivity is intrinsically low compared to for instance fluorescence. It is generally very rare to detect

chemical species below the milli-molar range. In cells it is difficult to address concentrations in a similar way as in solution. Although 60% of the cytosol is made up of water, various compounds can aggregate in cellular organelles. It is well known that retinol aggregates in hepatic stellate cells. Testerink et al. report concentrations of 10% (estimated mass percentages) localized in lipid droplets, which corresponds to concentrations well measurable by Raman spectroscopy. Interestingly, Galler et al. observe a retinol decrease with ongoing proliferation and no detection of retinol in HSCs already 5 days after isolation. It is therefore reasonable to assume that unlike freshly isolated HSCs, LX-2 cultured cells do not exhibit retinol derivatives at concentrations measurable by Raman spectroscopy.

2.4. Intravital microscopy

Intravital microscopy is a powerful technique to monitor physiologic effects in real-time in vivo. FVB/N mice were injected with DY590 during imaging and its distribution pattern is analyzed at different time points (Figure 4A). Hepatocytes are identified by their high intracellular NAD(P)H concentration which is visualized by excitation at 375 to 405 nm. DY590 quickly occurs in portal vein distributing though sinusoids. Already after 30 s a hepatic lining of the dye occurs. After 5 min the dye is internalized into hepatocytes and after 20 min line structure on the hepatocytes get visible while the dye disappeared from the blood vessels. DY590 accumulates further in periportal area (Figure 4B) suggesting a transporter mediated transport into hepatocytes. After approximately 40 min most of the dye is eliminated into the canalicular system which drains into bile ducts and subsequently process in the duodenum. DY590 thereby allows the reconstruction of the canalicular network in the liver under most physiologic conditions (Figure 4C).

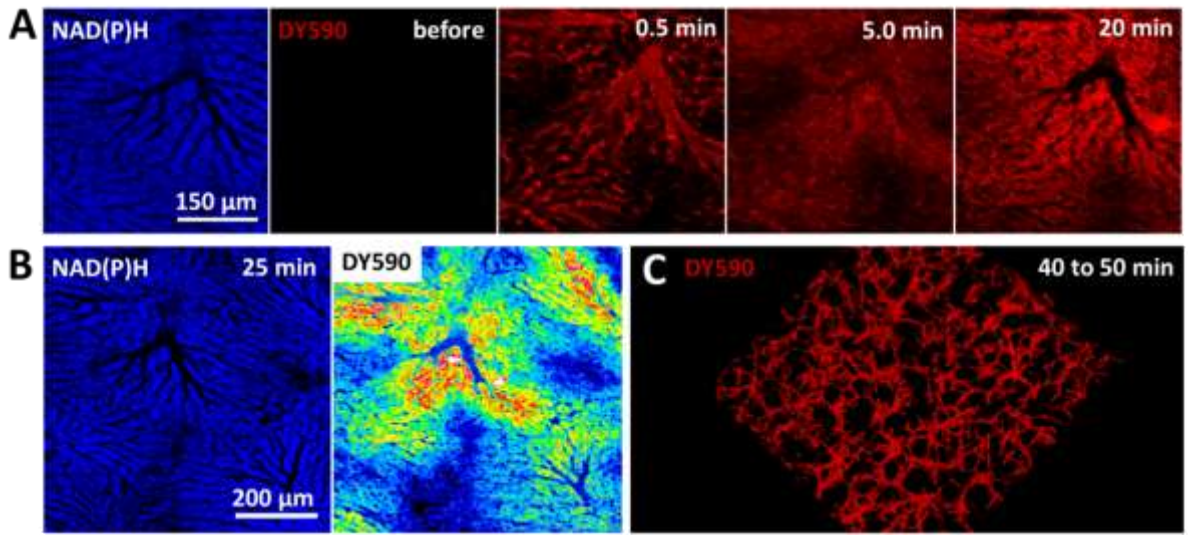

Figure 4. Intravital microscopy of DY590 in the murin liver. A) Uptake and elimination of DY590 in the murine liver. B) Zonal uptake of DY590. C) Reconstruction of a *in vivo* z-stack depicting the DY590 filled canalicular network indicating the hepatic elimination of the dye.

When DY590 is conjugated to the cationic polymers $\mathbf{P^{OH}}$ and $\mathbf{P^{RA}}$ and formed to nanoparticles, it loses its hepatobiliary clearance (Fig. 5). Both nanoparticles $\mathbf{P^{DY590}}$ and $\mathbf{P^{RA\text{-}DY590}}$ did not enter hepatocytes but are instead uptaken by cells located in the sinusoids. Greater occurring accumulations, especially in the curves of the sinusoids, can be contributed to Kupffer cells and HSC. Smaller accumulations scattered along the sinusoids can be assigned to liver sinusoidal endothelia cells (LSECs). Kupffer cells represent the largest population of local macrophages in the liver and are together with LSECs the immunological line of defense in the liver. It is known for nanoparticles exhibiting cationic charge to be recognized and eliminated quickly by immune cells in particular in the liver. Interestingly, the conjugation of retinoic acid did not alter pharmacokinetics of the nanoparticles. This indicates the importance of a carefully engineered surface to employ targeting moieties.

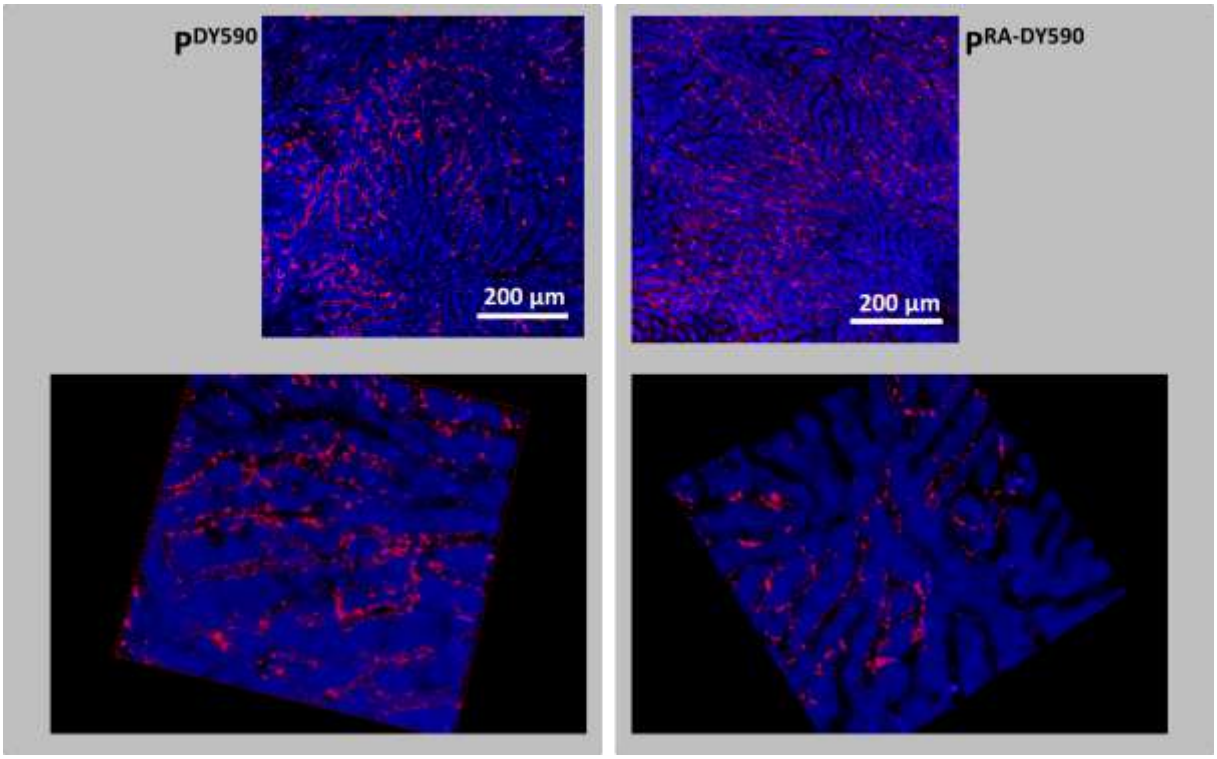

Figure 5. Hepatic uptake of DY590 conjugated polymeric nanoparticles without ($\mathbf{P}^{\mathbf{DY590}}$) and with ($\mathbf{P}^{\mathbf{RA\text{-}DY590}}$) retinoic acid after 40 min.

3. Conclusions

In conclusion, polymeric nanoparticles were prepared by using a cationic methacrylate based polymer, which is functionalized with RA and/or a fluorescent dye (DY590). Raman imaging of RA functionalized nanoparticle ($\mathbf{P}^{\mathbf{RA}}$) uptake was studied on human liver cells. The in vitro studies of the retinoic acid modified PMMA particles on LX-2 cells show a very high intracellular uptake efficacy. Initial endocytosis is on the order of less than an hour. After one hour, the presence of the particles was evident randomly distributed throughout the cytosol. Longer incubation times lead to continuous uptake, whereby large areas of the cytosol are apparently filled with endocytotic vesicles until a maximum capacity is reached within several hours. It was possible to monitor the uptake of the RA-PMMA particles in a completely label free manner using Raman microscopy. The advantage of the technique is that the addition of fluorescence labels can be avoided. Fluorescence labels are of significant molecular size and often change the chemical or biochemical properties of the molecules or in this case

nanoparticles. For further development and optimization of such particle systems, Raman spectroscopy has great potential, as it is an analytical tool, which also offers the possibility of quantification of the intracellular uptake and therefore the possibility to compare the efficacy of different polymeric systems. Potentially Raman microscopy can also be applied on dissected liver tissue. In the quiescent state, HSC store 90% of body vitamin A and regulate nutritive perfusion at the level of individual sinusoids. It is therefore expected (and has been shown) that untreated liver tissue contains to a great extent vitamin A, which has to be accounted for in carful comparative studies, which will be subject to further investigations in the near future.

Intravital microscopy is utilized to monitor the distribution of free DY590 and nanoparticles $\mathbf{P}^{\mathbf{DY590}}$ and $\mathbf{P}^{\mathbf{RA\text{-}DY590}}$ *in vivo*. In case of only injection of free DY590, it is internalized in hepatocytes and eliminated into the canalicular system. Whereas in the case of DY590, conjugated nanoparticles ($\mathbf{P}^{\mathbf{DY590}}$ and $\mathbf{P}^{\mathbf{RA\text{-}DY590}}$), hepatobiliary clearance was not evident as the nanoparticles did not enter hepatocytes but are instead uptaken by cells located in the sinusoids. The results clearly show that modification of polymers with RA for the formulation of nanoparticles for targeted delivery to HSC can be monitored by Raman microscopy. Consequently, further uptake and selectivity studies are planned to investigate the potential of RA modified polymeric nanoparticles for treating liver diseases.

Acknowledgements

The authors acknowledge the German Federal Ministry of Education and Research (BMBF, 13N13416) for funding. We further acknowledge funding from the Carl-Zeiss Foundation (JCSM Strukturantrag), the Collaborative Research Center SFB ChemBioSys (SFB 1127) and the Thüringer Ministerium für Wirtschaft, Wissenschaft, und Digitale Gesellschaft (TMWWDG, ProExzellenz II (Nanopolar) and ProExzellenz I (NanoConSens)).

Keywords: polymeric nanoparticles, Raman imaging, intravital microscopy, retinoic acid, liver cell targeting.

References

[1] J. Nicolas, *Chem. Mater.* **2016**, *28*, 1591-1606.

[2] K. Wake, *Proc. Jpn. Acad., Ser. B, Phys. Biol. Sci.* **2006**, *82*, 155-164.

[3] D. F. Brandão, L. N. Z. Ramalho, F. S. Ramalho, S. Zucoloto, A. d. L. C. Martinelli, O. d. Castro e Silva, *Acta Cir. Bras.* **2006**, *21*, 54-57.

[4] Y. Sato, K. Murase, J. Kato, M. Kobune, T. Sato, Y. Kawano, R. Takimoto, K. Takada, K. Miyanishi, T. Matsunaga, T. Takayama, Y. Niitsu, *Nat. Biotechnol.* **2008**, *26*, 431-442.

[5] R. Kawaguchi, J. Yu, J. Honda, J. Hu, J. Whitelegge, P. Ping, P. Wiita, D. Bok, H. Sun, *Science* **2007**, *315*, 820-825.

[6] S. F. El-Mashtoly, H. K. Yosef, D. Petersen, L. Mavarani, A. Maghnouj, S. Hahn, C. Kötting, K. Gerwert, *Anal. Chem.* **2015**, *87*, 7297-7304.

[7] M. Hedegaard, C. Matthäus, S. Hassing, C. Krafft, M. Diem, J. Popp, *Theor. Chem. Acc.* **2011**, *130*, 1249-1260.

[8] C. Matthäus, T. Chernenko, J. A. Newmark, C. M. Warner, M. Diem, *Biophys. J.* **2007**, *93*, 668-673.

[9] H.-J. van Manen, Y. M. Kraan, D. Roos, C. Otto, *Proc. Natl. Acad. Sci. U.S.A.* **2005**, *102*, 10159-10164.

[10] C. Stiebing, T. Meyer, I. Rimke, C. Matthäus, M. Schmitt, S. Lorkowski, J. Popp, *J. Biophotonics* **2017**, DOI: 10.1002/jbio.201600279.

[11] C. Stiebing, C. Matthäus, C. Krafft, A.-A. Keller, K. Weber, S. Lorkowski, J. Popp, *Anal. Bioanal. Chem.* **2014**, *406*, 7037-7046.

[12] C. Matthäus, C. Krafft, B. Dietzek, B. R. Brehm, S. Lorkowski, J. Popp, *Anal. Chem.* **2012**, *84*, 8549-8556.

[13] C. Matthäus, A. Kale, T. Chernenko, V. Torchilin, M. Diem, *Mol. Pharm.* **2008**, *5*, 287-293.

[14] C. Matthäus, S. Schubert, M. Schmitt, C. Krafft, B. Dietzek, U. S. Schubert, J. Popp, *ChemPhysChem* **2013**, *14*, 155-161.

[15] K. Galler, R. P. Requardt, U. Glaser, R. Markwart, T. Bocklitz, M. Bauer, J. Popp, U. Neugebauer, *Sci. Rep.* **2016**, *6*, 24155.

[16] W. S. Blaner, S. M. O'Byrne, N. Wongsiriroj, J. Kluwe, D. M. D'Ambrosio, H. Jiang, R. F. Schwabe, E. M. C. Hillman, R. Piantedosi, J. Libien, *Biochim. Biophys. Acta* **2009**, *1791*, 467-473.

[17] K. L. Penniston, S. A. Tanumihardjo, *Am. J. Clin. Nutr.* **2006**, *83*, 191-201.

[18] J. E. Puche, Y. Saiman, S. L. Friedman, in *Comprehensive Physiology*, John Wiley & Sons, Inc., **2011**.

[19] K. Abshagen, M. Brensel, B. Genz, K. Roth, M. Thomas, V. Fehring, U. Schaeper, B. Vollmar, *Curr. Gene Ther.* **2015**, *15*, 215-227.

[20] Alnylam Pharmaceuticals. Available at: http://www.alnylam.com/web/wp-content/uploads/2012/11/ALNY-AASLD-FibrosisPosterXPanel-Nov2012.pdf, accessed on February 1, 2017.

[21] H. T. T. Duong, Z. Dong, L. Su, C. Boyer, J. George, T. P. Davis, J. Wang, *Small* **2015**, *11*, 2291-2304.

[22] R. Omar, J. Yang, H. Liu, N. M. Davies, Y. Gong, in *Reviews of Physiology, Biochemistry and Pharmacology, Vol. 172* (Eds.: B. Nilius, P. de Tombe, T. Gudermann, R. Jahn, R. Lill, O. H. Petersen), Springer International Publishing, Cham, **2016**, pp. 1-37.

[23] T. Yildirim, A. C. Rinkenauer, C. Weber, A. Traeger, S. Schubert, U. S. Schubert, *J. Polym. Sci., Part A: Polym. Chem.* **2015**, *53*, 2711-2721.

[24] M. Dietrich, M. Glassner, T. Gruendling, C. Schmid, J. Falkenhagen, C. Barner-Kowollik, *Polym. Chem.* **2010**, *1*, 634-644.

[25] I. Washington, S. Jockusch, Y. Itagaki, N. J. Turro, K. Nakanishi, *Angew. Chem. Int. Ed.* **2005**, *44*, 7097-7100.

[26] S. Schubert, J. J. T. Delaney, U. S. Schubert, *Soft Matter* **2011**, *7*, 1581-1588.

[27] T. Yildirim, I. Yildirim, R. Yanez-Macias, S. Stumpf, C. Fritzsche, S. Hoeppener, C. Guerrero-Sanchez, S. Schubert, U. S. Schubert, *Polym. Chem.* **2017**.

[28] T. Yildirim, A. Traeger, E. Preussger, S. Stumpf, C. Fritzsche, S. Hoeppener, S. Schubert, U. S. Schubert, *Macromolecules* **2016**, *49*, 3856-3868.

[29] N. Testerink, M. Ajat, M. Houweling, J. F. Brouwers, V. V. Pully, H.-J. van Manen, C. Otto, J. B. Helms, A. B. Vaandrager, *PLOS ONE* **2012**, *7*, e34945.

[30] K. Galler, F. Schleser, E. Frohlich, R. P. Requardt, A. Kortgen, M. Bauer, J. Popp, U. Neugebauer, *Integr. Biol.* **2014**, *6*, 946-956.

For table of contents only:

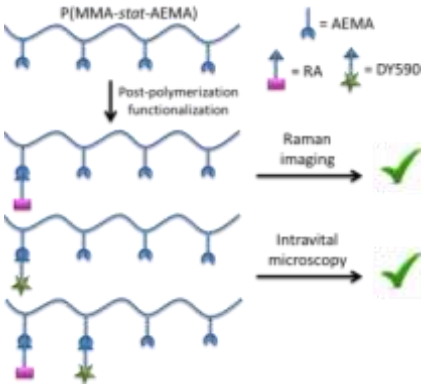

Text for table of contents:

The cellular uptake of retinoic acid functional cationic nanoparticles on human liver cells could be monitored using Raman imaging in a completely label free manner. Additionally, covalent conjugation of a fluorescent dye allowed monitoring the distribution of nanoparticles *in vivo* using intravital microscopy.

Uptake of retinoic acid-modified PMMA nanoparticles in LX-2 and liver tissue by Raman imaging and intravital microscopy[a]

Turgay Yildirim,[#] Christian Matthäus,[#] Adrian T. Press, Stephanie Schubert, Michael Bauer, Jürgen Popp,* Ulrich S. Schubert*

_____

Turgay Yildirim, Prof. Ulrich S. Schubert
Laboratory of Organic and Macromolecular Chemistry (IOMC), Friedrich Schiller University Jena, Humboldtstr. 10, 07743 Jena, Germany
Jena Center for Soft Matter (JCSM), Friedrich Schiller University Jena, Philosophenweg 7, 07743 Jena, Germany
E-mail: ulrich.schubert@uni-jena.de

Dr. Christian Matthäus, Prof. Dr. Jürgen Popp
Leibniz Institute of Photonic Technology (IPHT), Albert-Einstein-Straße 9, 07745 Jena, Germany
Institute of Physical Chemistry and Abbe Center of Photonics, Friedrich Schiller University Jena, Helmholtzweg 4, 07743 Jena, Germany

Dr. Adrian T. Press, Prof. Dr. Michael Bauer
Jena University Hospital, Department of Anesthesiology and Intensive Care Medicine, Am Klinikum 1, 07747 Jena, Germany

Dr. Stephanie Schubert
Jena Center for Soft Matter (JCSM), Friedrich Schiller University Jena, Philosophenweg 7, 07743 Jena, Germany
Institute of Pharmacy, Department of Pharmaceutical Technology, Friedrich Schiller University Jena, Otto-Schott-Str. 41, 07745 Jena, Germany

_____

EXPERIMENTAL SECTION

Materials

All-*trans*-retinoic acid (RA), dicyclohexylcarbodiimide (DCC), azobisisobutyronitrile (AIBN), triphenylphosphine (PPh_3), and Amberlyst® A21 were purchased from Sigma Aldrich and used as received. DY590 was obtained from Dyomics GmbH (Germany).

Instruments and methods

Proton nuclear magnetic resonance (^{1}H NMR) spectra were recorded at room temperature in $CDCl_3$ or CD_3OD on a Brucker Avance 300 MHz. The chemical shifts are given in ppm.

Size-exclusion chromatography (SEC) measurements were performed on a Shimadzu system equipped with a SCL-10A system controller, a LC-10AD pump, a RID-10A refractive index detector, and a PSSSDV-linear S column (5 μm particle size; Polymer Standards Service GmbH, Mainz, Germany) at 40 °C using a chloroform ($CHCl_3$), triethylamine and 2-propanol (94:4:2) mixture as eluent at a flow rate of 1 mL min^{-1}. The system was calibrated with a linear calibration curve built from poly(methyl methacrylate) (PMMA) standards of narrow dispersity (M_p = 410 to 88,000 g mol^{-1}).

Dynamic light scattering was performed on a Zetasizer Nano ZS (Malvern Instruments, Herrenberg, Germany). After an equilibration time of 180 s, 3 × 30 runs were carried out at 25 °C (λ = 633 nm). The counts were detected at an angle of 173°. Each measurement was performed in triplicate. The mean particle size was approximated as the effective (Z-average) diameter and the width of the distribution as the polydispersity index of the particles (PDI) obtained by the cumulants method assuming a spherical shape of the nanoparticles.

Electrophoretic light scattering was used to measure the electrokinetic potential, also known as ζ-potential. The measurements were performed on a Zetasizer Nano ZS (Malvern Instruments, Herrenberg, Germany) by applying laser Doppler velocimetry. For each measurement, 10 runs

were carried out using the slow-field and fast-field reversal mode at 150 V. Each experiment was performed in triplicate at 25 °C.

Raman measurements

Raman images were acquired using a confocal Raman Microscope Model alpha300 R (WITec, Ulm, Germany) and a Nikon water immersion objective with a magnification of 60x and a numerical aperture of 1.00. An excitation wavelength of 785 nm was provided by a cw diode laser (Toptica Photonics, Gräfelingen, Germany). Raman images were taken at a step size of 0.5 µm with an integration time of 0.5 s. Each pixel in an image represents one spectrum. If not declared otherwise, a grating of 300 grooves/mm was used, leading to a spectral resolution of around 6 cm^{-1}.

Data analysis of Raman measurements

All spectra were cleared from cosmic rays before analysis using the software CytoSpec (Cytospec, Berlin, Germany). Image analysis and spectral quantification was then performed in MatLab (MathWorks, Natick, MA). Baseline correction with a second order polynomial and vector normalization was implemented. Images acquired with Raman microspectroscopy were analyzed by the N-FINDR spectral unmixing algorithm described by Winter et al.[1,2] A wavenumber region from 500 to 3100 cm^{-1} was used.

Cell culture:

Human LX2 (cell line CCL-2, ATCC, Manassas, VA) were grown in 75-cm^3 culture flasks with 7 mL of Dulbecco's modified Eagle's medium/Nutrient mixture F-12 DMEM/F12 and 2% fetal kalf serum at 37°C and 5% CO_2. 100 µL of 1% Pen/Strep was added. Cells were seeded onto and allowed to attach to polished CaF_2 substrates (Wilmad LabGlass, Buena, NJ), which were chosen to avoid background scattering that is observed from regular glass windows. The CaF_2 substrates were removed from the culture medium after incubation with , and the cells were fixed in a 10% phosphate buffered formalin solution and washed in phosphate buffered saline.

Animals

Animal studies were conducted in accordance with animal welfare legislation under pathogen-free conditions in the animal facility of the Jena University Hospital. During all procedures and imaging methods, animals remained under deep general anesthesia using Isoflurane and pain-reflexes were assessed to gauge the depth of anesthesia. The body temperature further was permanently kept on 37 °C using feed-back controlled heating plate.

Intravital microscopy

Intravital microscopy was performed as described before.[3] Briefly, a sterile tail-vein catheter was placed in the tail-vein of male FVB/NRj mice. Afterwards the left lateral abdomen was shaved and opened and the left lateral liver lobe was exposed on a cover slip and subsequently fixed on it by a drop of n-butyl-2-cyanoacrylat (Histoacryl, B. Braun Melsungen AG, Germany). For the analysis an inverted confocal laser scanning microscope (LSM-780, Zeiss AG, Jena, Germany) was used. The liver architecture was visualized using the NAD(P)H/H+ autofluorescence (excitation 375 to 405 nm, emission 410 to 556 nm band-pass on photomultiplier tube). DY590 was excited at 561 nm and emitted light detected on a GaAsP Detector through a 566 to 704 nm band-pass filter.

Synthesis

RAFT end group transformation

A solution of 900 mg p(MMA-*stat*-AEMA·HCl) ($\mathbf{P^{RAFT}}$) and 300 mg of AIBN in 200 mL of THF and 2 mL of triethylamine was stirred vigorously at 60 °C under ambient atmosphere. After the discoloration of the solution (~ 3 h), the temperature was reduced to 40 °C and 150 mg of triphenylphosphine was added. After 30 min, the polymer was purified by precipitating in hexane (3 times). The reader is referred to the note of caution in the followed literature due to the possible formation of small amounts of potentially explosive THF-peroxides during the reaction.[4]

***In situ* deprotonation of $\mathbf{P^{OH}}$**

Ion exchange resin Amberlyst® A21 was used to deprotonate $\mathbf{P^{OH}}$. $\mathbf{P^{OH}}$ was dissolved in dichloromethane, mixed with Amberlyst® A21 and stirred for 10 min at room temperature. Subsequently, Amberlyst® A21 beads filtered and the resulting solution was used for the coupling reactions.

Coupling of the retinoic acid to $\mathbf{P^{OH}}$

28.4 mg DCC (0.138 mmol) and 46 mg of RA (0.153 mmol) were dissolved in 4 mL of CH_2Cl_2 and gently stirred for 30 min at room temperature in the dark. 270 mg of $\mathbf{P^{OH}}$ (0.054 mmol) dissolved in 10 mL of CH_2Cl_2 was then added to the solution. The resulting reaction mixture was stirred in the dark for 90 min at room temperature. Thereafter, the reaction mixture was filtered to get rid of the *N*,*N*'-dicyclohexylurea. Subsequently, the corresponding polymer $\mathbf{P^{RA}}$ was obtained precipitation into hexane (5 times) and by removal of the volatiles under reduced pressure at room temperature.

Coupling of DY590 to $\mathbf{P^{OH}}$ or $\mathbf{P^{RA}}$

240 mg $\mathbf{P^{OH}}$ or $\mathbf{P^{RA}}$ and 1 mg of DY590 were dissolved in 8 mL of CH_2Cl_2 and stirred for overnight at room temperature in the dark. The resulting products were obtained by precipitating in hexane and drying under reduced pressure.

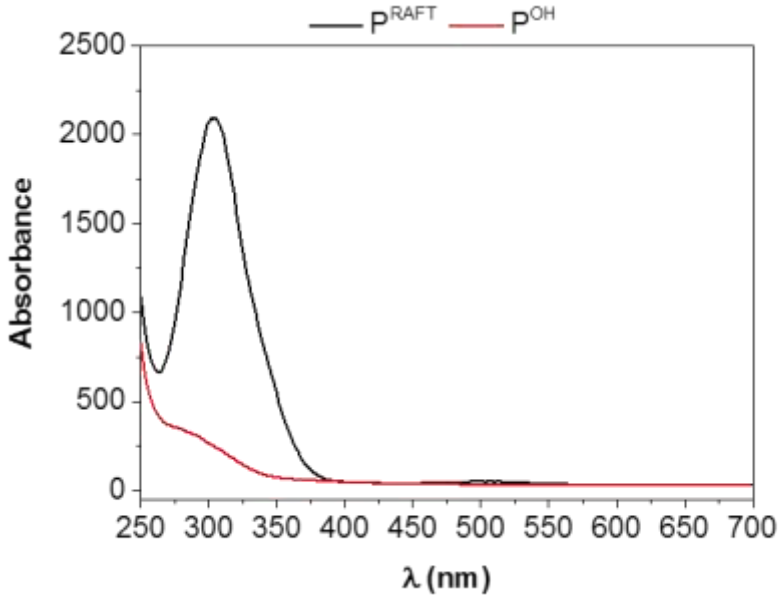

Figure S1. UV/vis spectra of $\mathbf{P^{RAFT}}$ and $\mathbf{P^{OH}}$ in $CHCl_3$.

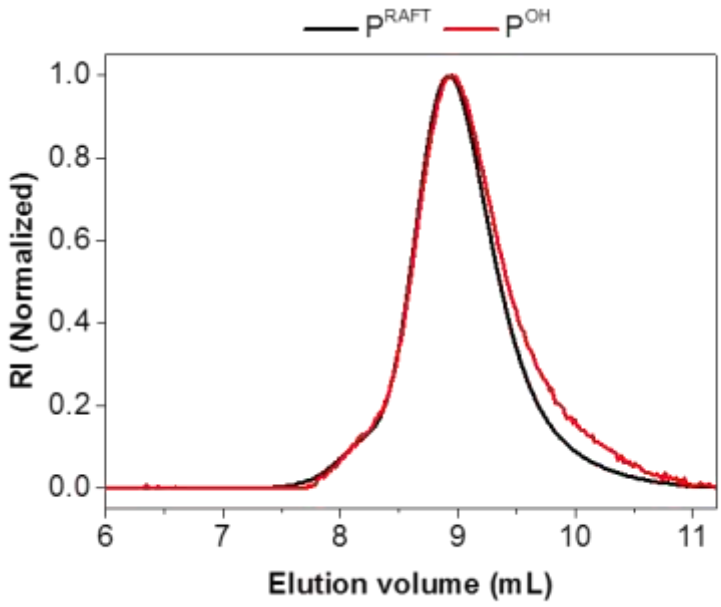

Figure S2. Normalized SEC (RI detection) traces in $CHCl_3$ of $\mathbf{P^{RAFT}}$ and $\mathbf{P^{OH}}$.

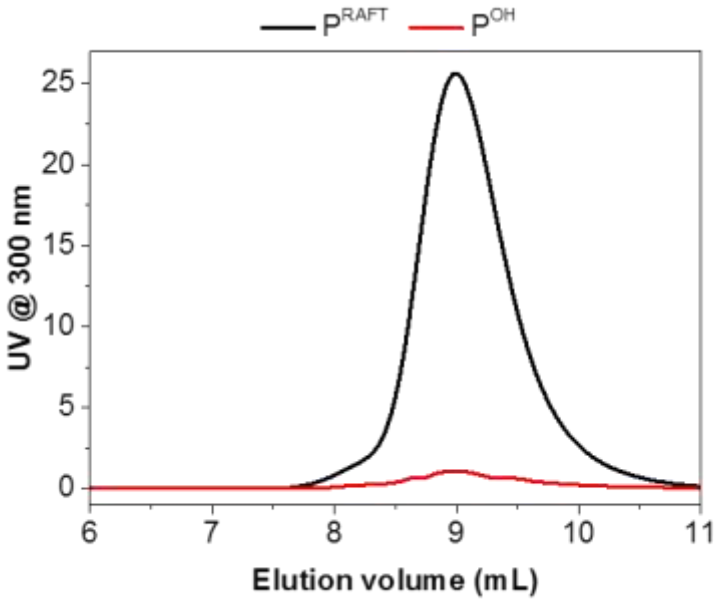

Figure S3. Calibrated SEC (UV detection) traces in $CHCl_3$ of $\mathbf{P^{RAFT}}$ and $\mathbf{P^{OH}}$.

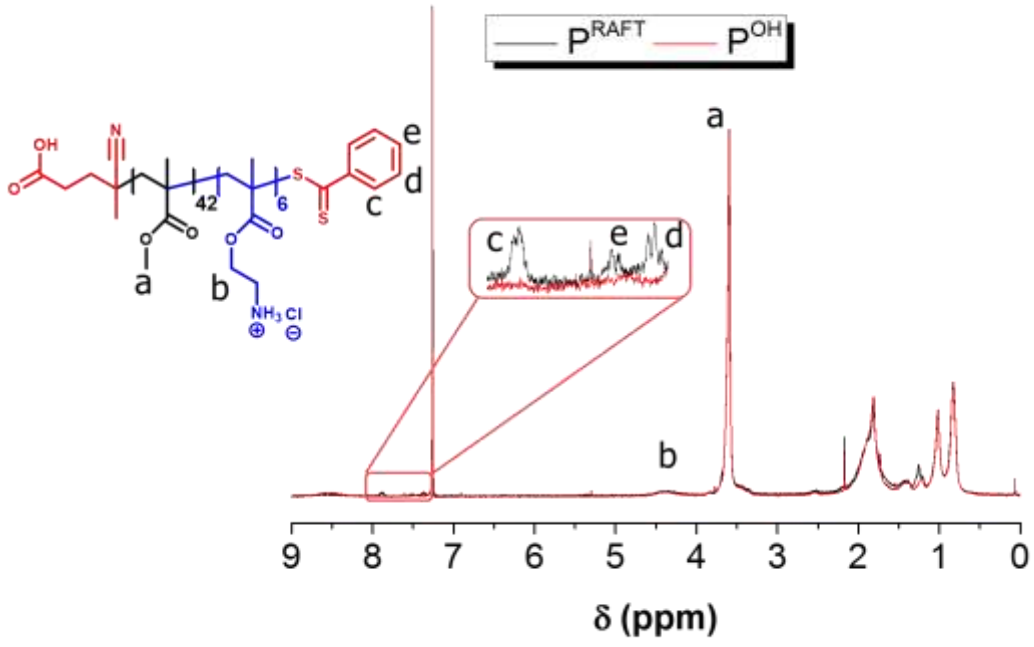

Figure S4. ^{1}H NMR overlay spectra (300 MHz, $CDCl_3$) of $\mathbf{P^{RAFT}}$ and $\mathbf{P^{OH}}$.

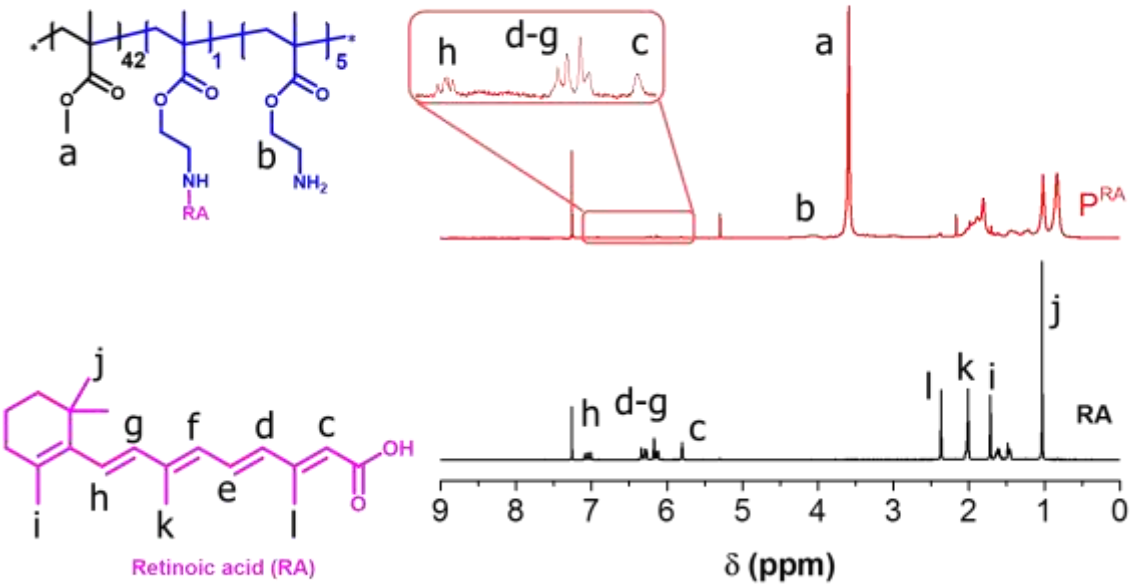

Figure S5. ^{1}H NMR spectra (300 MHz, $CDCl_3$) of retinoic acid (RA) and RA coupled polymer ($\mathbf{P^{RA}}$).

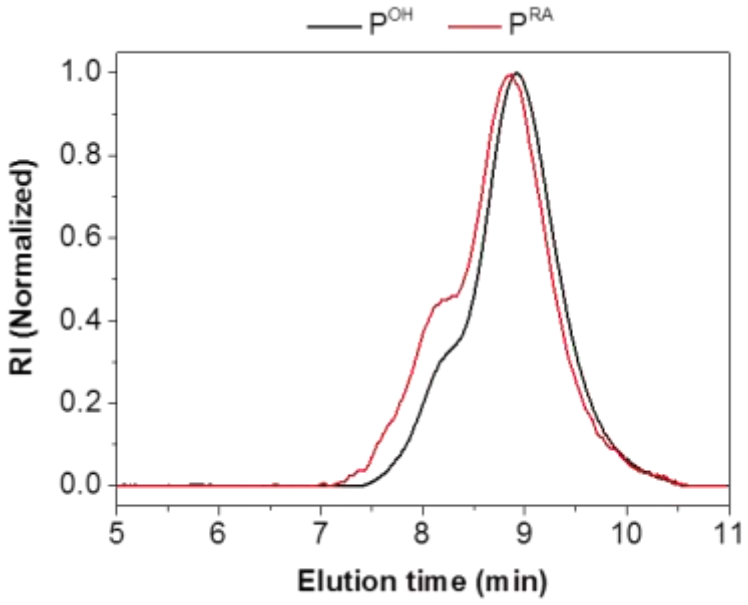

Figure S6. Normalized SEC (RI detection) traces in $CHCl_3$ of $\mathbf{P^{RAFT}}$ and $\mathbf{P^{OH}}$.

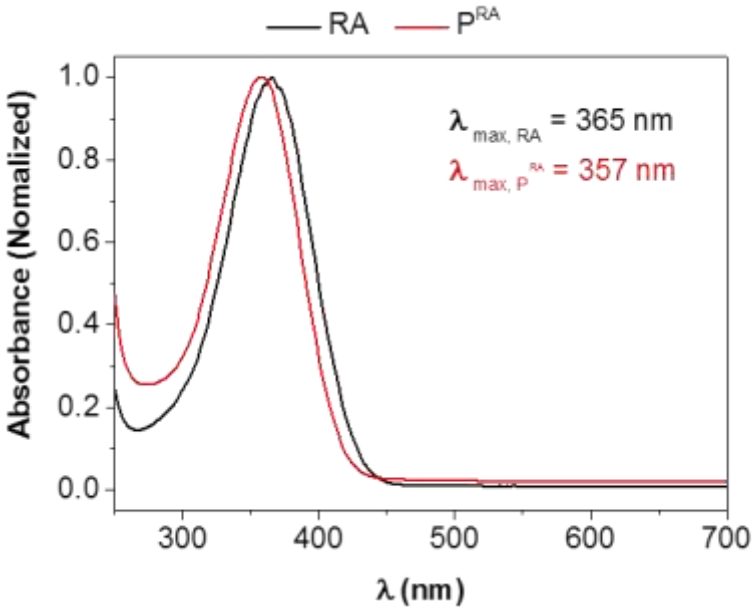

Figure S7. Normalized UV/vis spectra of retinoic acid (RA) and retinoic acid coupled polymer $\mathbf{P^{RA}}$ in $CHCl_3$.

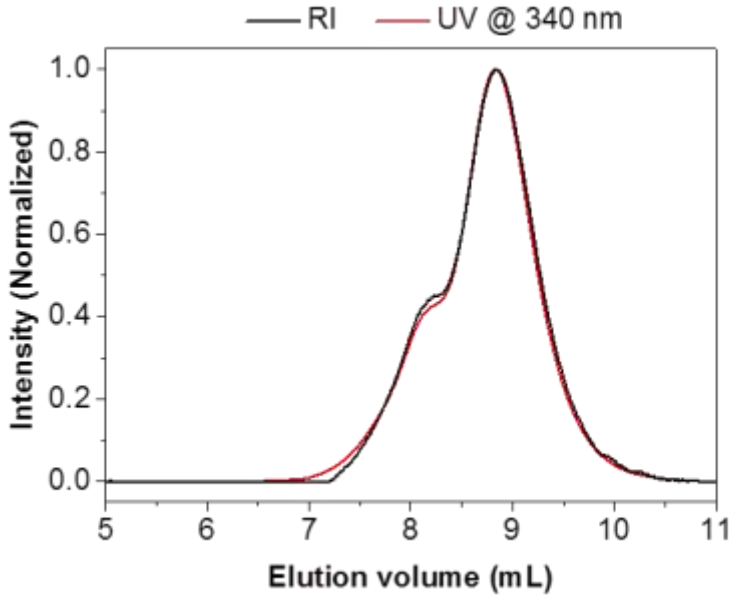

Figure S8. Normalized SEC traces in $CHCl_3$ of $\mathbf{P^{RA}}$ (RI and UV at 340 nm).

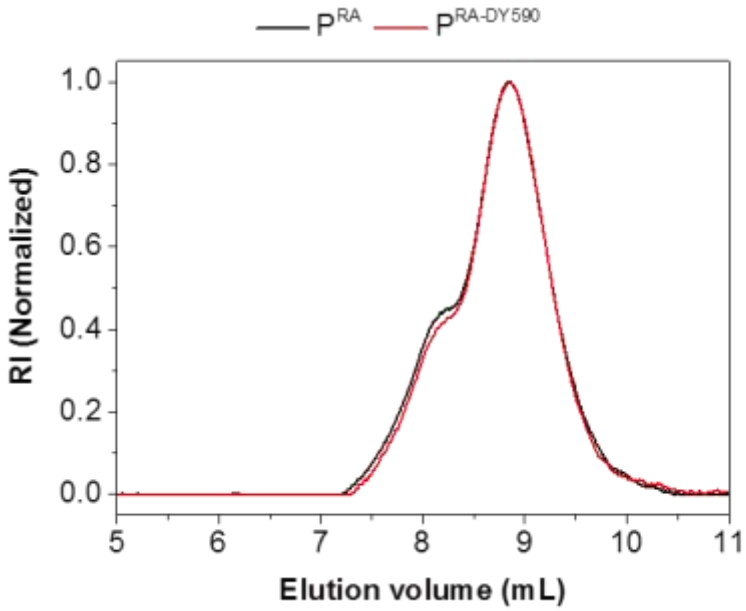

Figure S9. Normalized SEC (RI detection) traces in $CHCl_3$ of $\mathbf{P^{RA}}$ and $\mathbf{P^{RA\text{-}DY590}}$.

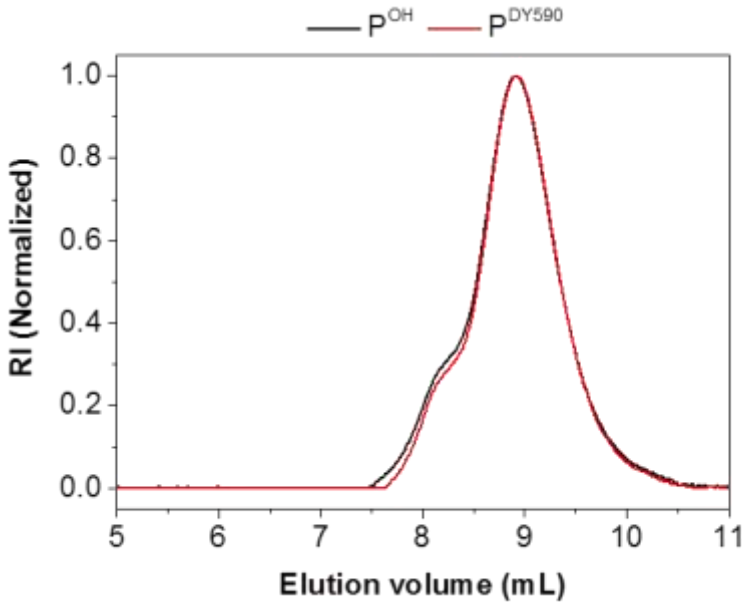

Figure S10. Normalized SEC (RI detection) traces in $CHCl_3$ of $\mathbf{P^{OH}}$ and $\mathbf{P^{DY590}}$.

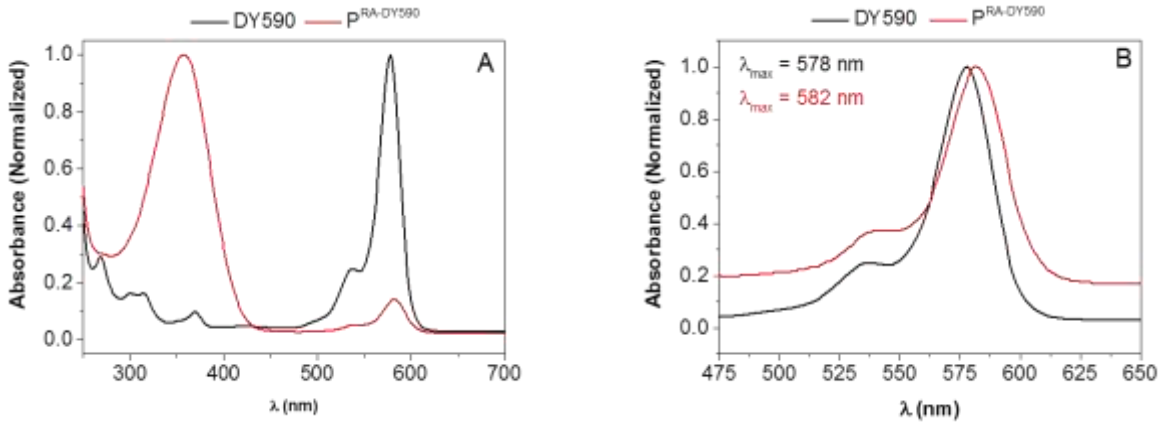

Figure S11. (A) Normalized UV/vis spectra of DY590 and retinoic acid (RA) as well as DY590 coupled polymer $\mathbf{P^{RA\text{-}DY590}}$ in $CHCl_3$. (B) Normalized UV/vis spectra (between 475-650 nm) of DY590 and retinoic acid (RA) as well as DY590 coupled polymer $\mathbf{P^{RA}}$.

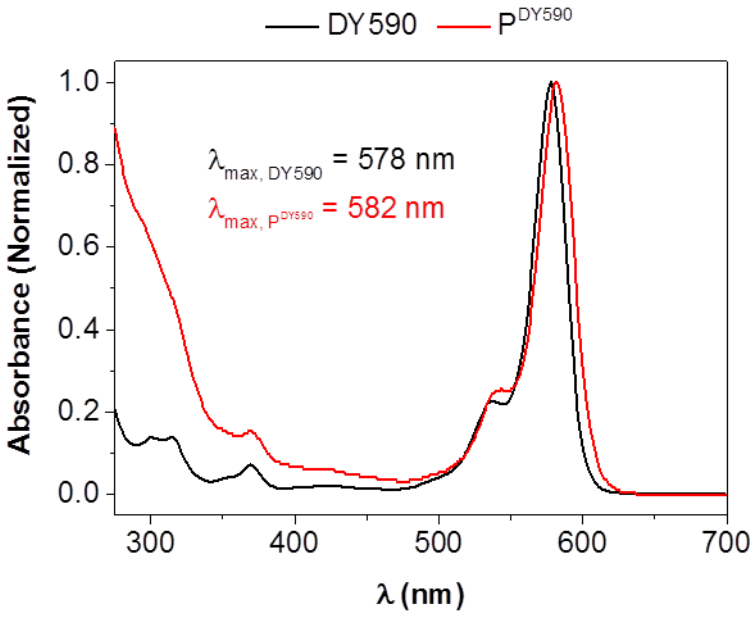

Figure S12. Normalized UV/vis spectra of DY590 and DY590 coupled polymer $\mathbf{P^{DY590}}$ in $CHCl_3$.

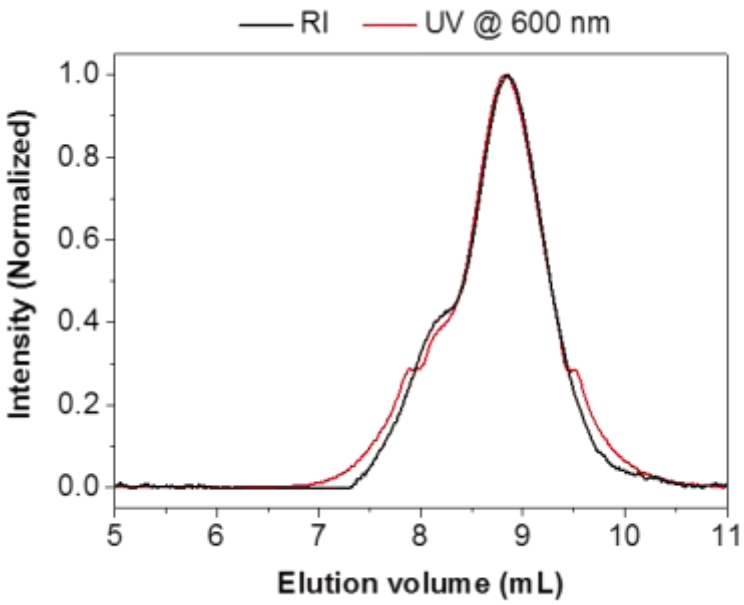

Figure S13. Normalized SEC traces in $CHCl_3$ of $\mathbf{P}^{\mathbf{RA\text{-}DY590}}$ (RI and UV at 600 nm).

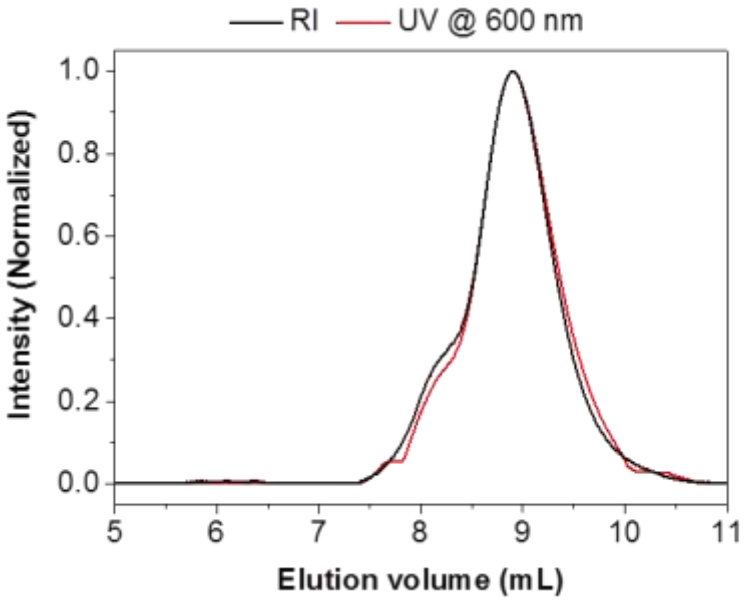

Figure S14. Normalized SEC traces in $CHCl_3$ of $\mathbf{P}^{\mathbf{DY590}}$ (RI and UV at 600 nm).

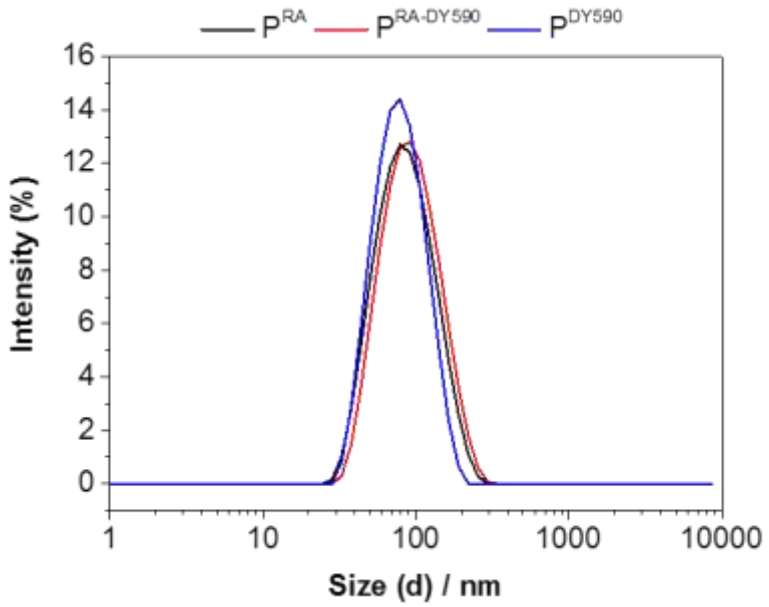

Figure S15. Intensity size distributions of the nanoparticles in water with an initial acetone-polymer concentration of 4 mg mL^{-1}, prepared by dropping acetone-polymer solution to water.

Table S1. Selected characterization results of the prepared nanoparticles.

Entry	Z-average [d, nm][a]	PDI[a]	ζ-potential[b]
P^{RA}	78 ± 1	0.17 ± 0.01	+ 28 ± 7
$P^{RA\text{-}DY590}$	85 ± 1	0.18 ± 0.01	+ 49 ± 3
P^{DY590}	72 ± 1	0.12 ± 0.02	+ 30 ± 5

[a] Average values of three DLS measurements. [b] Average values of three ζ-potential measurements in pure water.

References

1. M. E. Winter, *Proc. SPIE*, 1999, **3753**, 266-275.
3. A. T. Press, A. Traeger, C. Pietsch, A. Mosig, M. Wagner, M. G. Clemens, N. Jbeily, N. Koch, M. Gottschaldt, N. Bézière, V. Ermolayev, V. Ntziachristos, J. Popp, M. M. Kessels, B. Qualmann, U. S. Schubert and M. Bauer, *Nature Communications*, 2014, **5**, 5565.
4. M. Dietrich, M. Glassner, T. Gruendling, C. Schmid, J. Falkenhagen and C. Barner-Kowollik, *Polym. Chem.*, 2010, **1**, 634-644.

Publication P4

“Dual responsive nanoparticles from a RAFT copolymer library for the controlled delivery of doxorubicin”

T. Yildirim, A. Traeger, E. Preussger, S. Stumpf, C. Fritzsche, S. Hoeppener, S. Schubert, U. S. Schubert

Macromolecules **2016**, *49*, 3856-3868.

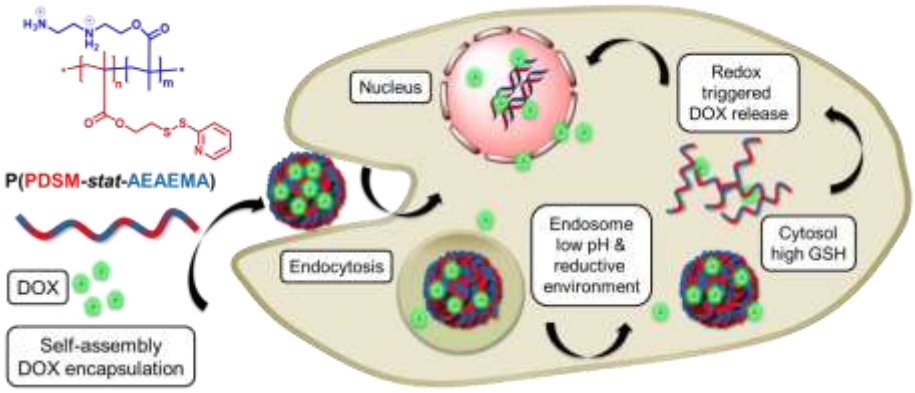

Macromolecules

Article

pubs.acs.org/Macromolecules

Dual Responsive Nanoparticles from a RAFT Copolymer Library for the Controlled Delivery of Doxorubicin

Turgay Yildirim,[†,‡] Anja Traeger,[†,‡] Elisabeth Preussger,[†,‡] Steffi Stumpf,[†,‡] Carolin Fritzsche,[†,‡] Stephanie Hoeppener,[†,‡] Stephanie Schubert,[*,‡,§] and Ulrich S. Schubert[*,†,‡]

[†]Laboratory of Organic and Macromolecular Chemistry (IOMC), Friedrich Schiller University Jena, Humboldtstrasse 10, 07743 Jena, Germany

[‡]Jena Center for Soft Matter (JCSM), Friedrich Schiller University Jena, Philosophenweg 7, 07743 Jena, Germany

[§]Institute of Pharmacy, Department of Pharmaceutical Technology, Friedrich Schiller University Jena, Otto-Schott-Strasse 41, 07745 Jena, Germany

Supporting Information

ABSTRACT: In this study, we designed, synthesized, and characterized a novel pH- and redox responsive nanoparticle system for the enhanced spatial delivery of hydrophobic drugs. A statistical copolymer library of pyridyldisulfide ethyl methacrylate (PDSM) with different compositions of 2-((*tert*-butoxycarbonyl)(2-((*tert*-butoxycarbonyl)amino)ethyl)amino)-ethyl methacrylate (BocAEAEMA) was synthesized using the reversible addition−fragmentation chain transfer (RAFT) polymerization process. The controlled nature of the radical polymerization was demonstrated by a kinetic study. The Boc-groups were cleaved to obtain the desired amino functional copolymers. Nanoparticles were prepared by nanoprecipitation and characterized by dynamic light scattering (DLS), scanning electron microscopy (SEM), and transmission electron microscopy (TEM). Differently sized nanoparticles that have monomodal size distributions ranging from 50 to 460 nm with positive ζ-potential values were obtained by varying initial conditions of the formulations. The pH- and redox responsiveness of the nanoparticle systems was investigated by the DLS and ζ-potential measurements. The pH-responsiveness test results demonstrated that the obtained nanoparticles reveal a pH response, such as changes in the size and ζ-potential values upon pH value change. Moreover, redox responsiveness tests revealed the stability of the nanoparticles at a glutathione (GSH) concentration found in the plasma of the human body (10 μM) and the disassembly ability of the nanoparticles in a mimicking intracellular reductive environment (10 mM GSH). The antitumor drug doxorubicin (DOX) was used to investigate the encapsulation and release capability of the nanoparticles. Release studies showed that the DOX release was significantly accelerated in the presence of 10 mM GSH compared to the physiological conditions. Confocal laser scanning microscopy (CLSM) studies indicated that DOX-loaded nanoparticles were taken up efficiently by HEK cells, and DOX was released from the nanoparticles and interacted with the chromosomes in the cell nuclei after 6 h. Cytotoxicity tests revealed that DOX-loaded nanoparticles decreased the cell viability in a concentration and time dependent manner comparable or even better as the free DOX, whereas pure particles are biocompatible.

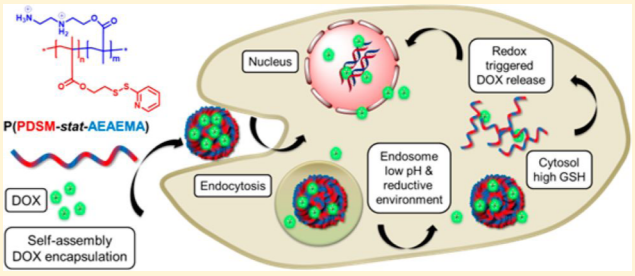

INTRODUCTION

In the past few decades, increasing attention has been drawn on stimuli responsive polymeric nanoparticles, also called "smart nanoparticles", based on their potential applications in life sciences.[1] Smart polymeric nanoparticles respond to various physical (light,[2] temperature,[3] ultrasound,[4] magnetic,[5] and mechanical[6]), chemical (ionic strength,[7] pH value,[8] and redox[9]), or biological (enzyme[10] and receptor[11]) stimuli. Among these, pH- and redox-responsive nanoparticles are regarded as highly promising vehicles for the selective delivery of pharmaceutical agents to the desired sites, in response to specific microenvironmental conditions. Because of the pH value gradients in intracellular pathways (5.0 to 6.0 for endosomes and 4.0 to 5.0 for lysosomes), pH-sensitive polymeric nanoparticles can enhance the therapeutic activity of loaded drugs by spatially controlled release.[12] One of the main strategies to obtain pH-responsive polymeric nanoparticles is incorporating ionizable segments in the backbone of the polymers, such as amino and/or carboxyl groups,[13−15] which can render tunable pH sensitivity to the corresponding nanoparticles. On the other hand, endo-/lysosomes and the cytosol have reductive environments compared to the extracellular compartments due to the active accumulation of proteinogenic cysteine and the presence of reductive enzymes,

Received: December 1, 2015
Revised: April 27, 2016
Published: May 10, 2016

ACS Publications © 2016 American Chemical Society

DOI: 10.1021/acs.macromol.5b02603
Macromolecules 2016, 49, 3856−3868

Scheme 1. Schematic Representation of the RAFT Copolymerization of PDSM with BocAEAEMA

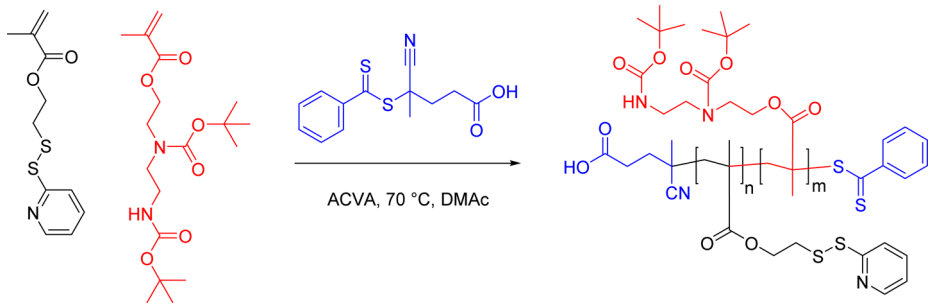

such as gamma-interferon inducible lysosomal thiol reductase (GILT), in lysosomes and the higher glutathione (GSH) concentrations in the cytosol (100−1000 times higher than the extracellular GSH).[16,17] Therefore, redox-sensitive polymeric nanoparticles that respond to reductive environments of endo-/lysosomes or cytosol provide a rationale for the intracellular delivery of pharmaceutical payloads. Accordingly, polymers containing disulfide groups have been intensively investigated for the design of redox responsive nanocarriers for drug delivery applications due to their ability to undergo reduction in the endocytotic pathway and/or in the cytosol.[18−21]

In this study, a library of well-defined statistical copolymers of pyridyldisulfide ethyl methacrylate (PDSM) with different compositions of 2-((*tert*-butoxycarbonyl)(2-((*tert*-butoxycarbonyl)amino)ethyl)amino)ethyl methacrylate (BocAEAEMA) were synthesized using the RAFT polymerization process (Scheme 1) to obtain a novel pH- and redox responsive drug delivery vehicle for the controlled release of doxorubicin (DOX) in the intracellular environment.[22] DOX is a potent anticancer drug used for the treatment of various cancers, such as lung, ovarian, and breast cancer. However, in clinical therapy it suffers from poor aqueous solubility, rapid elimination, severe side effects, low selectivity, and multidrug resistance.[23,24] To overcome these limitations, various drug delivery systems such as dendrimers, micelles, liposomes, and polymeric nanoparticles have been developed. Among these, stimuli-responsive polymeric nanoparticles have emerged as promising candidates for the controlled delivery of DOX owing to their reduced side effects, prolonged circulation time, and increased drug concentration in tumor tissues by the enhanced permeability and retention effect (EPR).[25,26] Dual responsive nanoparticles are designed in such a way that (i) PDSM is used as GSH responsive moiety,[27−30] which is well-known for exhibiting a GSH response due to the pyridyldisulfide groups that undergo direct coupling with free thiols under ambient conditions; (ii) additionally AEAEMA is used as pH-responsive functionality since it contains primary and secondary amino groups in the side chain. The relatively new amino methacrylate (BocAEAEMA) was chosen, which has been recently polymerized for the first time via the RAFT polymerization technique by the groups of Bulmus and Becer.[31] To investigate the effect of the amino content on the size and stimuli response of the corresponding nanoparticles, the copolymer composition was varied by using different monomer feed ratios. The AEAEMA content in the copolymers was kept low (up to 50%) because of the required hydrophobicity of the copolymers to form nanoparticles.[32,33] The reported polymer design has the following advantages over previously reported drug delivery systems based on amphiphilic block copolymers. First, a statistical monomer distribution within the polymers was chosen because block copolymers with an amphiphilic character may self-assemble into micelles. However, beyond their critical micelle concentration (CMC), polymeric micelles can disintegrate into unimers *in vivo*, resulting in premature release of their payloads in undesired locations.[34] Moreover, statistical copolymer assemblies may provide a certain fraction of surface exposed functional hydrophobic moieties, which can enable decoration of corresponding assemblies with ligands and/or functional molecules, unlike the block copolymer assemblies, where the hydrophobic units are hidden in the core of the micelles or bilayer of the vesicles.[35,36] Additionally, our synthetic approach involves only a facile one-step reaction. This is an advantage over the block copolymer synthesis, which involves sequential controlled polymerizations or postpolymerization treatments.[37,38] Second, AEAEMA moieties in the copolymers render cationic surface charge to the corresponding nanoparticles. This can enhance the cell internalization of the nanoparticles. It is known that cationic nanoparticles are more rapidly internalized by the cells compared to negatively charged and neutral ones due to their high affinity for the negatively charged phospholipid bilayer of cell membranes.[39] Moreover, primary amino functionality of the AEAEMA can allow conjugation to other molecules such as proteins and polypeptides.[40] Third, a serious challenge for successful drug delivery into the cytosol of cells is the endosomal escape.[41] Disruption of endosomal membranes via the proton-sponge effect is one approach to overcome this challenge. AEAEMA's half spermine/spermidine like structure, which possibly causes the proton-sponge effect in the acidic environment of endosomes,[42] can provoke endosomal rupturing. Finally, the ability of the PDSM-based nanoparticles to encapsulate and release guest molecules using the redox trigger can sustain the targeted spatial drug delivery in the endo-/lysosomes or in the cytosol.

EXPERIMENTAL SECTION

Materials. The monomers pyridyldisulfide ethyl methacrylate (PDSM) and 2-((*tert*-butoxycarbonyl)(2-((*tert*-butoxycarbonyl)amino)ethyl)amino)ethyl methacrylate (BocAEAEMA) were synthesized according to the procedures reported elsewhere (see Supporting Information for detailed NMR studies).[31,43] *N*-Hydroxyethylethylenediamine, di-*tert*-butyldicarbonate, methacryloyl chloride, aldrithiol-2, 2-mercaptoethanol, glacial acetic acid, 4,4′-azobis(4-cyanopentanoic acid) (ACVA), 4-cyano-4-(phenylcarbonothioylthio) pentanoic acid (CPADB), 1,3,5-trioxane, *N*,*N*-dimethylacetamide (DMAc), reduced L-glutathione and pyrene were purchased from Sigma-Aldrich. Doxorubicin hydrochloride (DOX) was purchased from Cayman Chemical. AlamarBlue and Hoechst 33342 were obtained from Thermo Fischer. If not stated otherwise, cell culture materials, cell culture media, and solutions were obtained from Biochrom. All other

DOI: 10.1021/acs.macromol.5b02603
Macromolecules 2016, 49, 3856−3868

Table 1. Selected Characterization Data of the PDSM (M1) Copolymers with BocAEAEMA (M2)

entry	total monomer/CTA/ACPA	f(M1/M2)[a]	F(M1/M2)[b]	convn [%][c] M1/M2	$M_{n,theo.}$[d] [g mol^{-1}]	DP[c] M1/M2	M_n[c] [g mol^{-1}]	$M_{n,SEC}$[e] [g mol^{-1}]	$Đ_M$[e]	$M_{n,SEC}$[f] [g mol^{-1}]	$Đ_M$[f]
P1[g]	38.07/1/0.25			76/0	7700	24/0	6400	7200	1.22	7300	1.18
P2	37.19/1/0.25	19.0	19.1	78/60	7700	23/1.2	6600	6600	1.15	7000	1.13
P3	36.40/1/0.25	9.0	11.1	73/62	7200	21/1.9	6300	7200	1.20	7400	1.15
P4	35.62/1/0.25	5.7	7.5	87/67	8300	24/3.2	7600	8300	1.14	8300	1.14
P5	34.86/1/0.25	4.0	5.5	75/60	7200	21/3.8	7000	7500	1.17	8000	1.14
P6	33.42/1/0.25	2.3	3.5	78/70	7600	19/5.5	7200	8600	1.16	9200	1.13
P7	32.17/1/0.25	1.5	2.5	78/68	7400	17/6.8	7200	9100	1.10	10 000	1.09
P8	29.86/1/0.25	0.7	1.0	83/74	7700	11/11	7200	8600	1.13	9700	1.12
P9[h]	25.92/1/0.25			0/69	6900	0/18.3	7100	6100	1.07	7600	1.08

[a]Initial monomer feed ratio. [b]Monomer ratio in the isolated copolymer. [c]Determined by ^{1}H NMR spectroscopy. [d]Determined by the formula $M_{n,theo.} = [([M]_{M1}/[CTA] \times convn \times M_{M1}) + ([M]_{M2}/[CTA] \times convn \times M_{M2}) + (M_{CTA})]$. [e]Determined by SEC in $CHCl_3$ analysis (RI detection, PS calibration). [f]Determined by SEC in DMAc analysis (RI detection, PS calibration). [g]Homopolymer of the PDSM. [h]Homopolymer of the BocAEAEMA.

chemicals were obtained from standard suppliers and used without purification unless specified.

Instruments and Methods. Proton nuclear magnetic resonance (^{1}H NMR) spectra were recorded at room temperature in $CDCl_3$ or CD_3OD on a Bruker Avance 300 or 400 MHz using the residual solvent resonance as an internal standard. The chemical shifts are given in ppm.

Size-exclusion chromatography (SEC) measurements were performed on two different set-ups. SEC in $CHCl_3$: Shimadzu system equipped with a SCL-10A system controller, a LC-10AD pump, a RID-10A refractive index detector, SPD-10AD VP (UV detector), and a PSSSDV-linear S column (5 μm particle size; Polymer Standards Service GmbH, Mainz, Germany) at 40 °C using a chloroform, triethylamine, and 2-propanol (94:4:2) mixture as eluent at a flow rate of 1 mL min^{-1}. The system was calibrated with polystyrene (PS) standards (M_p = 370 to 128 000 g mol^{-1}). SEC in DMAc: Agilent 1200 series equipped with a G1310A pump, a G1315D DA detector, a G1362A RI detector, and PSS GRAM 30 Å/1000 Å (10 μm particle size) columns in series at 40 °C using *N*,*N*-dimethylacetamide (DMAc) with 2.1 g L^{-1} LiCl as eluent at a flow rate of 1 mL min^{-1}. The system was calibrated with polystyrene (PS) standards (M_p = 100 to 1 000 000 g mol^{-1}).

Dynamic light scattering was performed on a Zetasizer Nano ZS (Malvern Instruments, Herrenberg, Germany). After an equilibration time of 180 s, 3 × 30 runs were carried out at 25 °C (λ = 633 nm). The counts were detected at an angle of 173°. Each measurement was performed in triplicate. The mean particle size was approximated as the effective (*Z*-average) diameter and the width of the distribution as the polydispersity index of the particles (PDI) obtained by the cumulants method assuming a spherical shape of the nanoparticles.

Electrophoretic light scattering was used to measure the electrokinetic potential, also known as ζ-potential. The measurements were performed on a Zetasizer Nano ZS (Malvern Instruments, Herrenberg, Germany) by applying laser Doppler velocimetry. For each measurement, 10 runs were carried out using the slow-field and fast-field reversal mode at 150 V. Each experiment was performed in triplicate at 25 °C.

For scanning electron microscopy (SEM), 5 μL of the suspensions were placed on a mica surface and dried overnight at room temperature under atmospheric pressure. Afterward, samples were investigated using a Sigma VP field emission scanning electron microscope (Carl-Zeiss AG, Germany). The samples were coated with a thin layer (4 nm) of platinum via sputter coating using a Bal-TEC 020 HR Sputtering Coater.

Transmission electron microscopy (TEM) was carried out on a FEI Technai G^2 20 transmission electron microscope.

The fluorescence spectra of pyrene solutions were recorded on a Jasco FP-6500 fluorometer applying an excitation wavelength of 335 nm. The emission spectra were recorded from 350 to 600 nm. The excitation and emission bandwidths were 5.0 and 5.0 nm, respectively.

Synthesis. *RAFT Polymerization.* PDSM was copolymerized with BocAEAEMA using CPADB as chain transfer agent (CTA) and ACVA as initiator. The initial monomer feed ratios of the monomers and overall monomer to CTA ratio was varied. All polymerizations were carried out at 70 °C for 8 h in an oil bath. The polymerizations were performed in a 0.5 M DMAc solution. The used initial feed ratios are summarized in Table 1. An exemplary RAFT copolymerization procedure (Table 1, **P5**) is as follows: 400 mg PDSM (1.567 mmol), 146 mg BocAEAEMA (0.392 mmol), 15.7 mg CPADB (0.056 mmol) and 3.94 mg ACVA (0.014 mmol) were dissolved in DMAc in a Biotage microwave reaction vial (5 mL) equipped with a magnetic stir bar. The total volume of the reaction mixture was 3.92 mL. After the reaction was degassed for 40 min by argon purging, the t_0 sample for ^{1}H NMR was taken, and the flask was immersed in a preheated oil bath under stirring at 70 °C. After 8 h, the polymerization was stopped by cooling to room temperature and exposing to air. Monomer conversions were determined via ^{1}H NMR by using 1,3,5-trioxane as internal standard. The polymer was purified by precipitating in cold diethyl ether (2 times). The resulting pink colored polymer was dried under high vacuum at room temperature until constant weight to produce an overall yield of 70%. The number-average molar mass (M_n) and molar mass dispersity ($Đ_M$) were determined by two different SEC systems by using PS standards. SEC in $CHCl_3$: M_n = 7,500 g mol^{-1} and $Đ_M$ = 1.17. SEC in DMAc: M_n = 8,000 g mol^{-1} and $Đ_M$ = 1.14. ^{1}H NMR ($CDCl_3$, 300 MHz): δ = 8.45, 7.65, and 7.08 (Ar−H, PDSM), 7.87, 7.52, and 7.36 (Ar−H, CPADB), 4.22 (−OC*H*2CH2−S−S−), 4.02 (−OCH_2CH$_2$−N−), 3.30 (−CH_2−N(COO(CH$_3$)$_3$−CH_2−CH_2−NH(COO(CH$_3$)$_3$)), 3.01 (−OCH$_2$CH_2−S−S−), 2.50 (−CH$_2$CH_2CO$_2$OH, CPDB), 2.4−0.7 (backbone), 1.41 (−CO$_2$OC(CH_3)$_3$) ppm.

The degree of polymerization (DP) for each polymer was calculated from the signal integrals in the ^{1}H NMR spectrum (Figure S5) of the purified copolymer using the following equations:

$$DP_{PDSM} = \frac{I(peak\ b)/2}{I(peak\ f)/2} \quad (1)$$

$$DP_{BocAEAEMA} = \frac{I(peak\ b')/6}{I(peak\ f)/2} \quad (2)$$

with *I(peak b)* corresponding to the integral of the methylene proton peaks of the PDSM at 3.02 ppm, *I(peak b′)* corresponding to the integral of methylene proton peaks of the BocAEAEMA at 3.31 ppm, and *I(peak f)* corresponding to the integral of two methylene protons of the dithiobenzoate end group at 2.52 ppm. Molar mass values were calculated by using the following equation:

$$M_{n,NMR} = (DP_{PDSM} \times M_{PDSM}) + (DP_{BocAEAEMA} \times M_{BocAEAEMA}) + M_{CTA} \quad (3)$$

DOI: 10.1021/acs.macromol.5b02603
Macromolecules 2016, 49, 3856−3868

in which the molar masses of the PDSM, BocAEAEMA, and RAFT agent are 255.35 g mol^{-1}, 372.46 g mol^{-1}, and 279.38 g mol^{-1}, respectively.

Kinetic Study of the Polymerization. During polymerization of **P7**, aliquots of 0.2 mL were taken periodically from the reaction mixture by a syringe purged with argon. From each sample, conversions were calculated via ^{1}H NMR by using 1,3,5-trioxane as internal standard. Molar masses and dispersities were determined via SEC analysis (DMAc, RI detection).

Deprotection of the Polymers. Trifluoroacetic acid was used for the removal of Boc-groups from BocAEAEMA containing polymers (**P2**–**P9**). An exemplary deprotection reaction procedure (Table 1, **P5**) is as follows: **P5** was dissolved in CH_2Cl_2 (2 mL). Trifluoroacetic acid (1 mL) was added dropwise into the solution at 0 °C. The final solution was stirred at room temperature for 40 min. The volatiles were removed by purging N_2 at room temperature. The residue was redissolved in a minimum amount of methanol and precipitated in diethyl ether. The resulting polymer was dried under high vacuum at room temperature. M_n and $Đ_M$ values were determined by SEC in DMAc by using PS standards. SEC in DMAc: M_n = 8,000 g mol^{-1} and $Đ_M$ = 1.14. ^{1}H NMR ($CDCl_3$, 300 MHz): δ = 8.45, 7.65, and 7.08 (Ar–H, PDSM), 7.87, 7.52, and 7.36 (Ar–H, CPADB), 4.22 ($-OCH_2CH_2-S-S-$), 4.02 ($-OCH_2CH_2-N-$), 3.30 ($-CH_2-N-(COO(CH_3)_3-CH_2-CH_2-NH(COO(CH_3)_3)$), 3.01 ($-OCH_2CH_2-S-S-$), 2.50 ($-CH_2CH_2CO_2OH$, CPDB), 2.4–0.7 (backbone) ppm.

Preparation of the Nanoparticle Suspensions. For nanoprecipitation, the corresponding polymers (deprotected form of **P2**, **P3**, and **P4**) were dissolved in acetone at a final concentration of 5 or 3 mg mL^{-1}, respectively, and subsequently added dropwise to deionized water under continuous stirring at 500 rpm (acetone to water, AW method). For the water to acetone (WA) method, deionized water was added dropwise to the acetone polymer solution under stirring at 500 rpm. The acetone/water (solvent/nonsolvent) ratio was kept constant at 0.5 for all suspensions. After removal of the acetone by stirring overnight at room temperature (GC analysis ensured complete removal of the acetone), the nanoparticles were characterized by DLS (performed in pure water) and SEM without filtration.

pH-Response Test of the Nanoparticles. For the pH-response test of the nanoparticles, nanoparticle suspensions that were derived from the deprotected form of **P2**, **P3**, and **P4** by the WA method with an initial acetone polymer concentration of 5 mg mL^{-1} were used. In a typical experiment, the **P2** nanoparticle suspension (2 mL, c = 2.5 mg mL^{-1}) was diluted to a final volume of 50 mL (c = 0.1 mg mL^{-1}), and the pH value was recorded. The final suspension was divided into two equal volumes. The resulting suspensions were titrated with 0.01 M HCl or 0.01 M NaOH. During titrations, 650 μL suspensions were taken periodically. For each sample, DLS and ζ-potential measurements were performed.

Redox-Response Test of the Nanoparticles. For the redox response test of the nanoparticles, nanoparticle suspensions that were derived from the deprotected form of **P2**, **P3**, and **P4** by utilizing the WA method with an initial acetone polymer concentration of 5 mg mL^{-1} or 3 mg mL^{-1} were used. In a typical experiment, the **P2** nanoparticle suspension (50 μL, c = 2.5 mg mL^{-1}) was diluted to a final volume of 325 μL (c = 0.385 mg mL^{-1}). The final suspension was mixed with 325 μL of 20 mM or 20 μM glutathione in a DLS cuvette. The temperature of the DLS was set to 37 °C and the attenuation level was set to 7. DLS measurements were performed periodically to follow the change in size distribution and signal strength.

Fluorescence Spectroscopic Study of the Nanoparticles. A 100 μL aliquot of stock solution of pyrene (120×10^{-5} mol L^{-1}) in acetone was added to 1 mL of the nanoparticle suspensions (1.5 mg mL^{-1}). The samples were incubated at 37 °C for 24 h to remove acetone and to give a final pyrene concentration of 12×10^{-5} mol L^{-1}. 50 μL of the final suspensions were mixed with 950 μL of pure water and 1 mL of 20 mM glutathione in Eppendorf vials to give a final pyrene concentration of 6×10^{-6} mol L^{-1}. The temperature of the vials was set to 37 °C. Fluorescence measurements were performed periodically to follow the change in fluorescence emission intensity.

For the pH dependent pyrene fluorescence intensity study, 40 μL of a **P2** nanoparticle suspension with a pyrene concentration of 12×10^{-5} mol L^{-1} was mixed with 1950 mL 0.1 M buffer solutions at various pH values to give a final pyrene concentration of 4.8×10^{-6} mol L^{-1} and to give a nanoparticle concentration of 0.060 mg mL^{-1}. Fluorescence measurements were performed to follow the change in fluorescence emission intensity.

Encapsulation of DOX. For DOX encapsulation, **P3-d** (30 mg) and DOX (3 mg) were dissolved in 3 mL DMF. Subsequently, 6 mL of deionized water was added dropwise to the DMF solution under continuous stirring at 500 rpm. Excess drug and DMF were removed by dialysis (1 L, 24 h; MWCO: 3500 g/mol) against deionized water. External medium was renewed four times in the course of dialysis. Total concentration of the DOX-loaded nanoparticle suspension concentration after dialysis was found as 1.39 mg/mL. The amount of DOX in the nanoparticles was calculated by two different methods allowing a cross-check. First, DOX-loaded nanoparticle suspensions were freeze-dried, dissolved in DMF, and analyzed by UV–vis spectroscopy. Second, fluorescence emission intensity of the DOX-loaded nanoparticle suspension at $\lambda_{ex}/\lambda_{em}$ 478/598 nm was measured in deionized water. Quantification was performed using UV-vis absorbance calibration function of DOX in DMF (Figure S6) and fluorescence intensity calibration function of DOX in deionized water (Figure S7).

Drug loading efficiency (DLE) and drug loading content (DLC) were calculated according to the following equations:

$$\text{DLE} = \frac{\text{mass of the loaded drug}}{\text{mass of the drug in feed}} \times 100\% \quad (4)$$

$$\text{DLC} = \frac{\text{mass of the loaded drug}}{\text{total mass of polymer and loaded drug}} \times 100\% \quad (5)$$

Release Studies of DOX. The release of the DOX from the nanoparticle suspensions were investigated at 37 °C under three different conditions: (i) Acetate buffer (100 mM, pH 5.0) containing 10 mM GSH, (ii) PBS buffer (100 mM, pH 7.4) containing 10 mM GSH. A 3 mL aliquot of DOX-loaded nanoparticle suspensions in deionized water was added into a dialysis bag (MWCO: 3500 g/mol) and soaked in a glass bottle containing 55 mL of appropriate buffer and gently stirred. At various time intervals, 1 mL of the release media was taken out and replenished with an equal volume of fresh media. The amount of released DOX was calculated by fluorescence measurements as mentioned above.

Cell Lines and Culture Conditions. The cell lines L929 (CCL-1, ATCC) and HEK-293 (CRL-1573, ATCC) were cultured in DMEM culture media and RPMI 1640 medium supplemented with 10% fetal calf serum (FCS), 100 μg mL^{-1} streptomycin and 100 IU mL^{-1} penicillin, respectively. The cells were cultured at 37 °C in humidified 5% CO_2 atmosphere.

Cytotoxicity Test of Pure and DOX-Loaded Nanoparticles. The cytotoxicity was tested with L929 cells, as this sensitive cell line is recommended by ISO10993–5 (n = 3 × 6). In detail, cells were seeded at 10^4 cells per well in a 96-well plate and were incubated for 24 h. No cells were seeded in the outer wells. Afterward, the media were replaced by fresh media and incubated for 30 min. The nanoparticle suspensions were added in the indicated end concentration range, and the cells were incubated at 37 °C for 24 and 48 h. Subsequently, the medium was replaced by fresh medium and AlamarBlue as recommended by the supplier. After incubation for 4 h, the fluorescence intensity was measured at Ex 570/Em 610 nm, with untreated cells on the same well plate serving as controls.

Live Cell Imaging of Pure and DOX-Loaded Nanoparticles. As recommended, HEK-293 cells were used for uptake studies. Therefore, cells (10^5 cells mL^{-1}) were seeded on glass-bottomed dishes and cultured for 24 h in a humidified atmosphere. One hour prior to the addition of nanoparticles, the medium was replaced with fresh one. Nanoparticles were added to the cells and incubated for 6 and 24 h. Afterward, Hoechst 33342 for nucleus staining was added to the media. Imaging was performed with a LSM880, Elyra PS.1 system

DOI: 10.1021/acs.macromol.5b02603
Macromolecules 2016, 49, 3856–3868

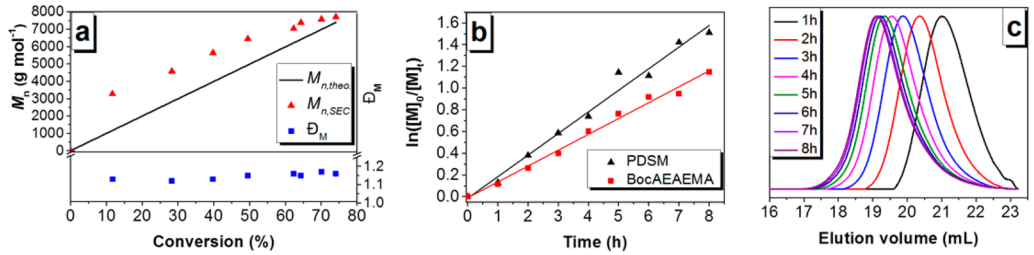

Figure 1. Kinetic studies of the RAFT copolymerization of PDSM with BocAEAEMA. [PDSM]/[BocAEAEMA]/[CPADB]/[AIBN] = 23.42/10.05/1/0.25; $[M]_0$ = 0.5 mol L^{-1}. Polymerization conditions: Solvent DMAc, T = 70 °C. (a) M_n and $Đ_M$ evolution with total monomer conversion. (b) Semilogarithmic kinetic plot. (c) SEC in DMAc overlay curves.

(Zeiss, Oberkochen, Germany) applying a 63 × 1.4 NA plan apochromat oil objective. Excitation wavelengths of 405 nm (excitation grating 23.0 μm) and 488 nm (excitation grating 28.0 μm) were used.

RESULTS AND DISCUSSION

A library of statistical copolymers of PDSM and BocAEAEMA was synthesized via the RAFT polymerization process. In order

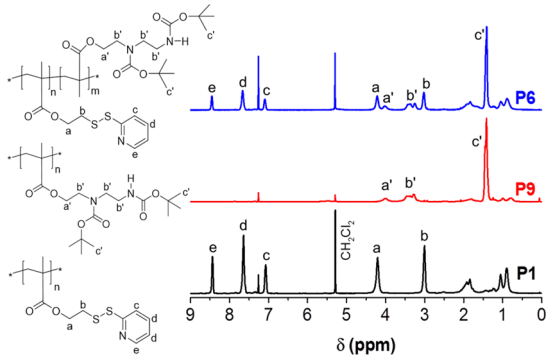

Figure 2. ^{1}H NMR spectra (300 MHz, $CDCl_3$) of **P1**, **P6**, and **P9** and the assignment of the peaks used to calculate the degree of polymerization (DP).

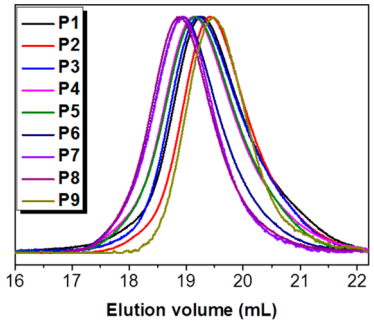

Figure 3. Normalized SEC traces in DMAc of isolated copolymers of **P1** to **P9**.

to investigate the possible effect of the monomer composition on the physical properties and stimuli response of the corresponding nanoparticles, a number of copolymers with similar molar mass values but varying monomer compositions were synthesized. To the best of our knowledge, the RAFT copolymerization of PDSM and BocAEAEMA has never been reported in the open literature so far. Yet, the CTA used in these experiments has previously shown a good behavior in RAFT polymerizations of both monomers.[31,43] In accordance to previous research, the [CTA]/[ACVA] ratio was kept at 1/

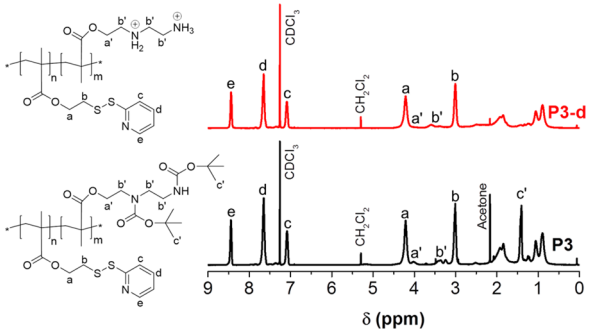

Figure 4. ^{1}H NMR spectra (300 MHz, $CDCl_3$) of **P3** and deprotected form of **P3** (**P3-d**).

0.25 regarding the polymerization rate to gain control over the molar mass.[44] Different initial monomer feed ratios were applied for each copolymerization to vary the amino content in the copolymers. The targeted molar mass value was $M_{n,tg}$ = 10 000 g mol^{-1} at 100% conversion. All polymerizations were carried out in DMAc at 70 °C with a monomer concentration of 0.5 mol L^{-1}.

Kinetic Study. The distribution of the monomers among the polymer chains could potentially affect the particle morphology. To obtain information about the sequence of the monomers in the copolymer chains, a kinetic study was performed for the copolymerization of **P7**. The kinetic study plots of the RAFT copolymerization of **P7** are displayed in Figure 1. Analysis of the kinetic samples by means of SEC in DMAc revealed monomodal molar mass distributions that shift to lower elution volumes in the course of the polymerization (Figure 1c). The evolution of M_n and $Đ_M$ versus conversion is shown in Figure 1a. At zero conversion, M_n could not be extrapolated to a zero molar mass value. This phenomenon has been observed by a number of researchers and is attributed to a low chain-transfer constant of the utilized CTA in the polymerizations.[45−47] However, the molar mass M_n was found to increase linearly with respect to the total monomer conversion with $Đ_M$ lower than 1.2 suggesting a RAFT-controlled mechanism. The semilogarithmic kinetic plots are linear (Figure 1b) for both monomers, indicating a pseudo first order polymerization rate with respect to the monomer concentration and a constant concentration of the propagating radicals during the RAFT polymerization. No induction period was observed for both monomers. The slope of PDSM was steeper than for BocAEAEMA in the semilogarithmic plot, which indicates that PDSM was consumed faster than BocAEAEMA. Indeed, the compositions in the isolated polymer deviated from the initial monomer feed ratio.

DOI: 10.1021/acs.macromol.5b02603
Macromolecules 2016, 49, 3856−3868

Table 2. Selected Characterization Results of the Prepared Nanoparticles

	Z-average [d, nm][a]			PDI[a]			ζ-potential[b]		
entry	c = 3 g L^{-1}	c = 5 g L^{-1}	c = 5 g L^{-1}	c = 3 g L^{-1}	c = 5 g L^{-1}	c = 5 g L^{-1}	c = 3 g L^{-1}	c = 5 g L^{-1}	c = 5 g L^{-1}
P2	264 ± 1[c]	466 ± 4[c]	74 ± 1[d]	0.07 ± 0.02[c]	0.07 ± 0.02[c]	0.20 ± 0.01[d]	74 ± 2[c]	72 ± 5[c]	69 ± 3[d]
P3	240 ± 1[c]	274 ± 1[c]	51 ± 1[d]	0.06 ± 0.02[c]	0.11 ± 0.02[c]	0.26 ± 0.01[d]	54 ± 2[c]	62 ± 2[c]	72 ± 5[d]
P4	117 ± 1[c]	180 ± 1[c]	[e]	0.15 ± 0.01[c]	0.05 ± 0.01[c]	[e]	52 ± 2[c]	59 ± 3[c]	[e]

[a]Average values of three DLS measurements. [b]Average values of three ζ-potential measurements. [c]WA, dropping water to acetone. [d]AW, dropping acetone to water. [e]No well-defined nanoparticles.

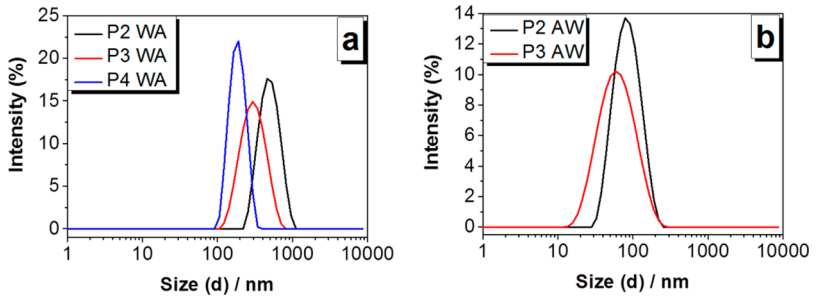

Figure 5. (a) Intensity size distributions of nanoparticles in water (**P2**, **P3**, and **P4**) with an initial acetone-polymer concentration of 5 mg mL^{-1}, prepared by dropping acetone-polymer solution to water (WA). (b) Intensity size distributions of nanoparticles in water (**P2** and **P3**) with an initial acetone-polymer concentration of 5 mg mL^{-1}, prepared by dropping acetone-polymer solution to water (AW).

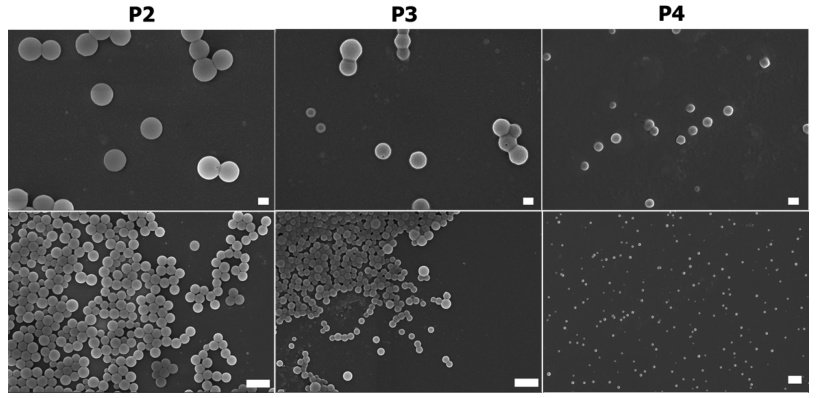

Figure 6. SEM images of nanoparticles that were prepared from **P2**, **P3**, and **P4** (5 mg mL^{-1}) by dropping water to acetone-polymer solution (WA). Upper scale bars represent 200 nm; lower scale bars represent 1000 nm.

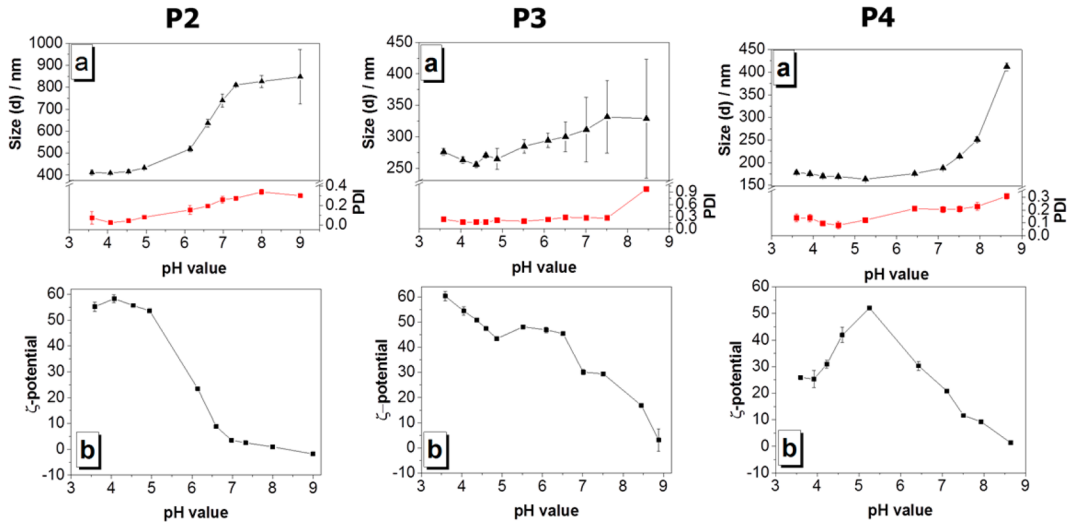

Figure 7. (a) Z-Average diameter and PDI values of nanoparticles as a function of the pH value. (b) ζ-Potentials of the nanoparticles as a function of the pH value.

DOI: 10.1021/acs.macromol.5b02603
Macromolecules 2016, 49, 3856−3868

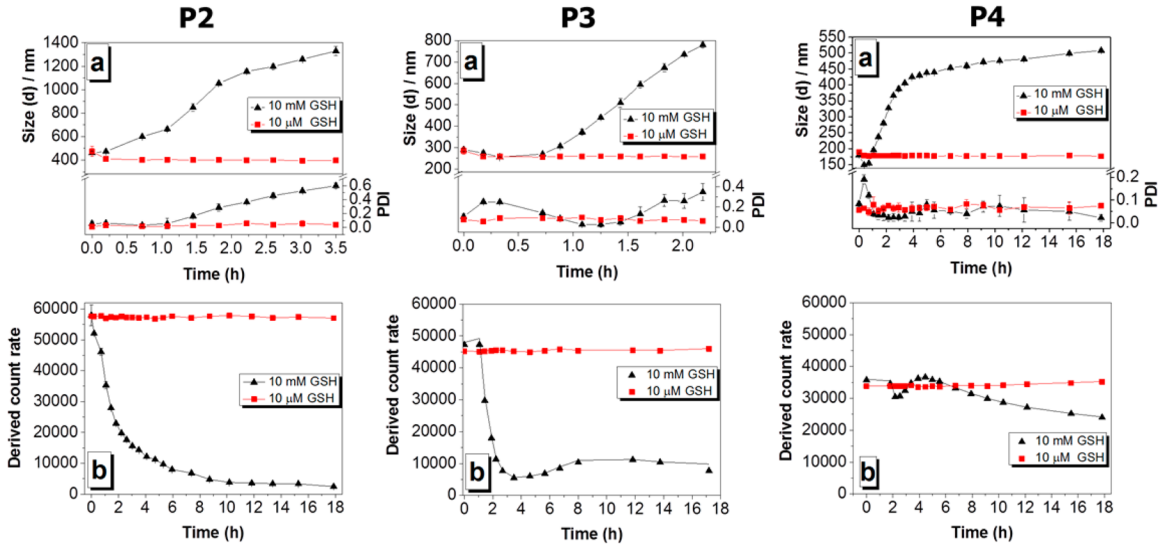

Figure 8. (a) *Z*-Average diameter and PDI values of nanoparticles as a function of 10 μM and 10 mM GSH. (b) Derived count rate of the nanoparticles as a function of 10 μM and 10 mM GSH.

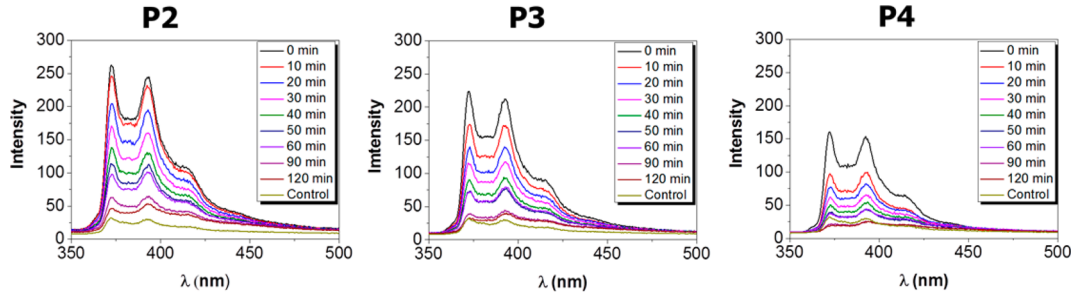

Figure 9. Fluorescence emission spectra of pyrene (6×10^{-6} mol L^{-1}) against **P2**, **P3**, and **P4** nanoparticles (0.075 mg mL^{-1}) as a function of time. Pyrene in pure water was used as control.

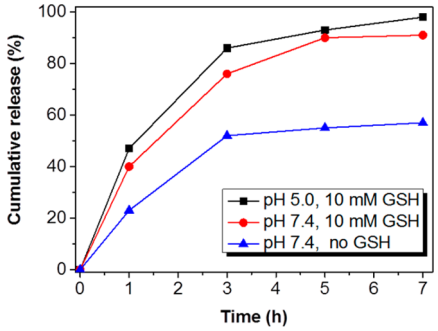

Figure 10. Drug release of DOX-loaded nanoparticles at pH 7.4 (blue), pH 7.4 with 10 mM GSH (red), and pH 5.0 with 10 mM GSH (black).

Copolymer Synthesis and Characterization. The resulting copolymer library was characterized by ^{1}H NMR spectroscopy (Figure 2) and SEC measurements on two systems (Table 1). ^{1}H NMR spectra of the isolated copolymers revealed the presence of the α (δ = 2.50 ppm) and ω (δ = 7.84, 7.48, and 7.35 ppm) RAFT end groups (Figure S5). The ω RAFT end group proton signals overlap with the pyridyldisulfide proton signals (δ = 8.45, 7.65, and 7.08 ppm), whereas the α RAFT end group protons enable the estimation of the degree of polymerization (DP) for each monomer (see Experimental Section for details). The according number-average molar mass (M_n) values calculated by ^{1}H NMR are in good agreement with the theoretical values that were calculated from the [monomer] to [CTA] ratio and the monomer conversions. The compositions of the isolated copolymers (F(**M1**/**M2**)) were calculated by comparing the DP values for each monomer (Table 1). The integrals of the pyridyldisulfide protons and the methylene protons of the polymer side groups of the PDSM (δ = 8.45 and 3.02) are in good agreement with each other indicating the absence of side transfer reactions during the polymerization.

The isolated copolymers were analyzed using two different SEC systems (Figure 3, Figure S8). Both systems revealed monomodal traces and low dispersities ($Đ_M$ < 1.3) for all polymers. In general, SEC in DMAc revealed higher molar mass values compared to the SEC investigations in $CHCl_3$. This is caused by the increased hydrodynamic volume of the BocAEAEMA containing polymers in polar solvents, which results in higher apparent molar mass values. Both SEC systems revealed slightly higher molar mass values than the molar mass values determined by ^{1}H NMR spectra due to the PS calibration in the SEC systems, resulting in a relative molar mass value.

Deprotection of the Polymers and Long-Term Stability Test. Prior to the nanoparticle formulation, the polymers were treated with trifluoroacetic acid to obtain the desired primary and secondary amino containing copolymers. The ^{1}H NMR spectrum indicates the complete removal of the Boc-groups by the disappearance of the peak at 1.41 ppm,

DOI: 10.1021/acs.macromol.5b02603
Macromolecules 2016, 49, 3856−3868

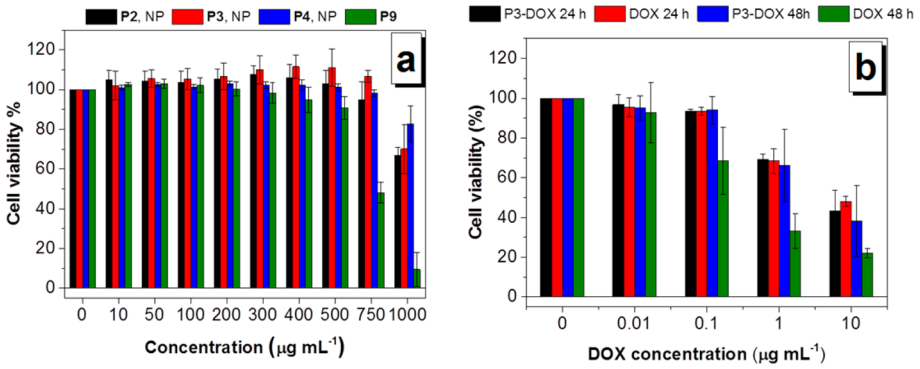

Figure 11. (a) Cytotoxicity test of nanoparticles (NPs) that were prepared from **P2**, **P3**, **P4**, and AEAEMA homopolymer **P9** in L929 cells. (b) Cytotoxicity test of DOX-loaded nanoparticles and free DOX in L929 cells. The relative viability is expressed as percentage to control cells not treated with NPs. Untreated cells on the same well plate were used as positive controls.

which corresponds to the *tert*-butoxy carbonyl protons (Figure 4). SEC in DMAc reveals a slight increase in the molar mass values after deprotection of the Boc-groups (Figure S16–22) caused by the increased hydrodynamic volume of the copolymers in DMAc after deprotection. To investigate the long-term stability of the polymers, **P6** and its deprotected form **P6-d** were stored at room temperature for six months. Then, ^{1}H NMR and SEC measurements were performed. A change cannot be observed for **P6** in the SEC trace or in the ^{1}H NMR spectrum. However, SEC in $CHCl_3$ reveals an appearance of a small shoulder at around double molar mass region for **P6-d** (Figure S23a). This is attributed the nucleophilic attack of primary amino groups of AEAEMA to the thiocarbonylthio RAFT end groups, which is a well-known reaction between the RAFT-generated polymers and the primary amino groups leading to thiol terminated polymers.[48] A significant reduction of the characteristic UV absorbance in the SEC at 340 nm (calibrated relating to the maximum of the corresponding RI curves) of the thiocarbonylthio end group proves this assumption (Figure S23b). Such a reaction would be expected to cause a polymer–polymer coupling via disulfide formation and/or coupling with the pyridyldisulfide groups of the polymer side chains via thiol disulfide exchange reactions. However, the ^{1}H NMR spectrum shows no change in the ratio of the integral values between the pyridyldisulfide protons and the methylene protons of the polymer side groups of the PDSM (δ = 8.45 and 3.02) (Figure S24), suggesting that the appearance of the shoulder in the SEC trace is due to the polymer–polymer coupling via disulfide formation. These results also suggest the stability of the pyridyldisulfide units in the presence of amino groups.

Nanoparticle Formulation and Characterization. Polymeric nanoparticles were prepared from the deprotected copolymers of **P2**, **P3**, and **P4**, which contain 5, 8, and 12 mol% AEAEMA functionality, respectively, by means of nanoprecipitation with subsequent solvent evaporation without any need of stabilizers/surfactants. No nanoparticles could be obtained using higher mol% AEAEMA containing polymers (**P5–P9**) due to their insufficient hydrophobicity. In order to obtain differently sized nanoparticles, two different initial acetone-polymer solution concentrations (3 and 5 mg mL^{-1}) and two different dropping methods (dropping acetone polymer solution to water (AW) as well as dropping water to acetone polymer solution (WA)) were applied for each polymer. By dropping water to acetone polymer solution (WA), nanoparticles with monomodal size distributions and low polydispersity (PDI) values were obtained with both initial acetone-polymer solution concentrations (Table 2, Figure 5). Smaller nanoparticles (*Z*-average diameter between 117 and 264 nm) were formed at a lower initial acetone-polymer concentration of 3 mg mL^{-1} compared to 5 mg mL^{-1} (*Z*-average diameter between 180 and 466 nm) for all polymers, which is a common phenomenon in nanoprecipitation.[49] Moreover, it could be observed that there is a correlation between the mol% of AEAEMA content of the polymers and the size of the corresponding nanoparticles: An increase of the AEAEMA content results in a decrease of the nanoparticles size of both initial polymer concentrations. It is well-known that preparation variables, such as the choice of organic solvent and initial polymer concentration in the organic phase, influence the properties of the final nanoparticles.[50] However, to the best of our knowledge, there has been no literature example which describes the influence of the polymer composition on the size of the nanoparticles. Nevertheless, very recently Reisch et al. reported that the presence of charged groups in polymer chains can reduce the size of polymer nanoparticles fabricated by nanoprecipitation.[51] By dropping acetone-polymer solution (AW) to water, nanoparticles with monomodal intensity size distributions and acceptable polydispersity (PDI) values were obtained from **P2** and **P3** with an initial acetone-polymer solution concentration of 5 mg mL^{-1} (Table 2, Figure 5). In contrast, **P4** yielded multiple intensity distributions and relatively high PDI values by utilizing the AW method and an initial polymer concentration of 5 mg mL^{-1}. This is attributed to the higher hydrophilicity of the **P4** compared to the **P3** and **P2** which pushes **P4** out of the Ouzo region under the applied conditions. It is known that production of metastable dispersions or emulsions is limited to a small region of the composition map, called the Ouzo region.[33,52] In accordance, the lower initial acetone-polymer concentration (3 mg mL^{-1}) used in AW method, did not result in the formulation of well-defined nanoparticles with any of the polymers. The dropping method affected particle size significantly. By AW method, relatively smaller nanoparticles were obtained compared to WA method at an initial acetone-polymer concentration of 5 mg mL^{-1} for **P2** and **P3**, which is commonly observed for the nanoprecipitation method.[53] The ζ-potential of all suspensions shows positive values higher than +50 mV as a consequence of the amino functionality of the copolymers, indicating a high colloidal stability. The long-term stability of the nanoparticle suspensions was tested at room temperature for 6 weeks, showing no change in size and size distributions. SEM (Figure

DOI: 10.1021/acs.macromol.5b02603
Macromolecules 2016, 49, 3856–3868

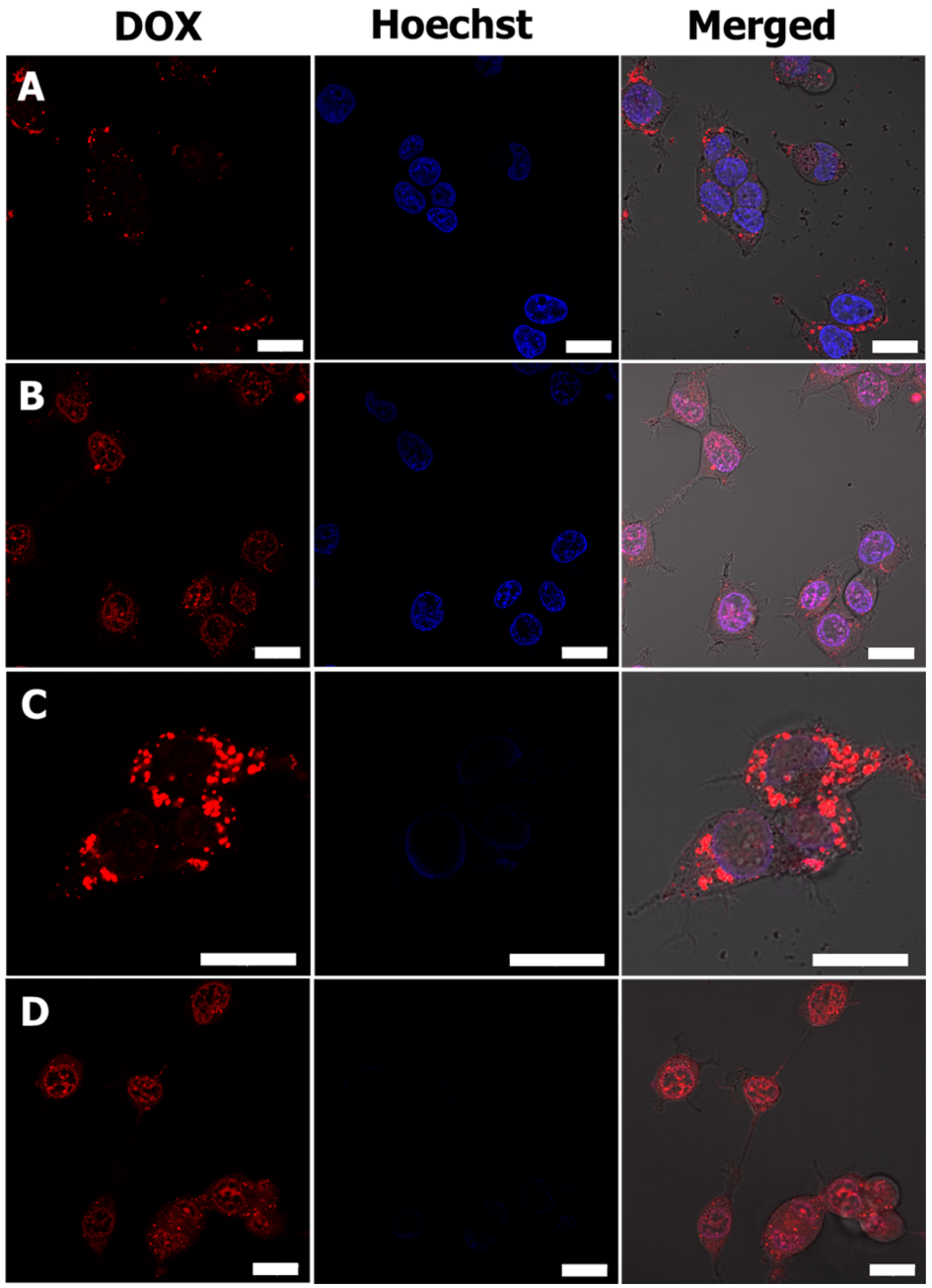

Figure 12. Live cell CLSM images of HEK cells incubated with DOX-loaded nanoparticles and free DOX at 1 μg/mL pure and encapsulated DOX. For each panel, the images from left to right show DOX fluorescence in cells (red), cell nuclei stained by Hoechst (blue), and overlays of the two images and a brightfield image. The scale bars correspond to 20 μm in all the images. Key: (A) DOX-loaded nanoparticles, 6 h incubation; (B) free DOX, 6 h incubation; (C) DOX-loaded nanoparticles, 24 h incubation; (D) free DOX, 24 h incubation.

6 and Figure S26) and TEM (Figure S25) investigations revealed that all nanoparticles have uniform spherical shapes.

pH-Response Test of the Nanoparticles. For the understanding of the pH-responsive behavior of the nanoparticles, nanoparticle suspensions were titrated in the pH value range from 3.5 to 9. Simultaneous size and ζ-potential measurements were applied (Figure 7). **P2** nanoparticle suspensions possess stable size values at low pH values (pH $\leq$ 5.0). At higher pH values, the size of the nanoparticles gradually increases and they start to precipitate above a pH value of 7.5. This is due to the deprotonation of the amino groups at high pH values. In agreement with this, the ζ-potential is inversely proportional to the pH with the ζ-potential reaching 0 mV at the isoelectric point (IEP) at a pH value of around 7.5. The nanoparticles derived from **P3** and **P4** show higher IEP values, at a pH value of above 8.5, compared to the **P2** nanoparticles. This is due to the higher AEAEMA content of the corresponding polymers compared to **P2**. In contrast to **P2** and **P3** nanoparticles, the ζ-potential profile of **P4** nanoparticles displays a maximum at around pH 5. At lower pH values, a reduction in the ζ-potential can be observed. This is attributed to the amount of HCl that is used for the titration of **P4** nanoparticles, which is higher than for the titration of **P2** and **P3** nanoparticles due to the high AEAEMA content. It is known that excess HCl could act as a salt and screen the positive charge arising from the amino groups, which could

DOI: 10.1021/acs.macromol.5b02603
Macromolecules 2016, 49, 3856−3868

result in a decrease in the ζ-potential.[40] It should also be noted that **P4** nanoparticles that contain the highest AEAEMA content have stable size values up to a pH value of 6.5.

Redox Response Test of the Nanoparticles. The redox responsive behavior of the nanoparticles was tested via the addition of the reducing agent glutathione (GSH) at a concentration of 10 μM and 10 mM to the nanoparticle suspensions at 37 °C. The changes in particle size were recorded by DLS at various time intervals (Figure 8). At a GSH concentration similar like in the plasma of the human body (10 μM), no change was observed neither in the nanoparticle size distribution nor in the derived count rate for all nanoparticle suspensions implying the stability of the nanoparticle suspensions in the plasma. However, in a mimicking intracellular reductive environment (10 mM GSH), **P2** nanoparticles underwent rapid aggregation, meaning the average particles size was increased from 460 to 660 nm just after 1 h and up to 1330 nm after 3.5 h as well as broader distributions, indicating the disassembly of the nanoparticles. This is due to the reaction of GSH with the disulfide functionality of the PDSM that converts the amphiphilic copolymer into a more hydrophilic polymer. This conversion causes nanoparticles to disassemble. In accordance, a rapid decrease in the derived count rate was observed in the presence of 10 mM GSH. Moreover, the **P2** nanoparticle suspension turned from an opalescent into a colorless solution over time in the presence of 10 mM GSH, confirming the disassembly of the nanoparticles. Unlike **P2**, **P3** nanoparticles revealed an induction period of around 1 h to respond to 10 mM GSH. However, after this induction period again a fast increase in the particle size with broader distributions and a rapid decrease in the derived count rate were observed. **P3** nanoparticles also became colorless after being treated with 10 mM GSH. Like **P3**, **P4** nanoparticles revealed an induction period of around 1 h before showing any response to the 10 mM GSH. After approximately 1 h, a rapid increase in the particle size without aggregation was observed. In accordance, an increase in the derived count rate for the **P4** nanoparticles was observed between 2 and 6 h. This is due to the rapid increase in size of the **P4** nanoparticles. However, after about 6 h a slower decrease in the derived count rate compared to **P2** and **P3** nanoparticles was observed, indicating partial disassembly of the nanoparticles. This phenomenon, slower disassembly of **P4** nanoparticles compared to **P2** and **P3** nanoparticles, is attributed to the slower diffusion of the polar GSH within the most hydrophilic **P4** nanoparticles, having the highest AEAEMA content.

Fluorescence Spectroscopic Study of the Nanoparticles. In order to confirm the ability of the nanoparticles to encapsulate hydrophobic guest molecules and to release them under elevated GSH concentration, pyrene as hydrophobic fluorescent probe was encapsulated as a model drug in **P2**, **P3**, and **P4** nanoparticles by utilizing the WA technique using polymer concentrations of 3 mg mL^{-1}. The fluorescence emission spectra of pyrene encapsulated **P2**, **P3**, and **P4** nanoparticles at 10 mM GSH concentration as a function of time are shown in Figure 9 with a fixed excitation wavelength of 335 nm. Pyrene in pure water at 10 mM GSH concentration is used as control. The total intensities of the emission spectra of the nanoparticle suspensions at time zero are significantly higher compared to the emission intensity of the control. This indicates that pyrene is transferred into the hydrophobic domains of the nanoparticles. Moreover, it could be observed that an increase of the AEAEMA content results in a decrease in the fluorescence intensity of the nanoparticles at time zero. This can be explained by the increased hydrophilicity of the nanoparticles with increasing AEAEMA content, which might cause a decrease in the encapsulation efficiency of hydrophobic pyrene. Moreover, the total intensities of the emission spectra of the nanoparticle suspensions showed a gradual decrease over time. Indeed, after 120 min the emission intensity of the pyrene decreased to the intensity of the control for each system, which indicates the capability of the nanoparticles to release their hydrophobic cargos in response to the GSH stimulus. Moreover, the fluorescence emission spectra of pyrene against **P2** nanoparticles at various pH values was investigated (Figure S27). A gradual decrease in the emission intensity of the pyrene can be observed as the pH value of the medium decreases from 7.4 to 5. This can be explained by the protonation of the amino groups, which makes the corresponding polymers more hydrophilic and thus results in a lower pyrene encapsulation. Notably, a change in the pH value from 5 to 4 did not result in a decrease in the emission intensity of the pyrene. This is attributed to the complete protonation of amino groups above a pH value of 5, which did not cause any physical change to the **P2** nanoparticles. This conclusion is in accordance with the pH-response test of the **P2** nanoparticles, which revealed no change of the size of a pH value of 4 and 5 (see above).

Loading and Release Studies of DOX. DOX was encapsulated in **P3** nanoparticles using the nanoprecipitation method. The resulting DOX-loaded nanoparticles have a *Z*-average diameter of 130 nm, a PDI value of 0.1 and a ζ-potential of +30 mV (Figure S28). The target drug loading content was 10%. The drug loading efficiency and drug loading content were calculated as 19.2% and 1.9%, respectively. The release of the DOX was investigated at 37 °C using three different conditions as reported in Figure 10. The results reveal that 91% DOX is released in 7 h under a reducing environment containing 10 mM GSH at pH 7.4, which is due to the disassembly of the nanoparticles caused by the reaction of GSH with the disulfide functionality of the PDSM. The release of DOX is slightly accelerated at pH 5.0 in the presence of 10 mM GSH, in which 98% DOX was released in 7 h. This is due to the protonation of the amino groups of AEAEMA. These results indicate that an acidic pH value and a high GSH concentration have a synergetic effect on the DOX release of the nanoparticles. Under physiological conditions (pH 7.4), the release of DOX is slower with 57% DOX in 7 h. It should be noted, that although the release of DOX under physiological conditions is slightly higher than previously reported DOX delivery systems based on amphiphilic block copolymers, it is still in an acceptable range.[54]

Cytotoxicity of the Nanoparticles, AEAEMA Homopolymer, DOX-Loaded Nanoparticles, and Free DOX. In order to evaluate the cytotoxicity of the systems, nanoparticle samples of **P2**, **P3**, and **P4** prepared from 5 mg mL^{-1} by the WA technique and the water-soluble AEAEMA homopolymer **P9** were investigated at the indicated concentrations (Figure 11a). The cytotoxicity assay results showed that the nanoparticles did not have any significant cytotoxic effect on L929 cells after 48 h of incubation at concentrations up to 0.75 mg mL^{-1}. However, a slight cytotoxic effect at 1 mg mL^{-1} with a cell viability of about 70% was observed (general threshold for cytotoxicity is 70% cell viability). The AEAEMA homopolymer **P9** revealed no toxic effect on the cells up to 0.5 mg mL^{-1}, but a significant loss in cell viability of about 50% at 0.75 mg mL^{-1} and a severe loss in cell viability of about 90% at 1 mg mL^{-1}

DOI: 10.1021/acs.macromol.5b02603
Macromolecules 2016, 49, 3856−3868

could be observed. This is due to the primary and secondary amino functionalities of AEAEMA, which can be associated with toxic effects in cell studies.[15,55,56] The higher cell viability of the nanoparticles compared to the AEAEMA homopolymer at increased concentrations can be explained by the lower amino content (up to 12 mol% AEAEMA) in the corresponding copolymers compared to the AEAEMA homopolymer. Moreover, the cytotoxicity of the DOX-loaded nanoparticles was evaluated to compare with the DOX-free nanoparticles by using free DOX as a control. Though DOX-free nanoparticles show no cytotoxic effects at similar particle concentrations, the cell viability decreased with an increasing concentration of the DOX-loaded nanoparticles even after 24 h incubation (Figure 11b). Similar results were observed for free DOX. Prolonged incubation of 48 h resulted in a slightly lower cell viability of free DOX. These results indicate the efficient release of DOX from the nanoparticles in the intracellular environment, which inhibits the proliferation of the cells.

Cellular Uptake and Intracellular Drug Release. The cellular uptake and intracellular drug release profiles of the DOX-loaded nanoparticles in comparison with free DOX were studied in HEK cells using confocal laser scanning microscopy (CLSM). After 6 h of incubation, DOX fluorescence can mainly be observed in the cytosol and in the nuclei for cells treated with DOX-loaded nanoparticles (Figure 12A) indicating that DOX-loaded nanoparticles have been taken up efficiently by the cells (no aggregation of nanoparticles at the cell surface) and some of the DOX released from the nanoparticles by the intracellular triggers meaning an acidic and reductive environment of the endosomes and/or a high GSH concentration of the cytosol. Within the same incubation time, free DOX mainly accumulated in the nuclei with higher fluorescence intensity than DOX-loaded nanoparticles (Figure 12B). This can be attributed to a time dependent cell internalization of the nanoparticles by energy-dependent endocytosis in contrast to the free DOX, which is rapidly internalized through diffusion.[57] Furthermore, although the DOX release of the nanoparticles was not complete, the intensity of the DOX fluorescence inside the cell nuclei increased by prolonging the incubation time to 24 h (Figure 12C), which is similar to the free DOX (Figure 12D). Taking the CLSM results into account, a triggered release caused by a change in the pH value or the reductive environment can be assumed. Furthermore, the images show that to some extend the DOX is not fully released from the nanoparticles but the toxic effect is comparable to free DOX. These results are promising for the targeted cancer therapy since it is known that the accumulation of DOX in the cell nuclei is crucial to induce cell death.[58]

CONCLUSIONS

In this study, a well-defined statistical copolymer library of PDSM and BocAEAEMA was prepared via RAFT polymerization. Copolymerization was shown to proceed with a first order kinetics and a linear evolution of the molar mass versus conversion. In order to alter the amino content in the copolymers and in the corresponding nanoparticles, the initial monomer feed ratios were varied. Boc-groups were cleaved prior to the nanoparticle formulation to obtain desired primary and secondary amino functional polymers. Copolymers that contain up to 12 mol% AEAEMA functionality were shown to self-assemble into nanoparticles in aqueous solution via nanoprecipitation with application of the subsequent solvent evaporation method. The corresponding nanoparticles have been demonstrated to be dual responsive to both pH value and glutathione content. The ability of the nanoparticles to encapsulate DOX and release it under various triggered conditions was confirmed. CLSM studies showed that DOX-loaded nanoparticles were efficiently taken up by HEK cells. The acidic pH value in the endosomes and the high glutathione concentration inside the cytosol caused intracellular DOX release, showing a comparable cytotoxicity of free and encapsulated DOX. In comparison, none of the DOX-free nanoparticles exhibited any significant cytotoxic effect on L929 cells at concentrations up to 0.75 mg mL^{-1}. Consequently, these nanoparticles may serve as promising smart drug delivery vehicles for the controlled delivery of DOX.

ASSOCIATED CONTENT

Supporting Information

The Supporting Information is available free of charge on the ACS Publications website at DOI: 10.1021/acs.macromol.5b02603.

^{1}H NMR spectra of PDSM, BocAEAEMA, **P2, P2-d**, **P4**, **P4-d**, **P5**, **P5-d**, **P6**, **P6-d**, **P7**, **P7-d**, **P8**, **P8-d**, and **P9-d**, ^{13}C spectra of BocAEAEMA at 25 and 0 °C, additional comments on ^{1}H and ^{13}C NMR spectra of (BocAEAEMA), normalized SEC traces in $CHCl_3$ of isolated copolymers of **P1**−**P9**, normalized SEC overlay traces in DMAc of **P2** with **P2-d, P4** with **P4-d, P5** with **P5-d, P6** with **P6-d, P7** with **P7-d**, **P8**, and **P8-d**, further SEM images, and fluorescence emission spectra of pyrene in **P2** nanoparticles as a function of pH value (PDF)

AUTHOR INFORMATION

Corresponding Authors

*(S.S.) Fax: +49(0) 3641 9482 02. E-mail: stephanie.schubert@uni-jena.de.

*(U.S.S.) E-mail: ulrich.schubert@uni-jena.de.

Notes

The authors declare no competing financial interest.

ACKNOWLEDGMENTS

We acknowledge funding from the Carl-Zeiss Foundation (JCSM Strukturantrag, grant for A.T.), the Thüringer Ministerium für Wirtschaft, Wissenschaft, und Digitale Gesellschaft (TMWWDG, ProExzellenz I, NanoConSens), and the German Federal Ministry of Education & Research (BMBF, #031A518B). The SEM facilities of the Jena Center for Soft Matter (JCSM) were provided by grants from the German Research Council (DFG) and the European Fonds for Regional Development (EFRE). We also express our gratitude to Dr. Wolfgang Günther for helpful discussion.

REFERENCES

(1) Cheng, R.; Meng, F.; Deng, C.; Klok, H.-A.; Zhong, Z. Dual and multi-stimuli responsive polymeric nanoparticles for programmed site-specific drug delivery. *Biomaterials* **2013**, *34*, 3647−3657.

(2) Yan, B.; Boyer, J.-C.; Habault, D.; Branda, N. R.; Zhao, Y. Near Infrared Light Triggered Release of Biomacromolecules from Hydrogels Loaded with Upconversion Nanoparticles. *J. Am. Chem. Soc.* **2012**, *134*, 16558−16561.

(3) Jeong, B.; Bae, Y. H.; Kim, S. W. Drug release from biodegradable injectable thermosensitive hydrogel of PEG−PLGA−PEG triblock copolymers. *J. Controlled Release* **2000**, *63*, 155−163.

(4) Chen, Y.; Yin, Q.; Ji, X.; Zhang, S.; Chen, H.; Zheng, Y.; Sun, Y.; Qu, H.; Wang, Z.; Li, Y.; Wang, X.; Zhang, K.; Zhang, L.; Shi, J.

DOI: 10.1021/acs.macromol.5b02603
Macromolecules 2016, 49, 3856−3868

Manganese oxide-based multifunctionalized mesoporous silica nanoparticles for pH-responsive MRI, ultrasonography and circumvention of MDR in cancer cells. *Biomaterials* **2012**, *33*, 7126−7137.
(5) Wang, Y.; Wang, G.; Xiao, Y.; Yang, Y.; Tang, R. Yolk−Shell Nanostructured Fe3O4@NiSiO3 for Selective Affinity and Magnetic Separation of His-Tagged Proteins. *ACS Appl. Mater. Interfaces* **2014**, *6*, 19092−19099.
(6) Hsu, L.; Weder, C.; Rowan, S. J. Stimuli-responsive, mechanically-adaptive polymer nanocomposites. *J. Mater. Chem.* **2011**, *21*, 2812−2822.
(7) Gambinossi, F.; Chanana, M.; Mylon, S. E.; Ferri, J. K. Stimulus-Responsive Au@(MeO2MAx-co-OEGMAy) Nanoparticles Stabilized by Non-DLVO Interactions: Implications of Ionic Strength and Copolymer (x:y) Fraction on Aggregation Kinetics. *Langmuir* **2014**, *30*, 1748−1757.
(8) Du, J.-Z.; Mao, C.-Q.; Yuan, Y.-Y.; Yang, X.-Z.; Wang, J. Tumor extracellular acidity-activated nanoparticles as drug delivery systems for enhanced cancer therapy. *Biotechnol. Adv.* **2014**, *32*, 789−803.
(9) Wang, Y.-C.; Wang, F.; Sun, T.-M.; Wang, J. Redox-Responsive Nanoparticles from the Single Disulfide Bond-Bridged Block Copolymer as Drug Carriers for Overcoming Multidrug Resistance in Cancer Cells. *Bioconjugate Chem.* **2011**, *22*, 1939−1945.
(10) Nguyen, M. M.; Carlini, A. S.; Chien, M.-P.; Sonnenberg, S.; Luo, C.; Braden, R. L.; Osborn, K. G.; Li, Y.; Gianneschi, N. C.; Christman, K. L. Enzyme-Responsive Nanoparticles for Targeted Accumulation and Prolonged Retention in Heart Tissue after Myocardial Infarction. *Adv. Mater.* **2015**, *27*, 5547−5552.
(11) Zhang, P.; Chiu, Y.-C.; Tostanoski, L. H.; Jewell, C. M. Polyelectrolyte Multilayers Assembled Entirely from Immune Signals on Gold Nanoparticle Templates Promote Antigen-Specific T Cell Response. *ACS Nano* **2015**, *9*, 6465−6477.
(12) Oishi, M.; Kataoka, K.; Nagasaki, Y. pH-Responsive Three-Layered PEGylated Polyplex Micelle Based on a Lactosylated ABC Triblock Copolymer as a Targetable and Endosome-Disruptive Nonviral Gene Vector. *Bioconjugate Chem.* **2006**, *17*, 677−688.
(13) Ko, J.; Park, K.; Kim, Y.-S.; Kim, M. S.; Han, J. K.; Kim, K.; Park, R.-W.; Kim, I.-S.; Song, H. K.; Lee, D. S.; Kwon, I. C. Tumoral acidic extracellular pH targeting of pH-responsive MPEG-poly(β-amino ester) block copolymer micelles for cancer therapy. *J. Controlled Release* **2007**, *123*, 109−115.
(14) Lackey, C. A.; Press, O. W.; Hoffman, A. S.; Stayton, P. S. A Biomimetic pH-Responsive Polymer Directs Endosomal Release and Intracellular Delivery of an Endocytosed Antibody Complex. *Bioconjugate Chem.* **2002**, *13*, 996−1001.
(15) Yildirim, T.; Rinkenauer, A. C.; Weber, C.; Traeger, A.; Schubert, S.; Schubert, U. S. RAFT made methacrylate copolymers for reversible pH-responsive nanoparticles. *J. Polym. Sci., Part A: Polym. Chem.* **2015**, *53*, 2711−2721.
(16) Arunachalam, B.; Phan, U. T.; Geuze, H. J.; Cresswell, P. Enzymatic reduction of disulfide bonds in lysosomes: characterization of a gamma-interferon-inducible lysosomal thiol reductase (GILT). *Proc. Natl. Acad. Sci. U. S. A.* **2000**, *97*, 745−50.
(17) Gainey, D.; Short, S.; McCoy, K. L. Intracellular location of cysteine transport activity correlates with productive processing of antigen disulfide. *J. Cell. Physiol.* **1996**, *168*, 248−254.
(18) Bulmus, V.; Woodward, M.; Lin, L.; Murthy, N.; Stayton, P.; Hoffman, A. A new pH-responsive and glutathione-reactive, endosomal membrane-disruptive polymeric carrier for intracellular delivery of biomolecular drugs. *J. Controlled Release* **2003**, *93*, 105−120.
(19) Wu, L.; Zou, Y.; Deng, C.; Cheng, R.; Meng, F.; Zhong, Z. Intracellular release of doxorubicin from core-crosslinked polypeptide micelles triggered by both pH and reduction conditions. *Biomaterials* **2013**, *34*, 5262−5272.
(20) Klaikherd, A.; Nagamani, C.; Thayumanavan, S. Multi-Stimuli Sensitive Amphiphilic Block Copolymer Assemblies. *J. Am. Chem. Soc.* **2009**, *131*, 4830−4838.
(21) Zhang, J.; Wu, L.; Meng, F.; Wang, Z.; Deng, C.; Liu, H.; Zhong, Z. pH and Reduction Dual-Bioresponsive Polymersomes for Efficient Intracellular Protein Delivery. *Langmuir* **2012**, *28*, 2056−2065.
(22) Moad, G.; Rizzardo, E.; Thang, S. H. Radical addition−fragmentation chemistry in polymer synthesis. *Polymer* **2008**, *49*, 1079−1131.
(23) Gottesman, M. M.; Fojo, T.; Bates, S. E. Multidrug resistance in cancer: role of ATP-dependent transporters. *Nat. Rev. Cancer.* **2002**, *2*, 48−58.
(24) Yeh, E. T. H.; Tong, A. T.; Lenihan, D. J.; Yusuf, S. W.; Swafford, J.; Champion, C.; Durand, J.-B.; Gibbs, H.; Zafarmand, A. A.; Ewer, M. S. Cardiovascular Complications of Cancer Therapy: Diagnosis, Pathogenesis, and Management. *Circulation* **2004**, *109*, 3122−3131.
(25) Taurin, S.; Nehoff, H.; Greish, K. Anticancer nanomedicine and tumor vascular permeability; Where is the missing link? *J. Controlled Release* **2012**, *164*, 265−275.
(26) Bae, Y. H.; Park, K. Targeted drug delivery to tumors: Myths, reality and possibility. *J. Controlled Release* **2011**, *153*, 198−205.
(27) Car, A.; Baumann, P.; Duskey, J. T.; Chami, M.; Bruns, N.; Meier, W. pH-Responsive PDMS-b-PDMAEMA Micelles for Intracellular Anticancer Drug Delivery. *Biomacromolecules* **2014**, *15*, 3235−3245.
(28) K. C., R. B.; Thapa, B.; Xu, P. pH and Redox Dual Responsive Nanoparticle for Nuclear Targeted Drug Delivery. *Mol. Pharmaceutics* **2012**, *9*, 2719−2729.
(29) Jia, L.; Cui, D.; Bignon, J.; Di Cicco, A.; Wdzieczak-Bakala, J.; Liu, J.; Li, M.-H. Reduction-Responsive Cholesterol-Based Block Copolymer Vesicles for Drug Delivery. *Biomacromolecules* **2014**, *15*, 2206−2217.
(30) Jia, Z.; Wong, L.; Davis, T. P.; Bulmus, V. One-Pot Conversion of RAFT-Generated Multifunctional Block Copolymers of HPMA to Doxorubicin Conjugated Acid- and Reductant-Sensitive Crosslinked Micelles. *Biomacromolecules* **2008**, *9*, 3106−3113.
(31) Kurtulus, I.; Yilmaz, G.; Ucuncu, M.; Emrullahoglu, M.; Becer, C. R.; Bulmus, V. A new proton sponge polymer synthesized by RAFT polymerization for intracellular delivery of biotherapeutics. *Polym. Chem.* **2014**, *5*, 1593−1604.
(32) Fessi, H.; Puisieux, F.; Devissaguet, J. P.; Ammoury, N.; Benita, S. Nanocapsule formation by interfacial polymer deposition following solvent displacement. *Int. J. Pharm.* **1989**, *55*, R1−R4.
(33) Schubert, S.; Delaney, J. J. T., Jr.; Schubert, U. S. Nanoprecipitation and nanoformulation of polymers: from history to powerful possibilities beyond poly(lactic acid). *Soft Matter* **2011**, *7*, 1581−1588.
(34) Jiang, J.; Qi, B.; Lepage, M.; Zhao, Y. Polymer Micelles Stabilization on Demand through Reversible Photo-Cross-Linking. *Macromolecules* **2007**, *40*, 790−792.
(35) Ryu, J.-H.; Bickerton, S.; Zhuang, J.; Thayumanavan, S. Ligand-Decorated Nanogels: Fast One-Pot Synthesis and Cellular Targeting. *Biomacromolecules* **2012**, *13*, 1515−1522.
(36) Li, L.; Raghupathi, K.; Song, C.; Prasad, P.; Thayumanavan, S. Self-assembly of random copolymers. *Chem. Commun.* **2014**, *50*, 13417−13432.
(37) Wong, C.-H.; Zimmerman, S. C. Orthogonality in organic, polymer, and supramolecular chemistry: from Merrifield to click chemistry. *Chem. Commun.* **2013**, *49*, 1679−1695.
(38) Quemener, D.; Davis, T. P.; Barner-Kowollik, C.; Stenzel, M. H. RAFT and click chemistry: A versatile approach to well-defined block copolymers. *Chem. Commun.* **2006**, 5051−5053.
(39) Arvizo, R. R.; Miranda, O. R.; Thompson, M. A.; Pabelick, C. M.; Bhattacharya, R.; Robertson, J. D.; Rotello, V. M.; Prakash, Y. S.; Mukherjee, P. Effect of Nanoparticle Surface Charge at the Plasma Membrane and Beyond. *Nano Lett.* **2010**, *10*, 2543−2548.
(40) Penfold, N. J. W.; Lovett, J. R.; Warren, N. J.; Verstraete, P.; Smets, J.; Armes, S. P. pH-Responsive non-ionic diblock copolymers: protonation of a morpholine end-group induces an order-order transition. *Polym. Chem.* **2016**, *7*, 79−88.

DOI: 10.1021/acs.macromol.5b02603
Macromolecules 2016, 49, 3856−3868

(41) de Bruin, K. G.; Fella, C.; Ogris, M.; Wagner, E.; Ruthardt, N.; Bräuchle, C. Dynamics of photoinduced endosomal release of polyplexes. *J. Controlled Release* **2008**, *130*, 175−182.
(42) Akinc, A.; Thomas, M.; Klibanov, A. M.; Langer, R. Exploring polyethylenimine-mediated DNA transfection and the proton sponge hypothesis. *J. Gene Med.* **2005**, *7*, 657−663.
(43) Wong, L.; Boyer, C.; Jia, Z.; Zareie, H. M.; Davis, T. P.; Bulmus, V. Synthesis of Versatile Thiol-Reactive Polymer Scaffolds via RAFT Polymerization. *Biomacromolecules* **2008**, *9*, 1934−1944.
(44) Fijten, M. W. M.; Paulus, R. M.; Schubert, U. S. Systematic parallel investigation of RAFT polymerizations for eight different (meth)acrylates: A basis for the designed synthesis of block and random copolymers. *J. Polym. Sci., Part A: Polym. Chem.* **2005**, *43*, 3831−3839.
(45) Mueller, A. H. E.; Zhuang, R.; Yan, D.; Litvinenko, G. Kinetic Analysis of ″Living″ Polymerization Processes Exhibiting Slow Equilibria. 1. Degenerative Transfer (Direct Activity Exchange between Active and ″Dormant″ Species). Application to Group Transfer Polymerization. *Macromolecules* **1995**, *28*, 4326−4333.
(46) Uzulina, I.; Kanagasabapathy, S.; Claverie, J. Reversible addition fragmentation transfer (RAFT) polymerization in emulsion. *Macromol. Symp.* **2000**, *150*, 33−38.
(47) Lejars, M.; Margaillan, A.; Bressy, C. Synthesis and characterization of diblock and statistical copolymers based on hydrolyzable siloxy silylester methacrylate monomers. *Polym. Chem.* **2014**, *5*, 2109−2117.
(48) Willcock, H.; O'Reilly, R. K. End group removal and modification of RAFT polymers. *Polym. Chem.* **2010**, *1*, 149−157.
(49) Vollrath, A.; Pretzel, D.; Pietsch, C.; Perevyazko, I.; Schubert, S.; Pavlov, G. M.; Schubert, U. S. Preparation, Cellular Internalization, and Biocompatibility of Highly Fluorescent PMMA Nanoparticles. *Macromol. Rapid Commun.* **2012**, *33*, 1791−1797.
(50) Beck-Broichsitter, M.; Nicolas, J.; Couvreur, P. Solvent selection causes remarkable shifts of the ″Ouzo region″ for poly(lactide-co-glycolide) nanoparticles prepared by nanoprecipitation. *Nanoscale* **2015**, *7*, 9215−9221.
(51) Reisch, A.; Runser, A.; Arntz, Y.; Mély, Y.; Klymchenko, A. S. Charge-Controlled Nanoprecipitation as a Modular Approach to Ultrasmall Polymer Nanocarriers: Making Bright and Stable Nanoparticles. *ACS Nano* **2015**, *9*, 5104−5116.
(52) Aubry, J.; Ganachaud, F.; Cohen Addad, J.-P.; Cabane, B. Nanoprecipitation of Polymethylmethacrylate by Solvent Shifting:1. Boundaries. *Langmuir* **2009**, *25*, 1970−1979.
(53) Vollrath, A.; Schallon, A.; Pietsch, C.; Schubert, S.; Nomoto, T.; Matsumoto, Y.; Kataoka, K.; Schubert, U. S. A toolbox of differently sized and labeled PMMA nanoparticles for cellular uptake investigations. *Soft Matter* **2013**, *9*, 99−108.
(54) Bui, Q. N.; Li, Y.; Jang, M.-S.; Huynh, D. P.; Lee, J. H.; Lee, D. S. Redox- and pH-Sensitive Polymeric Micelles Based on Poly(*β*-amino ester)-Grafted Disulfide Methylene Oxide Poly(ethylene glycol) for Anticancer Drug Delivery. *Macromolecules* **2015**, *48*, 4046−4054.
(55) Zhang, H.; Xia, T.; Meng, H.; Xue, M.; George, S.; Ji, Z.; Wang, X.; Liu, R.; Wang, M.; France, B.; Rallo, R.; Damoiseaux, R.; Cohen, Y.; Bradley, K. A.; Zink, J. I.; Nel, A. E. Differential Expression of Syndecan-1 Mediates Cationic Nanoparticle Toxicity in Undifferentiated versus Differentiated Normal Human Bronchial Epithelial Cells. *ACS Nano* **2011**, *5*, 2756−2769.
(56) Yue, Y.; Jin, F.; Deng, R.; Cai, J.; Chen, Y.; Lin, M. C. M.; Kung, H.-F.; Wu, C. Revisit complexation between DNA and polyethylenimine — Effect of uncomplexed chains free in the solution mixture on gene transfection. *J. Controlled Release* **2011**, *155*, 67−76.
(57) Xu, Z.; Liu, S.; Kang, Y.; Wang, M. Glutathione-Responsive Polymeric Micelles Formed by a Biodegradable Amphiphilic Triblock Copolymer for Anticancer Drug Delivery and Controlled Release. *ACS Biomater. Sci. Eng.* **2015**, *1*, 585−592.
(58) Gewirtz, D. A critical evaluation of the mechanisms of action proposed for the antitumor effects of the anthracycline antibiotics adriamycin and daunorubicin. *Biochem. Pharmacol.* **1999**, *57*, 727−741.

DOI: 10.1021/acs.macromol.5b02603
Macromolecules 2016, 49, 3856−3868

Dual responsive nanoparticles from a RAFT copolymer library for the controlled delivery of doxorubicin

Turgay Yildirim,[a,b] *Anja Traeger,*[a,b] *Elisabeth Preussger,*[a,b] *Steffi Stumpf,*[a,b] *Carolin Fritzsche,*[a,b] *Stephanie Hoeppener,*[a,b] *Stephanie Schubert,**[b,c] *Ulrich S. Schubert**[a,b]

[a] Laboratory of Organic and Macromolecular Chemistry (IOMC), Friedrich Schiller University Jena, Humboldtstr. 10, 07743 Jena, Germany

[b] Jena Center for Soft Matter (JCSM), Friedrich Schiller University Jena, Philosophenweg 7, 07743 Jena, Germany

[c] Institute of Pharmacy, Department of Pharmaceutical Technology, Friedrich Schiller University Jena, Otto-Schott-Str. 41, 07745 Jena, Germany

Corresponding Author

*Fax: +49(0) 3641 9482 02; E-mail: stephanie.schubert@uni-jena.de; ulrich.schubert@uni-jena.de

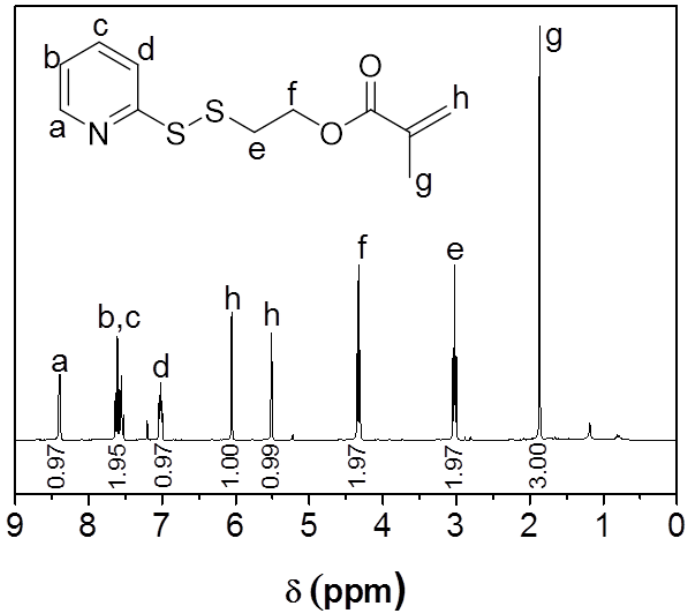

Figure S1. ^{1}H NMR spectrum (300 MHz, $CDCl_3$) of pyridyldisulfide ethylmethacrylate (PDSM) and the assignment of the peaks.

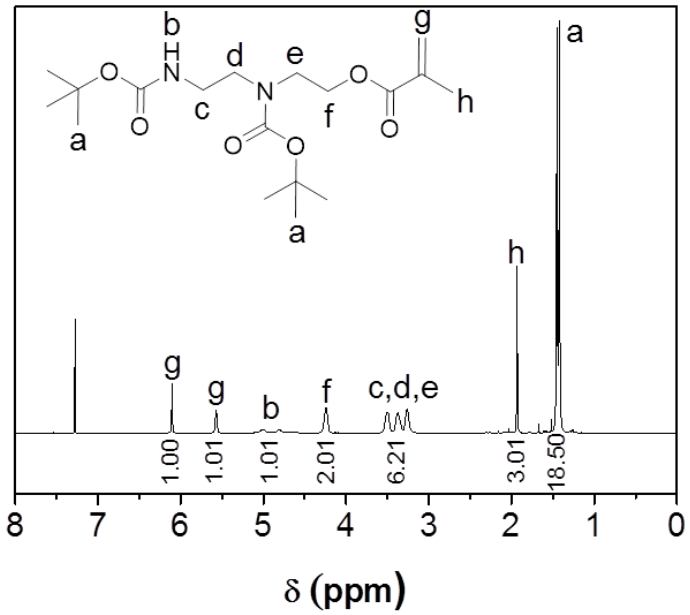

Figure S2. ^{1}H NMR spectrum (400 MHz, $CDCl_3$) of 2-((*tert*-butoxycarbonyl)(2-((*tert*-butoxycarbonyl)amino)ethyl)amino)ethylmethacrylate (BocAEAEMA) and the assignment of the peaks.

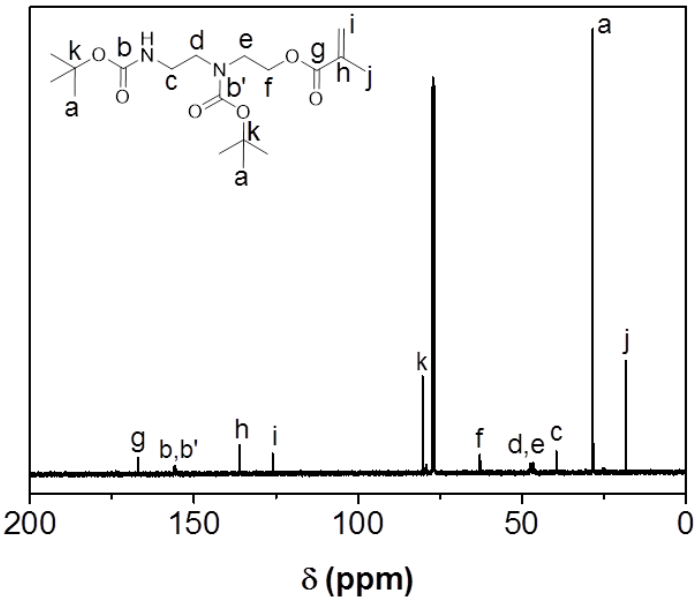

Figure S3. ^{13}C NMR spectrum (400 MHz, $CDCl_3$) of 2-((*tert*-butoxycarbonyl)(2-((*tert*-butoxycarbonyl)amino)ethyl)amino)ethylmethacrylate (BocAEAEMA) at 25 °C and the assignment of the peaks.

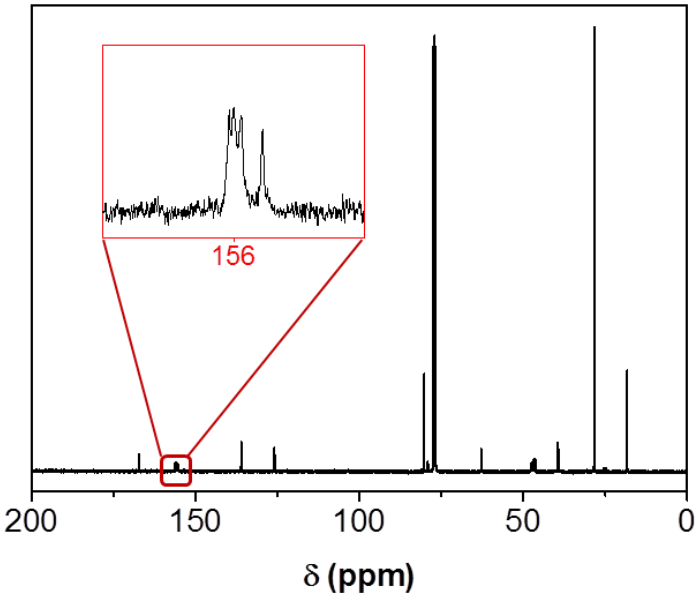

Figure S4. ^{13}C NMR spectrum (400 MHz, $CDCl_3$) of 2-((*tert*-butoxycarbonyl)(2-((*tert*-butoxycarbonyl)amino)ethyl)amino)ethylmethacrylate (BocAEAEMA) at 0 °C.

Additional comments on ^{1}H and ^{13}C NMR spectrum of 2-((*tert*-butoxycarbonyl)(2-((*tert*-butoxycarbonyl)amino)ethyl)amino)ethylmethacrylate (BocAEAEMA): The characteristic signal of amide proton ,-NH, is observed as duplicate (at 4.79 and 4.99 ppm) instead of a singlet (Figure S2). This is attributed to the presence of two possible isomers (E/Z) of the Boc protection groups. To prove this assumption, we applied ^{13}C NMR experiments at 25 and 0 °C. Figure S3 demonstrate a ^{13}C NMR spectrum of BocAEAEMA at 25 °C. All characteristics carbon peaks of the BocAEAEMA at 25 °C can be assigned. However, at 156 ppm carbonyl carbon peaks of the Boc protecting groups (b and b', Figure S3) overlap and were not separated well. Therefore, ^{13}C NMR at 25 °C is found to be not informative to prove the isomerization. However, at 0 °C carbonyl carbon peaks of the Boc groups at around 156 ppm were separated well (Figure S4). Indeed, four separated peaks can be observed, which proves the (E/Z) isomerization of both Boc groups.

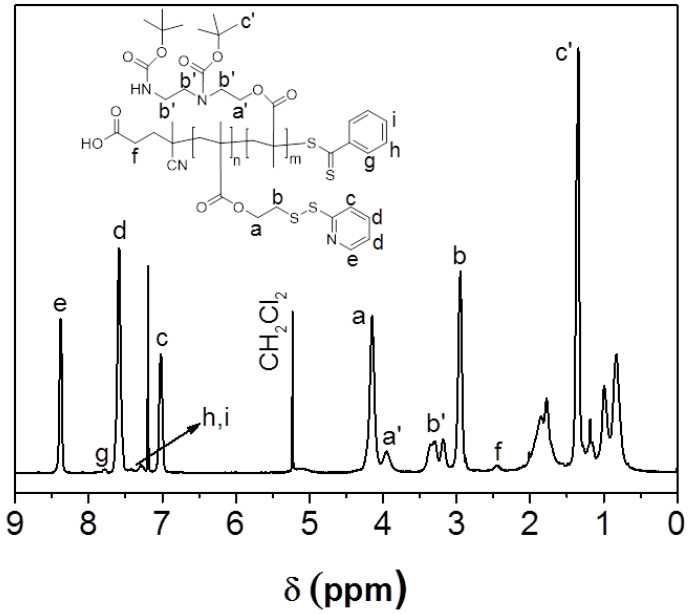

Figure S5. ^{1}H NMR spectrum (300 MHz, $CDCl_3$) of **P5** and the assignment of the peaks used to calculate the degree of polymerization (DP).

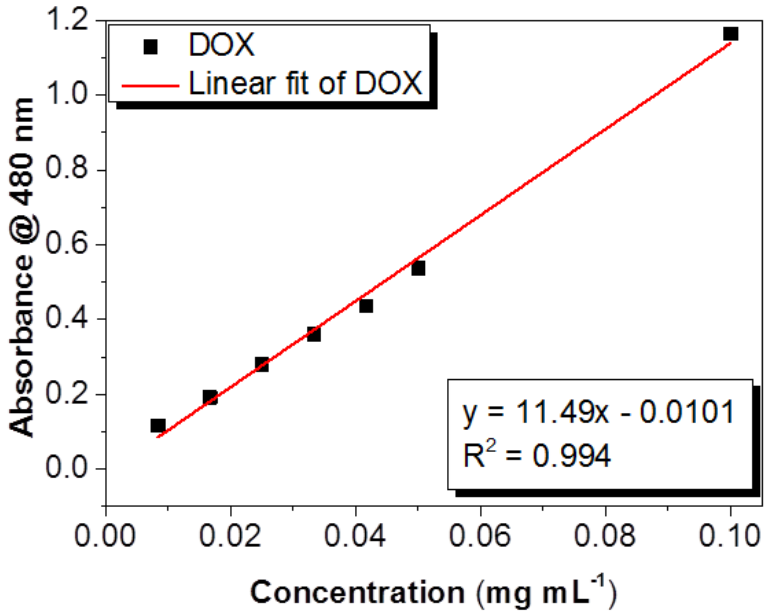

Figure S6. The UV-vis absorbance intensity of DOX in DMF at a wavelength of 480 nm as a function of DOX concentration.

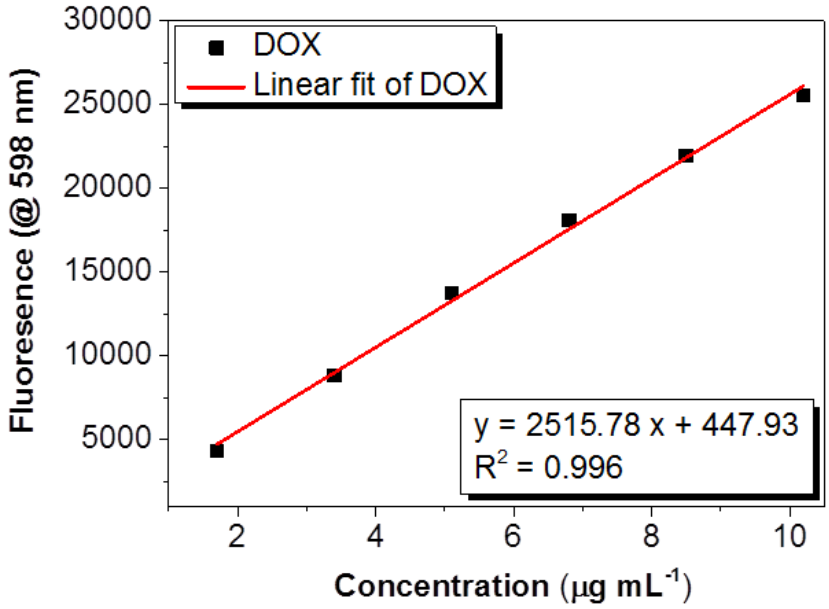

Figure S7. The fluorescence intensity of DOX in deionized water at emission wavelength of 598 nm, excitation wavelength of 488 nm, as a function of DOX concentration.

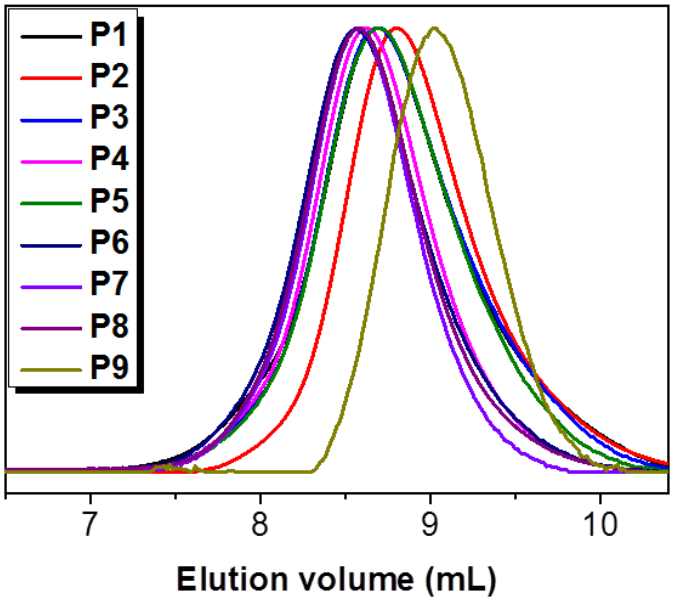

Figure S8. Normalized SEC traces in $CHCl_3$ of isolated copolymers of **P1** to **P9**.

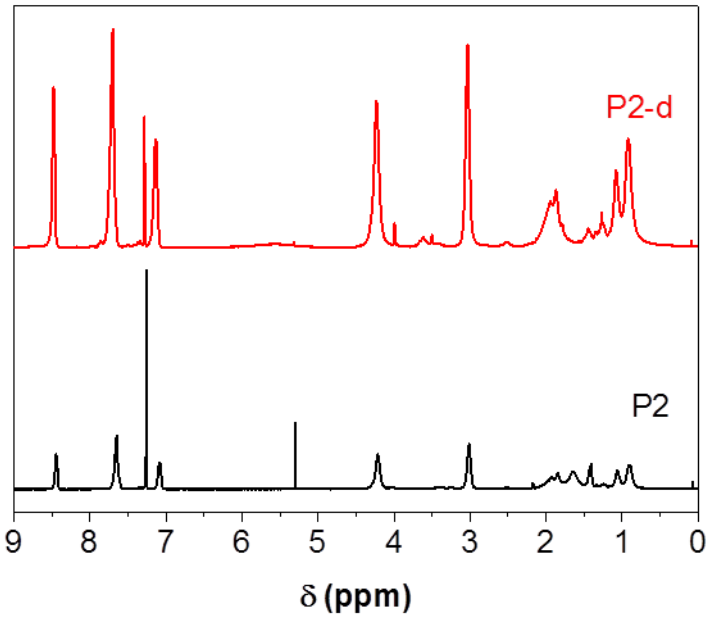

Figure S9. ^1H NMR spectra (300 MHz, $CDCl_3$) of **P2** and deprotected form of **P2** (**P2-d**).

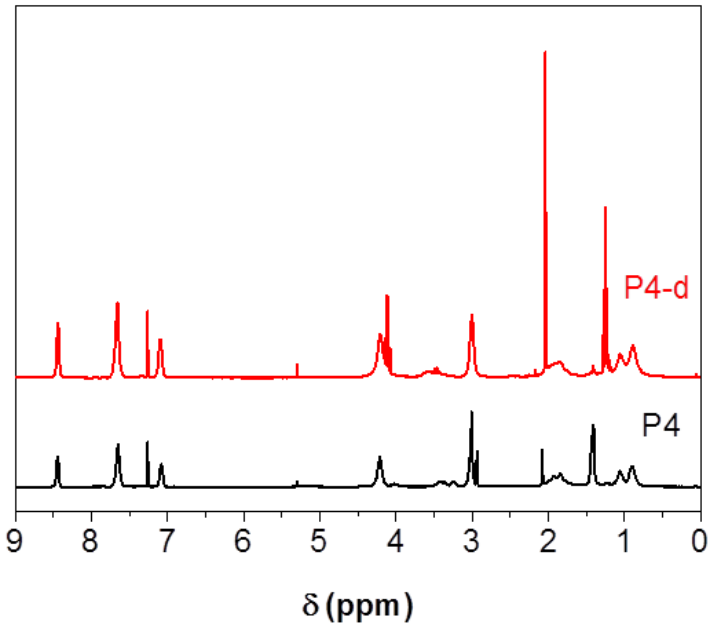

Figure S10. ^{1}H NMR spectra (300 MHz, $CDCl_3$) of **P4** and deprotected form of **P4** (**P4-d**).

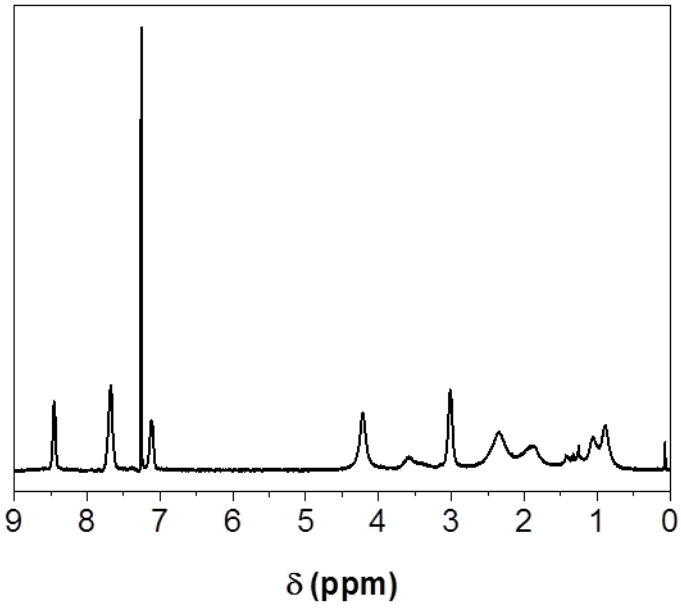

Figure S11. ^{1}H NMR spectrum (300 MHz, $CDCl_3$) of deprotected form of **P5** (**P5-d**).

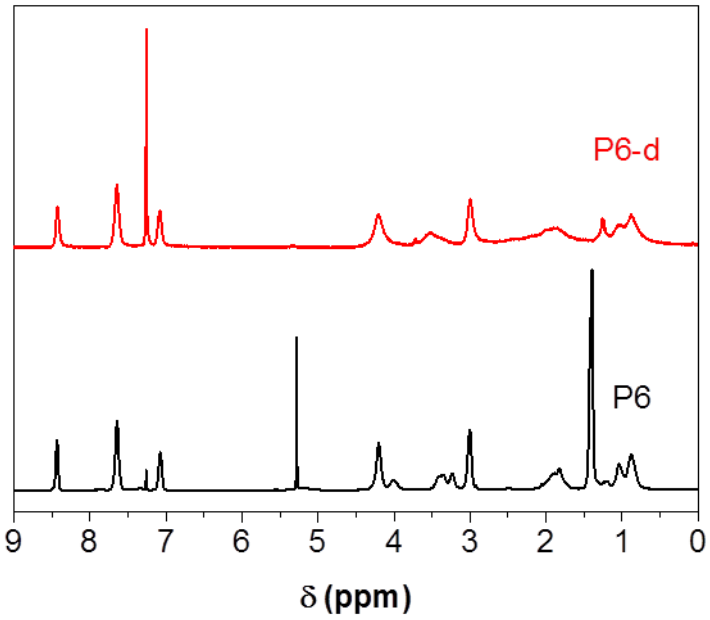

Figure S12. ^{1}H NMR spectrum (300 MHz, $CDCl_3$) of deprotected form of **P6** (**P6-d**).

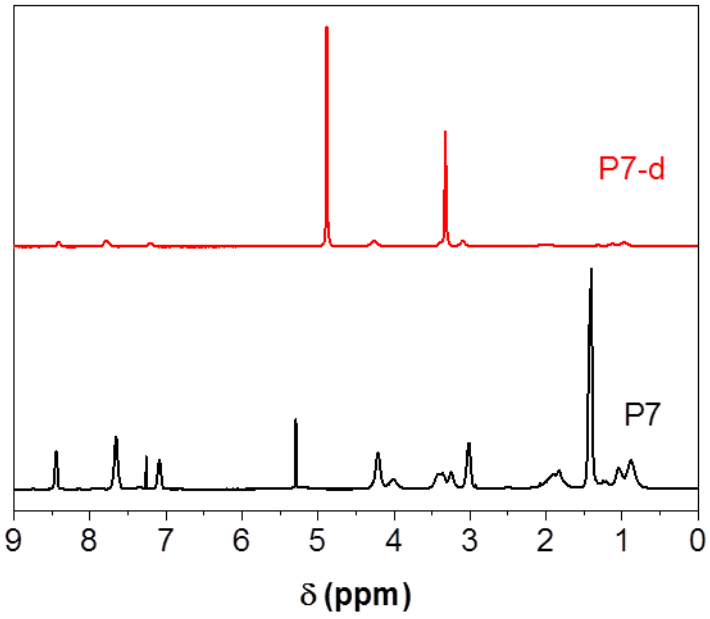

Figure S13. ^{1}H NMR spectrum of **P7** (300 MHz, $CDCl_3$) and ^{1}H NMR spectrum (300 MHz, MeOD) of deprotected form of **P7** (**P7-d**).

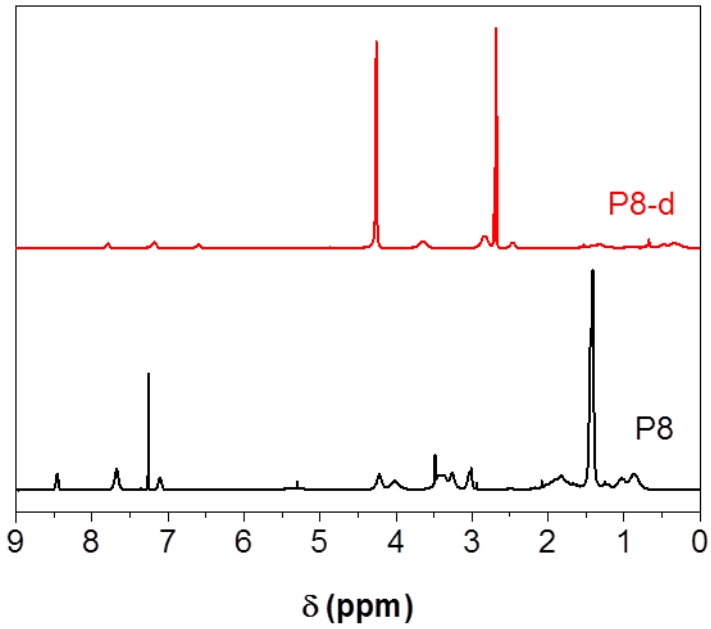

Figure S14. ^{1}H NMR spectrum of **P8** (300 MHz, $CDCl_3$) and ^{1}H NMR spectrum (300 MHz, MeOD) of deprotected form of **P8** (**P8-d**).

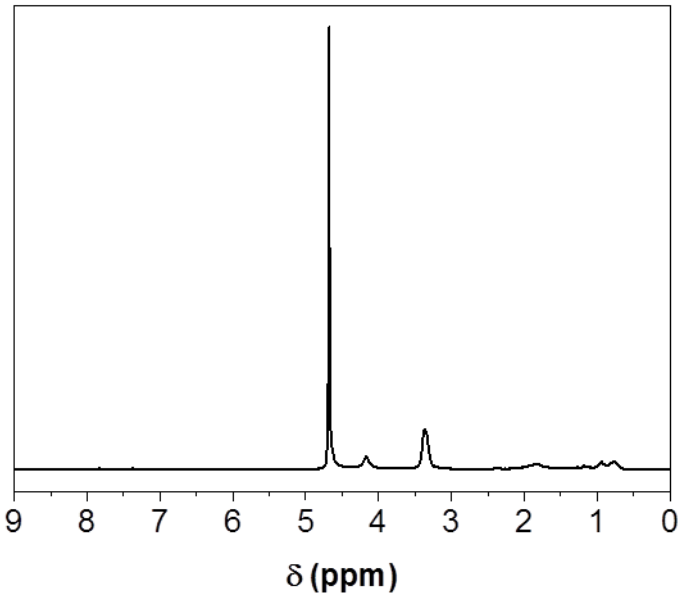

Figure S15. ^{1}H NMR spectrum (300 MHz, D_2O) of deprotected form of **P9** (**P9-d**).

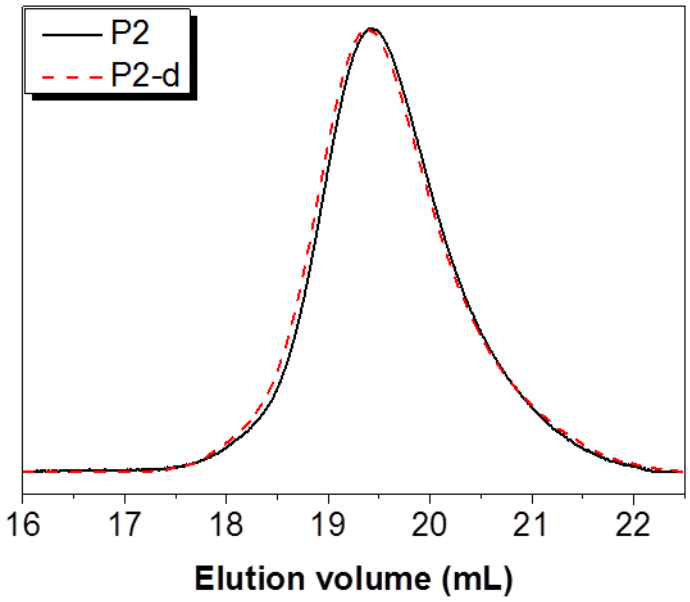

Figure S16. Normalized SEC traces in DMAc of **P2** and deprotected form of **P2** (**P2-d**).

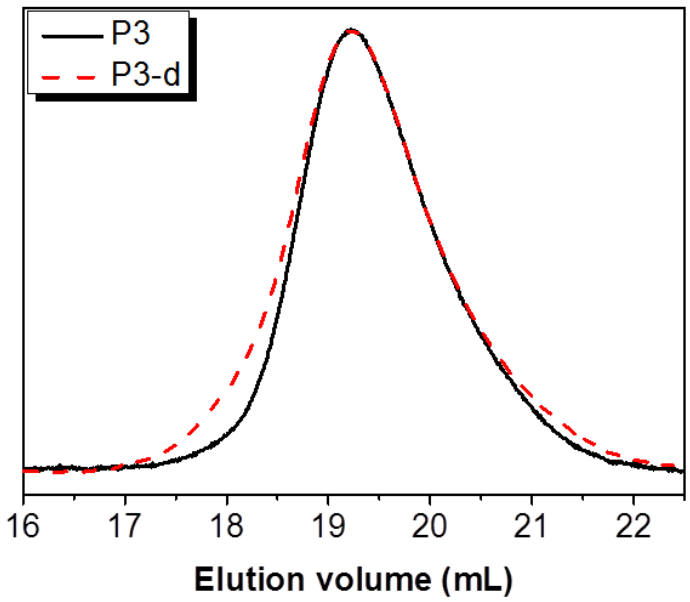

Figure S17. Normalized SEC traces in DMAc of **P3** and deprotected form of **P3** (**P3-d**).

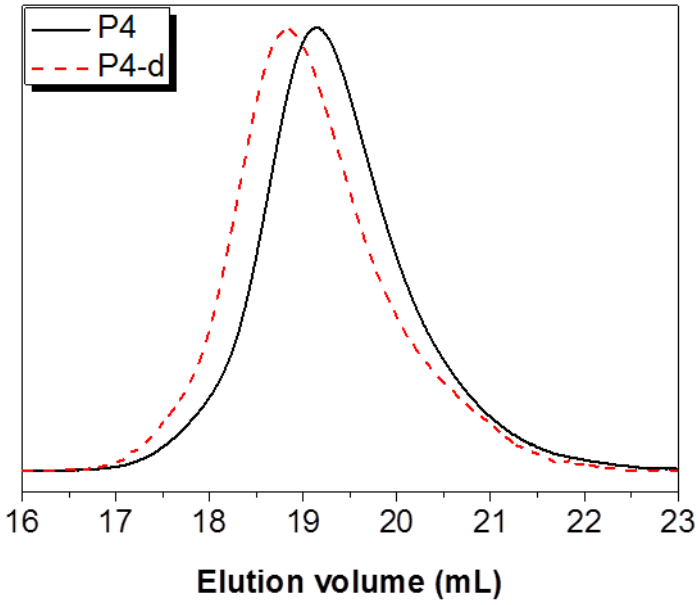

Figure S18. Normalized SEC traces in DMAc of **P4** and deprotected form of **P4** (**P4-d**).

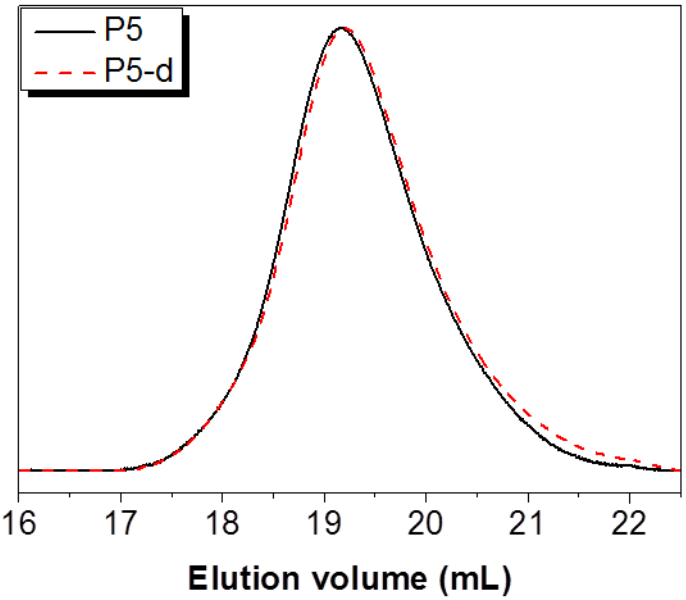

Figure S19. Normalized SEC traces in DMAc of **P5** and deprotected form of **P5** (**P5-d**).

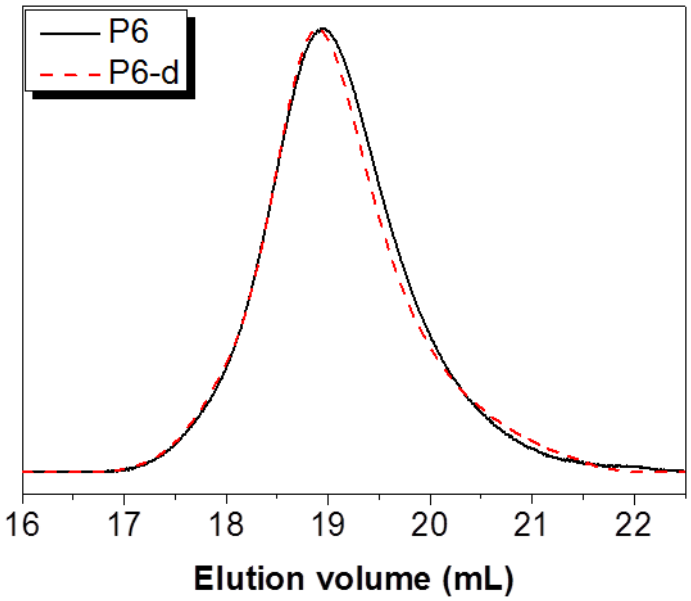

Figure S20. Normalized SEC traces in DMAc of **P6** and deprotected form of **P6** (**P6-d**).

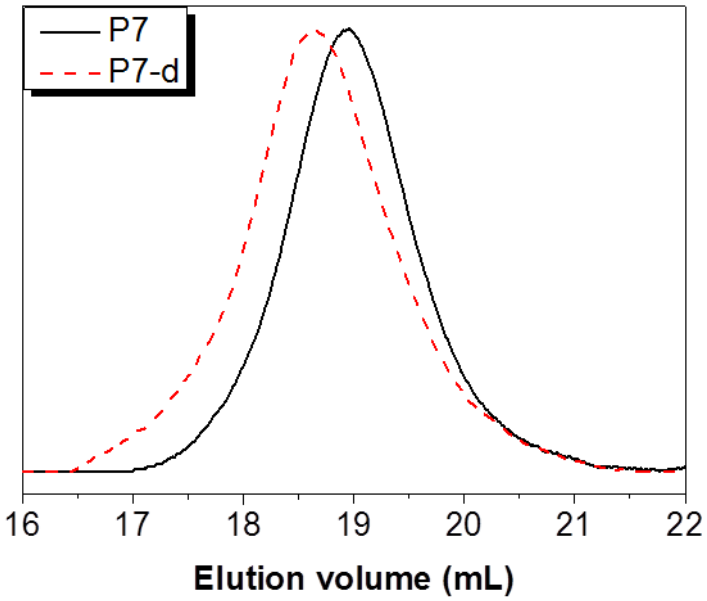

Figure S21. Normalized SEC traces in DMAc of **P7** and deprotected form of **P7** (**P7-d**).

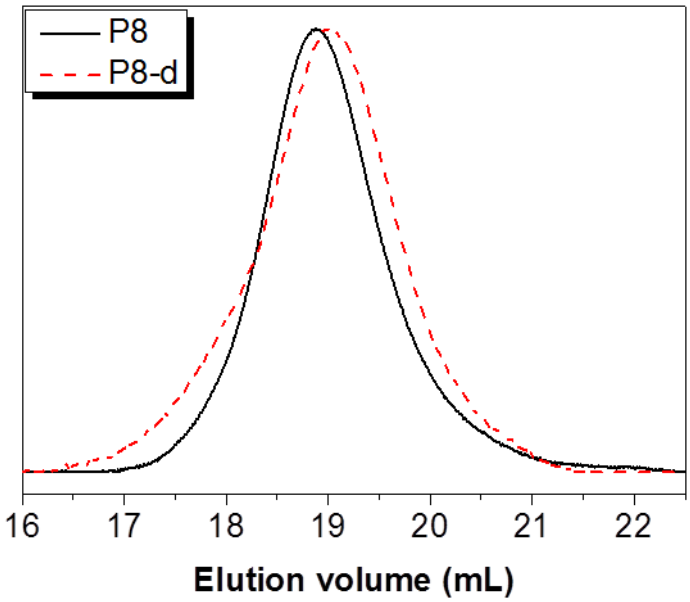

Figure S22. Normalized SEC traces in DMAc of **P8** and deprotected form of **P8** (**P8-d**).

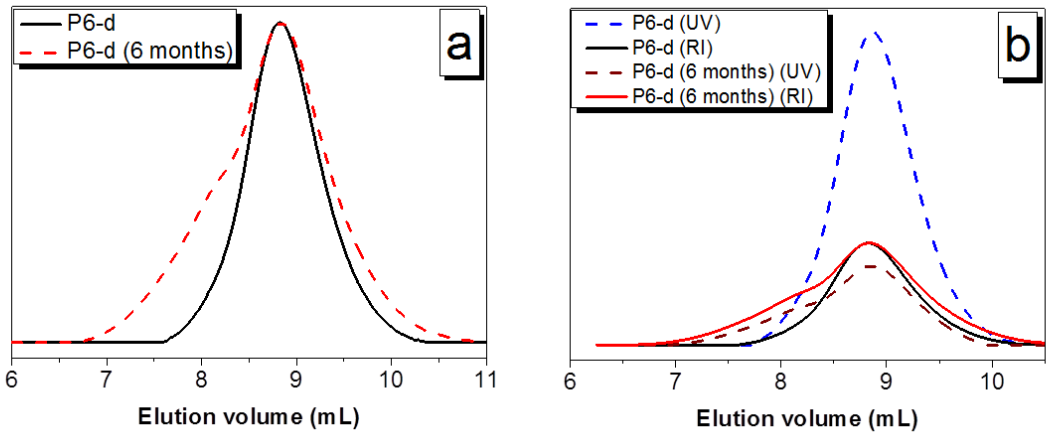

Figure S23. (a) Normalized SEC (RI) traces in $CHCl_3$ of **P6-d** before and after six months storage at room temperature. (b) Calibrated SEC (UV) traces in $CHCl_3$ of **P6-d** before and after six months storage at room temperature.

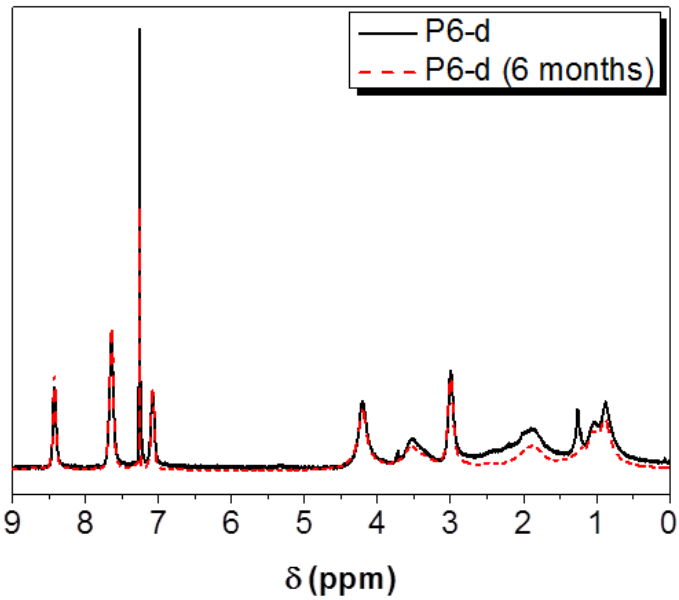

Figure S24. ^{1}H NMR spectrum of **P6-d** (300 MHz, $CDCl_3$) before and after six months storage at room temperature.

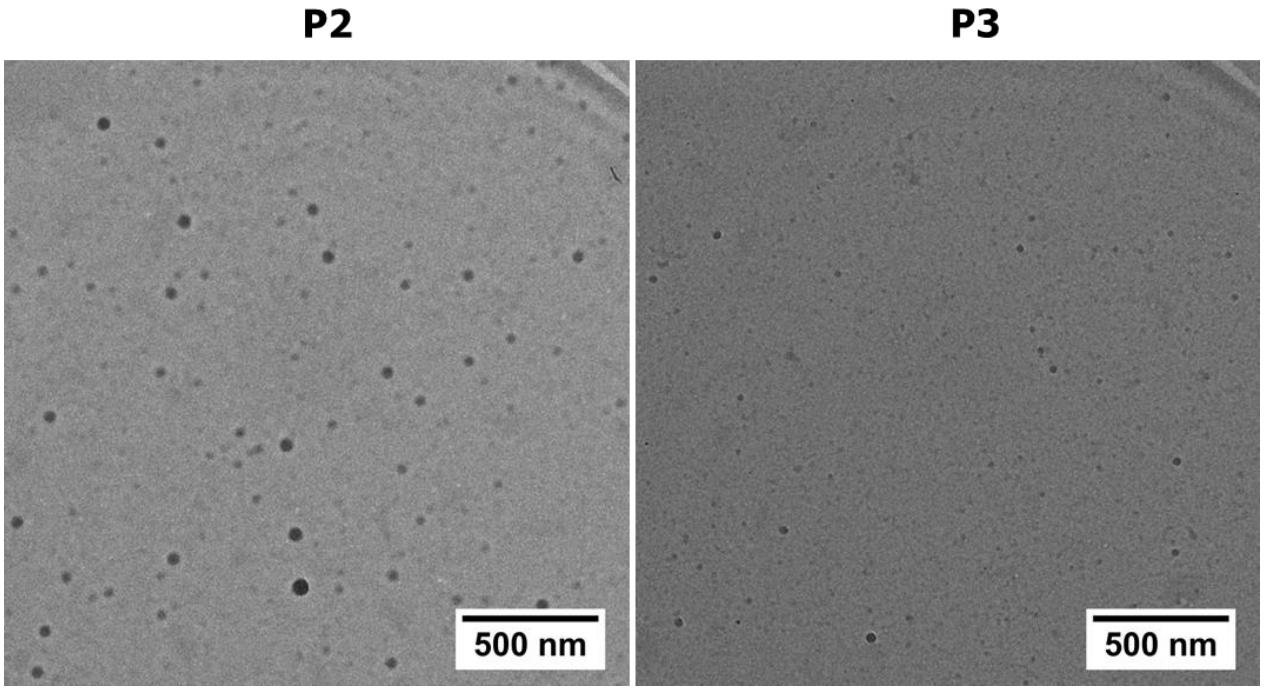

Figure S25. TEM images of nanoparticles that were prepared from **P2** and **P3** (5 mg mL^{-1}) by dropping acetone-polymer solution to water (AW).

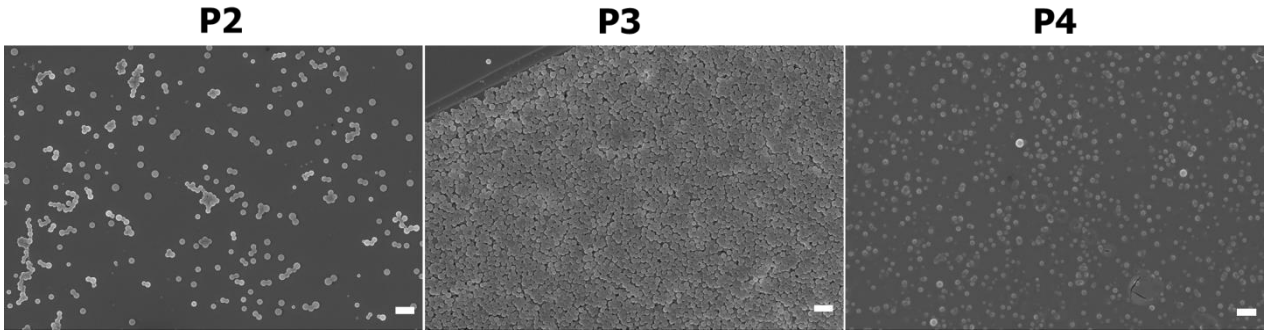

Figure S26. SEM images of nanoparticles that were prepared from **P2**, **P3** and **P4** (3 mg mL^{-1}) by dropping water to acetone-polymer solution (WA). Scale bars represent 1000 nm.

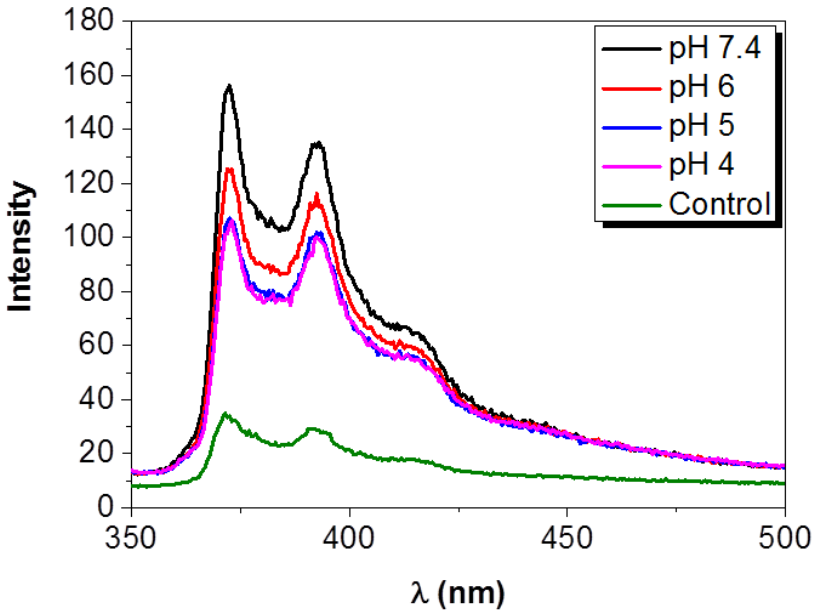

Figure S27. Fluorescence emission spectra of pyrene (4.8×10^{-6} mol L^{-1}) in **P2** nanoparticles (0.060 mg mL^{-1}) as a function of the pH value. Pyrene in pure water was used as control.

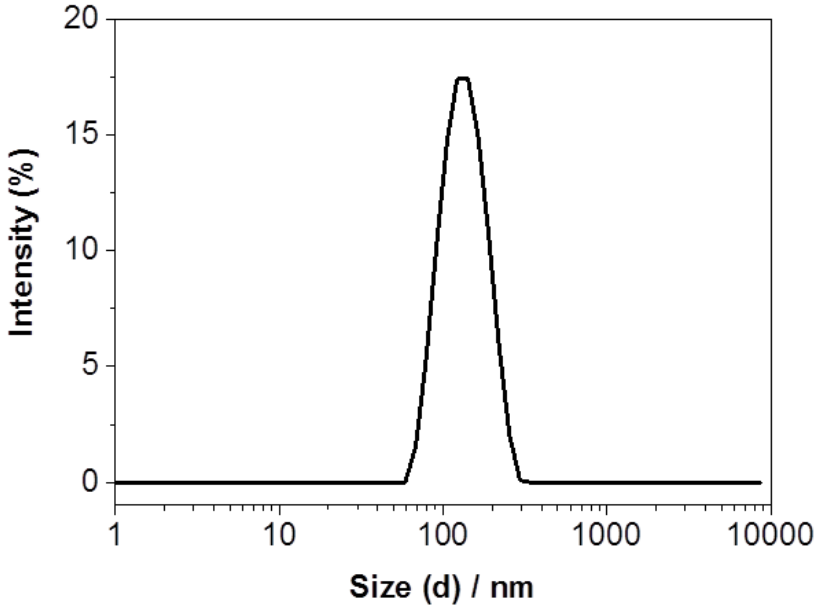

Figure S28. Intensity size distribution of DOX-loaded nanoparticles in water.

Publication P5

"Dual pH and ultrasound responsive nanoparticles with pH triggered surface charge-conversional properties"

T. Yildirim, I. Yildirim, R. Yanez-Macias, S. Stumpf, C. Fritzsche, S. Hoeppener, C. Guerrero-Sanchez, S. Schubert, U. S. Schubert

Polym. Chem. **2017**, *8*, 1328-1340.

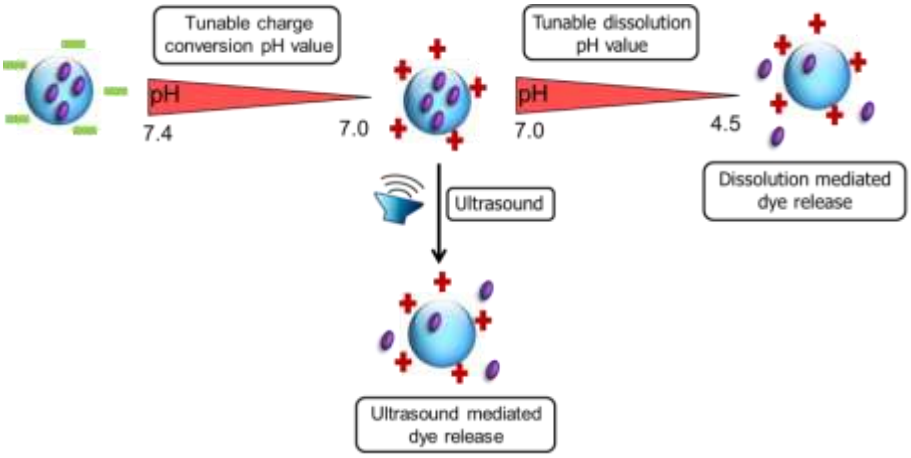

Published on 16 January 2017. Downloaded by Thueringer Universitats Landesbibliothek Jena on 26/06/2017 08:02:15.

Polymer Chemistry

PAPER

View Article Online
View Journal | View Issue

Cite this: *Polym. Chem.*, 2017, **8**, 1328

Dual pH and ultrasound responsive nanoparticles with pH triggered surface charge-conversional properties†

Turgay Yildirim,[a,b] Ilknur Yildirim,[a,b] Roberto Yañez-Macias,[b,c] Steffi Stumpf,[a,b] Carolin Fritzsche,[a,b] Stephanie Hoeppener,[a,b] Carlos Guerrero-Sanchez,[a,b] Stephanie Schubert*[b,d] and Ulrich S. Schubert*[a,b]

A series of dual pH- and ultrasound responsive statistical copolymers were synthesized *via* the reversible addition–fragmentation chain transfer (RAFT) polymerization of 3,4-dihydro-2*H*-pyran (DHP) protected HEMA 2-((tetrahydro-2*H*-pyran-2-yl)oxy)ethyl methacrylate (THP-HEMA) and 2-(dimethylamino)ethyl methacrylate (DMAEMA). The RAFT-controlled nature of the (co)polymerizations was verified by detailed kinetic studies. The chemical structure and the co-monomer composition of the copolymers were confirmed by ^{1}H NMR spectroscopy. The number-average molar mass values (M_n) and dispersities ($Đ_M$ = M_w/M_n) of the copolymers were estimated by size exclusion chromatography (SEC). The thermal properties of the (co)polymers were analyzed by means of thermogravimetric analysis (TGA) and differential scanning calorimetry (DSC). Additionally, the DMAEMA moieties of the copolymers were quaternized with an excess of methyl iodide. The synthesized polymers self-assemble into nanoparticles in aqueous media *via* the nanoprecipitation method and were characterized by dynamic light scattering (DLS) and transmission electron microscopy (TEM). Zeta potential measurements revealed that all DMAEMA containing nanoparticles undergo a surface charge conversion from positive to negative at slightly acidic pH values. However, quaternized DMAEMA nanoparticles possess pH independent positive surface charges. At acidic pH values, the nanoparticles disassemble and dissolve in water due to the protonation of the DMAEMA moieties and/or due to the acidic hydrolysis of the THP-HEMA groups. It was found that the surface charge and the stability of the nanoparticles were greatly affected by the DMAEMA content of the polymers, meaning that the isoelectric point (IEP), at which the charge is reversed and the pH value at which the disassembly occurs, increased with the higher DMAEMA content in the copolymer. Moreover, it was proven that the ionization of the carboxyl RAFT end-group of the polymers enhanced the anionic character and the stability of the nanoparticles at neutral pH values. DLS and scanning electron microscopy (SEM) measurements revealed that these nanoparticles can be further disrupted by ultrasound exposure. Nile Red was encapsulated into nanoparticles as a model hydrophobic drug. The release profile of the Nile Red was significantly accelerated in acidic media or under ultrasound exposure. The cytotoxicity assay results showed that negatively charged nanoparticles are non-toxic and biocompatible, whereas positively charged nanoparticles are extremely toxic to L929 cells.

Received 3rd November 2016,
Accepted 14th January 2017

DOI: 10.1039/c6py01927g

rsc.li/polymers

Introduction

Over the past few decades, a large number of nanoparticle based drug delivery systems have been used in various stages of clinical applications.[1] These carriers improve drug treatments by altering their pharmacokinetics and biodistribution profiles. Nevertheless, uncontrolled drug release and poor cellular internalization are still issues limiting the therapeutic efficacy. To overcome these limitations, increasing attention has been drawn to stimuli responsive polymeric nanoparticles, also called "smart nanoparticles". The surface charge of the

[a]*Laboratory of Organic and Macromolecular Chemistry (IOMC), Friedrich Schiller University Jena, Humboldtstr. 10, 07743 Jena, Germany. E-mail: stephanie.schubert@uni-jena.de, ulrich.schubert@uni-jena.de*
[b]*Jena Center for Soft Matter (JCSM), Friedrich Schiller University Jena, Philosophenweg 7, 07743 Jena, Germany*
[c]*Centro de Investigación en Química Aplicada, Departamento de Síntesis de Polímeros, Blvd. Enrique Reyna H. 140, 25100 Saltillo, Mexico*
[d]*Institute of Pharmacy, Department of Pharmaceutical Technology, Friedrich Schiller University Jena, Otto-Schott-Str. 41, 07745 Jena, Germany*
† Electronic supplementary information (ESI) available: Additional ^{1}H NMR, SEC and DLS data. See DOI: 10.1039/c6py01927g

This journal is © The Royal Society of Chemistry 2017

Published on 16 January 2017. Downloaded by Thueringer Universitats Landesbibliothek Jena on 26/06/2017 08:02:15.

nanoparticles has a significant influence on the blood circulation, cellular uptake and the safety of the nanocarriers. For instance, it is known that positively charged nanoparticles are more rapidly internalized by the cells than neutral and negatively charged ones as a result of their high affinity for the negatively charged phospholipid bilayer of cell membranes.[2] However, the positive charge of the nanoparticles can cause nonspecific cellular uptake and strong interaction with proteins in the bloodstream, which causes severe aggregation and rapid clearance from circulation. Moreover, positively charged nanoparticles can perturb the structure of the plasma membrane, which induces high cytotoxicity and excessive immune response.[3] In contrast, neutral and negatively charged nanoparticles have shown prolonged circulation times and less interactions with serum proteins in *in vivo* experiments.[4] As a consequence, considering the slightly acidic pH value of the tumor extracellular environment (6.5 to 7.2) and the above mentioned facts, the development of stimuli responsive, charge-conversional nanoparticle systems, which have negative or neutral surface charge values under physiological conditions but become positively charged under a slightly acidic environment, would yield interesting candidates for intravenous antitumor drug delivery systems. Such systems are expected to improve the targeting efficiency by combining the advantages of positively and negatively charged nanoparticles.[5,6] There are two main strategies for the fabrication of polymeric surface charge-conversional nanoparticle systems. The first and most intensively investigated strategy relies on the tumor pH-triggered cleavage of the amide bond between an amino and 2,3-dimethylmaleic anhydride at the tumor site, which results in a charge conversion from negative to positive.[7–10] The second strategy involves polymers that have ionizable segments such as amino and/or carboxyl groups in the backbone. In this case, the charge conversion ability of the nanoparticles is sustained by the protonation and deprotonation of the ionizable groups of the polymer upon change of pH value.[11–13] These studies demonstrated the enhanced cellular uptake of the surface charge-conversional nanoparticles. However, to improve the therapeutic efficiency the loaded cargo should additionally be released rapidly when the desired destination is reached. Therefore, several surface charge-conversional nanoparticles combined with stimuli responsive drug release profiles have been investigated. Stimuli responsive nanoparticles can enhance the therapeutic activity of loaded drugs by spatially controlled release *via* responding to various exogenous (light,[14] temperature,[15] ultrasound,[16] and magnetic field[17]) or endogenous (pH value,[18] redox,[19] enzyme,[20] and receptor[21]) stimuli. Among these stimuli, pH value and redox responsiveness are the most frequently used ones due to the pH gradients in tissues (*e.g.* normal *vs.* tumor tissue) and intracellular pathways (during endocytosis pH value decreases from 7.4 to 5.0–6.0 in endosomes and to 4.0–5.0 in lysosomes) and the reductive environment of the cytosol compared to extracellular environments (100 to 1000 times higher glutathione (GSH) concentration than the extracellular GSH).[22] Though most of the reported drug release mechanisms depend on the endogenous stimuli triggered release mechanisms like endosomal pH value or redox potential, they are complicated and limit the control over drug release.[23] In contrast, exogenous stimuli are independent of the complex conditions of the biological environment that can enable a precise control over the release of encapsulated cargo. Among the exogenous stimuli ultrasound has recently attracted much attention since ultrasound is noninvasive and can penetrate deep into the interior of the body.[16,24–26] Moreover, ultrasound can be localized in space and time, which prevents damage to healthy tissue.

In this contribution, a library of well-defined statistical copolymers of 2-((tetrahydro-2*H*-pyran-2-yl)oxy)ethyl methacrylate (THP-HEMA) with different compositions of 2-(dimethylamino)ethyl methacrylate (DMAEMA) were synthesized using the RAFT polymerization process (Scheme 1) to develop a novel pH value and an ultrasound responsive drug delivery system, which possesses the following features: (i) a charge conversion from negative to positive under slightly acidic conditions and (ii) nanoparticle disassembly at endosomal pH values or by ultrasound exposure. We used THP-HEMA as a hydrophobic moiety of the polymers because its cyclic acetal functionality can be cleaved under acidic conditions.[27] This converts the hydrophobic part of the polymer into hydrophilic HEMA leading to an imbalance of the hydrophilic/lipophilic ratio resulting in the disassembly of the corresponding nanoparticles. Additionally, it is known that THP functional nanoparticles can be disrupted by ultrasound treatment.[28,29]

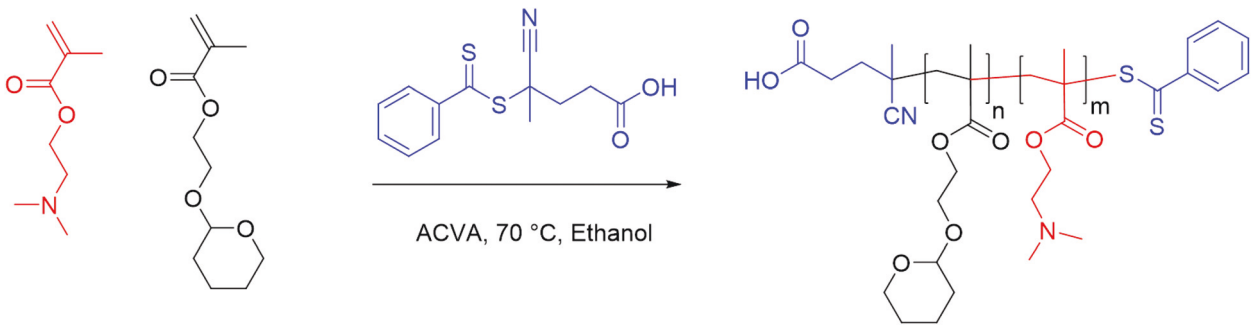

Scheme 1 Schematic representation of the RAFT copolymerization of THP-HEMA with DMAEMA.

Published on 16 January 2017. Downloaded by Thueringer Universitats Landesbibliothek Jena on 26/06/2017 08:02:15.

DMAEMA was used as a hydrophilic moiety since it is a weak polyelectrolyte in water with a pK_a value of ~7.4. Therefore, it is expected that partial protonation of DMAEMA groups can render the surface charge conversion at slightly acidic pH values and complete protonation of the DMAEMA groups at endosomal pH values may cause nanoparticle disassembly. Findings on the synthesis and self-assembly behavior of these polymers in aqueous media, pH value and ultrasound responsiveness of the corresponding nanoparticles, the release kinetics of the encapsulated Nile Red in response to pH value and ultrasound, and the effect of surface charge on the cytotoxicity of nanoparticles are discussed below.

Experimental section

Materials

The THP-HEMA was synthesized according to the procedure reported elsewhere (see Fig. S1† for the ^{1}H NMR spectrum).[27] 4,4′-Azobis(4-cyanovaleric acid) (ACVA), 4-cyano-4-(phenylcarbonothioylthio)pentanoic acid (CPADB), 4-cyano-4-[(dodecylsulfanylthiocarbonyl)sulfanyl]pentanol (CDP), 1,3,5-trioxane, *N*,*N*-dimethylaminoethyl methacrylate (DMAEMA), methyl iodide (MeI), and Nile Red were purchased from Sigma Aldrich. AlamarBlue was obtained from Life Technologies. Consumables for cell culture, like pipettes and cell culture plates (96 well) were obtained from Corning (USA) and Greiner Bio-one (Austria/Germany). If not stated otherwise, cell culture media and supplements (L-glutamine, antibiotics) were obtained from Biochrom (Merck Millipore, Germany). Poly(methyl methacrylate) (PMMA) (M_n = 13 500 g mol^{-1}, $Đ_M$ = 1.13) was obtained from Polymer Libraries GmbH (Germany). All other chemicals were purchased from standard suppliers and used without further purification.

Instruments and methods

Proton nuclear magnetic resonance (^{1}H NMR) spectra were recorded at room temperature in $CDCl_3$ or DMSO-d_6 on a Bruker Avance 300 MHz. The chemical shifts are given in ppm.

Size-exclusion chromatography (SEC) measurements were performed on a Shimadzu system equipped with a SCL-10A system controller, a LC-10AD pump, a RID-10A refractive index detector, and a PSSSDV-linear S column (5 μm particle size; Polymer Standards Service GmbH, Mainz, Germany) at 40 °C using a $CHCl_3$, triethylamine and 2-propanol (94 : 4 : 2) mixture as the eluent at a flow rate of 1 mL min^{-1}. The system was calibrated with a linear calibration curve built from poly(methyl methacrylate) (PMMA) standards of narrow dispersity (M_p = 410 to 88 000 g mol^{-1}).

Differential Scanning Calorimetry (DSC) measurements were performed on a Netzsch DSC F1 Phoenix under a nitrogen atmosphere using a heating rate of 20 K min^{-1} from −50 to +150 °C. 2 cycles were recorded for each sample. The glass transition temperature (T_g) values are reported for the second heating run.

Thermogravimetric analysis (TGA) was performed under a nitrogen atmosphere on a Netzsch TG 209 F1 Iris in the range of room temperature to 800 °C with a heating rate of 20 K min^{-1}. The corresponding decomposition temperatures were determined at the decay point of the curves.

Solubility of the polymers was tested on a Crystal 16™ from Avantium Technologies being connected to a chiller (Julabo FP 40) using a wavelength of 500 nm.

Dynamic light scattering was performed using a Zetasizer Nano ZS (Malvern Instruments, Herrenberg, Germany). After an equilibration time of 180 s, 3 × 30 runs were carried out at 25 °C (λ = 633 nm). The counts were detected at an angle of 173°. Each measurement was performed in triplicate. The mean particle size was calculated applying the nonlinear least-squares fitting mode. The *Z*-average diameter and the width of the distribution as the polydispersity index of the particles (PDI) were obtained by the cumulants method assuming a spherical shape of the particles.

Electrophoretic light scattering was used to measure the electrokinetic potential, also known as ζ-potential. The measurements were performed on a Zetasizer Nano ZS (Malvern Instruments, Herrenberg, Germany) by applying laser Doppler velocimetry. For each measurement, 10 runs were carried out using the slow-field and fast-field reversal mode at 150 V. Each experiment was performed in triplicate at 25 °C.

For scanning electron microscopy (SEM), 5 μL of the suspensions were placed on a mica surface and dried overnight at room temperature under atmospheric pressure. Afterwards, samples were investigated using a Sigma VP field emission scanning electron microscope (Carl-Zeiss AG, Germany). The samples were coated with a thin layer (4 nm) of platinum *via* sputter coating using a Bal-TEC 020 HR Sputtering Coater.

Transmission electron microscopy (TEM) was carried out utilizing a FEI Technai G2 20 transmission electron microscope.

The fluorescence spectra of Nile Red were recorded on a Jasco FP-6500 fluorometer applying an excitation wavelength of 549 nm. The emission spectra were recorded from 560 to 800 nm. The excitation and emission bandwidths were 3.0 and 3.0 nm, respectively. For Nile Red release experiments a Tecan M200 Pro fluorescence microplate reader was used.

Synthesis

RAFT polymerization. A Chemspeed Swing-SLT automated parallel synthesizer was utilized for the synthesis of **P1–P5**. For more details about the automated parallel synthesizer readers are referred to the literature.[30–32] Neat chemicals (THP-HEMA, DMAEMA and ethanol (solvent reservoir)), stock solutions of ACVA (13.3 mg mL^{-1} in ethanol), and of the RAFT agent (53.0 mg mL^{-1} in ethanol) were prepared, degassed by purging with nitrogen for 15 min, and placed inside the automated synthesizer. Aliquots of THP-HEMA, DMAEMA, ACVA, RAFT agent stock solutions, and the solvent from the reservoirs were transferred into parallel reactors with the automated liquid handling system of the equipment to provide the desired concentrations of reagents. In all cases, a total monomer concen-

 This journal is © The Royal Society of Chemistry 2017

Published on 16 January 2017. Downloaded by Thueringer Universitats Landesbibliothek Jena on 26/06/2017 08:02:15.

tration of 1 M was maintained. Different initial monomer feed ratios were applied for each copolymerization to vary the amino content in the copolymers. The targeted molar mass value was $M_{n,tg}$ = 10 000 g mol^{-1} at 100% conversion. In all cases a [RAFT]/[initiator] = 1/0.25 was used. The initial feed ratios used are summarized in Table 1. After all the liquid transfers were completed, the reaction solutions were additionally degassed through one automated cooling–evacuate–heating cycle carried out as follows: the reaction mixtures were cooled to 0 °C, a vacuum (~5 millibar) was then applied to the reactor block while heating the reactors up to 0 °C and maintained for 2 minutes. After that, the reactors were sealed under a nitrogen atmosphere and heated to the reaction temperature (70 °C); the temperature of the reflux condensers on top of the reactors was set to 5 °C. The onset of the polymerizations was considered once the reaction temperature in the reactors was reached. At the pre-established times, an aliquot of 200 μL was withdrawn with the automated liquid handling system from the reaction mixtures and placed into NMR tubes and SEC vials (75 μL each and 50 μL excess) to follow the monomer conversion and molar mass of the formed polymers, respectively. SEC and NMR samples for analysis were prepared with the automated liquid handling system of the synthesizer at the end of each sampling sequence by adding the corresponding SEC and NMR solvents. Once the pre-established reaction time elapsed, the polymerization mixtures were cooled to 20 °C. Monomer conversions were determined *via* ^{1}H NMR by using 1,3,5-trioxane as an internal standard. The polymers were purified by precipitation in cold hexane : diethyl ether (4 : 1). The resulting pink colored polymers were dried under high vacuum at room temperature until constant weight to produce an overall yield of around ~80%. The number average molar mass (M_n) and molar mass dispersity ($Đ_M$) were determined by SEC using PMMA standards. The degree of polymerization (DP) for each polymer was calculated from the signal integrals of the ^{1}H NMR spectrum (Fig. 2) of the purified copolymer using the following equations:

$$\mathrm{DP_{THP\text{-}HEMA}} = \frac{I(\text{signal e})}{I(\text{signal a})/2} \quad (1)$$

$$\mathrm{DP_{DMAEMA}} = \frac{I(\text{signal h})/6}{I(\text{signal a})/2} \quad (2)$$

with I(signal e) corresponding to the integral of the methine proton peaks of the THP-HEMA at 4.65 ppm, I(signal h) corresponding to the integral of methyl proton peaks of the DMAEMA at 2.30 ppm, and I(signal a) corresponding to the integral of two aromatic protons of the dithiobenzoate end group at 7.84 ppm. Number average molar mass values were calculated by using the following equation:

$$M_{n,NMR} = (\mathrm{DP_{THP\text{-}HEMA}} \times M_{\mathrm{THP\text{-}HEMA}}) + (\mathrm{DP_{DMAEMA}} \times M_{\mathrm{DMAEMA}}) + M_{CTA} \quad (3)$$

in which the molar mass of the THP-HEMA, DMAEMA and RAFT agent is 214.26 g mol^{-1}, 157.21 g mol^{-1}, and 279.38 g mol^{-1}, respectively.

Quaternization of the polymers. For quaternization, each 50 mg of the polymer (**P2** to **P5**) were dissolved in 5 mL of acetone. Methyl iodide (MeI) was added at room temperature at a molar ratio of 3 compared to DMAEMA groups. The mixture was stirred overnight to ensure quantitative conversion. Excess MeI was removed by precipitation in cold hexane. The resulting quaternized polymers (**P2q** to **P5q**) were dried under high vacuum at room temperature.

Nanoprecipitation of the polymers. For nanoprecipitation, two different methods were used. For the acetone to water (AW) method, corresponding polymers (**P1** to **P5**, **P2q** to **P5q**, **P1OH**, **P5OH**) were dissolved in acetone at a final concentration of 1 mg mL^{-1} and subsequently added dropwise to deionized water under continuous stirring at 500 rpm. For the water to acetone (WA) method, deionized water was added dropwise to the acetone polymer solution (1 mg mL^{-1}) under stirring at 500 rpm. The acetone/water (solvent/non-solvent) ratio was kept constant at 0.5 for all suspensions. After removal of the acetone by stirring overnight at room temperature in an open vial, the nanoparticles were characterized by DLS (performed in pure water) and TEM without filtration.

pH-Response test of the nanoparticles. For the pH-response test of the nanoparticles, 0.1 M acetic acid for a pH value of 3.1, 0.1 M acetate buffer for pH values of 4, 5, 6, 6.25, 6.50 and

Table 1 Selected characterization data of the THP-HEMA (M1) (co)polymers with DMAEMA (M2)

Entry	Monomer/CTA/ACPA	f(M1/M2)[a]	F(M1/M2)[b]	Conv.[c] [%] M1/M2	$M_{n,theo.}$[d] [g mol^{-1}]	DP[c] M1/M2	M_n[c] [g mol^{-1}]	$M_{n,SEC}$[e] [g mol^{-1}]	M_w/M_n[e]	T_g[f] [°C]
P1	45.37/1/0.25			85/0	8500	40/0	8800	6300	1.13	29.4
P1OH	45.37/1/0.25			90/0	9000			6800	1.24	—
P2	45.98/1/0.25	19	15.7	85/84	8500	36/2.3	8300	5700	1.18	30.6
P3	46.61/1/0.25	9	8.2	80/90	8100	33/4	7800	5600	1.18	28.0
P4	47.26/1/0.25	5.7	5.6	76/84	7800	31/5.5	7800	6200	1.17	29.9
P5	47.92/1/0.25	4	4	84/87	8500	29/7.3	7600	6300	1.18	29.1
P5OH	47.92/1/0.25	4	4	82/90	8600			6400	1.27	—

[a] Initial monomer feed ratio. [b] Monomer ratio in the isolated copolymer. [c] Determined by ^{1}H NMR spectroscopy. [d] Determined by the formula $M_{n,theo.} = [([M]_{M1}/[CTA] \times Conv. \times M_{M1}) + ([M]_{M2}/[CTA] \times Conv. \times M_{M2}) + (M_{CTA})]$. [e] Determined by SEC in $CHCl_3$ analysis (RI detection, PMMA calibration). [f] Determined by DSC analysis.

Published on 16 January 2017. Downloaded by Thueringer Universitats Landesbibliothek Jena on 26/06/2017 08:02:15.

0.1 M tris buffer for the pH values 7, 7.4, 8, and 9 were used. In a typical experiment, 100 μL of **P1** nanoparticle suspension (0.5 mg mL^{-1}) were mixed with 900 μL acetic or corresponding buffer solutions in Eppendorf tubes and stored at 37 °C for 1 h while mixing at 200 rpm. Then, DLS and ζ-potential measurements were performed.

Ultrasound-response test of the nanoparticles. Ultrasound response tests of the nanoparticles were performed by generating ultrasound using a Hielscher UP 200St instrument. The general procedure is as follows: 1 mL of nanoparticle suspension (0.5 mg mL^{-1}) was diluted to a final volume of 5 mL in a glass vial. The ultrasonic probe was immersed in the middle of the nanoparticle suspension. In order to minimize the temperature change during the ultrasound exposure, the glass vial was cooled in an ice bath. After a certain time of ultrasound treatment, the temperature of the suspensions was monitored and 100 μL of samples were taken for characterization.

Nile Red encapsulation and release. Nile Red was encapsulated into the polymers by utilizing the co-precipitation technique. An exemplary procedure is as follows: **P1** (10 mg) was dissolved in 10 mL acetone. Then, 40 μL Nile Red stock solution (1 mM in acetone) was added. Subsequently, 20 mL of deionized water was added dropwise to the acetone solution under continuous stirring at 500 rpm. The mixed solutions were stirred overnight at room temperature in an open vial to remove the acetone.

To test the ultrasound mediated release of Nile Red from the nanoparticles, 1 mL of dye encapsulated nanoparticle suspensions was mixed with 9 mL of deionized water. After every 1 minute of ultrasound exposure (40 W), 300 μL of the sample were taken for the fluorescence spectroscopy analysis.

To test the pH value mediated release of Nile Red from the nanoparticles, 100 μL of dye encapsulated nanoparticles were mixed with 900 μL of three different buffers: (i) acetate buffer (0.1 M, pH 4.0), (ii) acetate buffer (0.1 M, pH 6.0), and (iii) tris buffer (0.1 M, pH 8.0) in an Eppendorf tube and stored at 37 °C. 300 μL of the sample were taken periodically and analyzed by fluorescence spectroscopy. The % release of Nile Red was calculated by using the following equation:

$$\text{Release}\,(\%) = \frac{I_0 - I_t}{I_0} \times 100 \qquad (4)$$

where I_0 corresponds to the initial fluorescence intensity of Nile Red at 610 nm and I_t corresponds to the fluorescence intensity of Nile Red at each time point.

Determination of cytotoxicity. Cytotoxicity studies were performed with the mouse fibroblast cell line L929 (CCL-1, ATCC), as recommended by ISO10993-5. The cells were routinely cultured in Dulbecco's modified eagle's medium supplemented with 10% fetal calf serum (FCS, Capricorn Scientific, Germany), 100 U mL^{-1} penicillin and 100 μg mL^{-1} streptomycin at 37 °C under a humidified 5% (v/v) CO_2 atmosphere. In detail, cells were seeded at 10^4 cells per well in a 96-well plate and incubated for 24 hours. No cells were seeded in the outer wells. Afterwards, nanoparticles were added to the cells at indicated concentrations (from 10 μg mL^{-1} to 1000 μg mL^{-1}), and the plates were incubated for further 24 hours. Subsequently, the medium was replaced by a mixture of fresh culture medium and the assay reagent AlamarBlue (resazurin-based solution, Thermo Fisher, Germany, prepared according to the manufacturer's instructions). After a further incubation of 4 hours at 37 °C under a humidified 5% (v/v) CO_2 atmosphere, the fluorescence was measured at Ex 570/Em 610 nm, with untreated cells on the same well plate serving as negative controls. The negative control was standardized as 0% of metabolism inhibition and referred to as 100% viability. Cell viability below 70% was considered to be indicative of cytotoxicity. Data are expressed as mean ± standard deviation (SD) of three independent determinations.

Results and discussion

In order to obtain an ultrasound responsive nanoparticle system with surface charge-conversional properties, a series of statistical copolymers of THP-HEMA and DMAEMA were synthesized by utilizing the RAFT polymerization process.[33] To the best of our knowledge, the copolymerization of THP-HEMA and DMAEMA has never been reported so far. However, both monomers have been successfully polymerized with RAFT using CPADB as a chain transfer agent (CTA).[18,27] For the comprehensive understanding of the effect of monomer composition on the stimuli response of the corresponding nanoparticles, one homopolymer of THP-HEMA (**P1**) and four copolymers of THP-HEMA and DMAEMA (**P2** to **P5**) with similar molar mass values but varying compositions were synthesized using ACVA as an initiator and CPADB as a CTA in ethanol at 70 °C with a monomer concentration of 1 mol L^{-1} (Scheme 1 and Table 1). Regarding the polymerization rate and to gain control over the molar mass, the [CTA]/[ACVA] ratio was kept at 1/0.25.[34] To vary the monomer composition, different monomer feed ratios were applied with a targeted molar mass value of $M_{n,tg}$ = 10 000 g mol^{-1} at 100% conversion for each polymerization. Concerning the possible toxicity of tertiary amino groups, the DMAEMA content in the copolymers was kept below 20 mol%. In addition, since the ionizable carboxylic acid end-group of the CPADB could potentially affect the pH-responsive behavior of the corresponding nanoparticles, analogues of **P1** and **P5** (**P1-OH** and **P5-OH**) were synthesized by using a non-ionizable hydroxyl functional chain transfer agent 4-cyano-4-[(dodecylsulfanylthiocarbonyl)sulfanyl]pentanol (CDP) (Scheme S1† and Table 1) to investigate the effect of functional groups in the chain transfer agents on the pH-responsive behavior of the nanoparticles.

Kinetic studies

To verify the RAFT-controlled nature of the (co)polymerizations, kinetic investigations were performed for **P1** to **P5**. The kinetic plots are displayed in Fig. 1 and S2.† SEC analysis revealed that molar mass distributions of the kinetic samples remain monomodal while shifting to lower elution volumes in the course of each polymerization (Fig. S2†). The molar mass

 This journal is © The Royal Society of Chemistry 2017

Published on 16 January 2017. Downloaded by Thueringer Universitats Landesbibliothek Jena on 26/06/2017 08:02:15.

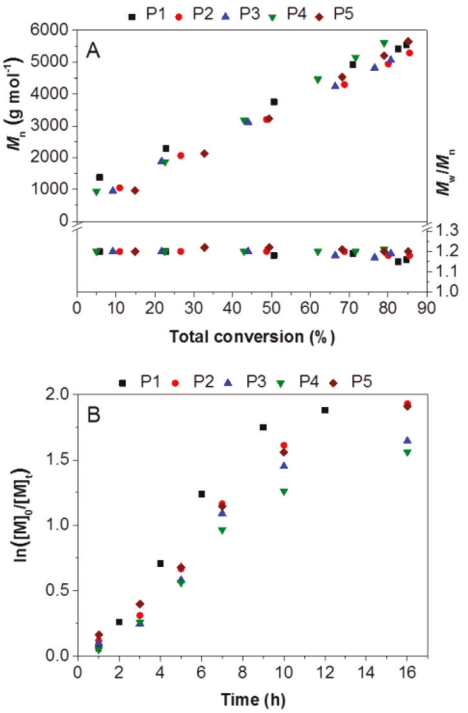

Fig. 1 Kinetic studies of the RAFT homopolymerization of THP-HEMA (**P1**) and RAFT copolymerization of THP-HEMA with DMAEMA (**P2** to **P5**). Polymerization conditions: solvent = ethanol, T = 70 °C, $[M]_0$ = 1 mol L^{-1}. (A) M_n and $Đ_M$ evolution with total monomer conversion. (B) Semilogarithmic kinetic plots.

M_n increases linearly with respect to the total monomer conversion with $Đ_M$ values below 1.3 suggesting a controlled polymerization mechanism (Fig. 1A). Fig. 1B depicts the semilogarithmic kinetic plots. An induction period of around 30 min was observed for both polymerizations as often reported for RAFT polymerizations. After this induction time, semilogarithmic plots increase linearly for about 10 h, indicating a pseudo first order polymerization rate with respect to the total monomer concentration and a constant concentration of the propagating radicals during the RAFT polymerization. Finally, the slopes of the curves are no longer linear, which is attributed to a decrease in the rate of radical generation caused by a decrease in the initiator concentration.

Polymer characterization

The resulting (co)polymers were characterized by ^{1}H NMR spectroscopy and SEC measurements (Table 1). ^{1}H NMR spectroscopy analysis of the isolated (co)polymers (**P1** to **P5**) clearly revealed the presence of the ω-RAFT end groups (δ = 7.84, 7.48, and 7.35 ppm), and the characteristic signals that are derived from THP-HEMA (δ = 4.65 to 3.50 ppm) and DMAEMA (δ = 2.58 and 2.30 ppm) (Fig. 2). This enables the estimation of the degree of polymerization (DP) for each monomer and the number average molar mass values for **P1** to **P5**. The signal corresponding to the aromatic protons of the ω-RAFT end groups were used to calculate the DP of each monomer in the

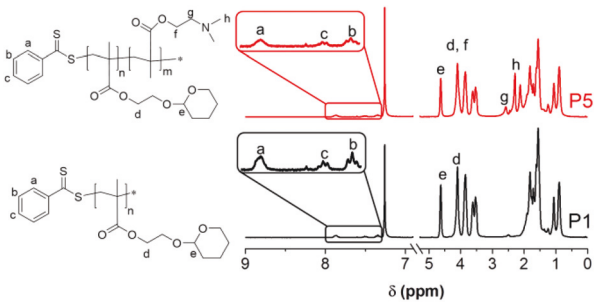

Fig. 2 ^{1}H NMR spectra (300 MHz, $CDCl_3$) of **P1** (bottom) and **P5** (top) and the assignment of the peaks used to calculate the DP.

corresponding polymer. For this purpose, the integral values were compared with the integral value of the methine proton peak of the THP-HEMA side chains (peak "e" in Fig. 2) and the methylene peak of the DMAEMA side chains (peak "h" in Fig. 2) (see the Experimental section for details). The resulting M_n values calculated by ^{1}H NMR are in good agreement with the theoretical values that were calculated from the [monomer] to [CTA] ratio and the monomer conversions. The monomer compositions in the isolated copolymers (F(M1/M2)) were calculated by comparing the integral values of peak "e" and peak "h". Since the characteristic ^{1}H NMR peaks of the CDP overlap with the backbone of the polymers, DP and M_n values cannot be estimated by ^{1}H NMR for **P1OH** and **P5OH**.

The isolated copolymers were analyzed using SEC (Fig. 3 and S5†). SEC analysis revealed monomodal traces and low dispersities ($Đ_M$ < 1.3) for all polymers. Molar mass values obtained by SEC are lower than the molar mass values determined by ^{1}H NMR spectra due to the PMMA calibration in the

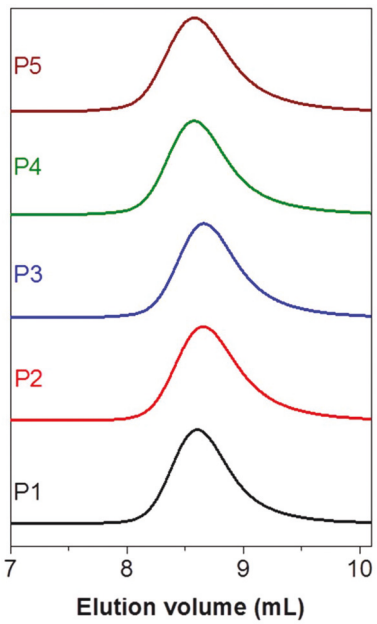

Fig. 3 Normalized SEC traces in $CHCl_3$ of isolated copolymers of **P1** to **P5**.

Published on 16 January 2017. Downloaded by Thueringer Universitats Landesbibliothek Jena on 26/06/2017 08:02:15.

SEC systems, resulting in a relative molar mass value. Moreover, molar mass values determined by SEC are similar for all polymers, which is expected since the same molar mass values were targeted, and similar total monomer conversions were obtained for all polymers.

Thermal properties

Thermogravimetric analysis (TGA) was used to study the decomposition pattern and the thermal stability of the (co) polymers under a nitrogen atmosphere (Fig. 4A). It can be observed that the homopolymer **P1** undergoes a two-step degradation. The first step is between 170 and 265 °C (~45% of mass loss), which presumably corresponds to the loss of the pendant THP groups (~40% of calculated mass loss). This converts **P1** to poly(2-hydroxyethyl methacrylate) (PHEMA). The second step occurs between 290 and 450 °C and is attributed to the degradation of the PHEMA. This is consistent with the reported thermal stability studies of PHEMA (stable up to ~300 °C, a one-step degradation between ~300 °C and ~450 °C).[35] Similar results were obtained with the copolymers **P2** to **P5**. However, an increase of the DMAEMA content resulted in a decrease of the rate of mass loss, which is attributed to the better thermal stability of the PDMAEMA than P(THP-HEMA). Thermal transitions of the (co)polymers (**P1** to **P5**) were studied by differential scanning calorimetry (DSC) under a nitrogen atmosphere (Fig. 4B). The homopolymer **P1** exhibits a T_g point at 29.4 °C (Table 1). The copolymers **P2** to **P5** exhibit single T_g temperatures between 28.0 and 30.6 °C, which are similar to **P1**, without apparently any correlation with the DMAEMA content of the polymer. This is attributed to the low content of DMAEMA moieties (up to 20%), which are randomly distributed along the polymer chains.

Quaternization of the polymers

The pendant amino groups of the copolymers (**P2** to **P5**) were treated with an excess of methyl iodide in acetone in order to investigate the effect of the quaternization of the DMAEMA moieties on stimuli response of the corresponding nanoparticles (**P2q** to **P5q**) (Scheme S2†). The quantitative quaternization was verified by the disappearance of the proton signals of DMAEMA in the ^{1}H NMR spectrum (δ = 2.58 and 2.30 ppm) (Fig. 5). The more deshielded protons of the DMAEMA after quaternization cause a shift of the proton peaks to a lower field.[36] SEC reveals a slight increase in the molar mass values after quaternization caused by the increased hydrodynamic volume of the copolymers in $CHCl_3$ (Fig. S7†).

Nanoparticle formulation and characterization

Polymeric nanoparticles were prepared from the synthesized (co)polymers (**P1** to **P5**, **P1OH**, **P5OH**, **P2q** to **P5q**) by nanoprecipitation with subsequent solvent evaporation without any need for stabilizers/surfactants. Two different dropping methods (dropping the acetone–polymer solution into water (AW) as well as dropping water into the acetone–polymer solution (WA)) were applied for each polymer in order to obtain differently sized nanoparticles. Well-defined nanoparticles with monomodal size distributions and low polydispersity index (PDI) values were obtained with both dropping methods for all polymers except **P2** (Table 2 and Fig. S8†). As commonly seen, larger nanoparticles with lower PDI values for all polymers were obtained with the WA method in comparison with the AW method.[37,38] Moreover, smaller nanoparticles were obtained with quaternized polymers (**P2q** to **P5q**) than with unquaternized ones (**P3** to **P5**) for both dropping methods. These results are consistent with the recent report of Reisch *et al.*, which states that the presence of charged groups in polymer chains can reduce the size of polymer nanoparticles fabricated by nanoprecipitation.[39] Well-defined nanoparticles could not be obtained using **P2**, which contains a 5% DMAEMA functionality. This is attributed to the insufficient cationic character of the nanoparticles, which is presumably

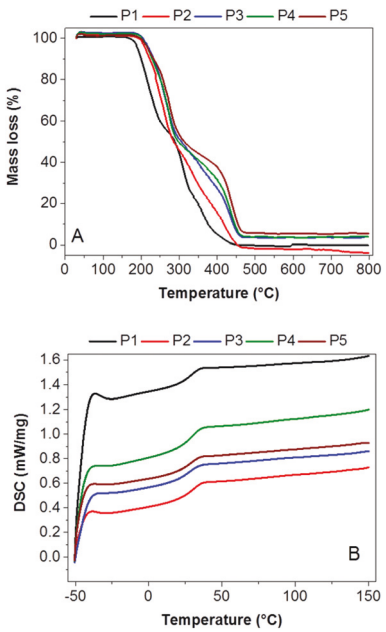

Fig. 4 (A) TGA thermograms of **P1** to **P5**. (B) DSC heating runs of **P1** to **P5** (heating rate: 20 K min^{-1}).

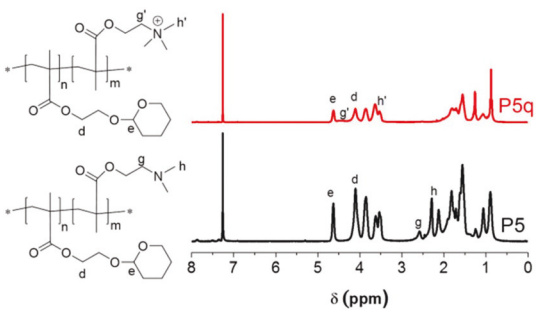

Fig. 5 ^{1}H NMR spectra (300 MHz, $CDCl_3$) of **P5** and **P5q** (quaternized form of **P5**).

This journal is © The Royal Society of Chemistry 2017

Published on 16 January 2017. Downloaded by Thueringer Universitats Landesbibliothek Jena on 26/06/2017 08:02:15.

Table 2 Selected characterization results of the prepared nanoparticles

	Z-Average[a] [*d*, nm]		PDI[a]		ζ-Potential[b]	
Entry	AW[c]	WA[d]	AW[c]	WA[d]	AW[c]	WA[d]
P1	108 ± 1	242 ± 3	0.14 ± 0.01	0.01 ± 0.01	−31 ± 1	−26 ± 1
P1OH	119 ± 1	223 ± 3	0.08 ± 0.02	0.08 ± 0.02	−33 ± 1	−25 ± 1
P2q	57 ± 1	182 ± 1	0.23 ± 0.01	0.06 ± 0.01	+29 ± 1	+37 ± 2
P3	98 ± 1	216 ± 3	0.13 ± 0.02	0.03 ± 0.01	+42 ± 1	+46 ± 6
P3q	42 ± 1	172 ± 2	0.26 ± 0.01	0.07 ± 0.02	+54 ± 3	+57 ± 1
P4	130 ± 1	233 ± 1	0.13 ± 0.01	0.01 ± 0.01	+48 ± 1	+30 ± 1
P4q	38 ± 1	120 ± 1	0.28 ± 0.01	0.11 ± 0.01	+65 ± 3	+48 ± 1
P5	120 ± 1	247 ± 2	0.11 ± 0.01	0.02 ± 0.01	+45 ± 1	+47 ± 1
P5OH	89 ± 1	229 ± 3	0.15 ± 0.11	0.05 ± 0.03	+42 ± 1	+51 ± 1
P5q	51 ± 1	138 ± 2	0.28 ± 0.01	0.01 ± 0.01	+48 ± 5	+63 ± 2
PMMA	—	187 ± 1	—	0.03 ± 0.03	—	−18 ± 1

[a] Average values of three DLS measurements. [b] Average values of three ζ-potential measurements in pure water. [c] Dropping acetone into water. [d] Dropping water into acetone.

not high enough to stabilize the nanoparticles. This assumption is reasonable, since there are about 2.3 DMAEMA units in average (estimated by ^{1}H NMR) in a **P2** chain, which are not completely protonated in pure water (pH ~ 7). Moreover, there is one carboxylic acid unit in every **P2** chain due to the α end group of the utilized RAFT agent that is completely ionized in pure water due to its low pK_a value (~5) leading to a decrease in the cationic character of the nanoparticles. In contrast to this, **P2q** (quaternized form of **P2**) yielded well-defined nanoparticles, due to having an appreciable cationic character (pH independent cationic charge). The ζ-potential measurements in pure water revealed that **P3** to **P5**, **P5OH**, and **P2q** to **P5q** nanoparticles exhibit positive ζ-potential values higher than +29 mV with small differences for AW and WA methods, which is commonly seen for the nanoprecipitation method.[19] The positive ζ-potential values are due to the protonated or quaternized amino groups of the polymers. **P1** nanoparticles show negative ζ-potential values of around −30 mV due to the presence of carboxyl groups in the polymer. Although there are no ionizable groups in **P1OH** it also has negative ζ-potential values around −30 mV. To understand the source of the negative ζ-potential of the **P1OH** further pH dependent ζ-potential measurements were conducted (see the next section). TEM analysis (Fig. 6) revealed homogeneous spherical nanoparticles with diameters in agreement with the DLS measurements. A long term stability test at room temperature for three weeks shows no change in the particle size and size distribution (determined by DLS).

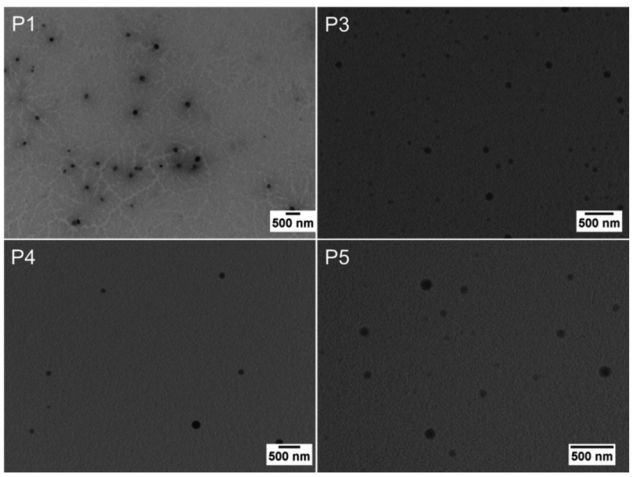

Fig. 6 TEM images of nanoparticles that were prepared from **P1**, **P3**, **P4**, and **P5** (1 mg mL^{-1}) by dropping acetone–polymer solution to water (AW).

pH-Response test of the nanoparticles

The nanoparticle suspensions were stored at various pH values for 1 h, and the changes in particle size and ζ-potential values were recorded. DLS measurements revealed that **P1** nanoparticle suspensions possess stable size and PDI values at neutral and basic pH values (pH = 7.4, 8, and 9). Below 7.4 the size and PDI values of the nanoparticles gradually increase whereas they precipitate below a pH value of 6.25 (Fig. 7) due to the decrease in the ζ-potential values in the acidic pH regime from −66 mV at a pH value of 9 to −19 mV at a pH value of 6.2. In general, stable polymeric nanoparticles have ζ-potential values beyond ±25 mV.[40] Upon decreasing the pH below its IEP, **P1** nanoparticles show a surface charge conversion from negative to positive. Armes and coworkers reported that RAFT based carboxyl end-groups of the nanoparticles can be ionized at neutral pH values and protonated in acid media leading to a nanoparticle ζ-potential conversion.[41] Therefore, we first hypothesized that the conversion of the ζ-potential values of **P1** upon change in the pH value could be due to the protonation of the carboxyl end-group of the polymer. To examine this hypothesis, the pH responsive behavior of the **P1OH**, which is synthesized by using a hydroxyl functional CTA instead of a carboxyl functional one, was also investigated as a control experiment. Unexpectedly, **P1OH** nanoparticles showed similar size and ζ-potential value changes like **P1** nanoparticles upon pH value change, suggesting that both **P1** and **P1OH** nanoparticles exhibit IEPs due to having

Published on 16 January 2017. Downloaded by Thueringer Universitats Landesbibliothek Jena on 26/06/2017 08:02:15.

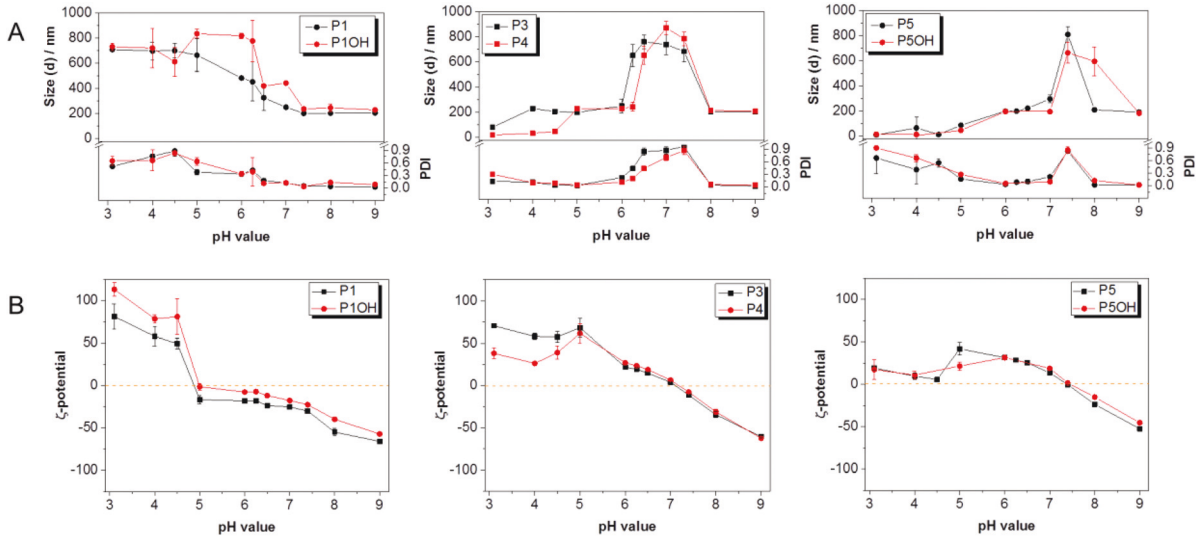

Fig. 7 (A) Intensity-weighted size and PDI values of nanoparticles as a function of the pH value. (B) ζ-Potentials of the nanoparticles as a function of the pH value.

THP-HEMA moieties. However, **P1** nanoparticles start aggregating at lower pH values than **P1OH** nanoparticles. This is attributed to the ionization of the carboxyl end-group of the **P1** leading to a better ionic character of **P1** than in the case of **P1OH**. Moreover, the pH responsive behavior of control PMMA nanoparticles (Table 2) was also investigated under the same conditions as a second control experiment; in this case, PMMA nanoparticles aggregated at the entire pH range presumably due to the action of buffer solutions that screen the weak repulsive forces between the PMMA nanoparticles. The low absolute ζ-potential values of the PMMA nanoparticles at all pH values support this assumption. In contrast to **P1** and **P1OH**, **P3** nanoparticles that contain 10% DMAEMA functionality show stable size and PDI values in the pH range from 4 to 6 with ζ-potential value higher than +58 mV, due to an adequate cationic character of the polymer as a result of protonated DMAEMA groups. However, at a pH value of 3.1, **P3** nanoparticles showed a significant decrease in size from 200 to 80 nm. This is presumably due to the protonation of DMAEMA and THP-HEMA groups. The protonation of the THP-HEMA groups would be expected to cause the cleavage of the cyclic acetal functionality of the THP-HEMA side chain. To confirm this assumption, the **P3** nanoparticle solution was treated with 0.1 M acetic acid (pH = 3.1) and stored at 37 °C for 24 h. The resulting solution was freeze-dried and a ^{1}H NMR spectrum was recorded (Fig. S9†). After treatment with acetic acid, a new small signal was observed at 4.9 ppm corresponding to the hydroxyl (–OH) group of poly(2-hydroxyethyl methacrylate) (PHEMA) and suggesting the slow cleavage of acetal groups.[27] Therefore, the quick decrease in size at pH value 3.1 is attributed to the protonation of DMAEMA chains. An increase of the pH value from 5 to 6 resulted in a significant decrease in the ζ-potential of **P3** nanoparticles from +68 mV to +21 mV. This is due to the partial deprotonation of the DMAEMA groups. At higher pH values, the ζ-potential value of the **P3** nanoparticles further decreases and reaches its IEP at a pH value of ~7.1. Above its IEP, ζ-potential values of the nanoparticles show a surface charge conversion from positive to negative. Due to the insufficient ζ-potential values (lower than ±20 mV), **P3** nanoparticles form aggregates between the pH values from 6.25 to 7.4. At a pH value of 8, **P3** nanoparticles reveal a ζ-potential value of −37 mV; hence, they are stable in their size and PDI value. A further increase of the pH value from 8 to 9 resulted in an increase of the absolute value of the ζ-potential to −60 mV. In contrast to **P3** nanoparticles, **P2q** nanoparticles revealed stable size and PDI values, no IEP, and ζ-potential values higher than +20 mV over the entire pH range. This is due to the quaternization of the DMAEMA groups (Fig. S11†), which imparts a pH independent cationic character to the nanoparticles. In agreement with this, although **P3** nanoparticles form aggregates at a pH value of 7.4, **P3q** nanoparticles showed no change in size even after 23 h storage at 37 °C (Fig. S12†). Although **P3** nanoparticles are stable at pH values of 4.5 and 4.0, the size of the **P4** nanoparticles that contain a higher DMAEMA content than **P3** decreased from 200 nm to 47 nm at pH 4.5 and to 33 nm at pH 4 (Fig. 7). Moreover, an increase of the incubation time to 6 h resulted in no detectable DLS signals. This is attributed to the dissolution of the **P4** nanoparticles at these pH values as a result of the completely protonated DMAEMA moieties. In accordance with this, **P5** nanoparticles that contain the highest DMAEMA content revealed dissolution even at pH 5. The dissolution abilities of **P4** and **P5** at these pH values, at a concentration of 1 mg mL^{-1}, were further confirmed by turbidity measurements with 100% transmittance (Fig. S10†). Moreover, it was found that the IEP of the nanoparticles in relation to the pH value increases with the DMAEMA content in the copolymer. The IEP of **P4** nanoparticles was found to be

 This journal is © The Royal Society of Chemistry 2017

Published on 16 January 2017. Downloaded by Thueringer Universitats Landesbibliothek Jena on 26/06/2017 08:02:15.

7.2, whereas **P5** nanoparticles reached IEP at 7.4. These results suggest that the dissolution pH as well as the IEP of the nanoparticles can simply be tuned by varying the DMAEMA content in the copolymers. Moreover, although **P5** nanoparticles are stable at pH 8 with a ζ-potential of −24 mV, the **P5OH** nanoparticles are not stable at a lower ζ-potential value (−18 mV). This may be due to the ionization of the carboxyl end-group of the **P5**, resulting in a better anionic character.

Ultrasound response test of the nanoparticles

To investigate the ultrasound responsive behavior of the nanoparticles, ultrasound with a power of 20 W and a frequency of 26 kHz was applied to the nanoparticle suspensions. In order to prevent the thermal hydrolysis of the THP-HEMA moieties, the temperature of the suspensions was kept constant in the range of 32 to 34 °C during the ultrasound treatment. The changes in particle size and PDI values were recorded by DLS at intervals of 5 minutes of ultrasound exposure. Fig. 8 shows the DLS results of **P1**, **P3**, and **P5** nanoparticles subjected to ultrasound treatment. The size and PDI values of the nanoparticles increase upon prolonged ultrasound exposure together with a rapid decrease in the derived count rate of the nanoparticles due to the formation of larger aggregates. However, the DLS traces of the nanoparticles also reveal the appearance of some smaller aggregates (Fig. S13†). Moreover, SEM images of **P1** and **P5** nanoparticles showed that, although nanoparticles have uniform spherical shapes prior to ultrasound exposure, smaller nanoparticles and irregular larger aggregates were formed after ultrasound treatment for 30 minutes (Fig. 9). It was found that an increase in the power of the ultrasound from 20 to 40 W resulted in a faster aggregate formation and a faster decrease in the derived count rate (Fig. S14†). As a control experiment, ultrasound was also applied to the PMMA nanoparticles, where no change in size and the derived count rate of the PMMA nanoparticles was observed (Fig. S15 and S16†). This confirms that the ultrasound response of the nanoparticles is caused by the THP-HEMA groups in the polymers. To understand the origin of the nanoparticle disruption, ^{1}H NMR spectra of the freeze-dried nanoparticles after ultrasound treatment (5 min, 40 W) were analyzed. However, no change could be observed in the

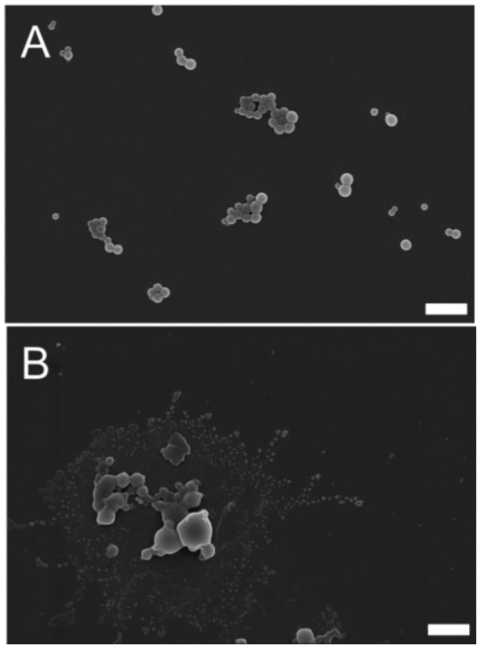

Fig. 9 SEM images of **P1** nanoparticles before (A) and after (B) ultrasound exposure. Scale bars represent 1 μm.

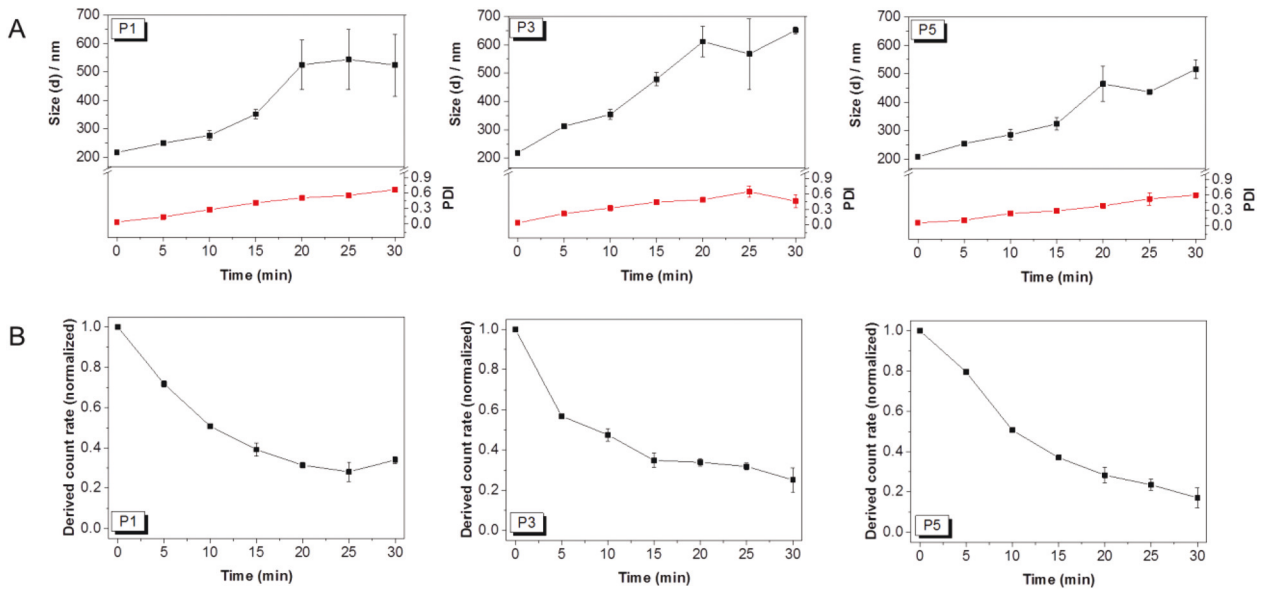

Fig. 8 (A) Intensity weighted size and PDI values of nanoparticles as a function of the ultrasound (20 W) exposure time. (B) Normalized count rate of the nanoparticles as a function of the ultrasound (20 W) exposure time.

Published on 16 January 2017. Downloaded by Thueringer Universitats Landesbibliothek Jena on 26/06/2017 08:02:15.

^{1}H NMR spectrum of the nanoparticles (Fig. S17†), meaning that a physical process disrupted the nanoparticles instead of a chemical reaction. Therefore, the ultrasound responsive behavior of the nanoparticles was ascribed to their relatively low T_g values and lack of any crystallization temperatures (T_c) (Table 1 and Fig. 4), which enable nanoparticles to have high motion abilities that result in sensitivity to ultrasound.[26] To verify this assumption, a control experiment was conducted with a poly(methyl acrylate) (PMA) nanoparticle suspension (see the ESI† for the synthesis details), which has a T_g value of 16 °C (Fig. S19†), under the same conditions. In this case, some of the PMA nanoparticles were aggregated just after 1 min of ultrasound exposure (40 W). The aggregation of the nanoparticles was visualized by a color change of the suspension from turbid to a more clear solution and deposition of some aggregated polymers on the wall of the glass vial (Fig. S20†). Moreover, DLS measurements revealed the formation of smaller aggregates upon ultrasound treatment (Fig. S21†). These results correlate well with our findings with THP-HEMA nanoparticles and prove that ultrasound responsive behavior of the THP-HEMA nanoparticles originated from their elastic nature.

Fluorescence spectroscopic studies of the nanoparticles

To examine the ability of the nanoparticles to encapsulate a hydrophobic guest molecule, Nile Red was used as a model drug to be encapsulated into the hydrophobic domains of the nanoparticles.[42] Nile Red exhibits an environmentally sensitive fluorescence behavior. Fig. 10 depicts the fluorescence emission spectra of Nile Red encapsulated into the nanoparticles that are formed by unquaternized (Fig. 10A) and quaternized (Fig. 10B) polymers. The total intensities of the emission spectra of the nanoparticle suspensions from unquaternized polymers show similar emission intensities. Moreover, the emission wavelength maximum of Nile Red is comparable for all nanoparticles. This indicates that the cores of the nanoparticles have similar hydrophobicities without any correlation with the DMAEMA content in the polymers, which is reasonable as most of the DMAEMA moieties are deprotonated at the pH value of pure water. However, the emission intensity of Nile Red gradually decreases upon increasing the ratio of the quaternized DMAEMA content in the nanoparticles. Additionally, the emission wavelength maximum of Nile Red is consistently red-shifted from **P1** to **P5q** indicating that the hydrophilicity of the core of the nanoparticles can be manipulated by simply varying the quaternized DMAEMA content of the nanoparticles. Additionally, the influence of the pH change and ultrasound exposure on the dye release profiles of the nanoparticles was investigated. Fig. 11(A) shows the release profiles of the Nile Red from **P5** nanoparticles at three different pH values. 45% of the Nile Red was released at a pH value of 8.0 in 8 h. The release was slightly accelerated at a pH value of 6.0, in which 49% of the Nile Red was released in 8 h. This is attributed to the partially protonated DMAEMA moieties. At a pH value of 4.0, 75% of the Nile Red was released due to the dissolution of nanoparticles as a result of complete protonation of the DMAEMA groups. Fig. 11(B) reveals the

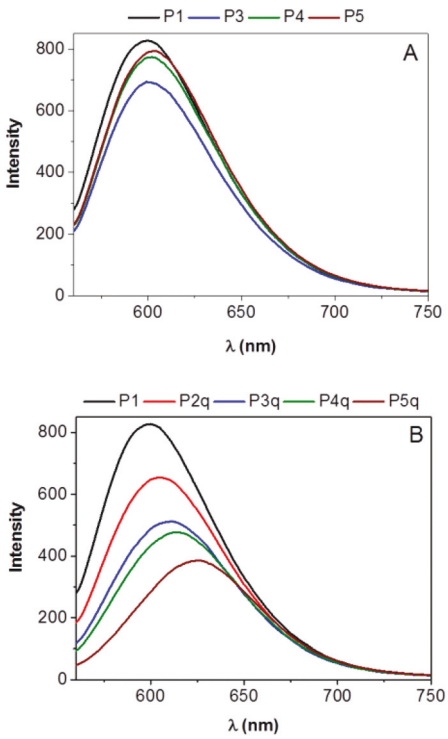

Fig. 10 Fluorescence emission spectra of Nile Red encapsulated into nanoparticles (0.5 mg mL^{-1}) formed by **P1**, **P3–P5** (A); **P1**, **P2q** to **P5q** (B).

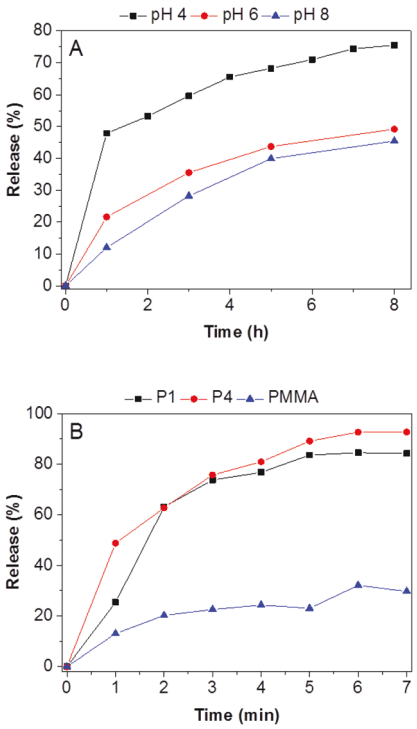

Fig. 11 (A) Nile Red release from **P5** nanoparticles at pH 8.0, pH 6.0, and pH 4.0. (B) Nile Red release from **P1**, **P4**, and PMMA nanoparticles with ultrasound treatment (40 W, 26 kHz).

This journal is © The Royal Society of Chemistry 2017

Published on 16 January 2017. Downloaded by Thueringer Universitats Landesbibliothek Jena on 26/06/2017 08:02:15.

release of Nile Red from **P1**, **P4** and PMMA nanoparticles with ultrasound exposure. For all nanoparticles, the release of Nile Red increases with the cumulative ultrasound exposure time. PMMA nanoparticles released 29% Nile Red after 7 minutes, whereas 84% and 92% Nile Red was released from **P1** and **P4** nanoparticles, respectively. In a control experiment almost no Nile Red release was observed under the same conditions but without ultrasound exposure (Fig. S22†). Therefore, the observed fast release of Nile Red was attributed to the disruption of the THP-HEMA based nanoparticles with ultrasound treatment.

Cytotoxicity of the nanoparticles in L929 cells

It is known that cationic polymers and nanoparticles frequently show toxic effects in cells, mainly due to their undesired interactions with negatively charged cell membranes. Therefore, the cytotoxicity of the nanoparticles was investigated using L929 cells (Fig. 12). No significant reduction of cell viability was observed when treated with up to 1 mg mL^{-1} **P1**, **P3**, and **P4** nanoparticles for 24 h incubation. Consequently, **P1**, **P3**, and **P4** nanoparticles are nontoxic to the cells and possess excellent biocompatibility, which can be attributed to the negative surface charge of the corresponding nanoparticles in the pH value of the cell media (~7.4). However, cell viability decreased to 44% at 1 mg mL^{-1} **P5** nanoparticles. The more positive surface charge leads to a relatively higher toxicity and poor biocompatibility. In accordance with this, **P3q** nanoparticles that show pH value independent positive surface charge revealed a severe loss in cell viability of about 96% at a concentration of 0.25 mg mL^{-1}. Moreover, cytotoxicity becomes even more pronounced in the case of **P5q** nanoparticles compared to **P3q** nanoparticles with an almost quantitative cell death at 0.10 mg mL^{-1}. The cytotoxicity of the nanoparticles correlates well with the trend that the more positive the surface potential is the more toxic effects of the nanoparticles are observed.

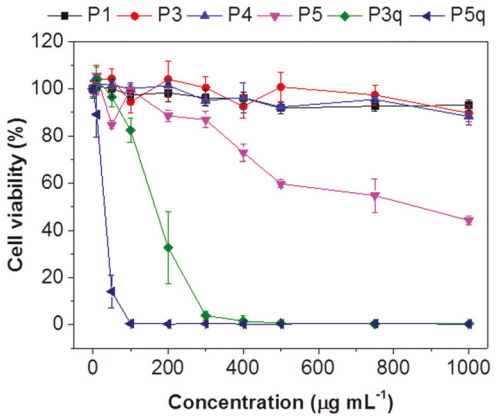

Fig. 12 Cytotoxicity test of nanoparticles that were prepared from **P1–P5**, **P3q**, and **P5q**. The relative viability is expressed as percentage to control cells not treated with nanoparticles. Untreated cells on the same well plate were used as positive controls.

Conclusion

In this study, novel surface charge-conversional nanoparticles at slightly acidic pH values (7 to 7.4) that also show disassembly at acidic pH values (4 to 5) have been presented. The nanoparticles based on a well-defined statistical copolymer library of THP-HEMA and DMAEMA with different monomer compositions were prepared by RAFT polymerization by varying initial feed ratios. Kinetic studies demonstrated the pseudo-first order kinetics. The synthesized polymers self-assembled into spherical nanoparticles in aqueous solution *via* nanoprecipitation. It was demonstrated that the incorporation of DMAEMA units into THP-HEMA based nanoparticles can sustain effective pH-dependent surface charge conversion properties. Moreover, the IEP and the disassembly pH value of the DMAEMA nanoparticles can be systematically tuned by varying the DMAEMA content of the nanoparticles. The ability of the nanoparticles to encapsulate Nile Red and release it under acidic pH values and by ultrasound treatment was confirmed. Moreover, it was verified that negatively charged nanoparticles are non-toxic and biocompatible. However, the increased DMAEMA content or quaternization of DMAEMA units in the nanoparticles led to a more positive surface charge and resulted in toxic effects on L929 cells. The results indicate the potential of these polymeric nanoparticles as novel tumor extracellular pH triggered charge-conversional drug delivery systems for cancer therapy. Therefore, our future investigations will focus on the encapsulation and controlled release of anticancer drugs.

Acknowledgements

We acknowledge funding from the Carl-Zeiss Foundation (JCSM Strukturantrag) and the Thüringer Ministerium für Wirtschaft, Wissenschaft, und Digitale Gesellschaft (TMWWDG, ProExzellenz I, NanoConSens). The SEM and TEM facilities of the Jena Center for Soft Matter (JCSM) were established with a grant from the German Research Council (DFG) and the European Fonds for Regional Development (EFRE). RYM acknowledges the financial support from CONACyT (Consejo Nacional de Ciencia y Tecnologia, Mexico) and the Centro de Investigacion en Quimica Aplicada (Mexico) to pursue his Ph.D. RYM and CGS thank CONACyT and DAAD (Deutscher Akademischer Austauschdienst, Germany) for financial support within the framework of the funding program for international mobility PROALMEX 2015 (CONACyT project: 267752 and DAAD project: 57271725)

References

1 O. C. Farokhzad and R. Langer, *ACS Nano*, 2009, **3**, 16–20.
2 R. R. Arvizo, O. R. Miranda, M. A. Thompson, C. M. Pabelick, R. Bhattacharya, J. D. Robertson,

Published on 16 January 2017. Downloaded by Thueringer Universitats Landesbibliothek Jena on 26/06/2017 08:02:15.

V. M. Rotello, Y. S. Prakash and P. Mukherjee, *Nano Lett.*, 2010, **10**, 2543–2548.
3 Y. Lee, K. Miyata, M. Oba, T. Ishii, S. Fukushima, M. Han, H. Koyama, N. Nishiyama and K. Kataoka, *Angew. Chem., Int. Ed.*, 2008, **47**, 5163–5166.
4 E. C. Cho, J. Xie, P. A. Wurm and Y. Xia, *Nano Lett.*, 2009, **9**, 1080–1084.
5 J.-Z. Du, T.-M. Sun, W.-J. Song, J. Wu and J. Wang, *Angew. Chem., Int. Ed.*, 2010, **49**, 3621–3626.
6 S. Chen, L. Rong, Q. Lei, P.-X. Cao, S.-Y. Qin, D.-W. Zheng, H.-Z. Jia, J.-Y. Zhu, S.-X. Cheng, R.-X. Zhuo and X.-Z. Zhang, *Biomaterials*, 2016, **77**, 149–163.
7 Y.-Y. Yuan, C.-Q. Mao, X.-J. Du, J.-Z. Du, F. Wang and J. Wang, *Adv. Mater.*, 2012, **24**, 5476–5480.
8 S.-X. Li, L. Liu, L.-J. Zhang, B. Wu, C.-X. Wang, W. Zhou, R.-X. Zhuo and S.-W. Huang, *Polym. Chem.*, 2016, **7**, 5113–5122.
9 Y. Wang, S. Lv, M. Deng, Z. Tang and X. Chen, *Polym. Chem.*, 2016, **7**, 2253–2263.
10 J.-Z. Du, X.-J. Du, C.-Q. Mao and J. Wang, *J. Am. Chem. Soc.*, 2011, **133**, 17560–17563.
11 K. Raghupathi, L. Li, J. Ventura, M. Jennings and S. Thayumanavan, *Polym. Chem.*, 2014, **5**, 1737–1742.
12 Y. Huang, Z. Tang, X. Zhang, H. Yu, H. Sun, X. Pang and X. Chen, *Biomacromolecules*, 2013, **14**, 2023–2032.
13 L. Li, K. Raghupathi, C. Yuan and S. Thayumanavan, *Chem. Sci.*, 2013, **4**, 3654–3660.
14 H. Kang, A. C. Trondoli, G. Zhu, Y. Chen, Y.-J. Chang, H. Liu, Y.-F. Huang, X. Zhang and W. Tan, *ACS Nano*, 2011, **5**, 5094–5099.
15 T. Kaiden, E. Yuba, A. Harada, Y. Sakanishi and K. Kono, *Bioconjugate Chem.*, 2011, **22**, 1909–1915.
16 J. L. Paris, M. V. Cabañas, M. Manzano and M. Vallet-Regí, *ACS Nano*, 2015, **9**, 11023–11033.
17 W. Zhao, K. Odelius, U. Edlund, C. Zhao and A.-C. Albertsson, *Biomacromolecules*, 2015, **16**, 2522–2528.
18 T. Yildirim, A. C. Rinkenauer, C. Weber, A. Traeger, S. Schubert and U. S. Schubert, *J. Polym. Sci., Part A: Polym. Chem.*, 2015, **53**, 2711–2721.
19 T. Yildirim, A. Traeger, E. Preussger, S. Stumpf, C. Fritzsche, S. Hoeppener, S. Schubert and U. S. Schubert, *Macromolecules*, 2016, **49**, 3856–3868.
20 J. W. Woodcock, X. Jiang, R. A. E. Wright and B. Zhao, *Macromolecules*, 2011, **44**, 5764–5775.
21 N. Yamaguchi, L. Zhang, B.-S. Chae, C. S. Palla, E. M. Furst and K. L. Kiick, *J. Am. Chem. Soc.*, 2007, **129**, 3040–3041.
22 W. Gao, J. M. Chan and O. C. Farokhzad, *Mol. Pharm.*, 2010, **7**, 1913–1920.
23 Q. Jin, T. Cai, Y. Wang, H. Wang and J. Ji, *ACS Macro Lett.*, 2014, **3**, 679–683.
24 S. Mura, J. Nicolas and P. Couvreur, *Nat. Mater.*, 2013, **12**, 991–1003.
25 Y. Li, R. Tong, H. Xia, H. Zhang and J. Xuan, *Chem. Commun.*, 2010, **46**, 7739–7741.
26 W. Chen and J. Du, *Sci. Rep.*, 2013, **3**, 2162.
27 A. Klaikherd, C. Nagamani and S. Thayumanavan, *J. Am. Chem. Soc.*, 2009, **131**, 4830–4838.
28 J. Xuan, M. Pelletier, H. Xia and Y. Zhao, *Macromol. Chem. Phys.*, 2011, **212**, 498–506.
29 J. Wang, M. Pelletier, H. Zhang, H. Xia and Y. Zhao, *Langmuir*, 2009, **25**, 13201–13205.
30 J. J. Haven, C. Guerrero-Sanchez, D. J. Keddie, G. Moad, S. H. Thang and U. S. Schubert, *Polym. Chem.*, 2014, **5**, 5236–5246.
31 C. Guerrero-Sanchez, L. O'Brien, C. Brackley, D. J. Keddie, S. Saubern and J. Chiefari, *Polym. Chem.*, 2013, **4**, 1857–1862.
32 C. Guerrero-Sanchez, D. J. Keddie, S. Saubern and J. Chiefari, *ACS Comb. Sci.*, 2012, **14**, 389–394.
33 G. Moad, J. Chiefari, Y. K. Chong, J. Krstina, R. T. A. Mayadunne, A. Postma, E. Rizzardo and S. H. Thang, *Polym. Int.*, 2000, **49**, 993–1001.
34 M. W. M. Fijten, R. M. Paulus and U. S. Schubert, *J. Polym. Sci., Part A: Polym. Chem.*, 2005, **43**, 3831–3839.
35 T. Çaykara, C. Özyürek, Ö. Kantoğlu and B. Erdoğan, *Polym. Degrad. Stab.*, 2003, **80**, 339–343.
36 K. Grygiel, J.-S. Lee, K. Sakaushi, M. Antonietti and J. Yuan, *ACS Macro Lett.*, 2015, **4**, 1312–1316.
37 A. Vollrath, D. Pretzel, C. Pietsch, I. Perevyazko, S. Schubert, G. M. Pavlov and U. S. Schubert, *Macromol. Rapid Commun.*, 2012, **33**, 1791–1797.
38 S. Schubert, J. J. T. Delaney and U. S. Schubert, *Soft Matter*, 2011, **7**, 1581–1588.
39 A. Reisch, A. Runser, Y. Arntz, Y. Mély and A. S. Klymchenko, *ACS Nano*, 2015, **9**, 5104–5116.
40 C. Pietsch, U. Mansfeld, C. Guerrero-Sanchez, S. Hoeppener, A. Vollrath, M. Wagner, R. Hoogenboom, S. Saubern, S. H. Thang, C. R. Becer, J. Chiefari and U. S. Schubert, *Macromolecules*, 2012, **45**, 9292–9302.
41 J. R. Lovett, N. J. Warren, L. P. D. Ratcliffe, M. K. Kocik and S. P. Armes, *Angew. Chem., Int. Ed.*, 2015, **54**, 1279–1283.
42 J.-H. Ryu, R. Roy, J. Ventura and S. Thayumanavan, *Langmuir*, 2010, **26**, 7086–7092.

 This journal is © The Royal Society of Chemistry 2017

Electronic Supplementary Material (ESI) for Polymer Chemistry.
This journal is © The Royal Society of Chemistry 2017

Dual pH- and ultrasound responsive nanoparticles with pH-triggered surface charge conversional properties

Turgay Yildirim,[a,b] Ilknur Yildirim,[a,b] Roberto Yañez-Macias,[b,d] Steffi Stumpf,[a,b] Carolin Fritzsche,[a,b] Stephanie Hoeppener,[a, b] Carlos Guerrero-Sanchez,[a,b] Stephanie Schubert,[b,c]*

Ulrich S. Schubert[a,b]*

[a] Laboratory of Organic and Macromolecular Chemistry (IOMC), Friedrich Schiller University Jena, Humboldtstr. 10, 07743 Jena, Germany

[b] Jena Center for Soft Matter (JCSM), Friedrich Schiller University Jena, Philosophenweg 7, 07743 Jena, Germany

[c] Institute of Pharmacy, Department of Pharmaceutical Technology, Friedrich Schiller University Jena, Otto-Schott-Str. 41, 07745 Jena, Germany

[d] Centro de Investigación en Química Aplicada, Departamento de Síntesis de Polímeros, Blvd. Enrique Reyna H. 140, 25100 Saltillo, Mexico

KEYWORDS: RAFT polymerization; pH-responsive polymers; polymerization kinetics; nanoprecipitation; pH-responsive nanoparticles; ultrasound responsive nanoparticles.

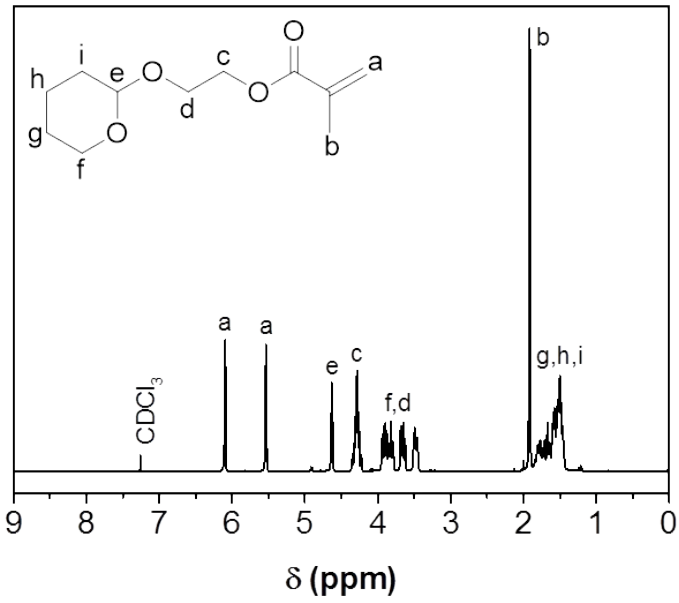

Figure S1. ^{1}H NMR spectrum (300 MHz, $CDCl_3$) of monomer THP protected HEMA (THP-HEMA) and assignment of the signals.

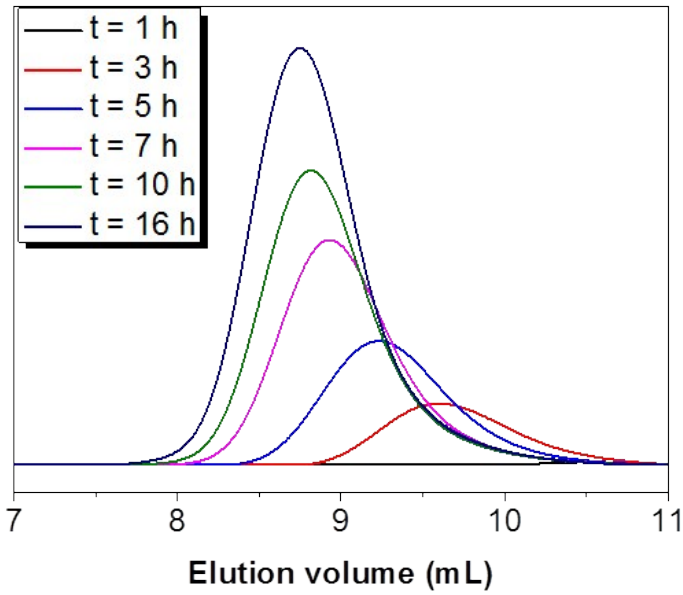

Figure S2. Overlay of the SEC traces ($CHCl_3$) from kinetic studies of the RAFT copolymerization of **P5**.

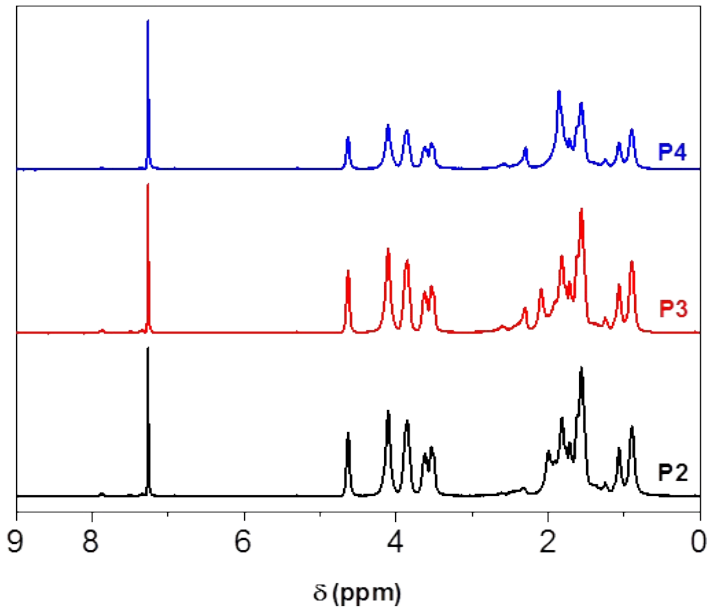

Figure S3. ^{1}H NMR spectra (300 MHz, $CDCl_3$) of **P2**, **P3** and **P4**.

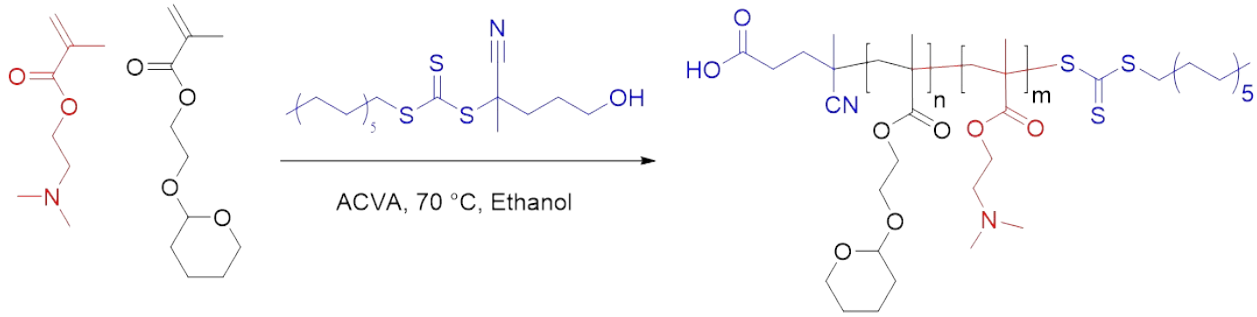

Scheme S1. Schematic representation of the RAFT copolymerization of THP-HEMA and DMAEMA by using CDB as CTA.

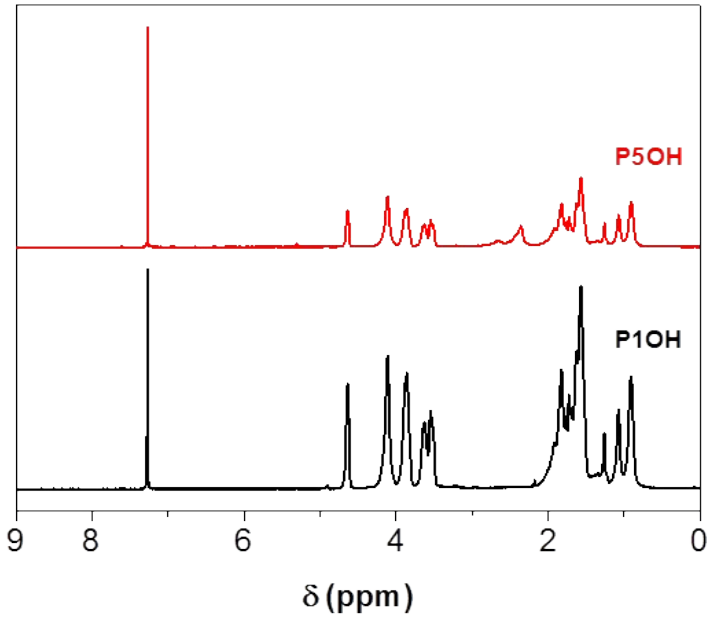

Figure S4. ^{1}H NMR spectra (300 MHz, $CDCl_3$) of **P1OH** and **P5OH**.

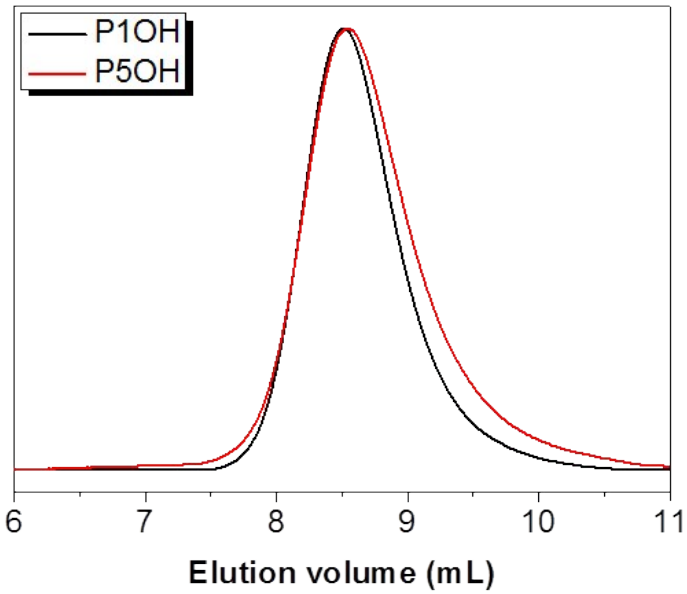

Figure S5. Normalized SEC traces ($CHCl_3$) of the isolated copolymers **P1OH** and **P5OH**.

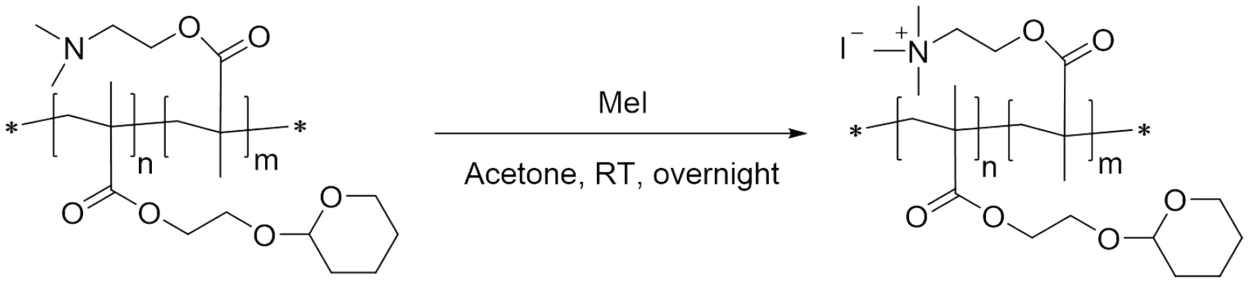

Scheme S2. Schematic representation of the quaternization of the synthesized copolymers (**P2** to **P5**).

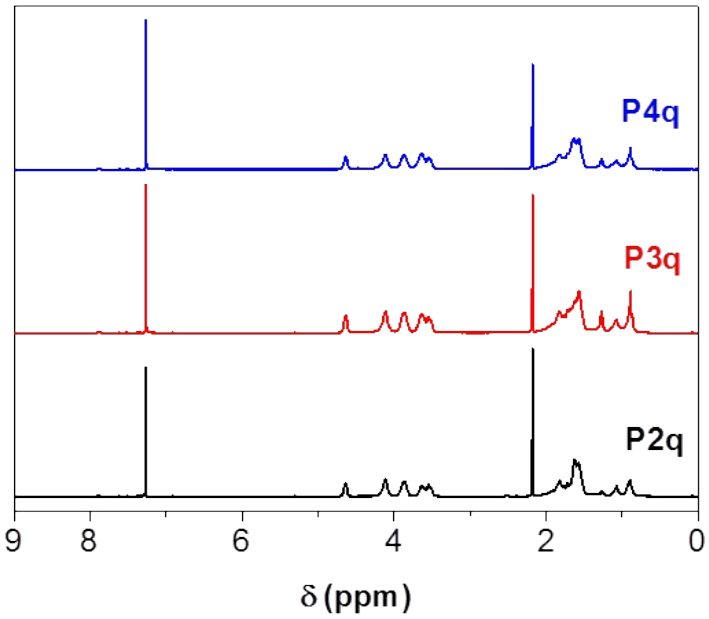

Figure S6. ^{1}H NMR spectra (300 MHz, $CDCl_3$) of **P2q** to **P4q**.

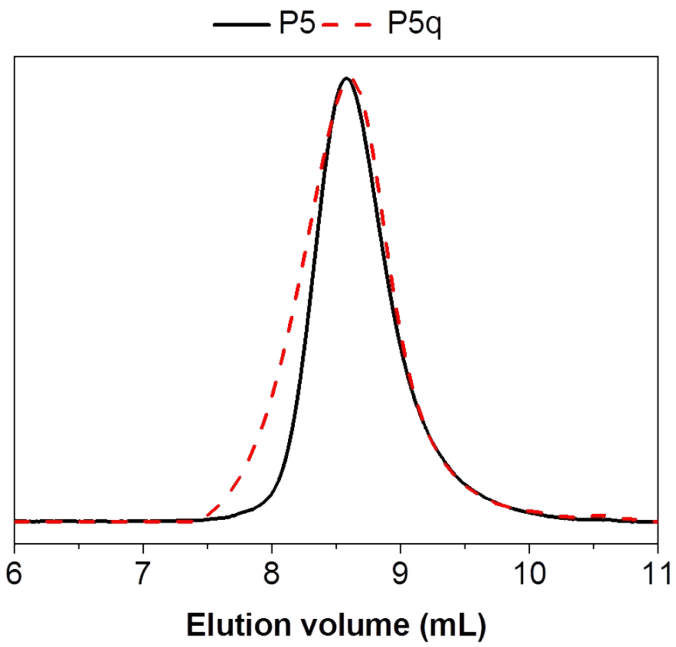

Figure S7. Normalized SEC traces ($CHCl_3$) of the isolated copolymers **P5** and **P5q**.

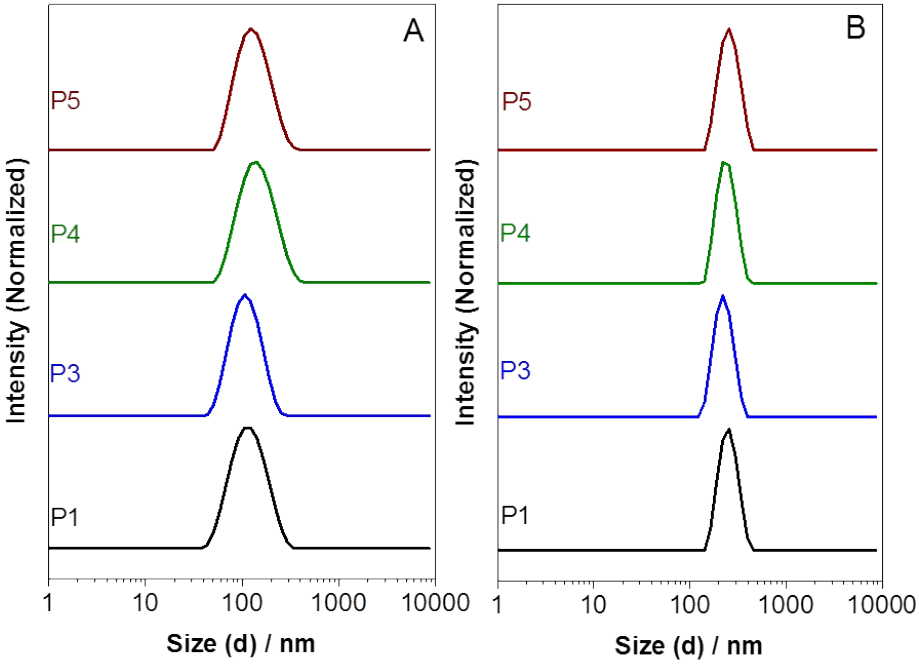

Figure S8. Normalized intensity size distributions of nanoparticles in water (**P1**, **P3**, **P4**, and **P5**) with an initial acetone-polymer concentration of 1 mg mL^{-1}, (A) prepared by dropping acetone-polymer solution to water (AW), (B) dropping water to acetone-polymer solution (WA).

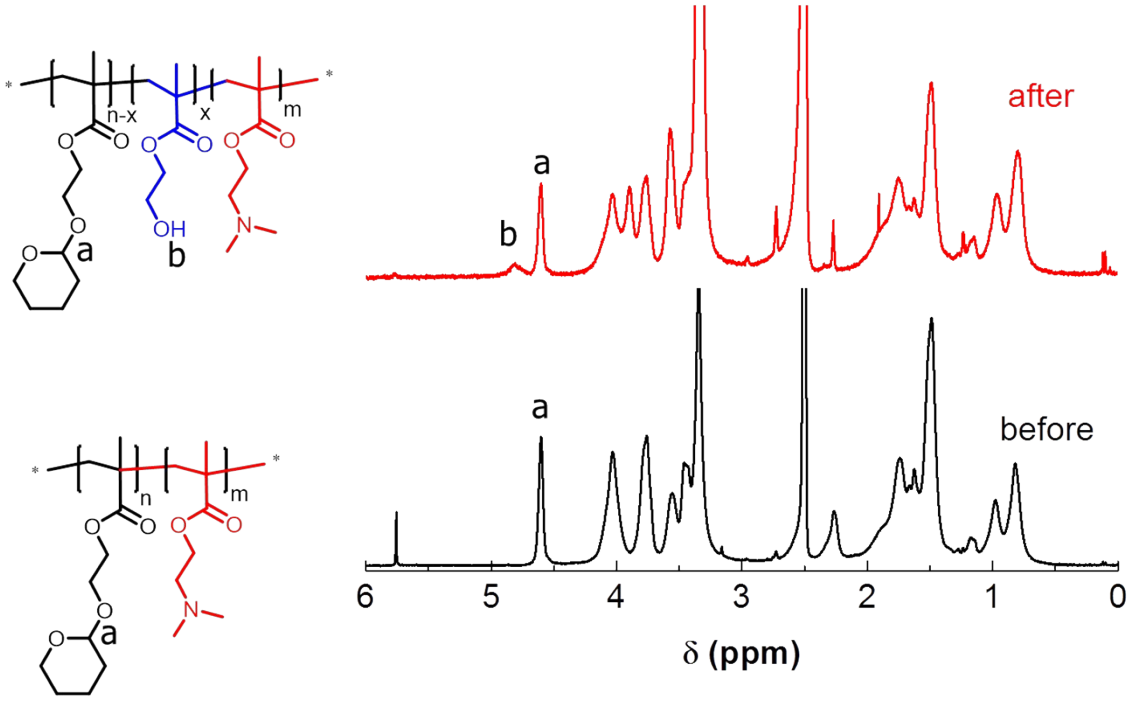

Figure S9. ^{1}H NMR spectrum (300 MHz, DMSO-d6) of **P3** nanoparticles before and after treatment with 0.1 M acetic acid (pH = 3.1, stored at 37 °C for 24 h).

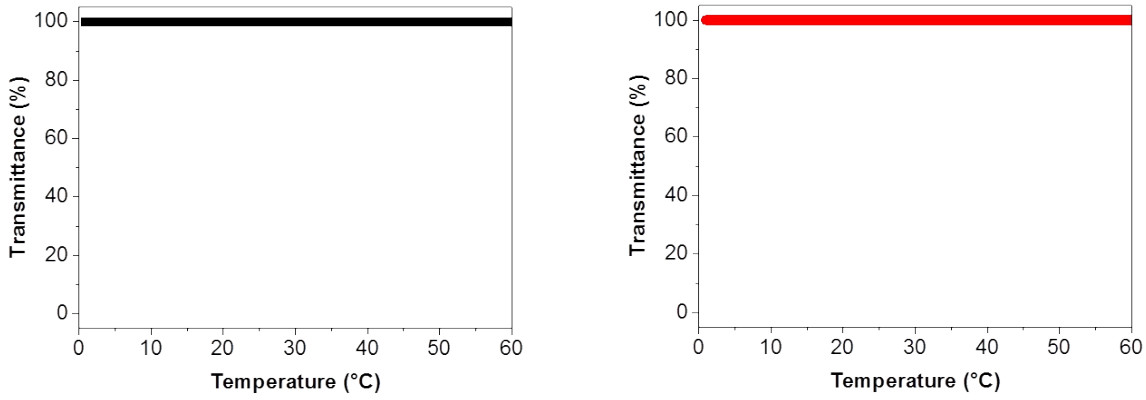

Figure S10. (Left) Transmittance curve of **P4** solution at pH 4.0 during heating from 0 to 60 °C (c = 1 mg mL^{-1}, heating rate 1 K min^{-1}). (Right) Transmittance curve of **P5** solution at pH 5.0 during heating from 0 to 60 °C (c = 1 mg mL^{-1}, heating rate 1 K min^{-1}).

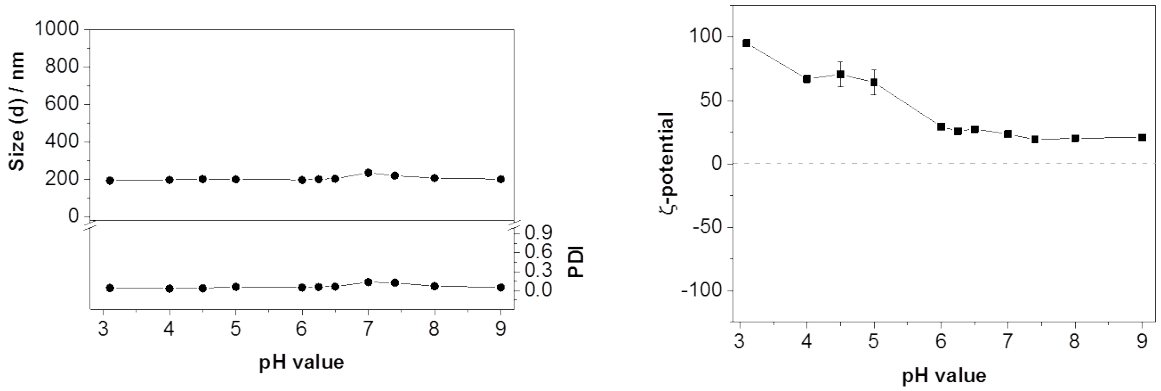

Figure S11. (Left) Intensity weighted diameters and PDI values of **P2q** nanoparticles as a function of the pH value. (Right) ζ-Potentials of the **P2q** nanoparticles as a function of the pH value.

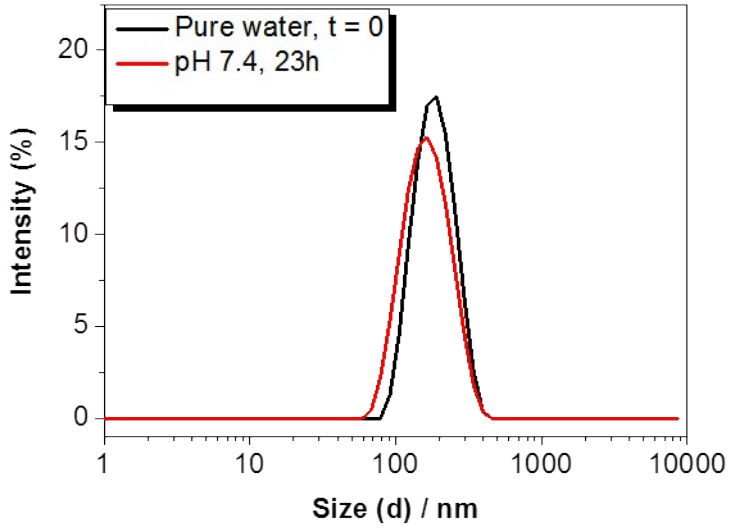

Figure S12. Intensity weigted size distributions of **P3q** nanoparticles in water before and after storage at pH value of 7.4 for 23 h at 37 °C.

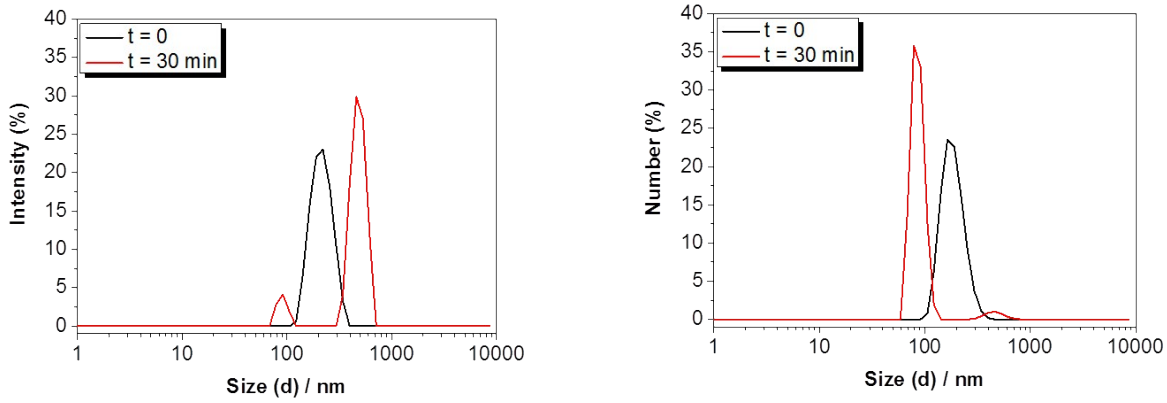

Figure S13. (Left) Intensity weigted size distributions of **P1** nanoparticles in water before and after 30 min. ultrasound treatment (20 W). (Right) Number % size distributions of **P1** nanoparticles in water before and after 30 min. ultrasound treatment (20 W).

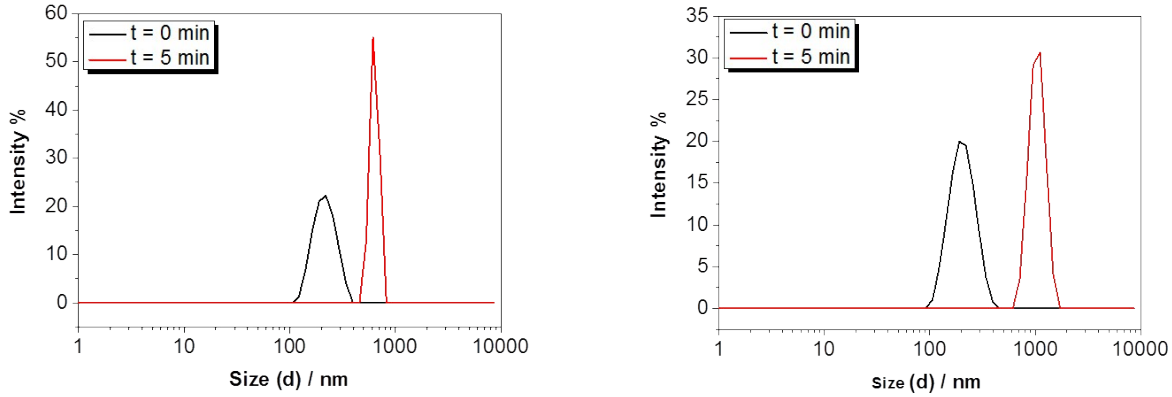

Figure S14. (Left) Intensity weighted size distributions of **P1** nanoparticles in water before and after 5 min. ultrasound treatment (40 W). (Right) Intensity weighted size distributions of **P5** nanoparticles in water before and after 5 min. ultrasound treatment (40 W).

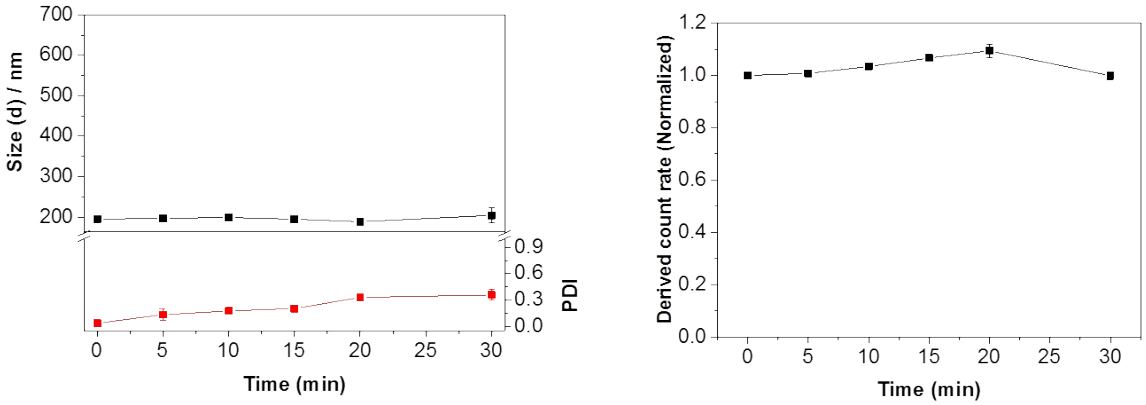

Figure S15. (Left) Intensity weighted size and PDI values of **PMMA** nanoparticles as a function of the ultrasound irradiation time (20 W). (Right) Normalized count rate of the **PMMA** nanoparticles as a function of the ultrasound irradiation time (20 W).

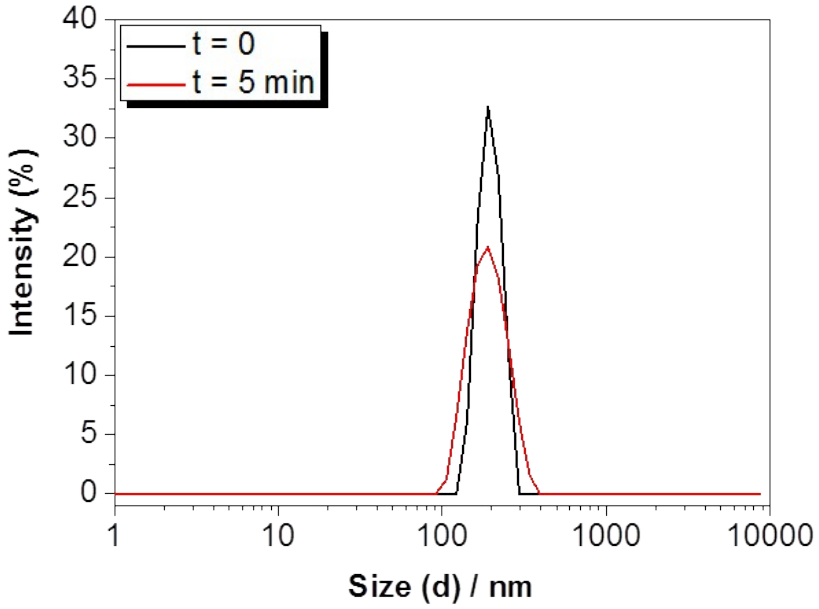

Figure S16. Intensity weighted size distribution of **PMMA** nanoparticles in water before and after 5 min. ultrasound treatment (40 W).

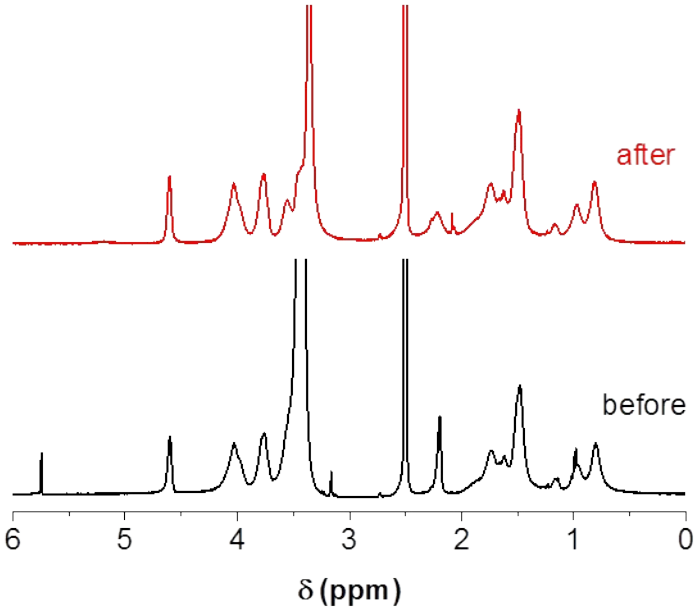

Figure S17. ^{1}H NMR spectrum (300 MHz, DMSO-d6) of **P5** nanoparticles before and after ultrasound treatment (5 min, 40 W).

Synthesis of poly(methyl acrylate) (PMA) and synthesis of PMA nanoparticles:

400 mg methyl acrylate (4.646 mmol), 11.5 mg CPADB (0.041 mmol) and 2.88 mg ACVA (0.010 mmol) were dissolved in DMF in a Biotage microwave reaction vial (5 mL) equipped with a magnetic stir bar. The total volume of the reaction mixture was 4.65 mL. After the reaction was degassed for 40 min by argon purging, the t0 sample for ^{1}H NMR was taken, and the flask was immersed in a preheated oil bath under stirring at 70 °C. After 16 h, the polymerization was stopped by cooling to room temperature and exposing to air. Monomer conversion was determined via ^{1}H NMR as 38%. The polymer was purified by precipitating in cold diethyl ether (2 times). The resulting polymer was dried under high vacuum at room temperature until constant weight. The number average molar mass (M_n) and dispersity ($Đ_M$) were determined SEC in $CHCl_3$ by using PMMA standards. SEC in $CHCl_3$: M_n = 3,200 g mol^{-1} and $Đ_M$ = 1.26 (Figure S17). The number average molar mass (M_n) was calculated as 3,700 g mol^{-1} via ^{1}H NMR by comparing the ω-RAFT end groups signals and the methyl proton signal of **PMA** (Figure S17). **PMA** nanoparticles were prepared by nanoprecipitation method by dropping water into acetone-polymer solution.

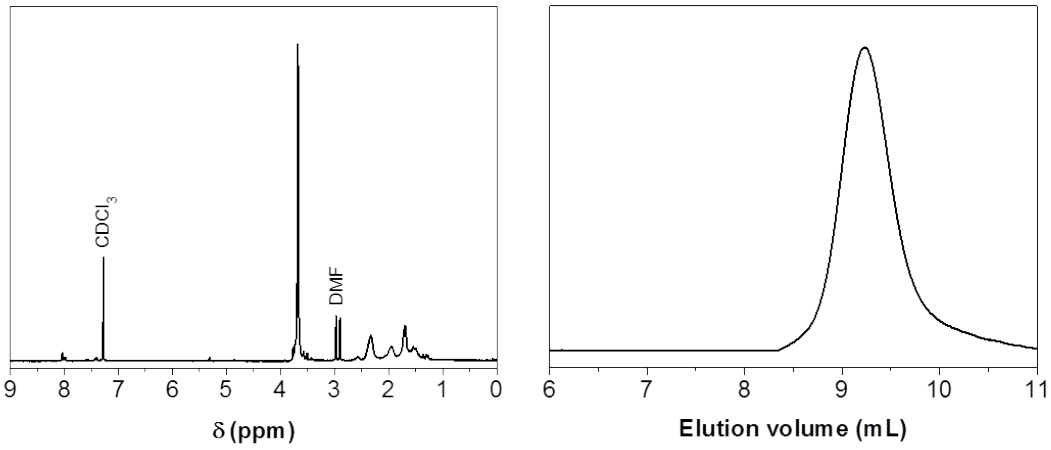

Figure S18. (Left) ^{1}H NMR spectrum (300 MHz, $CDCl_3$) of **PMA**. (Right) SEC trace ($CHCl_3$) of the isolated **PMA**.

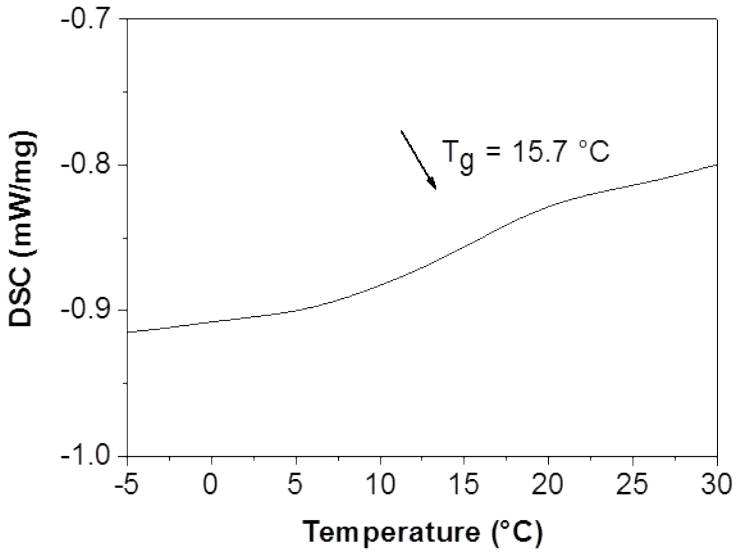

Figure S19. DSC heating run of **PMA** (heating rate 20 K min^{-1}).

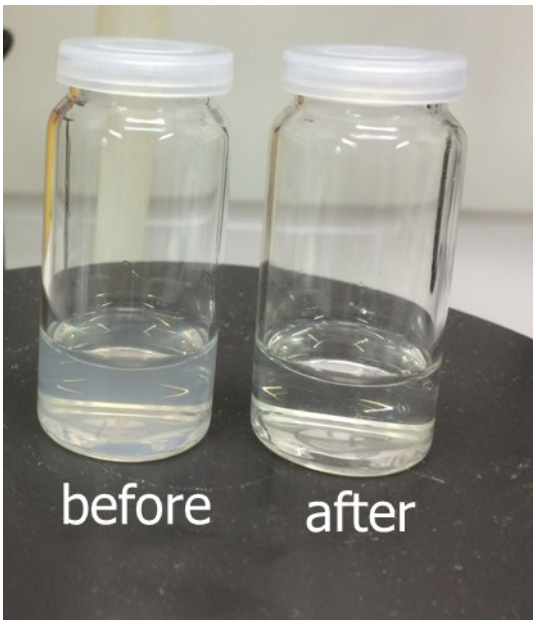

Figure S20. Photograph of **PMA** nanoparticle suspension before and after 2 min. ultrasound treatment (40 W).

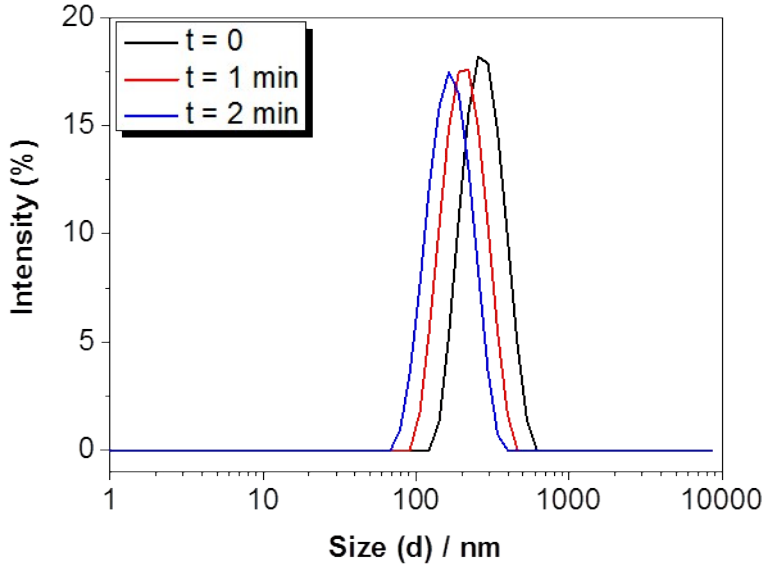

Figure S21. Intensity weighted size distribution of **PMA** nanoparticles in water before and after 1 and 2 min. ultrasound treatment (40 W).

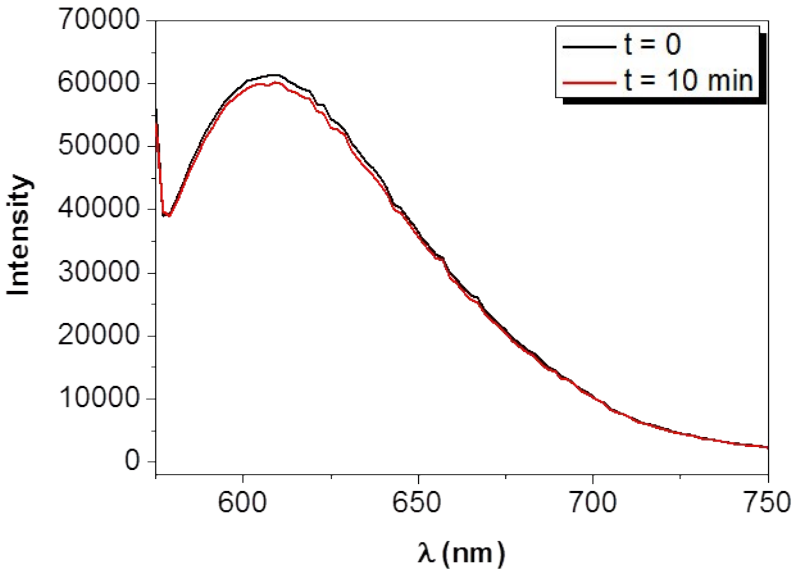

Figure S22. Fluorescence emission spectra of Nile Red encapsulated **P4** nanoparticles (0.5 mg mL^{-1}) before and after storage at 37 °C for 10 min. in pure water.

Publication P6

“Polymersomes with endosomal pH induced vesicle-to-micelle morphology transition and a potential application for controlled doxorubicin delivery”

T. Yildirim, A. Traeger, P. Sungur, S. Hoeppener, C. Fritzsche, I. Yildirim, D. Pretzel, S. Schubert, U. S. Schubert

Manuscript, submitted.

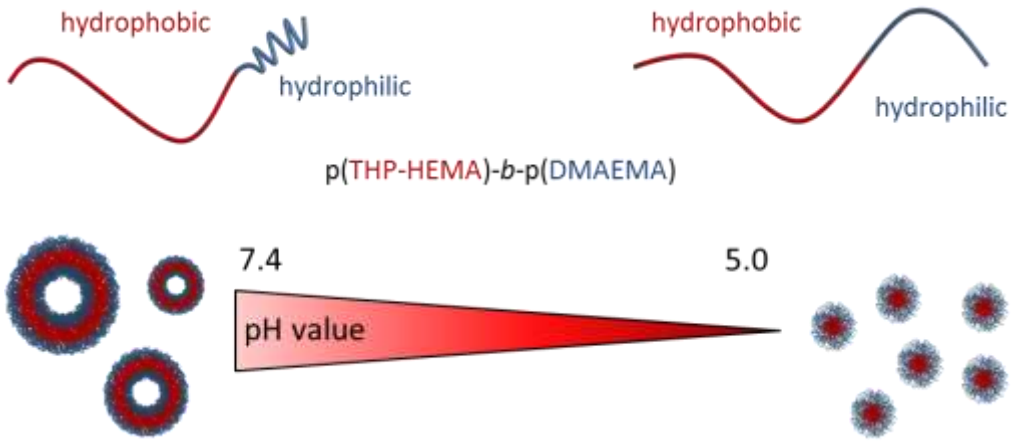

Polymersomes with endosomal pH-induced vesicle-to-micelle morphology transition and a potential application for controlled doxorubicin delivery

Turgay Yildirim,[a,b] Anja Traeger,[a,b] Pelin Sungur,[a,b] Stephanie Hoeppener,[a,b] Carolin Fritzsche,[a,b] Ilknur Yildirim,[a,b] David Pretzel,[a,b] Stephanie Schubert,[b,c] Ulrich S. Schubert*[a,b]*

[a] Laboratory of Organic and Macromolecular Chemistry (IOMC), Friedrich Schiller University Jena, Humboldtstr. 10, 07743 Jena, Germany

[b] Jena Center for Soft Matter (JCSM), Friedrich Schiller University Jena, Philosophenweg 7, 07743 Jena, Germany

[c] Institute of Pharmacy, Department of Pharmaceutical Technology, Friedrich Schiller University Jena, Otto-Schott-Str. 41, 07745 Jena, Germany

KEYWORDS: RAFT polymerization; block copolymers; pH-responsive polymers; nanoprecipitation; pH-responsive polymersomes; vesicle-to-micelle morphology transition; drug delivery.

ABSTRACT

A series of pH responsive block copolymers were synthesized *via* the reversible addition-fragmentation chain transfer (RAFT) polymerization of 3,4-dihydro-2H-pyran (DHP) protected 2-hydroxyethyl methacrylate (HEMA) (2-((tetrahydro-2H-pyran-2-yl)oxy)ethyl methacrylate (THP-HEMA)) and 2-(dimethylamino) ethyl methacrylate (DMAEMA) using p(THP-HEMA) as a macro chain transfer agent (mCTA). The degree of polymerization (DP) of the p(THP-HEMA) block was fixed to 35, whereas the DP of the p(DMAEMA) block was systematically varied from 21 to 50. In aqueous solution, the block copolymer with the shortest p(DMAEMA) block (DP = 21) self-assembled into vesicles, while the polymer with 30 units of p(DMAEMA) formed a mixture of micelles and vesicles. The polymer with the longest p(DMAEMA) block (DP = 50) formed exclusively micelles. The morphology change as a function of monomer composition was verified by dynamic light scattering (DLS) and cryo-transmission electron microscopy (cryo-TEM) studies. Moreover, the corresponding polymersomes exhibited a morphology transition from vesicles at neutral pH values to micelles upon lowering the pH value down to endosomal pH value as evidenced by the decrease in the hydrodynamic diameter of the formed structures investigated by DLS and cryo-TEM. The capability of polymersomes to encapsulate both hydrophobic (*e.g.,* Nile Red) and hydrophilic (*e.g.*, doxorubicin hydrochloride (DOX·HCl)) cargos was verified by *in vitro* studies. Drug release studies demonstrated that the DOX·HCl release is significantly accelerated under acidic pH values compared to physiological conditions. Cytotoxicity studies revealed that DOX·HCl loaded polymersomes exhibited an efficient cell death in L929 cells comparable to free DOX·HCl. Confocal laser scanning microscopy (CLSM) and flow cytometry studies showed that DOX·HCl loaded vesicles were easily taken up by L929 cells and were mainly located in the cytoplasm and cell nuclei after 2 h of incubation.

INTRODUCTION

Self-assembly of amphiphilic polymers, particularly block copolymers, has become a versatile and widely used method for the formation of nanostructures with different morphologies such as nanospheres, rods, micelles, and vesicles.[1] Among other, polymeric vesicles, also known as polymersomes, have gained great interest due to their potential applications in a broad range of areas including as mimics of biological membranes, as microreactors and drug carriers.[2, 3] Regarding the latter application, polymersomes are under intense scrutiny due to their ability, like lipid-based vesicles (liposomes), to offer hydrophilic aqueous cavities that are suitable for encapsulation of hydrophilic molecules as well as a hydrophobic membrane that can incorporate hydrophobic species and protect the payloads from the external media.[4] Compared to liposomes, polymersomes have thicker and more stable membranes as a result of higher molar mass values of the polymers than lipids. This can remarkably diminish the premature release of the payloads during circulation and accordingly decrease the systemic cytotoxicity. Moreover, to improve the therapeutic efficiency and to avoid drug resistance in cells the loaded drugs should be released rapidly in a controlled way when the target site is reached. Therefore, several stimuli responsive polymersomes, which target to release the encapsulated therapeutics in respond to several endogenous (pH value,[5] redox,[6] and enzyme[7]) and exogenous (temperature,[8] light,[9] magnetic field,[10] and ultrasound[11]) stimuli, have been developed by incorporating different responsive building blocks into polymers. Among all the stimuli, pH responsiveness is the most intensively investigated one due to the pH value gradients found within the physiological environment. For instance, tumor and inflammatory tissues are slightly more acidic (pH = 6.5 to 7.2) than normal ones (pH = 7.4).[12, 13] Even within cell compartments there is a pH value gradient. Cytosol has a comparable pH value like blood (7.4), whereas the endosome features a pH value between 6.5 to

5.0. The pH value even decreases to 4.5 in the lysosome.[14] The pH responsiveness of the polymersomes usually relies on the change in hydrophilicity of the corresponding polymers by protonation/deprotonation of ionizable pendant groups or by the cleavage of the pH sensitive moieties. The change in hydrophilicity mediates the cargo release, commonly caused by dissolution, precipitation, swelling or collapsing of the polymers.[15] However, a change in hydrophilicity can also induce a morphology transition. For instance, several examples of micelle-to-vesicle transitions in response to a stimulus have been reported.[16-20] However, polymersomes that can exhibit vesicle-to-micelle transitions are of particular interest for the controlled delivery of hydrophilic drugs due to offering a loss of aqueous cavities within the vesicles, which can trigger the hydrophilic cargo release. Nevertheless, polymersomes with vesicle-to-micelle transition abilities have been rarely observed.[21-23]

In this study, three well-defined diblock copolymers of poly((THP-HEMA)-*b*-DMAEMA) with a fixed degree of polymerization (DP) of p(THP-HEMA) and a variable p(DMAEMA) block length were synthesized by reversible addition-fragmentation chain transfer (RAFT) polymerization using a macro chain transfer approach (Scheme 1). It is believed that polymersomes can undergo shape transformations in response to stimuli when the membrane has a sufficient chain mobility.[24-27] Previous work within our group has shown that p(THP-HEMA) based nanoparticles are responsive to ultrasound due to their high chain mobilities as a result of their elastic nature (T_g ~30 °C).[28] As a consequence, hydrophobic p(THP-HEMA) is selected as a building block for the membrane of the polymersomes, which can possibly feature a morphology transition upon a change in the hydrophilicity of the polymer. Additionally, the weak polyelectrolyte p(DMAEMA) was used as pH responsive hydrophilic block since it can be protonated under its pK_a value (~7.4) and, hence, change the hydrophobic/hydrophilic ratio of the

corresponding copolymer. The findings on the self-assembly behavior of these polymers in aqueous media, the pH responsive behavior of the polymersomes, encapsulation studies of both hydrophobic Nile Red and hydrophobic doxorubicin hydrochloride (DOX·HCl), and additional biological studies to evaluate the capability of the polymersomes as smart DOX·HCl carriers are presented herein.

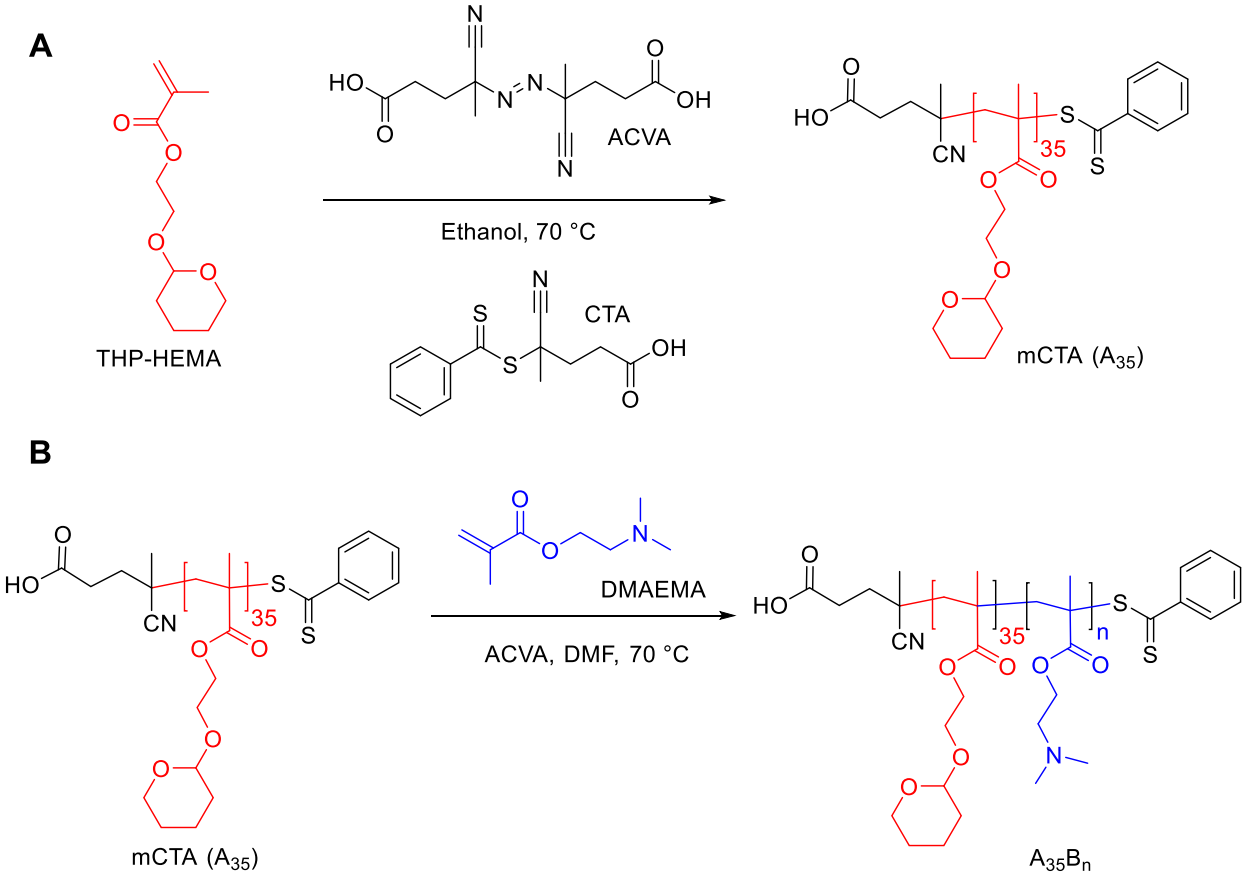

Scheme 1. (A) Schematic representation of the synthesis of **mCTA** via RAFT polymerization of THP-HEMA and (B) its subsequent chain extension with DMAEMA.

EXPERIMENTAL SECTION

Materials

The monomer THP (3,4-dihydro-2H-pyran) protected HEMA (THP-HEMA) 2-((tetrahydro-2H-pyran-2-yl)oxy)ethyl methacrylate was synthesized according to the procedure reported elsewhere.[29] 4,4'-Azobis(4-cyanovaleric acid) (ACVA), 4-cyano-4-(phenylcarbonothioylthio) pentanoic acid (CPADB), 1,3,5-trioxane, *N*,*N*-dimethylaminoethyl methacrylate (DMAEMA), and Nile Red were purchased from Sigma Aldrich. Doxorubicin hydrochloride (DOX·HCl) was purchased from Cayman Chemical. AlamarBlue was obtained from Life Technologies. Consumables for cell culture, like pipettes and cell culture plates (96 well), were obtained from Corning (USA) and Greiner Bio-one (Austria/Germany). If not stated otherwise, cell culture media and supplements (L-glutamin, antibiotics) were obtained from Biochrom (Merck Millipore, Germany).

Instruments and methods

Proton nuclear magnetic resonance (^{1}H NMR) spectra were recorded at room temperature in $CDCl_3$ or CD_3OD on a Brucker Avance 300 MHz. The chemical shifts are given in ppm.

Size-exclusion chromatography (SEC) measurements were performed on a Agilent 1200 series equipped with a G1310A pump, a G1315D DA detector, a G1362A RI detector, and PSS GRAM 30 Å/1000 Å (10 μm particle size) columns in series at 40 °C using *N*,*N*-dimethylacetamide (DMAc) with 2.1 g L^{-1} LiCl as eluent at a flow rate of 1 mL min^{-1}. The system was calibrated with polystyrene (PS) standards (M_p = 100 to 1 000 000 g mol^{-1}).

Dynamic light scattering (DLS) was performed on a Zetasizer Nano ZS (Malvern Instruments, Herrenberg, Germany). After an equilibration time of 180 s, 3 × 30 runs were carried out at 25 °C (λ = 633 nm). The measurements were performed at an angle of 173°. Each measurement

was done in triplicate. The size distribution of suspensions were calculated applying the nonlinear least-squares fitting mode.

Electrophoretic light scattering was used to measure the electrokinetic potential, also known as ζ-potential. The measurements were performed on a Zetasizer Nano ZS (Malvern Instruments, Herrenberg, Germany) by applying laser Doppler velocimetry. For each measurement, 10 runs were carried out using the slow-field and fast-field reversal mode at 150 V. Each experiment was performed in triplicate at 25 °C.

Transmission electron microscopy (TEM) was carried out on a FEI Technai G2 20 cryo-transmission electron microscope. Samples were prepared with a Vitrobot Mark IV system. 8 µL of the sample solution (2.5 mg mL^{-1}) were transferred onto Quantifoil (R2/2, Quantifoil) grids, which were cleaned by Ar plasma cleaning for 2 min prior to preparation. Samples were plunged into liquid ethane, transferred, and kept at temperatures below 170 °C by using a Gatan cryo-stage. Images were recorded with a Mega View G2 CCD camera (OSIS, 1392 × 1040 pixels) or an Eagle CCD camera (Eagle 4k HS 200 kV, 4096 × 4096 pixels).

A Tecan M200 Pro fluorescence microplate reader was used for fluorescence measurements.

Synthesis

Synthesis of the macro chain transfer agent (mCTA)

6 g THP-HEMA (28 mmol), 172 mg CPADB (0.616 mmol) and 12 mg ACVA (0.041 mmol) were dissolved in ethanol in a Biotage microwave reaction vial (30 mL) equipped with a magnetic stir bar. The total volume of the reaction mixture was 14 mL. After the reaction mixture was degassed for 40 min by argon purging, the t_0 sample for ^{1}H NMR was taken, and the vial was immersed in a preheated oil bath under stirring at 70 °C. After 8 h, the polymerization was stopped by cooling to room temperature and exposing to air. Prior to precipitation, t_f sample

was taken to calculate the monomer conversion. Monomer conversion was determined via ^{1}H NMR by using 1,3,5-trioxane as internal standard. The polymer was purified by precipitating in cold diethyl ether (four times). The resulting polymer was dried under high vacuum at room temperature until constant weight. An overall yield of 60% was obtained. The number average molar mass (M_n) and dispersity ($Đ_M$) were determined by SEC using PS standards. The degree of polymerization (DP) for **mCTA** was calculated from the signal integrals of ^{1}H NMR spectrum (Figure 1) of the purified polymer using the following equation:

$$DP_{mCTA} = \frac{I(signal\ e)}{I(signal\ a)/2} \qquad (1)$$

with *I(signal e)* corresponding to the integral of the methine proton peaks of the THP-HEMA at 4.65 ppm and *I(signal a)* corresponding to the integral of two aromatic protons of the dithiobenzoate end group at 7.84 ppm. The number average molar mass value of the **mCTA** was calculated by using the following equation:

$$M_{n,NMR} = (DP_{THP\text{-}HEMA} \times M_{THP\text{-}HEMA}) + M_{CTA} \qquad (2)$$

in which the molar mass of the THP-HEMA, and RAFT agent are 214.26 g mol^{-1} and 279.38 g mol^{-1}, respectively.

RAFT polymerization of $\mathbf{A_{35}B_{21}}$ to $\mathbf{A_{35}B_{50}}$

For each polymerization, the [mCTA]/[ACVA] ratio was kept as 15/1, and the initial monomer concentration was 1 mol L^{-1} in DMF. All polymerizations were carried out at 70 °C. The DMAEMA to **mCTA** ratio and polymerization times were varied as summarized in Table 1. An exemplary RAFT block copolymerization procedure (Table 1, $\mathbf{A_{35}B_{50}}$) is as follows: 830 mg DMAEMA (28 mmol), 402 mg mCTA (0.052 mmol), 90 mg 1,3,5-trioxane (0.999 mmol), and 10 mg ACVA (0.036 mmol) were dissolved in DMF (5.28 mL) in a microwave vial. The reaction mixture was subsequently flushed with argon for 40 min. After taking the t_0 sample for the

determination of the monomer conversion, the vial was immersed in a preheated oil bath at 70 °C and stirred for 8 h. The reaction mixture was cooled to room temperature, exposed to air, and a sample for determination of monomer conversion (t_f) was taken. The polymer was purified by precipitation in hexane (four times). The M_n and $Đ_M$ values were determined by SEC using PS standards. The degree of polymerization (DP) for the DMAEMA block was calculated from the signal integrals of the ^{1}H NMR spectrum (Figure 2) of the purified copolymer using the following equation:

$$DP_{DMAEMA} = \frac{I(signal\ h)/6}{I(signal\ e)/\ 35} \qquad (3)$$

with *I(signal h)* corresponding to the integral of methyl proton peaks of the DMAEMA at 2.30 ppm, and *I(signal e)* corresponding to the integral of the methine proton peaks of the THP-HEMA at 4.65 ppm. M_n values of the block copolymers were calculated by using the following equation:

$$M_{n,NMR} = M_{mCTA} + (DP_{DMAEMA} \times M_{DMAEMA}) \qquad (4)$$

in which the molar mass of the mCTA and DMAEMA are 7,800 g mol^{-1} and 157.21 g mol^{-1}, respectively.

Nanoprecipitation of the block polymers

The corresponding block polymers were dissolved in acetone at a final concentration of 5 mg mL^{-1}. Subsequently, pure water was added dropwise to the acetone polymer solution under stirring at 500 rpm. The acetone/water (solvent/nonsolvent) ratio was kept constant at 0.5 for all suspensions. The acetone was evaporated by stirring the open vial for at least 24 h to yield aqueous suspensions with a final polymer concentration of 2.5 mg mL^{-1}.

pH-response test of the vesicles

For the pH-response tests of the nanoparticles, 0.1 M acetic acid (for a pH value of 3.1), 0.1 M acetate buffers (for pH values of 4, 5, 6, 6.25, 6.50), and 0.1 M tris buffers (for the pH values 7, 7.4, 8, and 9) were used. 200 µL of suspension (2.5 mg mL^{-1}) were mixed with 800 mL acetic acid and corresponding buffer solutions in Eppendorf tubes and stored at 37 °C for 3 h while mixing at 200 rpm. Then, DLS and ζ-potential measurements were performed.

Nile Red encapsulation and determination of critical aggregation concentration (CAC)

To encapsulate Nile Red to vesicles, $\mathbf{A_{35}B_{21}}$ (25 mg) was dissolved in 5 mL acetone. Then, 20 µL Nile Red stock solution (1 mM in acetone) was added. Subsequently, 10 mL of deionized water was added dropwise to the acetone solution under continuous stirring at 500 rpm. The mixed solutions were stirred overnight at room temperature in an open vial to remove the acetone. Excess Nile Red was removed using a 0.45 µm syringe filter. To calculate the CAC, the Nile Red encapsulated $\mathbf{A_{35}B_{21}}$ suspension was diluted to a series of concentrations. The corresponding fluorescence emission spectra were recorded with an excitation wavelength at 549 nm. The maximum emission intensity at a wavelength of 605 nm was plotted as a function of log 10 of polymer concentration. The CAC was calculated using the antilog of the intersection point value of two linear curves.

Encapsulation of DOX·HCl

DOX-loaded vesicles were prepared by the nanoprecipitation method. Briefly, $\mathbf{A_{35}B_{21}}$ (50 mg) and DOX·HCl (3 mg) were dissolved in 5 mL DMF. The solution was equilibrated for 20 min under stirring. Subsequently, 10 mL of pure water was added dropwise to the DMF solution under continuous stirring at 500 rpm. DMF was removed by dialysis (3 L, 48 h; MWCO: 3,500 g mol^{-1}) against tris buffer (pH = 7.4, 0.1 M). The unloaded doxorubicin was removed using a 0.45 µm syringe filter and stored at 4 °C until used. 500 µL of suspension was lyophilized to

determine the suspension concentration. For drug loading quantification, fluorescence intensity calibration functions of DOX·HCl in deionized water were used as reported elsewhere.[30]

Drug loading efficiency (DLE) and drug loading content (DLC) were calculated according to the following equations:

$$\mathrm{DLE} = \frac{\text{weight of the loaded drug}}{\text{weight of the drug in feed}} \times 100\% \qquad (5)$$

$$\mathrm{DLC} = \frac{\text{weight of the loaded drug}}{\text{total weight of polymer and loaded drug}} \times 100\% \qquad (6)$$

Release studies of DOX·HCl

Drug release from DOX·HCl encapsulated vesicles was performed in two different buffers: (i) Acetate buffer (100 mM, pH 5.0), (ii) Tris buffer (100 mM, pH 7.4) using a dialysis tube. Briefly, 3 mL of DOX-loaded vesicle suspensions in deionized water were added into a dialysis tube (MWCO: 3,500 g mol^{-1}). Subsequently, the dialysis tube was closed and exposed to 65 mL of appropriate buffer solutions at 37 °C in the dark. At predetermined time intervals, 1 mL of the buffer was taken out and an equal volume of buffer was added. The amount of released drug was calculated using a fluorescence intensity calibration function of DOX·HCl in water.

Determination of cytotoxicity

Cytotoxicity studies were performed with the mouse fibroblast cell line L929 (CCL-1, ATCC), as recommended by ISO10993-5. The cells were routinely cultured in Dulbecco's modified eagle's medium supplemented with 10% fetal calf serum (FCS, Capricorn Scientific, Germany), 100 U mL^{-1} penicillin and 100 µg mL^{-1} streptomycin at 37 °C in a humidified 5% (v/v) CO_2 atmosphere. In detail, cells were seeded at 10^4 cells per well in a 96-well plate and incubated for 24 h. No cells were seeded in the outer wells. Afterwards, the testing substances (polymeric

suspensions) were added to the cells at indicated concentrations (from 50 to 500 µg mL^{-1}), and the plates were incubated for additional 48 h. Subsequently, the medium was replaced by a mixture of fresh culture medium and the assay reagent AlamarBlue (resazurin based solution, Thermo Fisher, Germany, prepared according to the manufacturer's instructions). After a further incubation of 4 h at 37 °C in a humidified 5% (v/v) CO_2 atmosphere, the fluorescence was measured at Ex 570 / Em 610 nm, with untreated cells on the same well plate serving as negative controls. The negative control was standardized as 0% of metabolism inhibition and referred to as 100% viability. Cell viability below 70% was considered to be indicative for cytotoxicity. Data are expressed as mean ± standard deviation (SD) of three independent determinations.

Comet assay

Cells were plated in multi-well plates at a density of 1×10^4 cells/cm^2 and allowed to attach for 24 h at 37 °C and 5% CO_2. Then medium was replaced by culture medium containing free or encapsulated DOX·HCl at concentrations of 1, 2.5 or 5 µg mL^{-1}. Duplicate cultures were incubated at 37 °C for 24 h and 5% CO_2. Following incubation, cells were harvested by trypsin treatment and resuspended in PBS to a final concentration of 5×10^5 cells/mL. A 1% low melting point agarose solution was prepared in TBE-buffer (90 mM Tris-HCl, 90 mM boric acid, 2 mM EDTA, pH 7.5), tempered to 37 °C, and aliquots were mixed with cell-suspensions in a volume ratio of 10:1. For each sample, 100 µL of agarose-cell mixture were subjected to a plastic agarose gel support (GelBond film agarose support media, Lonza) and immediately covered with a coverslip to ensure an even distribution of the cell containing gel. After cooling for 30 min at 4 °C, the coverslip was removed from the formed gel. Each cell sample was prepared in triplicates. Gel-supports were placed in chambers of a 4 well plate, immersed with ice-cold lysis buffer and incubated in the dark for 2 hours at 4 °C. After washing with TBE-buffer to remove

salts from the lysis buffer, gel-supports were placed into a horizontal electrophoresis chamber filled with chilled alkaline electrophoresis buffer (3 mM NaOH, 1 mM EDTA, pH 13). After 30 min equilibration to allow DNA unwinding and double strand separation, electrophoresis was then performed at 1.5 V cm^{-1} for 30 min. Next, gel supports were removed and rinsed with icecold distilled water. SYBR Green dye was added to the gels at a concentration of 1 μg mL^{-1} in order to stain the DNA. DNA damage was measured using a epifluorescence microscope (Cell observer Z1, Zeiss, Oberkochen, Germany) equipped with a 10 × 0.45 NA plan-apochromat objective, the appropriate filter set for excitation and emission wavelengths as well as integrated software tools. Results are given as the mean tail length of individual comets captured from 100 cells of triplicate samples. During the whole assay, direct light was excluded from cell samples to avoid uncontrolled DNA damage due to UV light. All steps were performed with chilled solutions to exclude thermal induction of DNA alterations.

Live cell imaging

L929 cells were used for uptake studies. Therefore, cells (10^5 cells mL^{-1}) were seeded on glass-bottomed dishes and cultured for 24 h in a humidified 5% (v/v) CO_2 atmosphere. One hour prior to the addition of polymers and drugs, the medium was replaced with fresh one. Loaded polymersomes and free DOX were added to the cells and incubated for 2 and 24 h. Imaging was performed with an LSM880, Elyra PS.1 system (Zeiss, Oberkochen, Germany) applying a 63 × 1.4 NA plan apochromat oil objective. Furthermore, excitation wavelengths of 488 nm (exc. grating 28.0 μm) were used to detect DOX.

Flow cytometry study

According to the CLSM studies, the uptake of free and encapsulated DOX·HCl was quantified by flow cytometry. For this purpose, 2 × 10^5 L929 cells mL^{-1} were seeded on glass-bottomed

dishes and cultured for 24 h in a humidified 5% (v/v) CO_2 atmosphere. One hour prior to the addition of polymers and drugs, the medium was replaced with fresh one. Loaded polymersomes and free DOX·HCl were added to the cells and incubated for 2 and 24 h. To determine the relative uptake of DOX·HCl, 10,000 cells were measured by flow cytometry using a Cytomics FC 500 (Beckman Coulter). The amount of DOX·HCl taken up by the cells were measured by the mean fluorescence intensity (MFI) of all cells. The experiments were performed at least three times independently.

Table 1. Selected characterization data of the **mCTA**.

Entry	THP-HEMA/CTA[a]	CTA/ACVA[b]	Polym. time (h)	Conv. [%][c]	$DP_{theo.}$[d]	$M_{n,theo.}$[e] [g mol^{-1}]	DP[f]	M_n[g] [g mol^{-1}]	$M_{n,SEC}$[i] [g mol^{-1}]	M_w/M_n[i]	T_g[j]
mCTA	47.71/1	15/1	8	65	31	6,900	35	7,800	5,800	1.08	24.6

[a]Monomer to CTA ratio. [b]CTA to ACVA ratio. [c]Determined by ^{1}H NMR spectroscopy. [d]Determined by the formula $DP_{theo.} = [([M]/[CTA] \times Conv.]$. [e]Determined by the formula $M_{n,theo.} = [([M]/[CTA] \times Conv. \times M_{THP\text{-}HEMA}) + (M_{CTA})]$. [f]Determined by ^{1}H NMR spectroscopy of isolated mCTA. [g]Determined by the formula $M_{n,theo.} = [(DP \times M_{THP\text{-}HEMA}) + M_{CTA}]$. [i]Determined by SEC in DMAc analysis (RI detection, PS calibration). [j]Determined by DSC analysis.

Table 2. Selected characterization data of the block copolymers (**$A_{35}B_{21}$** to **$A_{35}B_{50}$**).

Entry	DMAEMA/mCTA[a]	mCTA/ACVA[b]	Polym. time (h)	Conv. [%][c]	$DP_{theo.}$[d]	$M_{n,theo.}$[e] [g mol^{-1}]	DP[f]	M_n[g] [g mol^{-1}]	$M_{n,SEC}$[i] [g mol^{-1}]	M_w/M_n[i]	T_g[j]
$A_{35}B_{21}$	49.62/1	15/1	4	36	18	10,600	21	11,100	8,300	1.09	24.9
$A_{35}B_{30}$	49.62/1	15/1	8	58	29	12,400	30	12,500	9,300	1.08	23.4
$A_{35}B_{50}$	102.54/1	15/1	7	49	50	15,700	50	15,700	11,200	1.10	20.7

[a]Monomer to mCTA ratio. [b]mCTA to ACVA ratio. [c]Determined by ^{1}H NMR spectroscopy. [d]Determined by the formula $DP_{theo.} = [([M]/[mCTA] \times Conv.]$. [e]Determined by the formula $M_{n,theo.} = [([M]/[mCTA] \times Conv. \times M_{mCTA}) + (M_{mCTA})]$. [f]Determined by ^{1}H NMR spectroscopy of isolated polymers. [g]Determined by the formula $M_{n,theo.} = [(DP \times M_{DMAEMA}) + M_{mCTA}]$. [i]Determined by SEC in DMAc analysis (RI detection, PS calibration). [j]Determined by DSC analysis.

RESULTS AND DISCUSSION

A macro chain transfer agent (**mCTA**) was prepared by RAFT polymerization of THP-HEMA in ethanol using CPADB as CTA at 70 °C with a monomer concentration of 1 mol L^{-1} (see

Scheme 1 and Table 1).[31] ACVA that generates the same radical as the R group of the CPADB was used as initiator to avoid defects that are caused by the initiator derived chains.[32] To minimize the formation of dead chains and to obtain an acceptable polymerization rate, the [CTA]/[ACVA] ratio was kept at 15/1.[33] In order to ensure chain end retention, the polymerization was stopped at 65% monomer conversion after 8 h. After purification, the **mCTA** was characterized by ^{1}H NMR spectroscopy and SEC analysis (Table 1). By comparing the integral values of the aromatic protons of the ω-RAFT end group at δ = 7.84 ppm (peak "a" in Figure 1) and the integral value of the methine proton peak of the THP-HEMA side chains at δ = 4.65 ppm (peak "e" in Figure 1), the mean DP of the **mCTA** was estimated to be 35 (see equation 1). The resulting M_n value calculated by ^{1}H NMR (7,800 g mol^{-1}) is close to the theoretical M_n (6,900 g mol^{-1}) calculated by the monomer conversion, and they are higher compared to the M_n = 5,800 g mol^{-1} obtained by SEC analysis (Table 1). The underestimated molar mass by SEC is probably due to the PS calibration of the SEC system. It is known that copolymers with hydrophobic to hydrophilic ratios higher than 2:1 favor a vesicle formation. However, this is not a definitive rule and exceptions can be observed.[3] Therefore, the length of the p(THP-HEMA) block was kept constant and the p(DMAEMA) block was systematically varied to identify the optimal composition for a vesicle formation. Diblock copolymers were synthesized via RAFT polymerization by utilization of the **mCTA** as CTA and ACVA as initiator in DMF at 70 °C with a monomer concentration of 1 mol L^{-1} (Scheme 1). Three different diblock copolymers were synthesized by variation of the [**mCTA**] to [DMAEMA] ratio or the polymerization time (Table 2). For the sake of the simplicity, a shorthand notation is used throughout this contribution to describe the various block copolymers. The letters A and B are used to represent the THP-HEMA and DMAEMA blocks, respectively. Thus, A_xB_y denotes

p(THP-HEMA)-*b*-p(DMAEMA) where x and y indicates the mean DP values of the respective blocks. Table 2 summarizes the polymerization conditions and characterization data of the isolated AB diblock copolymers that were obtained by ^{1}H NMR spectroscopy as well as by SEC measurements. The overlay of ^{1}H NMR spectra of the **mCTA** and $\mathbf{A_{35}B_{50}}$ are depicted in Figure 1. The mean DPs of the DMAEMA block of the copolymers were estimated via ^{1}H NMR spectroscopy by comparing integral value of the methylene peak of the DMAEMA side chains (peak "g") with the methine proton peak of the THP-HEMA side chains (peak "e"), which is calibrated to be 35 units (see equation 3). The resulting M_n values (calculated according to equation 4) are in good agreement with the theoretical M_n values that were estimated from the DMAEMA conversion. The SEC traces of the purified **mCTA** and the block copolymers are shown in Figure 2. SEC analysis revealed monomodal traces and narrow dispersities ($Đ_M < 1.10$) for all polymers, which indicates the effectiveness of **mCTA** for the controlled RAFT polymerization of DMAEMA. A shift to lower elution volumes and the increase of the molar mass values were observed as the DMAEMA block length increases with no tailing in the low molar mass region. The molar mass values determined by SEC are slightly lower than the calculated ones. However, SEC represents a relative method for molar mass determination, which relies on the calibration with standard linear PS polymers.

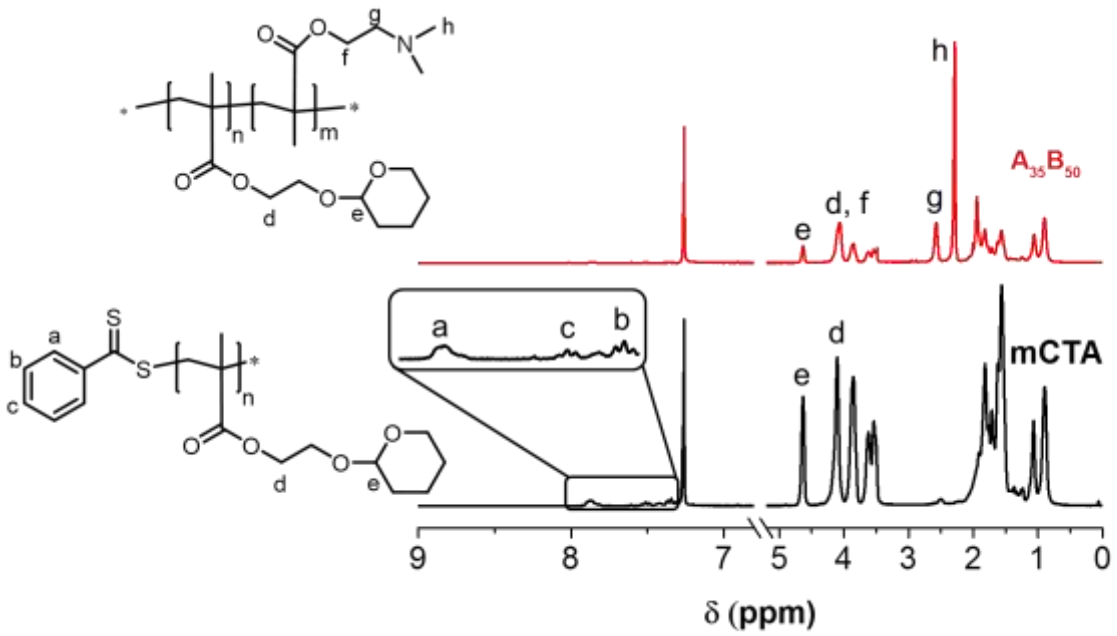

Figure 1. ^{1}H NMR spectra (300 MHz, $CDCl_3$) of **mCTA** (bottom) and **$A_{35}B_{50}$** (top) and the assignment of the peaks used to calculate the DP.

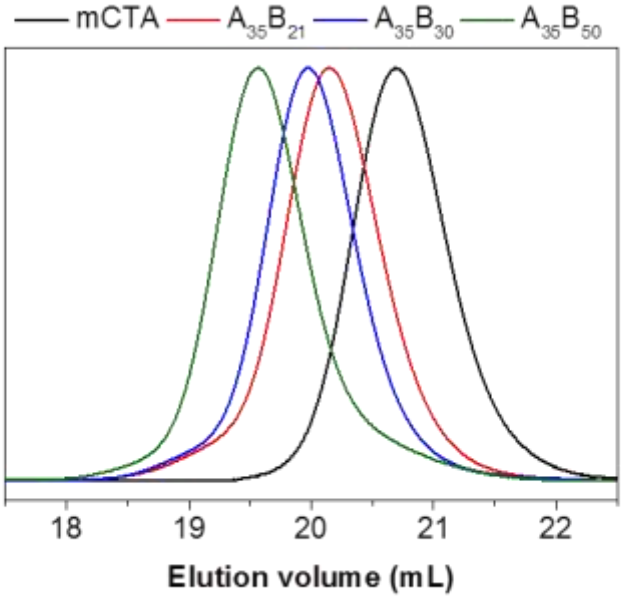

Figure 2. Normalized SEC traces in DMAc of isolated **mCTA** and block copolymers (**$A_{35}B_{21}$** to **$A_{35}B_{50}$**).

Thermal transitions of the **mCTA** and block copolymers (**$A_{35}B_{21}$** to **$A_{35}B_{50}$**) were studied by differential scanning calorimetry (DSC) under nitrogen atmosphere (Figure S3). The **mCTA** exhibits a T_g at 24.6 °C (Table 1), as expected based on our previous report.[28] All the block copolymers have single T_gs, suggesting that the components of block copolymers are thermodynamically miscible. The block copolymer **$A_{35}B_{21}$** with the shortest p(DMAEMA) block has a T_g value of 24.9 °C, which is similar to the **mCTA**, this may be ascribed to the small DP of the p(DMAEMA) block. However, the T_g values of the **$A_{35}B_{30}$** and **$A_{35}B_{50}$** decrease with increasing p(DMAEMA) block length to 23.4 and 20.7 °C, respectively, which could be ascribed to a lower T_g value of the p(DMAEMA) (~14 °C) compared to p(THP-HEMA).[34]

Self-assembly behavior in aqueous media

To investigate the self-assembly behavior of the amphiphilic diblock copolymers in water, aqueous suspensions were prepared by nanoprecipitation (dropping water into acetone polymer solutions).[35] Subsequently, DLS and cryo-TEM measurements were performed. Figure 3 summarizes the resulting number and volume distributions obtained from DLS and cryo-TEM images of the copolymer assemblies **$A_{35}B_{21}$**, **$A_{35}B_{30}$**, and **$A_{35}B_{50}$**. The corresponding DLS intensity distributions of the suspensions are shown in Figure S4 to S6. For the most hydrophobic copolymer **$A_{35}B_{21}$**, DLS measurements revealed a monomodal number distribution with an average hydrodynamic diameter (D_{av}) of 30 nm. However, the volume and intensity distributions exhibited a bimodal distribution of small (D_{av} ~40 nm) as well as medium sized aggregates (D_{av} ~300 nm). In agreement with DLS measurements, cryo-TEM measurements revealed predominantly polydisperse vesicles of 20 to 90 nm diameter exhibiting a clear membrane as well as

some larger spherical aggregates (~200 nm) (Figure 3, Figure S7). The thickness of the vesicle membrane was found to be around 8 ± 2 nm.

A monomodal number distribution with a D_{av} of 15 nm was observed from DLS for the suspension of the $\mathbf{A_{35}B_{30}}$ block copolymer. Some larger structures are also visible in the DLS volume and intensity distributions with a D_{av} of 120 nm. Cryo-TEM analysis showed that spherical micelles with diameters around 12 nm coexist with some polydisperse vesicles which have diameters ranging from 30 to 180 nm which might be the larger aggregates found by DLS (Figure 3, Figure S8). These observations are in accordance with the hydrodynamic diameters obtained from DLS measurements.

Monomodal number and volume distributions with an D_{av} of 11 and 13 nm, respectively, were obtained from DLS measurements for the suspension of the $\mathbf{A_{35}B_{50}}$ with the highest DMAEMA content. However, intensity distribution exhibited a bimodal size distribution of small (D_{av} ~13 nm) as well as medium sized aggregates (D_{av} ~130 nm). In accordance with the bimodal intensity size distribution obtained from DLS, cryo-TEM analysis revealed densely packed homogeneous spherical micelles with diameters around 10 nm as well as a small number of larger spherical aggregates (D_{av} ~100 nm) (Figure 3, Figure S9). It is known that copolymers with a hydrophilic-to-hydrophobic ratio less than 1:2 usually form vesicular aggregates, whereas copolymers with a ratio greater than 1:1 favor micelle formation.[3] Therefore, the observed morphology change from vesicles to spherical micelles as the hydrophilicity increrases from $\mathbf{A_{35}B_{21}}$ to $\mathbf{A_{35}B_{50}}$ correlates to literature. Since the aim of this contribution is the investigation of the vesicles as drug delivery vehicles the next sections mainly focuses on $\mathbf{A_{35}B_{21}}$ self-assemblies, since it features vesicular structures.

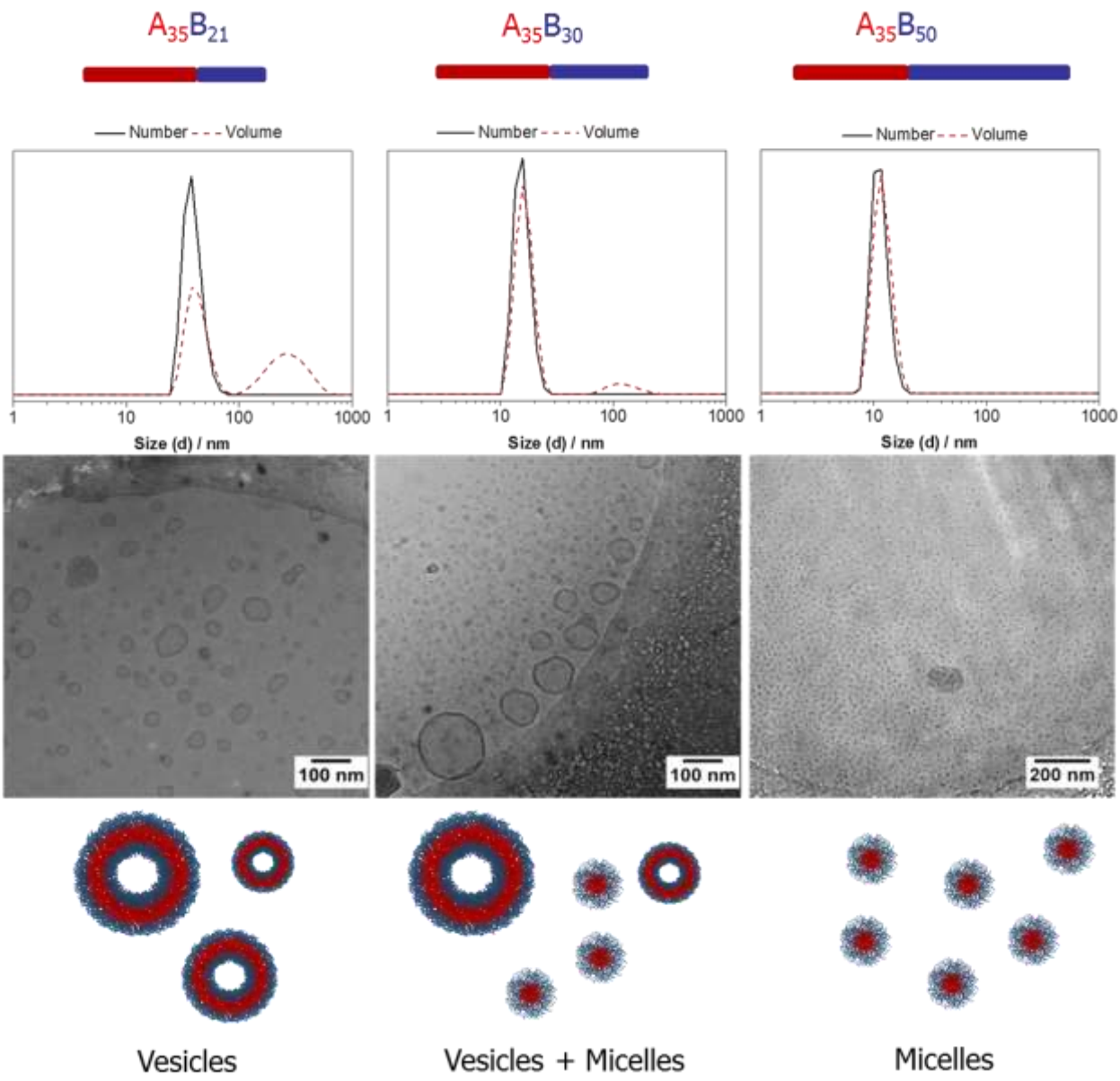

Figure 3. DLS plots and cryo-TEM images of the suspensions obtained from $\mathbf{A_{35}B_{21}}$, $\mathbf{A_{35}B_{30}}$, and $\mathbf{A_{35}B_{50}}$ in water (c = 2.5 mg mL^{-1}).

pH-Response test and determination of critical aggregation concentration of the vesicles

As already demonstrated above, the hydrophilic-to-hydrophobic ratio of the copolymers plays a critical role on the morphology and the sizes of the self-assembled structures.

PDMAEMA is a weak polyelectrolyte in water with a pK_a value of ~ 7.4.[14] Below its pK_a value, PDMAEMA is hydrophilic due to the protonation of the tertiary amino moieties. In contrast, above its pK_a PDMAEMA becomes hydrophobic as a consequence of the deprotonation of the amino groups. This pH dependent protonation/deprotonation ability of the PDMAEMA can alter the hydrophilic-to-hydrophobic ratio of the corresponding copolymers and accordingly can change the morphology as well as the size of the self-assembled structures at different pH values. For this purpose, the pH responsive behavior of the vesicles was explored by storing the $\mathbf{A_{35}B_{21}}$ suspension at various pH values for 3 h. The changes in size and ζ-potential values were recorded. Number size distributions and ζ-potentials of the $\mathbf{A_{35}B_{21}}$ suspension as a function of the pH value are demonstrated in Figure 4**.** The corresponding volume and intensity distributions of the $\mathbf{A_{35}B_{21}}$ suspension as a function of the pH value are shown in Figure S10 and S11. DLS measurements revealed that the $\mathbf{A_{35}B_{21}}$ suspension showed stable size distribution at neutral pH values (pH = 7.0 and 7.4) (Figure 4). An increase of the pH value from 7.4 to 8.0 resulted in an increase of the diameter of the vesicles. This is due to the partial deprotonation of the DMAEMA groups.[36] A decrease in the ζ-potential from +33 mV at pH 7.4 to +20 mV at pH 8.0 proves this assumption. In accordance with this, an additional increase of the pH value from 8.0 to 9.0 resulted in a further decrease of the ζ-potential from +20 mV to -11 mV leading to precipitation of the vesicles. In contrast, upon decreasing the pH value from neutral to acidic pH values a continuous decrease in the particle diameter together with an increase in the ζ-potential was observed. Moreover, the suspension lost its turbidity and became transparent at acidic pH values. To understand the origin of the decrease in the size of the aggregates, cryo-TEM investigations of the suspensions were performed at pH 7.4 and 5.0,

respectively. At pH 7.4, exclusively vesicular aggregates with clear membranes can be seen (Figure 5, Figure S12). On the other hand, only homogeneous spherical micelles were observed at pH 5.0 (Figure 5, Figure S13). At both pH values the observed diameters correlate well with the DLS measurements. Recently, we showed that cleavage of the THP groups in acidic media is relatively slow; after treatment with acetic acid (0.1 M, pH = 3.1) at 37 °C for 24 h a negligible amount of THP group cleavage was observed.[28] In agreement with this, ^{1}H NMR spectrum of the freeze dried suspensions after treatment with acetate buffer (0.1 M, pH = 4) at 37 °C for 3 h exhibited no change in the ^{1}H NMR spectrum of the $\mathbf{A_{35}B_{21}}$ polymer (Figure S14). As a consequence, the decrease in the size at acidic pH values is attributed to the morphology transition from vesicles to micelles at acidic pH values as a result of the protonation of the DMAEMA groups, which increases the hydrophilic-to-hydrophobic ratio. A subsequent increase of the pH value to 7.4 resulted in an increase in diameter, which is only slightly lower than the original polymersomes (Figure S15). This hints toward the reversibility of the morphology change.

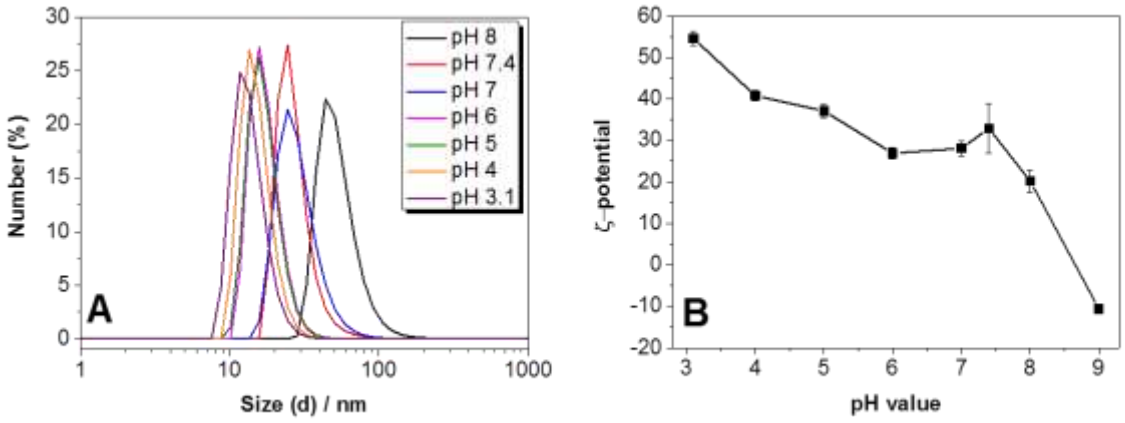

Figure 4. (A) Number size distributions and (B) ζ-potentials of the $\mathbf{A_{35}B_{21}}$ suspension as a function of the pH value.

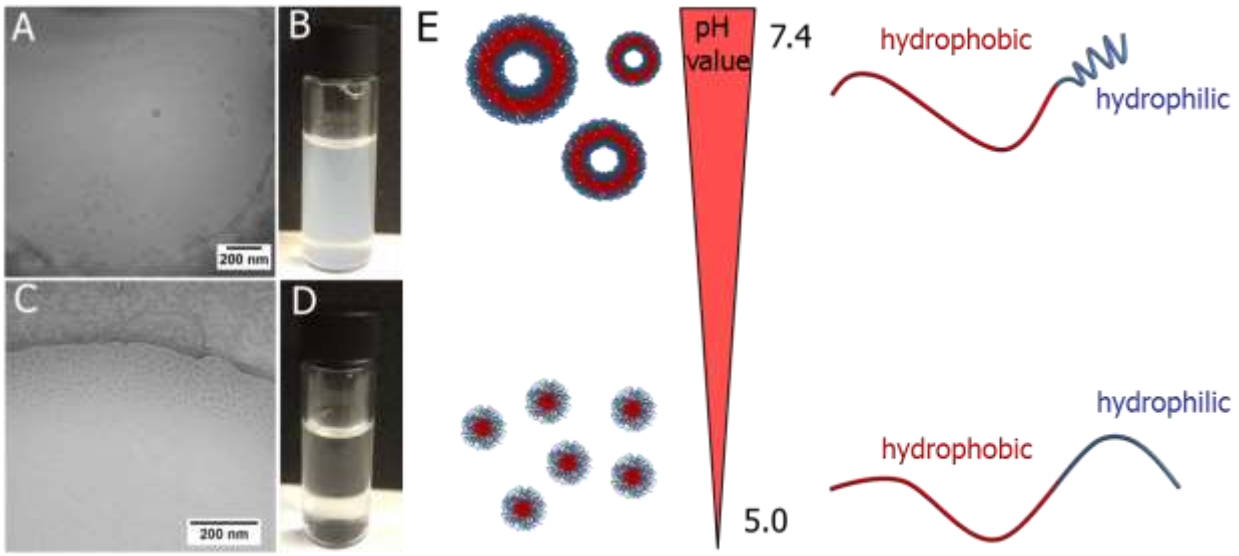

Figure 5. (A) Cryo-TEM image of the $\mathbf{A_{35}B_{21}}$ suspension at pH 7.4. (B) Photograph of vial containing the $\mathbf{A_{35}B_{21}}$ suspension at pH 7.4. (C) Cryo-TEM image of the $\mathbf{A_{35}B_{21}}$ suspension at pH 5.0. (D) Photograph of vial containing the $\mathbf{A_{35}B_{21}}$ suspension at pH 5.0. (E) Schematic illustration of the pH value change induced vesicle-to-micelle morphology transition as a result of an increase of the volume of hydrophilic block at acidic pH values.

The critical aggregation concentration of the $\mathbf{A_{35}B_{21}}$ suspension at pH 7.4 was estimated using hydrophobic Nile Red as a fluorescent probe. It is well know that Nile Red has negligible fluorescence intensity in water but its fluorescence intensity significantly increases when it is encapsulated in a hydrophobic environment such as in the membrane of polymersomes or in the core of micelles.[37, 38] To estimate the CAC, the Nile Red encapsulated $\mathbf{A_{35}B_{21}}$ suspension was diluted and the corresponding fluorescence emission spectra were recorded. Figure 6 depicts the Nile Red fluorescence intensity at the emission maxima (λ_{max} = 605 nm) *versus* the polymer concentration. At low concentrations there is almost no change in emission intensity, but above a certain polymer concentration the emission intensity increases substantially. The CAC of the $\mathbf{A_{35}B_{21}}$ was calculated as 0.084 mg mL^{-1} by using the antilog of the intersection point value of the base line and the steep curve. The calculated CAC is in good agreement with before reported values for p(THP-HEMA) copolymer based micelles.[29]

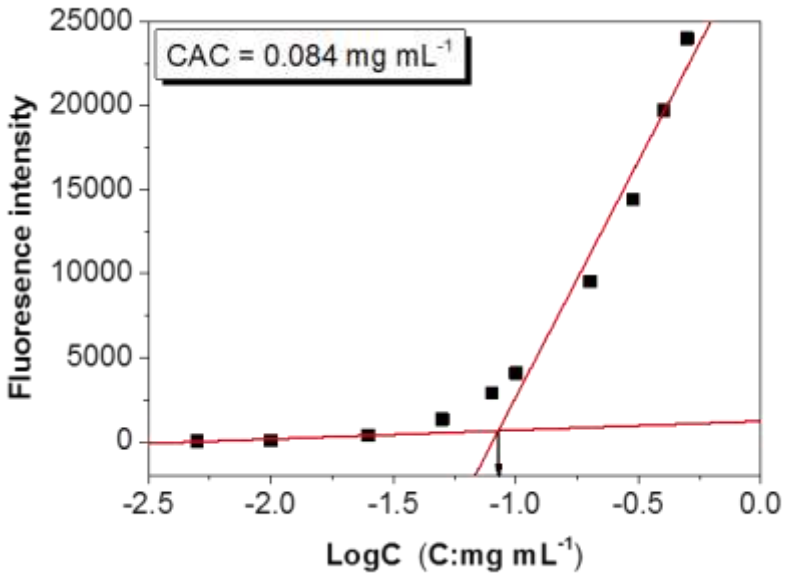

Figure 6. Nile Red fluorescence intensity at the emission maxima (λ_{max} = 605 nm) *versus* the log of polymer concentration.

DOX·HCl loading and release studies

The encapsulation ability of hydrophilic molecules in the vesicular hydrophilic cavity was tested using the water soluble anticancer drug DOX·HCl. The DOX·HCl was encapsulated in $\mathbf{A_{35}B_{21}}$ vesicles using nanoprecipitation. DLS measurements revealed that the resulting DOX-loaded vesicles have a number average diameter of 30 nm and a ζ-potential of +30 mV (Figure S16). Cryo-TEM images showed relatively uniform vesicular morphology (Figure S17). A drug loading efficiency of 30.7% was obtained at a target drug loading content of 4.8%. The drug loading content was calculated as 1.5%. The DOX·HCl release was studied at 37 °C in two different media, i.e., tris buffer (pH 7.4, 100 mM) and acetate buffer (pH 5.0, 100 mM). Figure 7 shows the cumulative DOX·HCl release over time. At pH 7.4, 50% DOX·HCl was released in 24 h. In contrast,

78% DOX·HCl was released at pH 5.0 in 24 h. The faster DOX·HCl release at pH 5.0 is attributed to the loss of the hydrophilic reservoirs of the vesicles.

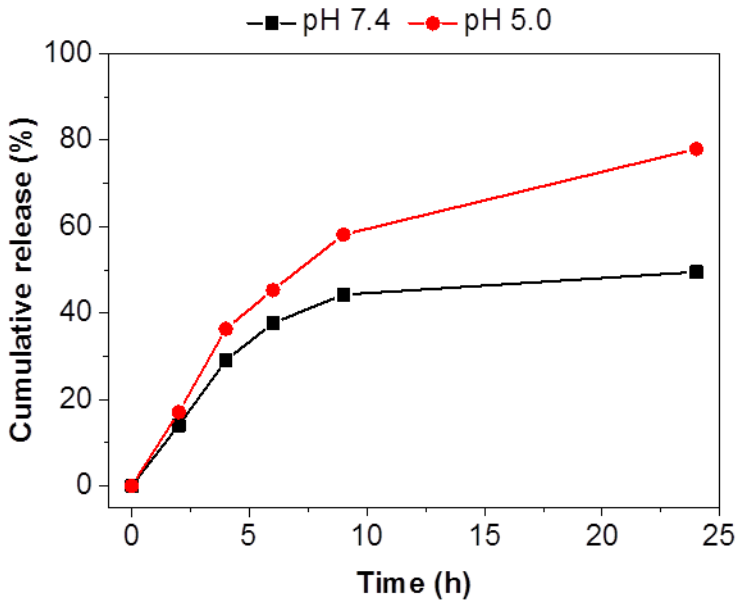

Figure 7. Drug release of DOX·HCl loaded vesicles at pH 7.4 and pH 5.0.

Cytotoxicity studies

Cationic polymers and their self-assembled aggregates may induce toxic effects to the cells as a result of their disruptive interaction with the plasma membrane.[39] Hence, the cytotoxicity of $\mathbf{A_{35}B_{21}}$, $\mathbf{A_{35}B_{30}}$, and $\mathbf{A_{35}B_{50}}$ as aqueous suspensions were investigated using L929 cells (Figure 8 A). The cytotoxicity assay revealed that the $\mathbf{A_{35}B_{21}}$ suspension has no significant cytotoxic effect on L929 cells after 48 h incubation at up to a concentration of 250 μg mL^{-1} with a cell viability above 70%, which is considered as the general threshold for cytotoxicity. However, an increase of the $\mathbf{A_{35}B_{21}}$ concentration to 300 μg mL^{-1} resulted in a decrease of the cell viability to 65%, and it continuously decreases with an increasing concentration of the $\mathbf{A_{35}B_{21}}$. Our recent study showed that p(THP-HEMA) is biocompatible and not cytotoxic.[28] Therefore, the cytotoxicity of the

$A_{35}B_{21}$ suspension can be attributed to the cationic p(DMAEMA) block, which usually exhibits toxic effects at high polymer concentrations.[40, 41] The **$A_{35}B_{30}$** suspension that contains a slightly longer p(DMAEMA) block than **$A_{35}B_{21}$** exhibited a similar cell viability compared to **$A_{35}B_{21}$** at all tested concentrations. The **$A_{35}B_{50}$** suspension exhibited the most toxic effect to the cells due to the presence of the longest p(DMAEMA) block.

Additionally, the cytotoxicity of the DOX·HCl encapsulated **$A_{35}B_{21}$** polymersomes on the L929 cells after 24 and 48 h of incubation were investigated and compared with the cytotoxicity of the free DOX·HCl (Figure 8 B) to evaluate the anticancer efficacy. To avoid the toxic effect of the **$A_{35}B_{21}$** suspension at high polymer concentrations, the maximum polymer concentration was kept at 250 μg mL^{-1}. The DOX·HCl encapsulated polymersomes could decrease the cell viability gradually with increasing concentration of encapsulated DOX·HCl and with increasing incubation time, which is comparable to the free DOX·HCl. Specifically, 60% of the cells died after 48 h of exposure to DOX·HCl encapsulated polymersomes with 5 μg mL^{-1} DOX·HCl. The significantly increased cytotoxicity of the DOX·HCl loaded polmersomes compared to the blank ones can be attributed to vesicle-to-micelle morphology transitions triggered by the endosomal pH values, which can induce the release of encapsulated DOX·HCl within the cells. It is known that molecular mechanisms of cytotoxic action of DOX·HCl rely on a) intercalation into DNA, b) direct induction of DNA strand breaks and c) evolution of radical species provoking DNA strand breaks. All modes of action result in a disruption of DNA and RNA synthesis finally leading to cell death.[42, 43] The comet assay was performed to quantify the amount of DNA damage resulting from single and double strand breaks as well as from abasic sites.[44] For the assay, L929 fibroblast cells were

treated with three different concentrations of free DOX·HCl and DOX·HCl encapsulated **$A_{35}B_{21}$** polymersomes for 24 h. In comet assay, small and fragmented DNA molecules show a higher mobility in an electric field than larger intact DNA molecules. The comet assay results show that (Figure S18 and S19) DOX·HCl encapsulated **$A_{35}B_{21}$** vesicles induce remarkable DNA damages in a concentration dependent manner, which is comparable with free DOX·HCl. These results are in agreement with the cytotoxicity studies.

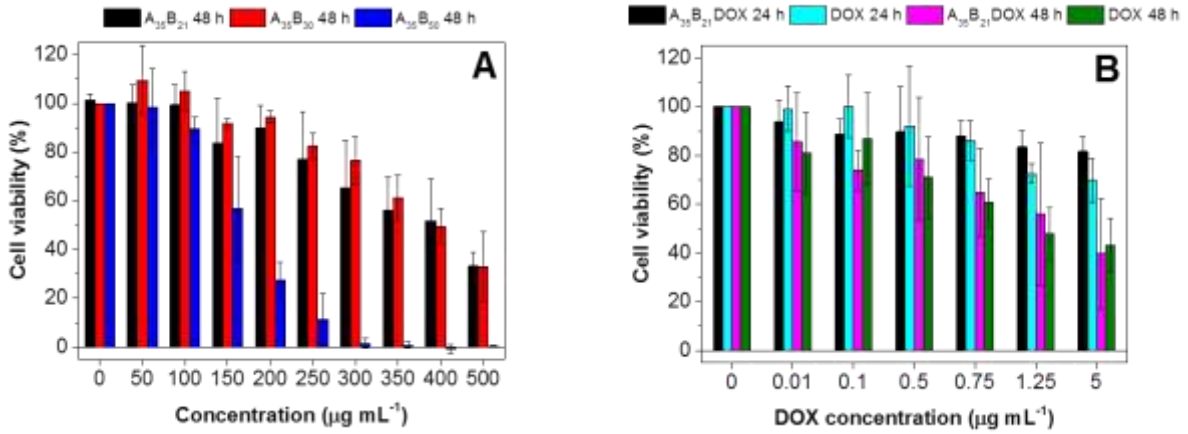

Figure 8. (A) Cytotoxicity test of **$A_{35}B_{21}$**, **$A_{35}B_{30}$**, and **$A_{35}B_{50}$** aqueous suspensions in L929 cells after 48 h incubation. (B) Cytotoxicity test of DOX·HCl encapsulated **$A_{35}B_{21}$** suspension and free DOX·HCl in L929 cells. The relative viability is expressed as percentage to control cells not treated with NPs. Untreated cells on the same well plate were used as positive controls.

Cellular uptake studies

The cellular uptake of the DOX·HCl loaded polymersomes and the free DOX·HCl were qualitatively monitored in L929 cells at different time points (2 to 24 h) by confocal laser scanning microscopy (CLSM). The red fluorescence of the DOX·HCl enabled the visualization of the cells. Figure 9 shows the representative CLSM images of L929 cells treated with free DOX·HCl and DOX·HCl loaded polymersomes. After 2 h of incubation, the DOX·HCl

fluorescence is clearly visible in the nucleus of the cells (white arrows). This indicates that DOX·HCl loaded polymersomes are efficiently taken up by the cells and subsequently DOX·HCl is released from the polymersomes in the endo/lysosomes due to morphology change. An increase of incubation time of DOX·HCl loaded polymersomes to 24 h resulted in stronger DOX·HCl fluorescence, which is similar to the free DOX·HCl. The cellular uptake of the DOX·HCl loaded polymersomes and the free DOX·HCl were further quantitatively investigated by flow cytometry. Figure 10 illustrates the mean fluorescence intensity ratio of the DOX·HCl loaded polymersomes and the free DOX·HCl. Flow cytometry results indicated that the intracellular DOX·HCl content released from the polymersomes is higher than that of the free DOX·HCl after 2 h and this even becomes more pronounced for longer incubation times. This is explained by the faster internalization of the DOX·HCl loaded polymersomes compared to the free DOX·HCl. It is known that nanocarriers featuring diameters between 20 and 500 nm are taken up by the cells usually by an endocytosis pathway which is energy and time dependent,[45, 46] whereas small drugs enter the cells rapidly through passive diffusion.[47, 48] Therefore, free DOX·HCl is usually uptaken by the cells faster than the DOX·HCl loaded nanoparticles. However, positive surface charges can significantly enhance the cellular uptake of the nanoparticles due their high affinity for the negatively charged phospholipid bilayer of cell membranes.[49] Indeed, several literature examples have demonstrated that cationic nanoparticles can enter the cells even faster than the free DOX·HCl.[50-52] Therefore, the enhanced cellular uptake of the polymersomes is attributed to their cationic character. These preliminary results demonstrate that $\mathbf{A_{35}B_{21}}$ polymersomes represent promising candidates as effective drug delivery platform for the fast and controlled delivery of hydrophilic DOX·HCl within cancer cells.

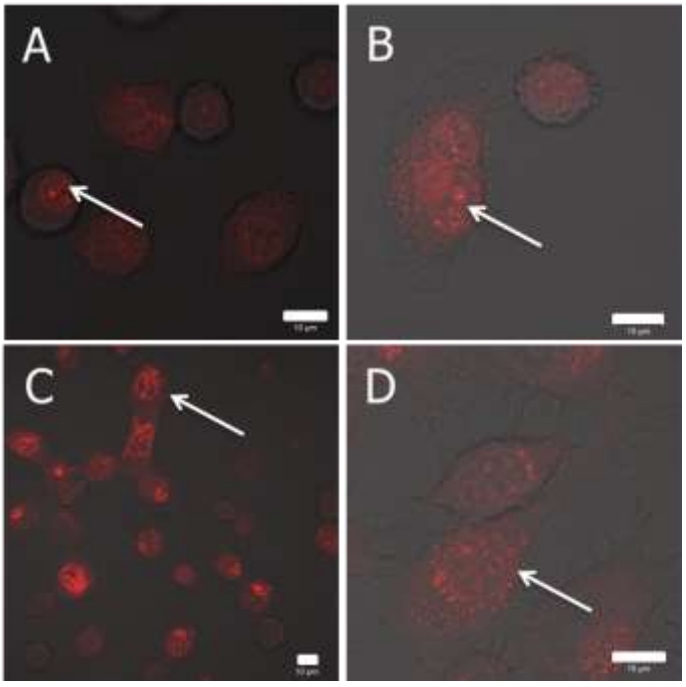

Figure 9. Live cell CLSM images of L929 cells incubated with DOX·HCl-loaded polymersomes and free DOX·HCl at 1 μg mL^{-1} pure and encapsulated DOX·HCl. (A) free DOX·HCl, 2 h incubation; (B) DOX·HCl-loaded polymersomes, 2 h incubation; (C) free DOX·HCl, 24 h incubation; (D) DOX·HCl-loaded polymersomes, 24 h incubation. The scale bars correspond to 10 μm in all the images.

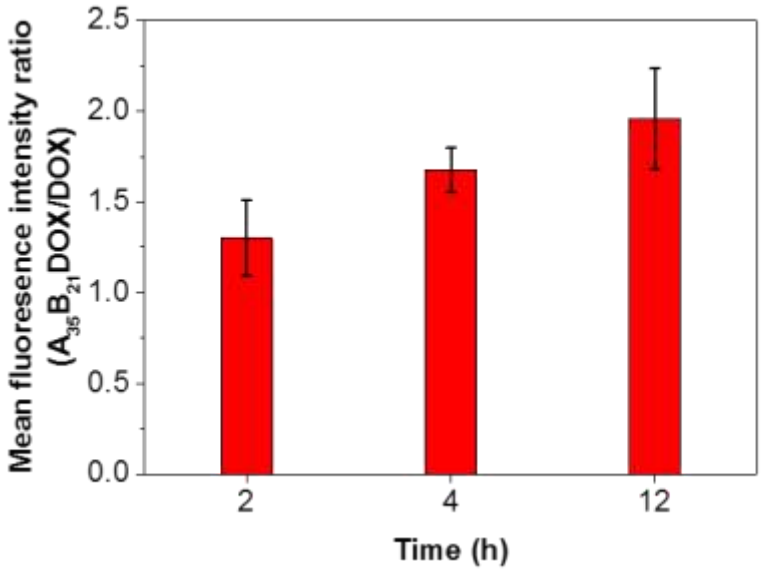

Figure 10. Mean fluorescence intensity ratio of DOX·HCl loaded polmersomes ($A_{35}B_{21}$DOX) to free DOX·HCl after incubating for 2, 4, and 24 h as observed by flow cytometry.

CONCLUSIONS

In conclusion, a novel, pH responsive polymersome system with a facile synthetic route has been developed. For this purpose, a well-defined diblock copolymer library of p(THP-HEMA) and p(DMAEMA) was prepared *via* RAFT polymerization utilizing p(THP-HEMA) as a macro-chain transfer agent. The DP of the p(THP-HEMA) block was fixed and the DP of the p(DMAEMA) block was systematically varied. It was shown that the copolymer with the shortest p(DMAEMA) block self-assembled into polymersomes, whereas an increase of the p(DMAEMA) block length led to the formation of micellar structures. In addition, the polymersomes exhibited a morphology transition from vesicles to micelles upon lowering the pH value. The ability of polymersomes to encapsulate the hydrophobic model drug (Nile Red) into the membrane and a hydrophilic anticancer drug (DOX·HCl) in the aqueous cavities were verified. Drug release studies demonstrated that DOX·HCl release was accelerated in response to a decrease in pH value from 7.4 to 5.0. Cytotoxicity studies revealed that DOX·HCl loaded polymersomes exhibited an efficient cell death comparable to free DOX·HCl, while the blank polmersomes showed no cytotoxic effect up to a tested concentration of 250 μg mL^{-1}. Furthermore, cell studies revealed that DOX·HCl loaded polymersomes were efficiently taken up by cells faster than free DOX·HCl. This novel pH responsive polymersome system offers dual loading ability for both hydrophobic and hydrophilic guest molecules and is, therefore, suitable to target multiple drug delivery applications.

ASSOCIATED CONTENT

Supporting Information.

The supporting information is available free of charge on the ACS Publications website at DOI: ^{1}H NMR spectra of $\mathbf{A_{35}B_{21}}$ and $\mathbf{A_{35}B_{30}}$, DSC heating runs of the polymers, DLS size distributions of DOX·HCl loaded polymersomes in water, a representative cryo-TEM image of the DOX·HCl loaded polymersomes.

AUTHOR INFORMATION

Corresponding Author

E-mail: stephanie.schubert@uni-jena.de; ulrich.schubert@uni-jena.de

Author Contributions

The manuscript was written through contributions of all authors. All authors have given approval

ACKNOWLEDGMENT

We acknowledge funding from the Carl-Zeiss Foundation (JCSM Strukturantrag, grant for Dr. Anja Traeger), the Thüringer Ministerium für Wirtschaft, Wissenschaft, und Digitale Gesellschaft (TMWWDG, ProExzellenz I (NanoConSens), ProExzellenzII (NanoPolar), and the German Federal Ministry of Education & Research (BMBF, #031A518B Vectura, #13N13416 smart-dye-livery). The TEM facilities of the Jena Center for Soft Matter (JCSM) were established with a grant from the German Research Council (DFG) and the European Fonds for Regional Development (EFRE). The LSM880 ELYRA PS.1 was further funded with a grant from the DFG.

REFERENCES

1. Mai, Y.; Eisenberg, A., Self-assembly of block copolymers. *Chem. Soc. Rev.* **2012**, *41*, 5969-5985.
2. Discher, D. E.; Eisenberg, A., Polymer vesicles. *Science* **2002**, *297*, 967-973.

3. Du, J.; O'Reilly, R. K., Advances and challenges in smart and functional polymer vesicles. *Soft Matter* **2009**, *5*, 3544-3561.

4. Choucair, A.; Lim Soo, P.; Eisenberg, A., Active loading and tunable release of doxorubicin from block copolymer vesicles. *Langmuir* **2005**, *21*, 9308-9313.

5. Wang, L.; Liu, G.; Wang, X.; Hu, J.; Zhang, G.; Liu, S., Acid-disintegratable polymersomes of pH-responsive amphiphilic diblock copolymers for intracellular drug delivery. *Macromolecules* **2015**, *48*, 7262-7272.

6. Ren, T.; Wu, W.; Jia, M.; Dong, H.; Li, Y.; Ou, Z., Reduction-cleavable polymeric vesicles with efficient glutathione-mediated drug release behavior for reversing drug resistance. *ACS Appl. Mater. Interfaces* **2013**, *5*, 10721-10730.

7. Li, Y.; Liu, G.; Wang, X.; Hu, J.; Liu, S., Enzyme-responsive polymeric vesicles for bacterial-strain-selective delivery of antimicrobial agents. *Angew. Chem. Int. Ed.* **2016**, *55*, 1760-1764.

8. van Elk, M.; Deckers, R.; Oerlemans, C.; Shi, Y.; Storm, G.; Vermonden, T.; Hennink, W. E., Triggered release of doxorubicin from temperature-sensitive poly(N-(2-hydroxypropyl)-methacrylamide mono/dilactate) grafted liposomes. *Biomacromolecules* **2014**, *15*, 1002-1009.

9. Blasco, E.; Serrano, J. L.; Piñol, M.; Oriol, L., Light responsive vesicles based on linear–dendritic block copolymers using azobenzene–aliphatic codendrons. *Macromolecules* **2013**, *46*, 5951-5960.

10. Oliveira, H.; Pérez-Andrés, E.; Thevenot, J.; Sandre, O.; Berra, E.; Lecommandoux, S., Magnetic field triggered drug release from polymersomes for cancer therapeutics. *J. Control. Release* **2013**, *169*, 165-170.

11. Chen, W.; Du, J., Ultrasound and pH dually responsive polymer vesicles for anticancer drug delivery. *Sci. Rep.* **2013**, *3*, 2162.

12. Gao, W.; Chan, J. M.; Farokhzad, O. C., pH-responsive nanoparticles for drug delivery. *Mol. Pharm.* **2010**, *7*, 1913-1920.

13. Hu, X.; Zhang, Y.; Xie, Z.; Jing, X.; Bellotti, A.; Gu, Z., Stimuli-responsive polymersomes for biomedical applications. *Biomacromolecules* **2017**.

14. Car, A.; Baumann, P.; Duskey, J. T.; Chami, M.; Bruns, N.; Meier, W., pH-responsive PDMS-b-PDMAEMA micelles for intracellular anticancer drug delivery. *Biomacromolecules* **2014**, *15*, 3235-3245.

15. Meng, F.; Zhong, Z.; Feijen, J., Stimuli-responsive polymersomes for programmed drug delivery. *Biomacromolecules* **2009**, *10*, 197-209.

16. Sundararaman, A.; Stephan, T.; Grubbs, R. B., Reversible restructuring of aqueous block copolymer assemblies through stimulus-induced changes in amphiphilicity. *J. Am. Chem. Soc.* **2008**, *130*, 12264-12265.

17. Moughton, A. O.; O'Reilly, R. K., Thermally induced micelle to vesicle morphology transition for a charged chain end diblock copolymer. *Chem. Commun.* **2010**, *46*, 1091-1093.

18. Moughton, A. O.; Patterson, J. P.; O'Reilly, R. K., Reversible morphological switching of nanostructures in solution. *Chem. Commun.* **2011**, *47*, 355-357.

19. Cai, Y.; Aubrecht, K. B.; Grubbs, R. B., Thermally induced changes in amphiphilicity drive reversible restructuring of assemblies of ABC triblock copolymers with statistical polyether blocks. *J. Am. Chem. Soc.* **2011**, *133*, 1058-1065.

20. Sun, Z.; Tian, Y.; Hom, W. L.; Gang, O.; Bhatia, S. R.; Grubbs, R. B., Translating thermal response of triblock copolymer assemblies in dilute solution to macroscopic gelation and phase separation. *Angew. Chem. Int. Ed.* **2017**, *56*, 1491-1494.

21. Doncom, K. E. B.; Hansell, C. F.; Theato, P.; O'Reilly, R. K., pH-switchable polymer nanostructures for controlled release. *Polym. Chem.* **2012**, *3*, 3007-3015.

22. Maiti, C.; Banerjee, R.; Maiti, S.; Dhara, D., pH-induced vesicle-to-micelle transition in amphiphilic diblock copolymer: investigation by energy transfer between in situ formed polymer embedded gold nanoparticles and fluorescent dye. *Langmuir* **2015**, *31*, 32-41.

23. Lovett, J. R.; Warren, N. J.; Armes, S. P.; Smallridge, M. J.; Cracknell, R. B., Order–order morphological transitions for dual stimulus responsive diblock copolymer vesicles. *Macromolecules* **2016**, *49*, 1016-1025.

24. Salva, R.; Le Meins, J.-F.; Sandre, O.; Brûlet, A.; Schmutz, M.; Guenoun, P.; Lecommandoux, S., Polymersome shape transformation at the nanoscale. *ACS Nano* **2013**, *7*, 9298-9311.

25. Discher, B. M.; Won, Y.-Y.; Ege, D. S.; Lee, J. C.-M.; Bates, F. S.; Discher, D. E.; Hammer, D. A., Polymersomes: tough vesicles made from diblock copolymers. *Science* **1999**, *284*, 1143-1146.

26. Li, X.; Pivkin, I. V.; Liang, H.; Karniadakis, G. E., Shape transformations of membrane vesicles from amphiphilic triblock copolymers: A dissipative particle dynamics simulation study. *Macromolecules* **2009**, *42*, 3195-3200.

27. Yuan, H.; Huang, C.; Zhang, S., Dynamic shape transformations of fluid vesicles. *Soft Matter* **2010**, *6*, 4571-4579.

28. Yildirim, T.; Yildirim, I.; Yanez-Macias, R.; Stumpf, S.; Fritzsche, C.; Hoeppener, S.; Guerrero-Sanchez, C.; Schubert, S.; Schubert, U. S., Dual pH and ultrasound responsive nanoparticles with pH triggered surface charge-conversional properties. *Polym. Chem.* **2017**, *8*, 1328-1340.

29. Klaikherd, A.; Nagamani, C.; Thayumanavan, S., Multi-stimuli sensitive amphiphilic block copolymer assemblies. *J. Am. Chem. Soc.* **2009**, *131*, 4830-4838.

30. Yildirim, T.; Traeger, A.; Preussger, E.; Stumpf, S.; Fritzsche, C.; Hoeppener, S.; Schubert, S.; Schubert, U. S., Dual responsive nanoparticles from a RAFT copolymer library for the controlled delivery of doxorubicin. *Macromolecules* **2016**, *49*, 3856-3868.

31. Moad, G.; Chiefari, J.; Chong, Y. K.; Krstina, J.; Mayadunne, R. T. A.; Postma, A.; Rizzardo, E.; Thang, S. H., Living free radical polymerization with reversible addition – fragmentation chain transfer (the life of RAFT). *Polym. Int.* **2000**, *49*, 993-1001.

32. Keddie, D. J., A guide to the synthesis of block copolymers using reversible-addition fragmentation chain transfer (RAFT) polymerization. *Chem. Soc. Rev.* **2014**, *43*, 496-505.

33. Hill, M. R.; Carmean, R. N.; Sumerlin, B. S., Expanding the scope of RAFT polymerization: Recent advances and new horizons. *Macromolecules* **2015**, *48*, 5459-5469.

34. Chen, S.-C.; Kuo, S.-W.; Liao, C.-S.; Chang, F.-C., Syntheses, Specific interactions, and pH-sensitive micellization behavior of poly[vinylphenol-*b*-2-(dimethylamino)ethyl methacrylate] diblock copolymers. *Macromolecules* **2008**, *41*, 8865-8876.

35. Schubert, S.; Delaney, J. J. T.; Schubert, U. S., Nanoprecipitation and nanoformulation of polymers: From history to powerful possibilities beyond poly(lactic acid). *Soft Matter* **2011**, *7*, 1581-1588.

36. Yildirim, T.; Rinkenauer, A. C.; Weber, C.; Traeger, A.; Schubert, S.; Schubert, U. S., RAFT made methacrylate copolymers for reversible pH-responsive nanoparticles. *J. Polym. Sci., Part A: Polym. Chem.* **2015**, *53*, 2711-2721.

37. Pramod, P. S.; Shah, R.; Jayakannan, M., Dual stimuli polysaccharide nanovesicles for conjugated and physically loaded doxorubicin delivery in breast cancer cells. *Nanoscale* **2015**, *7*, 6636-6652.

38. Yang, F.; Cao, Z.; Wang, G., Micellar assembly of a photo- and temperature-responsive amphiphilic block copolymer for controlled release. *Polym. Chem.* **2015**, *6*, 7995-8002.

39. Lee, Y.; Miyata, K.; Oba, M.; Ishii, T.; Fukushima, S.; Han, M.; Koyama, H.; Nishiyama, N.; Kataoka, K., Charge-conversion ternary polyplex with endosome disruption moiety: A technique for efficient and safe gene delivery. *Angew. Chem. Int. Ed.* **2008**, *47*, 5163-5166.

40. Cai, J.; Yue, Y.; Rui, D.; Zhang, Y.; Liu, S.; Wu, C., Effect of chain length on cytotoxicity and endocytosis of cationic polymers. *Macromolecules* **2011**, *44*, 2050-2057.

41. Wang, Z. H.; Li, W. B.; Ma, J.; Tang, G. P.; Yang, W. T.; Xu, F. J., Functionalized nonionic dextran backbones by atom transfer radical polymerization for efficient gene delivery. *Macromolecules* **2011**, *44*, 230-239.

42. Gewirtz, D., A critical evaluation of the mechanisms of action proposed for the antitumor effects of the anthracycline antibiotics adriamycin and daunorubicin. *Biochem. Pharmacol.* **1999**, *57*, 727-741.

43. Pérez-Arnaiz, C.; Busto, N.; Leal, J. M.; García, B., New insights into the mechanism of the DNA/Doxorubicin interaction. *J. Phys. Chem. B* **2014**, *118*, 1288-1295.

44. Olive, P. L.; Banath, J. P., The comet assay: a method to measure DNA damage in individual cells. *Nat. Protocols* **2006**, *1*, 23-29.

45. Yildirim, I.; Bus, T.; Sahn, M.; Yildirim, T.; Kalden, D.; Hoeppener, S.; Traeger, A.; Westerhausen, M.; Weber, C.; Schubert, U. S., Fluorescent amphiphilic heterografted comb polymers comprising biocompatible PLA and PEtOx side chains. *Polym. Chem.* **2016**, *7*, 6064-6074.

46. Xiao, L.; Xiong, X.; Sun, X.; Zhu, Y.; Yang, H.; Chen, H.; Gan, L.; Xu, H.; Yang, X., Role of cellular uptake in the reversal of multidrug resistance by PEG-*b*-PLA polymeric micelles. *Biomaterials* **2011**, *32*, 5148-5157.

47. Lei, T.; Srinivasan, S.; Tang, Y.; Manchanda, R.; Nagesetti, A.; Fernandez-Fernandez, A.; McGoron, A. J., Comparing cellular uptake and cytotoxicity of targeted drug carriers in cancer cell lines with different drug resistance mechanisms. *Nanomedicine* **2011**, *7*, 324-332.

48. Misra, R.; Sahoo, S. K., Intracellular trafficking of nuclear localization signal conjugated nanoparticles for cancer therapy. *Eur. J. Pharm. Sci.* **2010**, *39*, 152-163.

49. Arvizo, R. R.; Miranda, O. R.; Thompson, M. A.; Pabelick, C. M.; Bhattacharya, R.; Robertson, J. D.; Rotello, V. M.; Prakash, Y. S.; Mukherjee, P., Effect of nanoparticle surface charge at the plasma membrane and beyond. *Nano Lett.* **2010**, *10*, 2543-2548.

50. Chen, Y.; Ai, K.; Liu, Y.; Lu, L., Tailor-made charge-conversional nanocomposite for pH-responsive drug delivery and cell imaging. *ACS Appl. Mater. Interfaces* **2014**, *6*, 655-663.

51. Hu, X.; Guan, X.; Li, J.; Pei, Q.; Liu, M.; Xie, Z.; Jing, X., Hybrid polymer micelles capable of cRGD targeting and pH-triggered surface charge conversion for tumor selective accumulation and promoted uptake. *Chem. Commun.* **2014**, *50*, 9188-9191.

52. Deng, H.; Zhao, X.; Liu, J.; Deng, L.; Zhang, J.; Liu, J.; Dong, A., Reactive oxygen species (ROS) responsive PEG-PCL nanoparticles with pH-controlled negative-to-positive charge reversal for intracellular delivery of doxorubicin. *J. Mater. Chem. B* **2015**, *3*, 9397-9408.

For table of contents only:

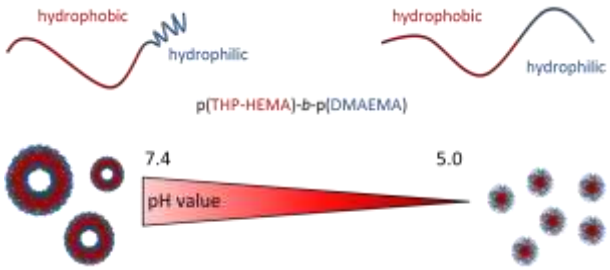

Polymersomes with endosomal pH-induced vesicle-to-micelle morphology transition and a potential application for controlled doxorubicin delivery

Turgay Yildirim,[a,b] Anja Traeger,[a,b] Pelin Sungur,[a,b] Stephanie Hoeppener,[a,b] Carolin Fritzsche,[a,b] Ilknur Yildirim,[a,b] David Pretzel,[a,b] Stephanie Schubert,[b,c] Ulrich S. Schubert*[a,b]*

[a] Laboratory of Organic and Macromolecular Chemistry (IOMC), Friedrich Schiller University Jena, Humboldtstr. 10, 07743 Jena, Germany

[b] Jena Center for Soft Matter (JCSM), Friedrich Schiller University Jena, Philosophenweg 7, 07743 Jena, Germany

[c] Institute of Pharmacy, Department of Pharmaceutical Technology, Friedrich Schiller University Jena, Otto-Schott-Str. 41, 07745 Jena, Germany

KEYWORDS: RAFT polymerization; block copolymers; pH-responsive polymers; nanoprecipitation; pH-responsive polymersomes; vesicle-to-micelle morphology transition; drug delivery.

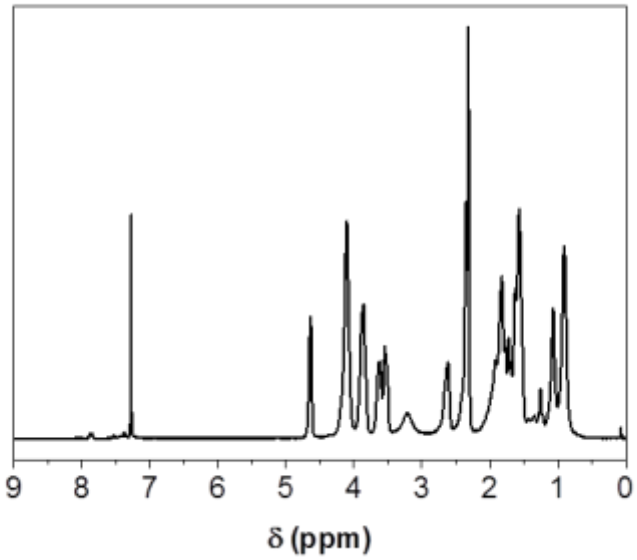

Figure S1. ^{1}H NMR spectrum (300 MHz, $CDCl_3$) of $\mathbf{A_{35}B_{21}}$.

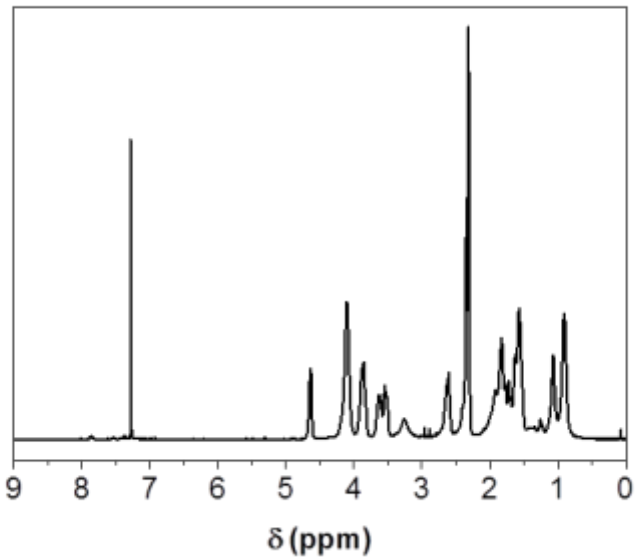

Figure S2. ^{1}H NMR spectrum (300 MHz, $CDCl_3$) of $\mathbf{A_{35}B_{30}}$.

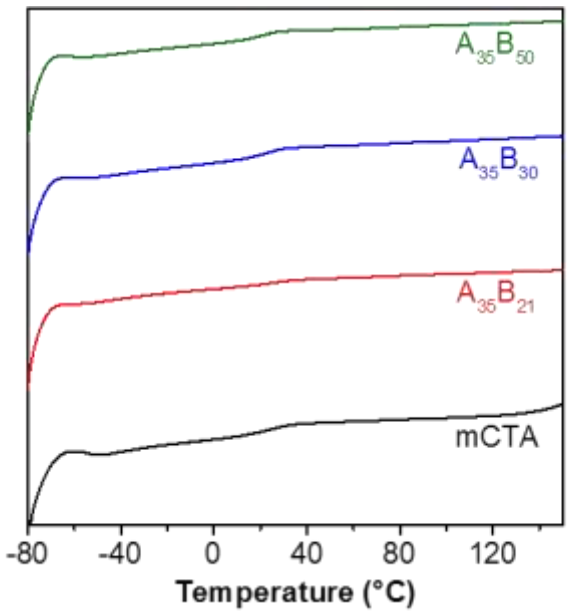

Figure S3. DSC heating runs of **mCTA** and the block copolymers $\mathbf{A_{35}B_{21}}$ to $\mathbf{A_{35}B_{50}}$ (heating rate 20 K min^{-1}).

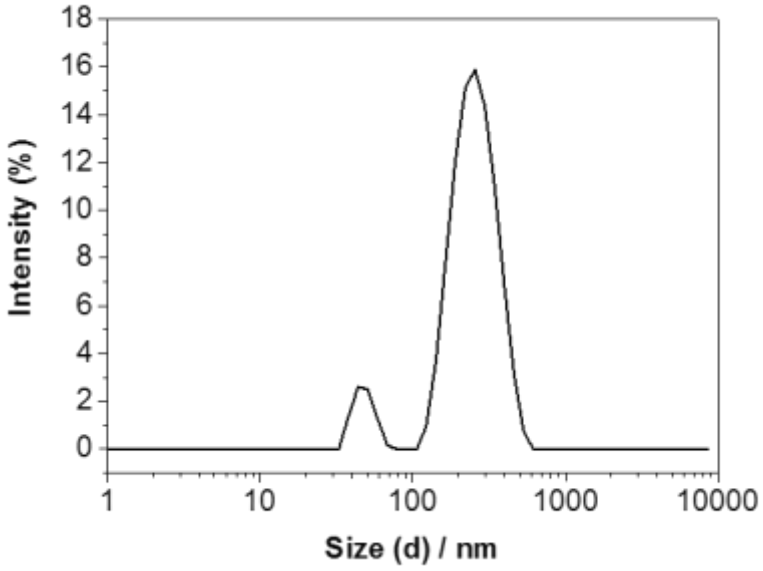

Figure S4. Intensity size distribution of the $\mathbf{A_{35}B_{21}}$ suspensions.

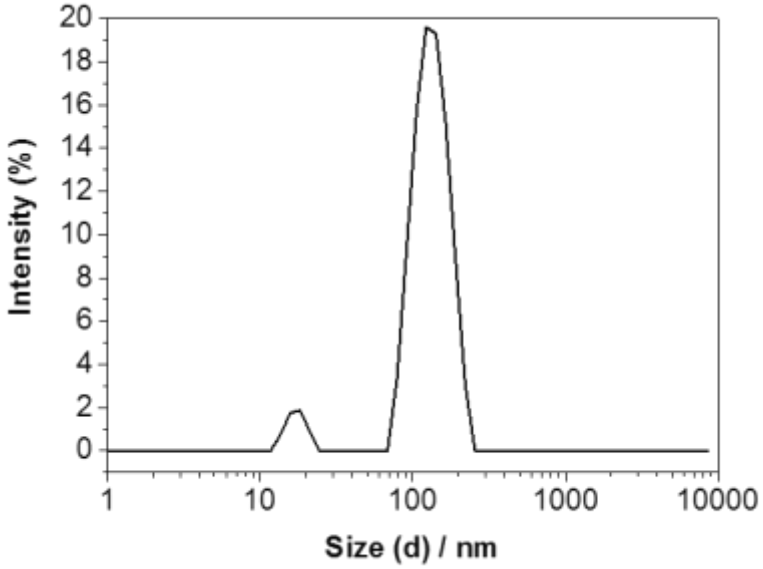

Figure S5. Intensity size distribution of the $\mathbf{A_{35}B_{30}}$ suspensions.

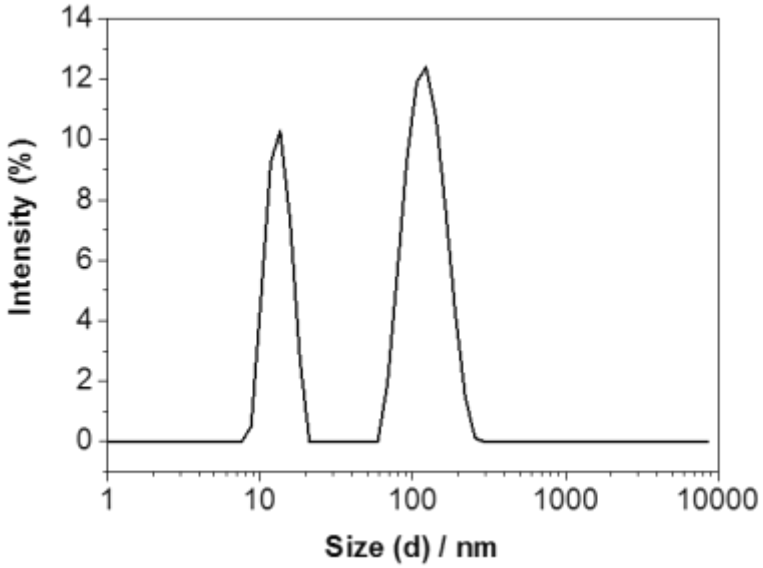

Figure S6. Intensity size distribution of the $\mathbf{A_{35}B_{50}}$ suspensions.

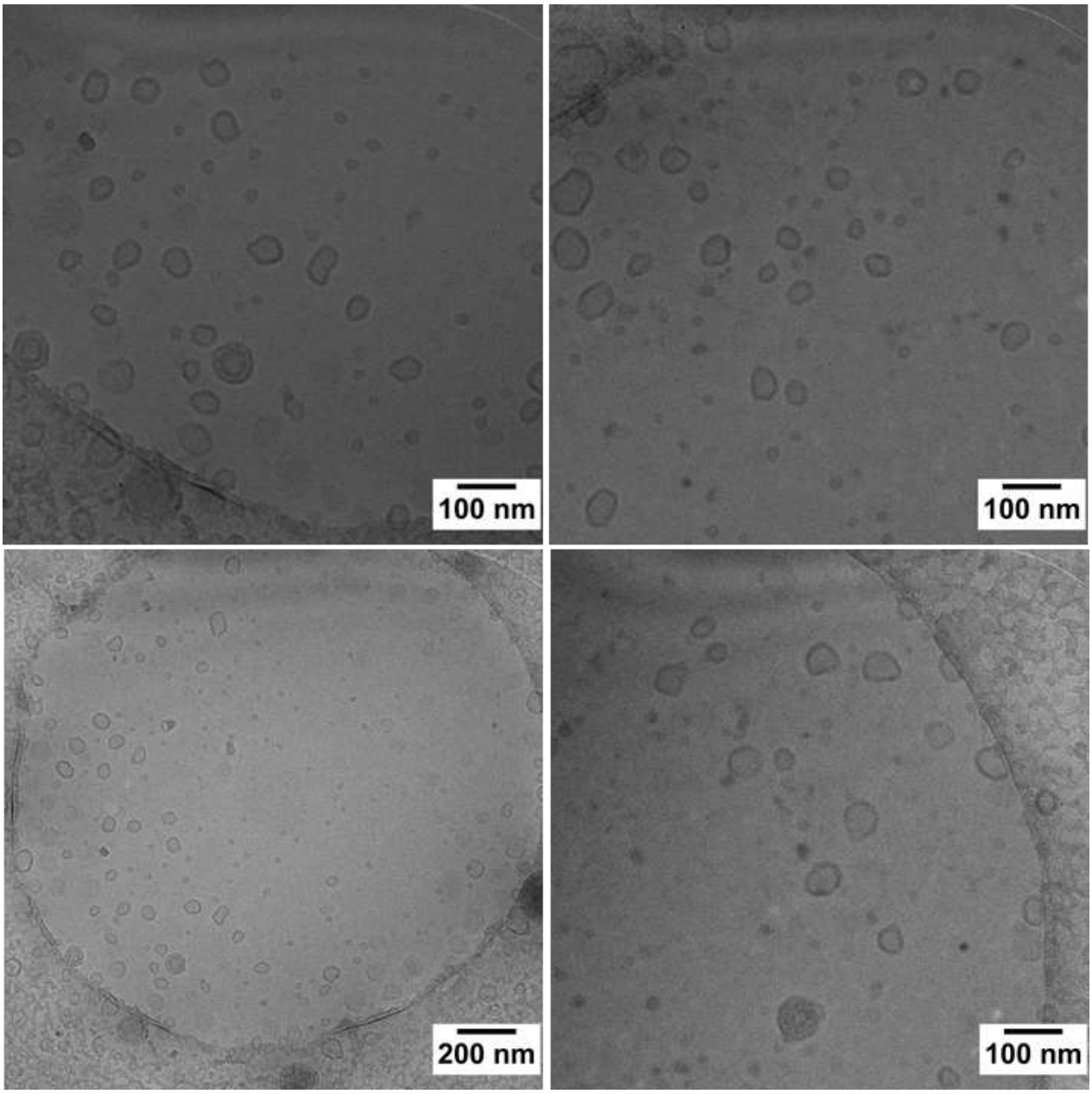

Figure S7. Cryo-TEM image of the $\mathbf{A_{35}B_{21}}$ suspension in pure water (c = 2.5 mg mL^{-1}).

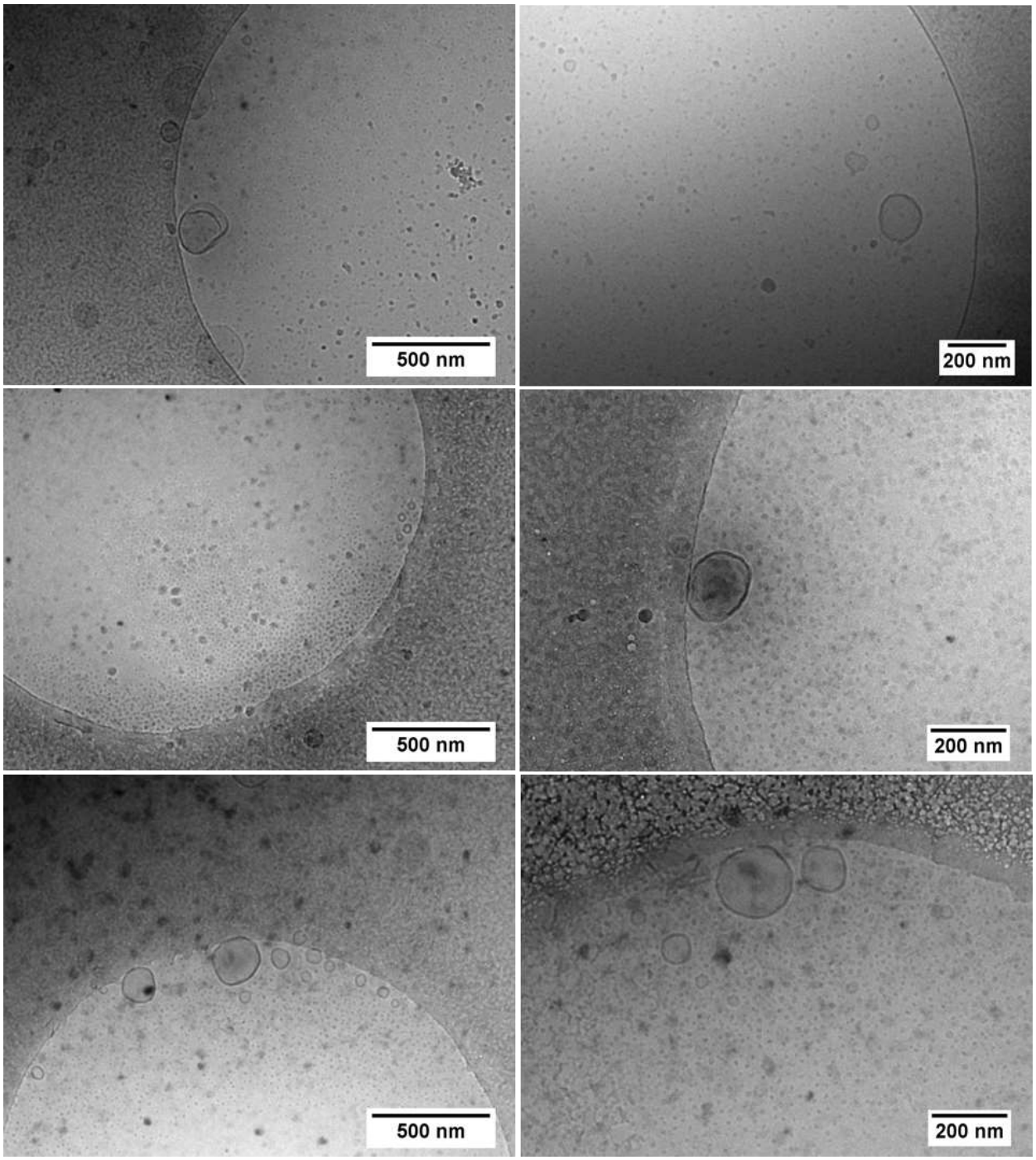

Figure S8. Cryo-TEM image of the $\mathbf{A_{35}B_{30}}$ suspension in pure water (c = 2.5 mg mL^{-1}).

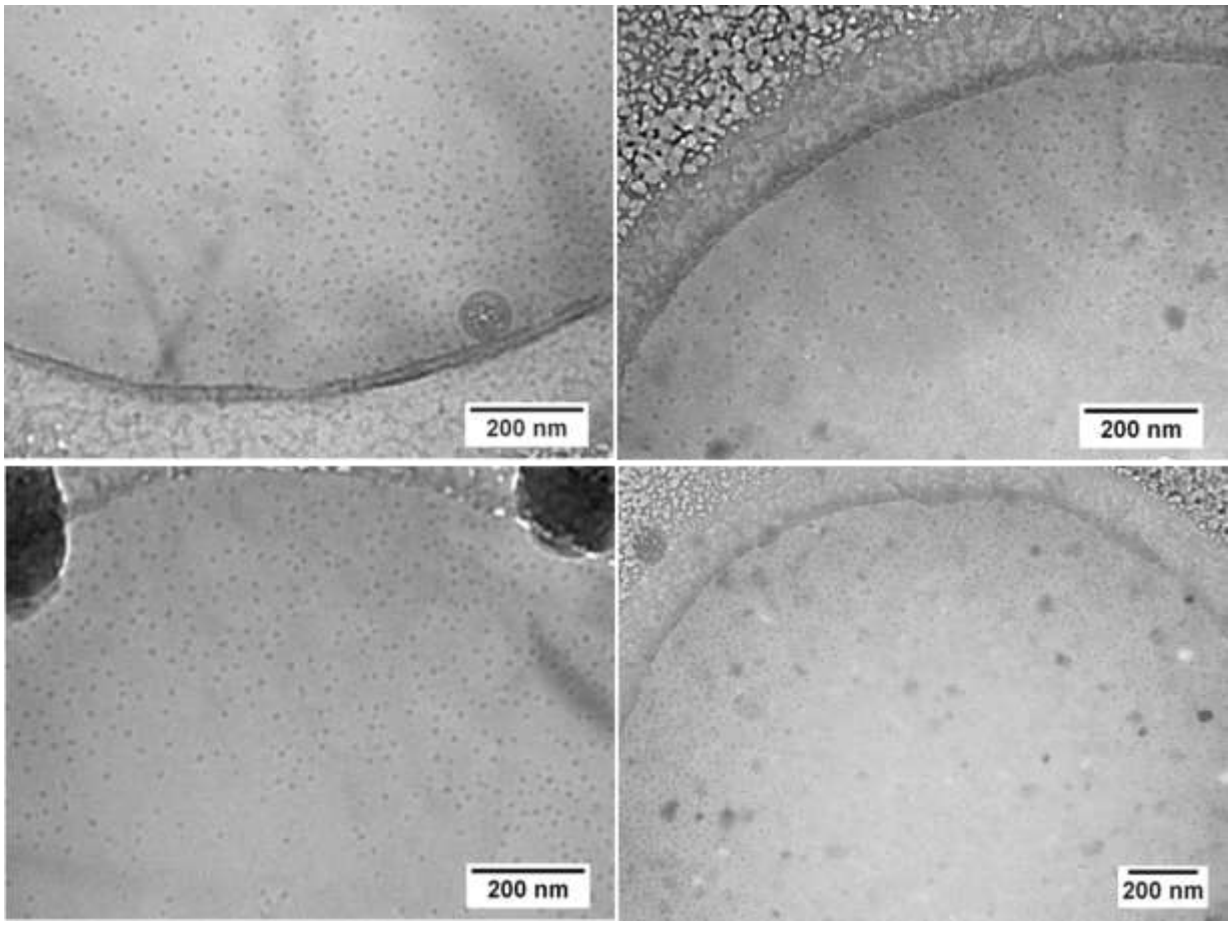

Figure S9. Cryo-TEM image of the $\mathbf{A_{35}B_{50}}$ suspension in pure water (c = 2.5 mg mL^{-1}).

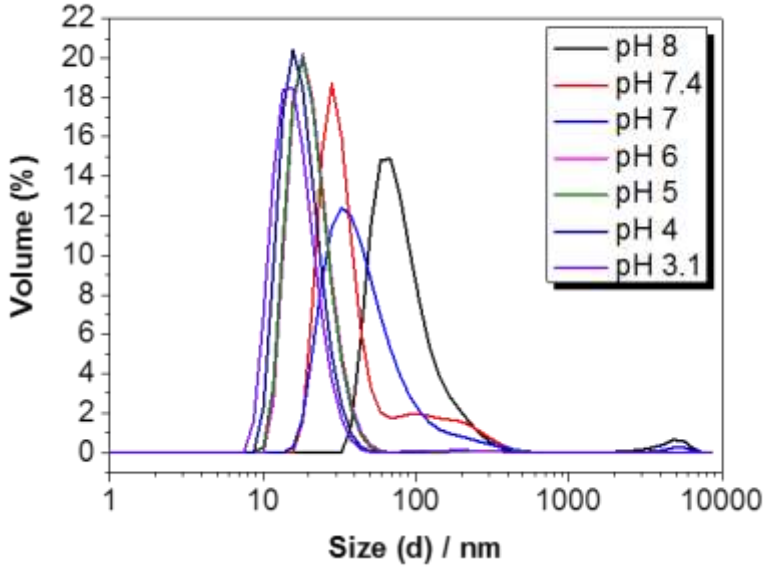

Figure S10. Volume size distributions of the $\mathbf{A_{35}B_{21}}$ suspension as a function of the pH value.

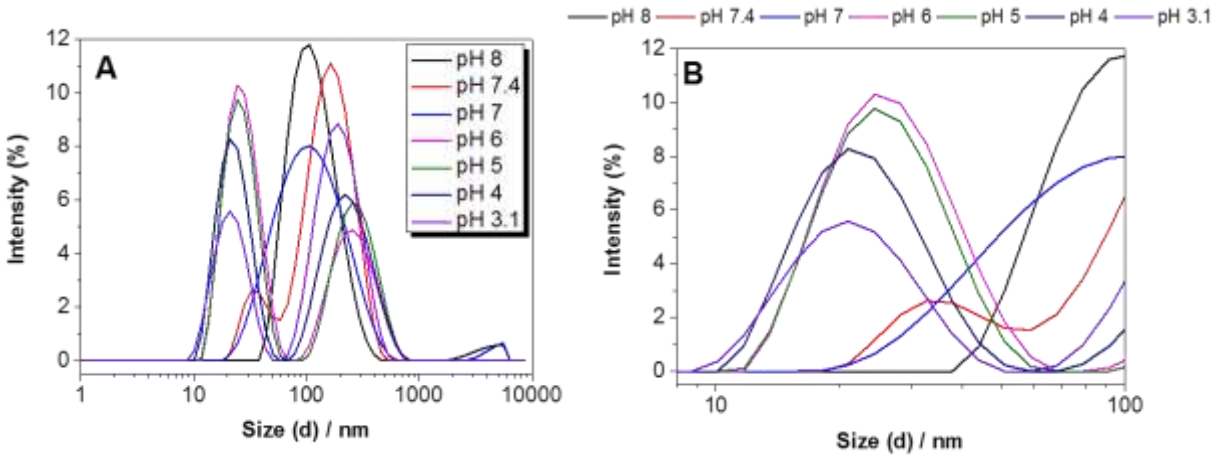

Figure S11. (A) Intensity size distributions of the $\mathbf{A_{35}B_{21}}$ suspension (A) between 1-10000 nm (B) between 8-100 nm as a function of the pH value.

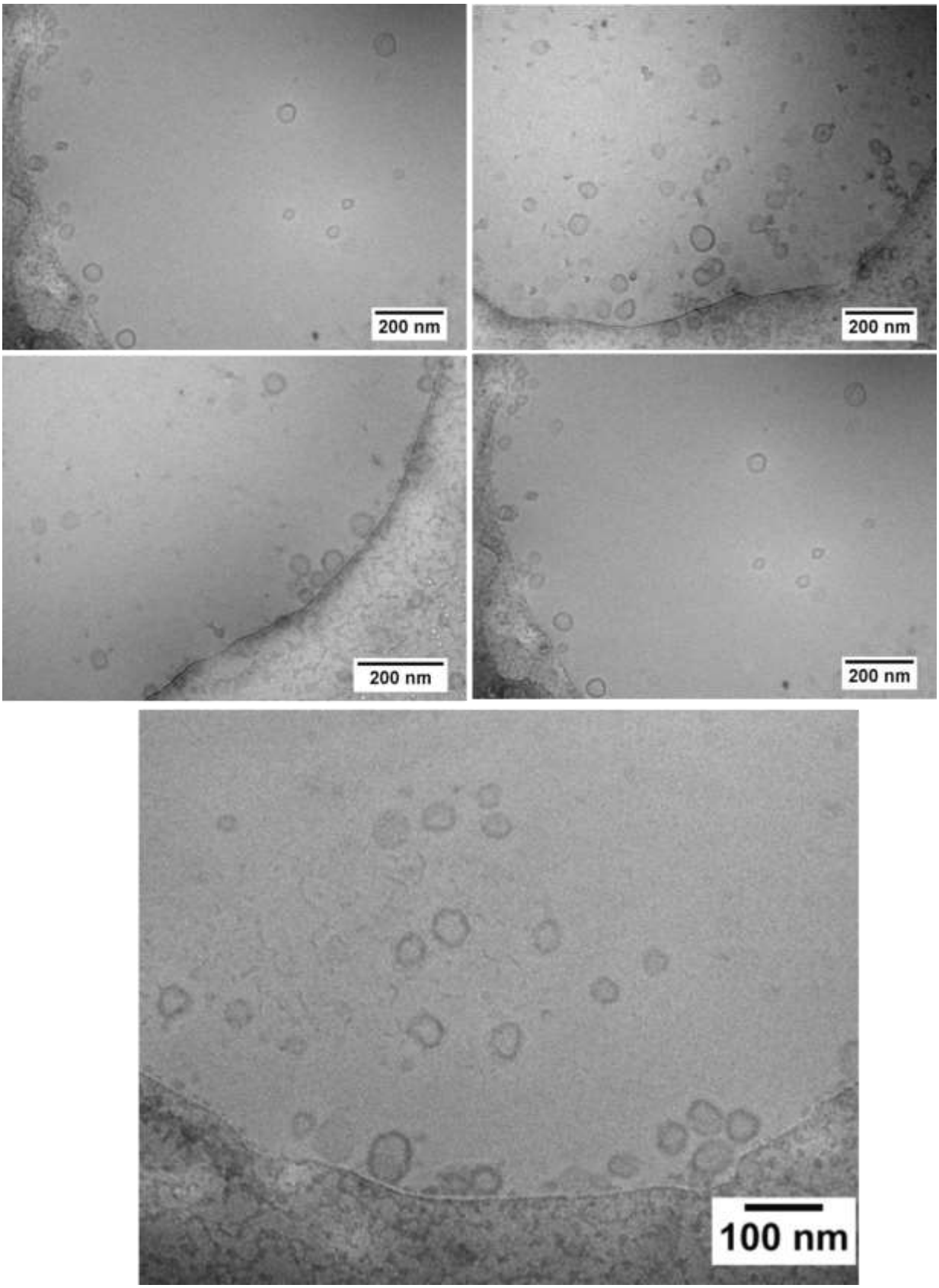

Figure S12. Cryo-TEM image of the $\mathbf{A_{35}B_{21}}$ suspension at pH 7.4.

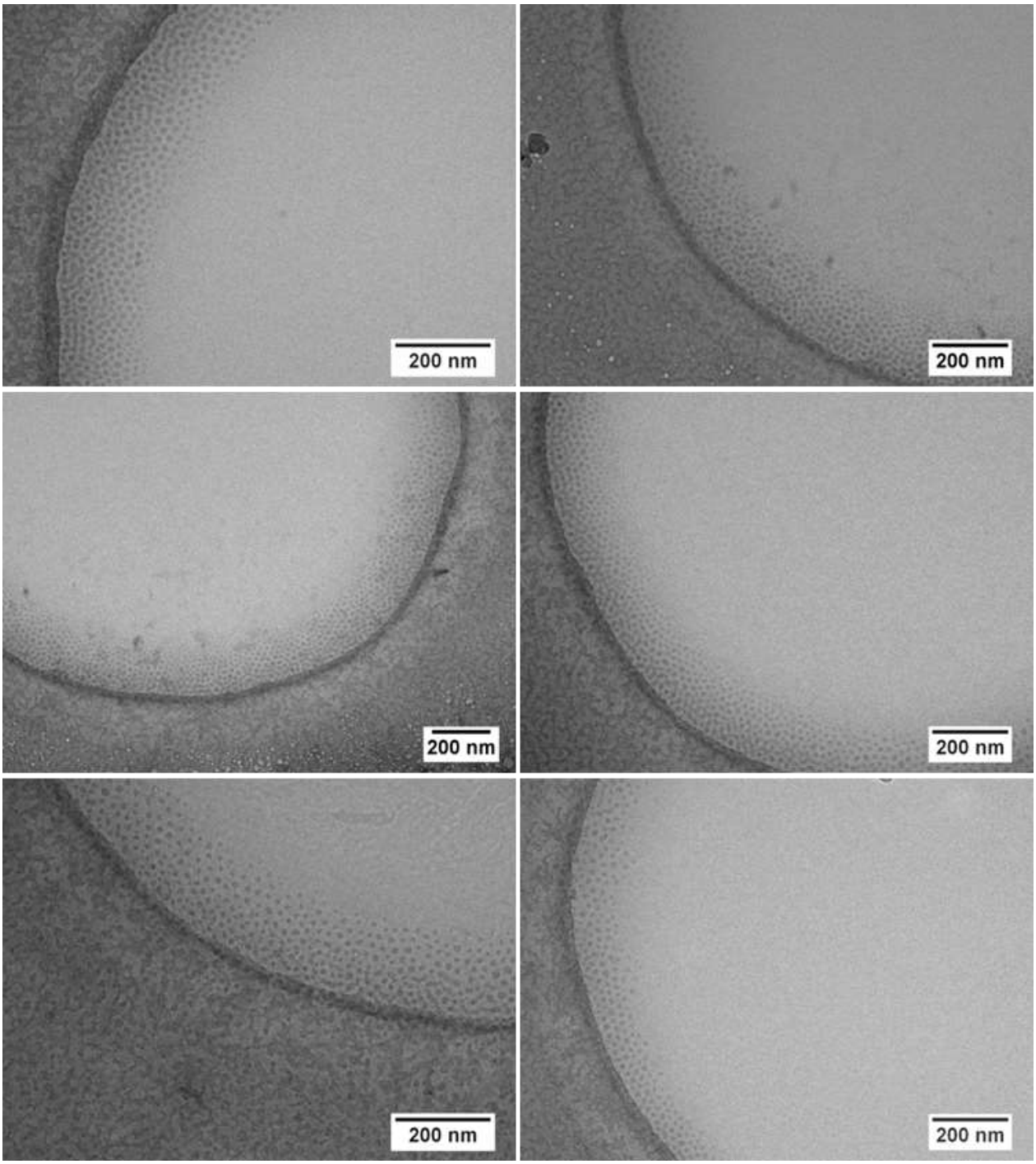

Figure S13. Cryo-TEM image of the $\mathbf{A_{35}B_{21}}$ suspension at pH 5.0.

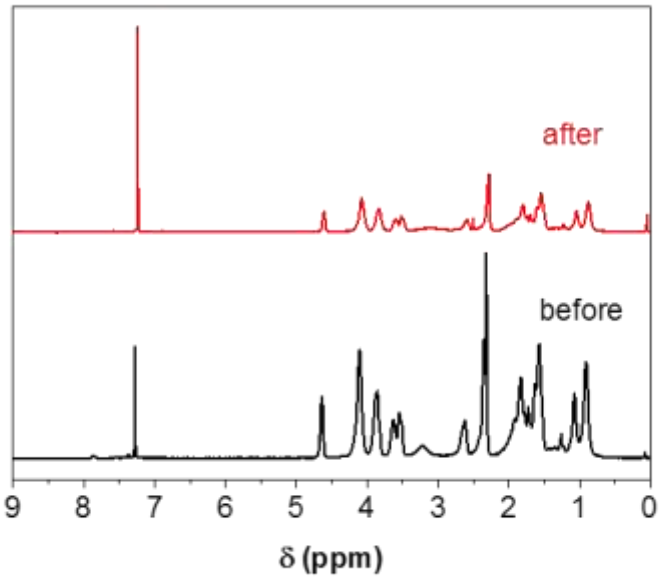

Figure S14. ^{1}H NMR spectrum (300 MHz, $CDCl_3$) of $\mathbf{A_{35}B_{21}}$ suspension before and after treatment with 0.1 M acetate buffer (pH = 4, stored at 37 °C for 3 h).

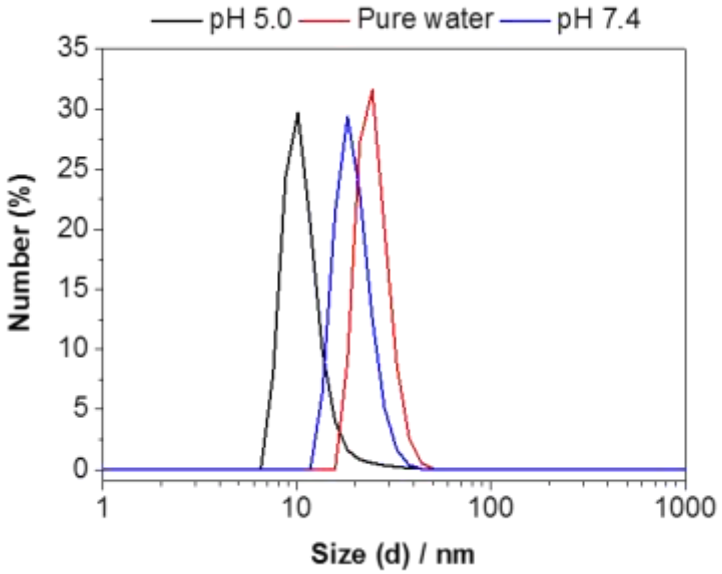

Figure S15. Number size distributions of $\mathbf{A_{35}B_{21}}$ suspensions in different media.

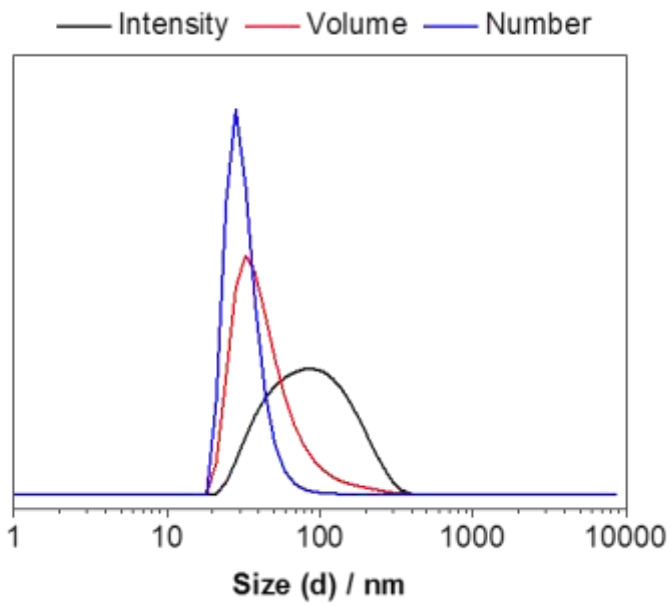

Figure S16. Intensity, volume and number size distributions of DOX·HCl loaded polymersomes in water.

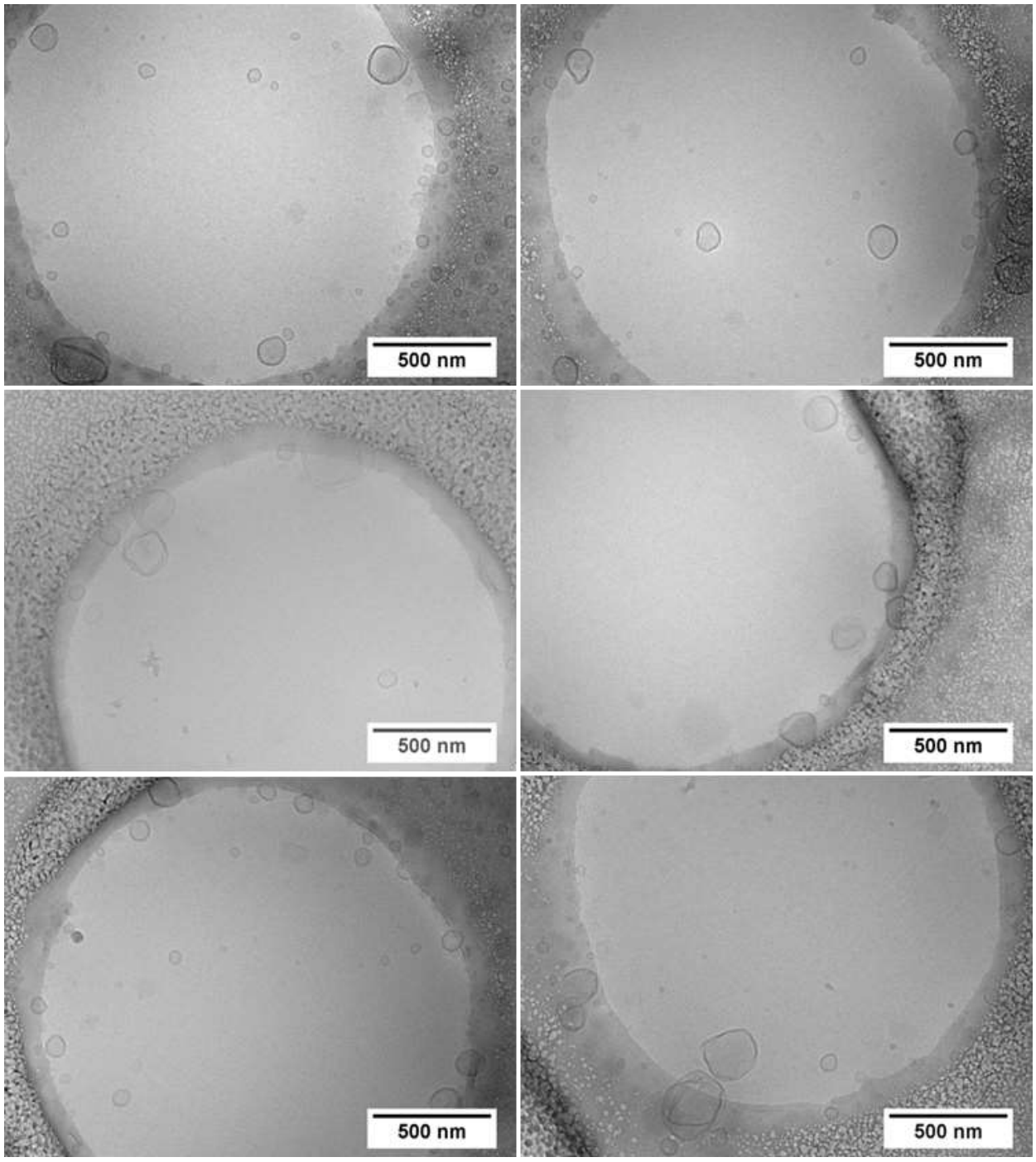

Figure S17. Representative cryo-TEM images of the DOX·HCl loaded polymersomes.

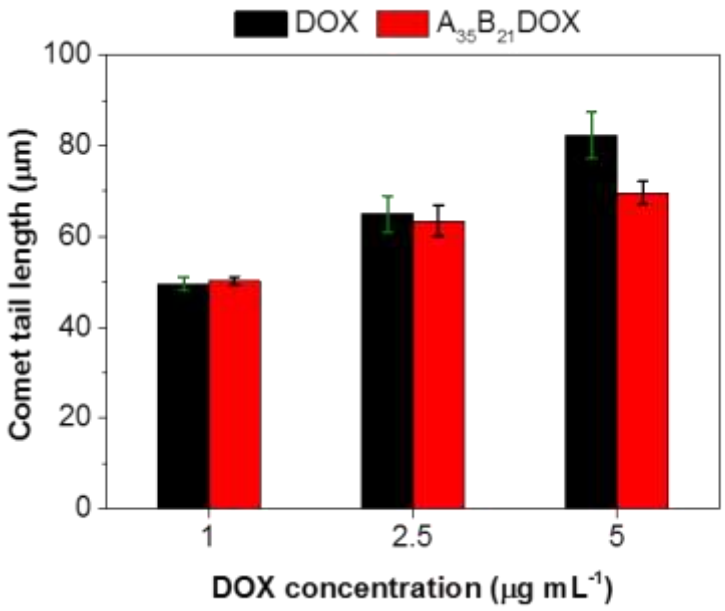

Figure S18. Mean tail length of 100 individual comets as a parameter of DNA damage in cells treated for 24 h with free DOX·HCl and DOX·HCl encapsulated $\mathbf{A_{35}B_{21}}$ suspension.

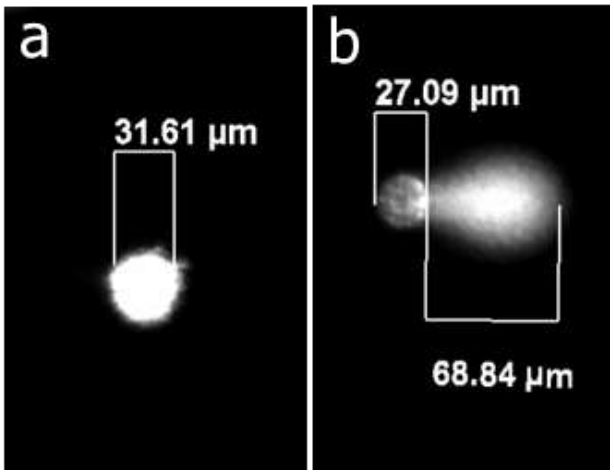

Figure S19. Pictures show a representative micrographs of an intact nucleus from a control sample (A) and the comet like tail of nucleic DNA in a sample treated with 2.5 μg DOX·HCl encapsulated $\mathbf{A_{35}B_{21}}$ suspension (B).